The Effect of Surgical Alignment and Soft Tissue Constraints on the Kinematics, Contact Pressure and Wear of a Total Knee Replacement

Helena E. Johnston

Submitted in accordance with the requirements for the degree of

Doctor of Philosophy

The University of Leeds

Mechanical Engineering

March 2019

The candidate confirms that the work submitted is their own, except where work which has formed part of jointly authored publications has been included. The contribution of the candidate and the other authors to this work has been explicitly indicated below. The candidate confirms that the appropriate credit has been given within the thesis where reference has been made to the work of others.

Some of the work in Chapters 4 and 5 of the thesis has appeared in publication as follows:

Representing the effect of variation in soft tissue constraints in the experimental simulation of total knee replacements, Journal of the Mechanical Behavior of Biomedical Materials, November 2018. H. Johnston, A. Abdelgaied, H. Pandit, J. Fisher and L.M. Jennings.

I was responsible for carrying out the experimental studies and the analysis of the results. The other authors contributed with feedback and comments on the paper.

Some of the work in Chapters 6 and 7 of the thesis has appeared in a publication currently under review:

The Effect of Surgical Alignment and Soft Tissue Conditions on the Kinematics and Wear of a Fixed Bearing Total Knee Replacement. H. Johnston, A. Abdelgaied, H. Pandit, J. Fisher and L.M. Jennings.

I was responsible for carrying out the experimental studies and the analysis of the results. The other authors contributed with feedback and comments on the paper.

Acknowledgements

I would like to thank everyone who helped me to complete this project. Thanks in particular to my supervisors Dr Louise Jennings, Dr Abdellatif Abdelgaied, Professor Hemant Pandit and Professor John Fisher for their helpful guidance and suggestions throughout the project. Particular thanks also to the iMBE lab technicians including Lee Wetherill, Rhys Moore and Phil Wood, your help with the experimental work was invaluable. I am thankful that I have been fortunate enough to have been supported throughout my PhD by EPSRC, the Leeds Alumni Fund and EPSRC Centre of Innovative Manufacturing of Medical Devices. I am grateful to have been lucky enough to meet many fantastic people in Leeds and elsewhere.

Abstract

As life expectancy and activity levels increase so does demand on total knee replacements (TKRs). Previous studies have determined that poor alignment can result in pain, lower knee scores or increased wear. However alignment alone may not result in early failure. Instead it may be the combination of alignment and the soft tissue conditions within the knee that are important.

The aim of this study was to investigate the effect of the soft tissues and surgical alignment on the kinematics and wear of a fixed bearing TKR. Experimental and computational studies were carried out under soft tissue and alignment conditions to reflect the range found in vivo. Previous studies have investigated the effect of soft tissues within the knee and the effect of component alignment as individual variables but not in combination.

The higher tension soft tissue conditions resulted in lower displacements and significantly lower wear. Surgical alignment also had a significant effect on the kinematics; a 10° posterior tibial slope dislocated under lower tension constraints. Rotational mismatch resulted in significantly higher tibial rotation and abduction-adduction displacements, which can lead to knee pain and instability.

The tibial slope and rotational mismatch alignment conditions resulted in significantly higher wear rates than mechanical alignment or 4° varus joint line. Rotational mismatch should be kept within 4°, the tibial slope should be lower than 4° and the angle between components in the coronal plane should be restricted under kinematic alignment to reduce the rotations and wear.

In conclusion, surgical alignment and soft tissue tensions significantly affected the kinematics and wear in this study. One limitation is that the effect of these conditions on patient satisfaction is unknown. Further investigations should be carried out to determine adverse biomechanical conditions in different TKR designs.

Contents

List of Figures

Nomenclature

AA abduction-adduction
ACL anterior cruciate ligament
AF axial force
AP anterior-posterior
ASTM American Society for Testing and Materials
BMI body mass index
CAS computer assisted surgery
CI confidence interval
CL collateral ligament
CR cruciate retaining
CS cruciate substituting
CVD curved tibial insert
FE flexion-extension
HKA hip knee ankle
IE internal-external
IKS international knee score
ISO International Organization for Standardization
KS knee simulator
KSS knee society score
LCL lateral collateral ligament
MC million cycles
MCL medial collateral ligament
NJR National Joint Registry
OA osteoarthritis
PCL posterior cruciate ligament
PLI partially lipped insert
TKR total knee replacement
TR tibial rotation
UHMWPE ultra high molecular weight polyethylene

Chapter 1

Introduction & Literature Review

1.1 Introduction

Over 100,000 primary total knee replacements (TKRs) were carried out in England, Wales and the Isle of Man in 2017 [150]. Wear is one of the main causes of failure in TKRs [75, 149, 150, 178]. Wear of the tibial insert can lead to bone resorption around the implant, aseptic loosening, leading to instability and early failure. As life expectancy and activity levels increase this could become more of an issue; demand is projected to increase in USA by more than 600% by 2030 [25, 122]. The risk of revision also increases as the age at primary implantation decreases, with the lifetime risk of revision at 35% for patients aged 50-54 years [25].

Experimental wear simulation has been used to predict the wear performance of total joint replacements. In addition to patient and surgical factors the wear of a TKR has been shown to depend on a number of factors including insert material (bearing), component design, surface geometry, contact area, stress and knee kinematics [6, 44, 97, 132]. Therefore understanding the factors that lead to abnormal mechanics and increased wear are vital in developing long lasting TKRs.

Currently standard conditions for knee simulation are a walking cycle with an ideally aligned knee, representing an average patient. Experimental simulation may generate the average wear found in vivo but not the range of outcomes found in retrievals [85, 95]. This may be due to factors not currently replicated in standard knee simulation.

Component alignment may result in early failure; it has been linked to knee pain, worse knee scores, higher contact stresses and increased wear rates [26, 31, 52, 56, 65, 66, 68, 126, 184, 201]. However few studies have compared the effects of alignment on wear, most of these have only looked at alignment in the coronal plane [65, 184]. So little is known as to the extent that alignment can affect wear of TKRs.

There are two main wear modes in TKRs; surface wear and fatigue wear. Surface wear occurs when some of the bearing material is moved by hard particles between two moving surfaces. Fatigue wear occurs under cyclic loading when the applied load is greater than the fatigue strength of the material. Many studies have shown that component alignment can lead

to higher contact stresses [52, 53, 126, 201], however if these stresses are below the fatigue stress of the tibial insert it may not increase the wear. Below the fatigue stress an increase in contact area between the tibial and femoral components will lead to a larger wear scar and therefore increased wear [6, 69, 76].

In experimental simulation the kinematics have also been shown to affect the wear rates with an increase in anterior-posterior (AP) motion and tibial rotation (TR) increasing wear [20, 132]. Experimental and cadaveric studies have shown that component alignment affects the movement of the joint and can change the AP displacement or TR rotation, therefore affecting the wear [92, 201].

Currently few studies have investigated the effect of alignment on wear. An experimental and a retrievals study both found that varus malalignment of 3° resulted in the wear rate almost doubling [65, 184]. While a computational study determined that rotational alignment may result in the greatest increase in wear [135]. This research aims to investigate the effect of alignment on the kinematics of the joint and the wear. The amount of alignment simulated in each plane will represent the variation found in patients.

Alignment of the TKR may not result in failure, often failure occurs due to a combination of factors such as alignment and body mass index (BMI) [32]. One cadaveric study determined that changes in the load distribution of the TKR were proportional to the angle of coronal alignment [201]. It was also determined that tight ligaments resulted in more balanced loading. This study suggested that alignment alone may not result in imbalanced loading, but it is the combination of alignment and soft tissue conditions that are important.

Patient factors have been shown to affect the wear of TKRs; patient weight [30], the activities they perform [97], soft tissues and muscles [140], the surgical alignment [65, 140, 184], and interactions between these factors, such as soft tissue and muscle mechanics producing different kinematics for specific activities. Patient factors are outside the control of the operating surgeon. The aim of a TKR is to provide a stable knee which will function optimally and last long. Stability of the TKR is partly dependent upon muscle strength, ligament integrity and TKR design. A more congruent tibial insert will result in a more stable knee. Increasing ligament laxity will introduce instability.

Simulating a wider range of patient conditions may replicate the range of outcomes that occur in vivo and increase our understanding of factors that lead to early or mid-term failure, or higher rates of failure in younger patients.

There are two approaches to experimental knee simulation; displacement control and force control. Displacement control defines the AP displacement and TR rotation during the gait cycle. Conversely, force control uses the AP force and TR torque profiles as inputs, allowing the joint to move in response to the test conditions such as the applied forces and design of the tibial insert. Both methods of simulation have their place, the choice between them depends on the research question. Force control results in more variation in the motions between the stations on the simulator, as differences such as component position or friction will affect the kinematics. In a study investigating predefined kinematics, for example a particular action

such as walking up stairs, displacement control would be the better option. Conversely under force control the motion of the knee can change in response to conditions such as the soft tissue constraints and insert design. For tests where the kinematics are not known, for example under different soft tissue conditions, force control would be used. However it must be recognised that in defining specific soft tissue constraints as an input in the force control situation, the kinematic output is being indirectly controlled. There are ISO [186, 188] standard TKR test conditions for both force and displacement control simulation. These define test conditions such as the input profiles and methodology.

Under force control simulation springs are used to replicate the soft tissues within the natural knee, including the ACL and PCL. As the soft tissues within the knee are not linear elastic The ISO standard [186] AP and TR springs profiles use linear springs but with a gap around the zero position [73, 113]. The size of this spring gap reflects the laxity within the knee.

As soft tissues within the knee vary between patients the spring gap and stiffness are difficult to choose. Ligament balance during surgery is a subjective process so can lead to unbalanced knees [17, 86]. Ligament balancing is an important factor in wear, range of motion, and pain [17] as it affects the mechanics of the knee, the kinematics and the resulting variation in performance and wear in individual patients.

Just as soft tissue tension and laxity influences kinematics in the natural knee the spring stiffness and spring gap will influence resultant kinematics in the force control knee simulator.

Experimental simulation is expensive with respect to time and cost therefore natural knees and TKRs have previously been modelled using finite element methods [6, 9, 94, 116, 126]. Computational modelling can provide outputs that are not available under experimental methods. For example dynamic measurement of contact area, contact pressure and shear forces. In this research a computational model was developed to simulate the experimental simulation conditions. The model was used to predict the output kinematics, contact pressure and contact area during the gait cycle under a wider range of alignment and soft tissue conditions.

The aim of this study was to experimentally and computationally investigate the effects of variation in the soft tissue constraints and component alignment on the output kinematics, contact area and wear of a fixed bearing TKR. A systematic investigation was carried out to address the following research questions:

1. What effect does the experimental and computational simulation of different soft tissue conditions have on the output kinematics with different tibial insert geometries?

2. What effect do soft tissue conditions have under mechanical alignment conditions on the kinematics, contact area and wear?

3. What effect do component alignment conditions have on the kinematics, contact area and wear?

4. What effect does the combination of different soft tissue conditions and component alignment have on the kinematics, contact area and wear?

In Chapter 2 the experimental methods used within the study will be detailed including the use of the knee simulator, the contact area measurements and analysis of the wear scars. This chapter will also detail the validation of the experimental methods and the knee simulator.

In Chapter 3 the development of the computational model will be detailed. Including initial validation of the computational model, such as mesh convergence. Further validation of the model using the experimental data will be detailed in later chapters.

In Chapter 4 the effect of different spring profiles, such as different spring gaps and tensions, will be investigated on different tibial insert geometries. This will investigate the effect of the experimental simulation of the soft tissue conditions on the output kinematics. The computational simulation of the soft tissue conditions will then be validated using the experimental results.

In Chapter 5 the effect of three different soft tissue conditions, representing a stiff knee, a resected ACL and a resected ACL & PCL, will be investigated under mechanical alignment conditions on the output kinematics, contact area and wear. The computational model will then be validated under the same simulation conditions using the experimental data. Further outputs such as the contact pressure and contact are throughout the cycle will be found using the computational model.

In Chapter 6 the effect of different component alignment conditions will be investigated. In the experimental study five different alignment conditions were studied; mechanical alignment, 4° femoral and tibial varus, 14° rotational mismatch, 10° posterior tibial slope and kinematic alignment conditions. These were studied under the soft tissue conditions representing a stiff knee. The computational model was then validated under the same study conditions using the experimental data. Further alignment conditions were then studied computationally including, 2° femoral and tibial varus, 8° and 4° rotational mismatch, 4° posterior tibial slope and kinematic alignment with half the values studied experimentally.

In Chapter 7 the effect of the combination of soft tissue conditions and alignment conditions was studied. The same three soft tissue conditions as those investigated in Chapter 5 were applied in combination with the five alignment conditions investigated in Chapter 6. Again the computational model was validated using the experimental data and the further alignment conditions studied in Chapter 6 under all three soft tissue conditions.

Finally in Chapter 8 there will be a discussion of the results, with a summary of the effect of each alignment condition. The clinical significance of the results will also be discussed along with the limitations of the research, further work and final conclusions.

1.2 Knee Anatomy and Function

The knee is made up of three bones; the tibia, femur and patella. The femur has a medial and lateral condyle; the medial is larger and more symmetrical whereas the lateral condyle is slightly shorter and wider. The intercondylar notch separates the two condyles on the distal and posterior sides. The lateral wall of the notch is flat, which is where the anterior cruciate ligament (ACL) is attached. The medial wall is larger, which is where the posterior cruciate ligament (PCL) originates.

The patella sits between the femoral epicondyles with the quadriceps tendon on its anterior side (Figure 1.1). It increases the arm of the quadriceps mechanism and ensures that the contact area increases as the load does during flexion, maintaining constant pressure.

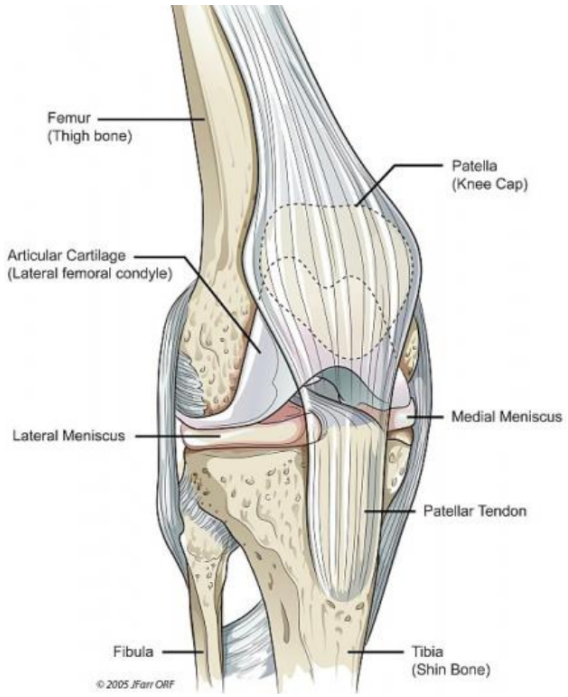

Figure 1.1: Anatomy of the knee. Image reprinted with kind permission by the OrthoIndy Knee Preservation and Cartilage Restoration Centre, Indianapolis, IN, USA [155]

The medial side of the tibial plateau is larger and nearly flat (Figure 1.2), whereas the lateral plateau is narrower and nearly convex. Both sides have a posterior slope of around 10° relative to the long axis of the tibia.

The menisci sit on the edges of the plateau and increase the contact area and conformity of the joint. The tibial spine is a depression that goes anteriorly along the plateau which the ACL and menisci are attached to.

In extension the ACL is taut and the PCL is relaxed, with the opposite in flexion. The ACL stops hyperextension and internal-external rotation it acts as a stabiliser against femoral anterior translation and provides up to 85% of the force resisting this movement [152]. The PCL prevents posterior instability when the knee is flexed. The PCL is the primary stabiliser

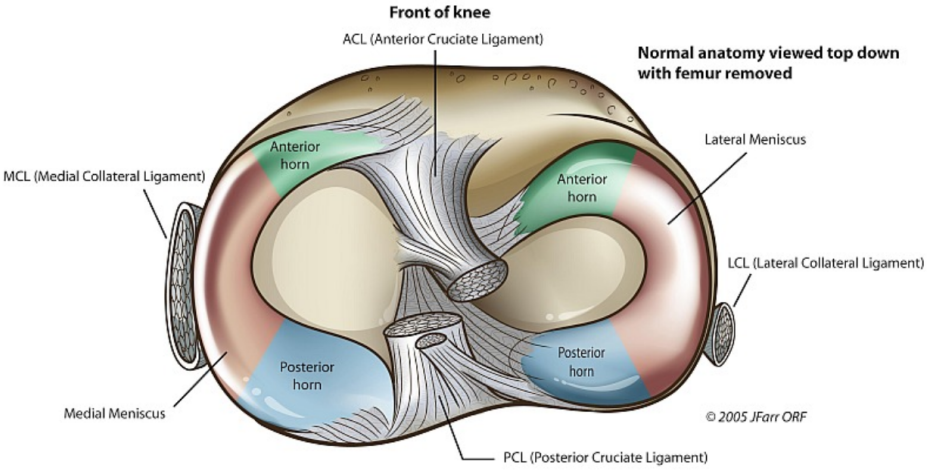

Figure 1.2: Diagram of the tibial plateau. Image reprinted with kind permission by the OrthoIndy Knee Preservation and Cartilage Restoration Centre, Indianapolis, IN, USA [155]

as it is nearly twice as long as the ACL and is close to the central axis of rotation. It provides around 95% of the total restraint to posterior translation [152]. It acts along with the lateral collateral ligament to stabilise the knee. They also perform a proprioceptive function by sending feedback on the position of the joint.

The collateral ligaments are on the medial and lateral sides of the knee and act to restrict abduction-adduction. The medial collateral ligament (MCL) resists abduction and controls rotation of the femur on the tibia in all joint positions. The lateral collateral ligament (LCL) restricts adduction and lateral rotation of the joint during extension. Medial-lateral (ML) translation of the joint is controlled by interaction between the tibial and femoral condyles as well as ligament tensions [141].

There are two main reference axes which are used to define the leg; the mechanical and anatomical axes (Figure 1.3). The anatomical axes follow the long axis of the tibia and femur whereas the mechanical axis goes from the centre of the femoral head, through the centre of the knee to the centre of the ankle. For the tibia the mechanical and anatomical axes are the same and are around 3° from vertical. The mechanical axis of the femur is the same as for the tibia so is 3° from vertical. Whereas the anatomical axis of the femur is 5-7° from the mechanical axis (8-10° from vertical) [163].

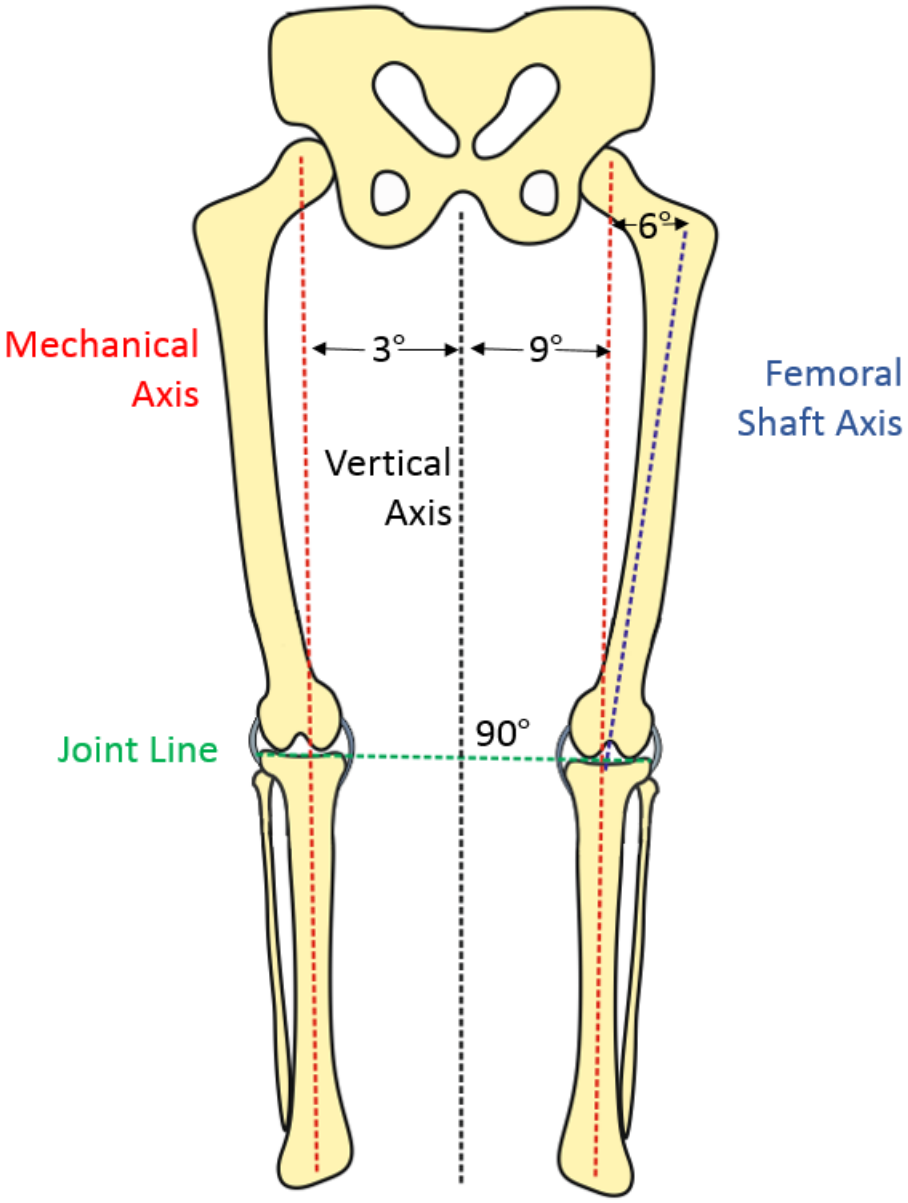

Figure 1.3: Anatomical (femoral shaft axis) and mechanical axes of the leg [83]

1.3 Natural Knee Motion

The knee forms a modified hinge joint, with limited stability from the conformity of the bones which allow six degrees of movement. There is translation in the medial-lateral (ML), anterior-posterior (AP) and proximal-distal directions and rotation in the flexion-extension (FE), tibial rotation (TR) and abduction-adduction (AA) directions (Figure 1.4). The stability and motion are controlled by static and dynamic stabilisers inside and around the joint; menisci, ACL, PCL, collateral ligaments (CL) and muscles.

The average pattern of flexion-extension is biphasic; slight flexion and extension during

Figure 1.4: Directions of motion in the knee

the stance phase then larger flexion and extension during swing. Knee flexion typically varies between 60° and 0° [49, 123] (Figure 1.5).

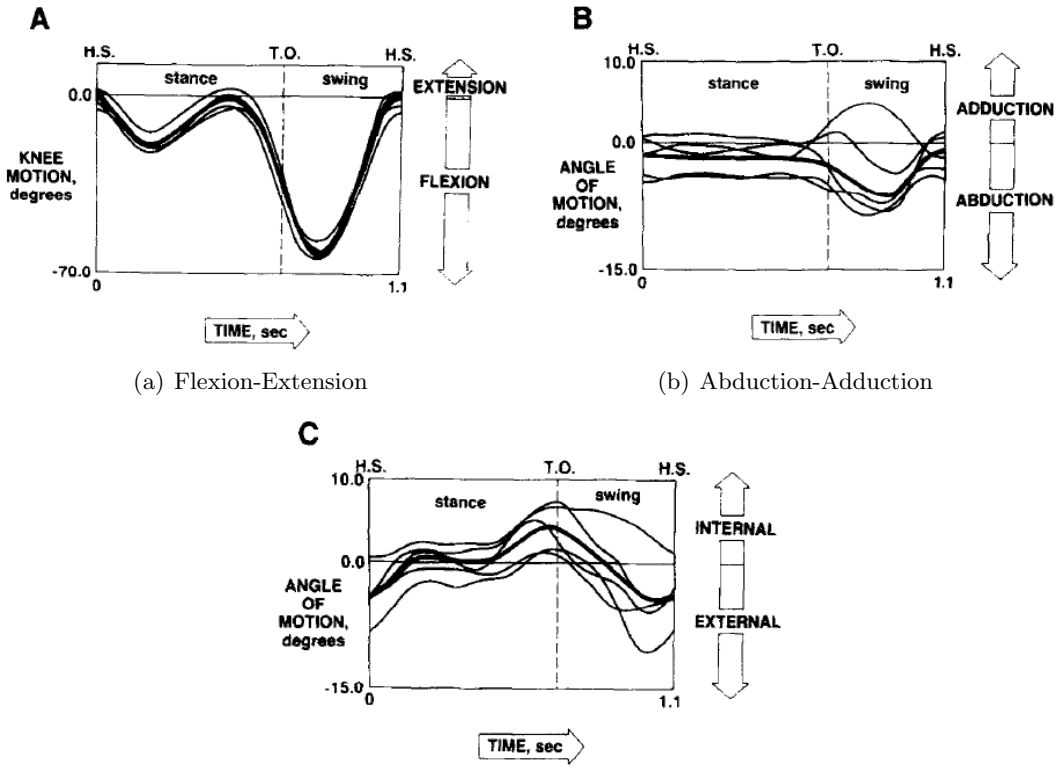

(a) Flexion-Extension

(b) Abduction-Adduction

(c) Internal-External Rotation

Figure 1.5: Motion of the knee in flexion-extension (a), abduction-adduction (b) and internal-external rotation (c) found by Lafortune et al. [123]

Average abduction rotation has a maximum of 5° with most abduction occurring during the swing phase [49, 123]. During both stance and the swing phases the knee rotates internally; at heel strike and just before toe off. The maximum internal rotation in both phases is around

5° [49, 123] .

Rotation of the knee occurs around the axis that passes through the centre of the medial femoral condyle. External rotation of the tibia causes forward movement of the lateral femoral condyle, stretching the PCL. The opposite happens from internal rotation. The ACL does not significantly restrain any internal rotation. The PCL carries a larger force than the ACL and the LCL more than the MCL [141].

As flexion begins there is external rotation of the tibia to "unlock" the knee. During the first 30° of flexion there is femoral rollback of the lateral condyle of the femur on the tibia. After 30° the femoral condyles rotate around one point on the tibial condyles. The medial condyle of the femur has a larger articular surface so when going from flexion to full extension the lateral side of the knee reaches full extension before the medial side. When the knee reaches full extension the femur rotates internally to "lock" the knee. During flexion more rotation is possible in the lateral side than the medial side. Previous studies have found that during gait the contact position of the lateral condyle moves posteriorly by around 4-5mm then moves anteriorly by around 2-3mm for toe off. The medial condyle's position is far more constant and only moves around 1-2mm during gait [98, 105, 117, 146] (Figure 1.6). This is the medial pivot movement.

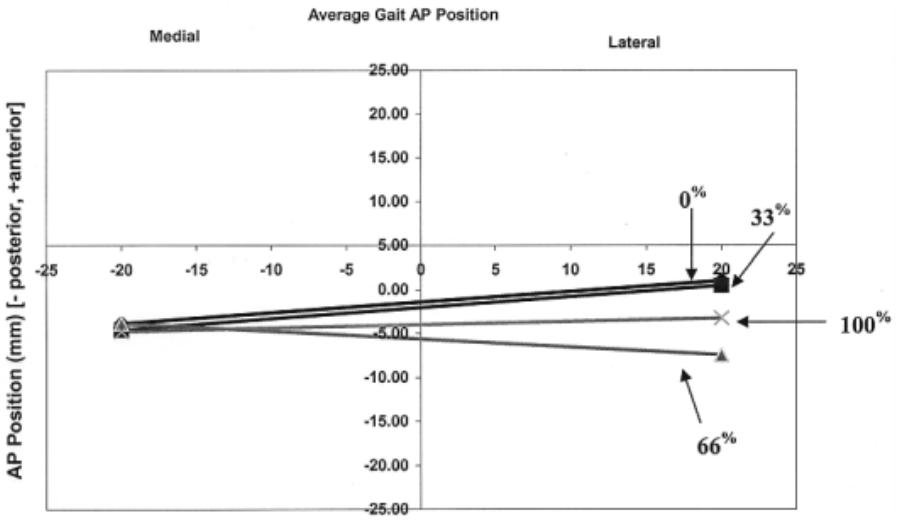

Figure 1.6: Average medial and lateral condyle positions during normal walking (0% heel strike to 100% toe off) as found by Komistek et al. [117]

The movement of the knee is carried out by the hamstrings, biceps emoris, gastrocnemius, popliteus, quadriceps and the soft tissues at the back of the knee. The hamstrings and biceps emoris are the main muscles involved in flexion of the knee. The soft tissues at the back of the knee limit flexion. The quadriceps perform the extension of the knee. The "locking" of the knee is caused by the shape of the ligament attachments and the articulation, making the femur rotate internally in extension [152].

The peaks in joint forces occur when the muscle forces are at a peak; the hamstrings just

after heel strike, the quadriceps femoris and then the gastrocnemius during the stance phase (Figure 1.7). The maximum joint forces vary between 2-4 times body weight [141]. Variations in the joint force between different people may be due to anthropometric and gait differences.

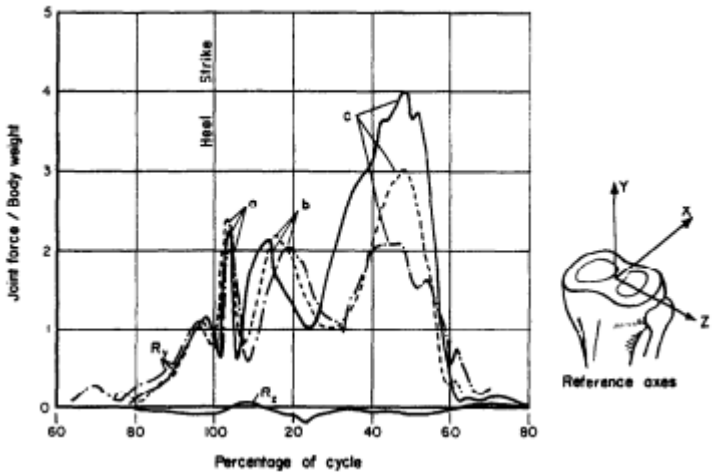

Figure 1.7: Joint forces during normal walking as found by Morrison et al. [141]

The shear force in the joint is relatively small with an average value of around 0.26 times body weight [141].

The kinematics of the knee vary between people, previous studies have found that subjects had similar flexion-extension gait patterns, however for internal-external rotation during stance there was more variation [29].

The measurement of knee kinematics can also be difficult, one of the main issues with gait laboratory studies is the effect of the skin movement that the markers are attached to. This skin artefact affects the output kinematics for the subject. A study using reflective markers to remove the skin artefact found different kinematics to those found previously [14]. This included lower amplitude of AA rotation and different profile shapes for TR rotation ML displacement and AP displacement.

The kinematics of the knee are different between a healthy subject and one with osteoarthritis (OA). One study found that patients with severe and moderate OA had lower flexion angles than normal patients and those with early OA [145]. Severe OA patients also had lower abduction angles. The patients with early, moderate and severe OA had significantly smaller external tibial rotation angles at heel strike than the normal patients.

1.4 TKR Motion

Previous studies have investigated the kinematics of TKR patients One study found that the kinematics of TKR patients were similar to studies with healthy patients, especially when considering the variation in gait between patients [72] (Figure 1.8). However the data for normal knees includes an initial peak at around 25% gait followed by a larger peak later in

the cycle whereas in this study the patient with the TKR just had the second peak of flexion without the smaller intimal peak being present.

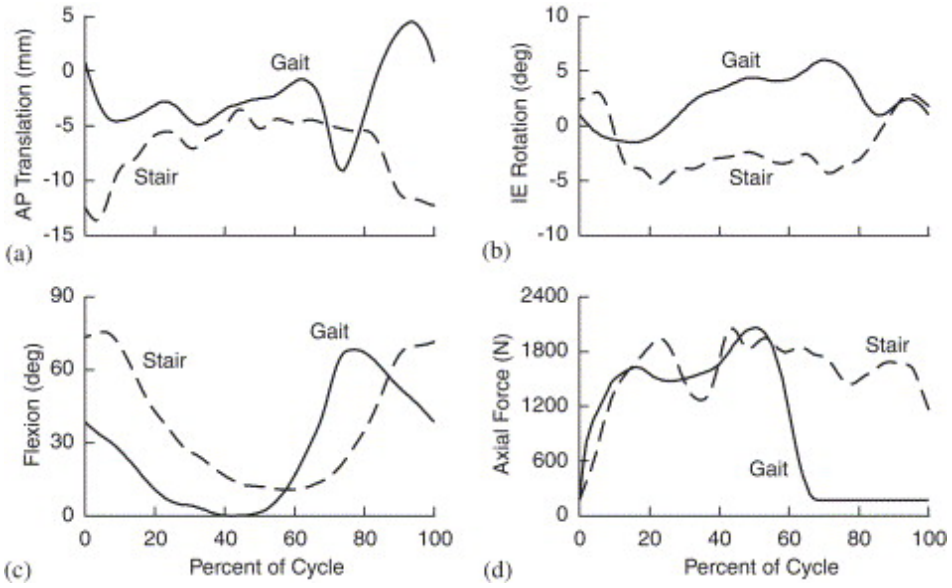

Figure 1.8: Knee kinematics of a subject with a CR TKR walking and climbing stairs as found by Fregly et al. [72]

Anther study into the kinematics of CR TKR patients found that the patients all had a slow walking speed and had a reduced stride length and knee flexion [28].

1.5 Design of Knee Replacements

Knee replacements are made up of femoral, tibial and patellar components (Figure 1.9).

The tibial component consists of a bearing surface and a stem that goes into the tibial bone. These may be made up of a bearing and a tibial tray or combined into one component. The tibial tray is usually made of titanium alloy, cobalt chrome or stainless steel and the bearing components are usually made of ultra high molecular weight polyethylene (UHMWPE). The femoral component is normally made of cobalt chrome and is designed to match the geometry of the knee. The UHMWPE insert is attached to the top of the tibial tray and sits between the femoral and tibial components providing a low friction surface. The patellar component may be used to resurface the back of the patellar and is usually made of UHMWPE. In the UK the patella is usually not replaced, whereas in the US the opposite is true [4].

1.5.1 UHMWPE

1.5.1.1 Formation

UHMWPE is a viscoplastic solid made up of crystalline phases within an amorphous matrix. Rows of carbon atoms in lamellae are surrounded by randomly positioned and entangled polymer chains. Tie molecules connect the lamellae and chains giving the material strength.

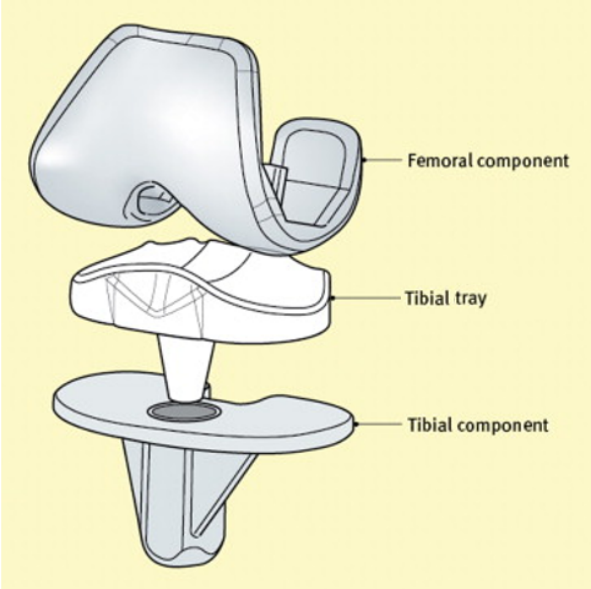

Figure 1.9: Components of fixed bearing total knee replacements. [180]

The chemical structure, molecular weight, crystalline organisation and thermal history all affect the mechanical properties [41, 120].

UHMWPE is formed as a powder by a chemical process and then compacted into a solid, by physical and chemical compaction. This involves the particles adhering to each other after melting and the polymeric chains becoming interpenetrated. The final properties depend on the temperature and the duration the pressure is applied. Compaction is carried out by ram extrusion, slab compression moulding or direct compression moulding, the first two of which may not result in uniform conditions throughout the mass. Air can enter the polyethylene and become trapped during compression or diffusion during storage affecting the production of cross-links. The diffusion of the air is faster in the amorphous phase [37].

1.5.1.2 Gamma Irradiation and Oxidation

UHMWPE can be sterilised using gamma irradiation, which causes scissions producing hydrogen atoms and alkyl radicals. If the irradiation is carried out in the absence of oxygen the alkyl radicals produced in the amorphous phase are mobile so have many opportunities to convert into double bonds within the polymer chain or to recombine and create the original, longer chains (Cross-linking). Within the crystalline phase the radicals are less mobile so remain there for a much longer time. With oxygen present a reaction between the alkyl radicals and the oxygen may occur; oxidative chain scission. This results in short oxidised polyethylene chains and a lower molecular weight of the material [37]. Once this process starts it cannot be interrupted and the rate will increase as more alkyls will be created which will then react with the oxygen. This means that degradation can also occur in vivo leading to weakening of the UHMWPE [37, 41, 42, 119].

Oxidative chain scission results in a lower molecular weight material which is less resistant

to delamination. It can be prevented by using a different sterilisation agent like ethylene oxide or by packaging the component in a vacuum or inert gas to remove the oxygen [37]. Ethylene oxide is a toxic gas that bonds with bacteria, disrupting their function and killing them [120]. During the sterilisation process there needs to be high control over a number of conditions including the temperature, humidity and duration. Gamma radiation has been found to increase the crystallinity of the polyethylene more than ethylene oxide, this is due to the magnitude of the radiation being larger than the bond energy in the UHMWPE [11]. The crystallinity of a polymer has a large impact on its mechanical properties with an increase in crystallinity and decrease in molecular weight attributed to a decrease in mechanical properties [11]. Ethylene oxide sterilised specimens have been found to have both a larger [11] and a lower wear rate [57, 202] than gamma-radiated in past research. This variation in results may be due to variations in the methods of radiation used, some were gamma radiated in air where as others were radiated in nitrogen. It may also be due to the use of different joints; knees [202] and hips [11, 57].

1.5.1.3 Cross-linking

The most common way to create cross-links within the material is by gamma irradiation. Cross-linking UHMWPE has been shown to significantly reduce the wear in joint replacements [75, 77]. During unidirectional motion the molecules in the UHMWPE orientate themselves so that they are aligned in the direction of motion. This makes the material stronger in that direction but weaker in other directions. Cross-linking results in more bonds between the molecules making them harder to split apart. This makes the material stronger as it is less susceptible to orientation hardening and softening and increases the resistance to cross shear. The extra bonds also provide more resistance against scratches and particle movement, reducing the wear [75, 166].

However some studies have shown that cross-linking reduces some mechanical properties of the material, such as strength, elastic modulus, fracture toughness and crack propagation resistance [42, 78]. It has been shown that cross-linking reduces wear however high levels of cross-linking should be avoided [18, 82, 166]. The cross-linked UHMWPE also produces a larger proportion of sub-micron debris, which are more biologically active [42]. Currently moderately cross-linked UHMWPE is commonly used for TKRs as it balances the material properties against the wear rate.

1.5.2 Cruciate Retaining and Cruciate Substituting

Previous studies have investigated the differences between cruciate retaining (CR) and cruciate substituting (CS) joint replacements. The PCL performs an important function within the joint, in stabilisation and femoral rollback. It can absorb some shear forces reducing the amount transmitted to the bone-implant interface and may maintain more natural joint motion [161, 191]. However proponents of PCL substitution believe that resection of the PCL during surgery can cause damage and impair its function [200]. It may also degenerate after

surgery, particularly in patients with osteoarthritis, reducing stability and making cruciate substitution more reliable [171].

The removal of the PCL can encourage posterior tibial subluxation, however a posterior post can help to regain stability and reduce femorotibial rollback (Figure 1.9 (b)). Some studies have found increased flexion and range of movement for CS replacements [129, 171]. However other studies have found no significant difference between CR and CS, with one finding that the final range of movement depends more on the pre surgical range of movement and the patients BMI [143]. A wear analysis study found that the cam-post attrition of the cruciate substituting replacement creates polyethylene debris [167]. This may increase osteolysis in the patient which could lead to early aseptic loosening.

1.5.3 Conformity

Increasing the conformity of the TKR components increases the contact area, which increases the stability. It has also been shown to reduce the fatigue wear and delamination by reducing the contact stresses, as well as reducing the demands on the ligaments [23, 71, 192]. However the improvement of the mechanical properties of the materials has increased the fatigue limit of UHMWPE [69, 76]. Recent studies have shown that if the stresses are lower than the fatigue limit increasing conformity increases the wear as the wear scars cover a larger area [6, 69, 76]. Earlier studies that found that conformity reduced wear, used polyethylene that was oxidised or degraded meaning that the fatigue limit was lower. The increase in contact area was therefore necessary to avoid more wear mechanisms, such as delamination, from occurring.

The conformity of the components also has an effect on the kinematics of the joint and therefore the cross shear. The higher the conformity the more cross shear and the higher the contact area, which increases wear of conventional UHMWPE [6]. Sagittal conformity may be more important than coronal conformity in terms of wear as the conformity in the sagittal plane has been found to have the greatest effect on the kinematics of the joint [71]. Different conclusions have been met about conformity, some believe that conformity should be increased to reduce the stresses and maintain stability. However others believe that the conformity should be reduced. The amount of conformity should maintain a sufficient level of stability and ensure that the stresses do not rise above the fatigue limit of the material [6, 192].

1.6 Causes of Failure

Knee replacements may fail due to factors such as; aseptic loosening, infection, fracture, joint stiffness, instability due to collateral ligament instability and wear or failure of the UHMWPE component [119, 178]. Wear is one of the main causes of failure in TKRs and was the main cause of failure in the 2018 NJR report [75, 150, 172, 178, 190].

1.6.1 Instability

Instability causes around 10-20% of TKR failures [3, 153, 157]. Instability soon after TKR may be due to poor component alignment or soft tissue imbalance. Instability that occurs later is often due to wear of the polyethylene insert [153].

Symmetrical instability occurs when the extension space is too large for the femoral and tibial components [153, 205]. This may be due to over resection of the distal femur, resulting in an elevated joint line. The change in the joint line will affect the patellar tracking, limit flexion and may cause mid flexion instability.

Asymmetrical instability often occurs due to inadequate correction of a preoperative deformity, commonly a varus deformity [153, 205]. If the soft tissues are not released and balanced correctly this may lead to a progressing varus deformity and increased medial stresses, wear, and a loosening of the soft tissues on the lateral side of the knee. This leads to asymmetrical wear of the polyethylene and instability of the knee.

Flexion instability is a result of the flexion gap being too large and is a cause of TKR failure [153, 205]. Early flexion instability is likely due to flexion and extension gap imbalance, whereas late flexion instability may be due to PCL loosening, resulting in wear and instability.

1.6.2 Poor range of motion

A low range of motion can be due to a number of causes including preoperative range of motion, preoperative diagnosis and patient factors such as low pain threshold [54, 112, 153]. Stiffness of the TKR limits motion as well as predisposing the patients to pain.

The positioning of the components is important in range of motion. Internal femoral rotation and patellar maltracking have been found to result in a limited range of motion as well as pain [153]. Stiffness in the knee can also be due to the formation of scar tissue [153].

1.6.3 Aseptic loosening

The wear debris from the UHMWPE can cause a biological response causing osteolysis. The wear debris activate macrophages, which in turn activate osteoclasts leading to bone reduction around the TKR causing it to become loose, this is called aseptic loosening. The bone loss increases the ease of transport of wear debris leading to more bone resorption [190]. The smaller the wear debris the higher the biological response so the greater the osteolysis [108].

The wear rate of the TKR is affected by a number of factors including materials, forces, kinematics and manufacturing processes [5, 6, 44]. The kinematics and contact area of the joint depend on the conformity of the replacement, the ligament tensions, muscle forces and the alignment of the components [6, 44, 92].

1.6.4 Patellofemoral complications

TKR failure may be due to subluxation or dislocation of the patellar or due to knee pain from patellar maltracking [153]. Patellar problems have been reported to occur in 5-30% of TKRs

[136].

The kinematics and alignment of the knee may affect the patellofemoral contact. Internal rotation of the components results in an increased quadriceps angle (Q angle). An increased Q angle reduces the efficiency of the quadriceps muscle and results in a lateral pull on the patella which may cause knee pain, instability and patella maltracking [22, 43, 64, 138, 153, 169, 175]. A previous study found that the mean Q angle was significantly higher for patients with knee pain than those without [64]. An overall valgus leg alignment will also result in an increased Q angle and therefore may lead to pain and instability [153].

Internal rotation of the femoral component will result in increased lateral soft tissue tensions during flexion and may cause patellar maltracking [22, 34, 136, 153]. The soft tissue balance of the knee will also affect the patellar motion; soft tissue imbalance may result in patellar instability [153].

1.7 Tribology

1.7.1 Types of Wear

Wear is the removal of a material because of impact or friction from another surface. There are five main types; abrasive, adhesive, fatigue, erosive and corrosive [108]. Common wear modes in TKRs include scratching (abrasive), burnishing (adhesive), pitting (fatigue) and delamination (fatigue) [108].

Abrasive wear is when the bearing material is moved by hard particles between moving surfaces [111]. If a hard particle is between the articulating surfaces it can cause damage to the softer surface. Abrasive wear can be minimised by using hard and smooth surfaces, like ceramics, and reducing the number of particles between the articulating surfaces by ensuring they are properly cleaned before surgery [108].

Adhesive wear is the transferral of material from one surface to another due to the relative motion of two surfaces and mainly occurs with metal surfaces [108]. There are three types of adhesive wear; severe, moderate and burnishing [168]. Burnishing is the most common adhesive wear in TKRs [108]. Burnishing only occurs in special situations, for example highly compatible surfaces and when there is a low pressure on the surfaces. The transitions between the wear regimes can be sudden as the conditions between the surfaces change [168]. Adhesive wear can be minimised with boundary and fluid-film lubrication (Figure 1.10). Boundary lubrication is when the fluid creates a boundary film between the two surfaces and fluid-film lubrication is when the two surfaces are completely separated with a fluid gap between the two boundary films [108].

Fatigue wear occurs under cyclic loading when the applied load is greater than the fatigue strength of the material. Fatigue cracks are formed at the surface which can then spread to the subsurface of the material, join and result in separation and delamination [118]. Even if the apparent contact stress is under the yield stress local yield can be achieved on the surface of the material due to discontinuities in the material [115]. Under sliding contact the

compressive stress on the surface can stop surface crack formation. Horizontal subsurface cracks can form around discontinuities in the material, these can grow, join and lead to thin sheets of the material detaching from the surface (delamination). Short term fatigue failure can be avoided by minimising the contact stress between the two surfaces [108].

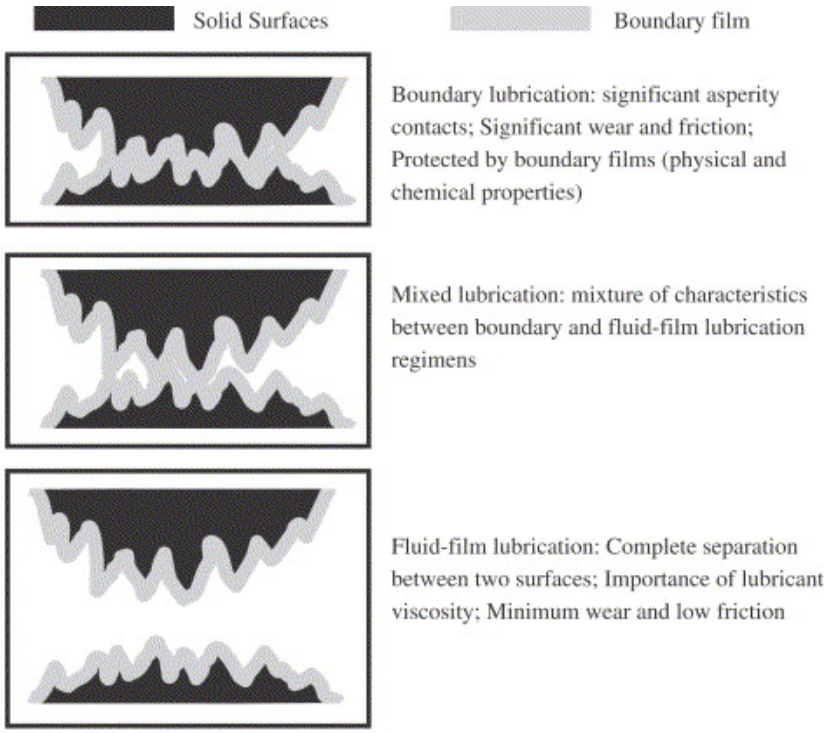

Figure 1.10: Boundary and fluid-film lubrication [108]

1.7.2 Wear Laws

There are three wear laws [108]:

1. As the load normal to the surface (P) increases the wear volume (V) increases
2. As the sliding distance (s) increases so does the wear
3. As the hardness (H) of the softer material increases the wear decreases

These laws can be combined to form equations for the wear coefficient (K_1) and the wear factor (K) (equations 1.1 and 1.2) . The wear factor is often used, as the hardness can be difficult to find for visco-elastic polymers.

$$K_1 = \frac{VH}{Ps} \tag{1.1}$$

$$K = \frac{V}{Ps} \tag{1.2}$$

The real contact area between two surfaces will be smaller than the apparent area as the contact will just be between the asperities on each surface [15, 111]. There is a high pressure in the contact between the asperities, which will cause them to deform until the contact area between the surfaces is large enough to support the applied load. The material that has been sheared off the surface forms debris and may remain between the two articulating surfaces, or if the shear causes a large enough increase in temperature the debris may attach to the surface [111].

1.7.3 Wear Particles

Wear debris can enter the periprosthetic tissue, here the macrophages try to phagocytose the debris. The macrophages release pro-inflammatory cytokines and other mediators, as the debris cannot be killed the cytokines and other particles result in a foreign-body granulomatous reaction [103]. In order to isolate the debris particles from the rest of the tissue the macrophages fuse together to form multi nucleated giant cells. In bone remodelling osteoclasts dissolve the bone and create a cavity, osteocytes then enter the cavity and get osteoblasts to create new bone. Cytokines have been shown to have an affect on the development or activation of osteoclast [35, 60, 84, 128]. The cytokines released by the macrophages stimulate osteoclastic bone resorption leading to osteolysis and loosening of the prosthesis [103].

The composition, number, size, surface area, shape and volume of debris are important factors in the biological response. For polyethylene the most biologically active particles have been found to be sub micron [103]. This size is the range that is phagocytable by the macrophages. The particles of other sizes result in fewer cytokines being released and therefore have a smaller effect on the bone resorption. In the knee the majority of debris particles have been found to be smaller than 1μm in size and therefore biologically active [70].

1.8 Experimental Simulation of Mechanics and Wear

Experimental knee simulators are designed to replicate the conditions within the knee in vivo. Different activities, such as walking, can be simulated on the knee replacement and the effect of these can be found on the mechanics of the joint. Knee simulators are used for pre-clinical simulation of TKRs in order to compare factors, such as the wear rate, to in use knee replacements.

Figure 1.11 shows the six axes of rotation and translation within the knee simulator. The tibial component can translate in the anterior-posterior (AP) and medial-lateral (ML) directions relative to the femoral component as well as rotate in the internal-external (IE) and abduction-adduction (AA) directions. The femoral component is mounted on a rocker allowing it to rotate in the flexion-extension (FE) direction relative to the tibial component. The centre of rotation of the femoral component is aligned with the FE axis and the top surface of the tibial insert is aligned with the AA axis.

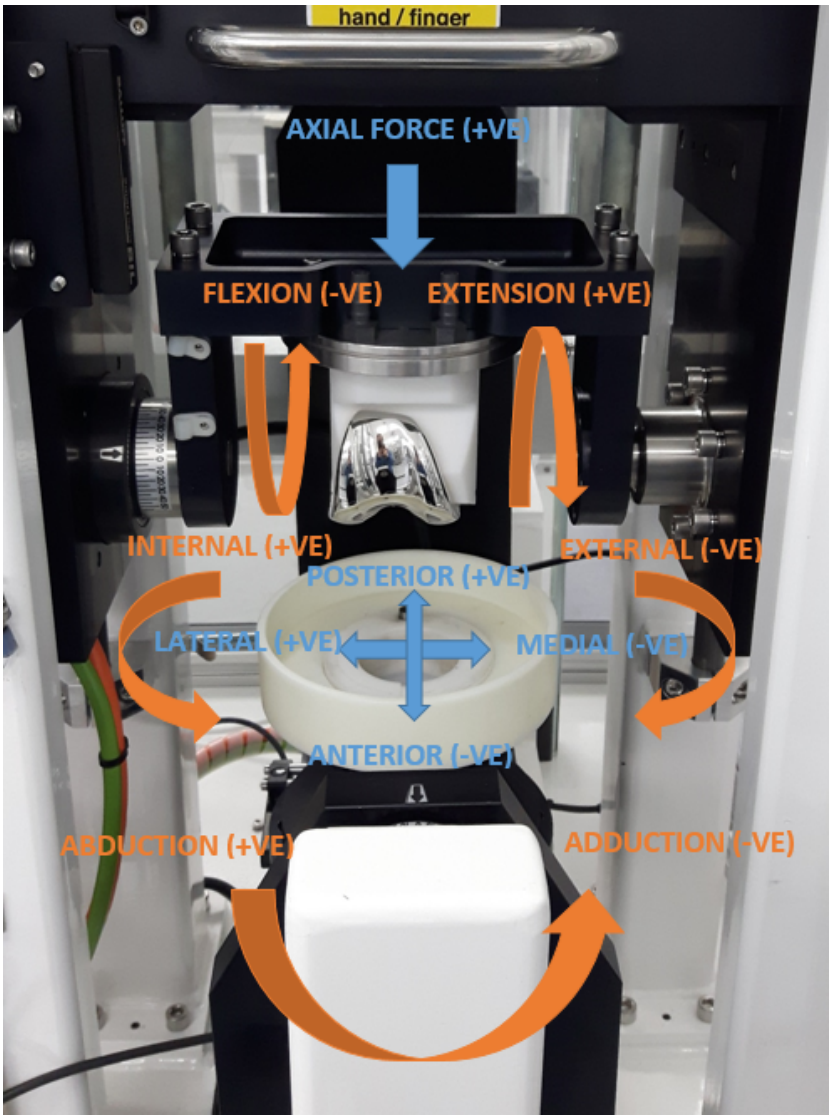

Figure 1.11: Axes of rotation and translation on a knee simulator for a right knee

The input profiles for the AP, FE and IE displacements along with the applied axial load can simulate different activities on the femoral and tibial components.

The ISO standard is made up of three parts; the first defining parameters for force control simulation [186], the second defining the measurement methods [187] and the third defining parameters for displacement control simulation [188]. These include the definition of the input force and displacement profiles for a walking cycle. The ISO standard input profiles simulate idealised conditions; assuming a standard patient, for instance in terms of their weight, ideal surgical procedure and only simulate a single activity. This can generate average wear rates similar to those found in vivo however it cannot reproduce the variation and spread of wear across patients [107]. The outliers can have up to 100 times the average wear rate so simulating these is important in determining which factors cause the increase in wear rate.

A stratified approach to knee simulation covers a wider range of conditions including

damage to the prosthesis, oxidative degradation, alignment, different activities and different patient anatomy and physiology [107]. Helping to determine the important factors in ensuring low failure rates in knee replacement. The effect of surgical positioning in the hip has been investigated and different alignments, such as offset in the medial-lateral direction, can result in dynamic separation between the head and the cup, increasing wear [12, 107, 147]. This may be one of the reasons for the variation in wear rates found in vivo compared to those found experimentally.

In order to simulate in vivo conditions fluid needs to surround the joint to simulate the synovial fluid present in vivo. Using distilled water has been shown to be insufficient as it creates different lubrication regimes, wear particles and wear patterns in the tibial insert [173]. Bovine serum is commonly used as it is similar to synovial fluid; with similar levels of protein and other biological components [173]. However there is no generally accepted level of proteins or composition ratio that has been suggested for joint simulation; different laboratories use different compositions of bovine serum. The ASTM standard F1715 does not specify any set protein level or dilution value however ISO standard 14243-1 [186] specifies the use of 25% bovine serum mixed with deionized water with a protein content of 20g/l [186]. Other chemicals are added to minimise the bacteria contamination, for example hydrochloric acid, sodium azide and antimyotics. The protein levels in serum can range from 50-80 g/l meaning there are variations in the final testing fluid.

The wear rates of the tibial components are found gravimetrically. They are weighed before testing and at defined intervals. Control inserts are immersed in the lubrication fluid for the same time the inserts are in the simulator. The control inserts are used to find the change in weight due to moisture uptake into the components. The change in weight of the test inserts are found minus the change in weight due to moisture uptake in the control inserts. The wear rate is then determined from this weight change.

There has been shown to be a difference in weight change between loaded and unloaded soak controls during a wear study. Over multiple wear studies the average correction from passive soak controls was found to be 0.89±0.85 mg/MC and from active soak controls the average correction was higher 1.65±0.88 mg/MC [93]. This difference may be due to the water within the polyethylene being squeezed out when under loading. Currently the ISO standard allows the use of either loaded or unloaded soak controls [186].

1.8.1 Displacement Controlled Simulation

In displacement controlled simulation the flexion-extension angle, tibial rotation angle, anterior-posterior displacement and axial force are all applied according to the input motion profile. The ISO standard profile for walking is shown in Figure 1.12. The standard input profiles create a range in flexion-extension of 0-58°, internal-external rotation of 2° external to 6° internal, a maximum anterior translation of 5.2mm and a maximum force of 2700N. This is based on a composite curve of loading in terms of body weight for an adult male with a weight of 101.6kg corresponding to a force of 996.4N (95th percentile) [109].

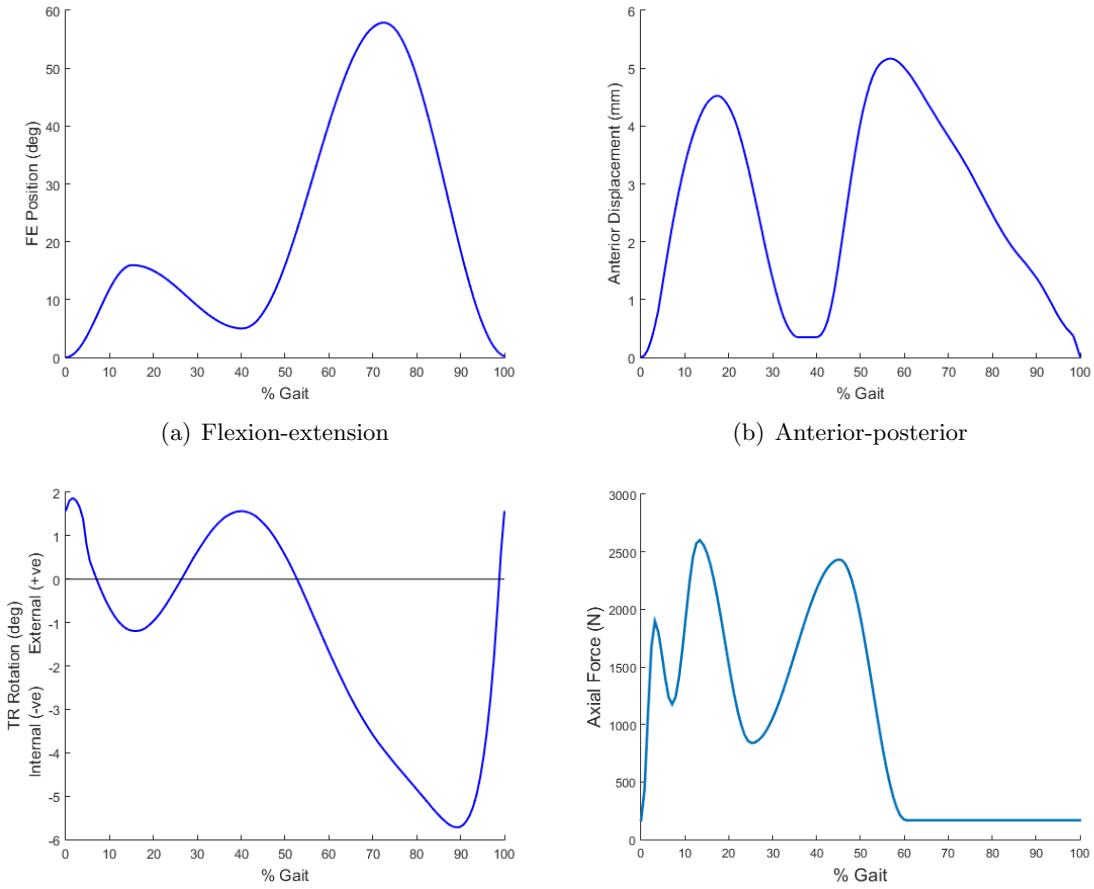

(a) Flexion-extension

(b) Anterior-posterior

(c) Tibial rotation

(d) Axial force

Figure 1.12: ISO standard displacement control input profiles [188]

Different input profiles can be used to simulate different activities such as walking or squatting. The AP displacement and TR rotation are controlled by a closed loop using the displacement feedback to follow the input profiles. Inputting a set motion profile makes it more repeatable as there is a consistent path, displacement and velocity between tests and the stations in the simulator.

Different TKR designs will result in different motion of the joint therefore a motion profile should be found for a specific design to ensure it represents the in vivo motion [10]. For low conforming TKR designs displacement control is acceptable, however for high conforming designs the motion profile may exceed what would naturally occur and therefore create areas of high stress and wear [10]. The force levels between the stations of the simulator may vary due to variations in the fixtures; the zero position, wear and deformation that has occurred to the components [10]. This can result in variations in the results across a test.

Some studies into the natural knee have found that there is a larger AP displacement and tibial rotation during walking than the ISO standard [123]. Some experimental wear tests are carried out under different inputs to the ISO standards with larger displacements in order to better replicate natural motion [20, 132]. McEwen et al [132] used inputs of tibial rotation

between ±5° and AP displacement from 0-10mm as was found by Lafortune et al [123] in the natural knee. This is around double the displacements from the ISO standard.

1.8.2 Force Controlled Simulation

Under force controlled conditions the tibial component is free to move relative to the femoral component according to the applied forces. This motion is sensitive and can be complex [10]. The axial force and flexion-extension angle are the same as those for displacement controlled simulation as described in the ISO standard [188] (Figure 1.12). AP force and TR torque are applied to represent the forces within the natural joint due to muscles and ligament tensions [186] (Figure 1.13). The AP force is cyclic but also varies in magnitude according to the displacement in the AP direction. The same applies to the TR torque; there is a cyclic component and it varies according to the TR rotation.

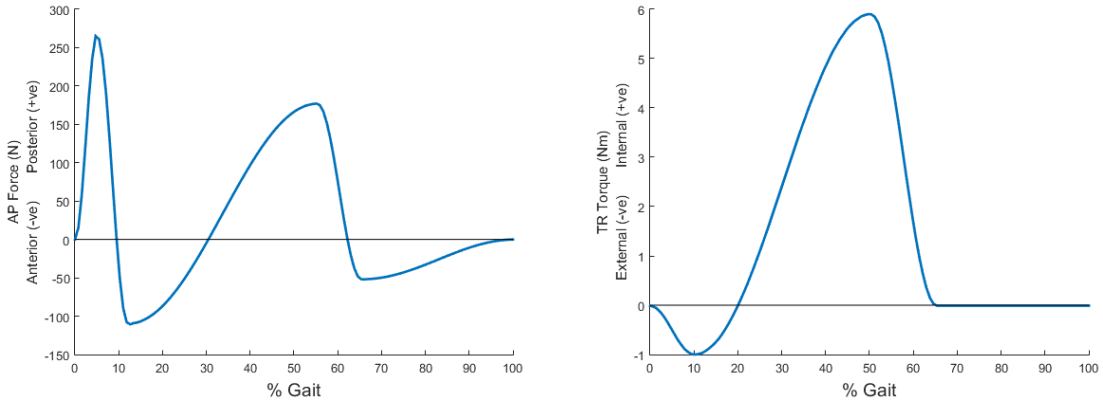

(a) Anterior-posterior Force

(b) Tibial rotation torque

Figure 1.13: ISO standard force control anterior-posterior force and tibial rotation torque input profiles [186]

For force controlled simulation soft tissue restraints must be included to generate realistic motion [10]. Many studies have used springs to restrict the AP translation and TR rotation (Figure 1.14) [62, 92, 196]. Natural ligaments are not linear elastic so the stiffness of the springs must be found from the gradient of the exponential curve of the ligament (Figure 1.15). This is difficult to find as the stiffness of ligaments will vary between people and will also vary before and after knee surgery [194].

The ISO standard for a cruciate retaining (CR) prosthesis has an AP spring with a gap of ±2.5mm and a linear restraint stiffness of 9.3N/mm and 44N/mm for anterior and posterior motion respectively. The ISO TR spring has a gap of ±6° and a rotational restraint stiffness of 0.36Nm/° [186]. For a cruciate substituting (CS) prosthesis the same AP and TR spring gaps are applied with a linear restraint stiffness of 9.3N/mm in both directions and a rotational restraint stiffness of 0.13 Nm/°.

Various stiffness values for the springs have been used in previous studies. Haider et al [91] investigated the effects of spring tensions on the AP displacement and tibial rotation using a

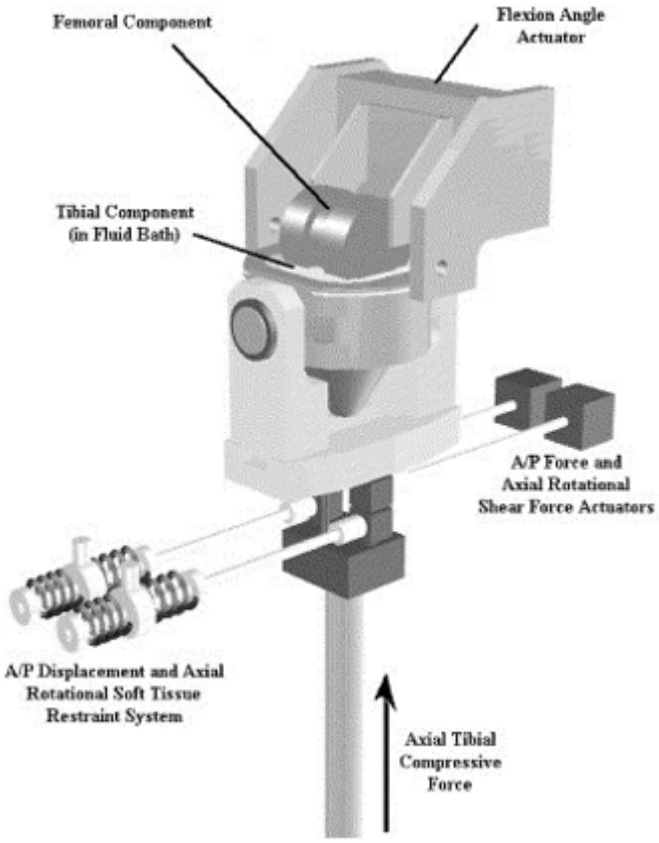

Figure 1.14: Knee simulator with soft tissue restraints [62]

mathematical model. In this study the optimum values for the spring stiffness were 7.24N/mm for the ACL side and 33.8N/mm on the PCL side, both with a gap of 2.55mm. These spring gaps were included in order to simulate the s-shaped response curve found previously (Figure 1.15). Isolated section of either PCL or ACL has been found to result in nearly 3 times more laxity than the intact knee [196].

Van Houtem et al [194] used soft springs (7.24 N/mm) and hard springs (33.8 N/mm) to prevent AP movement without the ACL and with and without the PCL respectively. These spring stiffness values were taken from measurements of soft tissue restraints with intact ligaments (hard springs) and with the ACL or PCL cut (soft springs) [91]. Both types of springs were used along with an Instron-Stanmore Knee Simulator, the resulting motion was compared to the kinematics from cadaveric specimens under the ISO Walking Cycle [186]. The hard springs resulted in realistic AP motion found in vivo but the soft springs resulted in more realistic rotation of the joint with the ACL cut. This study suggested use of springs of intermediate value between their hard and soft springs to get realistic kinematics.

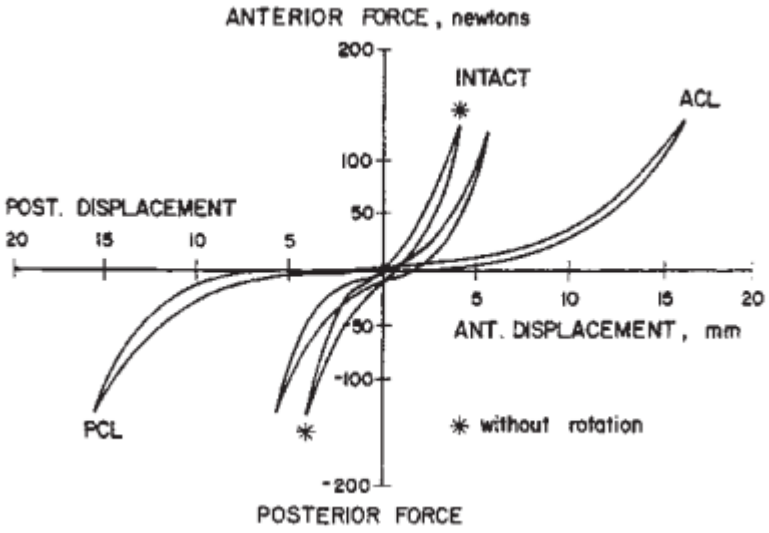

Figure 1.15: Anterior-posterior force vs displacement with the knee in 30^{o} flexion [196]

1.8.3 Force vs Displacement Control

Previous studies have investigated the difference in kinematics and wear rates between force and displacement control. The difference in kinematics has been found to vary substantially [90, 174]. However the wear rates have been found to be similar [21, 90] and significantly different [174].

For example Schwenke et al [174] investigated the difference in wear for a flat-on-flat, minimally constrained TKR under displacement and load controlled simulation according to the respective ISO standards. The wear rate for the load control group was double that of the displacement controlled group but also had a larger variance, 20.9±4.2 mg/million cycles (MC) compared to 9.2±0.9 mg/MC. Within the force controlled group there was more overall variation as one of the implants had a much lower wear rate than the other two. The main difference between the motions was an average posterior offset in the contact position of 3±0.8 mm in the force controlled test compared to displacement control (Figure 1.16). The rotations of both groups were more different; both had similar ranges in rotation but had different shapes of rotation profile (Figure 1.16). Under load control the tibia rotated more internally earlier, as soon as 25% of the gait cycle, with the rotation increasing up to 55% of the gait cycle. This means that the cross-shear conditions were created under the load of the third force peak of 800-2400N compared to the much lower swing phase loads for displacement control. The difference in the cross-shear motion may be what caused the differences in the wear rate.

Comparison between both the ISO force and displacement control standards are difficult as they were written independently of one another. Therefore the ISO force control input profiles do not result in the ISO displacement control displacement profiles.

Both methods of experimental simulation have drawbacks but neither is more accurate.

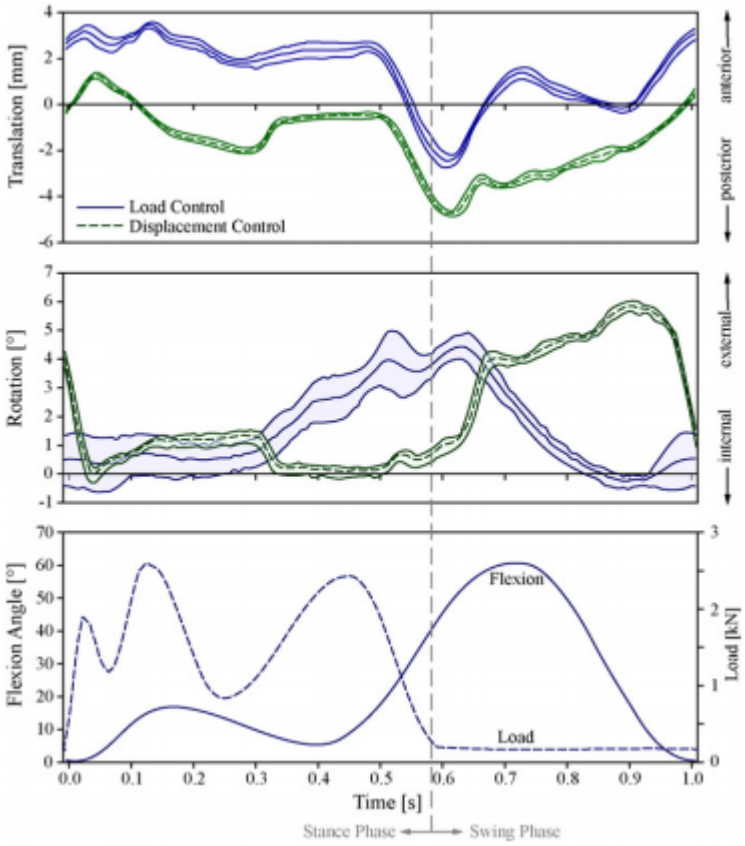

Figure 1.16: Difference in motion for load and displacement controlled simulation of the translation and rotation of the tibia relative to the femur [174]

Force controlled simulation applies forces to generate motion as in vivo, allowing the components to move how they would in vivo so may generate more accurate motion. However the restraints used are crucial in keeping the motion within the limits that occur in vivo. Force controlled simulation can result in motions that are more extreme than those which would be found in a patient. There is also more variation in the motions between the stations of a simulator which can mean that finding differences in wear rates under different conditions can be difficult. Displacement control however reduces the variation across the stations as the displacement is controlled. However this can lead to high forces and stresses in the components if the displacement inputs are not right for the design of the TKR.

1.9 Computational Simulation of Knee Mechanics

Computational modelling can be used to predict a range of outputs including the kinematics of knee replacements and natural knees. It can produce results faster than experimental methods, however creating a computational model requires information and understanding about the component design and test conditions. A wide range of variables can be studied in combination with one another due to the speed of the model.

Another benefit of computational modelling is dynamic measurement of values such as contact area, contact pressure and cross shear that are difficult to measure experimentally. A computational model can also remove some of the limitations with experimental studies, reduce errors and reduce variation between studies.They can be used in order to predict wear, however this is outside the scope of this research.

To have confidence in a computational simulation, validation must be carried out. This can be carried out during the development of the model by using simple geometry and comparing the results to mathematical solutions. Validation may also involve the comparison of the results from the computational model with experimental data of the same test conditions. Without validation of a model there can be no confidence in the veracity of the data.

Therefore the combination of both experimental and computational methods may provide the best results. The experimental data can be used to validate the computational model and provide confidence in the results. Parametric testing can then be carried out with the computational model faster and more cheaply than experimental studies. The computational simulation can also provide measurements of values such as cross shear which are not available experimentally. However without experimental validation the veracity of the results are unknown.

1.9.1 Soft Tissues

Previous studies have used computational models to simulate the natural knee, TKRs and the soft tissues within the knee. The simulation of soft tissues can be complex due to their non-linear and anisotropic nature. Different methods for the simulation of soft tissues within the body have been developed.

The ability to model the soft tissues allow studies to be carried out on the influence of the soft tissues and menisci on the loading of the knee. This is difficult to carry out experimentally. Experimental studies use cadaveric specimens which may not be representative of the dynamic response of soft tissues in vivo.

One such study used MRI data to develop the geometry of the model [160]. The articular cartilage and menisci were modelled as single-phase linear elastic, isotropic materials, this was deemed accurate for the prediction of short-term response. The long-term response was inaccurate due to the neglection of the material characteristics of the ligaments depending on time; visco-elasticity, creep and relaxation. With this model the loads in the ligaments and resulting displacements were able to be calculated over short time responses.

In another study a subject specific method of determining the zero load lengths of the PCL and collateral ligaments was defined [36]. Cadaveric knees were put under known loads and the ligament parameters within the computational model, such as the zero-load length and tension, were varied in order to reduce the difference between the model and experimental displacement. However the use of cadavers may not be representative of the soft tissues in vivo. This method can also only be used for subject specific models and not for a more general computational model.

Another study compared linear and non-linear visco-elastic computational models of eight ligaments within the ankle under step relaxation and ramp tests [74]. Ligament behaviour is non-linear visco-elastic however it was shown that natural ligaments could be adequately modelled up to 15% strain using a quasilinear visco-elastic computational model.

A linear visco-elastic model can be represented by a spring damper system, such as the generalized Maxwell model, which is simple and fast. However most soft tissues will behave linearly under small deformations but behave non-linearly at greater strains. Non-linear visco-elastic models can be used to replicate this change in behaviour. Fung's quasilinear visco-elastic model assumes that the material's response can be separated into a strain-dependent and time-dependent component (Equation 1.3).

$$R(\varepsilon, t) = G(t) \cdot T(\varepsilon) \tag{1.3}$$

G(t) is the reduced relaxation function and T(ε) is the instantaneous elastic response function, which may be non-linear. The functions for G(t) and T(ε) can be found by curve fitting experimental data.

The ISO standard spring profiles [186] attempt to replicate this non-linear behaviour by using the gaps around the zero position. Under small displacements there is no spring force, however under larger displacements this spring force increases. The computational simulation however allows for more complex soft tissue behaviour to be modelled, for example a change in the response due to flexion of the knee.

1.9.2 Total Knee Replacements

Previous studies have used finite element methods to study different TKR designs under a range of loading conditions. The use of computational modelling allows for parametric studies to be carried out and for a wider range of test conditions to be investigated both independently and in combination.

One study used a computational model to predict the kinematics of a TKR [81]. A DePuy Sigma TKR was modelled in order to simulate the Stanmore knee simulator. The femoral component was modelled as a rigid body and the polyethylene as an elastic-plastic material. The springs within the simulator were represented by applying a restraining force as a function of the displacements. These spring stiffness's were linear to replicate those in the simulator. A friction coefficient of 0.04 resulted in kinematics within a few percent of the experimental value.

Another study developed a computational model in order to determine the AP and TR constraint of a TKR [139]. The computational model was developed to replicate the experimental setup for determining the TKR constraint values. The experimental testing frame and the components of the TKR were modelled as rigid segments, with a deformable layer on the tibial insert. Experimental or estimated values were used for the segment masses, inertias, densities and damping. A rigid-body-spring-model was used to represent the contact between

the femoral and tibial components. There was some compliance in the loading frame under transverse loads. The computational model was validated using the experimental data and had good agreement when the compliance of the testing frame was included. This model provided a faster method of determining the constraint of a TKR.

Computational models have also been used in the optimisation of TKRs. One study investigated the relationship between durability and kinematics in the geometry of a TKR [203]. The shape of the femoral component and tibial insert were defined using 14 variables that were varied within a finite range. Durability was investigated using a previously validated wear model. This wear model was force controlled with springs used to simulate the soft tissues within the knee. The surface damage distribution and the volumetric wear was determined up to 3.5MC. The kinematics were predicted to assess the flexion range of motion and the AP and TR constraints of the TKR designs. With the results multi-objective design optimisation was carried out in order to determine the relationship between the durability and kinematics. The constraint from the geometry of the TKR was important for both the kinematics and durability. As TR laxity is necessary for proper kinematics and increased TR resulted in increased wear there was a trade off between the kinematics and durability. This suggests that a rotating platform TKR could be beneficial in removing this trade off.

Some computational studies have been carried out into the effect of component alignment, mainly the influence of varus-valgus alignment on the contact pressure of the tibial insert. Three computational studies have investigated the effect of varus-valgus alignment on contact pressure [52, 126, 189]. One previous computational study investigated the effect of the posterior tibial slope on the kinematics and contact pressure of a TKR [114]. There have been no previous computational studies into the effect of both soft tissue conditions and alignment conditions in the coronal, sagittal and transverse planes to the authors knowledge.

1.10 Surgical Procedure

There are two main surgical methods used for total knee arthroplasty; gap balancing and measured resection. The gap balancing technique aims to keep the flexion and extension gaps equal (Figure 1.17) and tends to be used with CS knee replacements and some CR devices. Ligament releases are carried out before bone cuts are made to put the limbs in approximate alignment [58]. The tibial cut is made perpendicular to the anatomical axis of the tibia. This is important to the alignment of the knee as it is used as a reference for the femoral bone cuts [2, 45, 58]. The flexion gap is balanced by cutting the anteroposterior femur parallel to the tibial cut [152]. The gap balancing technique uses the tension of the soft tissues to determine where the joint line lies (the axis where the femoral and tibial components come into contact).

Potential issues with this technique include movement of the joint line and midrange laxity in the joint [45, 152]. In order to balance the flexion gaps more of the distal femur may need to be cut which can make the joint line move proximally. This can be minimised by having a large range of femoral component sizes and by releasing the posterior capsule to correct

stiffness under extension [152]. The technique results in good soft tissue balance however there may be laxity between 0° and 90° flexion [2, 45]. If the posterior contracture is not adjusted the balance of the extension gap hinges on the posterior capsule rather than the collateral ligaments (CL). This means that the CL are not balanced throughout the range of motion, which may lead to instability of the knee [152].

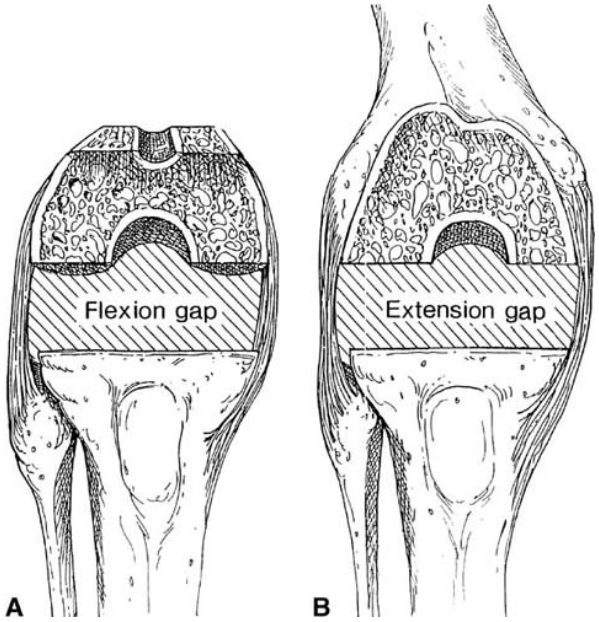

Figure 1.17: The flexion and extension gap are made to be equal for the gap balancing method [86]

The measured resection method aims to keep the joint line position constant, therefore trying to maintain natural motion. The femoral rotational alignment uses bony landmarks on the femur rather than ligament tension. This can be difficult due to differences in femoral shape between patients and if bone degradation has occurred. Placing the femoral component parallel to the transepicondylar axis results in better patellofemoral tracking and femorotibial motion however it can be difficult to determine this axis [45]. Using the AP axis has been found to result in fewer patellofemoral problems however using this axis can result in a range of errors and in patients with femorotibial osteoarthritis the femoral component will be rotated externally leading to instability [45]. The posterior condylar axis can also be used however there are shape differences between patients and degradation of the condyles makes it unreliable (Figure 1.18) [45, 152]. In measured resection the bone cuts are carried out before ligament releases, so that they can be carried out with the trial components in place [2, 45].

The main difference between the two techniques is the femoral rotation alignment. In general studies have found the use of the ligament tensions in the gap balancing method more reliable than bony landmarks [2, 58, 61]. The current preferred method for total knee arthroplasty involves using both the bony landmarks and the soft-tissue tensions reduces error during the alignment and balance of the joint [45]. The combined method focuses on the ligament tensions but also three gaps in the joint; flexion, extension and patellofemoral

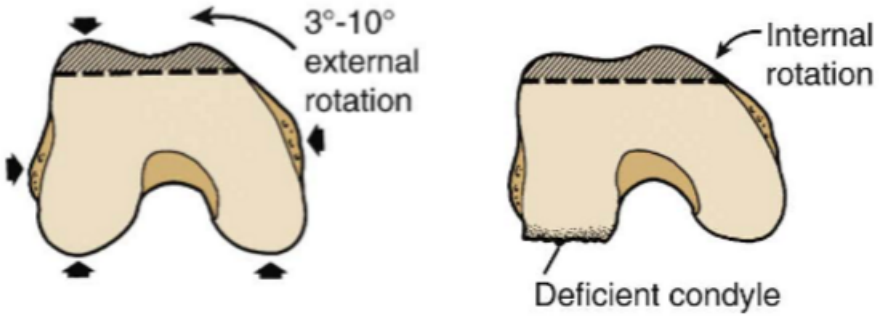

Figure 1.18: Erosion of the condyle can make rotational alignment more difficult [152]

gap [2]. Combining aspects from both methods can result in a more reliable procedure as more checks are made [2].

1.10.1 Alignment Methods and Instrumentation

Correct alignment is important for proper function of a TKR as it affects the stresses on the components and bone and helps balance the forces in the soft tissues [163]. Alignment guides are used to maintain the anatomical axis of the leg. Extramedullary guides are placed along the axis of the leg based on external landmarks, whereas intramedullary guides go down the diaphyseal canal in the bone. Commonly intramedullary guides are used for the femur as external landmarks are difficult to identify. For the tibia extramedullary guides are used as the landmarks are more distinct [152]. The position of the entry hole for intramedullary guides is important as it can result in a more varus femoral cut or make the knee more flexed or extended. This can cause problems with the soft tissue balance and lead to wear or fracture [163]. Mediolateral placement errors in the femoral head of 1mm can lead to 3-4.5° errors in the angle of the femoral cut [206].

Cutting blocks ensure that the bone cuts are aligned properly but can limit the surgeon's field of view, increasing the possibility of cutting structures like the MCL. The positioning of the cutting blocks is important in ensuring they are carried out correctly. Error has been decreased by using universal cutting blocks as there is no need to move the block between cuts [152].

The classic method of alignment involves cutting the distal femur with a valgus cut equal to the difference between the mechanical and anatomic axes (generally between 5-6°) [152]. A 7° valgus cut with 0° tibial alignment has been found to give the most even load across the knee replacement [100]. The anatomic method of alignment aims to maintain natural kinematics of the knee with a CR replacement. The femoral alignment is set to the anatomic axis which is around 9-10° valgus with the tibial cut at 2-3° varus creating an anatomic axis of 6-7° valgus [152]. These angles have been shown to create an even load distribution [100].

Femoral rotational alignment consists of using a combination of bony landmarks and ligament tensions as described previously. Tibial rotational alignment is based on the posterior

surface of the tibial cut, the anterior surface of the tibia, the tibial tubercle and the ankle mortise. If the tibial component is loose the position can be found relative to the femoral component by flexing and extending the knee with the components inserted. This is subject to errors from the position the leg is held in, the tourniquet on the thigh and the tightness of the flexion gap, which are not present when using anatomical landmarks.

The tibial and femoral components should be anatomically positioned with no overhang. Overhang can cause pain and stiffness due to stretching of the capsule [163]. The femoral component should align with the resected edge of the lateral femoral condyle, if it is too medial this can cause lateral patellar retinaculum stress [152].

1.10.2 Kinematic Alignment

Kinematic alignment is a method that is not widely used but that some surgeons believe results in better alignment and kinematics of the joint. Many studies have found that aligning the components to maintain the mechanical axis of the leg may not result in a good clinical knee score [63, 152]. The mechanical axis does not account for patient variation in the geometry of the femoral and tibial bones, for example bowing or natural varus. Aligning to the mechanical axis only aligns the components in the frontal plane, no alignment is carried out in the sagittal or transverse planes. A study into four different methods of mechanical alignment has shown that it can result in ligament instability and can change the mechanical axis of the knee and limb by more than 2° 58% of the time [87].

Kinematic alignment aims to maintain three different axes of the knee; the axis the tibia flexes and extends around, the axis the patellar flexes and extends around and the axis the tibia rotates around (Figure 1.19).

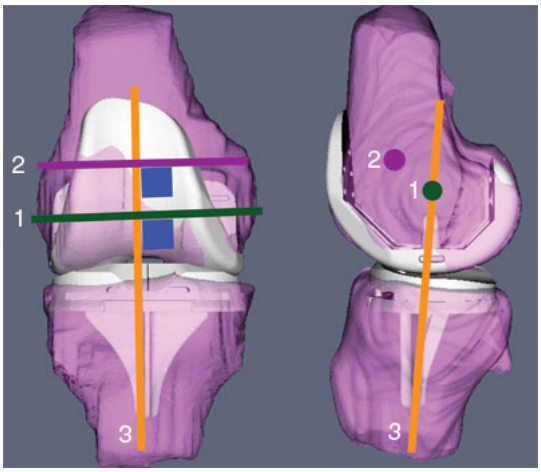

Figure 1.19: Kinematic alignment axes; axis the tibia flexes and extends around (1), axis the patellar flexes and extends around (2) and the axis the tibia rotates around (3) [1]

By maintaining these axes the function of the knee is thought to be maintained, keeping natural motion. The procedure also aims to preserve the ligaments as much as possible to ensure natural function and aims to maintain the original geometry of the femur and tibia in

order to keep the axes in the same positions. A study of 101 patients who underwent kinematic alignment knee replacement surgery found that in 93% of cases the alignment was within ±3° of the mechanical axis [99], compared to 68% for conventional mechanical alignment methods [130].

As it is not widely used the effects of using kinematic alignment rather than mechanical is unknown. Some studies have found that kinematic alignment results in better alignment and function [63, 99, 124] where as others have found more femoral rollback, external rotation and a more varus tibial placement which causes higher stresses [104] or that there was no significant difference between the two methods [133].

1.10.3 Computer Registration Methods

Newer computer navigation methods use bone surface landmarks as references. The surface topology is used to determine the correct alignment of the components using data on standard tibial or femoral anatomy. The computer system can then direct the surgeon to generate more accurate alignment [152]. However computer systems need to have accurate data entered to reliably calculate the mechanical axis. It also cannot take into account anatomical variations in the patient such as a bowed tibia or femur [163].

Many studies have compared the accuracy of conventional alignment and computer navigation. Some have found better accuracy with computational navigation whereas others have found no significant difference. One study found no significant difference between the standard guides and the computational system for the overall postoperative mechanical alignment [13]. But the computer navigation system had smaller variance in position, with more components within 3° of neutral. Apart from the femoral component in the sagittal plane, the component alignment was better with the computer system.

Another study found that computer assisted alignment was significantly better than the traditional methods for four parameters; femoral rotation, femoral flexion, tibial anteroposterior slope and matching of the femoral and tibial components [51]. One study found that computer assisted methods can reduce malalignment so that over 90% of total knee arthroplasties are within ±3° of the mechanical axis, however it was not significantly better than traditional methods [206].

1.10.4 Tibial Slope

The angle of the tibial slope has been shown to affect stability, range of motion, shear force and ligament forces [79, 80, 110, 131, 179]. An increase in tibial slope moves the femur posterior relative to the tibia. This has been found to alter the shear forces and ligament forces. PCL deficient knees have a more anterior tibiofemoral contact point so increasing the tibial slope is thought to help. Correspondingly, decreasing the tibial slope would help ACL deficient knees. Increasing the posterior tibial slope may reduce the quadriceps force, the contact stresses in the TKR as well as the forces on the PCL [114]. However an excessive posterior tibial slope may result in loosening of the joint due to the reduction in the collateral ligament forces [114].

A linear relationship has been found between the shear forces and ligament forces with the tibial slope (Figure 1.20) [179]. The tibial slope is thought to be one of the most important variables for range of motion [131, 164]. Previous studies have found that decreasing the tibial slope by 5° could reduce the range of flexion by 5° [131] and that increasing the tibial slope by 5° could increase the force in the ACL by 26% [179].

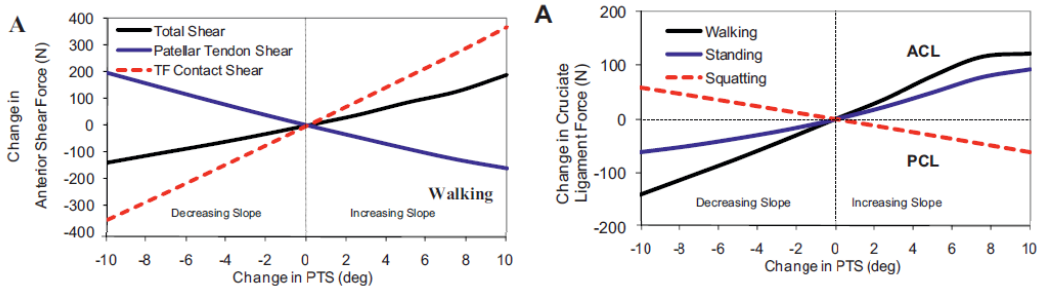

Figure 1.20: Effect of tibial slope on shear forces and ligament forces [179]

1.11 Alignment

Alignment of TKR components has been studied previously, both looking at alignment in vivo and the effect this alignment has on the TKR. However an in depth study into alignment in a range of planes in combination with different soft tissue conditions has not been carried out. As alignment can affect the loads, kinematics and contact area of a TKR it therefore may affect the wear rate [52, 53, 66, 92, 126, 184, 201].

This section will cover studies that have investigated the range of component positions that occur in vivo and the effect this has on the loading patterns, clinical results, kinematics and wear rates of the TKR.

1.11.1 Amount of Variation in Surgical Alignment

Previous studies have investigated the variation in alignment of total knee replacements after surgery. The axes of alignment they measure include the mechanical axis, varus-valgus component positions, tibial slope and rotational position. There is no clear consensus on the amount of variation in alignment.

A systematic review determined that the chance of the alignment being more than 3° out was 32% for the mechanical axis, 26% for femoral slope, 17% for tibial slope, 16% for femoral varus-valgus and 11% for tibial varus-valgus [130]. This showed that the variation in the flexion-extension was greater than for varus-valgus for both components, which is supported by other studies [13, 24, 164]. This also makes sense relative to surgical procedure; better alignment is possible in the coronal plane due to better field of view and the use of guides.

A systematic review on rotational alignment determined that the range in rotational alignment was 2° external to 3° internal for the femoral component and 6° external to 2° internal

for the tibial component [193].

Another study found that when using the epicondylar axis for femoral alignment, malalignment of the femoral component of >3° occurred in 10% of cases [156]. The preoperative alignment of the leg was determined to affect post-operative alignment; 7/64 (10.9%) of the varus knees, 3/22 (13.6%) valgus knees and 0/14 neutral knees were >3° malaligned.

Tables 1.1, 1.2 and 1.3 show the variation in component position found in the coronal, sagittal and axial planes in a number of studies. Studies were included that used the same surgical procedure; an intramedullary guide for the femoral and an extramedullary guide for the tibial alignment, did not include revision surgery or patients with large preoperative varus/valgus, did not use cadavers and measured the angles of the components in the same way.

For coronal alignment the angles were measured using a weight bearing, long leg radiograph. The angle of the tibial component was defined as the angle between the base of the tibial tray and the anatomical axis of the tibia. The angle of the femur was defined as the angle between the mechanical axis of the leg and the tangent to the femoral condyles.

Rotational alignment of knee components are measured using CT scans and only those using the Perth or Berger CT protocol were included as they use the same methods [33, 50].

For sagittal alignment CT scans were used to calculate the alignment angle according to the Perth CT protocol. The amount of variation found in the positions of TKR components varied between the studies, however by comparing the results there were some trends.

The component alignment in the coronal plane appears to have the least variation, this may be due to the fact that this plane is the easiest for the surgeon to view. The use of intramedullary, extramedullary and bone cutting guides in the coronal plane will also contribute to the lower variation. In most studies the femoral and tibial component positions are generally within ±4° and ±3° respectively of alignment and the mechanical axis of the leg is normally within ±4° (Table 1.1).

Table 1.1: Results from studies on the amount of variation in TKR position in the coronal plane. A negative value represents a varus alignment and a positive value valgus

Study	**Number of Subjects**	**Tibial (°)**	**Femoral (°)**
[89]	100	-6 to +2	-4 to +10
[13]	51	-4 to +4	-5 to +5
[38]	50	Not Reported	-5 to +4
[137]	39	-3.7 to +5.1	-6 to +1.8
[48]	29	-3 to +8	-1 to +6
[55]	30	-3 to +5	-6 to +3
[209]	29	-2 to +4	-5 to +8
[59]	50	-3 to +3	-4 to +3

The most variation in position occurs in the rotational position of the tibial component and in the tibiofemoral mismatch. From the results it appears that most positions are within ±14° of the ideal mechanical tibiofemoral alignment (Table 1.2). Whereas the femoral component

is normally within 5° external and 4° internal rotational alignment and the tibial component between 10° external and 8° internal rotation. The increased variation in the rotational position of the components compared to the coronal or sagittal alignment may occur due to the difficulty in aligning the tibial component as this relies on the use of bony landmarks.

The alignment of the tibial component in the sagittal plane should result in cut perpendicular to the anatomic axis. From the studies most tibial slopes are between 0° and 10° posterior slope (Table 1.3). For the femoral component in the sagittal plane there is a similar amount of variation with most being within 6° of neutral.

Table 1.2: Results from studies on the variation in the rotational alignment of TKR components. A negative value represents external rotation and positive an internal rotation

Study	**Number of Subjects**	**Tibiofemoral Mismatch (°)**
[127]	159	13
[51]	36	11
[96]	22	13.6
[26]	56	18.6
[148]	26	22.1

Table 1.3: Results from studies on the variation in TKR position in the sagittal plane. A negative value represents an anterior slope

Study	**Number of Subjects**	**Tibial Slope (°)**
[127]	159	-1 to +13
[51]	36	+1 to +10
[96]	22	+1 to +10
[101]	27	-1 to +10

1.11.2 Effect of Alignment

Some previous studies have investigated the effect of component alignment on the clinical outcomes, loading, kinematics and wear rates of TKRs. This section will cover the results of some of the clinical, experimental and computational studies.

1.11.2.1 Clinical Results

One study determined that there were four main factors for clinical and radiographic failure, two of which were; lower extremity malalignment (angle between the femoral and tibial components of <4° or >8° in the coronal plane) and tibial varus malalignment (varus tilt >5°) [68] . In this study 74.7% of patients had a neutral lower extremity alignment (between 4°-8°), 20.4% had a varus alignment (<4°) and 4.8% had valgus alignment (>8°). Nine patients had a varus tilt of the tibial component that was greater than 5°, and eight of these (88.9%) needed revision due to wear. The ninth patient from this group had evidence of femoral-tibial subluxation, this suggests that a large varus tilt can result in early failure. Of the varus knees

in the study, 44.1% were revised and 41.2% had radiographic evidence of progressive subluxation (dislocation). Of the valgus knees 37.5% had revision surgery and 50% had progressive subluxation. Whereas for the neutral group only 14.5% needed revision surgery and 15.3% had evidence of progressive subluxation. Another study compared the mechanical axis of the leg with functional knee scores [56]. There was a significant difference in the knee scores for those with a mechanical axis within 3° of neutral compared to those with a larger angle. Those with a mechanical axis close to neutral had better total IKS scores, Short-Form health survey (SF-12) physical and mental scores.

Bell et al [26] investigated the component rotational alignment in patients with knee pain and found there was a correlation between internal rotation of the tibial and femoral components with knee pain. Values for excessive internal rotation were 5.8°, 3.9° and 5.6° for the tibia, femur and femorotibial mismatch respectively. External rotation was not found to be a factor contributing to knee pain. For most patients internal rotation of the femoral component relative to the tibial component of 3°-6° or external rotation of up to 8° was found to be acceptable as it will not result in clinical problems such as knee pain [208]. Another study found that patients with a leg angle within 3° of the mechanical axis had a significantly higher Knee Society Score (KSS) than those with a greater angle [181]. However this correlation was only found with patients that did not have a preoperative varus alignment.

Alignment on its own may not result in failure of a TKR, failure often results from a combination of factors such as alignment, body mass index (BMI), implant size and depth of resection [32]. For example the combination of varus alignment with a high BMI can result in a high rate of failure. One study found a failure rate of 0.5% for alignment of the mechanical axis within one standard deviation of the mean (2.4°-7.2°) and failure rates outside of this range of 1.8% for varus alignment and 1.5% for valgus alignment [32].

1.11.2.2 Load Distribution

An unbalanced TKR has been defined as one with a difference in load of >9kg between the medial and tibial compartments [88, 158]. Imbalanced loading between the medial and lateral condyles has been shown to result in instability, increased pain, lift off and patient dissatisfaction [88, 153]. Increased lateral loading may result in increased peak bone strains on the medial compartment [162], which may result in tibial implant migration. One study found that if the medial and lateral loads were comparable there was no lift off greater than 1mm [199].

One computational study investigated the effect of medial, rotational and varus alignment on tibial loading [126]. A load of 3kN was applied using three different component types; high conformity flat-on-flat (HFF), high conformity curve-on-curve (HCC) and medium conformity curve-on-curve (MCC) (Figure 1.21). Table 1.4 shows the results for the maximum stresses for each malalignment condition. Both the maximum stresses were obtained for a varus rotation of 5° for all component types. The medial translation of 1mm resulted in higher stresses than the internal rotation. This data suggests that the effect of varus rotation is more significant

than that of medial translation or internal rotation. However this study only investigated the effect of alignment under 0° flexion and not a full gait cycle. The kinematics of the knee and the cyclic loading pattern were also not considered within this study.

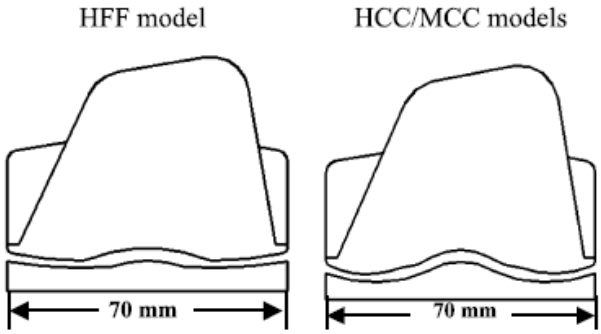

Figure 1.21: Line drawings of the flat-on-flat (HFF) and curve-on-curve (HCC) components used for testing by Liau et al [126]

Table 1.4: Maximum contact stresses and maximum von Mises stresses in different malalignment conditions [126]

	Maximum contact stress			Maximum von Mises stress		
	HFF	HCC	MCC	HFF	HCC	MCC
Neutral position	32.6	31.6	37.5	13.4	13.0	16.4
Med. Trans. 0.25 mm	40.1	39.9	49.0	20.3	16.8	17.8
Med. Trans. 0.50 mm	40.7	47.0	50.0	22.8	19.3	19.2
Med. Trans. 1.00 mm	43.4	53.0	49.1	25.7	20.6	21.9
Int. Rotation 1°	37.3	29.9	36.1	16.4	12.8	16.1
Int. Rotation 3°	34.9	29.6	32.7	15.4	13.5	16.1
Int. Rotation 5°	34.1	32.0	32.4	15.1	14.0	15.5
Varus Tilt 1°	56.6	51.8	52.3	25.9	23.3	23.3
Varus Tilt 3°	71.3	66.7	69.4	29.0	25.9	27.0
Varus Tilt 5°	80.2	74.3	76.2	39.5	27.0	27.9

Cheng et al [53] experimentally measured the pressure on the tibial component for different malalignment conditions using a Fuji pressure sensitive film. The contact pressure was measured with the components in neutral position, anterior-posterior translation of 2 and 4mm, medial-lateral translations of 0.5 and 1mm and internal rotation of 1°, 3°, 5° and 10° of the femoral component relative to the tibial component. All the pressures were measured with the knee in full extension and with an applied load of 3kN with a mobile and fixed bearing design. For most of the alignments the maximum contact pressure of the fixed bearing component was higher than the mobile bearing replacement. The contact pressures were highest for the internal-external rotations, where they reached 30MPa for the fixed bearing components. The anterior-posterior translation had the smallest increase in contact pressure as the load is evenly distributed between the medial and lateral sides of the component whereas for medial-lateral translation the load is unevenly distributed, increasing the contact stress. For internal-external rotation the load was evenly distributed however the conformity between the femoral and tibial components decreases, reducing the contact area. The use of the pressure film however may have affected the results due to it's thickness between the contact surfaces changing the contact. This study also only investigated the effect of a vertical load under 0°

flexion, however the contact will vary during flexion.

Another study investigated the effect of malrotation on the medial, lateral and peak contact forces using multi body dynamics modelling [52]. Internal-external rotation >5° of the femoral component and varus-valgus malalignment of the tibial or femoral components of >5° increased the medial, lateral and peak contact forces by 17.8-53.1%, 35-88.4% and 5.2-18.7% respectively. A 3° or 5° varus-valgus malalignment of the tibial component had a large effect on the load distribution on the tibial component. This supports the clinical results showing that >3° varus malalignment of the tibial component results in medial bone collapse [31]. However when the predicted and measured force data were compared using this model there were errors of 302N and 181N for the predicted maximum medial and lateral contact forces respectively. The changes in the medial and lateral contact forces during this study due to internal-external rotation were within these errors and therefore may not be significant.

Werner et al. [201] used pressure sensors on total knee replacements inserted inside cadaver legs to investigate the effect of varus-valgus malalignment on the stresses between the tibial tray and bearing. Loads were then applied to the knee using weights attached to the ankle to simulate a knee extension force of 66.7N. Five different inserts were used to simulate different malalignment positions; 0°, 3° and 5° of varus and valgus. A knee simulator was then used on the cadaver legs to apply hip load, tibial torque, tibial adduction-abduction and quadriceps loading to simulate walking conditions for a body weight of 400N. The changes in the load were proportional to the angle of the inserts used with the largest change occurring in the varus malaligned knees. During the gait cycle two different loading patterns were found; in four of the knees the ligaments were tight so the load was balanced across the medial and lateral tibial compartments but in two of the knees the ligaments were stretched resulting in uneven load distribution and instability. The healthy ligaments were able to help distribute the load more evenly counteracting the affect of the component alignment. However as they were cadaveric specimens the response may not be representative of the response in vivo.

Smith et al. [182] developed a three-body knee model using subject specific bone geometries from a single TKR patient along with the component geometries. This was incorporated into a musculoskeletal model and used experimental data from a motion analysis laboratory. Differences in the coronal alignment did not change the total force on the tibial insert, however it did affect the mediolateral position of the force. The ligament tensions had a larger effect; for all the ligaments there was a positive correlation with the ligament stiffness and reference strain with the total contact force. This implies that the ligament tensions are more important than alignment when it comes to the contact forces.

Norman et al. [151] found that varus and external rotation alignment had a significant effect on forces and moments in the knee, especially the medial-lateral force and abduction-adduction moment. The knee forces and moments were found under 0, 5, 10 and 25 degrees varus and 0, 5,10 and 25 degrees external rotation. The axial force through the TKR and anterior-posterior force were found to be very similar under all tests. However as the varus angle increased the medial-lateral force reduced significantly from 403N laterally to near zero.

The flexion-extension and internal-external rotation moments were also found to be very similar under all varus angles, and only increased slightly as external rotation increased. As the varus and external rotation angles increased the abduction-adduction moment went from abduction to adduction. The adduction moment resulted in a higher load in the medial side of the knee. The higher stresses in the medial compartment could result in higher wear rates. As this model did not include the soft tissues and forces at the hip and knee the forces in vivo may be different to those found in this study.

Another study used a computational model to find the contact stress, contact area and ligament forces under 0°, 3° and 5° varus and valgus alignments [189]. Higher contact stresses were found under varus alignment than valgus, especially on the medial condyle of the tibial insert. There was also an increase in the medial collateral ligament force under valgus alignment. The contact area remained similar under all the alignments on both the medial and lateral tibial condyles. However this computational model was developed using just one male patient, therefore the results may not be generalisable especially between different genders.

1.11.2.3 Kinematics

A cadaveric study found that coronal alignment affected the movement of the joint; varus inserts resulted in more external rotation during the walking cycle with the reverse being true for the valgus inserts [201] . The changes in rotation were found to be largest during the stance phase of the cycle (Figure 1.22). At maximum flexion the average increase in external rotation was 1.83° and 1.2° for the 5° and 3° varus inserts respectively. Smaller changes in motion were found with adduction-abduction with more abduction being seen in the valgus inserts at maximum load.

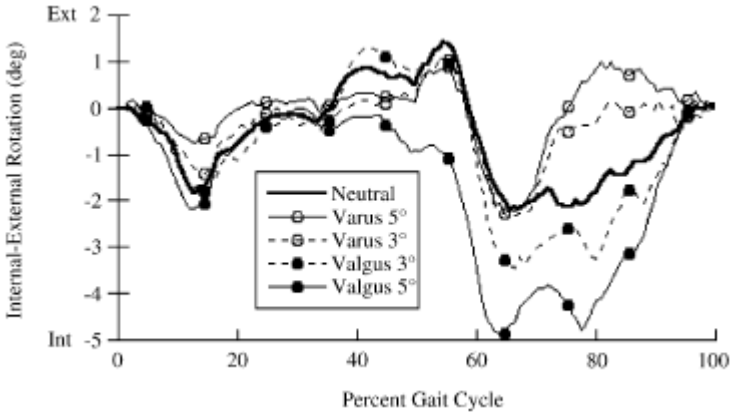

Figure 1.22: Internal-external rotation during a walking cycle for neutral, varus and valgus alignment [201]

An experimental study used the standard ISO walking cycle and an enhanced cycle with increased flexion, internal torque, anterior-posterior force and axial force on different TKR designs (Figure 1.23) [92]. Springs were used to simulate the ligaments of the knee to replicate a tight, standard and loose PCL. The tight PCL was represented with no gap, a standard

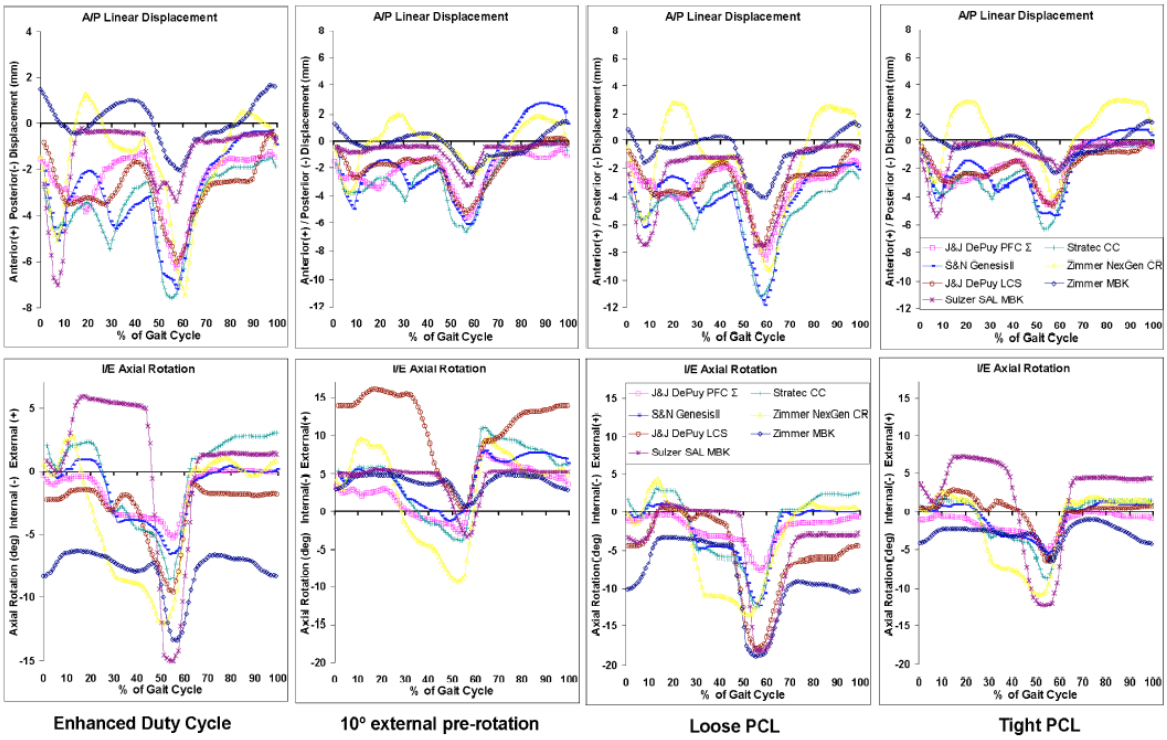

Figure 1.23: Kinematics of 7 TKR designs under enhanced walking cycle with varus, valgus, internal, external malalignment and PCL stiffness [92]

PCL with a 2.5mm gap and a loose PCL by a 2.5mm gap and a weaker spring. To simulate varus and valgus alignment this was varied out with the axial force down the centre line, 5mm medial of the centre line and 10mm medial to the centre line. The 5mm offset represents what happens in vivo with the 10mm offset representing a varus position of the knee of 7° and the load down the centreline representing 7° valgus angle. The tibial component was also rotated 10° externally and 10° internally.

The varus and valgus alignment had a minimal difference on the AP displacement and rotations of the TKR components (Figure 1.23). However this may be due to the method used, as the axial force was offset to simulate varus/valgus positioning but the force was still going between the femoral epicondyles so no lift off was occurring. There was also a minimal effect from the internal rotation of the tibial component however under external rotation the values of the rotation of the component changed. The range in the rotation was the same (around 15°), however the rotation went from -5-10° of rotation rather than -15-0°. The largest difference in the kinematics occurred with the change in PCL stiffness, particularly the increase in AP displacement with a loose PCL. This shows that the ligament tension has a large affect on the motion of the knee and is therefore an important factor to consider in experimental studies with respect to wear.

A computational study found that an increased posterior tibial slope resulted in a decreased quadriceps force, contact stress in the patellofemoral joint and PCL force [114]. An excessive posterior tibial slope could lead to loosening of the tibiofemoral joint gap during

flexion due to the reduction in tension in the collateral ligaments. As the posterior tibial slope increased there was an increase in posterior tibiofemoral translation. This is important as it allows more flexion in the TKR before tibiofemoral impingement occurs. It also improves the moment arm of the quadriceps which is associated with an improved knee society function score. Therefore this study suggests that a posterior tibial slope may be beneficial, particularly in CS TKR.

1.11.2.4 Wear

Simulation

Currently there are limited studies that have investigated the effect of alignment on the wear of knee replacements and only the effect of varus alignment has been studied experimentally. Ezzet et al [66] used a displacement controlled knee simulator to find the wear rates of knees under a varus alignment. The ISO standard inputs for axial force, tibial rotation and flexion extension were used. The anterior-posterior displacement was changed from the standard in order to simulate rollback during flexion (Figure 1.24).

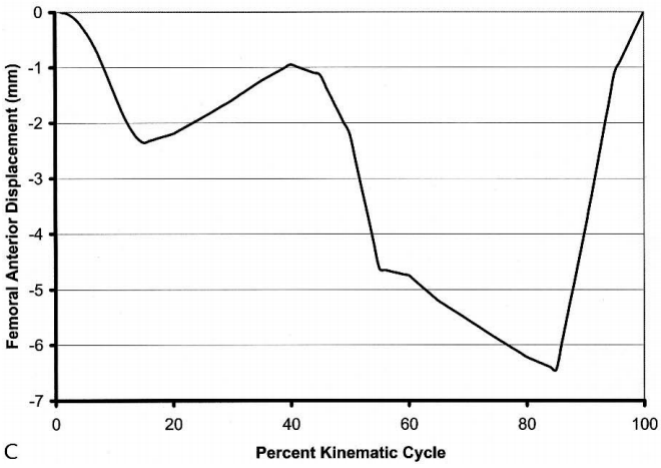

Figure 1.24: Anterior posterior input to simulate femoral rollback [65]

The wear rates were determined for both oxidized zirconium and cobalt-chrome femoral components against non-cross-linked, ethylene oxide-sterilized polyethylene. The components were simulated under an offset load to simulate a varus alignment of 3°, under a walking cycle with increased tibial rotation up to 20°. The gravimetric and volumetric wear rates for both types of components were found over 5 million cycles and compared to a previous study [65]. The wear with the alignment and increased kinematics resulted in nearly double the wear rate for the cobalt-chrome components (20-39 mg/MC) and increased the wear rate of the oxidized zirconium components by a smaller amount (12-17 mg/MC).

A computational study using a previously validated model was carried out into the effect of alignment in multiple planes on the wear rate of a TKR [135]. Alignment in the transverse plane was found to result in the highest increase in wear, however a posterior tibial slope was

also found to result in increased wear. Alignment in other planes, such as the tibial TR axis, only resulted in small changes in the wear rate. Internal tibial alignment was also found to result in edge loading on the tibial insert, this may result in increased damage and wear to the tibial insert [134].

Retrievals

One study found that tibial components which were placed in >3° of varus had almost double the volumetric penetration rate than those in <3° varus [184]. However there was no correlation between the femoral alignment or knee alignment with the wear rates.

In another study patients were separated into groups depending on their coronal alignment; valgus (Hip knee ankle (HKA) >3° valgus), neutral (HKA 0±3°), mild varus (HKA 3-6° varus) and moderate varus (>6° varus) [195]. For more varus alignments there was greater medial wear and for valgus alignments greater lateral wear. This may be due to condylar lift off in the lateral compartment in the valgus group and in the medial compartment for the varus group. However there were also higher damage scores in the lateral compartment for the mild and moderate varus groups compared to the valgus.

Another study [57] used radiographs to measure the tibial insert thickness of 416 knees. There was a significant increase in wear on the medial compartment for patients that had a more varus limb alignment after the TKR operation. A similar study found a significant correlation between the tibiofemoral and femoral angles with the difference in the polyethylene thickness between the medial and lateral compartments [47]. Varus alignments resulted in thinner medial compartments while valgus alignments resulted in thinner lateral compartments.

Some studies have found that alignment did not have a significant effect on wear [159]. This may be due to the differences in the patient morphology which can affect the loading in the knee. Some people have suggested using patient parameters such as weight and pelvic width to determine a patient specific “ideal alignment”[131]. However this may be subject to the ligament tensions and laxity, which may be hard to determine during surgery.

1.12 Aims and Objectives

Currently for mechanical alignment in TKR surgery the aim is to keep the alignment of the tibial and femoral components within 3° of the mechanical axis of the leg. Most alignment during surgery is carried out using the intramedullary and extramedullary rods in the coronal plane rather than the sagittal or axial planes. The envelope of ±3° has not been proven to be the range that results in better outcomes for TKRs. There is also no corresponding envelope in the sagittal or axial planes, in order to define this we must understand the effect of alignment on TKRs.

Previous studies that have investigated the effect of alignment on TKRs have tended to investigate the effect of alignment in the coronal plane on the loading of the tibial insert. This has provided an understanding of the impact that coronal alignment can have on contact pressures but the effect of alignment in multiple planes on contact pressure, kinematics and wear has not been carried out previously. Carrying out a study with a wider range of conditions will provide a wider understanding on the mechanical impact of alignment on the TKR.

One cadaveric study investigating varus-valgus alignment determined that changes in the load distribution of the TKR were proportional to the angle of the component alignment [201]. But that the cadaveric specimens with tight ligaments resulted in more balanced loading. This study suggested that alignment on its own may not result in imbalanced loading, but that it is the combination of alignment and the soft tissue conditions within the knee that are important.

The aim of this study was to investigate the effect of component alignment in the coronal, transverse and sagittal planes on the mechanics and wear of a fixed bearing, CR total knee replacement. This investigation of alignment in a number of planes has not been carried out previously. This project also investigated the effect of the soft tissue conditions within the knee in combination with component alignment in order to determine the relationship between the two factors. This may highlight why previous studies into just the effect of alignment have not found a relationship between knee scores and component alignment.

This was achieved by a number of objectives;

- The development and validation of a finite element computational model simulating the conditions within the experimental simulator in order to run parametric testing of additional alignment conditions.
- Experimental and computational simulation of different soft tissue conditions and the investigation of their effect with different tibial insert conformities.
- Investigating the effect of three different soft tissue conditions representing a patient with a stiff knee, resected ACL and resected ACL & PCL on the kinematics and wear of a TKR under mechanical alignment conditions.
- Understanding the effect of different component alignment conditions in the coronal, sagittal and transverse planes (4° varus, 14° rotational mismatch, 10° posterior tibial

slope and kinematic alignment) on the kinematics and wear of a TKR.

- Investigating the combination of the different alignment conditions and three soft tissue conditions on the kinematics and wear of a TKR.
- A parametric computational study investigating the effect of further alignment conditions (2° varus, 8° rotational mismatch, 4° rotational mismatch, 4° posterior tibial slope and half the kinematic alignment values studied experimentally) under the same three soft tissue conditions on the kinematics, contact mechanics and wear of a TKR.

Chapter 2

Experimental Methods and Validation

2.1 Introduction

This chapter will detail the methods used in experimental testing of the TKR. The experimental investigation was carried out using a knee simulator in order to determine the kinematics, contact pressure and wear rate of the TKR.

A Prosim six station force/displacement control electromechanical knee simulator (KS8) was used to perform the experimental studies. This was a new simulator so commissioning tests were carried out first in order to validate it. An electro-mechanical simulator was used as they provide better kinematic control (outputs following the demand inputs more closely) than the first generation pneumatic simulators [7].

Studies were carried out to simulate the effects of different soft tissues and alignment conditions on the contact pressure, kinematics and wear rates of a TKR.

In order to replicate the physiological conditions and show the influence of various soft tissue and alignment conditions on the output kinematics the simulator was run under force control conditions. This meant that the AP and TR displacements were not used as inputs as has historically been used at Leeds, instead AP force and TR torque input profiles were used. A two stage process was carried out; the first found the average output kinematics across the simulator and the second found the average wear rates for each test condition.

Wear studies were carried out in order to find the effect of different test conditions on the wear of the ultra-high molecular weight polyethylene (UHMWPE) tibial component.

In order to find the effect on the contact area a Tekscan (Tekscan Inc., Boston, USA) pressure sensor was used, this was placed between the femoral and tibial components in the simulator and representative displacements and loads applied to find the loading at different points within the gait cycle.

2.2 Materials

All the tests were carried out using DePuy Sigma fixed bearing, right knee (DePuy Synthes, Leeds, UK) components. The tibial inserts were size 3 moderately crosslinked UHMWPE (5MRad irradiated and re-melted GUR1020 XLK, part number 1581-13-110). Three different tibial insert designs were tested; curved (CVD), partially lipped (PLI), and custom flat inserts (Figure 2.1).

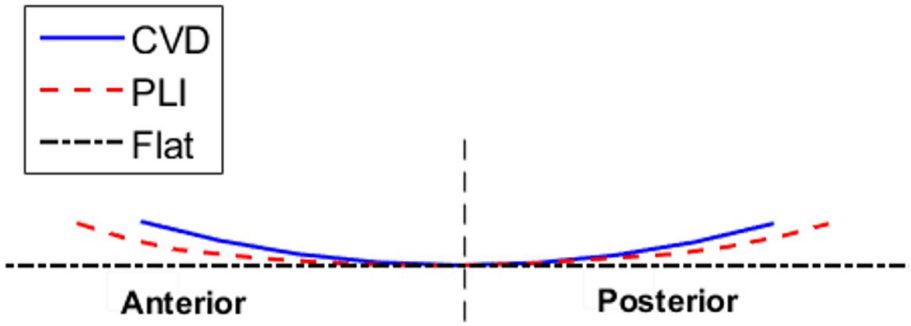

Figure 2.1: Three tibial insert designs tested; curved (CVD), lipped (PLI) and flat

The femoral components used had been used in previous studies, in order to ensure this would not affect the wear results the femorals were polished in order to remove any scratches.

The lubricant was 25% bovine serum (Life Technologies, New York, USA) in 0.04% sodium azide solution (Severn Biotech Ltd, Worcestershire, UK) and was changed approximately every 350,000 cycles. The contact area measurements were carried out using a Tekscan (Tekscan Inc., Boston, USA) pressure mapping sensor 4000 which was designed for use in knee joint applications, it has a total of 572 sensels with 62 sensels/cm^2 and a maximum pressure of 69.95 MPa.

The soft tissues were simulated using virtual springs within the simulator, the profiles of the virtual springs were changed to represent different soft tissue constraints. In order to represent different component alignments femoral and tibial fixtures were designed and made that allowed the tibial and femoral components to be inserted into the simulator in the desired positions.

2.3 Simulation Methods

The experimental study was carried out using a new generation electromechanical six station ProSim knee simulator (KS8). The simulator has five fully independently controlled axes and can be run in either force control or displacement control (Figure 2.2). Each station was individually controlled, has six degrees of freedom and can apply flexion-extension (FE), anterior-posterior (AP) displacement, abduction-adduction (AA), tibial rotation (TR) and axial force (AF) with the medial-lateral (ML) displacement either passive or fixed. The range

of movement within the simulator exceeds that used in the ISO standard input profiles [188]. AA can be active or passive, in all the tests it was passive to allow it to move freely.

The AP and TR displacements were defined in terms of the tibial insert; anterior displacement was anterior displacement of the tibial component. The AF was applied on the femoral component and the FE was defined in terms of the femoral component.

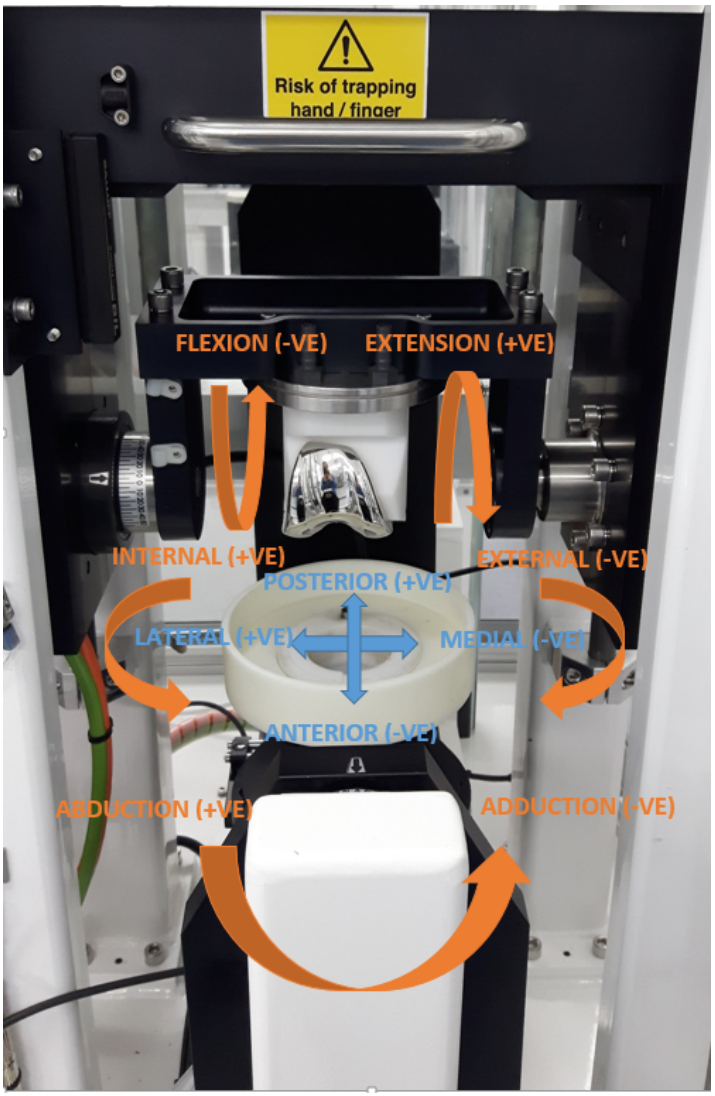

Figure 2.2: Simulator station with the axes and polarities labelled

2.3.1 Input Profiles

The ISO [186] force input profiles were used for all experimental simulation (Figure 2.3), with the AF varying between 268N and 2600N, the AP force between -111N and 265N and the TR torque from -1Nm to 5.9Nm. The FE varied between -30° and 30°, which resulted in values of 0° to 60° flexion of the femoral due to an offset of 30° applied to the femoral component with respect to the simulator axes. This was done to ensure that the FE position was within the

simulator FE displacement limits. The centre of rotation of the femoral component was set in accordance with the ISO standard [186] including the medial-lateral offset. The AF was applied medially to the centre of the joint by 7% of the width of the joint as stated in the ISO standard [188].

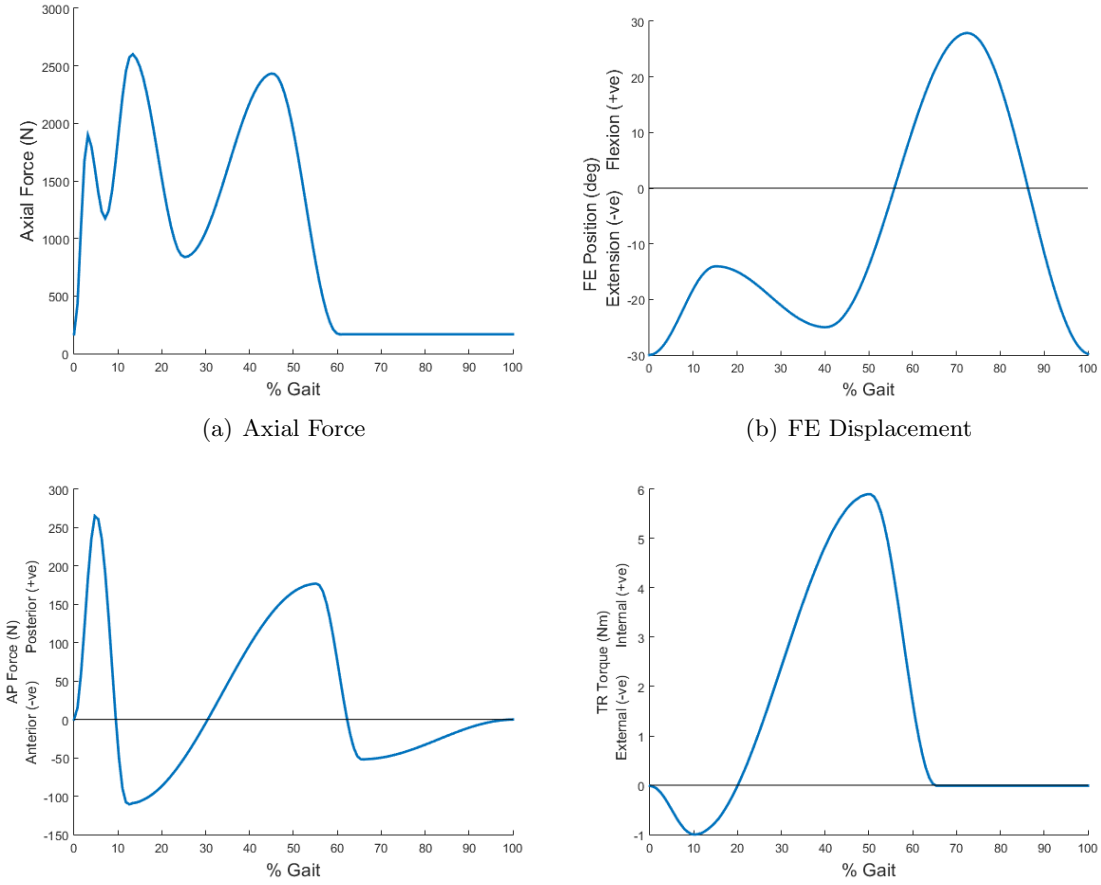

(a) Axial Force

(b) FE Displacement

(c) AP Force

(d) TR Torque

Figure 2.3: The input AF, FE displacement, AP force and TR torque profiles [186]

2.3.2 Soft Tissue Simulation

For this study force control was used as this allowed the kinematics in each test to be determined as an output of the study, enabling the effect of the soft tissue constraints and alignment on the kinematics to be investigated. In force control TKR simulation springs are used to represent the soft tissues in the knee [10, 62, 92, 196]. In this study virtual springs were used, this allowed any response profile including a non-linear one to be used. The desired spring profile for the AP and TR springs was uploaded into the simulator. This defined the force to be applied for a given displacement, which constrained the motion, replicating the effect of the soft tissues in the knee. The virtual springs within the simulator were validated experimentally by applying either an AP force or a TR torque and measuring the resulting

displacements (see Section 2.5.4).

The ISO standard spring profiles use linear springs with a gap around the zero position (Figure 2.4).

As the soft tissues within the natural knee do not have a linear response the gap around the zero position was added to the spring profile in order to generate a more representative profile of the soft tissues. All tests were carried out with spring profiles similar to the ISO standard, with variations in the spring gap size and the spring tension.

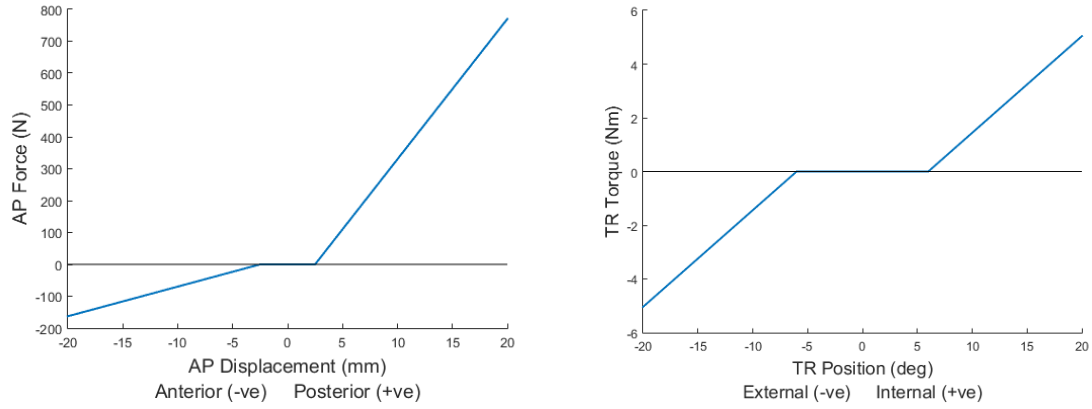

(a) AP Spring (b) TR Spring

Figure 2.4: The ISO standard AP and TR spring profiles for a CR TKR

2.3.3 Sensors

The simulator has 9 main sensors that are used for monitoring and feedback. A six axis load cell measures the AF, AP force, ML force, TR torque, FE torque and AA torque. The AP and vertical displacements are measured using magneto inductive position sensors mounted on the simulator. The FE, TR and AA displacements are measured using an optical encoder within the motor of the simulator.

2.3.4 Calibration

Before and after each wear study the simulator was calibrated; this was to ensure that the load and displacement sensors were measuring the correct load and displacement values over the range used during the study. The calibration was performed by comparing the output values of the in-situ simulator sensors with the output values of external and independently calibrated sensors.

The AP displacement was calibrated using slip gauges to measure the actual displacement between the values of -25mm and 25mm. An external calibrated load cell was used to calibrate the load cell within each station, different loads were applied in order to calibrate all the axes of the load cell. The axial force was calibrated within the range of 350N and 3kN, the AP force within the range of -500N and 500N, the TR torque within the range of -15Nm and

15Nm and the AA and FE torques within the ranges of -25Nm and 25Nm. These values are tuned for each station so there are some variations across the simulator but the ranges of values tested are similar. A digital inclinometer was also used to give an angular measure of the AA and FE displacements.

2.3.5 Stability Testing

To investigate the mechanical stability of the joint two, more extreme, spring conditions in addition to those used in the standard kinematics tests were applied to look at any change in the mechanics of the joint. This was done by changing the virtual spring profiles within the simulator. The first used the same spring tensions as the ISO Standard CS springs [186] but with increased spring gaps of ±5mm and ±9° rather than ±2.5mm and ±6°. The second test applied no spring restraints at all.

The simulator was run with no serum or gaiters attached so that the motion of the components could be seen, instead Vaseline was used to lubricate the joint. Dislocation of the joint or femoral lift off was noted and compared between alignment conditions.

2.3.6 Output Kinematics

The kinematic testing was run under conditions similar to the wear test; with 25% bovine serum and 0.04% sodium azide solution. One set of components was used on all stations to remove any effects due to differences in the component position or fixture weight. Each test was carried out on all six stations of the simulator with 10 consecutive cycles being recorded on each station once the simulator had stabilised after start up. The output kinematics for these cycles were then averaged across all the stations and the data was presented with 95% confidence interval (CI).

The output kinematics from each test were used to compare the test constraints as they have previously been shown to affect the wear rate of the TKR [132]. In order to do this minimum and maximum values at defined points throughout the gait cycle were assessed in order to characterize the profiles (Figure 2.5 and Table 2.1). For the AP displacement points A through to D were defined as the maximum from 0-20% gait, the minimum from 20-50% gait, the maximum from 50-70% gait and the minimum from 70-90% gait respectively. For the TR position points E through to H were defined as the maximum from 20-40% gait, the minimum from 40-50% gait, the maximum from 50-65% gait and the minimum from 65-80% gait. The AA displacement was only used as a comparison between alignment and soft tissue tests and not as a method to validate the simulator as it was not driven and was instead left free to move. Three points were defined on the AA displacement profile; point I was the maximum value from 0-15% gait, point J was the minimum value from 5-20% gait and point K was the maximum from 50-90% gait.

The range of motion in the cycles was also compared between tests. The range of motion was defined as the difference between the maximum and minimum points in the cycle.

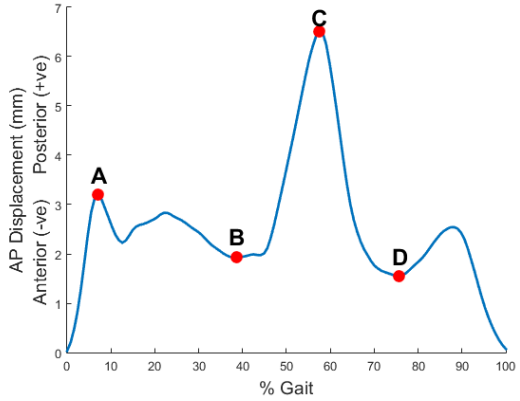

(a) AP Displacement

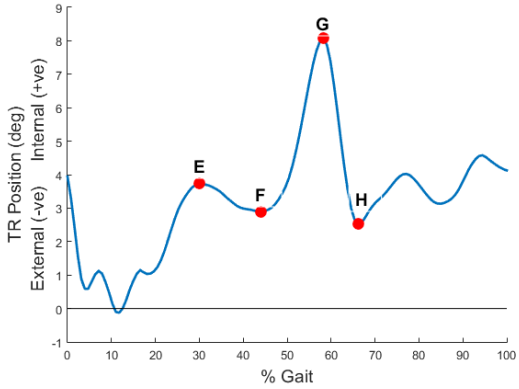

(b) TR Displacement

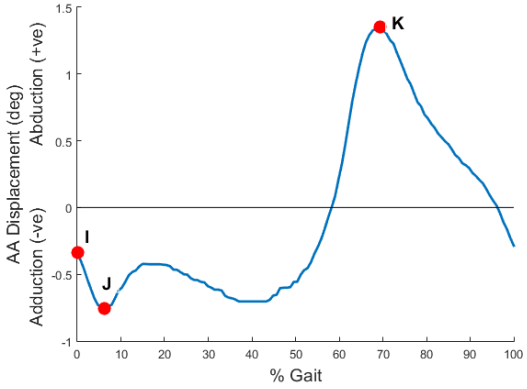

(c) AA Displacement

Figure 2.5: Maximum and minimum points on the AP, TR and AA displacement profiles that were used for statistical comparison between tests

Table 2.1: The definitions of the maximum and minimum points in the AP, TR and AA displacement profiles that were used for comparison between tests

AP Displacement			TR Displacement			AA Displacement		
A	max	0-20%	E	max	20-40%	I	max	0-15%
B	min	20-50%	F	min	40-50%	J	min	5-20%
C	max	50-70%	G	max	50-65%	K	max	50-90%
D	min	70-90%	H	min	65-80%			

The values of these points were then compared using a one way ANOVA with significance taken at $p<0.05$ using IBM SPSS Statistics 22. In cases where there were more than two groups a Welch's test with significance taken at $p<0.05$ was carried out to determine whether the variances between groups were homoscedastic. If this was found to be true a post hoc Tukey's test was used in order to confirm where the differences between the groups occurred, with significance taken at $p<0.05$, as this assumes equal variance. However if the variances were found to be too different a post hoc Games-Howell test was carried out, with significance taken at $p<0.05$, to determine the differences between the groups.

2.3.7 Wear Studies

During a wear study all six stations of the simulator were run at the same time under the same test conditions with 25% bovine serum and 0.04% sodium azide solution. The wear tests all had a frequency of 1Hz. After approximately every 350,000 cycles the lubricant was replaced and the components cleaned. Every million cycles the components were moved into different stations to help reduce the effects of the inter-station variability. The simulator was visually checked every 24 hours to ensure that it was working properly. During the test the kinematic data was periodically recorded. As the simulator would stabilise over time the number of cycles recorded decreased over time as the study was carried out. The first ten cycles were stored, then one in ten cycles until cycle 100, then one in 20 cycles until cycle 10,000 and after this one in every 10,000 cycles. This kinematic data was analysed at the end of the wear test to investigate any changes in kinematics during the wear test and to investigate the inter station variation.

Each study was run for 2MC and the tibial components were weighed after 0, 1 and 2 MC. The change in mass was used to determine the wear volume using a density value of 0.9346 kg/mm^3 [20]. A Mettler XP205 balance was used, which has a resolution of 10µg. Two unloaded control tibial components were soaked in lubricant for the duration of the tests and were used as a reference to compensate for moisture uptake [21, 76].

The surface roughness of the components was measured before and after testing using a Talysurf PGI-800. This was a stylus contact surface and form measuring instrument which was used to find the average roughness (Ra). A total of eight 10mm traces were taken along the superior surface of the tibial components, with four traces on the medial side and four on the lateral side. The traces had a 0.8mm cut off as the Ra value was between 0.1µm and 2µm [185], used a Gaussian filter and 100:1 bandwidth. The femoral components were mounted so that they could be rotated and the traces could be taken over the whole contact surface. Traces were taken on the medial and lateral sides at 0°, 12°, 18°, -27° and -40° from the reference point. The reference point was taken as the highest point of the component at each rotated position. The traces were 10mm long, had a 0.25mm cut off as the Ra value was between 0.02µm and 0.1µm [185] and used a Gaussian filter and 100:1 bandwidth.

The femoral components were re-used during testing, to ensure they were not too damaged only femoral components with an Ra value of less than 0.1µm were used for wear testing. Femoral components that had become too damaged were polished before being used again.

At the end of each wear study the change in the output kinematics over time was investigated. This was to determine whether the kinematics changed as the wear scar was formed. To do this 10 cycles from the start of the study, at around 1MC and at the end of the study were compared from each station. The minimum and maximum points in the cycles (points A-K in Figure 6.9) were compared to determine whether there were significant differences during the wear study. The wear rates between each of the inserts used in the study were then compared in order to determine whether there were similar differences in the wear rates over time.

The variation between the stations was also investigated. Using the same 30 cycles taken

at 0MC, 1MC and 2MC the output kinematics were compared between each of the 6 stations. Any significant differences in the kinematics were then compared to the wear rates on each station to determine whether the differences in kinematics may have affected the wear rates.

2.3.8 Fixture Design

In order to investigate the effect of alignment on the wear of knee replacements in KS8 different femoral and tibial fixtures needed to be designed or the input profiles altered to change the positioning of the components within the simulator. They were designed to simulate in vivo conditions where the components have not been aligned properly during implantation.

Under mechanical alignment the top of the tibial component surface was aligned with the AA axis of the simulator and the centre of rotation of the femoral head was aligned with the FE axis. As the simulator was run under force control the input profiles couldn't be altered to create the desired alignment conditions. Instead fixtures were used that had been designed to align the components at different angles.

The tibial component was cemented in place relative to the femoral component so that the maximum point on the femoral was in contact with the minimum point on the tibial surface. After set up the contact areas between the components were checked by applying microset to the femoral contact surface and placing the femoral and tibial components in contact by applying a load using the simulator. This was to ensure that the contact area between the components was in the centre of the tibial surface, at the dwell point, in the AP direction on both the medial and lateral side. This was carried out before all testing.

2.4 Simulator Validation Under Displacement Control

2.4.1 Methods

DePuy Sigma fixed bearing knee components were mounted in mechanical alignment; the centre of rotation of the femoral component was aligned with the FE axis of the simulator, the surface of the tibial component was aligned with the AA axis of the simulator and both were positioned so that they were centred within the knee simulator with respect to the AP, TR and ML axes.

The input profiles used in this test were the Leeds High Kinematics profiles (Figure 2.6) based on the AP and TR found in the natural knee by Lafortune et al [123]. Under this input profile the tibial rotation moved between $\pm 5°$, the flexion-extension from 0 - 58°, the anterior-posterior displacement from -10 - 0 mm and the axial force up to 2600N. The abduction-adduction was not driven and left to move freely and the medial-lateral displacements were fixed. The axial force and flexion-extension profiles were the same as those used in the ISO standard [188] (Figure 2.3).

The Leeds High Kinematic input profile was used under displacement control and the frequency of the test was 1Hz for the duration of six million cycle wear study. To find the

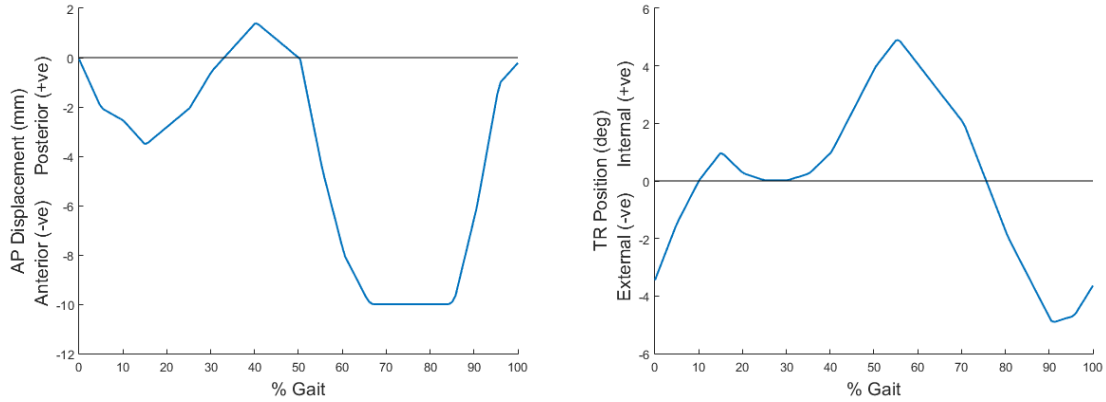

(a) AP Displacement (b) TR Displacement

Figure 2.6: Leeds High Kinematics AP and TR displacement input profiles

kinematic variation across the stations in the simulator the AP and TR cycles were split into stance and swing phases for the calculation. The maximum output values for each station were found over the six million cycles for the AP and TR. For the AP displacement the maximum absolute value at points B and D were found and for TR points F and G (Figure 2.7). The maximum values were averaged across the stations and compared to the input profile values. The mean output kinematics could then be found by finding the range of the total magnitude travelled by each implant over stance and swing phases. For the TR this was the maximum difference from point E-F and F-G and for the AP displacement from A-B and C-D. As before the values were averaged across the stations and compared to the input profile values. The input and output axial force profiles were also compared across the stations. An acceptable profile was one that was within ±5% of the maximum input profile value [186].

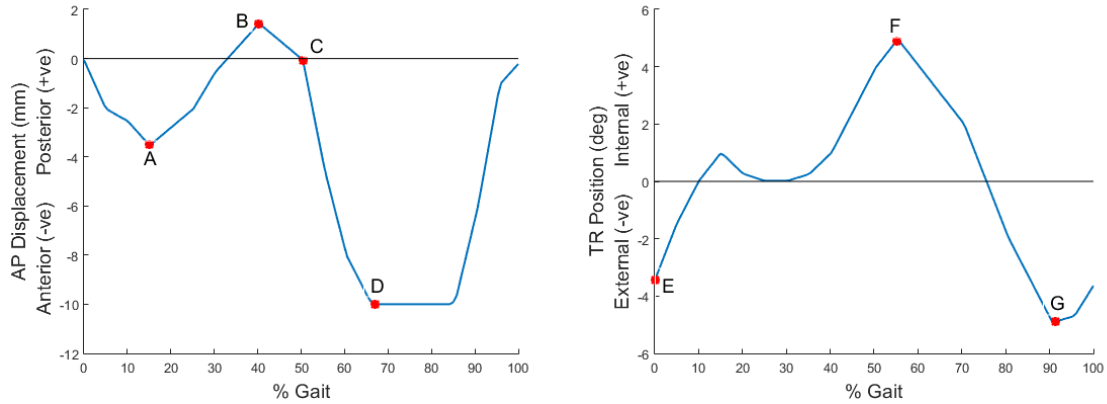

(a) AP Displacement (b) TR Position

Figure 2.7: Stance and swing phases of AP and TR displacements. The AP stance was defined as being from A-B and swing from B-D, while the TR stance was defined as being from E-F and swing from F-G.

2.4.2 Profile Following

The profile following of the simulator on the dummy and knee components were analysed to check whether the output profiles were acceptable, i.e. whether the applied forces and displacements were within ±5% of the maximum input value. Example cycles using knee components are shown in Figure 2.8. The axial force following was within ±5% of the input for most of the gait cycle, however during 60-100% gait the axial force oscillates around the demand value on all the stations. The oscillation in the axial force did not present in the dummy component profiles so may be due to the geometry of the components. Apart from the oscillations in the axial force the profile following was very similar between the dummy and knee components. The AP following was acceptable on most stations however there was an offset of around 1mm on station 5. There was also an offset of around 0.3° in the tibial rotation (TR) following on stations 1 and 6. Both of the offsets were rectified by recalibrating the AP displacement and TR position on the relevant stations.

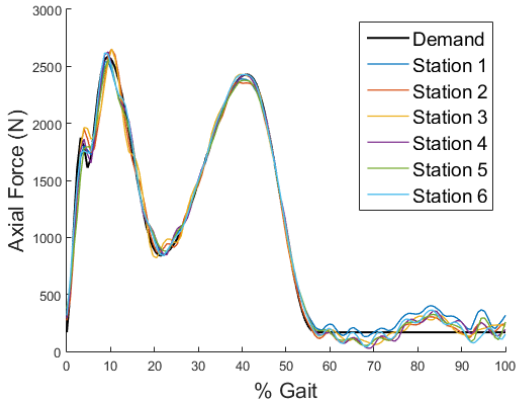

(a) Axial Force

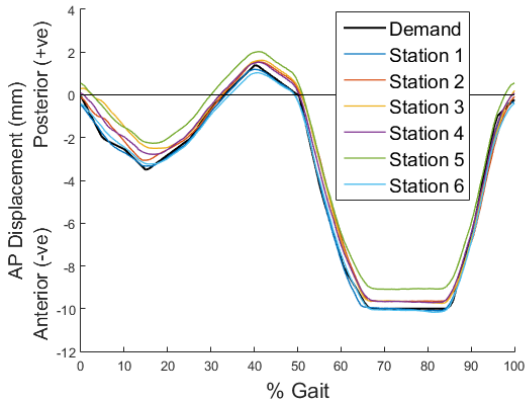

(b) AP Displacement

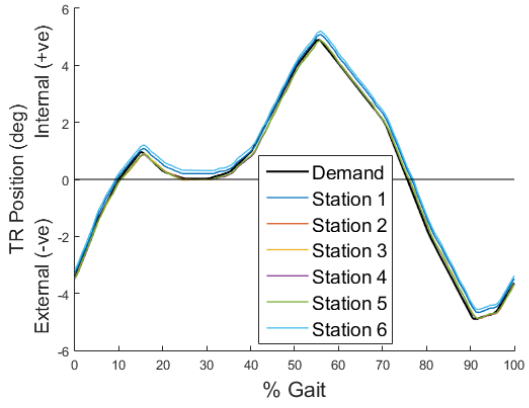

(c) TR Displacement

Figure 2.8: The demand and output profiles from the knee simulator running Sigma fixed bearing knee components

The maximum outputs for TR and AP displacement in the stance and swing phases were found for each station across all the cycles as described previously (Table 2.2). All the values were within 5% of the maximum input apart from the AP displacement during stance. This was 1.97mm compared to the input value of 1.4mm. This could have been due to the offset in the AP output compared to the input, station 5 had the largest offset however some of the other stations had an offset of around 0.5mm. The AP displacement was recalibrated on all stations to rectify the issue.

The maximum range of motion for TR and AP displacement was also found for the stance and swing phases across all the cycles as described previously (Table 2.3). All the values were within 5% of the input values. This showed that the output kinematics closely followed the input profiles to the simulator and achieved the demand values at the peaks.

Table 2.2: Average maximum input and output tibial rotation (°) and anterior-posterior displacement (mm) in the displacement control test

Displacement	**Gait Cycle Stage**	**Maximum Input**	**Maximum Output**
Tibial Rotation (°)	Stance	4.9	4.94
	Swing	-4.9	-4.80
Anterior-Posterior Displacement (mm)	Stance	1.4	1.97
	Swing	-10	-9.78

Table 2.3: Average maximum range of motion magnitudes for the TR and AP displacements in the displacement control test

Displacement	**Gait Cycle Stage**	**Maximum Input**	**Maximum Output**
Tibial Rotation (°)	Stance	8.37	8.37
	Swing	9.8	9.74
Anterior-Posterior Displacement (mm)	Stance	4.69	4.81
	Swing	11.4	11.38

2.4.3 Wear Rate

The average wear volume after each million cycles (KS8) is shown in Figure 2.9 compared to another simulator (KS6) for a similar wear study with the same conditions and components. A linear fit has been found for each simulator across the study to show the wear rate over the length of the study.

A student's t-test was carried out on the wear rates between the two simulators, a p value of less than 0.05 relates to a significant difference between the simulators. The null hypotheses for this test was that there was no significant difference between the simulators. After 3 MC the p value was above 0.47 and after 6 MC the average value was closer to that of KS6 and the CI decreased so the null hypotheses has not been rejected.

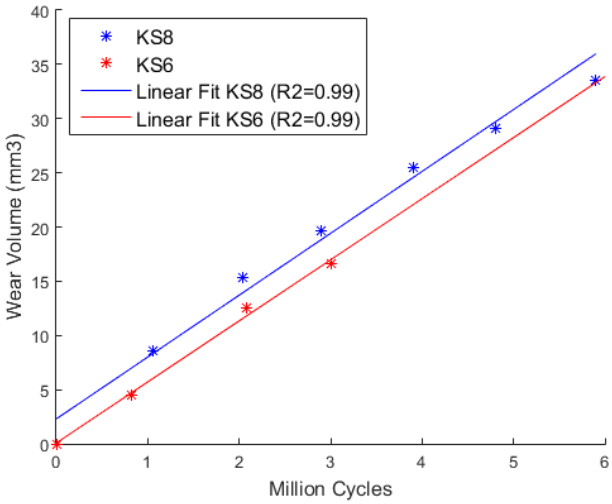

Figure 2.9: The average wear volume after each million cycles for KS8 and KS6 for the same wear study conditions along with a linear fit

2.5 Simulator Validation Under Force Control

2.5.1 Methods

In order to validate the simulator under force control a similar method was used as for the validation of displacement control using DePuy Sigma fixed bearing TKRs; the profile following was checked and the outputs (kinematics and wear) were validated against previous studies. The ISO standard force control inputs [186] were used in order to simulate walking motion with the ISO standard values for the AP displacement and TR restraints. For AP motion within ±2.5mm of the zero position no restraint was applied, for negative displacement greater than 2.5mm a restraint of 44 ± 2.2 N/mm was applied and 9.3 N/mm for positive motion. For TR no restraint was applied within ±6° of the zero position, past this there was a restraint of 0.36 ± 0.02 Nm/°. These restraints simulate the effects of the ligaments within the knee joint for a resected ACL and preserved PCL.

The input AP force and TR torque profiles were split into representative maximum and minimum points in order to investigate the profile following (Figure 2.10). The ISO standard specifies that the applied profile should be within ±5% of the maximum input value.

To investigate the inter-station variation one hundred consecutive cycles were recorded under wear test conditions on each station of KS8. These cycles were then averaged to give a mean AP and TR output for each station. The variation on each station across those 100 cycles was found as well as the variation between the six station means. To compare the kinematics the maximum and minimum points in the AP and TR displacement outputs were found (Figure 2.5). A students t-test was carried out using IBM SSPS Statistics 22 in order to test for significant differences with $p<0.05$ being taken for significance.

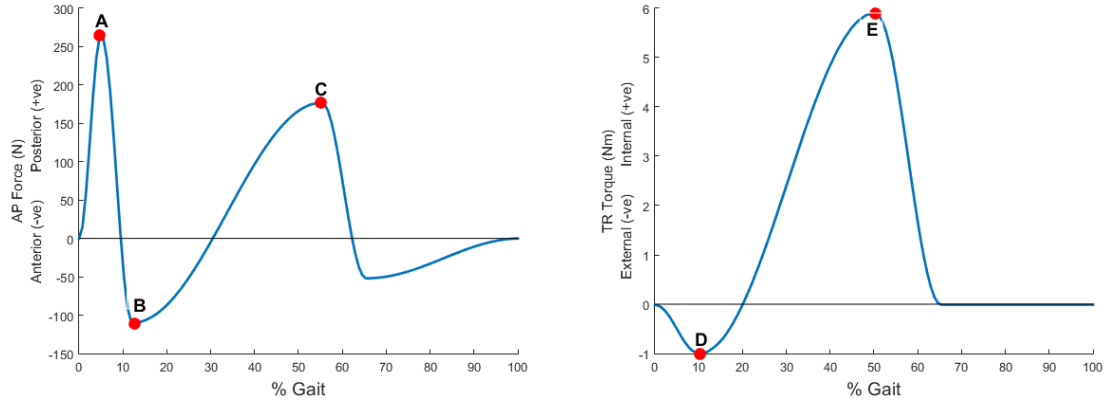

(a) AP Force (b) TR Torque

Figure 2.10: Maximum and minimum points in the AP force and TR torque input profiles used for comparison

2.5.2 Profile following

The corresponding points in the applied AP force and TR torque profiles were found for each station and averaged across the simulator (Table 2.4). For the AP force both points A and B were only just above 5% of the maximum input value and point C was below. For the TR torque point E was under 5% however it was very high at point D. This was due to the TR torque profiles being very unstable at this point in the cycle (Figure 2.11). This may be due to the sharp increase in the AP force between 0% and 10% gait (Figure 2.10 (a)), which would have affected the application of the TR torque. However for the rest of the cycle the TR torque was much more stable.

Table 2.4: Average maximum and minimum inputs and applied AP force and TR torque in force control test

		Input Profile	**Applied Profile**	**Difference (% of maximum input)**
AP (N)	A	265.1	279.64	5.5
	B	-110.7	-125.95	5.8
	C	177.16	180.6	1.3
TR (Nm)	D	-1	-2.2	20.3
	E	5.9	6.1	3.4

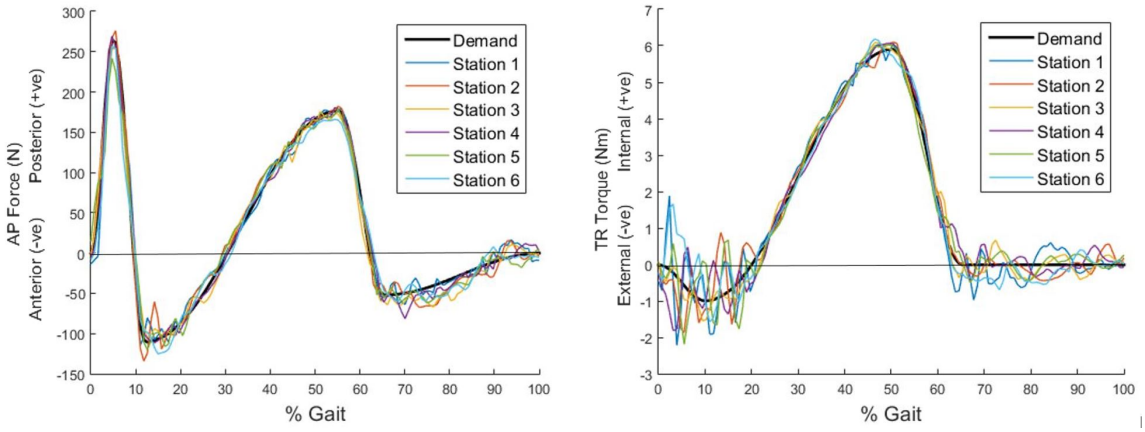

(a) AP Force (b) TR Torque

Figure 2.11: Input AP force and TR torque profiles from each station

2.5.3 Inter-station Variation

The maximum 95% confidence intervals for each of the stations were under 0.024 mm and 0.031° for the AP and TR respectively. This shows that for each station there was little variation between cycles, therefore in further kinematic testing only 10 consecutive cycles were recorded on each station.

However between the stations there was more variation, particularly in the last 30% of the cycle (Figure 2.12). The increased variation at the end of the cycle was probably due to a decrease in the applied AF resulting in lower friction between the components.

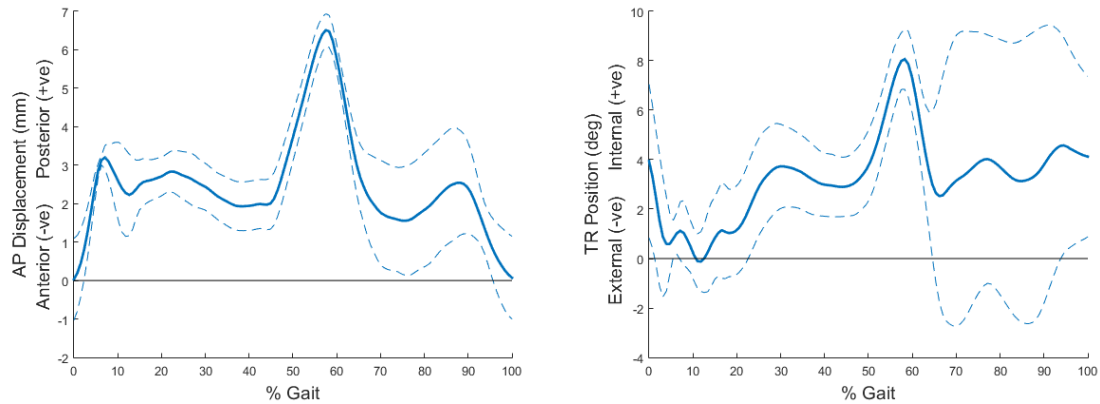

(a) AP Displacement (b) TR Displacement

Figure 2.12: Average AP and TR displacement under force control conditions with 95% confidence intervals

2.5.4 Virtual Springs

Under force control simulation virtual springs within the simulator were used to restrain the AP and TR motion, replicating the effect of the soft tissues within the knee. In order to check that the virtual springs were functioning properly the response to different loads was tested. Dummy components were inserted into the simulator and the ISO standard CR and CS springs uploaded. An AF of 50N was applied, this was the lowest AF value that could be applied during testing. Different AP forces and TR torques were applied to the dummy components and the resulting displacements recorded. These displacements were then compared to the expected values given the spring stiffness's and the average spring stiffness in each direction found for each station (Tables 2.5 and 2.6). The resulting displacements were close to the expected displacements, small differences were expected due to friction within the AP and TR motion and the applied AF.

Table 2.5: Virtual spring test results for ISO CR Springs

Station	Anterior (N/mm)	Posterior (N/mm)	External (Nm/°)	Internal (Nm/°)
	9.3	44	0.36	0.36
1	9.75	43.45	0.41	0.33
2	9.86	42.78	0.41	0.34
3	9.88	43.00	0.40	0.36
4	10.04	43.17	0.42	0.35
5	9.88	42.61	0.41	0.31
6	10.31	42.71	0.36	0.41
Average	9.96	42.95	0.40	0.35

Table 2.6: Virtual spring test results for ISO CS Springs

Station	Anterior (N/mm)	Posterior (N/mm)	External (Nm/°)	Internal (Nm/°)
	9.3	9.3	0.13	0.13
1	9.16	9.60	0.14	0.13
2	9.58	9.72	0.17	0.12
3	9.69	9.47	0.19	0.11
4	9.48	10.00	0.17	0.14
5	9.90	9.48	0.15	0.14
6	9.90	9.71	0.14	0.15
Average	9.62	9.66	0.16	0.13

2.5.5 Wear Rates

Three MC were run under force control conditions and the wear volume for each MC found (Figure 2.13). For the first MC under force control the data from only four stations could be used therefore an extra MC was carried out. The average wear rate for the first MC was significantly higher than the average wear rate after 3MC (p=0.025). There were some differences in the output kinematics during the study which may have resulted in different wear rates; point A in the AP displacement profile was significantly higher after 2MC than

at the start of the study (p=0.032), point D in the AP displacement profile was significantly lower after 1MC than at the start of the study and after 2MC (p<0.01). Point H in the TR displacement profile was also significantly lower at the start of the study than after 2MC (p<0.01).

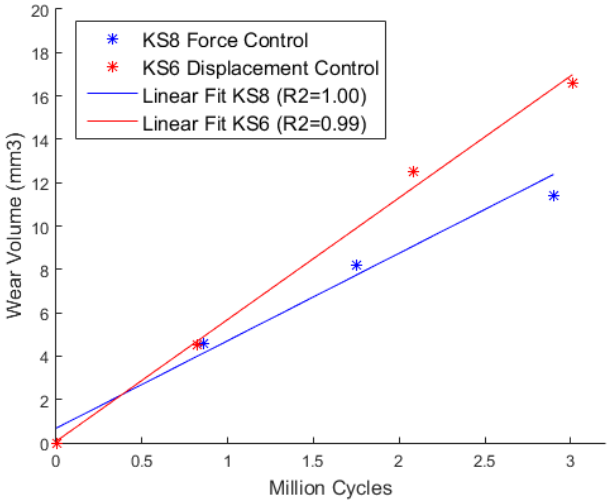

Figure 2.13: Wear volume for each million cycle for KS8 under force control conditions and KS6 under displacement control conditions with a linear trend

To validate the wear values under force control conditions they were compared to the wear rates found under displacement control. Under displacement control the AP displacement varied from -10mm to 2mm and the TR position from -5° to 5°. Under the force control test the AP displacement was between 0-6.5mm and the TR position between 0° and 8°. This meant the AP motion had about half the magnitude and the TR position about 0.8 of the magnitude under force control compared to displacement control. There was no significant difference between the wear rates after 3MC (p=1.26) although KS8 under displacement control conditions did result in a lower wear rate.

A previous study into the effect of kinematics on wear found that halving the AP magnitude resulted in the wear rate decreasing to 62% of the original value [132]. The force control wear rate after 3 MC was 54.9% of the displacement control values, which was a similar decrease as that found by the previous study. The difference in wear may be due to the UHMWPE used; conventional compared to moderately crosslinked in this study as cross-linking has been shown to significantly reduce the wear in joint replacements [75, 77]

2.5.6 Effect of tibial fixture weight

To test the effect of weight on the movement in the AP and TR positions the same profile was run with a PEEK tibial holder, weighing 1.9kg, and a steel tibial holder, weighing 2.4kg. The test was run on all six stations of the simulator under wear test conditions and 10 consecutive cycles were recorded on each station with both the Steel and PEEK tibial fixtures.

There was a minimal difference in the AP displacement, the PEEK holder resulted in around 1mm more posterior displacement than the steel holder during the first 80% of the cycle (Figure 2.14). This may be due to the extra weight of the steel holder so larger weight differences may result in a larger difference.

In the TR position there was a constant offset throughout the cycle of around 2 degrees (Figure 2.14). This offset could be due to differences in the cementing of the components into the tibial holders. Otherwise there was little difference between the two profiles. There was more variation in the TR position for both the Steel and PEEK holders compared to the AP. However there was more variation in the Steel holder TR position than for the PEEK.

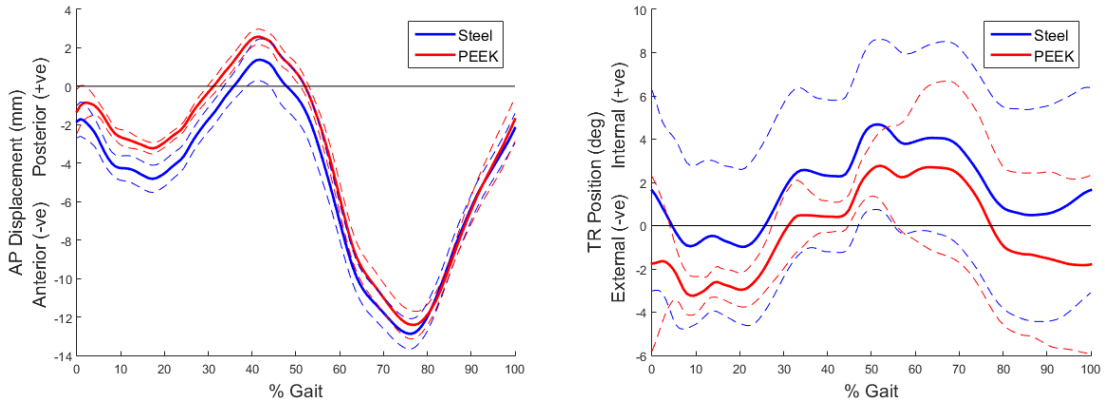

(a) AP Displacement (b) TR Displacement

Figure 2.14: The output AP and TR displacements with different weight tibial holders; steel (2.3kg) and PEEK (1.9kg) with the 95% CI shown by dotted lines

In order to reduce any differences in kinematics in any of the studies in this research the weight of the steel tibial fixtures were kept as close to 2.4kg as possible. Any tibial fixtures that weighed more than this were made lighter by removing any unnecessary sections of the tibial fixture surface.

2.6 Wear Scar Analysis

2.6.1 Purpose

The aim of this method was to be able to analyse and compare the wear scars between different experimental studies. After a wear study had been carried out on the simulator the area of the tibial insert which had worn away was visible, this method used an image of the tibial insert, where the wear scar had been outlined in pen, and digitised the position and shape relative to the tibial insert. The area of the wear scar could then be found and compared between tests.

2.6.2 Methods

2.6.2.1 Photographing the tibial insert and wear scars

After the experimental tests were complete a black, permanent pen was used to draw around the outside of each wear scar on the tibial inserts. This line was drawn so that the inner edge of the pen lined up with the outer edge of the wear scar (Figure 2.15).

The photographs were taken from above each tibial insert with a digital camera. A black background was used along with a light diffuser to reduce the amount of shine on the tibial insert and create a high contrast with the edge of the tibial insert. All the photographs were taken with the anterior side of the tibial insert at the top and with the medial-lateral plane of the tibial insert approximately horizontal.

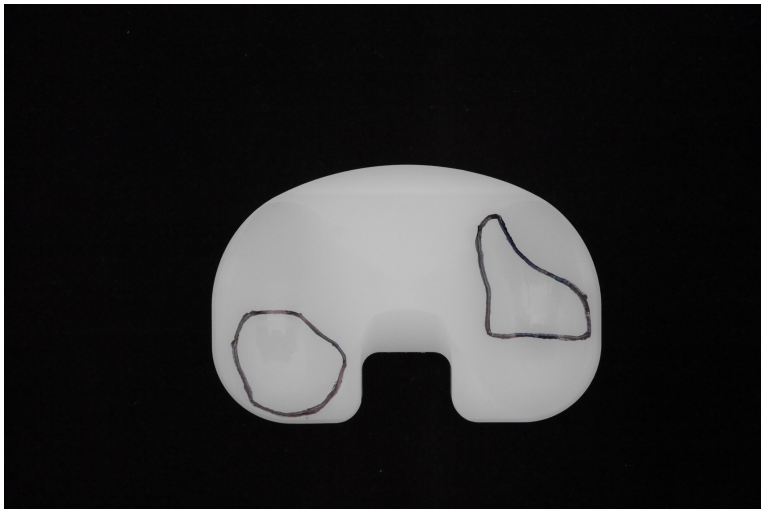

Figure 2.15: Example photograph showing a tibial insert with the wear scars

2.6.2.2 Generating the outlines

The digital image was imported into Matlab and converted to a greyscale image (Figure 2.16). The contrast of this image was then increased in order to increase the definition of the wear scars. The image was then converted into a binary image using a threshold value to determine whether each pixel would be black or white (Figure 2.17).

To find the outline of the tibial insert the threshold value was found using the Matlab function 'graythresh', this used the amount of dark/light pixels in the greyscale image to determine a threshold. This value was normally around 0.5 and varied depending on the amount of black background around the tibial insert. This resulted in a clean outline of the tibial insert.

However using the 'graythresh' function to determine the threshold did not generate clear outlines of the wear scars. As the lines used to draw around the wear scars were not as distinct as the background the threshold value often resulted in gaps in the outline of the wear scars.

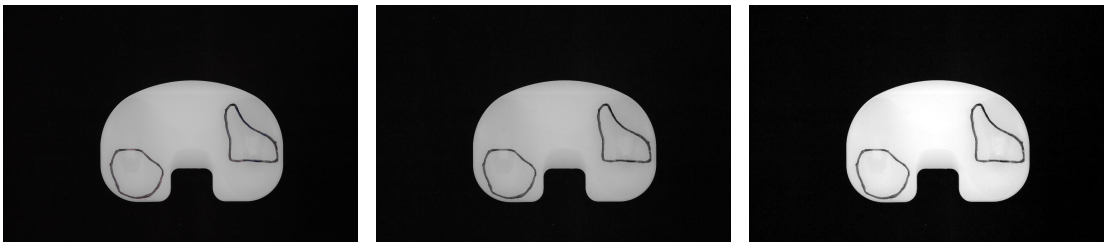

(a) Original image (b) Greyscale (c) High contrast

Figure 2.16: Original wear scar image, the greyscale version of the same image as well as the increased contrast image

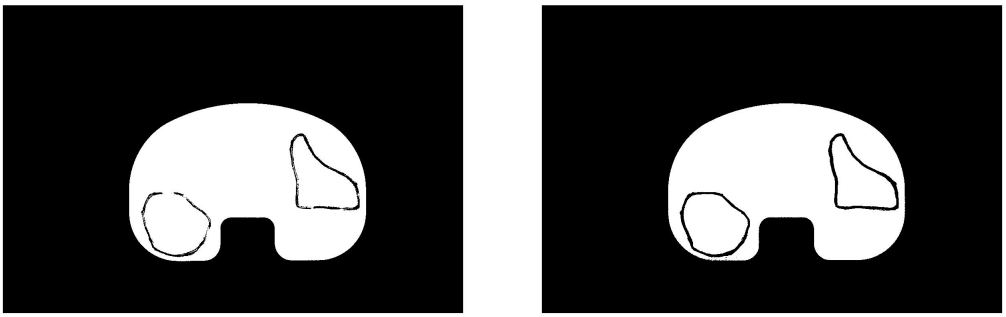

(a) Automated threshold (b) Manual threshold

Figure 2.17: Binary image using the automated threshold to find the edge of tibial insert and using the manual threshold to find the edge of the wear scars

A threshold value of 0.6-0.7 was found to work best in order to generate clean wear scar outlines. This value was changed depending on each image.

The Matlab function 'bwboundaries' was then used in order to find the coordinates of the boundaries; that was the regions between the black and white pixels. The largest boundary found from the binary image using the automated threshold was defined as the outline of the tibial insert. The location of the centre of the tibial insert was then found to determine which x coordinates would constitute a medial wear scar and which would constitute a lateral wear scar (Figure 2.18).

The Matlab function 'polyarea' was then used to find the area of each boundary, the boundary found on the medial and lateral sides of the tibial insert with the second largest areas (the inside edge of the drawn on black lines) were defined as the wear scar outlines.

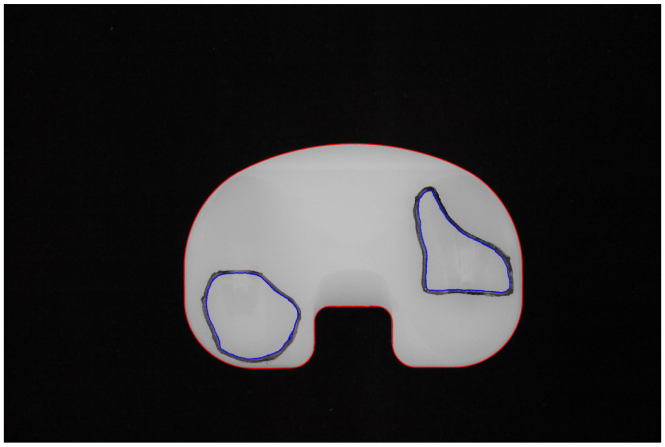

Figure 2.18: The generated outlines for the edge of the tibial insert and both wear scars

2.6.2.3 Normalisation

In order for the wear scar outlines to be comparable within and between tests the wear scar outlines needed to be normalised to ensure they were in the same location with the same orientation and size.

The centre of area of the tibial insert outline was found, the tibial outline and wear scar outlines were then moved so that (0,0) was at the centre of area of the tibial insert (Figure 2.19).

The principal moments of area of the outline were then found using the open source 'polygeom' function [183]. The tibial outline was then rotated about its centre of area so that the principal moment of area were at 90° and 180°, this resulted in the tibial outline being horizontal. The wear scar outlines were then rotated by the same angle. All the outlines were then scaled so that the width of the tibial insert was equal to 71mm and was to scale.

In order to ensure the wear scar outlines were smooth and did not contain inconsistencies from the boundary definition process the wear scar outlines were smoothed using Fourier analysis (Figure 2.20). As each outline was a closed loop standard smoothing functions in Matlab would not work; they do not allow repeated x values. The two functions used to generate the Fourier series and convert that into new coordinates were open source functions 'EllipticFourierDescriptor' and 'plotEllipticFourierDescriptor' respectively [165].

For the outlines to be directly comparable they were all down sampled so that they had the same number of points. For one set of 6 outlines the number of points making up each outline ranged from 1126-1254 points. All the outlines were therefore down sampled to 1000. In order to ensure that each outline started and ended at the same relative point and therefore that the first point on the outline will be comparable across all the outlines the start point of each outline was also changed so that they were in a similar position for all outlines. First each outline was moved so that the centre of area was at (0,0), the start point of the outline

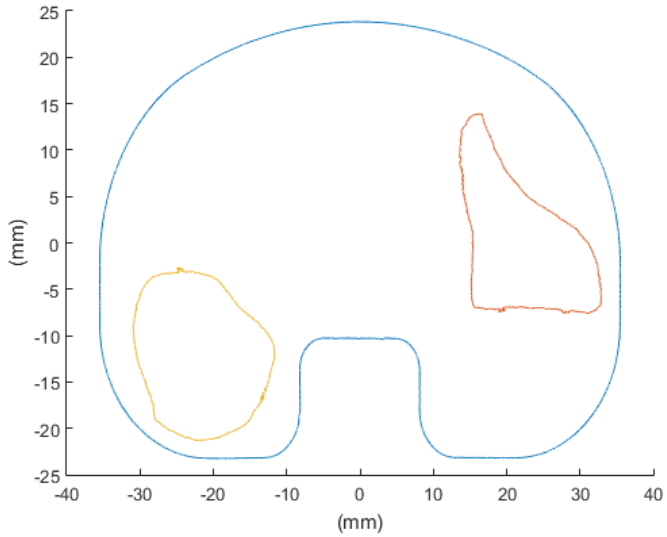

Figure 2.19: Scaled, centred and rotated tibial edge and wear scar outlines

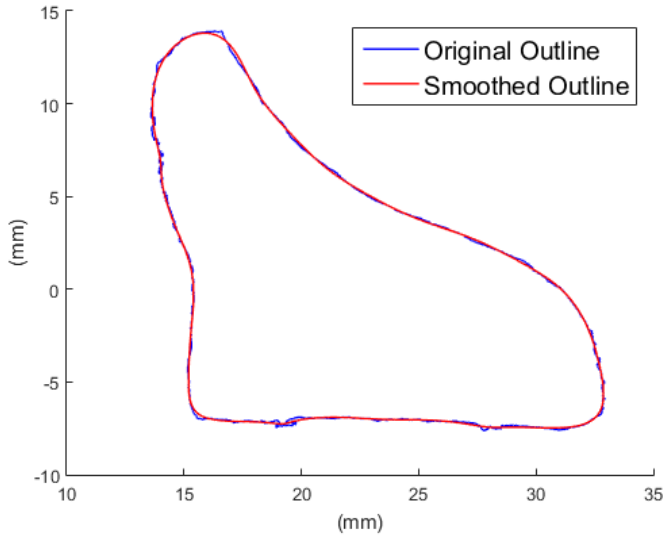

Figure 2.20: The original wear scar outline and the same outline after Fourier analysis

was then moved to the point where x=0 and with the highest value of y. After this process was completed the outlines were moved back to their original positions.

2.6.2.4 Average wear scar

As the wear scar outlines were different shapes the corresponding point in each outline was still not directly comparable; the differences in size and shape meant that the corresponding points could be in very different locations. In order to compare the outlines landmarks moved into comparable positions along each outline were used.

Bookstein defined three types of landmarks [40]; type 1 (fully defined) are where three

structures meet, type 2 are the maxima or minima of curves and type 3 (semi-landmarks) are less well defined; they fill in gaps away from any intersections. As there were no intersections in the wear scar outlines type 3 landmarks were used.

The method used to define the semi-landmarks was that explained by Bookstein [39]. The landmarks were first evenly spaced around one of the wear scar outlines; this was used as the reference outline (Figure 2.21). The next outline was then compared to the reference outline. For the first landmark on the reference outline the closest point along the new outline was found. This point was then set as the first landmark on the new outline. This process was then repeated for all the landmarks on the new outline.

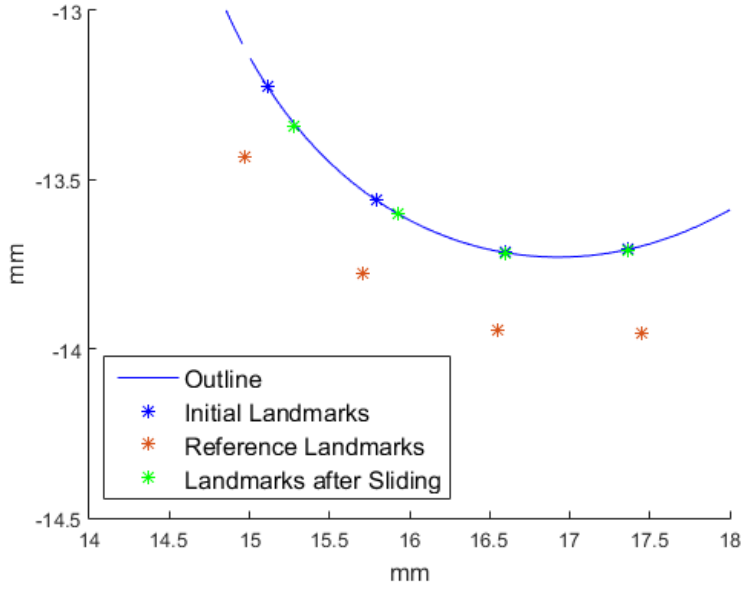

Figure 2.21: Landmarks on a wear scar when they were positioned based on the reference landmarks and after the landmarks have been moved relative to the average landmark position

Once this had been carried out on all 6 outlines the average landmark position across the outlines was found. This average was then used as the reference landmarks and the process was repeated. This allowed each outline to be defined by a number of points, in this case 100, in a way that made each set of points comparable regardless of the outline shape or size.

The average wear scar outline and the 95% confidence interval could then be calculated from the average position of each landmark across the 6 outlines (Figure 2.22).

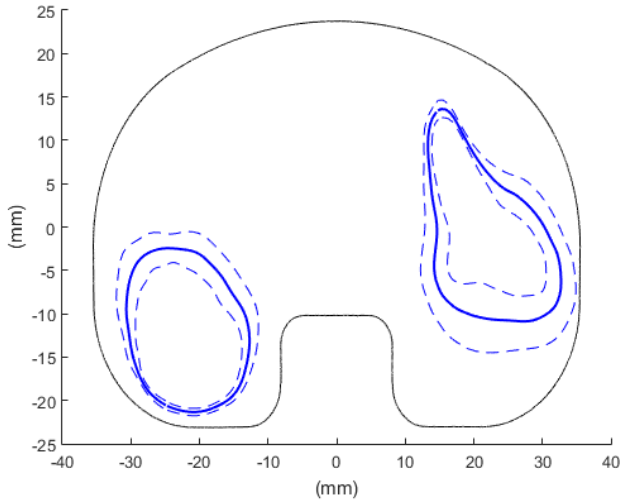

Figure 2.22: The average wear scar outlines with 95% confidence intervals (n=6)

2.6.2.5 Wear scar area

In order to calculate the contact area of the curved tibial surface using a 2D outline the proximal surface of the tibial insert was imported as an stl file from the solidworks part file of the whole insert. In order to get just the proximal tibial surface it was first exported as a parasolid, the surface was then meshed to generate triangular elements. The wear scar outline was then projected on top of the 3D tibial surface and the elements within the wear scar outline were found (Figure 2.23).

This was done by finding all the node points on the tibial surface that were within the wear scar outline (Figure 2.24). The nodes made up a triangular mesh, if one node of a triangular element was outside of the wear scar outline the element was removed from the wear scar surface. The 3D surface area was then calculated by summing the areas of each element, the area of each triangular element was calculated using Equation 2.1 where x, y and z are the coordinates for nodes 1, 2 and 3.

$$Area = 0.5 * \sqrt{\left| det \begin{vmatrix} x_1 & y_1 & 1 \\ x_2 & y_2 & 1 \\ x_3 & y_3 & 1 \end{vmatrix} \right|^2 + \left| det \begin{vmatrix} y_1 & z_1 & 1 \\ y_2 & z_2 & 1 \\ y_3 & z_3 & 1 \end{vmatrix} \right|^2 + \left| det \begin{vmatrix} z_1 & x_1 & 1 \\ z_2 & x_2 & 1 \\ z_3 & x_3 & 1 \end{vmatrix} \right|^2} \quad (2.1)$$

This area calculation using the 3D mesh resulted in an underestimate of the wear scar area due to the gaps occurring between the edge of the mesh and the edge of the outline (Figure 2.25).

Table 2.7 shows the calculations of the 2D and 3D surface areas of the wear scar outline. In order to make the calculation more accurate, the areas within the wear scar that were not represented by the 3D mesh were calculated as a 2D surface area. The total wear scar area was then calculated as the sum of the 3D surface made up of the mesh and the 2D area outside

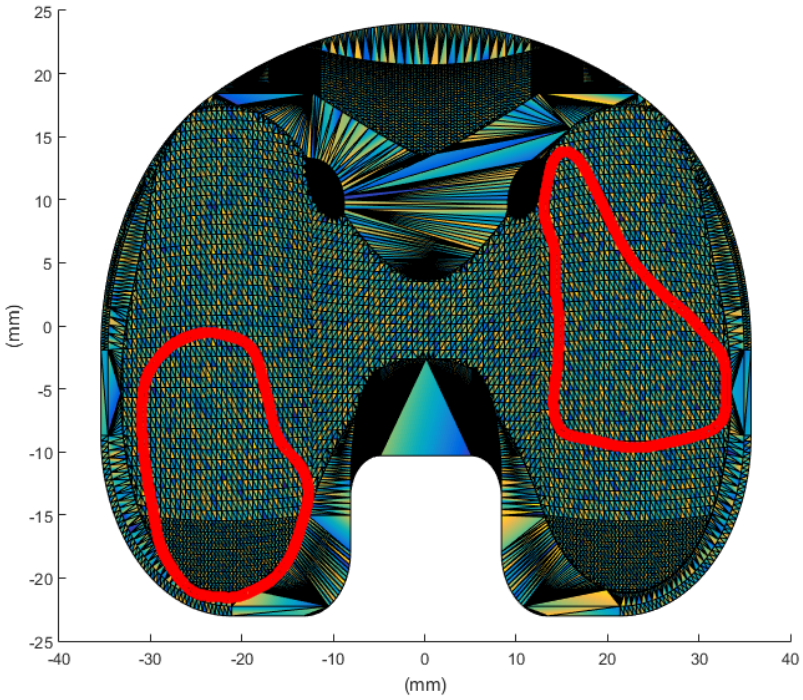

Figure 2.23: 3D proximal tibial surface imported into Matlab with wear scar outlines projected onto the top surface

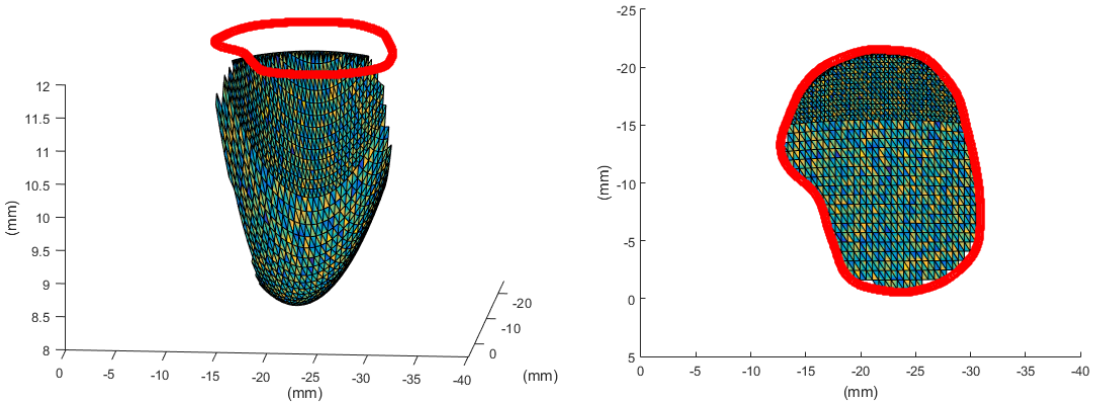

Figure 2.24: The 3D superior tibial surface within the wear scar outline

of the mesh that was still within the wear scar outline.

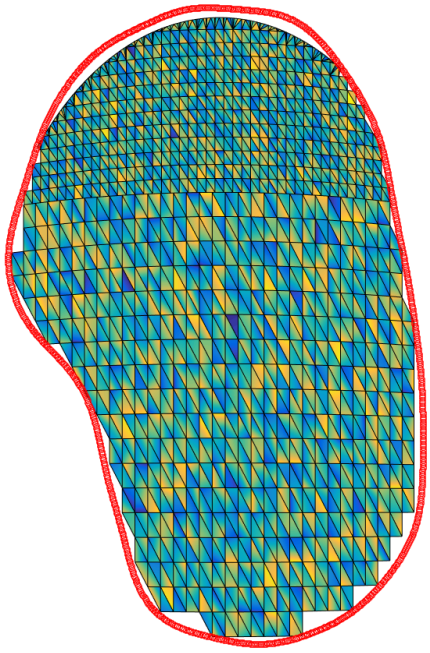

Figure 2.25: Zoomed in view of the 3D mesh elements to show the gaps between the mesh and the wear scar outline

Table 2.7: Calculated area for 6 wear scar outlines using three methods; calculating the area of the 2D wear scar outline, calculating the 3D area of the mesh within the wear scar outline and summing the 3D surface area with the 2D surface between the edge of the 3D mesh and with the wear scar outline.

Area (mm2)	1	2	3	4	5	6
2D Surface Area	234.20	266.05	269.31	237.21	245.07	244.44
3D Mesh Surface Area	244.63	277.04	281.03	247.03	255.89	255.63
Combined Area	261.50	295.33	306.54	267.18	279.31	272.49

2.6.2.6 Outline of conforming section of tibial

In order to investigate the amount of wear that occurs on the edge or over the edge of the tibial insert the outline of the conforming section of the tibial was found; this was the part of the tibial where contact with the femoral should occur (Figure 2.26).

An .stl file was generated of just this section of the tibial insert using the same method as described previously (Figure 2.27). The 2D outline of this section was then found using the Matlab function 'boundary' with a shrink factor of 1, this shrink factor gave the closest match to the outline of the data points in the .stl file.

This boundary was then added to the outline of the tibial insert (Figure 2.26). The area of the wear scars that overlapped this inner edge could then be found by finding the intersection between the inner edge and the average wear scar outline using the Matlab function 'polybool'. This returned the outline of the intersection and the area of this outline could be found.

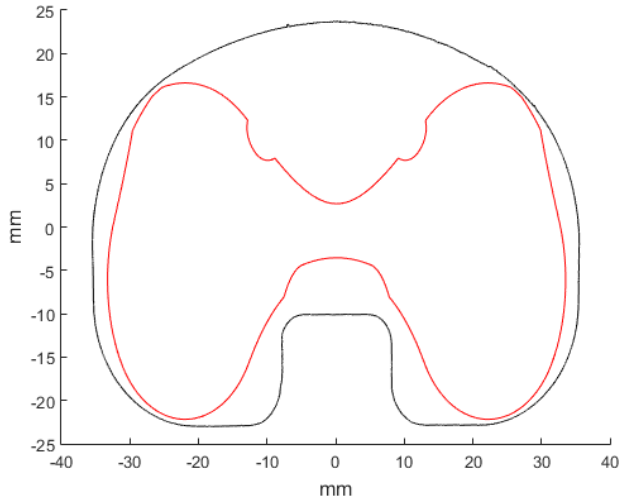

Figure 2.26: Edge of tibial insert with edge of conforming section shown in red

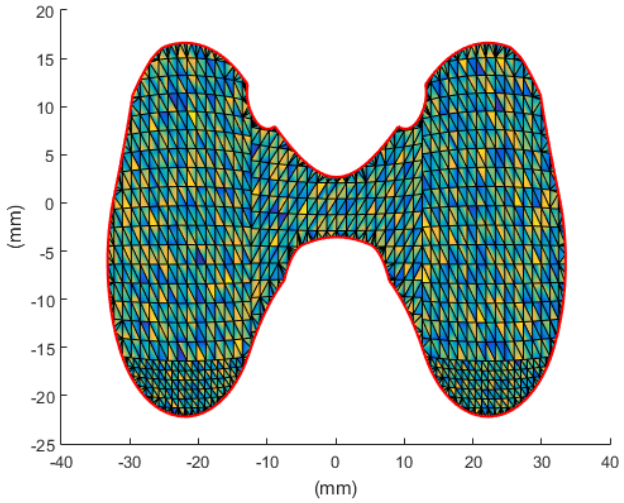

Figure 2.27: Mesh generated from the .stl file of the conforming section of the tibial with generated boundary shown in red

2.6.3 Validation

2.6.3.1 Wear scar generation

The generation of each of the outlines was validated by overlaying with the original image (Figure 2.18). The exact position of the boundaries depend on the threshold value used, however due to the error involved in drawing the lines on the insert originally the error in the position of the digitised boundary was negligible.

2.6.3.2 Normalisation

The tibial insert edges found from 6 different images once they had been normalised were very similar (Figure 2.28), this shows that the tibial edge definition and normalisation process across the different images resulted in comparable data.

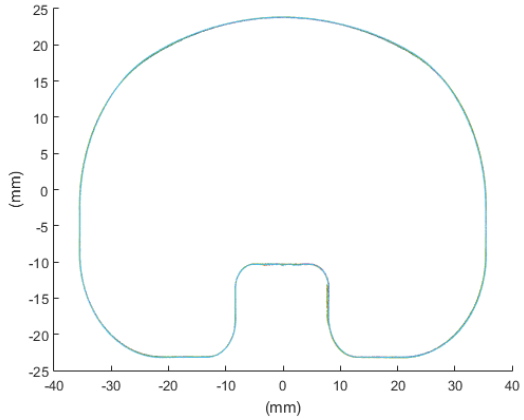

Figure 2.28: Normalised tibial outlines from 6 different images

Figure 2.29 (a) shows an image that has been rotated by 30 degrees, this has changed the size and orientation of the tibial insert in the image. The resulting tibial outline from the original image and from the rotated image is shown in Figure 2.29 (b); there was no difference between the two outlines. This shows that the scale, position and orientation of the tibial insert in the original image does not affect the digitised outline.

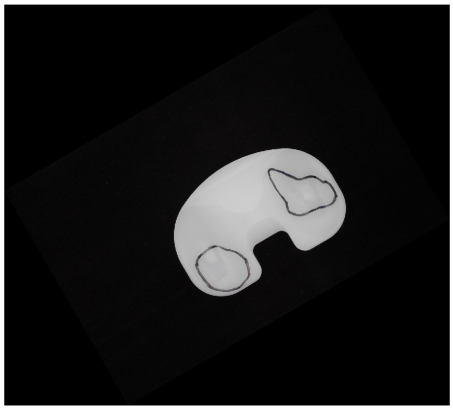

(a) Rotated image

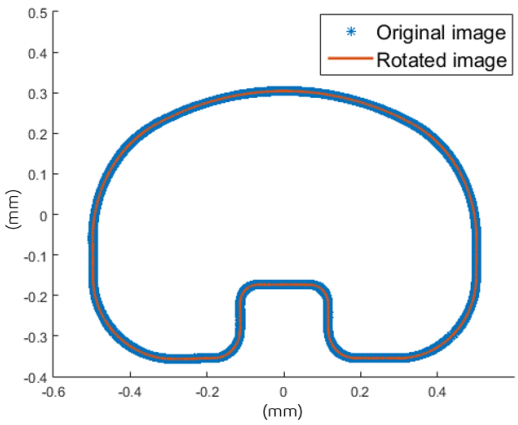

(b) Resulting outlines

Figure 2.29: A rotated image and the resulting tibial outlines from the original and rotated images

2.6.3.3 Average wear scar generation

The number of harmonics used for the Fourier analysis was chosen so that the position of the outline would remain the same but inconsistencies in the outline would be removed. The number of harmonics that best achieved this was found to be 15 for this data set. Figure 2.20 shows how close the Fourier outline was to the original outline.

In order to average the position of the landmarks they were moved along their respective outline until they were as close as possible to the reference/average landmark. This process was repeated and the sum of the differences in the locations across the average landmarks was found after each iteration (Figure 2.30). It took 10 iterations for the change in the average landmark positions to be zero for this data set. After 2 iterations the landmarks have been moved relative to the first outline, they were then moved relative to the average outline. In this test there was a total change in the coordinate positions of 0.31, given this was across all 100 landmarks in the average outline this was a small change. After another iteration this change had reduced down to 0.02, this code therefore used 3 iterations to define the positions of the landmarks on each outline.

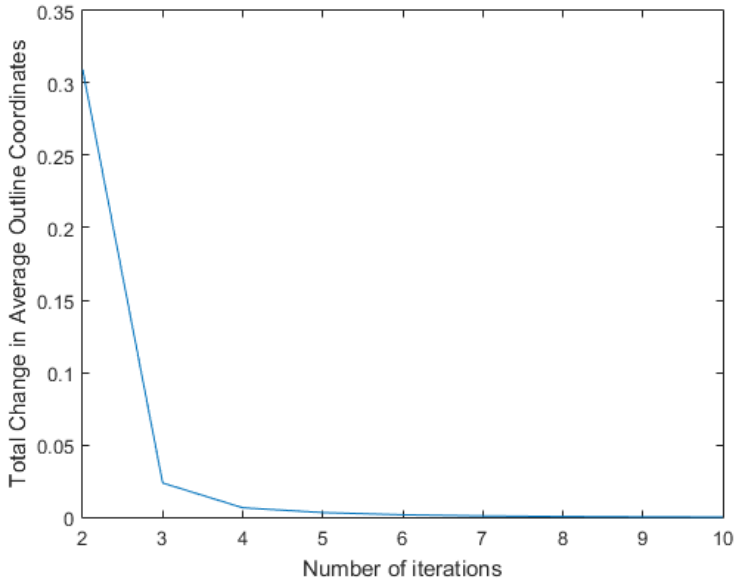

Figure 2.30: Change in average landmark positions after each iteration of the landmark sliding process

2.6.3.4 Wear scar area

In order to find the amount of error associated with the 3D area calculation using a triangular mesh rather than the actual curved surface a test was carried out. A sphere with a radius of 4mm was made as a solid part in Solidworks, the outer surface was then saved as an stl file and imported into Matlab (Figure 2.31).

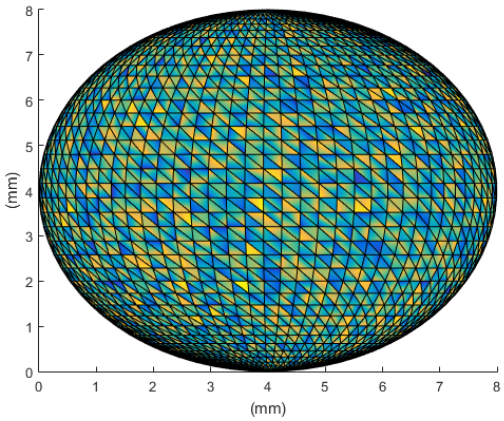

Figure 2.31: Sphere made up of a triangular mesh imported into Matlab

The area of the sphere was calculated using two different methods with Equation 2.1 in Section 2.6.2.5 and Equation 2.2.

$$A_{sphere} = 4\pi r^2 \tag{2.2}$$

The radius of the sphere was 4mm, this was chosen so that using Equation 2.2 the total area of the sphere would be similar to that of the wear scar outlines; 201.06mm^2. The area calculated using the triangular mesh in Matlab and Equation 2.1 was found to be 200.79mm^2. The percentage error between these two values was less than 1% and was therefore a valid method for the area calculations being carried out.

Mesh convergence was carried out on the .stl file of the tibial surface that was imported into Matlab. The average wear scar area calculated for 6 tibial inserts was calculated for fine and coarse meshes (Figure 2.32).

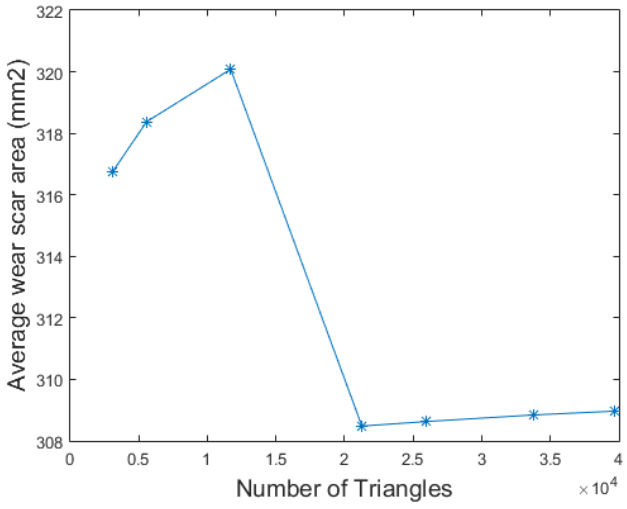

Figure 2.32: Mesh convergence carried out on the tibial insert surface used for the wear scar area calculation

The calculated wear scar area was found to converge after 22,000 triangles were used to represent the tibial surface. Therefore the imported tibial surface used for analysis had a total 25,939 triangles (deviation 0.008mm and tolerance 15°).

2.6.4 Limitations

When taking the image of the tibial insert with the wear scar outlines there are a number of factors that effect the final area calculation. For example if the image was taken at an angle and not from directly above the insert there would be a change in perspective which would affect the wear scar position and area.

There was also error involved in the drawing of the wear scar outlines. The code was set up to take the inside edge of the line drawn around the wear scar outline. However as the tibial insert was white and shiny the wear scar edges are sometimes difficult to see; this results in some error when drawing the edge of the wear scar. Any inaccuracies when drawing this outline and setting up the photograph will follow through into the analysis and area calculations.

To investigate the repeatability in drawing the wear scar outlines the outlines were drawn twice on the same set of tibial inserts and the average outline found each time (Figure 2.33). There were some differences in the outlines, especially near to the edge of the tibial insert on the medial, posterior side and the lateral, anterior side of the insert.

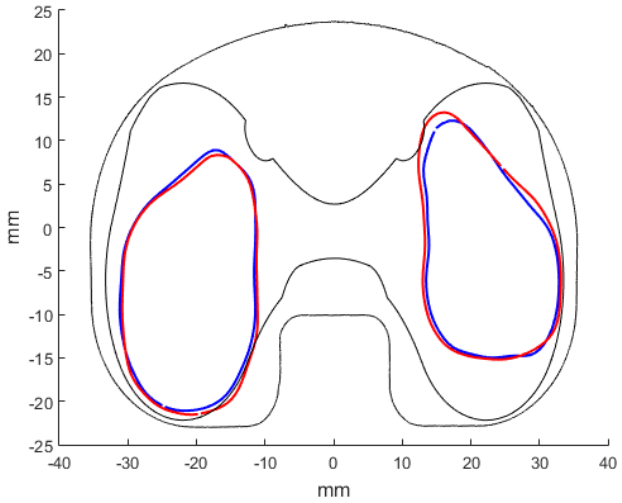

Figure 2.33: Average wear scar outlines for the same set of tibial inserts for repeats of wear scar outlines. The blue line shows the average outline for the first set of drawn outlines, and the red line shows the repeat carried out once the wear scar outlines had been drawn a second time

Another limitation was the calculation of the average wear scar using landmarks. The landmarks were moved along the wear scar outline to the position closest to a reference point. However for wear outlines which were a different shape to the others in the same test this can result in the landmarks being moved so that a section of the outline has no landmarks

on as there were other points on the outline closer to the reference point (Figure 2.34). This resulted in losing the true shape of the outlines due to clustering of the landmarks.

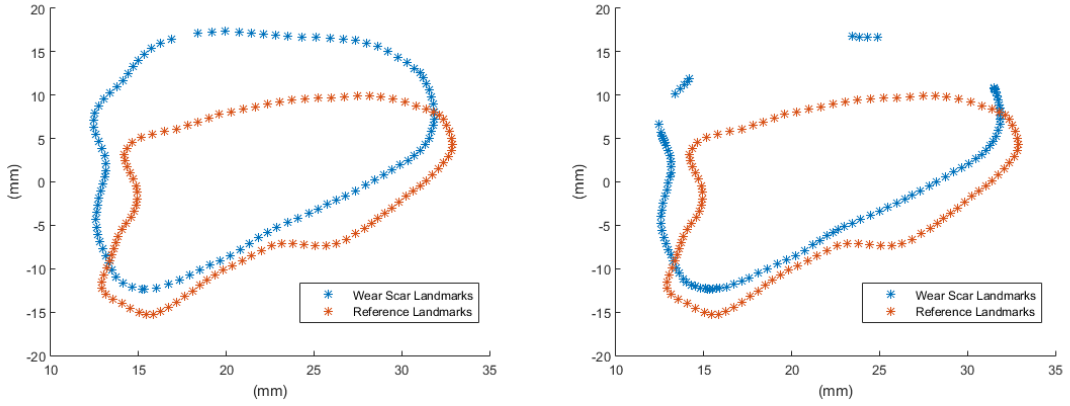

(a) Before Sliding (b) After Sliding

Figure 2.34: Landmark positions on a wear scar outline before sliding (a) and after sliding (b) if the landmarks were allowed to move too far from their original position along the wear scar outline

In order to prevent this from happening the distance that each landmark can move along the wear scar outline was restricted; this stopped the landmarks from clustering together and the shape of an outline being lost. However this may also result in the 95% confidence interval in the average wear scar outline increasing due to the landmarks being further from the reference landmarks.

The calculation of the wear scar area had some limitations due to the use of the mesh. However as the mesh convergence had been carried out the wear area calculation should be accurate. The calculation uses the geometry of a new insert as opposed to a worn insert, the actual surface area of the wear scar would be larger due to the change in geometry.

2.7 Contact Area Measurement

In order to measure the contact areas between the femoral and tibial components at different points in the gait cycle a Tekscan 4000 sensor was used. The sensor is designed for use in knees and has two sensors; one on the medial and one on the lateral condyle. There are a total of 572 sensels with a resolution of 62 sensels/cm^2 and a peak pressure of 68.95MPa.

The sensor was placed between the femoral and tibial components in the simulator and the displacements and loads of a particular point in the gait cycle were applied. This was carried out for each different alignment and spring condition.

The differences in the contact area aid in the understanding of the different wear rates and could be compared to previous computational and experimental studies into the effects of alignment on load distribution [52, 53, 126, 201].

2.7.1 Methods

2.7.1.1 Calibration

Before using the sensor it was first calibrated within one station of the simulator so that the sensor precision could be altered depending on the loading range applied. The sensors were placed between a pair of polyurethane shims between two flat surfaces (Figure 2.35). As there were a range of loads that were applied during gait a power law calibration was used; 80% and 20% of the peak load was applied to the sensor and measured for calibration. The polyurethane shims ensured that the sensors were evenly loaded and that the calibration was accurate.

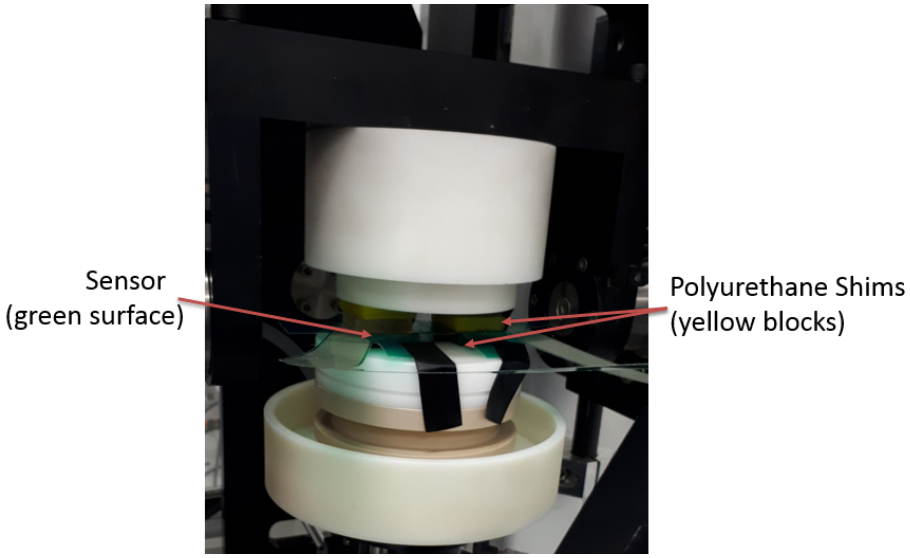

Figure 2.35: Tekscan calibration with the sensor between two polyurethane shims and the load being applied through a flat surface

When carrying out the calibration the sensitivity setting could be changed, this setting affected the saturation pressure set during calibration. The saturation pressure was set to correspond with the maximum pressure measured for the range of loads applied during calibration. The calibration was carried out at four different sensitivity settings; default, low 3, low 2 and low 1 (Table 2.8).

Table 2.8: Saturation pressure for different sensitivity settings using the Tekscan sensor

Sensitivity Setting	Saturation Pressure (MPa)
Default	5.98
Low 3	15.41
Low 2	20.48
Low 1	38.6

The default setting had the lowest saturation pressure of 5.98MPa, which would be too low for the testing, the low1 setting had the highest saturation pressure of 38.6MPa which would be higher than needed. The low2 setting was chosen as it had a saturation pressure

of 20.48MPa, ensuring that the expected contact pressures measured would all be lower than the saturation pressure.

2.7.1.2 Validation

In order to validate the pressure values from the Tekscan the sum of the pressure was determined and divided by the calculated contact area in order to find the measured force. This value of the measured force was then compared to the applied force at each point in the cycle.

The measured force values from the Tekscan sensor were significantly lower than the applied force values (Table 2.9). The large difference in values suggests that the contact pressure values were not accurate due to the high error in the applied force.

Table 2.9: Measured force (N) from the Tekscan compared to the applied force (N) at each point in the cycle

Point	Applied Force	Measured Force
1	1402	13.6±0.7
2	2433	14.7±0.6
3	367	13.8±3.9
4	168	5.7±0.8

This error could be due to issues during the calibration of the sensor; in order for calibration to occur there needed to be pressure over a large enough area of each of the sensors. The application of an even force across both sensors in the knee simulator was difficult to achieve using materials similar to the materials of the TKR. Instead more elastic materials were used in order to distribute the pressure over the sensors. This may have resulted in an error in the measurement of the force. With this calibration the values of the contact pressure measured were similar the values expected; around 12MPa. However if the large error in the measured force was taken into account the contact pressure values would be values around 100 times larger and would therefore be unrealistic.

The issue could also be due to the small contact areas with the TKR components compared to the larger contact area during calibration. During the calibration process the force measurement was close to the applied values, however with the TKR components this value was very different.

The measurement of the contact area using the Tekscan sensor was verified by applying a load on to two block of an area of 320mm^2 each. A load of 2kN was applied in order to ensure as much contact as possible and a contact pressure measurement taken. The contact area was then calculated by finding the area of all the sensels with a pressure reading of greater than 0MPa. The total contact area on the medial and lateral sensors was calculated to be 579mm^2 using the Tekscan sensor. This is slightly lower than the actual value of 640mm^2 however the differences could be due to the pixilated nature of the pressure reading or due to the there being incomplete contact between the surfaces. The measurement on the medial sensor was 305mm^2 which was closer to the actual value than the lateral sensor which resulted in a contact area of 274mm^2. This difference may be due to the slightly uneven loading in the

simulator; there was a larger load on the medial block and therefore a more accurate contact area measurement.

Due to the issues with the measurement of the force in combination with the potential error in the pressure calculation due to the measured force the pressure values measured by the Tekscan were not used. Instead the Tekscan measurements were taken in order to determine the contact area and the contact position at each point in the cycle.

2.7.1.3 Points Measured

The four points measured represented different points during the gait cycle (Figure 2.36); the first at 5% gait where the initial peak in the AP force occurs, the second at 45% gait where the last peak in the AF occurs, the third at the point in the cycle where the combined AP and TR displacement were at their maximum and the fourth point at 72% gait where the FE was at its peak (Table 2.10). These points were chosen to represent the range of pressures and contact points throughout the gait cycle.

To measure each point the Tekscan sensor was placed between the femoral and tibial components and the displacements applied to generate the desired positioning. The AF load was then applied and a measurement on the Tekscan sensor taken.

Table 2.10: Displacements and loads applied to the Tekscan sensor at four different points in the gait cycle

Measurement Point	AF (N)	FE (°)	AP Displacement (mm)	TR Rotation (°)	AA Rotation (°)
1	1402	-25	1.9	0.4	-0.7
2	2433	-22	0.6	3.6	-0.7
3	367	4	5.4	7.0	-0.1
4	168	28	-0.7	-0.3	1.2

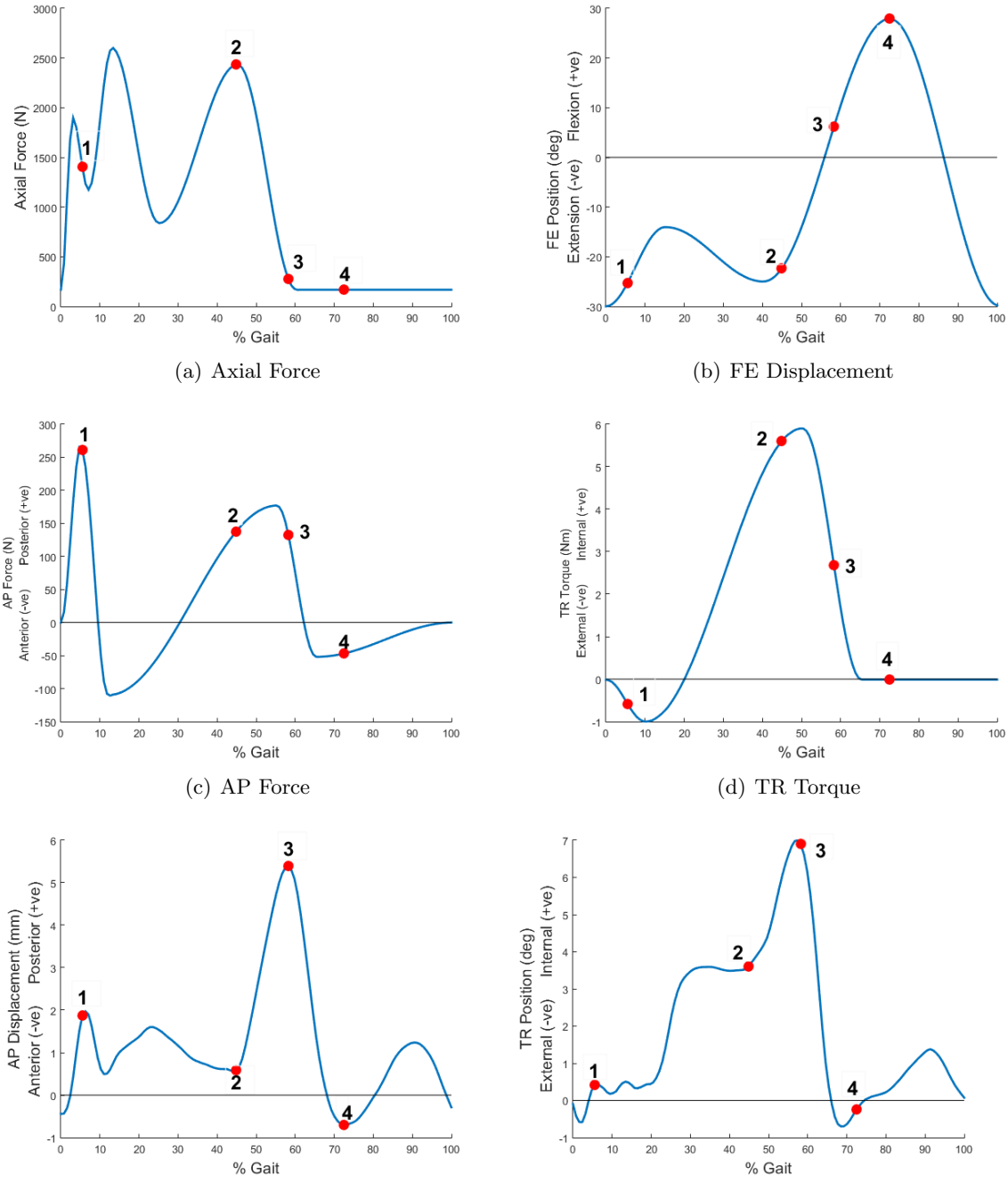

(a) Axial Force

(b) FE Displacement

(c) AP Force

(d) TR Torque

(e) AP Displacement

(f) TR Displacement

Figure 2.36: Points in the gait cycle measured using Tekscan

2.7.1.4 Analysis

For each measurement using the Tekscan sensor a file was generated with the loads of each sensel. Matlab was used to read these files and to find the contact area on each side and the position of the contact area. The data from the medial and lateral sensors were overlayed on an outline of the tibial insert in an approximation of their position during testing.

In order to find the contact area an outline was generated around all the sensors that had a pressure greater than 0. The outline was then smoothed using Fourier series (Figure 2.37) and the area and average outline found using the same method explained in Section 2.6. The average outline for each test and 95% confidence interval was then found, this allowed the position and shape of the contact areas between tests to be directly compared.

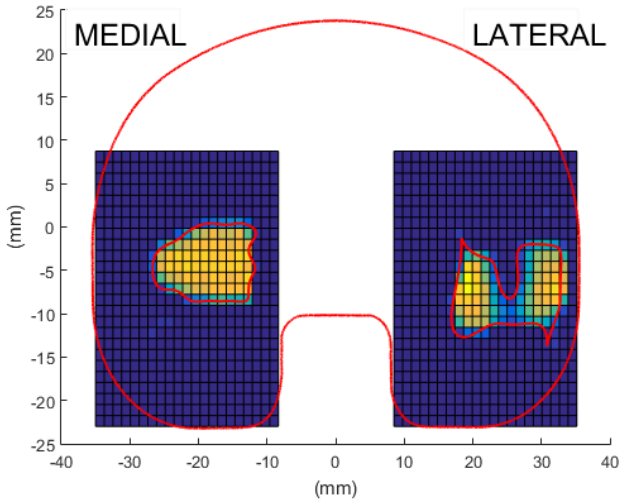

Figure 2.37: Tekscan data along with generated contact area outline shown in red

During testing some damage to the sensor occurred due to its fragile nature. Some of the rows and columns of sensels stopped producing any pressure values (Figure 2.38). In order to account for this data linear interpolation was carried out to approximate the unknown values. This insured that the damaged sensels did not affect the outline of the contact areas.

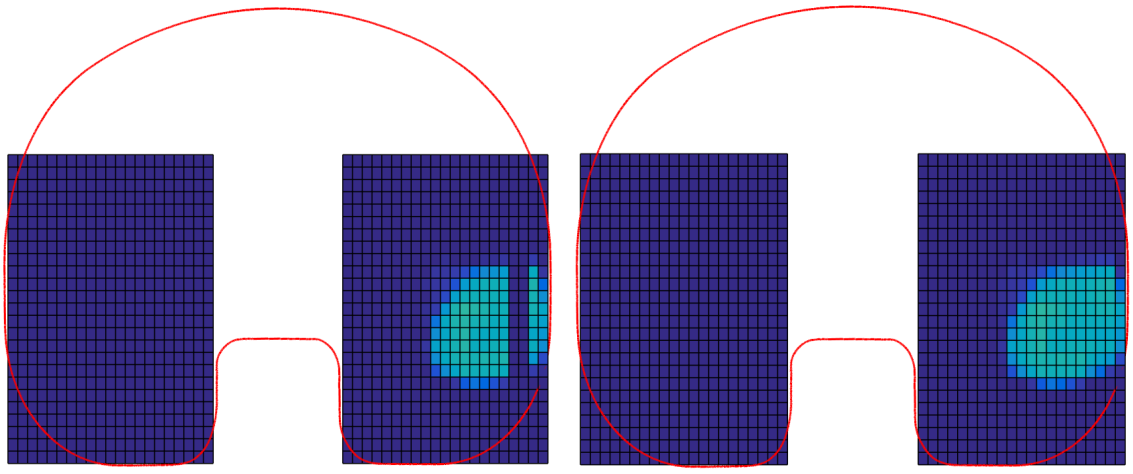

(a) Original Data (b) Interpolated Data

Figure 2.38: Tekscan data showing unresponsive sensels in two columns of the lateral sensor (a) and the approximated values for the damaged sensels after linear interpolation (b)

The contact areas were then compared between stations using a one way ANOVA with

significance taken at $p<0.05$ with post hoc testing as described previously.

2.7.2 Repeatability

To determine how repeatable the measurements would be given that the tibial surface was curved and therefore the sensor may be move slightly between readings the same measurements were repeated three times on five stations. The other station did not have a working AA motor and therefore could not be used for testing. The variation between these repeats and between each station were then found with respect to the contact areas and contact position.

For each measurement taken the outline of the contact area was found, Figure 2.39 shows the contact areas taken at gait cycle point 2 on all five stations. The outlines of each station were shown in a different colour with the 95% confidence intervals shown with dotted lines. Most of the confidence intervals were small enough that they were not visible in the image. The maximum 95% confidence intervals were found across the repeats on each station for each point measured. The confidence intervals were all within 7% of the average value; there was a minimal difference in the contact areas between repeats in terms of their position and shape.

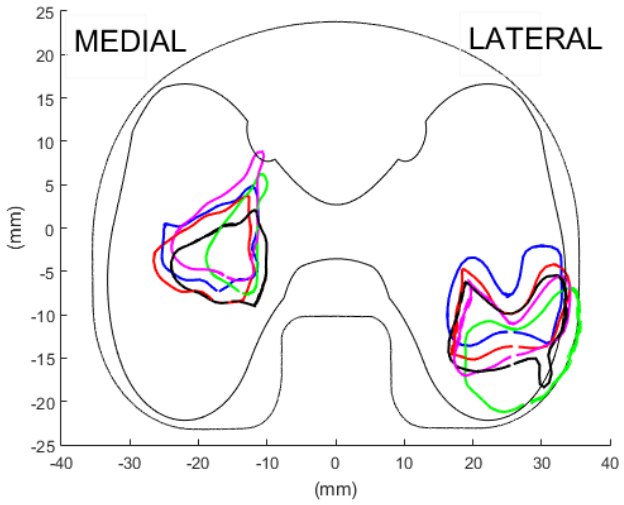

Figure 2.39: The average contact areas with 95% confidence intervals for three repeats on each station at gait cycle position 2

However between the stations there was much more variation, with some stations having a very different position of contact area. The maximum 95% confidence interval found was 30% of the average value. Figure 2.40 shows the average medial and lateral contact areas across all the stations on the simulator with the 95% confidence intervals, these were much larger than between the repeats on each station (Figure 2.39)

The average and 95% confidence interval in the contact area was found for each measurement point on each station. The 95% confidence intervals of the repeats on each station were within 7% of the average value.

Significant differences were found between the stations at all measurement points taken.

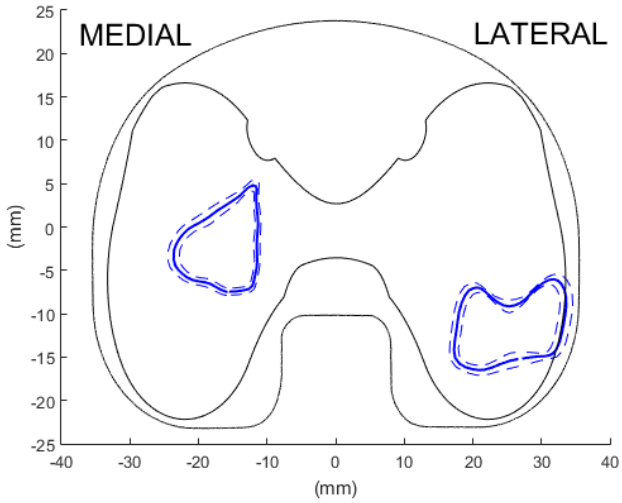

Figure 2.40: The average contact areas across the simulator for gait cycle position 2 and the 95% confidence intervals

There was no clear trends in which stations had higher or lower contact areas.

As there were minimal differences between repeats with respect to the contact area or contact position repeats were not carried out in further testing. However measurements were taken on all stations of the simulator as there was much higher inter station variation.

2.7.3 Limitations

One limitation due to use of the Tekscan sensor was due to the shape of the tibial and femoral components. As these are both curved and the Tekscan sensor was flat when a load was applied the sensor wrinkles around the components which may affect the accuracy of the measurements. The curvature of the tibial also means that the sensor cannot be applied flat to the insert, therefore there may be variation in its positioning between uses.

The variation between stations may be due to differences in the station set up which affect the positioning of the components relative to each other. Differences in the position of the tibial insert with respect to the simulator axes will affect the position of the centre of tibial rotation, therefore there will be differences in the contact positions after rotation. Some of the displacements being applied were also very small and therefore the variation in the actual applied position may also vary between stations.

The measurements were also taken statically with the Tekscan sensor as under dynamic loading the sensor would have moved during testing. This may result in the measured contact pressure being different to the dynamic contact pressure values.

The main limitation was due to the calculation of the applied force and the following calculation of the pressure values. The values of the measured force were found to be far lower than the applied force values, at some points by a factor of 100. This error may be due to the issues with calibration of the sensor within the knee simulator. However if this error

in the measured force were to be taken into account the pressure values would be around 1200MPa. As this is an unrealistic value for the conditions of this study there may also be an error in the calculation of the contact pressure by the sensor. Due to these issues the pressure values from the Tekscan sensor were not used in this study.

Chapter 3

Computational Methods

3.1 Introduction

Experimental simulation is expensive with respect to both time and cost therefore natural and prosthetic knee joints have previously been modelled using finite element methods [6, 9, 94, 116, 126]. Computational modelling can also provide extra outputs that are not available or difficult to measure under experimental methods. For example the measurement of contact pressure and area can only be measured statically under experimental methods, and at specific points in the gait cycle. Conversely using a computational model a more accurate measurement of contact pressure and area can be found throughout the gait cycle, at all points.

Computational modelling can also be used for parametric studies due to it being a faster and cheaper method than experimental studies. Therefore once a model has been validated by comparison with experimental results a wide range of test conditions, such as different component alignments, can be run in order to find the effect of incremental changes. This can provide more information and a greater depth of understanding of factors such as component alignment on a range of outputs such as contact area and kinematics throughout the gait cycle. Validated computational models can be used in comparative analysis and the design of new prostheses.

Previous studies have used computational models in order to predict the contact pressures on the tibial insert, the kinematics of the TKR and the wear rate [8, 9, 114, 126, 189]. In this study a computational model was developed in order to predict contact pressure and kinematics under force control conditions. In order to do this the model was validated under different soft tissue conditions and under different component alignment conditions using experimental data. This validation of the computational model under both soft tissues and component alignment with experimental data had not been carried out before. This was independent validation; validation of the computational outputs against outputs of independent and identical conditions. The model was then used to investigate the effect of a range of alignment and soft tissue conditions which had not been studied experimentally.

3.2 Methods

The computational model was developed in ABAQUS (ABAQUS 6.14-4) to replicate the conditions found within the simulator. The model was developed so that it could run under both displacement and force control conditions. A simplified cylinder on plate model was developed first in order to determine the correct contact properties by comparing to analytical solutions. A static knee model was then used for mesh convergence and finally a dynamic knee model used for validation and further studies (Figure 3.1).

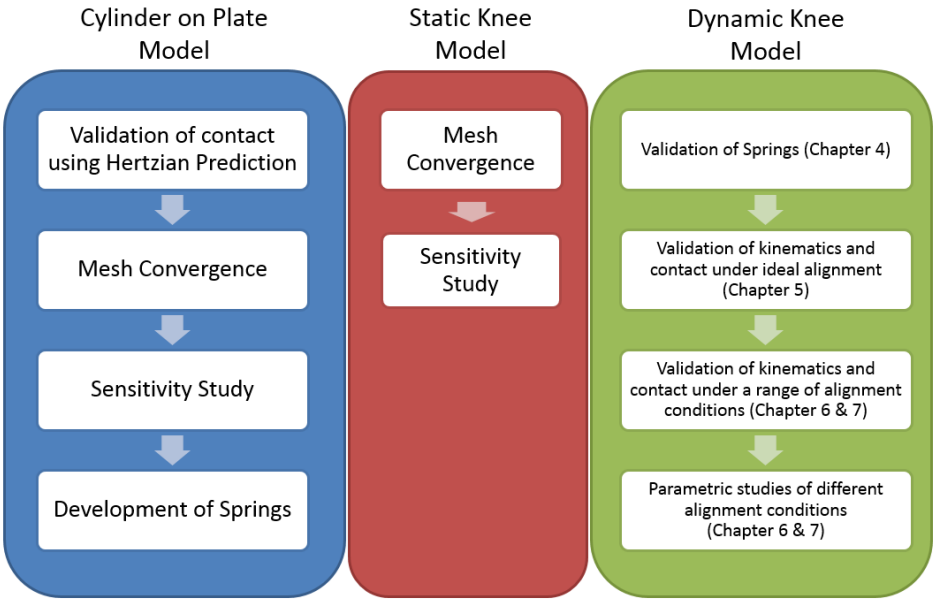

Figure 3.1: Flow chart showing the development of the simplified cylinder on plate model, the static knee component model and the dynamic knee model

A simplified model was developed first, using a cylinder and a plate with similar geometry and material properties as the knee components. This model was a static model as it was not run under the gait cycle conditions. The model was then validated by comparing the predicted stress to the Hertzian value. The validation was deemed successful if the predicted stress from the computational model was within 5% of the Hertzian value. The contact and interaction properties used in this simplified model were then used in all further models. Springs were added to the model in order to represent the virtual springs used within the simulator. The response of these springs were then validated by applying a force and measuring the resulting displacements.

A model using DePuy (DePuy Synthes, UK) Sigma knee components was then developed using the same methods as the simplified model. First a static model was developed and used to carry out mesh convergence and sensitivity studies. In a static model the acceleration is assumed to be zero, where as in a dynamic model the load is time dependent and the effects of inertia will be included in the calculation. A static model was used for the mesh convergence as a static load was being applied. Mesh convergence was carried out to ensure that the mesh

size was fine enough to generate accurate results. Once this had been completed a dynamic model was developed in order to run the gait cycle conditions.

The dynamic TKR model was then validated by comparing the output displacements and contact positions to the independent experimental data. The kinematic comparison was carried out by finding the correlation between the experimental and computational values of the AP, TR and AA displacements at each point in the gait cycle. The contact areas were also compared between the two methods in order to determine the validity of the measurements by looking at values of the total contact area and the contact position.

The springs within the computational model were also varied in order to determine whether the computational model would predict the same effect on the output kinematics due to changes in the soft tissues as under experimental studies. This validation of the springs within the computational model will be shown in Chapter 4. The validation under mechanical alignment conditions will be detailed in Chapter 5 and in Chapters 6 and 7 under different alignment conditions.

Once the model was validated it was used to run parametric testing to determine the effect of different alignment and soft tissue conditions on the kinematics and contact pressures. This parametric testing of the model enabled the understanding of smaller changes in the component alignment than those studied experimentally. The computational model could also provide a more accurate measure of the contact area and pressure than the experimental methods and this could be found for each step in the gait cycle. As increased contact area have been shown to result in higher surface wear rates this understanding of contact area during the gait cycle may be an important factor in the understanding of causes of early failure [6].

3.3 Cylinder on Plate Model

Before starting to develop a model using the femoral and tibial components a simplified cylinder on plate model was developed using ABAQUS (Figure 3.2).

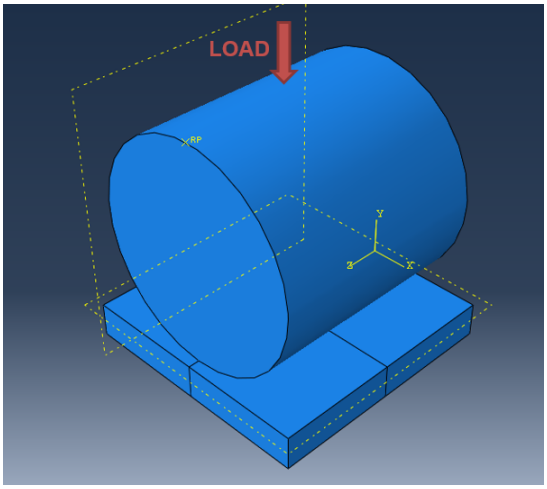

Figure 3.2: Cylinder on plate model in ABAQUS

It was developed to resemble a total knee replacement with respect to the geometry and material properties. The cylinder was modelled as a rigid body [46] and the plate was modelled as UHMWPE (E=400MPa, v=0.46) [23, 72, 121, 207]. The plate was 70mm square with a thickness of 10mm and the cylinder had a diameter and length of 63.5mm. These geometries were chosen to replicate the geometries of the knee components.

3.3.1 Boundary Conditions

The plate was fixed on its base so that it could not move in any direction. This boundary condition was only applied for the mesh convergence analysis, where there was no desired motion of the plate. For the spring verification the boundary conditions were edited in order to allow motion in the desired direction. For example when verifying the spring in the AP direction the plate was allowed to move in only that plane.

A vertical load of 2.52kN was applied to the top surface of the cylinder and the cylinder was constrained to only move in the direction of this load; normal to the surface of the plate. The interaction property between the two surfaces was defined as frictionless.

3.3.2 Element Type

The elements in both of the parts were linear, 3D stress, hex elements (C3D8R). As the model was used for stress analysis a 3D stress element was chosen. A linear element has nodes on each of its corners, while a quadratic element had corner and mid-side nodes. For the simplified cylinder on plate model the linear elements were chosen as they often result in an accurate solution in a shorter time [176]. The hex shape was chosen as it created a good mesh on both the cylinder and plate parts.

3.3.3 Hertzian Prediction

Hertzian contact is used for non-adhesive contact between two bodies in order to determine the resulting pressure. It assumes there is no friction, that the strains are within the elastic limit of the materials, that the surfaces are continuous and non-conforming and that each body can be considered an elastic half-space. This provides a simple equation that can be used to calculate the resulting pressure when a cylinder and plate are in contact based on the applied load, the material properties of each part and their geometries.

The Hertzian prediction was calculated using the applied force (F), the length of the cylinder (l), the diameter of the cylinder (d), the Poisson's ratio (ν) and Youngs modulus (E) of the materials. This gives the contact half width, b (Equation 3.1), and then the maximum contact stress, p_{max} (Equation 3.2). Where the subscript 1 denotes the cylinder and 2 the plate.

$$b = \sqrt{\frac{2Fd}{\pi l}\left[\frac{(1-\nu_1^2)}{E_1} + \frac{(1-\nu_2^2)}{E_2}\right]} \tag{3.1}$$

$$p_{max} = \frac{2F}{\pi bl} = 14.2MPa \tag{3.2}$$

3.3.4 Mesh Convergence

In order to generate accurate results using a computational model the mesh used on each of the parts must be fine enough for the measurements or loads used. However the finer a mesh is, and the more nodes there are in the model, the longer the model will take to run. Therefore a mesh convergence study was carried out where the total number of elements in the model (sum of the cylinder and plate elements) was plotted against the peak principal stress in the direction of the applied load (Figure 3.3). This was to determine the number of elements needed in order to generate accurate results once convergence on the peak contact stress had taken place.

The element size on the femoral and tibial components was kept at a ratio of 1:1. A previous study found that when two parts were in contact the calculated contact area on each part were closer when the meshing ratio was the same, e.g. 1:1 or 2:2 [106]. Therefore a ratio of 1:1 was chosen for this study in order to reduce the sensitivity of the contact area due to the mesh.

For the given applied load, geometry and material conditions the Hertzian prediction for the contact stress was 14.2MPa, this was close to the converged value using the ABAQUS model of 14.1MPa. The mesh convergence study showed that 535,392 elements in the model were sufficient and were used for any further studies with this model. Any further increase in the number of elements changed the predicted maximum contact stress by less than 5%.

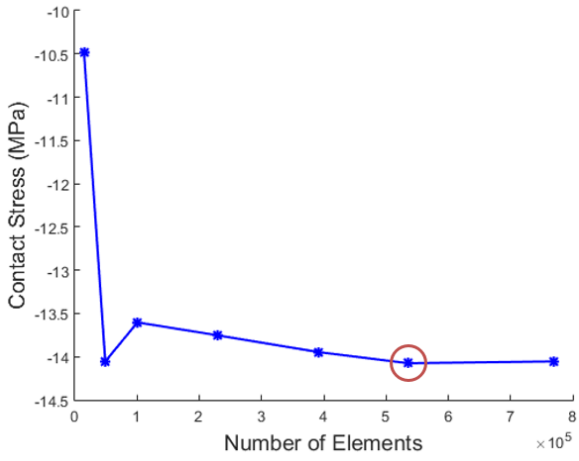

Figure 3.3: Mesh convergence carried out on cylinder on plate ABAQUS model showing the principal stress against the total number of elements in the model. Mesh convergence was taken as 535,392 elements

3.3.5 Sensitivity Study

A sensitivity study was carried out to investigate how well the ABAQUS model matched the Hertzian solution under different material properties. This was to understand the limitations of the model under a range of material properties.

The model was run with Youngs modulus values of 200, 300, 400 and 500 MPa and Poisson's ratio values of 0.46 and 0.3 for the plate, while the cylinder was kept as a rigid body (Figure 3.4). The predicted maximum contact stresses from the ABAQUS model were within ±5% of the Hertzian predictions.

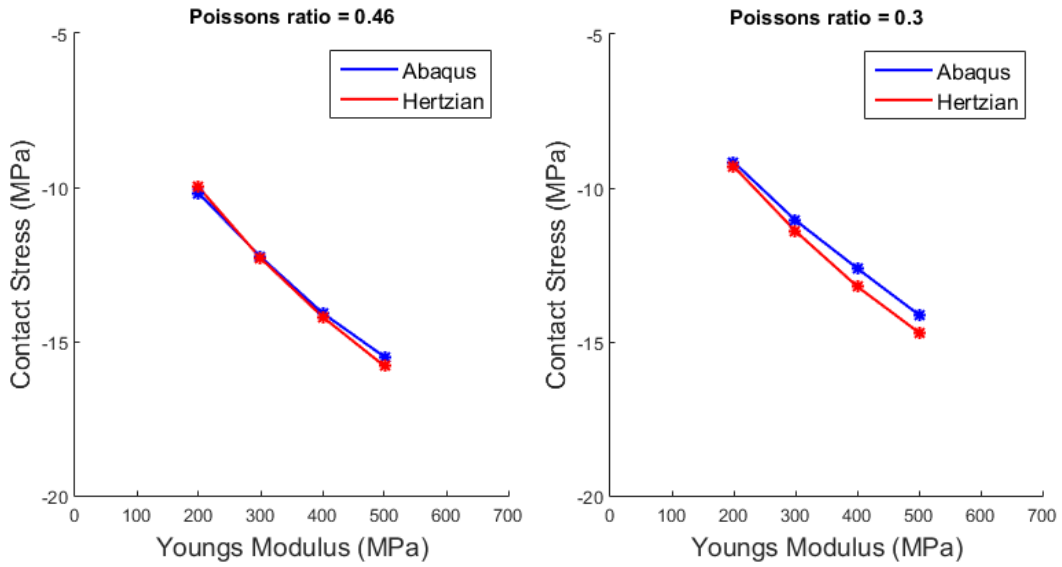

(a) (b)

Figure 3.4: Sensitivity study carried out on the cylinder on plate ABAQUS model showing the peak principal stress under different Youngs Modulus and Poisson's ratio values of 0.46 (a) and 0.3 (b)

3.3.6 Development of the Spring Model

In order to replicate the virtual springs within the simulator linear springs were added to the the model using connectors. Two connectors were attached to the plate in the model in order to replicate the AP and TR springs. The plate had a reference point at it's centre which both connectors were attached to. The other ends of each connector were attached to external reference points (RP-2 and RP-3 in Figure 3.5). For the AP spring a basic translational connection was used and for the TR spring a rotational connection. These allowed non-linear spring profiles to be input for the response of each spring.

In order to verify that the springs were responding as expected a load was applied in the direction of the spring and the resulting displacement was measured. This was then compared to the expected displacement, based on the stiffness of the spring. The equation used is shown by Equation 3.3 where x is the displacement, F is the force and k is the stiffness of the spring.

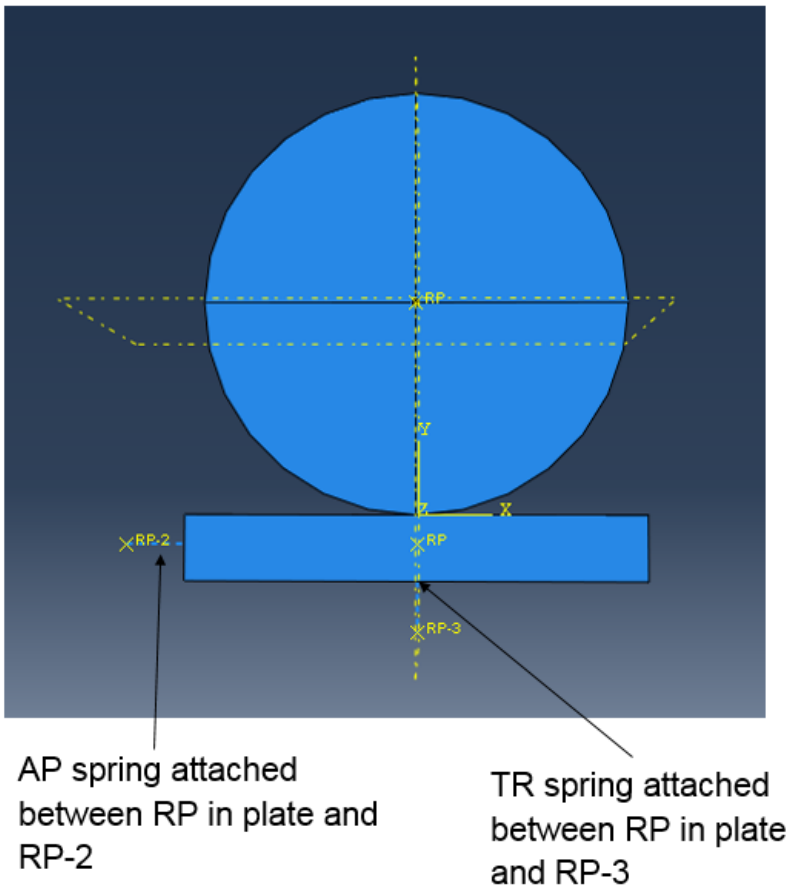

Figure 3.5: The cylinder on plate model with the AP and TR springs attached between reference points at the centre of the plate (RP) and reference points external to the plate (RP-2 and RP-3)

$$x = \frac{F}{k} \tag{3.3}$$

The connectors used in the model were found to respond to the loading as expected and were good representations of the virtual springs within the simulator.

3.4 Static Knee Model

The cylinder on plate model had been used in order to validate the contact definitions, interaction properties and the springs. Once this had been carried out a model was generated using the knee components with the same properties as the cylinder on plate model.

A static model using DePuy Sigma femoral and tibial knee components was developed first in order to carry out mesh convergence. A static model was used as a static load was applied for the mesh convergence study. Therefore the effects of inertia and acceleration were negligible.

3.4.1 Material Properties

Size 3 parts were generated with the same geometry as the DePuy Sigma CR knee femoral and tibial bearing insert knee components. The cobalt chrome of the femoral component was defined using the material properties of density=8.8g/cm^3, E=193000 MPa and ν=0.29. The UHMWPE of the tibial insert was defined using the following properties; density=0.934g/cm^3, E=553 MPa and ν=0.32 [8]. The Young's Modulus value was higher for this model than the cylinder on plate model as moderately crosslinked tibial inserts were used for experimental simulation, which had a higher Young's modulus value. Both were defined as being isotropic and homogeneous materials. The femoral part had a rigid body constraint applied as the cobalt chrome was much harder than the UHMWPE therefore any deformation would occur in the tibial insert and the femoral can be assumed rigid in comparison [46].

3.4.2 Alignment

The femoral component was aligned with the tibial component so that its superior surface, where the distal femoral cut would be made (red highlighted surface in Figure 3.6), was parallel with the distal surface of the tibial insert. The components were also aligned so that the femoral condyles matched with the dwell points of the tibial insert.

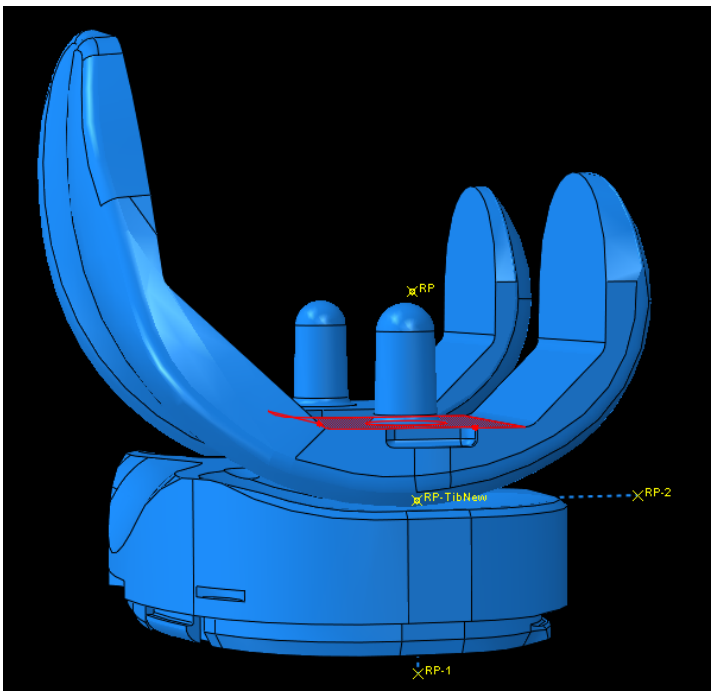

Figure 3.6: Alignment of the static ABAQUS model using the femoral and tibial components. The red, highlighted surface is the superior femoral surface which was alignment parallel to the posterior surface of the tibial insert

3.4.3 Boundary Conditions

The boundary conditions were defined in order to replicate the conditions within the simulator. The femoral component was fixed so that it could only move in an inferior-superior direction, in the same plane as the applied load. The tibial insert was fixed in all planes as this was a static loading model.

3.4.4 Element Type

The element types used on both the parts were 10 node quadratic tetrahedrons (C3D10). As with the cylinder on plate model the 3D stress elements were used. The tetrahedral elements were chosen as they were able to mesh well on both the femoral and tibial parts. Quadratic elements were chosen for this model as they tend to yield better results with a 3D tetrahedral element as it is a degenerate element [176]. A degenerate element is one which has at least one triangular face but has a quadrilateral characteristic face shape [177].

3.4.5 Mesh Convergence

To carry out the mesh convergence two steps were used; over the first step a displacement was applied to the femoral component in order to generate contact between the two parts. This was a static, general step with a time period of 1. The femoral component had a fixed vertical displacement to generate contact and all other boundary conditions were fixed. The displacement value was chosen so that the peak principal stress value in the proximal-distal direction would be less than 1MPa. The displacement was linearly applied over the first third of the step and maintained for the rest of the step, this was to allow some relaxation of the material once contact had been made.

The second step was a static, general step with a time period of 1. The femoral component was fixed in all directions apart from translation in the proximal-distal direction. A distal load of 220N was applied to the reference point of the femoral to generate a peak stress of around 14MPa as this was similar to the stresses found in a TKR in a previous study [8]. The load was applied in the same way as the displacement; it was linearly applied over the first 0.3 of the step and maintained until the end of the step. The resulting peak principal stress was then found in the direction of the load.

The mesh size was changed by varying the seed size on both the femoral and tibial components. The seed size is the approximate element size on each edge of the selected part. The seed size was kept the same for both parts and the total number of elements with a ratio of 1:1. The total number of elements in the model was plotted against the peak stress to determine convergence (Figure 3.7).

The number of elements used in all further testing was 749,034 (a seed size of 0.81 on both components) as this provided a balance between the time taken to run the model and the point of convergence.

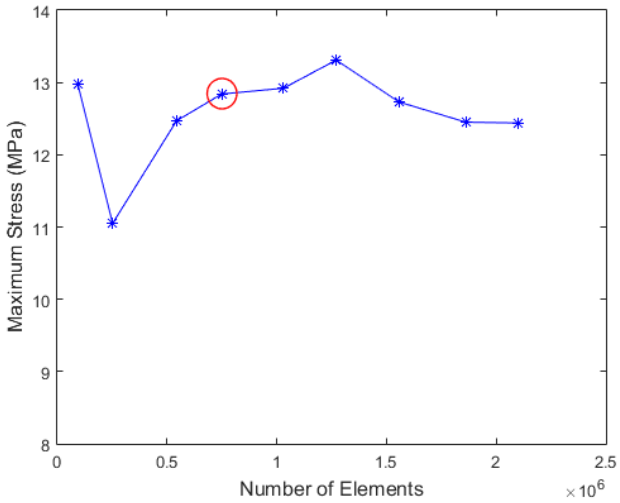

Figure 3.7: Mesh convergence carried out on the static knee component model showing the peak principal stress against the total number of elements in the model with the chosen mesh size circled in red

3.4.6 Sensitivity Study

A sensitivity study was then carried out on the model as with the cylinder on plate model; with Youngs Modulus values of 473, 573, 673 and 773MPa and Poisson's ratio values of 0.3 and 0.46 (Figure 3.8). The knee component model was more sensitive to changes in the material properties than the cylinder on plate model.

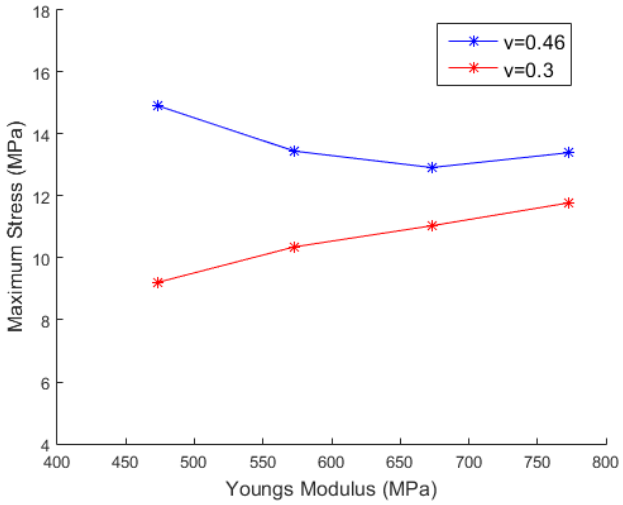

Figure 3.8: Sensitivity testing carried out on the static knee component model with varying Young's Modulus and Poisson's ratio values against the peak principal stress

3.5 Dynamic Knee Model

A dynamic, implicit model was then created using the same components and material properties as defined in the static model (Figure 3.9). An explicit dynamic model accounts for the propagation of dynamic effects in the material e.g. a stress wave. However an explicit model requires a very small step time, in the order of a microsecond, to be able to do this. Where as in an implicit dynamic model the propagation of dynamic effects are controlled by the inertia of the parts rather than the speed of sound. It therefore assumes that the speed of sound is infinite. As the model will not be simulating impact conditions where the propagations of the stresses are moving from one end of the part to another, and in order to generate a model with a shorter run time an implicit model was used.

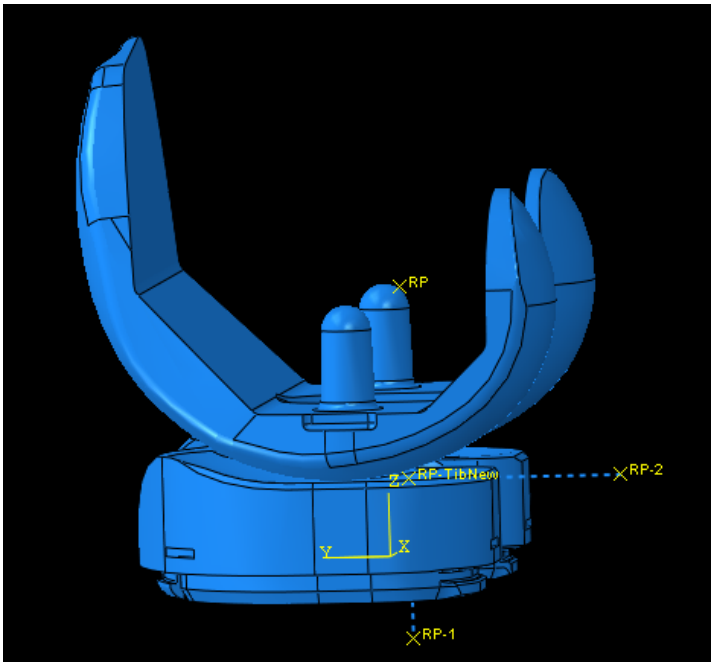

Figure 3.9: Dynamic, implicit ABAQUS model using the femoral and tibial bearing insert components and with the spring connections shown in dotted lines and reference points shown with a cross

3.5.1 Element Type

The elements used for both the femoral and tibial components were 10 node modified quadratic tetrahedron (C3D10M). This is the same element type used in the static model but with hourglass control applied. Hourglass modes are non-physical modes of deformation that can occur in under integrated elements. Under integrated elements are solid elements with only one integration point. Hourglass controls apply internal forces to each element to resist the deformation of the element.

3.5.2 Step Definitions

A total of 128 steps were defined; the first step had a period of 1s and applied a gradually increasing AF load from 0-167.6N and a gradually increasing TR torque from 0-0.01Nm over the step, this resulted in the forces being at the values for the start of the gait cycle. The next 127 steps replicated the steps in the simulator gait cycle; the 127 steps took a total time of 1s and used the same input profiles as the experimental simulation (Figure 2.3 in Section 2.3.1).

3.5.3 Boundary Conditions

The femoral component had a reference point in the same position as the centre of rotation in the experimental set up according to the ISO standard; the central axis of each implant was offset from the aligned axes of applied load and tibial rotation from the centre of the joint by 7% of its width [186] and a rigid body constraint was applied to the femoral component as before (Figure 3.10).

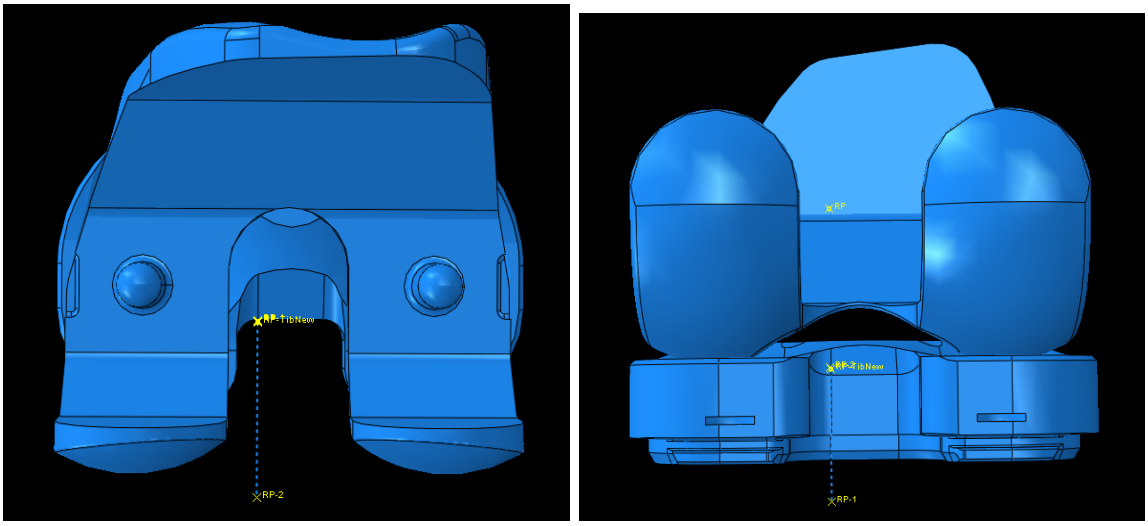

(a) Superior View (b) Posterior View

Figure 3.10: The positions of the tibial (RP-TibNew), femoral (RP) and spring (RP-1 and RP-2) reference points on the Dynamic knee model

Boundary conditions were applied to the femoral reference point and it was free to move in the superior-inferior direction with the AF profile applied in this direction. The FE displacement was applied to the centre of rotation of the femoral component using boundary conditions. The femoral component was not free to move in any of the other axes.

The reference point of the tibial was defined as directly below the reference point for the femoral component on the superior surface of the tibial insert so that it would be in line with the AA axis, this was the same position the centre of rotation for the tibial fixture would occur in the simulator (RP-TibNew in Figure 3.10). A coupling constraint was defined that coupled the reference point of the tibial to the posterior base of the tibial; the AP force and

TR torque were applied to the reference point. Boundary conditions were defined on the tibial reference point so that it was able to move in the AP, TR and AA directions but was fixed in all others, as in the simulator.

A friction coefficient of 0.04 was assumed between the femoral and tibial components [81, 204] with a penalty contact formulation.

3.5.4 Spring Definitions

Connector sections were defined to replicate the effect of the virtual springs within the simulator; one to restrain the AP displacement and one to restrain the TR displacement. These were applied to the tibial reference point and to external reference points (RP-1 and RP-2 in Figure 3.9) in order to generate springs in the correct axes as in the cylinder on plate model.

For the AP direction a Cartesian connector was defined with a non-linear elastic profile; the spring profile values from the virtual springs tested experimentally were applied (Figure 3.11). The TR spring was defined as rotation connection with a non-linear elastic profile; as for the AP spring this profile matched the ones tested experimentally.

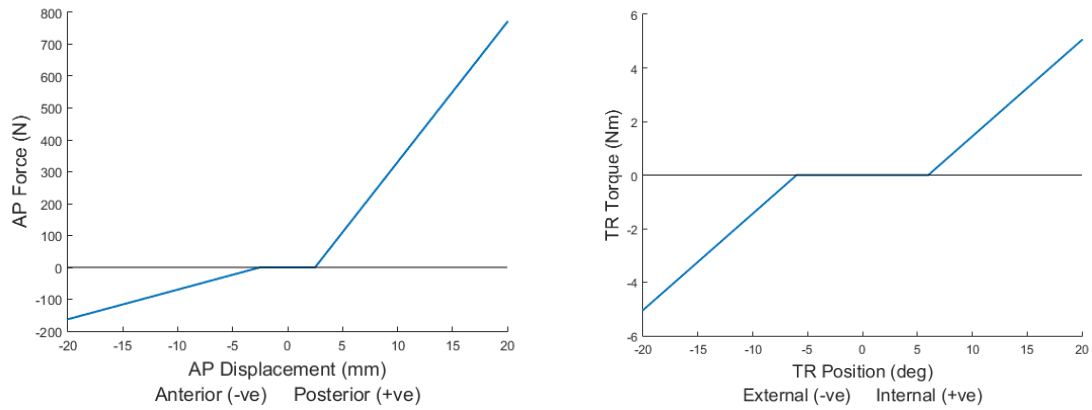

(a) AP Spring (b) TR Spring

Figure 3.11: The ISO standard AP and TR spring profiles for a CR TKR [186]

3.6 Comparison Between ABAQUS 6.14 and ABAQUS 2017

All of the models used within this study were developed in ABAQUS 6.14. However the models were then converted into ABAQUS 2017 in order to be run using one of the High Powered Computers (HPCs) within the university. This was so that a larger number of test conditions could be run in the time frame.

All of the results detailed in Chapter 4, where the effect of different spring conditions on the output kinematics were developed and run in ABAQUS 6.14. However all the other computational results, in Chapters 5-7, were models that were developed in ABAQUS 6.14 but were then converted and run in ABAQUS 2017 on one of the HPCs.

A model that was developed in ABAQUS 6.14 was run using both versions of ABAQUS in order to verify that the output kinematics were the same. The output AP, TR and AA kinematics were found to be exactly the same using both versions of the software (Figure 3.12). Therefore there should not be any difference in the kinematics in Chapter 4 compared to the other chapters.

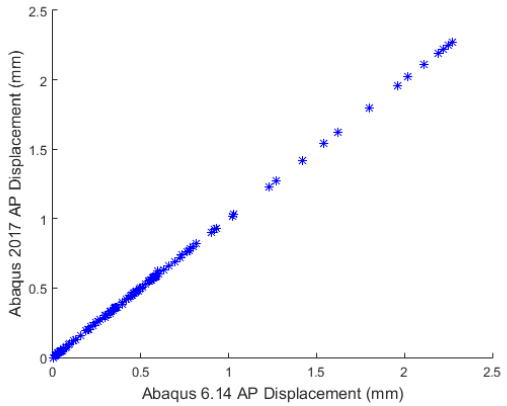

(a) AP Displacement

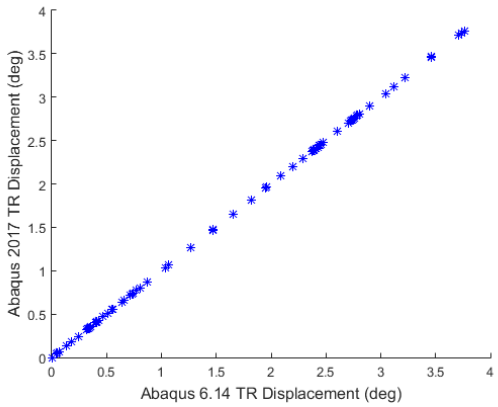

(b) TR Displacement

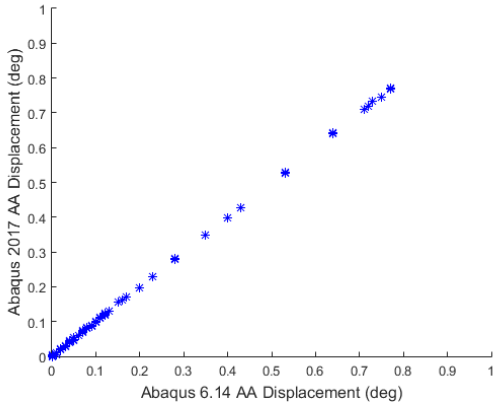

(c) AA Displacement

Figure 3.12: Correlation in the AP (a), TR (b) and AA (c) displacements between ABAQUS 6.14 and ABAQUS 2017

3.7 Limitations

The computational model allows for further alignment conditions to be studied than those studied experimentally. The model will be validated using the experimental results, however there are some differences between the computational and experimental simulations.

For example the masses and internal friction that exist within the experimental simulator have not been included in the computational model. As the weight of the tibial fixture was found to influence the output kinematics in the experimental simulation the lack of mass and friction in the computational model will likely result in different output kinematics.

However the weights and internal friction within the simulator are one of the limitations of the experimental simulation and therefore were not included within the computational model. But this difference between the simulations may make the validation of the computational model using the experimental data more difficult.

Chapter 4

Experimental and Computational Simulation of Soft Tissue Constraints

4.1 Introduction

Different patient factors have been shown to affect the wear of TKRs; patient weight [30], the activities they perform [97], soft tissues and muscles [140] and interactions between these factors, such as soft tissue and muscle mechanics producing different kinematics for specific activities. The majority of patient factors are outside the control of the operating surgeon. The aim of a TKR is to provide a stable knee which will function optimally and last a long time. Stability of the replaced knee is in part dependent upon muscle strength, ligament integrity and geometry of the polyethylene insert. A more congruent insert will result in a more stable knee. Increasing ligament laxity will introduce instability.

Simulating a wider range of patient conditions may replicate the wider range of outcomes that occur in vivo and increase our understanding of the factors that lead to early or mid-term failure, or higher rates of failure in younger patients.

Under force control simulation springs are used to replicate the effect of all the soft tissues within the natural knee, including the ACL and PCL. The ISO standard [186] AP and TR springs have a gap around the zero position to replicate the soft tissues within the knee as they are not linear elastic [73, 113]. The size of this spring gap reflects the soft tissue laxity within the knee.

As the tension of the tissues within the knee vary between patients the spring gap and stiffness values are difficult to choose. Ligament balance during surgery is a subjective process so can lead to unbalanced knees [17, 86]. Ligament balancing has been found to be an important factor in wear, range of motion, and pain [17]. The ligament balance affects the kinematics and mechanics of the knee and the resulting variation in performance and wear in individual patients.

Just as soft tissue tension and laxity influences joint kinematics in the natural knee, similarly soft tissue constraints, spring stiffness and spring gap will influence resultant kinematics in the force control knee simulator. The aim of this study was to experimentally and computationally investigate the effects of variation in the soft tissue constraints on the output kinematics of a TKR with different tibial insert geometries. A systematic investigation was carried out to address the following research questions about the effect on the output kinematics:

1. What effect do the AP force, TR torque and FE displacement input profiles have on the output kinematics?
2. What difference is there between a spring profile based on clinical data compared to the ISO standard linear profile?
3. What effect does the tibial insert geometry have on the kinematics?
4. What effect does the laxity of the knee, represented by the simulator AP and TR springs gaps, have on the output kinematics?
5. What effect does the ligament stiffness, represented by the simulator AP and TR spring tensions, have on the output kinematics?

The effect of the soft tissue constraints on the output AP and TR displacements will then be investigated using the computational model. Similar values of the AP and TR spring gaps and the AP and TR spring tensions will be used with the computational model. The output kinematics will then be compared between the experimental and computational results in order to validate the simulation of the soft tissues in the computational model.

4.2 Materials and Methods

All the investigations were carried out using DePuy Sigma fixed bearing TKR components (DePuy Synthes, UK). Three different tibial insert designs were tested; curved (CVD), partially lipped (PLI), and custom flat inserts (Figure 4.1). The CVD inserts are used most frequently clinically so were used as standard for all tests. Both the flat and PLI inserts were tested under standard ISO [186] input profiles (Figure 4.2) and test conditions in order to investigate the effect of tibial insert geometry (research question 3). The PLI inserts were also used for the spring gap and tension tests along with the CVD insert (research questions 4 and 5). The methods used for testing and analysis were those for kinematic testing outlined in Section 2.3.6.

For all studies a one way ANOVA with significance taken at $p<0.05$ using IBM SPSS Statistics 22 was used. A Welch's test with significance taken at $p<0.05$ was carried out to determine whether the variances between groups were homoscedastic. If this was determined to be true a post hoc Tukey's test was used in order to confirm where the differences between the groups occurred, with significance taken at $p<0.05$, as this assumes equal variance.

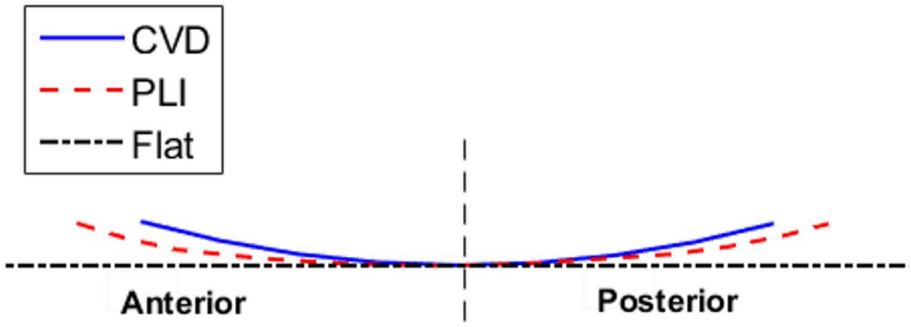

Figure 4.1: Conformity of the three tibial insert designs investigated; curved (CVD), lipped (PLI) and flat

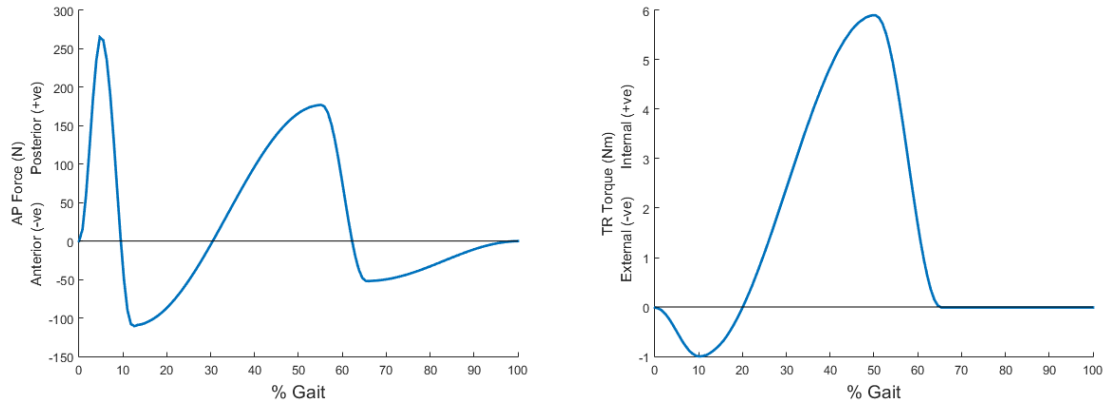

(a) AP Force (b) TR Torque

Figure 4.2: Input AP force and TR torque profiles [186]

However if the variances were determined to be too different a post hoc Games-Howell test was carried out, with significance taken at $p<0.05$, to determine the differences between the groups.

4.2.1 What effect do the AP force, TR torque and FE displacement input profiles have on the output kinematics?

In order to find the effect of the input profiles on the output kinematics different combinations of the FE, TR torque and AP force were applied (Table 4.1). The AF profile was always applied and the ISO standard CR [186] springs were used along with the CVD insert. This showed the effect of the absence of each profile on the output kinematics.

4.2.2 What difference is there between a spring profile based on clinical data compared to the ISO standard linear profile?

To investigate the difference between the ISO spring profiles and clinical data for a knee with no ACL and a knee with no ACL or PCL virtual springs were generated using clinical data

Table 4.1: Combinations of input profiles applied for research question 1

Test	AF	FE	AP	TR
1	✓	✓	✓	✓
2	✓	✓	✗	✗
3	✓	✗	✓	✗
4	✓	✗	✗	✓
5	✓	✓	✓	✗
6	✓	✓	✗	✓
7	✓	✗	✓	✓

(Figure 4.3).

For the AP spring profile the clinical data used was for a knee with a resected ACL and an intact PCL and with a resected ACL and PCL for knee flexion at 0° [73]. This study was used for the AP spring profile as it provided displacement values for knees with both a resected ACL and a resected ACL and PCL. This allowed comparison between the ISO CR and CS spring profiles. The ISO CS spring profiles are intended to represent a knee where both the ACL and PCL have been removed. For all the spring profiles studied an AP spring gap of ±2.5mm was assumed based on the ISO standard [186].

The clinical data used for the TR position was for a knee with no ACL [113]. This study was used for the TR position data as it provided a response profile across a range of applied TR torques. This clinical TR spring profile was used along with both of the clinical AP spring profiles.

All four spring conditions were tested on the simulator and their output kinematics compared (Research question 2 in Table 4.2).

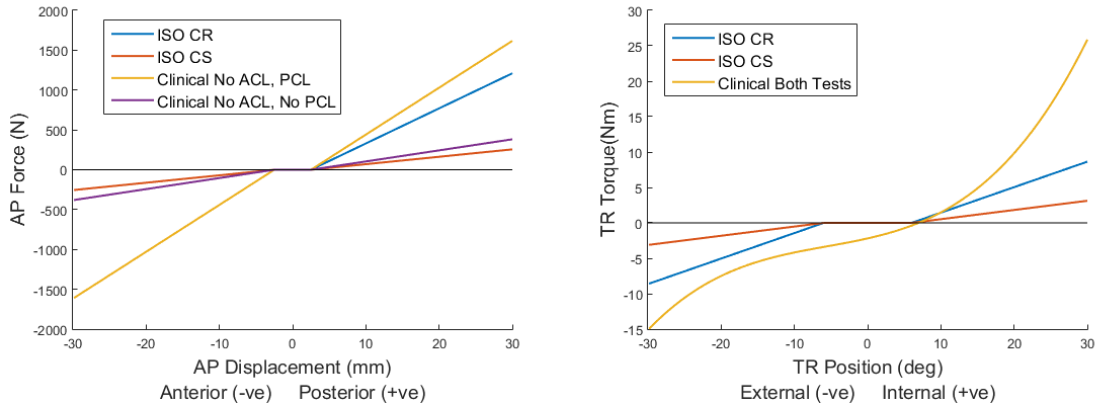

(a) AP Springs (b) TR Springs

Figure 4.3: The four spring conditions studied; linear and non-linear AP and TR spring profiles

4.2.3 What effect does the tibial insert geometry have on the kinematics?

To compare the kinematic outputs with different tibial insert designs each of the three inserts were tested with the ISO standard [186] CR springs (Research question 3 in Table 4.2).

4.2.4 What effect does the laxity of the knee, represented by the simulator AP and TR spring gaps, have on the output kinematics?

To determine the effect of the spring gaps on the output kinematics, the gap values were varied; for the AP spring the gap was varied from 0-9mm in 1mm increments, with the ISO spring gap of 2.5mm being used instead of 2mm. The TR spring gap was varied from 0-11° at 1° intervals (Research question 4 in Table 4.2). Only one spring was varied at a time with the other kept at the ISO standard [186] value (AP spring gap 2.5mm and TR spring gap 6°). The ISO CR spring tensions were used for both the AP and TR springs. The different tests were compared to the output kinematics using the ISO standard [186] spring gaps. This was carried out on both the CVD and PLI inserts to investigate the relationship between the spring gaps and the tibial inserts.

4.2.5 What effect does the ligament stiffness, represented by the simulator AP and TR spring tensions, have on the output kinematics?

To investigate the effect of the spring tensions on the output kinematics the AP spring tension was tested at 0, 20, 44, 60, 80, 100, 150, 200 and 250N/mm (Research question 5 in Table 4.2). The TR spring was tested at 0, 0.1, 0.36, 0.5, 0.8 and 1Nm/°. Only one was changed at a time with the other kept at the ISO standard value (44N/mm and 0.36Nm/°). The output kinematics from the different conditions were compared to the output kinematics using the ISO standard [186] spring tensions. This study was carried out using the CVD and PLI inserts to find the relationship between the spring tensions and the insert design.

4.2.6 Validation of the computational simulation

The computational model that was detailed in Chapter 3 will be validated using the experimental results. The same soft tissue conditions as those studied experimentally will be simulated computationally and the output kinematics compared.

The soft tissue conditions that will be compared will cover the range of the AP and TR spring gaps and spring tensions as those studied experimentally. The correlation between the experimental and computational output kinematics will be compared. A correlation coefficient of 0.7 or higher will be deemed as a good correlation.

Table 4.2: Spring tensions used for research questions 2-5

Research Question	Insert	Posterior AP Spring Tension (N)	AP Spring Gap (mm)	TR Spring Tension (Nm/°)	TR Spring Gap (°)
2	CVD	44	2.5	0.36	6
		Non-linear	0	Non-linear	0
3	CVD, PLI & Flat	44	2.5	0.36	6
4	CVD & PLI	44	9	0.36	6
			8		
			7		
			6		
			5		
			4		
			3		
			2.5		
			1		
			0		
		44	2.5	0.36	11
					10
					9
					8
					7
					6
					5
					4
					3
					2
					1
					0
5	CVD & PLI	250	2.5	0.36	6
		200			
		150			
		100			
		80			
		60			
		44			
		20			
		0			
		44	2.5	1	6
				0.8	
				0.5	
				0.36	
				0.1	
				0	

4.3 Experimental Results

4.3.1 What effect do the AP force, TR torque and FE displacement input profiles have on the output kinematics?

In order to investigate the effect of the FE, AP force and TR torque input profiles on the output kinematics, different combinations of the input profiles were applied using the CVD insert. This showed the effect of the absence of each profile.

With all profiles applied the AP displacement had three peaks during the gait cycle (Figure 4.4). The first two peaks occurred at the same points in the gait cycle as the peaks in the AP force profile (Figure 4.2).

The AP displacement was determined to be influenced by the AP force and the FE position. Without the AP force applied the first peak at 7% gait was not present. Instead there was a more gradual increase leading to a more rounded peak at 20% gait of 3mm. It also resulted in a significantly lower peak at 60% gait of 4.5mm rather than 6mm ($p<0.01$). The displacement at the end of the cycle was also higher with the third peak at 3.5mm. Without the FE input profile applied the AP displacement was significantly higher at the start of the cycle ($p<0.01$). The AP position then stayed relatively constant until 60% gait where it followed the same shape as with all the input profiles applied.

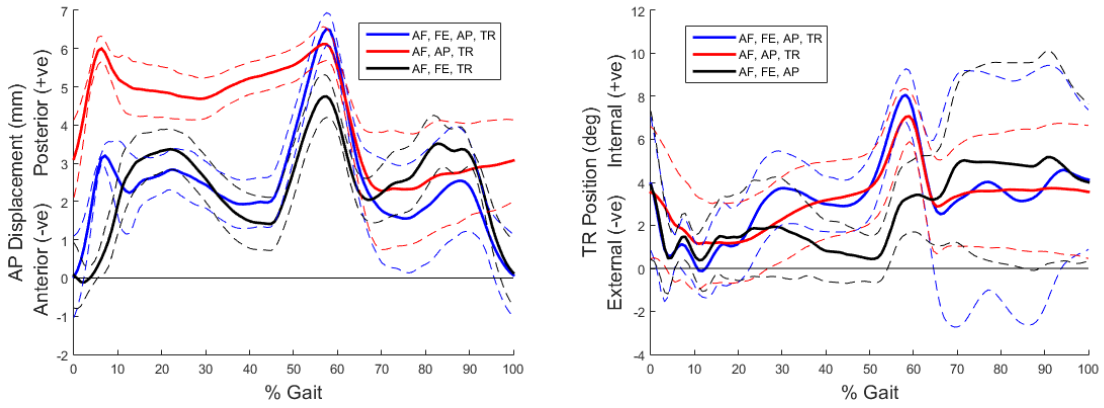

(a) AP Displacement

(b) TR Rotation

Figure 4.4: Effect of input profiles on the AP displacement (a) and TR rotation (b) with the 95% confidence interval shown by dotted lines

With all profiles applied the TR position had two peaks during the cycle (blue line in Figure 4.4 (b)). At 30% and 60% gait the contact was at the edge of the tibial component, which restricted further rotation and caused the two peaks in the TR output profile.

As anticipated the TR torque was determined to have the greatest effect on the TR position. With no TR torque applied the TR position remained between 0-4° throughout the cycle and was always within the TR spring gap of 6° (black line in Figure 4.4 (b)). There was a significant difference between the minima at 45% gait ($p<0.01$) and the peak at 60% gait with all profiles applied and with no TR torque applied ($p<0.01$). With no FE displacement

applied there was a reduction in the peak TR position; from 8° to 7° ('AF, FE, AP, TR' shown in blue compared to 'AF, AP, TR' shown in red in Figure 4.4). This same difference also occurred in the AP displacement when the FE was not applied (red line in Figure 4.4 (a)), without the FE motion there may be higher friction for the AP and TR displacements as the joint was more stationary resulting in lower displacement.For the TR position there was a large 95% CI during the last 30% of the cycle with a maximum of 6°.

The AP displacement was only minimally effected by the TR torque and the TR position was only minimally affected by the AP force so these were not shown in Figure 4.4 for clarity.

4.3.2 What difference is there between a spring profile based on clinical data compared to the ISO standard linear profiles?

The ISO standard springs use a linear spring with a gap around the zero position. Clinical data for the soft tissues in the knee, particularly for the TR, show a different profile [73, 113]. In order to compare the clinical data with the ISO profiles, springs were generated using clinical data (Figure 4.3). Two clinical data profiles were made; one with a resected ACL and intact PCL and one with a resected ACL and PCL. For the AP spring profile the clinical data used was for a knee with a resected ACL and an intact PCL and with a resected ACL and PCL for knee flexion at 0° [73]. For all the spring profiles studied an AP spring gap of ±2.5mm was assumed based on the ISO standard [186]. The clinical data used for the TR position was for a knee with no ACL [113]. This study was used for the TR position data as it provided a response profile across a range of applied TR torques. These were then run in the simulator and the output kinematics compared with the ISO springs for a CR and CS implant.

For each of the four spring conditions there were similar AP displacements for the first 50% of the cycle (Figure 4.5).

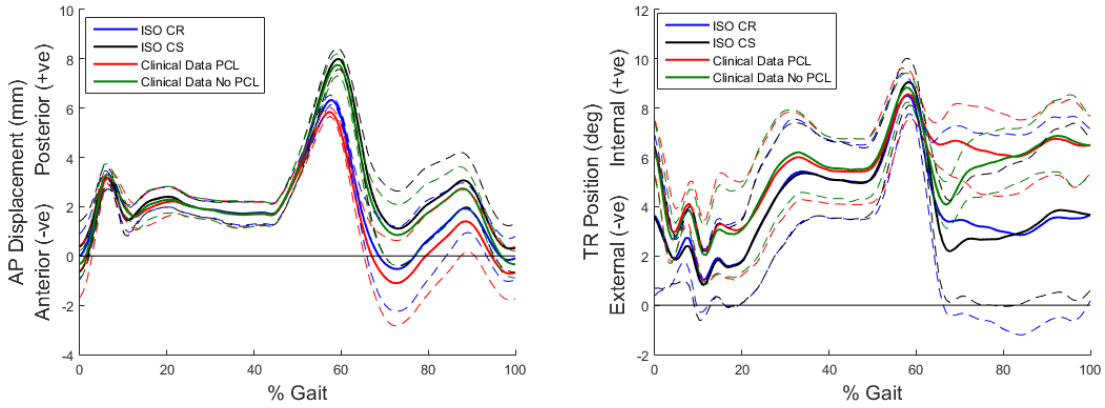

(a) AP Displacement (b) TR Rotation

Figure 4.5: Output AP displacement (a) and TR rotation (b) profiles with the ISO standard springs and springs based on clinical data

There was no significant difference between the ISO CS and the clinical data with no PCL.

But there was a significant difference between the peak AP values in the ISO CR and the clinical data with a PCL (p=0.001), however the difference was only 0.4mm.

For the TR position the output kinematics for each test were also similar. The peak TR values had no significant differences between any of the spring conditions (Figure 4.5). For the TR position there is more variation between the stations on the simulator than for the AP displacement. Therefore differences in the kinematics due to the different spring profiles were less clear.

4.3.3 What effect does the tibial insert geometry have on the kinematics?

Figure 4.6 shows the effect of tibial geometry on the output AP and TR displacements. Three insert designs were tested; CVD, PLI and flat. Each of the tibial insert designs resulted in a similar AP profile shape with peaks at 7% and 60% gait.

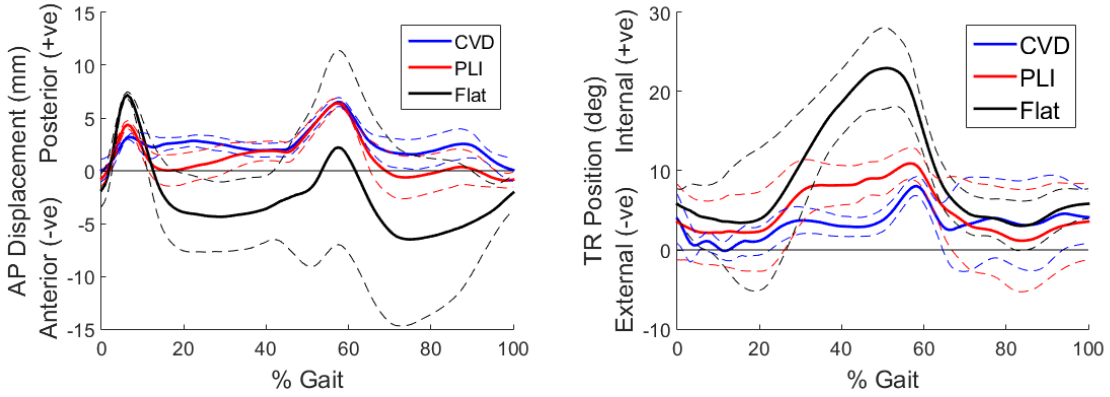

(a) AP Displacement

(b) TR Rotation

Figure 4.6: Effect of insert design on AP displacement (a) and TR rotation (b) with the 95% confidence intervals shown by dotted lines

The lower conformity inserts, particularly the flat insert, resulted in more anterior displacement. However there was also much more variation with the flat insert, resulting in a 95% CI of 9mm at 60% gait. The PLI and flat inserts had higher peaks at 7% gait compared to the CVD insert. At this point there was a significant difference between all three inserts (p<0.01). During the rest of the gait cycle the flat insert resulted in significantly lower AP displacements compared to the CVD insert (p=0.019).

The insert design had a large effect on the TR position profile shape and amplitude however the rotation remained in the internal direction for all designs (Figure 4.6). The lower the conformity of the insert the higher the peak TR position and the earlier in the cycle this peak occurred. For the first half of the cycle there was a significant difference between all three inserts (p<0.01). The flat insert had a peak of 23° at 50% gait which followed the profile shape of the TR torque profile (Figure 4.2) more closely than the PLI or CVD inserts, as the peak was larger and occurred earlier in the cycle.

At this point there was a significant difference between the flat insert and the CVD and PLI inserts ($p<0.01$).

At the peaks in the TR position at 30% and 60% gait cycle the femoral was up to the edge of the tibial insert. The curve of the insert at this point reduced any further rotation or displacement. For the CVD and PLI inserts the peak AP displacement stayed the same however the TR position increased from 8° to 11° from the CVD to the PLI insert.

4.3.4 What effect does the laxity of the knee, represented by the simulator AP and TR spring gaps, have on the output kinematics?

The AP and TR spring gaps were varied to find the effect on the output kinematics. The AP gap was tested from 0-9mm; the higher the AP gap the higher the AP displacement (Figure 4.7 (a)). This occurred throughout the cycle but particularly at the peak at 60% gait. For the CVD and PLI inserts there was a linear relationship between the peak AP displacement and the AP spring gap. The spring gap change had more of an effect on the PLI insert than the CVD insert; the gradient of the trend line for the PLI insert was significantly higher than for the CVD insert ($p=0.02$).

The TR spring gap was tested at 0-11° with 1° intervals. As with the AP spring the higher the TR gap the higher the TR rotation throughout the cycle (Figure 4.7 (b)). The relationship of TR spring gap to TR rotation had a similar linear trend on both the CVD and PLI inserts with the displacement increasing as the spring gaps increased; the gap increase from 0° to 11° resulted in an increase in the peak TR position of 4.5° and 4.7° for the CVD and PLI inserts respectively. The PLI insert had an offset of around 2° higher TR position throughout the test compared to the CVD insert. There was no significant difference between the gradients of the trend lines but the y-intercept was significantly higher on the PLI insert ($p=0.03$).

Changing the spring gaps did not affect the shape of the output profiles; it affected their magnitude and peak values. After these tests the spring gaps were kept at the ISO values of 2.5mm and 6°.

4.3.5 What effect does the ligament stiffness, represented by the simulator AP and TR spring tensions have on the output kinematics?

The AP spring tension was tested at 0, 20, 44, 60, 80, 100, 150, 200 and 250N/mm. This affected the magnitude of the AP displacement throughout the cycle but particularly from 50% gait onwards. The AP spring tensions had a minimal effect on the TR position and the only differences were present in the second half of the cycle when the axial force was at its lowest (Figure 4.8). The lower the AP spring tension the sharper and higher the decrease in TR position from the peak at 60%.

The relationship between the peak AP displacement and the AP spring tension is shown in Figure 4.9 for the CVD and PLI inserts.

There was a similar trend with both insert designs; as the spring tension increased the

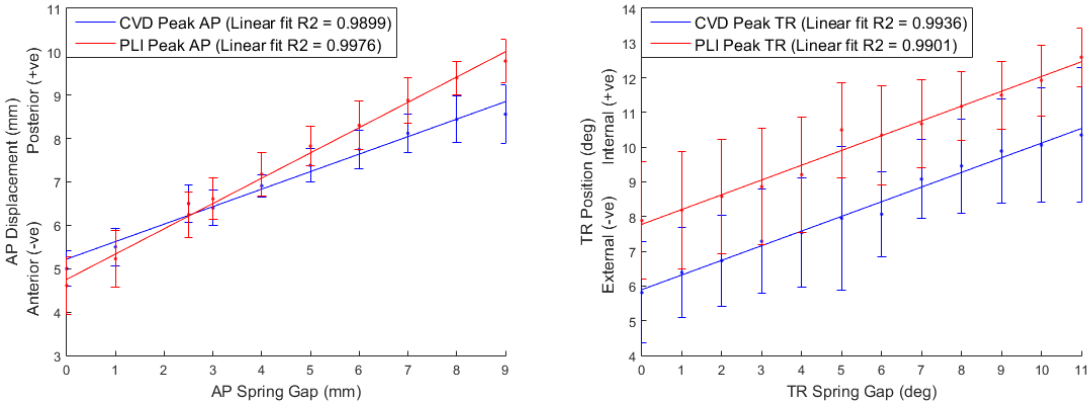

(a) AP Displacement (b) TR Rotation

Figure 4.7: Relationship between the peak AP displacement (a) and TR rotation (b) and the AP and TR spring gaps respectively for the CVD and PLI inserts

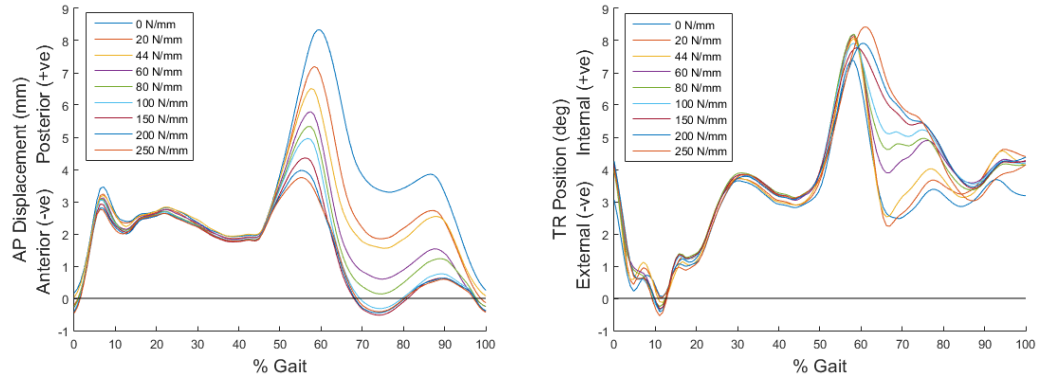

(a) AP Displacement (b) TR Rotation

Figure 4.8: The AP displacement and TR position with different AP spring tensions applied with the CVD insert

peak displacement decreased plateauing after 150N/mm at around 4mm. Increasing the spring tension also reduced the minimum at 75% gait. The minimum AP displacement at 75% gait followed a similar trend to the peak displacement; plateauing after 150N/mm. Varying the AP spring tension had a minimal effect on the TR position; the only difference occurred at 60-80% gait where a higher AP spring tension resulted in a more gradual decrease in the TR position from the peak at 60% gait.

The TR spring tensions were tested at 0, 0.1, 0.36, 0.5, 0.8 and 1 Nm/°. As with the AP springs this did not change the profile shape, however they changed the amplitude of the output profile. The TR spring tensions did not have an effect on the AP displacement (Figure 4.10).

The higher the TR spring tension the lower the TR position throughout the cycle. On the PLI insert the different spring tensions had more of an effect on the peak TR position; there was a larger range of 4.9° compared to 1.6° for the CVD insert from 0N/° to 1Nm/° (Figure

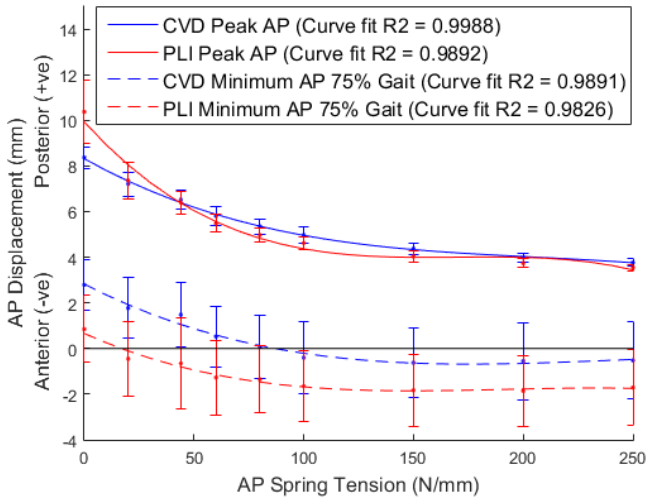

Figure 4.9: Relationship between the AP displacement and the AP spring tension for the CVD and PLI inserts

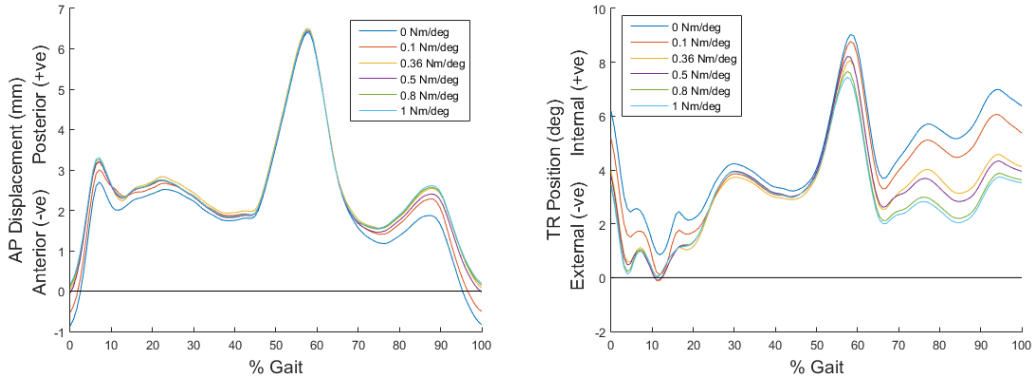

(a) AP Displacement (b) TR Rotation

Figure 4.10: The AP and TR displacements with different TR spring tensions with the CVD insert

4.11).

4.4 Validation of the Computational Simulation

The aim of this section was to validate the computational model described in Chapter 3 under a range of soft tissue conditions. To do this a study was carried out into the output AP and TR displacements under different spring gaps and tensions. The computational predictions for the AP and TR displacements were compared to those determined experimentally.

The AP spring gap was studied at values of 0mm, 2.5mm, 5mm, 7mm and 9mm and the TR spring gap at values of 0°, 2°, 4°, 6°, 8° and 10°. These were values covering a similar range that was tested experimentally.

The AP spring tension was varied to values of 0N/mm, 44N/mm, 80N/mm, 150N/mm

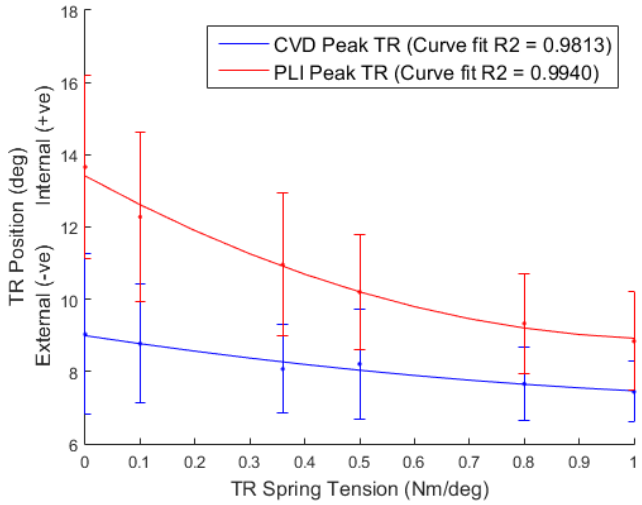

Figure 4.11: Relationship between the peak TR position and the TR spring tension for CVD and PLI inserts

and 250N/mm while the TR spring tension was studied under values of 0Nm/°, 0.1Nm/°, 0.36Nm/°, 0.5Nm/°, 0.8Nm/° and 1Nm/°.

As with the experimental study only one spring was changed at a time with the other kept at the ISO standard CR values for the spring gap and spring tension [186].

4.4.1 AP Spring Gap

The computational model was run with the AP spring gap of 0mm, 2.5mm, 5mm, 7mm and 9mm and using the ISO standard CR AP spring tensions of 44N/mm posteriorly and 9.3N/mm anteriorly. The peak AP displacements under these AP springs were determined and compared to those determined using the experimental methods described previously in this chapter (Figure 4.12).

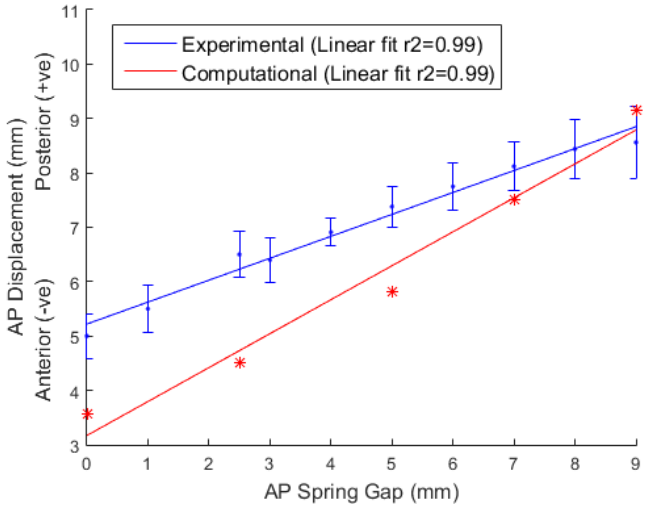

Figure 4.12: The peak AP displacement under a range of AP spring gaps using both experimental (mean ± 95%CI) and computational methods

Both the experimental and computational methods resulted in a linear relationship between the peak AP displacement and the spring gap. The computational model however resulted in lower peak AP displacement in the studies with a spring gap below 9mm.

For all of the AP spring gaps studied there was a good correlation between the two data sets (Figure 4.13). For all of the AP spring gaps the linear fit had a gradient less than 1; this showed that the computational model resulted in lower AP displacement values than the experimental model. With the 0mm and 2.5mm springs the linear fit passed close to the origin, this indicated that there was no offset between the two data sets. However for the other spring gap values there was an offset ranging between -0.3 and -1.5mm.

The higher spring gaps resulted in worse correlation between the two data sets. This may be due to the reduction in restraint resulting in a more unstable condition, differences between the computational and experimental methods may therefore have more of an effect on the output displacements.

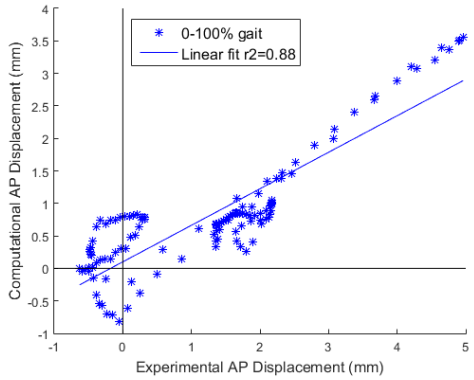

(a) 0mm gradient=0.56

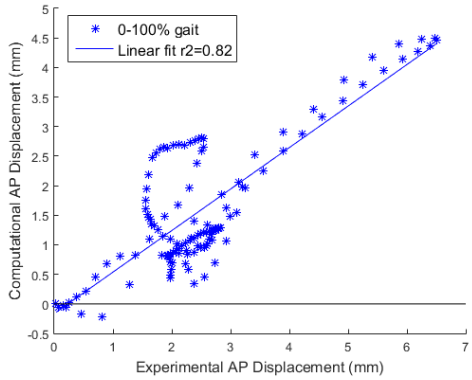

(b) 2.5mm gradient=0.7

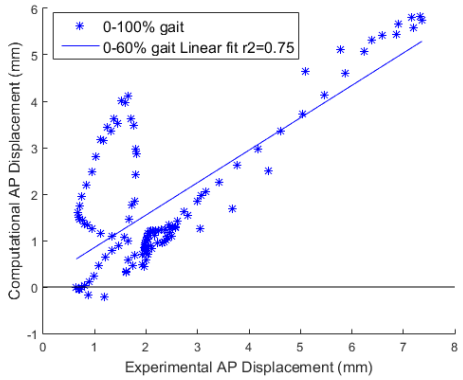

(c) 5mm gradient=0.70

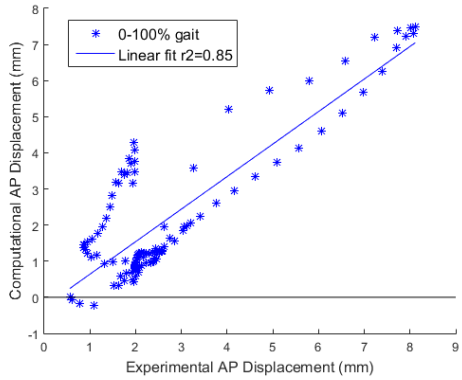

(d) 7mm gradient=0.90

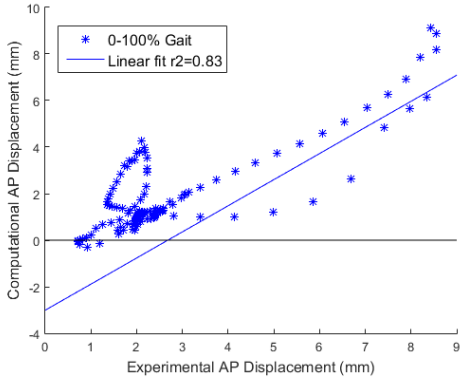

(e) 9mm gradient=0.82

Figure 4.13: The correlation of the AP displacement under a range of AP spring gaps between the computational and experimental methods

4.4.2 TR Spring Gap

The computational model was run with TR spring gap values of 0°, 2°, 4°, 6°, 8° and 10°, similar range of values studied experimentally. The peak TR rotation for each spring tested was determined and compared to the corresponding experimental result (Figure 4.14). The computational data resulted in a linear fit with a higher gradient than the experimental data.

However the peak TR rotations from the computational results were within the 95% CI of the experimental data (shown by the error bars) for all spring conditions tested.

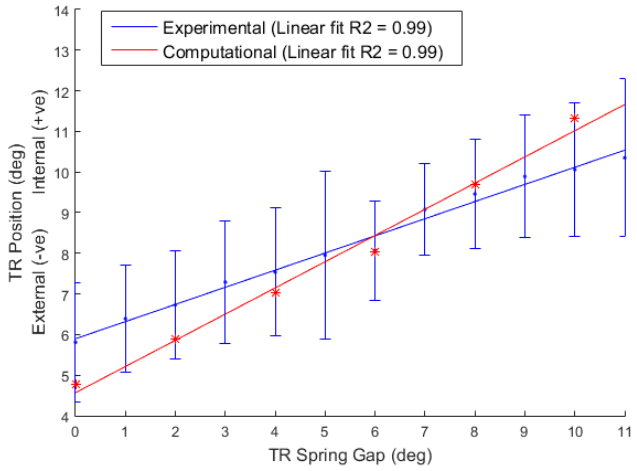

Figure 4.14: The peak TR rotation under a range of TR spring gaps using both experimental (mean ± 95%CI) and computational methods

For all of the TR spring gaps there was good correlation between the two data sets with the gradients of the linear fits varying between 0.82 and 1.08 (Figure 4.15). As this was close to 1 for all the spring gaps this showed that there was good agreement between the two data sets.

As with the AP displacement the best correlation occurred in the first half of the gait cycle. The most variation between the data sets occurred just after 60% gait; the increase in the TR rotation up to the peak value occurred later in the cycle with the computational data than the experimental data. This difference in the TR rotation profiles resulted in a worse correlation between the data sets at high TR rotation values. This occurred with all of the TR spring gap values studied.

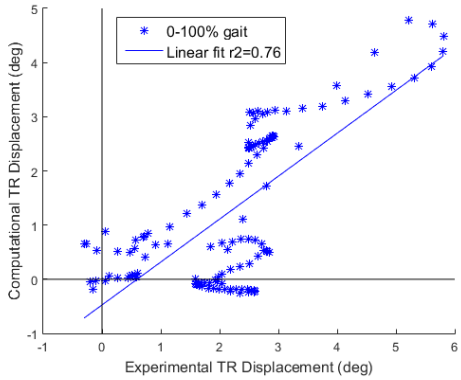

(a) 0deg gradient=0.79

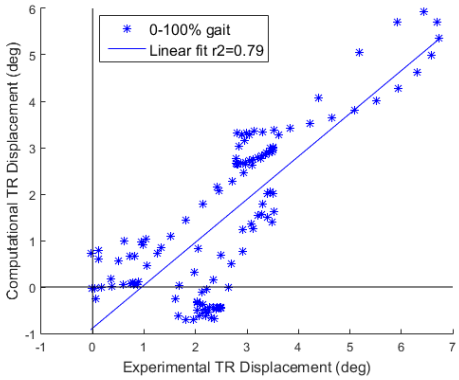

(b) 2deg gradient=0.92

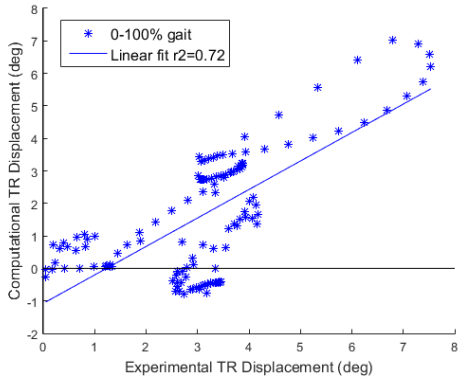

(c) 4deg gradient=0.88

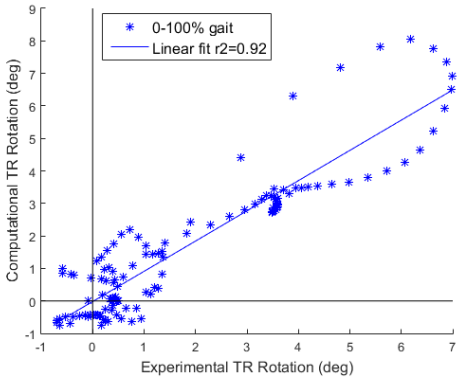

(d) 6deg gradient=0.93

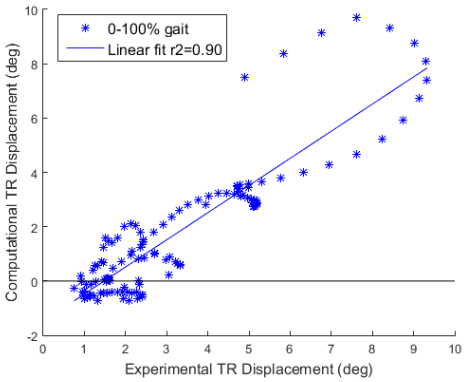

(e) 8deg gradient=1.00

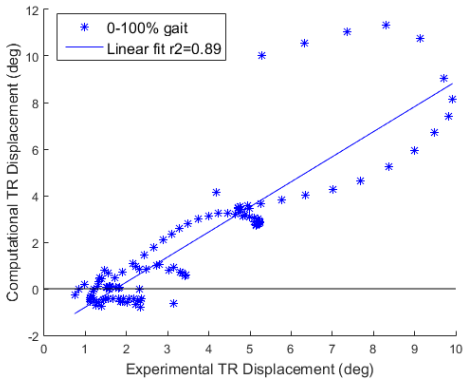

(f) 10deg gradient=1.08

Figure 4.15: The correlation of the TR rotation under a range of TR spring gaps between the computational and experimental methods

4.4.3 AP Spring Tension

The relationship between the peak AP displacement and the AP spring tension from both the experimental results and the computational prediction was determined for a range of AP spring tensions from 0N/mm to 250N/mm.

With an AP spring tension of 0N/mm the computational prediction resulted in the AP

displacement increasing to the point where the only tibiofemoral contact was on the medial, anterior tibial edge and the computational model could not be run for the whole cycle (Figure 4.16).

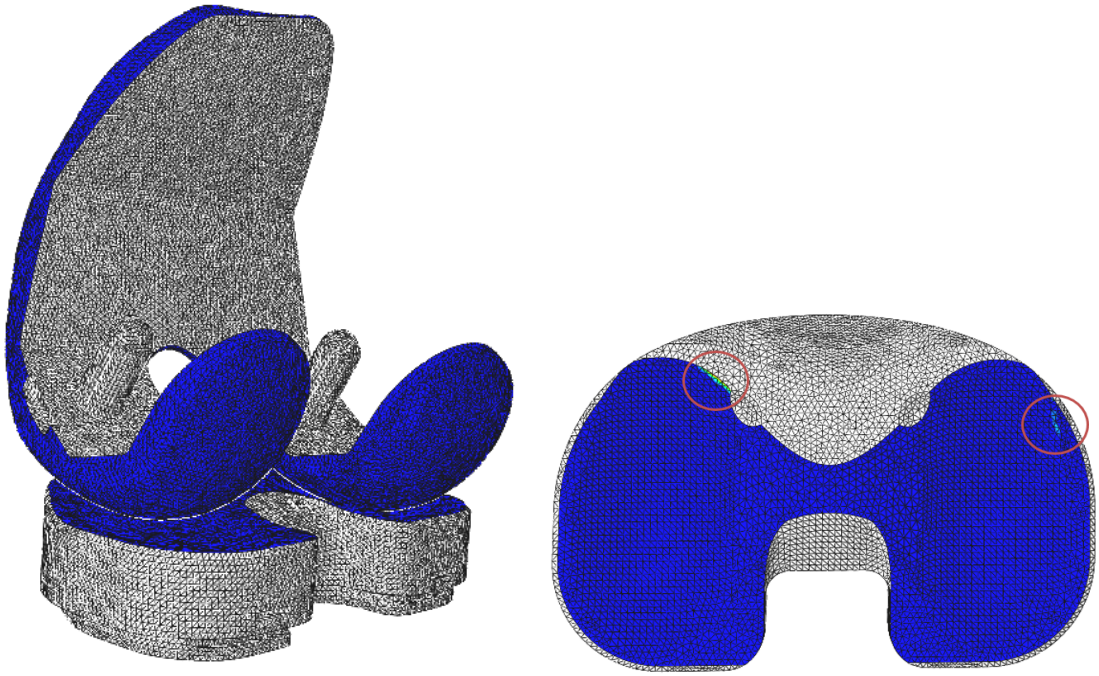

(a) Component Positions (b) Contact on Tibial Insert

Figure 4.16: Tibial and femoral component position after at the end of the computational model with an AP spring tension of 0N/mm

The computational prediction resulted in peak AP displacements lower than those from the experimental data (Figure 4.17). Both methods had a similar trend with the AP displacement increasing as the AP spring tension decreased with a plateau forming from 150N/mm and higher.

The AP and TR displacement profiles under a range of AP spring tensions using the experimental and computational methods were determined (Figure 4.18). In the experimental data the decrease in AP spring tension resulted in higher AP displacements from 50% gait onwards. The higher AP spring tensions also resulted in lower TR rotations from around 50-90% gait.

However with the computational model the lower AP spring tensions resulted in an increase in the AP displacement but only between 50-65% gait. In this section the AP displacement was higher than the size of the AP spring gap and therefore the springs were being applied. The lower AP spring tensions also resulted in lower TR rotations but between 50-65% gait rather than later in the cycle as with the experimental testing, this again was where the AP springs were being applied.

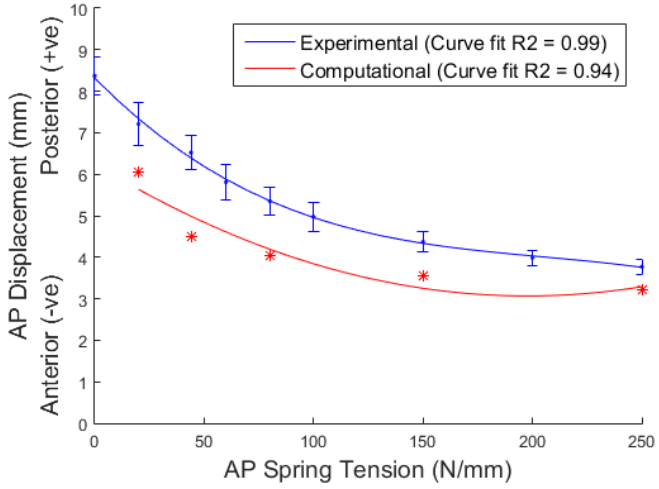

Figure 4.17: The peak AP displacement under a range of AP spring tensions using both experimental (mean ± 95%CI) and computational methods. Under a value of 0N/mm the AP displacement increased until contact was on the anterior edge of the tibial insert and the model could not finish running the gait cycle

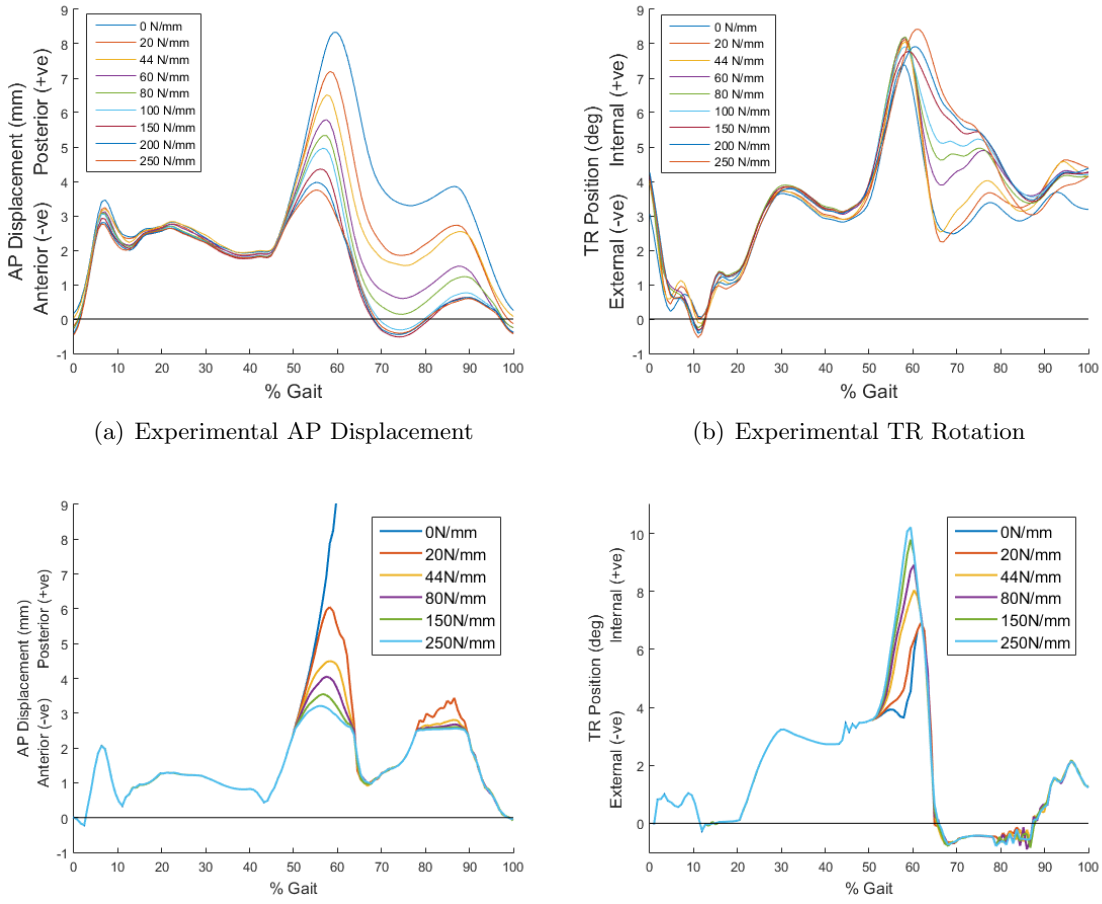

(a) Experimental AP Displacement

(b) Experimental TR Rotation

(c) Computational AP Displacement

(d) Computational TR Rotation

Figure 4.18: The AP and TR displacement under a range of AP spring tensions using the experimental and computational methods

The computational model only resulted in differences between the profiles where the AP spring tensions were being applied. The difference between this result and the experimental data may be due to the variation that occurs in experimental testing resulting in differences even when the springs were not applied. The differences may also be due to the computational model not including the momentum from the previous step; at each step the model finds equilibrium and therefore may have resulted in lower displacements and less variation between the spring conditions.

The computational prediction also resulted in a sharper decrease in the TR rotation at 65% gait, the TR rotation at this point decreased faster and to a lower point than the experimental data. As with the AP displacement the TR rotation begins to be the same for all the AP spring tensions as the AP displacement reached 2.5mm and therefore when the AP spring was not applied.

With the 0N/mm AP spring there was a good correlation between the two data sets for the first 60% of the gait cycle with a linear fit with a gradient of 1.1 and a high r squared value (Figure 4.19). The values for 60-100% gait is not shown on the figure as the computational prediction resulted in an increase in AP displacement causing the contact to occur on the medial, anterior tibial edge and the model to stop running.

Under AP spring tensions of 20N/mm and 44N/mm there was a good correlation between the experimental and computational data with r squared values of 0.87 and 0.82 and gradients of 0.8 and 0.7. The gradients were below 1, therefore the computational prediction resulted in lower AP displacement values than the experimental methods at higher AP displacements. This was shown in the computational model having a lower peak AP displacement than the experimental data. The end of the gait cycle was the section with the most difference between the two data sets; the computational prediction resulted in higher AP displacements between 70% and 90% gait.

With higher AP spring tensions there was lower correlation between the two data sets. Both the gradient of the linear fit and the r squared value decreased as the AP spring tension increased. However for all three of the highest AP spring tensions there was good correlation between the two methods between 0-60% gait (Figure 4.19), this correlation then decreased during the end of the gait cycle.

For each of the three higher spring tensions the y intercept of the linear fit was below zero with values of -0.84, -0.84 and -0.85 for 80N/mm, 150N/mm and 250N/mm respectively. This showed that there was an offset between the computational and experimental methods from 0-60% of around 0.8mm with the experimental data having a higher AP displacement.

Around 65% gait onwards is the where the computational and experimental models behaved differently to each other in response to the different AP spring tensions, this resulted in poor correlation. As explained previously this may be due to the differences in the AP and TR displacement values and the size of the AP spring gap.

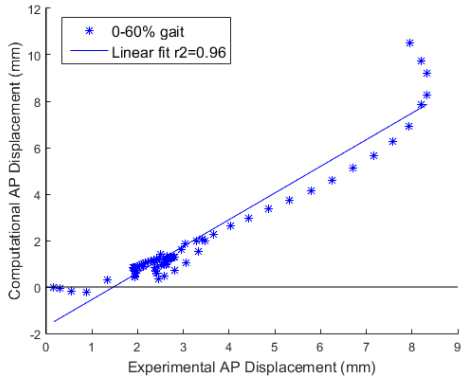

(a) 0N/mm gradient=1.15

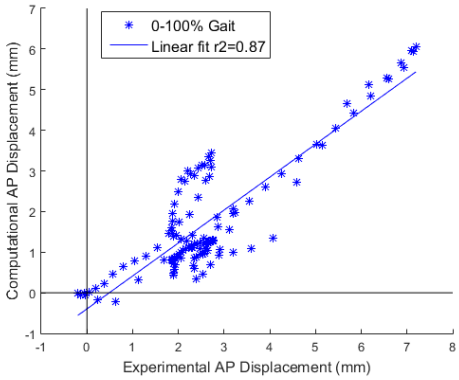

(b) 20N/mm gradient=0.8

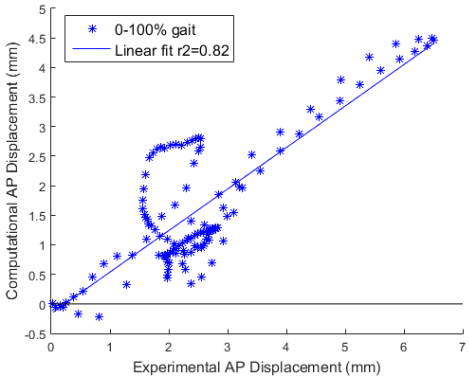

(c) 44N/mm gradient=0.7

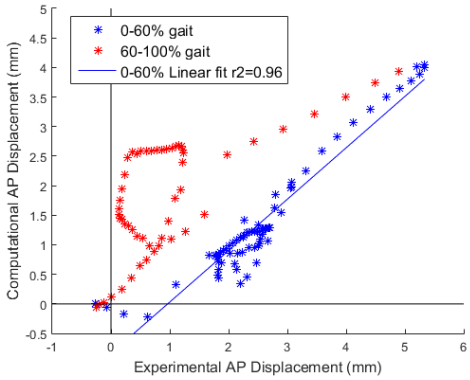

(d) 80N/mm gradient=0.87

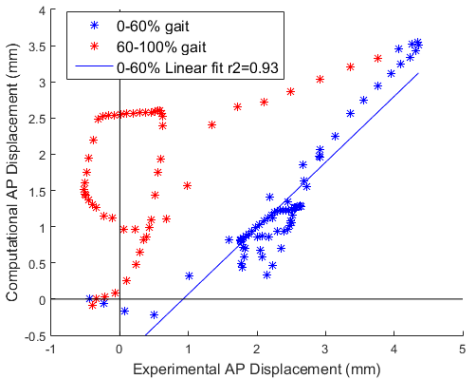

(e) 150N/mm gradient =0.91

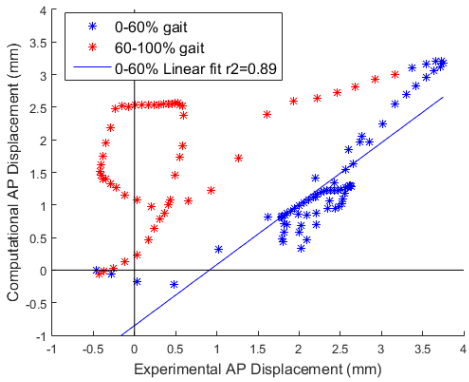

(f) 250N/mm gradient=0.94

Figure 4.19: The correlation of the AP displacement under a range of AP spring tensions between the computational and experimental methods

4.4.4 TR Spring Tension

A range of TR spring tensions were tested computationally; 0Nm/°, 0.1Nm/°, 0.36Nm/°, 0.5Nm/°, 0.8Nm/° and 1Nm/°. The peak TR rotations under each of these spring tensions were determined and compared to those determined by experimental methods (Figure 4.20).

For all the spring tensions tested apart from 0Nm/° the peak computational TR rotation

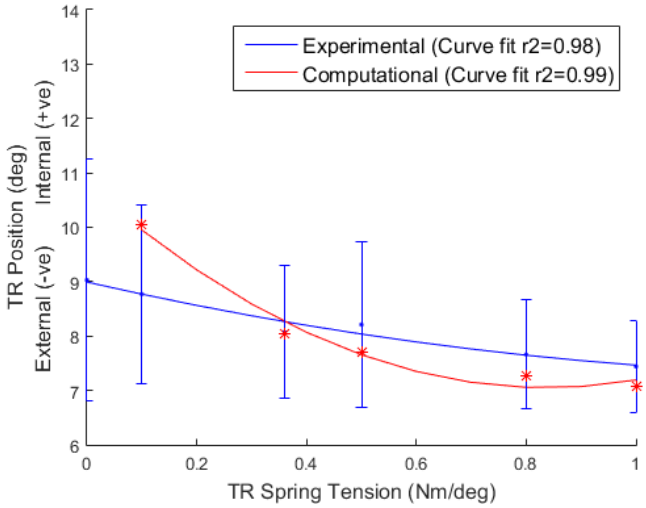

Figure 4.20: The peak TR rotation under a range of TR spring tensions using both experimental and computational methods

was within the 95% CI of the experimental data. However with the 0Nm/° TR springs the computational model resulted in dislocation after around 60% of the gait cycle due to the high external tibial rotation that resulted in the lateral femoral condyle rotating off the posterior edge of the tibial insert (Figure 4.21).

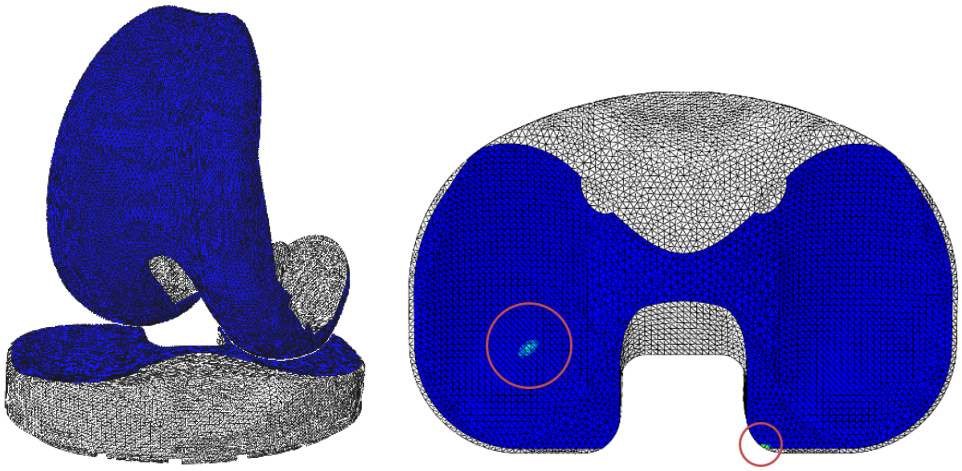

(a) Component Position (b) Contact on Tibial Insert

Figure 4.21: Tibial and femoral component position at the point of dislocation in the computational model with a TR spring tension of 0Nm/deg

The model could not run in order to complete the gait cycle with the 0Nm/° springs.

Under experimental testing the change in TR spring tension had a minimal effect on the output AP displacement, especially between 50-70% gait (Figure 4.22). Under the computational model there was no difference between the output AP displacements apart from the peak AP displacement, this was the opposite to the experimental methods. The higher TR

spring tensions resulted in higher peak AP displacements, however these differences were minimal. Overall there was good agreement between the AP displacements for the computational and experimental methods.

The higher TR spring tensions resulted in lower TR rotations throughout the gait cycle when tested experimentally. However in the computational model there was no difference in the TR rotations for most of the gait cycle. But the higher tension TR springs did result in lower peak TR rotations, as with the experimental simulation. The differences in the TR rotation with the computational model only occurred when the TR rotation was greater than the TR spring gap of 6°. The differences in the TR rotation under experimental simulation that occurred when the TR springs were not being applied (i.e. when the TR rotation was

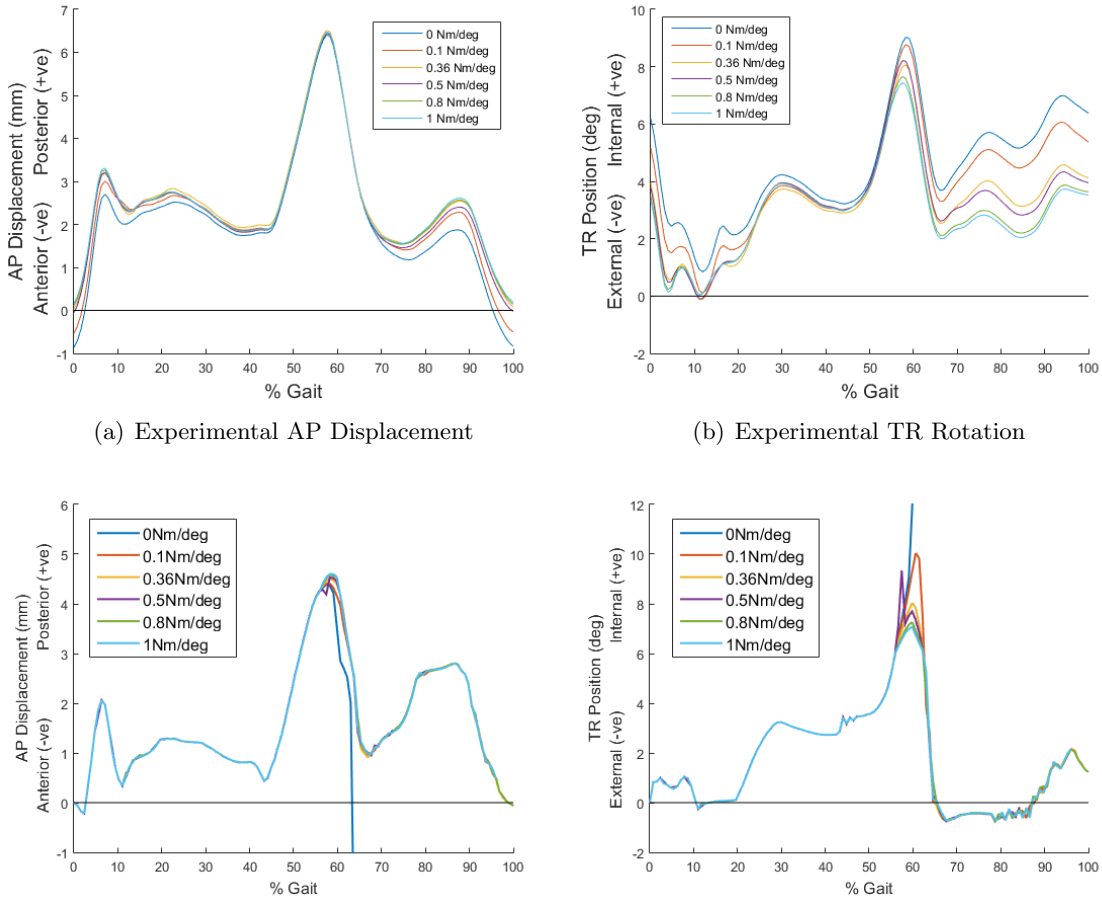

(a) Experimental AP Displacement

(b) Experimental TR Rotation

(c) Computational AP Displacement

(d) Computational TR Rotation

Figure 4.22: The AP and TR displacement under a range of TR spring tensions using the experimental and computational methods

lower than 6°) may have been due to experimental error or variation between stations.

With a TR spring tension of 0Nm/° the joint dislocated at around 60% gait, however before this point there was good correlation between the two data sets with a linear fit of gradient 0.88 and a high r squared value (Figure 4.23).

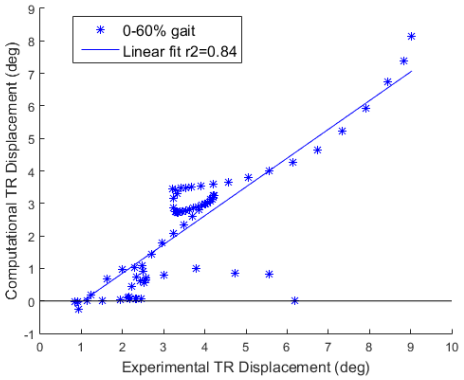

(a) 0Nm/deg gradient=0.88

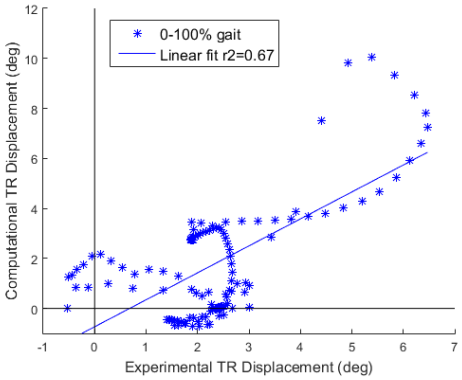

(b) 0.1Nm/deg gradient = 1.08

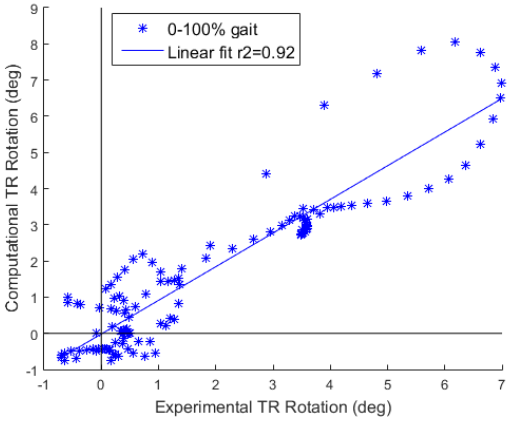

(c) 0.36Nm/deg gradient = 0.93

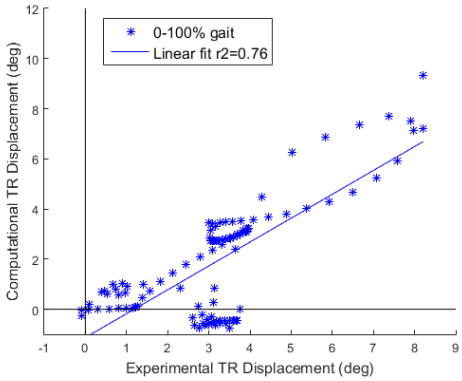

(d) 0.5Nm/deg gradient = 0.95

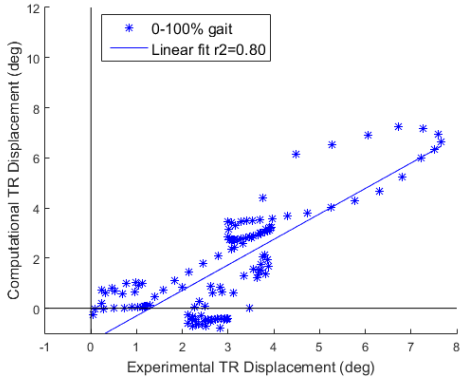

(e) 0.8Nm/deg gradient = 1.02

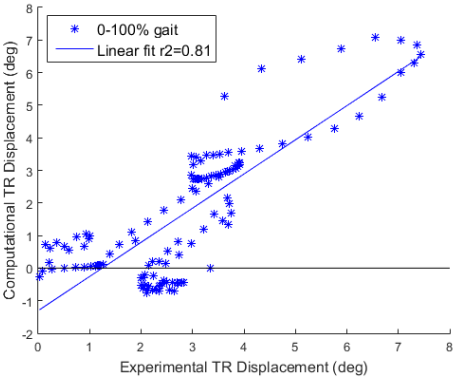

(f) 1Nm/deg gradient = 1.05

Figure 4.23: The correlation of the TR rotation under a range of TR spring tensions between the computational and experimental methods

With a TR spring tension of 0.1Nm/° the correlation was not as strong especially with high TR rotation values. This showed the difference in the peak TR rotation between the two results. The difference between the two TR profiles at around 30% gait where the computational prediction increased to the peak TR rotation later in the cycle was shown in the

weaker correlation with TR rotation values of around 2-3°.

With the higher TR spring tensions there was a better correlation between the data sets, especially at lower TR rotation values. The computational prediction resulting in a peak TR rotation later in the cycle is shown in each of the correlations, where the computational prediction resulted in higher TR rotations than the experimental data with values between 5-7°. However otherwise there was a strong correlation between the two data sets with linear fits of gradients 0.93, 1.03 and 1.05 along with high r squared values.

4.5 Discussion

Ligament tensions vary between patients and ligaments degrade as part of the disease process and aging and may be damaged or removed during TKR surgery. Currently standard simulation of TKRs does not take into account the range of soft tissue tensions found in vivo. A study into the soft tissue tensions after TKR determined that the soft tissue force ranged from 70.8-182N in extension and 70.8-169.4N in flexion across 77 TKR patients [16]. This study investigated the effect of soft tissue constraints on the kinematics of TKRs using experimental and computational simulation.

4.5.1 Methods

The use of force control for this study allowed the different soft tissue constraints, represented by the springs, to control the output kinematics of the joint. Differences between each station in the simulator, such as internal friction, affected the output kinematics especially when lower spring tensions were used. In order to reduce these differences the same component was used on each station and 100 cycles were recorded on each station. This removed offsets in the output AP and TR displacements across the stations. For the AP displacement this offset was up to 3mm and up to 4° on the TR position. The output kinematics from the tests gave an indication of the stability of the knee.

The ISO standard [186] force control input profiles are intended to mimic the muscle and joint forces that occur during walking, while the spring tensions and gaps represent the restraint and laxity of the soft tissues. These ISO standard test conditions represent an average patient, with mechanical alignment, and does not simulate a range of patient groups.

Previous studies have investigated the laxity and ligament tensions of the knee in TKR patients [198] or cadaveric specimens [73, 113, 144]. Due to the variation in ligament stiffness and laxity between patients there is a range of results. The AP displacement under a given load also depends on the flexion position of the knee [73]. Under 100N posterior load the displacement of the knee was determined to be around 2.5mm-2.8mm for TKR patients at 15-20° flexion [198]. Under the same load another study determined posterior displacements of 4mm and 10mm at 0° flexion for an intact knee and a knee with no PCL respectively [73]. For an intact knee the posterior displacement under 100N was determined to be relatively constant across different flexion positions. However with the PCL removed the posterior displacement

varied from around 9-18mm from 0-90° flexion [73].

As with the AP tension there is variation in the rotational stiffness of the knee. Previous studies have applied a TR torque to cadaveric specimens and measured the rotation. One study applied a TR torque of 6Nm and determined rotation of around 10° and 20° for 0° and 90° flexion respectively [144]. Another study determined that the response under a range of applied TR torques was approximately linear within 10° of the zero position, with tension values of around 0.34Nm/° and 0.3Nm/° for an intact and ACL resected knee [113].

4.5.2 Input Profiles

The first part of this study investigated the effect of the input profiles on the output kinematics. The absence of the FE motion had a large effect on the AP displacement. This was likely because as the FE moved from flexion to extension a posterior force was generated on the tibial component. The converse being true when moving from extension to flexion. For most of the gait cycle the FE motion and input AP force balanced each other; as the knee extended an anterior AP force was being applied. Therefore the AP displacement changed significantly if either the AP force or FE displacement was not applied. No such relationship was determined for the TR position; only the absence of the TR torque significantly changed the profile.

4.5.3 Tibial Insert Design

Three different tibial insert designs were tested to find the effect of the tibial insert design on the output kinematics. The design of the tibial insert particularly affected the TR position. A lower conformity insert had a higher peak position which occurred earlier in the cycle. This was due to the lower conformity inserts allowing the TR position to follow the shape of the TR torque profile more closely. The lower conformity inserts also resulted in more anterior AP displacement.

4.5.4 Spring Gap and Spring Tension

The effect of the laxity, represented by the spring gaps, and soft tissue tensions, represented by the spring tensions, within the knee were investigated. The spring gaps and tensions affected the peak displacements in both the AP and TR positions, particularly in the second half of the cycle. This was due to the AF decreasing to its minimum from 50% gait, the applied AF in the first half of the cycle restricted the AP displacement.

The increased spring gaps resulted in a linear relationship with the peak AP and TR displacements on both the CVD and PLI inserts. Changing the AP spring gap had more of an effect on the PLI insert; this may be due to the high conformity of the CVD insert restricting the motion. However changing the TR spring gap resulted in a similar response on both inserts, with the only difference being that the PLI insert had 2° more rotation across all the tests.

Increasing the AP spring tension reduced the peak AP motion on both the CVD and PLI inserts. The peak AP displacement plateaued at around 4mm from 150N/mm onwards. This may have been due to the spring gap of ±2.5mm; as the spring tension increased and the peak AP decreased the springs were only applied over a short section of the gait cycle. Therefore the difference in spring tension had less of an effect. The TR spring tension had very little effect on the CVD insert; the conformity of the insert may have been restricting the TR motion so that the effect of the spring was minimal. However with the PLI insert the peak TR position decreased as the tension increased. Further testing with tensions higher than 1Nm/° may show the same plateau as with the AP spring; the data collected showed a trend line that started to plateau at around 9°.

4.5.5 Computational Simulation

The soft tissues within the computational model were validated by comparing the output displacements to those found experimentally. There was good correlation between the experimental and computational results, especially during the first half of the gait cycle when the axial force was at its highest.

Both the computational and experimental data determined a linear relationship between the peak AP displacement and the size of the AP spring gap, however the gradient was slightly higher with the computational data. The correlation between the data sets for the TR profile was not as strong as with the AP displacement, mainly due to the peak TR rotation occurring slightly later in the cycle in the computational predictions. However the computational results for the peak TR rotation with a range of TR spring gaps was within the 95% CI of the experimental data.

The computational data resulted in a similar relationship between the spring tensions and the peak displacements as the experimental data, however it resulted in lower values. The model could not run under an AP spring tension of 0N/mm or TR spring tension of 0Nm/° as there was tibiofemoral contact occurring on the medial, anterior edge of the tibial insert. As discussed previously this may be due to the ability of the computational model to run unstable motion and the increased flexibility of the experimental simulators in comparison For all the spring tensions studied there was a good correlation between the two data sets during the first 60% of the gait cycle. This section of the gait cycle is where the axial force is highest so differences between the experimental and computational models, such as the mass as discussed previously, may have had less of an effect. There were some differences between the computational prediction and the experimental results however there was good overall agreement.

4.5.6 Comparison With Previous Work

A previous study [92] investigated the effect of different spring tensions and gaps on the output kinematics under force control. A four station Instron-Stanmore knee simulator with DePuy PFC Sigma Fixed bearing knee components were used. Two springs were attached

to the simulator to restrain the AP motion, they were separated by 47mm and therefore also applied restraint to the TR motion. High tension springs (anterior restraint of 7.24N/mm and posterior restraint of 33.8N/mm) were tested with a 2.5mm and 0mm gap. Both high and low tension springs (anterior and posterior restraint of 7.24N/mm) with a 2.5mm gap were used to investigate the effect of spring tension.

The spring gap tests had similar results to this study. The low tension spring resulted in a similar kinematic profile but with a higher amplitude. For the low tension TR springs the maximum TR position in the previous study was higher than that determined in this study (17° compared to 8°). This may have been due to the offset between the sets of results of around 6°. However there was less of a difference between the previous study and this study's peak TR rotation for a high tension spring with a 0mm or 2.5mm gap.

Differences in the results between studies may be due to differences in the test conditions and simulators. For example this study used virtual springs rather than the two physical springs used previously to apply both AP and TR restraint. Different knee simulators have also been used; this study used a ProSim simulator compared to the Instron-Stanmore simulator used in the previous study. The Instron-Stanmore simulator is pneumatic [197] compared to the electro-mechanical simulator used for this study. Electro-mechanical simulators can provide better kinematic following than the first generation pneumatic simulators [7].

The weight of the tibial fixtures were also determined to affect the output kinematics, especially that of the AP displacement. The heavier the tibial fixture the lower the AP displacement. Differences in the tibial fixture weights between any tests could result in differences in the results and is an important consideration. This could also be a cause for differences in this study and the previous study.

4.5.7 Limitations

There are some limitations to the experimental study, firstly there was some variation between the stations of the simulator, particularly when the low tension springs were applied. The high variation meant that differences were less clear. This study also only investigated the effect of the tibial insert surface geometry, further testing would investigate the effect of component design more thoroughly, for example the effect of different femoral designs.

Although the impact on kinematics has been examined, it is possible that there was a significant impact on forces going through implant-cement or cement-bone interface with varying restraints introduced by changes in ligament tension as well as surface geometry of the insert. These can manifest in a stable knee in the short-term but with a high risk of implant loosening in the mid to long-term. In this study we could not measure the magnitude of forces (shear in particular) going through these interfaces and therefore cannot comment upon the associated risk of implant loosening.

4.5.8 Conclusions

The soft tissue response in the knee varies between patients [16, 113]. The choice of these restraint values is an important factor for the kinematics and wear. When choosing the values for a test a specific patient group should be chosen. For a patient with an unstable knee due to the soft tissue tensions a high conformity insert would be used. Therefore, when choosing test conditions, the insert design and the soft tissue constraints should be matched so that they are clinically relevant. There are also other patient factors such as patient body mass index (BMI) and component position that may affect the kinematics but have not been investigated in this study.

Soft tissue constraints had a significant effect on the kinematics of the TKRs of varying geometries investigated in this study. Simulating the average soft tissue tensions will not represent the variation across different patients. Patient variation should be represented in experimental simulation; in order to simulate a patient with increased laxity in the knee an increased spring gap should be used. The difference in spring tensions were determined to have a lower effect on the high conformity tibial inserts. To ensure a test is clinically relevant the spring conditions should be considered with the tibial insert design in mind. For example a low conformity insert would not be used in a patient with high laxity. In order to replicate the range of outcomes that occur in vivo, experimental simulation must include a range of patient factors such as different soft tissue constraints.

Chapter 5

The Influence of Simulated Soft Tissue Constraints on the Mechanics and Wear of a TKR Under Mechanical Alignment

5.1 Introduction

This study was carried out in order to determine the influence of simulated soft tissue constraints on the output kinematics, contact pressure and wear rate of a TKR. In order to do this three different soft tissue conditions were defined in order to represent the range of conditions found in vivo. They were chosen to represent a knee where both the ACL and PCL have been resected, where the ACL has been resected but the PCL is intact and to represent a patient with a stiff knee.

Experimental simulation was carried out with a knee simulator (as described in Chapter 2) in order to find the output AP, TR and AA displacements under each of the soft tissue conditions. The soft tissues within the knee were represented using virtual springs within the simulator and the spring profiles were varied in order to represent the different soft tissue conditions. The resulting output displacements were then compared between the soft tissue conditions in order to determine their effect.

The contact area was also measured at four different points in the gait cycle for each soft tissue condition. The four points in the cycle were defined to cover the range of motion and loading that occurred. The contact areas were compared between the soft tissue conditions.

Then three studies of mechanical function and wear were run for 2MC with each of the soft tissue conditions to determine whether they influenced wear.

The computational model was then validated using the experimental data described in this chapter. The output kinematics and contact areas were compared between the experimental and computational data for the mechanical alignment condition under the three soft tissue

conditions studied experimentally. The output kinematics, contact area and peak contact pressure values from the computational model were then compared between the soft tissue conditions.

5.2 Materials

All the simulations were carried out using DePuy Sigma fixed bearing, right knee (DePuy Synthes, Leeds, UK) components. The tibial inserts were moderately crosslinked UHMWPE (5MRad irradiated and re-melted GUR1020 XLK, part number 1581-13-110).

The femoral components had been used in previous studies, in order to ensure this would not affect the wear results the femorals were polished in order to remove any scratches. The pre-test surface roughness was verified using a Form Talysurf to ensure the Ra was below 0.1µm.

The lubricant was 25% bovine serum (Life Technologies, New York, USA) in 0.04% sodium azide solution (Severn Biotech Ltd, Worcestershire, UK) and was changed approximately every 350,000 cycles. The contact area measurements were carried out using a Tekscan (Tekscan Inc., Boston, USA) pressure mapping sensor 4000 which was designed for use in knee joint applications, it has a total of 572 sensels with 62 sensels/cm^2 and a maximum pressure of 69.95 MPa.

The soft tissues were simulated using virtual springs within the simulator, the profiles of the virtual springs were changed to represent different soft tissue constraints.

5.3 Methods

To investigate the effect of ligament tension on the kinematics and wear of a TKR the virtual springs within the simulator, that replicate the effect of the soft tissues within the knee, were varied. The size of the spring gaps and the tension of the springs were changed in order to replicate 3 soft tissue conditions; a knee without an ACL or PCL, a knee with no ACL and a stiff knee (Table 5.1). The ISO standard force control inputs and centre of rotation were used for all studies [186] (Figure 2.3).

Table 5.1: The AP and TR spring tensions and spring gaps for the three soft tissue conditions studied

Condition	AP		TR	
	Gap (mm)	Tension (N/mm)	Gap (°)	Tension (Nm/°)
Resected ACL (ISO CR)	±2.5	44 posteriorly, 9.3 anteriorly	±6	0.36
Resected ACL & PCL (ISO CS)	±2.5	9.3	±6	0.13
Stiff	0	127	0	0.7

The first two soft tissue conditions were defined using the ISO standard virtual springs for a CS and CR prosthesis respectively to represent a resected ACL & PCL and a resected ACL.

The ISO CS springs have an AP tension of 9.3N/mm in the anterior and posterior directions, while the CR springs have a tension of 44N/mm in the posterior direction and 9.3N/mm in the anterior direction. The CS springs have a TR spring tension of 0.13Nm/° and the CR springs have a tension of 0.36Nm/°. Both the CR and CS springs had AP and TR spring gaps of 2.5mm and 6° respectively.

The third soft tissue condition was based on clinical data for the motion of the natural knee under AP and TR forces. One study found the average posterior displacement under a 100N posterior load was 1.84±1.05mm [198]. The value of 0.79mm, one standard deviation from the mean, was used in order to represent a patient with a stiffer than average knee. Assuming there was no laxity within the knee and therefore no spring gap, this gave an AP spring tension of 127N/mm.

Another study that investigated the rotation of the knee under 10Nm internal torque found that the average rotation was 19.3±4.6° [113]. Values were taken one standard deviation from the mean in order to represent a stiff knee. Assuming there was no laxity within the knee, this gave a mean TR spring tension of 0.7Nm/°. These spring values were used for the third soft tissue condition.

5.3.1 Stability

In order to determine the stability of the TKR under a wider range of soft tissue conditions the TKR was studied under more extreme soft tissue conditions. Along with studying the TKR with the three soft tissue conditions defined previously two other soft tissue conditions were studied; the resected ACL & PCL spring tensions with increased spring gaps of ±5mm and ±9° for the AP and TR springs respectively along with applying no spring restraints at all. The motion of the TKR was observed and any signs of lift off, dislocation of the joint or loading on the edges of the tibial insert were noted. Lift off was defined as any point where the femoral and tibial components were not in contact during the gait cycle.

The TKR was run with Vaseline used as lubricant and without the gaiters attached so that the mechanics of the joint could be observed.

5.3.2 Kinematics

As the knee simulator was run under force control conditions the output kinematics were able to vary in response to the different soft tissue conditions. For each of the three soft tissue conditions 10 consecutive cycles were recorded on each of the 6 stations of the simulator. The output AP, TR and AA profiles were then averaged across the simulator in order to determine the mean displacements and 95% CI.

The mean output profiles were then compared between the different soft tissue conditions using minimum and maximum points in the output profiles as defined in Section 2.3.6 (Figure 5.1). Points A-D were defined in the AP profile, points E-H in the TR profile and points I-K in the AA rotation profile.

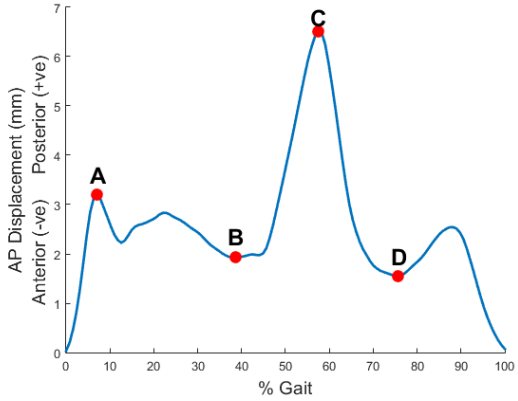

(a) AP Displacement

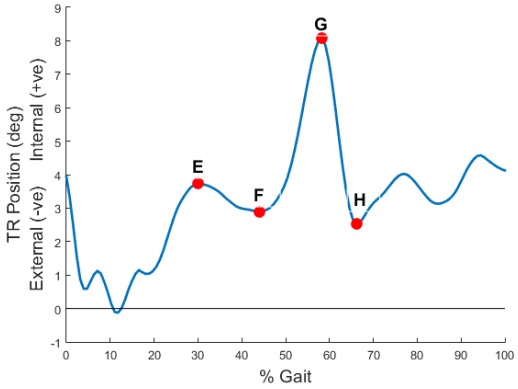

(b) TR Rotation

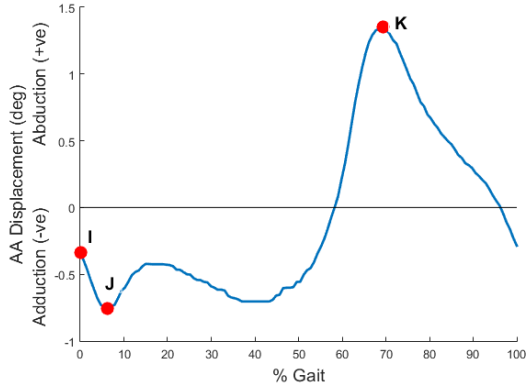

(c) AA Rotation

Figure 5.1: The maximum and minimum points in the AP, TR and AA displacement profiles used for comparison between studies

The range of motion in the displacement profiles was also compared between studies. The range of motion was defined as the difference between the maximum and minimum point in the displacement profile.

5.3.3 Contact Area

For each soft tissue condition the contact area at four points within the gait cycle were measured using the Tekscan sensor; the first at 5% gait where the initial peak in the AP force occurs, the second at 45% gait where the last peak in the AF occurs, the third at the point in the cycle where the combined AP and TR displacement were at their maximum and the fourth point at 72% gait where the FE was at its peak (Figure 5.2).

The displacements and loads at these points were found for each soft tissue condition (Table A.1). Each point was measured on all the stations of the simulator and the results averaged across them.

The contact area was measured on 5 of the stations of the simulator for each soft tissue condition and the mean contact areas were found for each point in the gait cycle. The AA

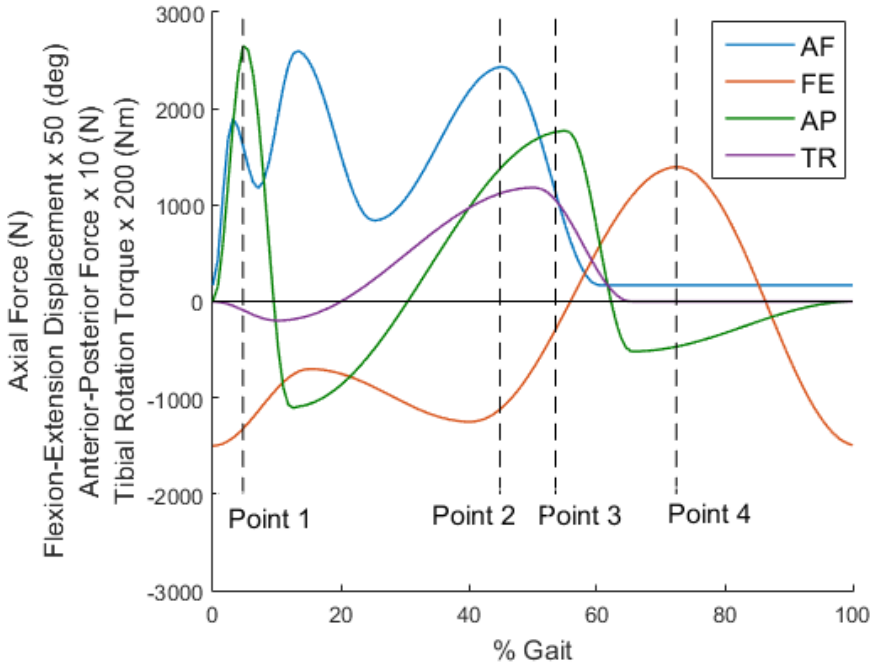

Figure 5.2: The input axial force, flexion-extension, AP force and TR torque profiles with the four points in the cycle where the contact area was measured

motor was not functional on the 6th station and was therefore not used for the study. The mean contact area was found by calculating the area of the sensor where the pressure value was greater than 0MPa and accounting for the curvature of the insert at that point. The average and 95% CI of the contact area position and size was then determined for each point in the cycle.

5.3.4 Wear rate

In order to investigate the effect of the soft tissue constraints on the wear rates 3 different wear studies were carried out. A wear study of 2MC was carried out for each of the three soft tissue conditions; resected ACL, resected ACL & PCL and a stiff knee.

At the end of each wear study the change in the output kinematics over time was investigated. This was to determine whether the kinematics changed as the wear scar was formed. To do this 10 cycles from the start of the study, at around 1MC and at the end of the study were compared from each station. The minimum and maximum points in the cycles (points A-K in Figure 5.1) were compared to determine whether there were significant differences during the wear study. The wear rates between each of the inserts used in the study were then compared in order to determine whether there were similar differences in the wear rates over time.

The variation between the stations was also investigated. Using the same 30 cycles taken at 0MC, 1MC and 2MC the output kinematics were compared between each of the 6 stations. Any significant differences in the kinematics were then compared to the wear rates on each

station to determine whether the differences in kinematics may have affected the wear rates.

The size, position and areas of the wear scars at the end of each wear study were also found and compared between wear studies.

Before and after each wear study the surface roughness of the superior surface of the tibial inserts and inferior surface of the femoral component were measured. Any significant change in surface roughness may be due to third body damage to the components. Over time this damage may result in increased wear. The surface roughness values and the change in the values were compared between the wear studies to investigate whether any of the soft tissue conditions resulted in damage to the contact surfaces.

During each wear study the bulk temperature of the serum was measured in order to determine any differences in running temperatures. The mean and 95% CI of the station and soak serum temperatures were compared between the different wear studies.

A one way ANOVA with significance taken at $p<0.05$ using IBM SPSS Statistics 22 was used. Depending on the homoscedasticity either a post hoc Tukey's test or a Games-Howell test was carried out, with significance taken at $p<0.05$, to determine the differences between the groups.

5.3.5 Validation of Computational Model

The experimental and computational data was compared for the mechanical alignment and the three soft tissue conditions studied experimentally; resected ACL, resected ACL & PCL and a stiff knee.

This was first done by comparing the output AP, TR and AA displacements between the experimental and computational results. The correlation between the experimental and computational displacements was determined and a correlation coefficient above a value of 0.7 was determined to be a good correlation.

The position of the tibiofemoral contact and the contact area were compared between the computational and experimental results at the four points in the gait cycle where the contact area was measured experimentally. A static computational model was also run under the experimental displacements at each of these points in the cycle. This was to verify whether any differences in the contact area under the dynamic computational model were due to the differences in kinematics or due to the static experimental measurements.

5.3.6 Computational results

Once the computational model was validated it was used to compare the contact areas and peak contact pressures between the three soft tissue conditions. The calculation of the contact area was carried out throughout the gait cycle. The peak contact pressure was found at each of the four points in the gait cycle where the experimental Tekscan measurements were carried out. The output AP, TR and AA kinematics from the computational model were also compared between the soft tissue conditions to determine any differences that may not have

appeared in the experimental methods. For example due to limitations in the experimental simulation such as the internal friction within the simulator.

5.4 Experimental Results

5.4.1 Stability

The same set of components was studied under a range of soft tissue conditions including with larger gaps of 5mm and 9° for the AP and TR springs respectively as well as with no springs applied. Under these different soft tissue conditions the effect on the stability and mechanics of the joint was observed.

The TKR under mechanical alignment was found to be stable under all the soft tissue conditions studied. Even with no springs attached it did not dislocate and there was no lift off of the femoral component relative to the tibial component.

5.4.2 Effect on Kinematics

The mean anterior-posterior, tibial rotation and abduction-adduction displacement profiles were found for each of the three soft tissue conditions.

5.4.2.1 Anterior-Posterior Displacement

Changing the spring tensions changed the kinematics of the joint. For the first 50% of the gait cycle there was no difference between the resected ACL and the resected ACL & PCL soft tissue conditions in the output AP displacement. However after 50% gait the resected ACL & PCL soft tissue condition resulted in a significantly higher peak AP displacement compared to the resected ACL soft tissue condition ($p<0.01$) (Figure 5.3).

Under the stiff knee soft tissue condition the initial peak in the AP displacement and the overall peak was significantly lower than the other two soft tissue conditions ($p<0.01$).

The stiff knee soft tissue condition also resulted in a significantly lower range of motion across the gait cycle compared to the other two soft tissue conditions ($p<0.01$).

There was no significant difference between the range of motion for the resected ACL and resected ACL & PCL soft tissue conditions ($p=0.27$). Although the resected ACL & PCL soft tissue condition resulted in a higher peak AP displacement the resected ACL soft tissue condition resulted in a lower minimum value at 70% gait, which may be why the range of motion was similar.

As the restraint of the soft tissue condition decreased the peak AP displacement increased, as well as the range of motion across the gait cycle. This was particularly apparent during the swing phase from 50% gait onwards where the AF was much lower.

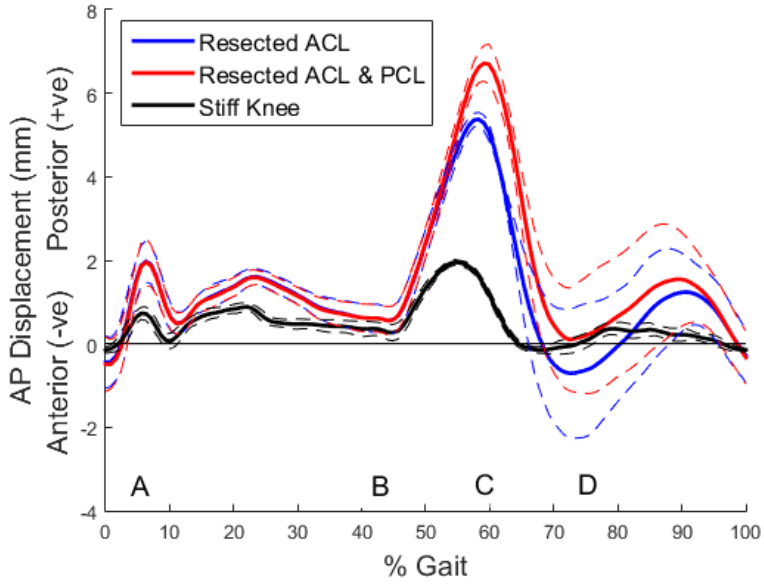

Figure 5.3: Mean AP displacement (mm) profiles with resected ACL, resected ACL & PCL and stiff knee soft tissue conditions with the 95% CI shown in dotted lines (n=6)

5.4.2.2 Tibial Rotation

There was no significant difference in the TR rotation between the resected ACL and resected ACL & PCL soft tissue conditions at any point in the cycle (Figure 5.4). As with the AP displacement for the first 50% of the cycle the output profiles were very similar, from 50% gait onwards the resected ACL & PCL soft tissue condition resulted in a higher TR rotation.

With the stiff knee soft tissue condition the TR rotation followed a similar shape, however had a significantly lower peak than the other soft tissue conditions ($p<0.03$).

The stiff knee soft tissue condition also resulted in a significantly lower range of motion across the gait cycle than the resected ACL soft tissue condition ($p=0.03$).

5.4.2.3 Abduction-Adduction Rotation

All three AA profiles followed a similar shape; there was a minima in the AA rotation just before 10% gait at around the same point in the gait cycle as the initial AP peak (Figure 5.5). The AA rotation then plateaued until around 50-60% gait. As the AP and TR displacements dropped from their peak values down to a minima at around 70% gait the AA rotation increased up to its peak value.

Up to 50% gait the resected ACL & PCL and stiff knee soft tissue conditions resulted in very similar AA rotation profiles. The resected ACL & PCL soft tissue condition followed a similar profile shape however it was around 1° offset towards adduction than the other AA profiles. The resected ACL & PCL soft tissue condition resulted in a significantly lower initial peak at the start of the gait cycle than the other soft tissue conditions ($p=0.01$). The resected ACL & PCL soft tissue condition also resulted in a significantly lower minima at point J

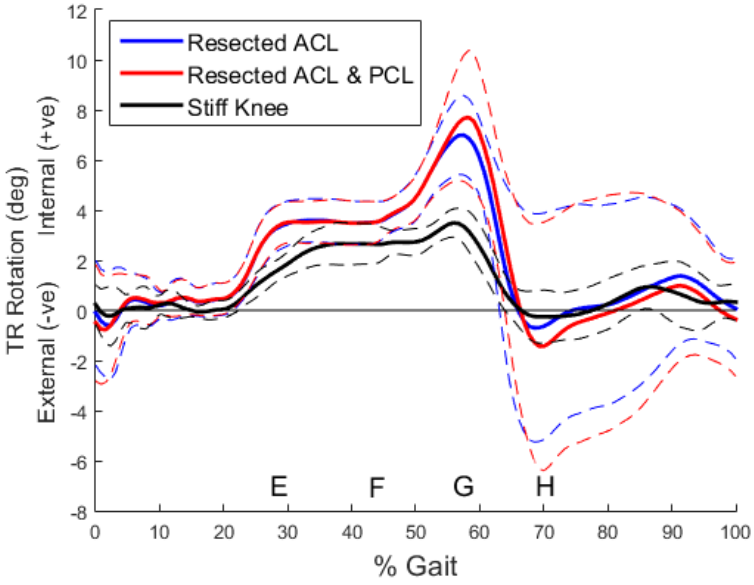

Figure 5.4: Mean TR rotation (°) profiles with resected ACL, resected ACL & PCL and stiff knee soft tissue conditions with the 95% CI shown in dotted lines (n=6)

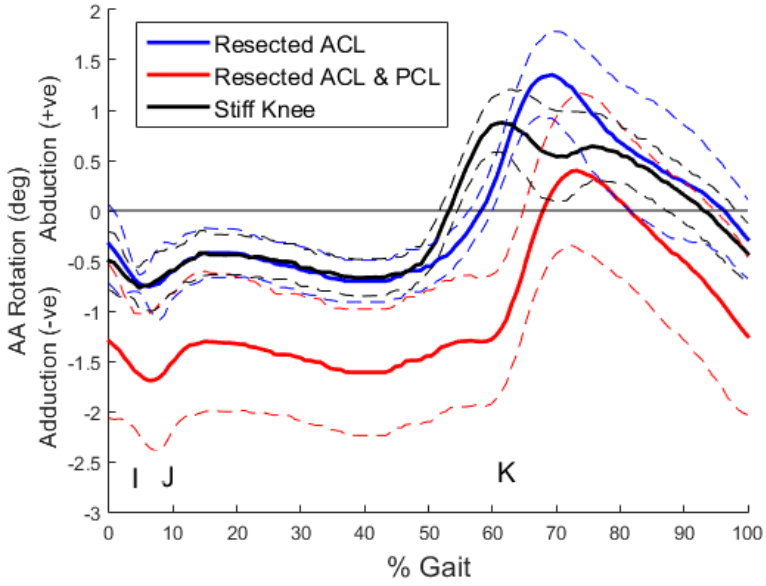

Figure 5.5: Mean AA rotation (°) profiles with resected ACL, resected ACL & PCL and stiff knee soft tissue conditions with the 95% CI shown in dotted lines (n=6)

compared to the resected ACL and stiff knee soft tissue conditions (p=0.03).

The stiff knee soft tissue condition reached the peak AA value earlier than the other two profiles, however it reached a lower peak value than the resected ACL soft tissue condition. The resected ACL & PCL soft tissue condition resulted in a significantly lower peak AA rotation than the resected ACL soft tissue condition (p=0.03).

There was no significant difference between any points I and J or J and K, or in the range of motion for any of the soft tissue conditions ($p>0.06$).

5.4.3 Effect on Contact Area

Figure 5.6 shows the contact areas for all the points measured for each soft tissue condition. All three soft tissue conditions resulted in a similar contact area pattern for the first half of the gait cycle. However the resected ACL & PCL soft tissue condition resulted in increased lateral loading.

At point 3 there was more variation; with the resected ACL & PCL soft tissue condition only resulting in lateral contact. The stiff knee soft tissue condition resulted in posterior motion of the medial contact which did not occur under the other soft tissue conditions.

At the end of the cycle the contact points had moved posteriorly from earlier in the cycle, with the resected ACL soft tissue condition only having a medial contact.

The resected ACL & PCL soft tissue condition also resulted in the most unbalanced contact with mainly lateral tibial loading. The resected ACL soft tissue condition resulted in some imbalance but with a higher contact area on the medial side rather than the lateral side. The stiff knee soft tissue condition resulted in both medial and lateral contact at all points measured.

The mean total contact areas on the tibia were found for each soft tissue condition at each point in the cycle (Figure 5.7).

At point 1 in the gait cycle the resected ACL & PCL soft tissue condition resulted in a significantly lower total contact area than the other two springs conditions ($p<0.01$).

At points 2 and 4 there was no significant difference in the total contact areas between the springs.

At point 3 in the cycle all the springs resulted in a significantly different total contact area, with the stiff knee having the highest and the resected ACL & PCL soft tissue condition the lowest areas ($p<0.01$).

5.4.4 Effect on Wear

Three wear studies were carried out each for 2MC with each of the three soft tissue conditions; resected ACL, resected ACL & PCL and the stiff knee soft tissue conditions.

5.4.4.1 Wear Rate

After 2MC the mean wear rates were $4.71\pm1.29 mm^3/MC$, $3.06\pm1.57\ mm^3/MC$ and $1.58\pm 1.20 mm^3/MC$ for the resected ACL, resected ACL & PCL and the stiff knee soft tissue conditions respectively (Figure 5.8). The wear with the stiff knee soft tissue condition was significantly lower than the resected ACL soft tissue condition ($p<0.01$). There was no significant difference between the wear rates for the resected ACL & PCL and resected ACL soft tissue conditions ($p=0.15$) or between the resected ACL & PCL and stiff knee soft tissue conditions

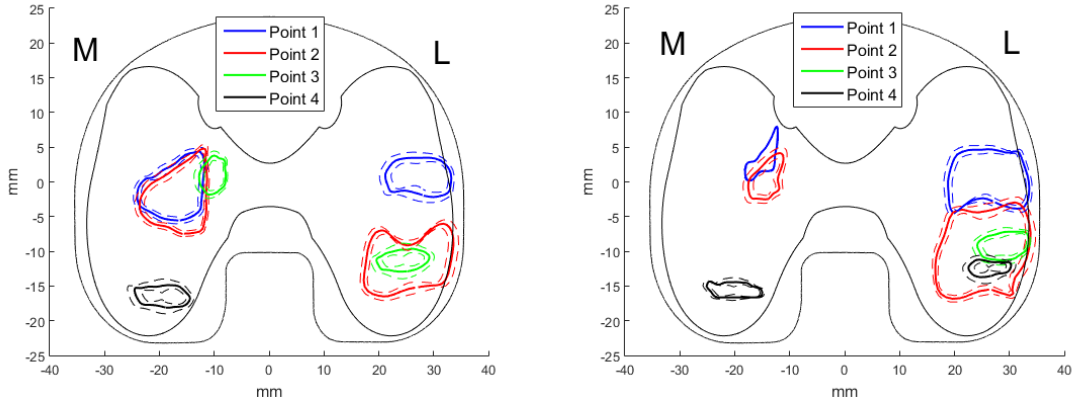

(a) Resected ACL

(b) Resected ACL and PCL

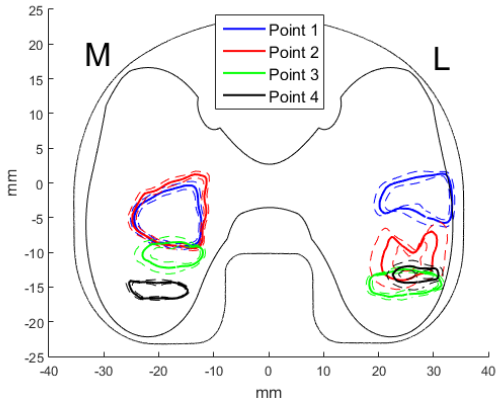

(c) Stiff Knee

Figure 5.6: Mean contact area and 95% confidence interval for each point in the cycle for each of the three soft tissue conditions

(p=0.15). However this may have been due to the increased variation in the kinematics with the resected ACL & PCL soft tissue condition; 3 stations that resulted in significantly higher displacements to the other 3 stations also resulted in significantly higher wear rates ($p<0.01$) with a mean of 5.2 mm^3/MC compared to 1.6mm^3/MC.

Under the resected ACL soft tissue condition the mean wear rate of the tibial inserts after 1MC was 5.3mm^3/MC and was 4.7mm^3/MC after 2MC. The wear rate of each station of the simulator is shown in Figure 5.9 (a). Each set of femoral and tibial components were moved to a different station in the simulator after every MC in order to reduce station variation.

Station 6 resulted in the highest wear rate after 1MC and 2MC with values of 6.5mm^3/MC and 6.9mm^3/MC respectively (Figure 5.9 (a)). After 1MC and 2MC the wear rate on station 2 was lower than all the other stations with a final value of 4.3mm^3/MC.

There was also some variation in the wear rates of the tibial inserts; tibials 4, 5 and 6, resulted in higher wear rates than the other three tibial inserts throughout the study (Figure 5.9 (b)). Two stations were run for slightly longer than the other four due to previous issues with them during the wear study. As with the tibial inserts three of the stations, stations 4, 5

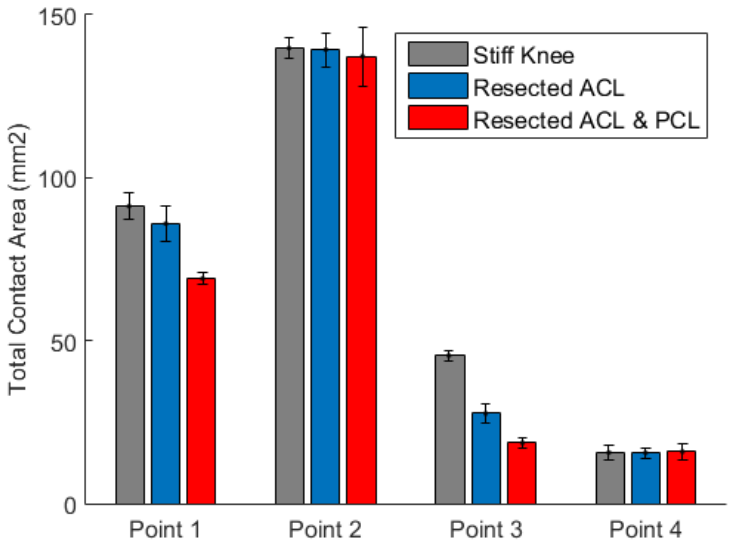

Figure 5.7: The mean contact area (mm2) with error bars showing the 95% CI (n=5) for mechanical alignment at each point in the cycle

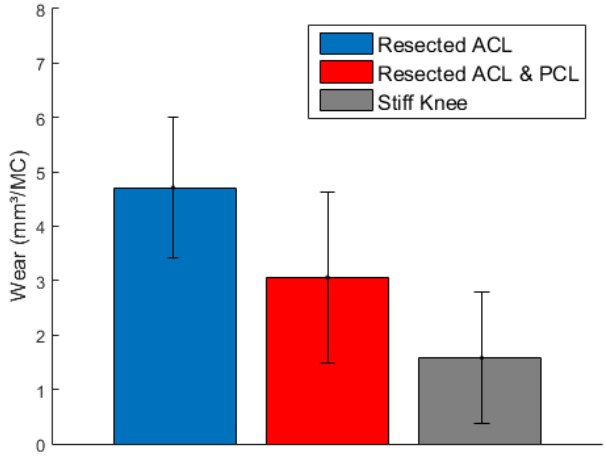

Figure 5.8: Mean wear rates over 2MC with the resected ACL, resected ACL & PCL and the stiff knee soft tissue conditions applied with the error bar showing the 95% CI

and 6, resulted in higher wear rates than the other 3 stations throughout the study. However there was less of a difference at 2MC between the stations than there was between the tibial insert wear rates.

Under the resected ACL & PCL soft tissue condition after 1MC three inserts resulted in higher wear rates than the other three; inserts 1, 4 and 5 (Figure 5.10 (b)).

After 2MC they still resulted in higher wear rates, however there was less of a difference due to a decrease in wear rate on these stations and an increase in wear rate on stations 2, 3 and 6. The mean wear rates across all the inserts were 3.4mm^3/MC and 3.1mm^3/MC after

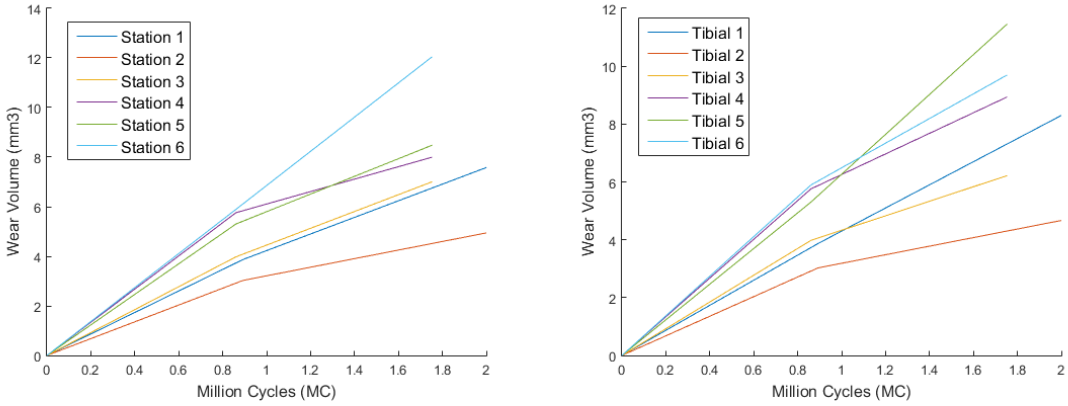

(a) Station Wear Volume (b) Tibial Insert Wear Volume

Figure 5.9: The wear volume (mm3) for each tibial insert and each station on the simulator over 1MC and over 2MC with the mechanical alignment and resected ACL soft tissue condition

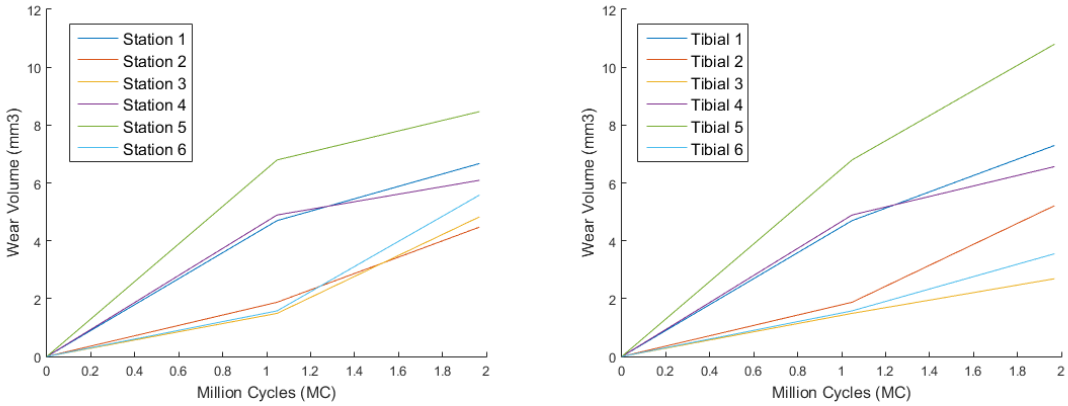

(a) Station Wear Volume (b) Tibial Insert Wear Volume

Figure 5.10: The wear volume (mm3) for each tibial insert and each station on the simulator over 1MC and over 2MC with the mechanical alignment and resected ACL & PCL soft tissue condition

1MC and 2MC respectively. The wear rate of each station of the simulator is shown in Figure 5.10 (a). Station 5 resulted in higher wear rates than all the other stations at 2MC, while stations 1, 4 and 5 resulted in higher wear rates than the other 3 stations after 1MC. The variation in wear rates found in this study was similar to that found under the resected ACL soft tissue condition.

On all the inserts that ran for the full study under the stiff knee soft tissue condition the wear volume was higher after 2MC than after 1MC (Figure 5.11). Station 4 was only run for the first MC in this study and could not be run for the second MC due to issues with the station. This difference in wear volume could be due to the formation of wear scars during the study. After 2MC insert 1 and insert 5 resulted in higher wear rates of 2.7mm^3/MC and 2.0mm^3/MC than the other inserts which resulted in values of around 1mm^3/MC.

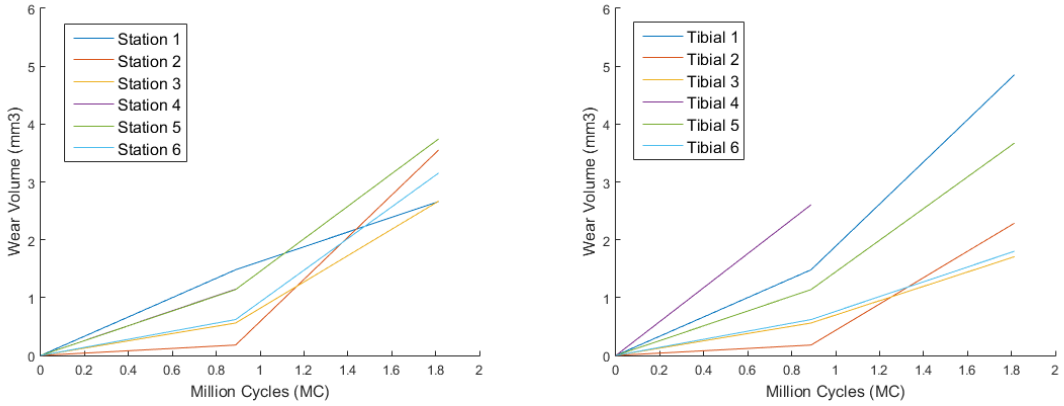

(a) Station Wear Volume

(b) Tibial Insert Wear Volume

Figure 5.11: The wear volume (mm3) for each tibial insert and each station on the simulator over 1MC and over 2MC with the mechanical alignment and stiff knee soft tissue condition

5.4.4.2 Kinematic Variation During Studies

Under the resected ACL soft tissue condition there were some significant differences in the ranges of motion however there was no distinct trend over time. The range of motion in the AP displacement was found to be significantly higher after 1MC compared to 0MC and 2MC ($p<0.01$). The range of motion increased from 5.1mm to 6.5mm then decreased to a value of 5.7mm during the study. The TR range of motion conversely was significantly higher at the start of the study with a value of 7.3° compared to 6.4° at 1MC and 6.0° and 2MC ($p<0.01$). There was no significant variation in the AA range of motion with values of 1.6°, 1.9° and 1.6° at 0MC, 1MC and 2MC respectively ($p=0.35$).

Under the resected ACL & PCL soft tissue condition there was no significant difference in the AP or TR ranges of motion during the wear study ($p=0.055$ and $p=0.38$). However the AA range of motion was significantly lower at 1MC, with a value of 0.8°, compared to at 0MC and 2MC with values of 1.1° and 1.0° respectively ($p<0.01$).

Under the stiff knee soft tissue condition there was no significant change in the AP range of motion during the wear study ($p=0.47$). However the range of motion of the TR rotation was significantly lower at 1MC with a value of 3.0° compared to 3.5° at 0MC and 3.3° at 2MC ($p<0.01$). The AA range of motion was significantly higher at 2MC with a value of 1.2° compared to 0.8° and 0.9° at 0MC and 1MC respectively ($p<0.01$). The differences in the range of motion during the wear study were small and did not follow an obvious trend.

5.4.4.3 Kinematic Variation Between Stations

Under the resected ACL soft tissue condition there was some kinematic variation between stations; station 1 resulted in a significantly higher AP, TR and AA range of motion than any of the other stations ($p<0.01$).

The correlation between the wear rate of each station and the range of motion in the AP, TR and AA displacement profiles was determined (Figure 5.12 (a)). There was found to be no positive correlation between the differences in kinematics and the differences in wear rates between stations. The same correlation was found between the ranges of motion and the wear rates for each tibial insert (Figure5.12 (b)). As with the stations there was no positive correlation between the two.

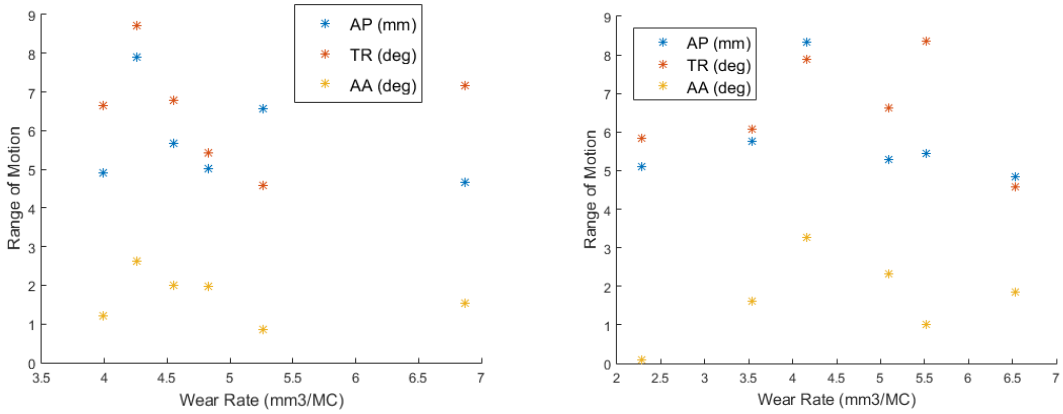

(a) Station Range of Motion vs Wear Rate (b) Tibial Insert Range of Motion vs Wear Rate

Figure 5.12: The correlation between the wear rate and range of motion under the resected ACL soft tissue condition for the stations (a) and the tibial inserts (b)

Under the resected ACL & PCL soft tissue condition three stations resulted in significantly different kinematics to the other three stations of the simulator. Stations 1, 2 and 3 all resulted in significantly higher and significantly different ranges of AP motion compared to the other stations and each other ($p<0.01$).

The correlation between the ranges of motion and the wear rates were determined (Figure 5.13).

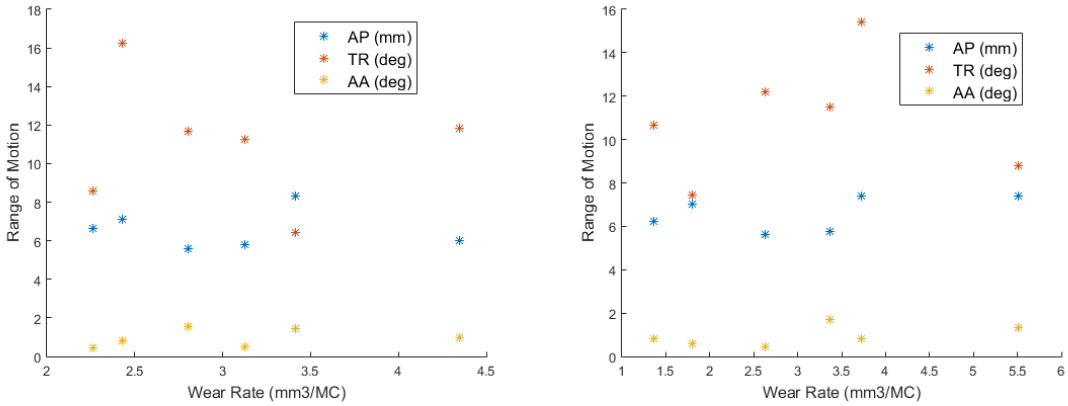

(a) Station Range of Motion vs Wear Rate (b) Tibial Insert Range of Motion vs Wear Rate

Figure 5.13: The correlation between the wear rate and range of motion under the resected ACL & PCL soft tissue condition for the stations (a) and the tibial inserts (b)

There was no positive correlation to show an increase in the wear rate along with an increase in any of the ranges of motion. The same lack of positive correlation was found between the ranges of motion and the wear rates for each tibial insert.

Under the stiff knee soft tissue condition three stations; stations 1, 2 and 5, resulted in significantly higher AP ranges of motion compared to the other three stations ($p<0.01$). There was more variation in the TR range of motion with stations 3 and 4 resulting in significantly higher values ($p<0.01$). Station 1 resulted in a significantly higher AA range of motion ($p<0.01$). However there was no positive correlation between the differences in wear rate and the differences in the ranges of motion between stations or between tibial inserts (Figure 5.14).

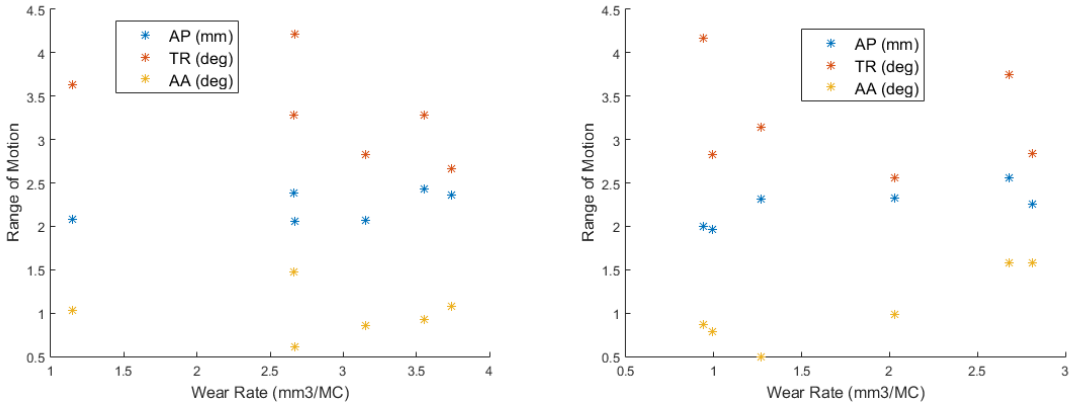

(a) Station Range of Motion vs Wear Rate (b) Tibial Insert Range of Motion vs Wear Rate

Figure 5.14: The correlation between the wear rate and range of motion under the stiff knee soft tissue condition for the stations (a) and the tibial inserts (b)

5.4.4.4 Running Temperature

During each wear study the bulk temperature of the serum in each station was measured in order to determine any differences in running temperature (Table 5.2). For each study the running temperatures across the stations and soak controls were similar with the station temperatures being within 0.3°c of each other and the soak controls being within 0.6°c of each other.

Table 5.2: Mean running temperature (°C) with the 95% CI across the simulator of the stations (n=6) and soak controls (n=2) during each wear study

Study	Station	Soak
Resected ACL	28.7±0.3	26.1±0.5
Resected ACL & PCL	29.0±0.4	26.7±0.4
Stiff Knee	28.7±0.3	26.5±0.6

During each study the station temperatures were higher than the soak controls by around 2°C, this was due to the friction and heat generated in each of the stations.

5.4.4.5 Surface roughness

The surface roughness of the femoral and tibial contact surfaces were measured at the start and end of each wear study. The same components were used for all three wear studies, the resected ACL study was carried out first, then the resected ACL & PCL wear study and finally the stiff knee soft tissue condition wear study. The roughness of the femoral components increased during the first study using the resected ACL soft tissue condition. The Ra value for the femoral components then remained stable at a value of 0.05µm. The opposite occurred with the tibial inserts; the Ra value of the tibial inserts decreased during each study by 0.04µm, 0.09µm and 0.01µm for the resected ACL, resected ACL & PCL and stiff knee soft tissue conditions respectively. However the 95% CI were all larger than the change in the mean Ra values therefore the differences in the Ra values were negligible.

Table 5.3: Mean surface roughness values (µm) (mean±95%CI, n=6) for the femoral and tibial components at the start and end of each wear study

Spring Condition	Femoral		Tibial	
	Start	End	Start	End
Resected ACL	0.023±0.002	0.051±0.002	0.470±0.184	0.427±0.168
Resected ACL & PCL	0.051±0.025	0.053±0.026	0.427±0.168	0.339±0.175
Stiff Knee	0.053±0.026	0.053±0.035	0.329±0.178	0.338±0.160

5.5 Validation of the Computational Model

The aim of this section was to validate the computational model by comparing the output kinematics and contact area to the experimental data in this chapter. The computational model was run using the same three soft tissue conditions as the experimental data; resected ACL, resected ACL & PCL and the stiff knee soft tissue conditions with the same AF, FE, TR and AP input profiles. The predicted computational results for each soft tissue condition were then compared to the experimental results from this study.

The output AP, TR and AA kinematics were compared between the computational and experimental data. The correlation between the experimental and computational values was then found. A correlation coefficient above 0.7 was deemed a good correlation between the two methods.

The contact area at the same four points in the cycle where the Tekscan measurements were carried out were also found (Figure 5.2). The tibiofemoral contact positions were compared between the experimental and computational data as well as the contact area values. A static computational model was also run under the experimental displacements at each point in the cycle measured with the Tekscan sensor. This was to verify whether any differences in the contact pressure results under the dynamic computational model were due to the differences in kinematics or due to the experimental data being measured statically.

5.5.1 Resected ACL

5.5.1.1 Kinematics

The output kinematics using the resected ACL soft tissue condition were determined and compared to the data collected using the experimental simulation. Figure 5.15 shows the output AP, TR and AA displacements for the computational model as well as the experimental results with 95% CI.

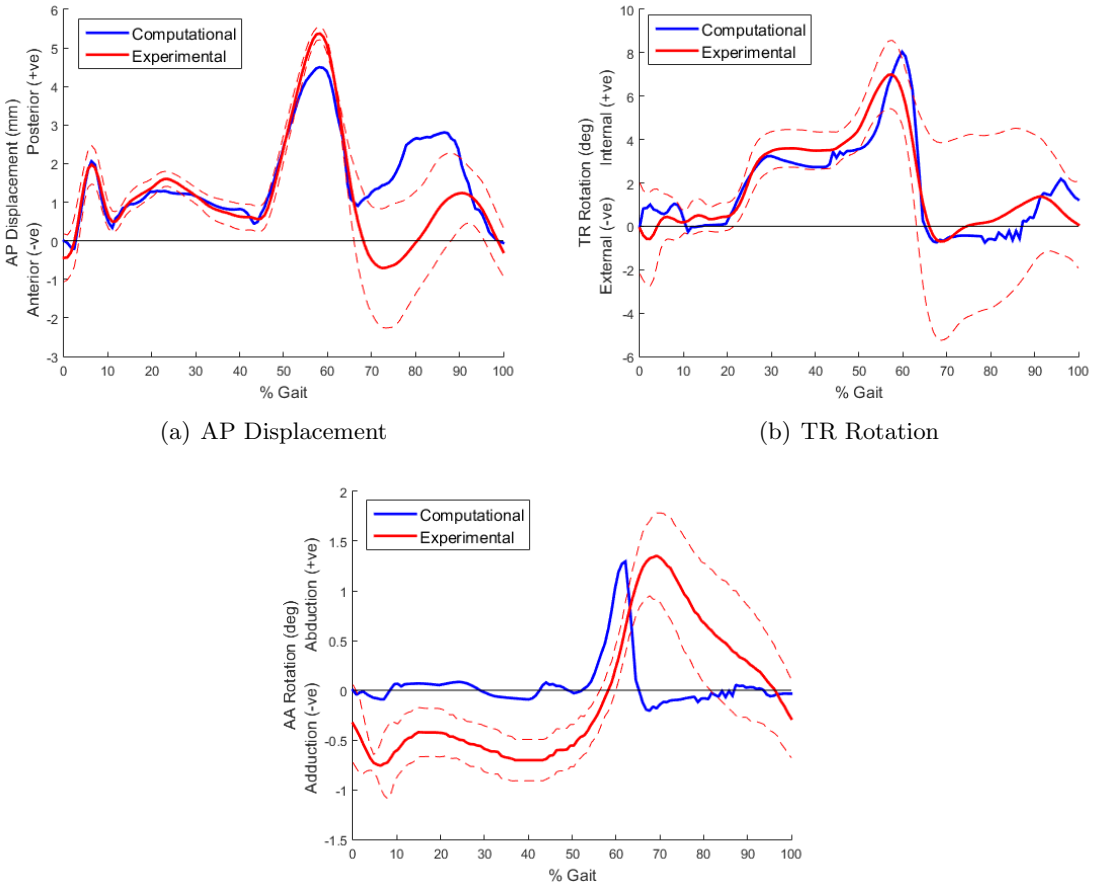

(a) AP Displacement

(b) TR Rotation

(c) AA Rotation

Figure 5.15: Output AP, TR and AA displacements under the resected ACL soft tissue condition from the computational model and from experimental study with a 95% CI shown in a dotted line (n=6)

The AP displacement profile from the computational model was similar to that from the experimental data; there was a peak before 10% gait then the highest peak at around 60% gait (Figure 5.15 (a)). The computational model resulted in a lower peak AP displacement compared to the experimental data. During the first half of the gait cycle the computational data was within the 95% CI of the experimental data. However between 50% and 60% gait the computational data was lower than the experimental data and outside of the 95% CI. Between 65% and 90% gait the computational data was higher than the 95% CI of the experimental

data.

The correlation between the experimental and computational AP displacements are shown in Figure 5.16 (a). Between 0-65% there was a strong linear correlation between the two methods with a gradient of 0.84, however the computational model resulted in lower AP displacements than the experimental methods. The data from 66-100% gait is shown in red, in this part of the gait cycle there was no trend between the two methods with the computational results being higher than the experimental data.

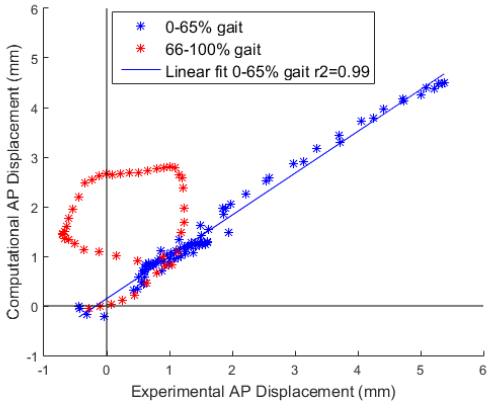

(a) AP Displacement gradient = 0.84

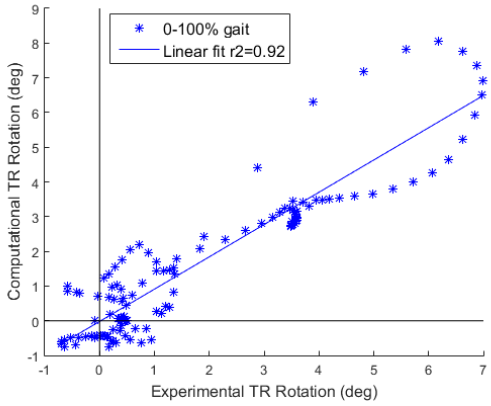

(b) TR Rotation gradient = 0.93

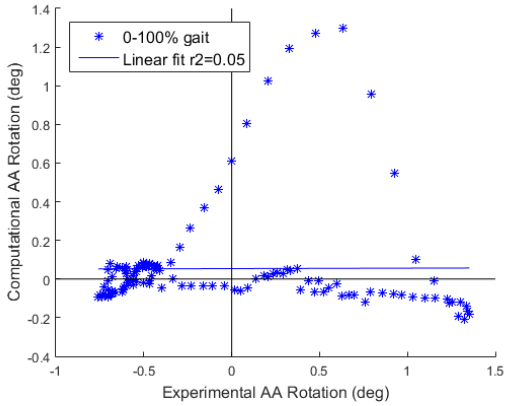

(c) AA Rotation gradient = 0.02

Figure 5.16: Correlation between the AP displacement (a), TR rotation (b) and AA rotation (c) values with the experimental and computational results with the resected ACL soft tissue condition

The computational prediction for the TR rotation was not as similar to the experimental data as the AP displacement, however it did follow a similar profile shape but with a lower displacement from 30-60% gait (Figure 5.15 (b)). The computational model resulted in a higher peak TR rotation than the experimental data. The computational prediction was within the 95% CI of the experimental data during most of the gait cycle. However at around 50% gait the computational data was lower than that from the experimental results as the peak TR rotation occurred later in the cycle. At around 60% gait the peak TR rotation with

the computational method was higher than the 95% CI of the experimental data.

The correlation between the experimental and computational TR rotations are shown in Figure 5.16 (b). A linear fit is shown on the data with a gradient of 0.93, showing there is a positive correlation that is close to 1 between the data. For TR values less than 4° the values are similar between the two methods. However with values of the TR rotation greater than that there was more variation. This shows the differences between the TR rotations between 50% and 65% gait.

The AA rotation from the computational mode resulted in lower AA rotation in the first half of the cycle compared to the experimental data (Figure 5.15 (c)). The AA rotation for the first half of the cycle was around 0° however it then increased at around 60% gait. The increase to the peak occurred slightly earlier in the cycle as the increase to the peak AA rotation in the experimental data. This difference may be a slight time delay in the experimental simulation due to the masses and friction of the simulator. The gradient of the increase in the AA rotation was similar between the two methods. However the computational AA rotation prediction was outside of the experimental 95% CI throughout most of the cycle.

The correlation between the experimental and computational AA rotations is shown in Figure 5.16 (c). As the experimental AA profile remained at around 0° for most of the gait cycle there was not a good agreement between the two profiles.

5.5.1.2 Contact Area

The contact areas in the computational model were found at the same points in the gait cycle that the measurements were taken experimentally under the resected ACL soft tissue condition (Figure 5.17).

At points 1, 2 and 3 the contact areas predicted computationally were similar in position to those found experimentally however the experimental methods resulted in the contact points occurring more laterally.

However at point 4 there was a difference between the computational and experimental measurements; the experimental data only showed contact on the medial condyle however the computational data showed contact on both the medial and lateral condyles. The computational contact areas at this point were also more posterior than those measured experimentally and were approximately equal in size on the medial and lateral condyles.

The measured contact area at each point in the cycle using the computational and experimental methods are shown in Table 5.4.

At each point in the cycle the computational model predicted a higher contact area than the experimental methods. However the values of the contact area followed a similar trend; the highest was found at point 2 in the cycle and the lowest at point 4 by both methods. Differences in the contact area may be due to differences in the kinematics and the loading. For example at point 4 in the cycle the experimental methods resulted in just medial contact while the computational methods resulted in both medial and lateral contact. In order to investigate this a static computational model was run under the experimental displacements.

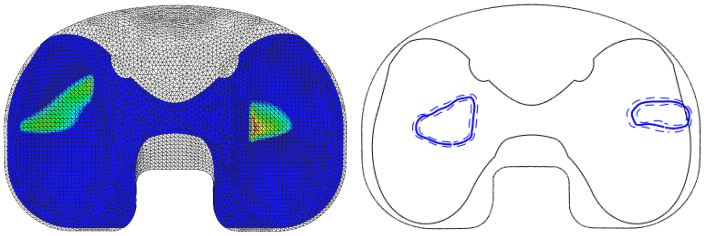

(a) Point 1

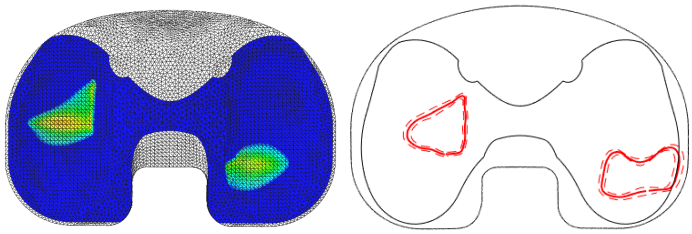

(b) Point 2

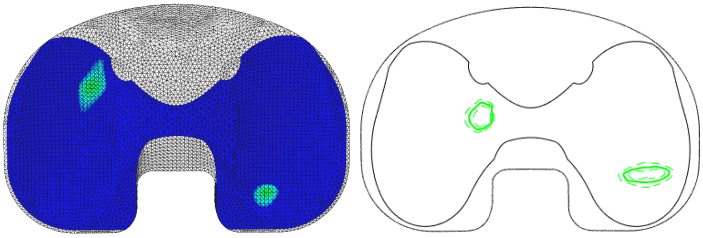

(c) Point 3

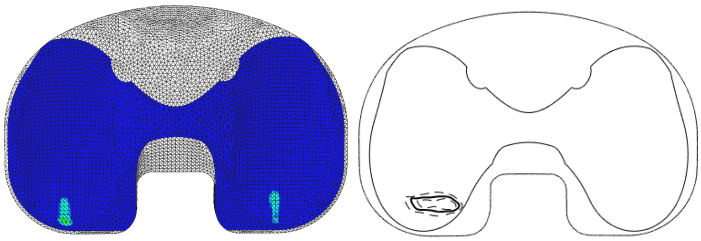

(d) Point 4

Figure 5.17: Contact pressures predicted by the computational model and experimental data under the resected ACL soft tissue condition with the pressure ranging from 0MPa (blue) to 25MPa (red) with the medial side on the left and lateral on the right

Table 5.4: Contact area (mm^2) at each point in the cycle under the resected ACL soft tissue condition using the computational and experimental (mean±95%CI) methods

Point	Experimental	Computational
1	85.9±5.3	168.9
2	139.3±5.2	226.0
3	27.7±3.1	82.6
4	15.6±1.6	26.1

5.5.1.3 Static Computational Model under the Experimental Output Displacements

In order to verify whether the differences between the computational and experimental contact pressure results were due to the differences in the output kinematics or due to the static measurement of the experimental data the contact pressure measurements were found using a static computational model and the experimental displacements.

The same static model was used as for the mesh convergence detailed in the Chapter 3. The experimental displacements under the resected ACL soft tissue condition were applied to the femoral and tibial components and the required axial load was applied to the femoral centre of rotation.

At points 1 and 2 in the cycle the contact points were similar between the dynamic model and the experimental data (Figure 5.18 (a) and (b)). At these points the static computational model resulted in just lateral contact. At point 2 in the cycle the static computational model resulted in a higher contact area on the lateral tibial condyle rather than on the medial condyle, as found in the dynamic model. The larger lateral contact area found under the static model is similar to the lateral contact area found using the experimental methods.

The difference between the two computational models may be due to the difference in AA rotation at this point. The experimental data resulted in contact on both condyles, this could be due to multiple factors including that the thickness of the pressure sensor was not included in the computational model. Therefore the experimental methods may have resulted in medial contact when the static computational model did not.

At point 3 in the cycle the dynamic computational model and the experimental data resulted in contact on the medial and lateral tibial condyles (Figure 5.18 (c)). The static computational model however resulted in just lateral contact, but this contact area was more similar in shape to the experimental data than the dynamic model.

At point 4 in the cycle the static computational model and the experimental results both resulted in just medial contact, while the dynamic model resulted in both medial and lateral contact (Figure 5.18 (d)).

The total contact area at each point in the cycle with the experimental, dynamic and static computational models were found (Table 5.5).

Table 5.5: The total contact area (mm^2) found under the resected ACL soft tissue condition using experimental (mean±95%CI, n=5) and two computational methods; a static and a dynamic model

Point	Experimental	Computational	
		Dynamic	Static
1	85.9±5.3	168.9	101.7
2	139.3±5.2	226.0	200.3
3	27.7±3.1	82.6	36.7
4	15.6±1.6	26.1	14.4

The computational models resulted in higher contact areas at points 1-3 in the cycle than

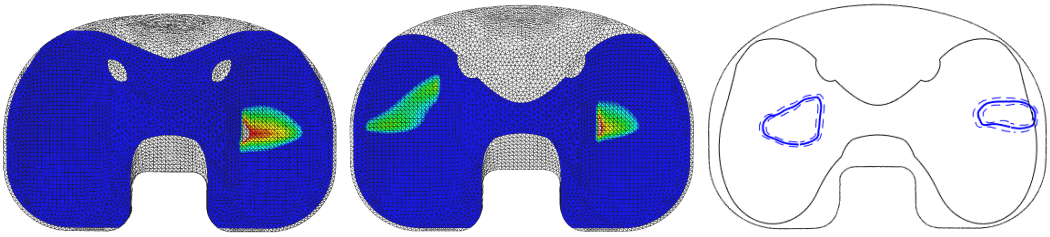

(a) Point 1

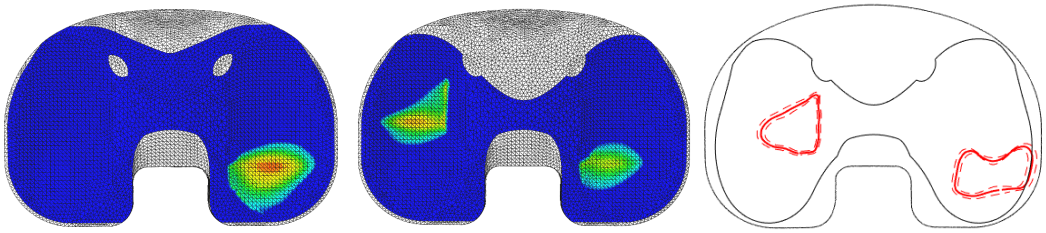

(b) Point 2

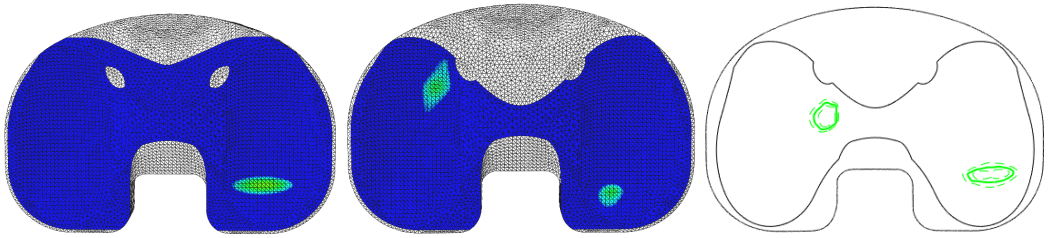

(c) Point 3

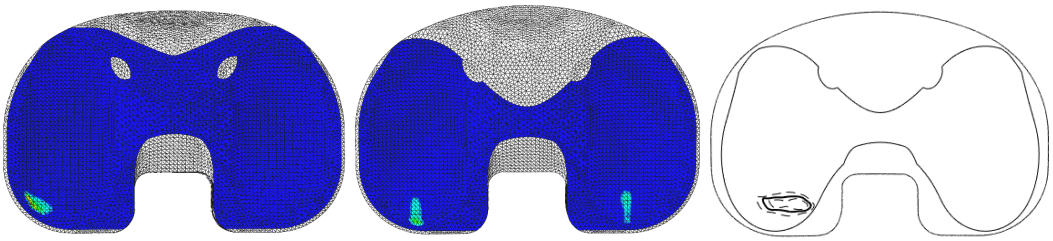

(d) Point 4

Figure 5.18: Contact pressures predicted by the static (left) and dynamic (centre) computational models and experimental data (right) under the resected ACL soft tissue condition with the pressure ranging from 0MPa (blue) to 25MPa (red) with the medial side on the left and lateral on the right

the experimental data. However the static model resulted in closer values to the experimental methods than the dynamic model. This shows that the differences between the dynamic computational model and the experimental methods may be partly due to the differences in kinematics and due to the static experimental measurements.

5.5.2 Resected ACL & PCL

5.5.2.1 Kinematics

During the first 50% gait the computational prediction for the AP displacement was mostly within the bounds of the 95% CI of the experimental data (Figure 5.19).

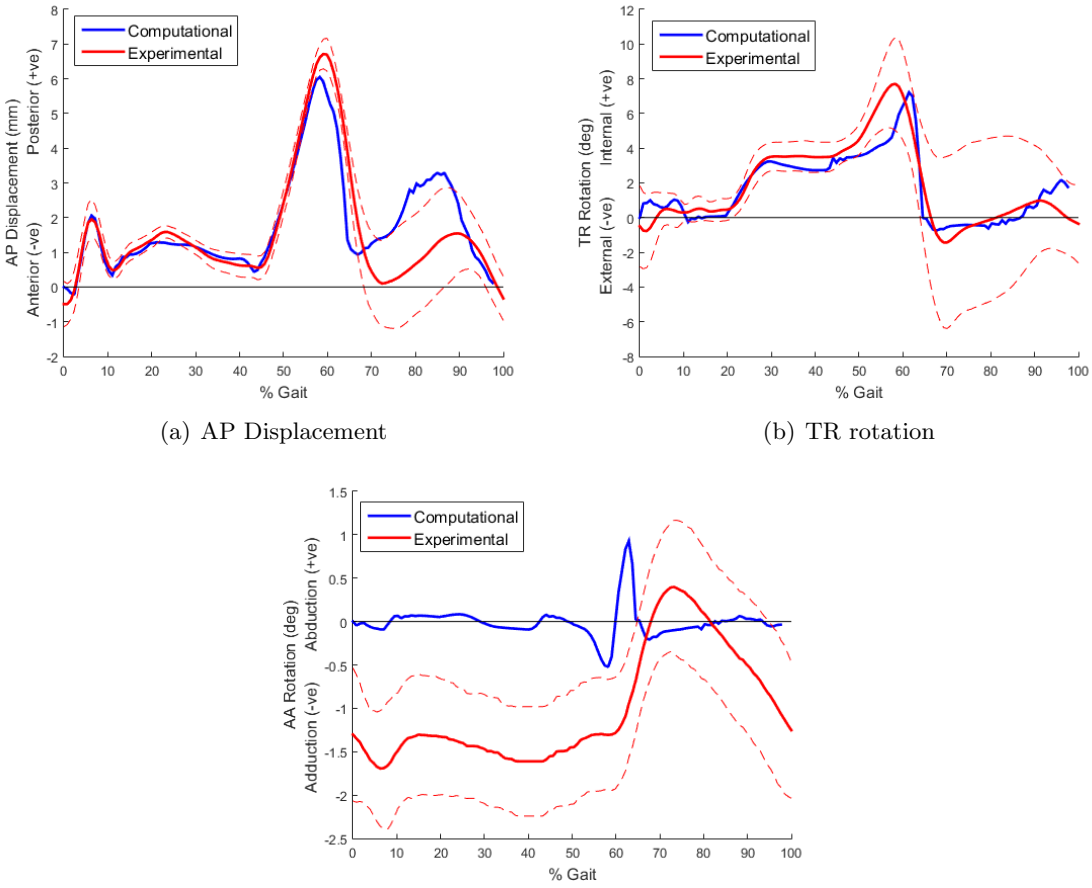

(a) AP Displacement

(b) TR rotation

(c) AA rotation

Figure 5.19: Output AP, TR and AA displacements under the resected ACL & PCL soft tissue condition for the computational and experimental methods with the 95% CI shown with a dotted line (n=6)

From 50-65% gait the computational prediction was lower than the experimental data, resulting in a lower peak AP displacement with the computational prediction. During the last section of the gait cycle the computational prediction was higher than that of the experimental data and was outside the bounds of the 95% CI for around 75-90% gait.

There was a good correlation between the computational and experimental results for the AP displacement value however the linear fit had a gradient of 0.7 and it did not pass through the origin (Figure 5.20 (a)).

This shows that the computational prediction was higher than the experimental data at low AP values and lower than the experimental data at high AP displacement values. The last

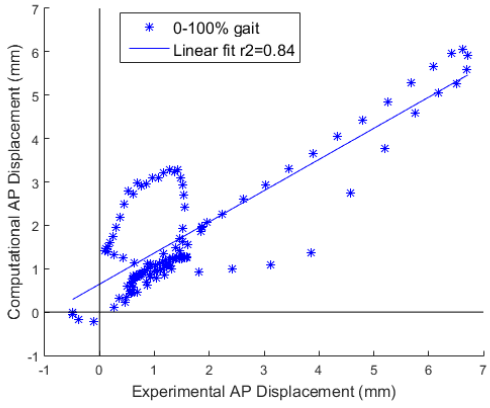

(a) AP Displacement gradient = 0.72

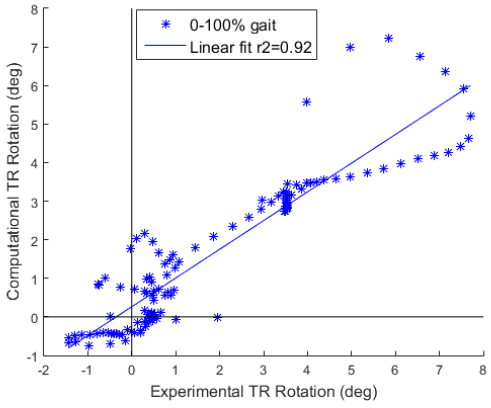

(b) TR rotation gradient = 0.74

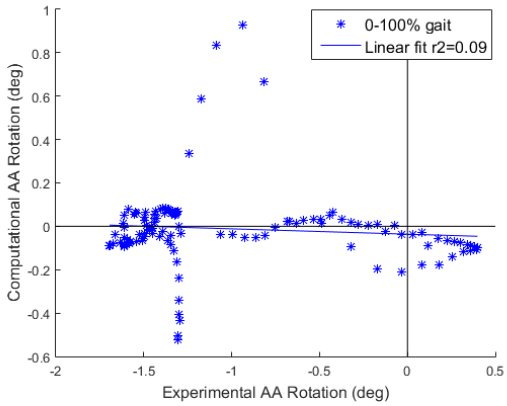

(c) AA rotation gradient = -0.02

Figure 5.20: Correlation between the AP displacement (a), TR rotation (b) and AA rotation (c) values with the experimental and computational results with the under the resected ACL & PCL soft tissue condition.

part of the gait cycle, where the computational prediction was higher than the experimental results shows as the circle of points above the linear fit.

There was more of a difference in the shape of the TR rotation profiles; the computational data resulted in lower values of TR rotation between 30% and 60% gait. The peak TR rotation also occurred later in the cycle in the computational data compared to the experimental data. However for nearly all of the gait cycle the computational prediction was within the bounds of the experimental data 95% CI.

There was some correlation between the experimental and computational results for the TR profile however at high TR rotation values there were some differences (Figure 5.20 (b)). The gradient of the linear fit was 0.74 showing there was a good agreement between the two data sets, however the computational prediction was lower than the experimental data. This was most obvious between 30% and 60% gait when the TR rotation values were highest.

As with the other soft tissue conditions the largest difference in the profiles occurred with the AA rotation. The computational data resulted in lower displacement values for the first

half of the gait cycle and resulted in the peak AA rotation occurring earlier in the cycle. For nearly all of the profile the computational prediction was not within the 95% CI of the experimental data.

There was poor correlation between the computational and experimental AA rotations with the linear fit having a gradient of -0.02 (Figure 5.20 (c)). This was similar to the other soft tissue conditions as the computational prediction of the AA rotation stayed around 0° for most of the cycle.

5.5.2.2 Contact Area

The contact areas were found using the computational model at the same points in the gait cycle that the contact area was found experimentally (Figure 5.21).

At points 1, 2 and 3 in the cycle the experimental data mostly resulted in contact on the lateral tibial condyle whereas the computational data resulted in more medial contact (Figure 5.21). Again this difference in the medial and tibial loading may be due to the differences in the AA rotation. The experimental lateral contact was also larger than that found computationally.

At point 4 in the gait cycle the computational model resulted in medial and lateral contacts of similar size on the posterior edge of the tibial insert. The experimental data resulted in a larger medial contact area that was more posterior than the lateral contact. Both the experimental contacts were more anterior than those found computationally.

The contact area at each point in the cycle was determined using both the experimental and computational methods (Table 5.6). As with the resected ACL soft tissue condition the computational model under the resected ACL & PCL soft tissue condition resulted in higher contact area values compared to the experimental methods. However the values of the contact areas followed a similar trend with the peak value occurring at point 2 in the cycle.

Table 5.6: Contact area (mm^2) at each point in the cycle under the resected ACL & PCL soft tissue condition using the computational and experimental (mean±95%CI) methods

Point	Experimental	Computational
1	69.1±1.7	168.9
2	137.3±9.0	227.6
3	18.6±1.5	78.4
4	15.9±2.4	26.1

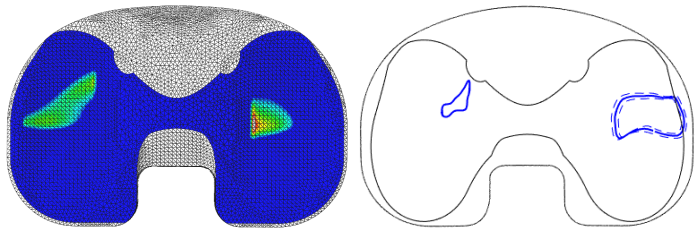

(a) Point 1

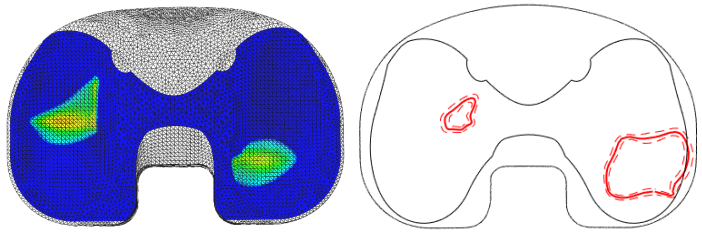

(b) Point 2

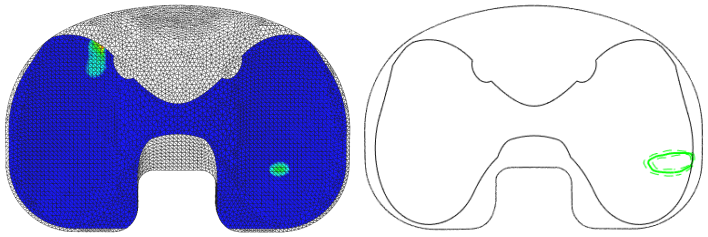

(c) Point 3

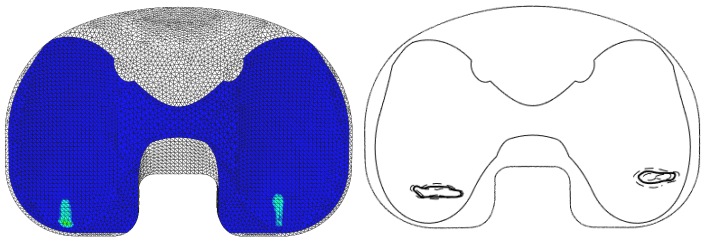

(d) Point 4

Figure 5.21: Pressure maps found using the computational model (left) and experimentally (right) under the resected ACL & PCL soft tissue condition ranging from 0MPa (blue) to 25MPa (red) with the medial side on the left and lateral on the right

5.5.3 Stiff Knee

5.5.3.1 Kinematics

Under the stiff knee soft tissue condition the kinematics for the AP and TR displacements were very similar between the computational and experimental results (Figure 5.22). For most of the cycle the computational prediction for the AP displacement was within the 95% CI of the experimental data. However the computational results resulted in a higher peak AP displacement of 2.3mm compared to 2.0m with the experimental methods.

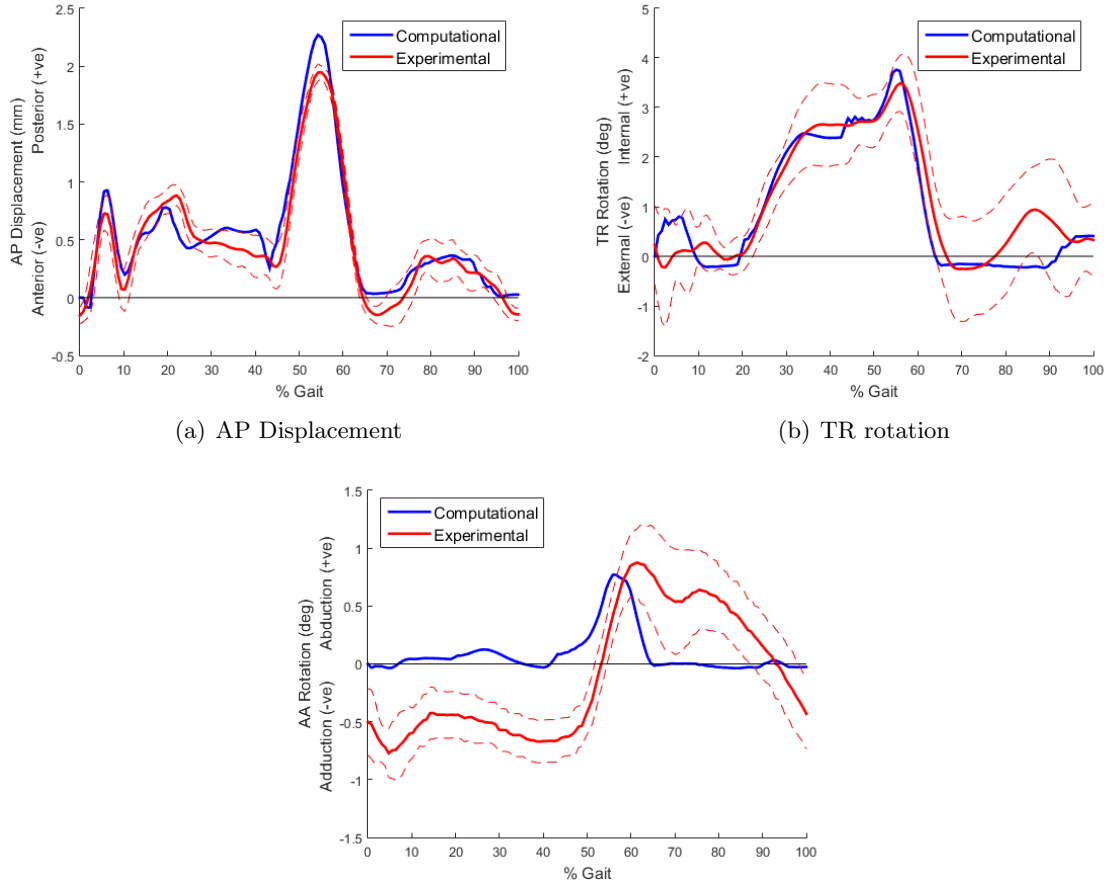

(a) AP Displacement

(b) TR rotation

(c) AA Displacement

Figure 5.22: Output AP, TR and AA displacements under the stiff knee soft tissue condition for the computational and experimental methods with the 95% CI shown with a dotted line (n=6)

There was a strong correlation between the AP displacement values of the two data sets, a linear fit was applied with a gradient of 1.01 and an r squared value of 0.97 showing the strong agreement between them (Figure 5.23 (a)).

The computational prediction of the TR rotation profile was also similar to the experimental data with the computational prediction being within the 95% CI for nearly all of the cycle.

The correlation between the computational and experimental results for the TR rotation was not as strong as with the AP displacement, however there was good agreement (Figure 5.23 (b)). The linear fit resulted in a gradient of 0.99 and the r squared value was 0.94. With the TR rotation values near 0° there was the most difference between the results, however these points in the gait cycle were the ones with the highest variation (Figure 5.22).

There was more of a difference in the output AA rotations between the experimental and computational data, with the computational data having lower displacement during the first half of the cycle. As with the resected ACL soft tissue condition the computational prediction

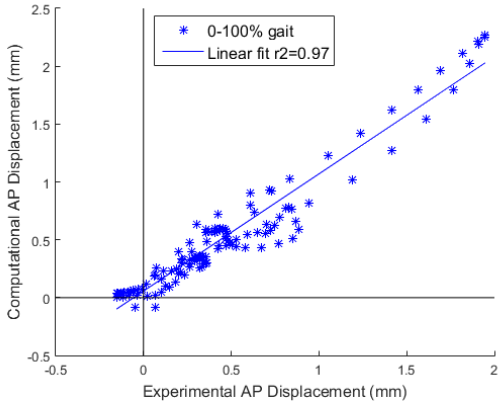

(a) AP Displacement gradient = 1.01

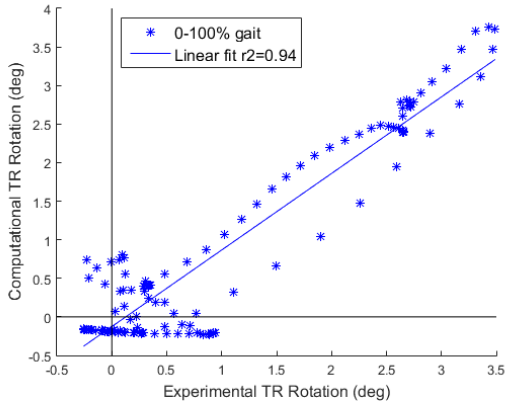

(b) TR rotation gradient = 0.99

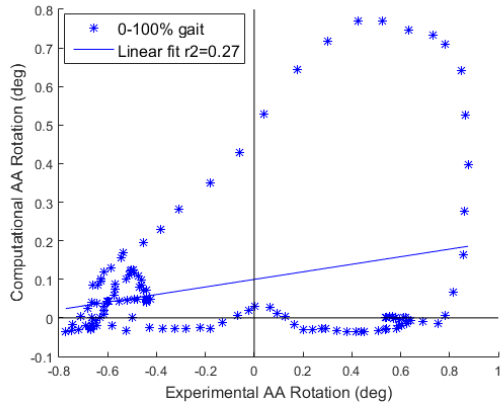

(c) AA rotation gradient = 0.1

Figure 5.23: Correlation between the AP displacement (a), TR rotation (b) and AA rotation (c) values with the experimental and computational results with the stiff knee soft tissue condition

for the AA rotation was not within the 95% CI of the experimental data for nearly all of the cycle.

The computational data resulted in abduction throughout the cycle where as the experimental data resulted in adduction during the first 50% gait. In the second half of the cycle the trend of the two output profiles was more similar with the peak AA rotation resulting at around 60% gait. However the experimental data resulted in higher abduction and adduction displacements, with a higher peak AA rotation of 0.9° compared to 0.8°.

There was not a strong correlation between the AA rotations in the experimental and computational results (Figure 5.23 (c)). There was also no systematic error or constant offset between the two data sets.

5.5.3.2 Contact Area

With the stiff knee soft tissue condition the femorotibial contact point was in a similar position in the computational data as it was using the Tekscan sensor (Figure 5.24).

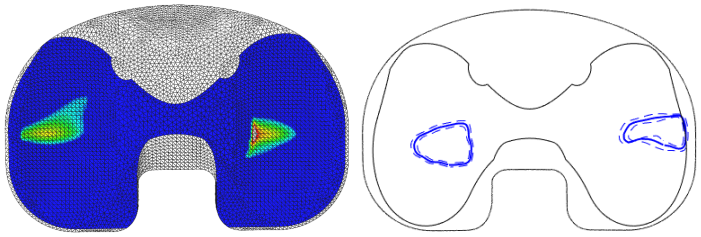

(a) Point 1

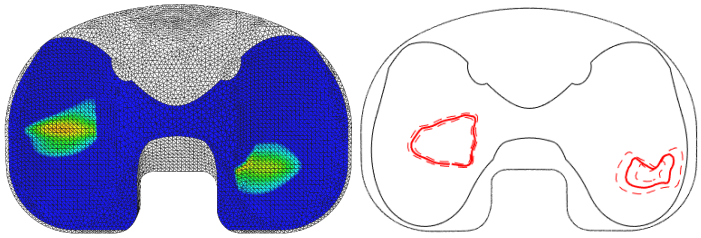

(b) Point 2

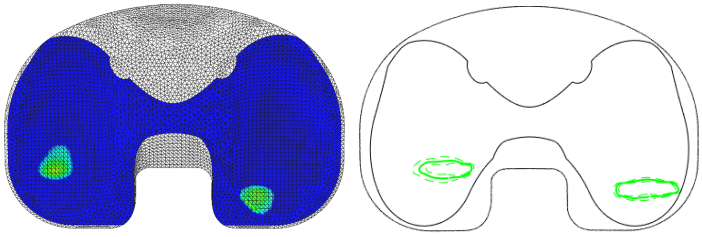

(c) Point 3

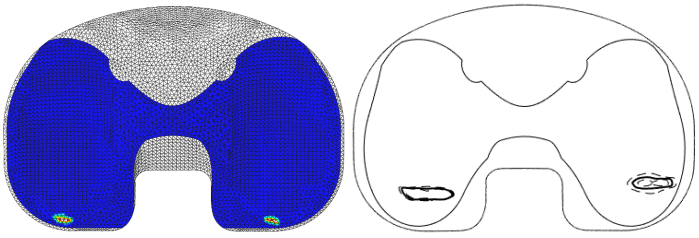

(d) Point 4

Figure 5.24: Contact areas found using the computational model (left) and experimentally (right) under the stiff knee soft tissue condition ranging from 0MPa (blue) to 25MPa (red) with the medial side on the left and lateral on the right

However at point 4 in the cycle the computational data predicted that the contact would occur more posteriorly, on the edge of the tibial insert. This did not occur when using the Tekscan sensor.

There were also some differences in the position of the contact points with the computational model resulting in more posterior lateral contact.

At point 1 in the cycle the computational data resulted in the medial and lateral contacts being in similar positions to each other while the experimental data resulted in a more anterior lateral contact. At this point the computational data resulted in higher internal TR, which

would result in a more posterior lateral contact (Figure 5.19).

At points 2 and 3 the experimental data resulted in the contact points being similar in position while the computational data resulted in a more posterior lateral contact. However the computational model resulted in lower internal tibial rotation than the experimental data at these points than the experimental data.

5.6 Computational Results

The computational model was then used to compare the output kinematics between the soft tissue conditions to determine any differences that may not have occurred in the experimental results due to limitations of the experimental simulation. For example without the limitation of the internal friction and the weight of the AA arm.

The output contact area and peak contact pressures from the computational model were compared between the soft tissue conditions. The contact area was calculated throughout the gait cycle, while the peak pressure values were found at the same four points in the gait cycle where the experimental Tekscan measurements were carried out.

5.6.1 Kinematics

The output AP, TR and AA displacement profiles from the computational model under each of the three soft tissue conditions are shown in Figure 5.25.

The difference in the AP displacement profiles between the soft tissue conditions was similar to that found under the experimental methods (Figure 5.25 (a)). The stiff knee soft tissue condition resulted in much lower AP displacements, while there was less of a difference between the resected ACL and resected ACL & PCL soft tissue conditions. However in the computational results the difference between the AP displacement profiles with the resected ACL and resected ACL & PCL soft tissue conditions occurred with AP displacement values greater than 2.5mm. This was the size of the AP spring gap for both of the soft tissue conditions and therefore was when the springs began to be applied. In the experimental results the difference between the two AP displacement profiles began at a similar point but continued for the rest of the gait cycle.

As with the AP displacement the differences in the TR rotation profiles were similar to those found experimentally (Figure5.25 (b)). The stiff knee soft tissue condition resulted in much lower rotations while the difference between the resected ACL and resected ACL & PCL profiles began at around 50% gait. This is the point in the cycle where the AF began to decrease and where the differences in the AP profiles began. However in the computational results the differences in the two TR profiles only occurred from 50% to 65% gait.

The greatest difference between the computational and experimental results occurred in the AA rotation profiles. The differences in comparison with the experimental data may be due to the weight of the AA arm in the experimental simulator. The stiff knee and resected ACL soft tissue conditions only resulted in abduction during the gait cycle (Figure 5.25 (c)).

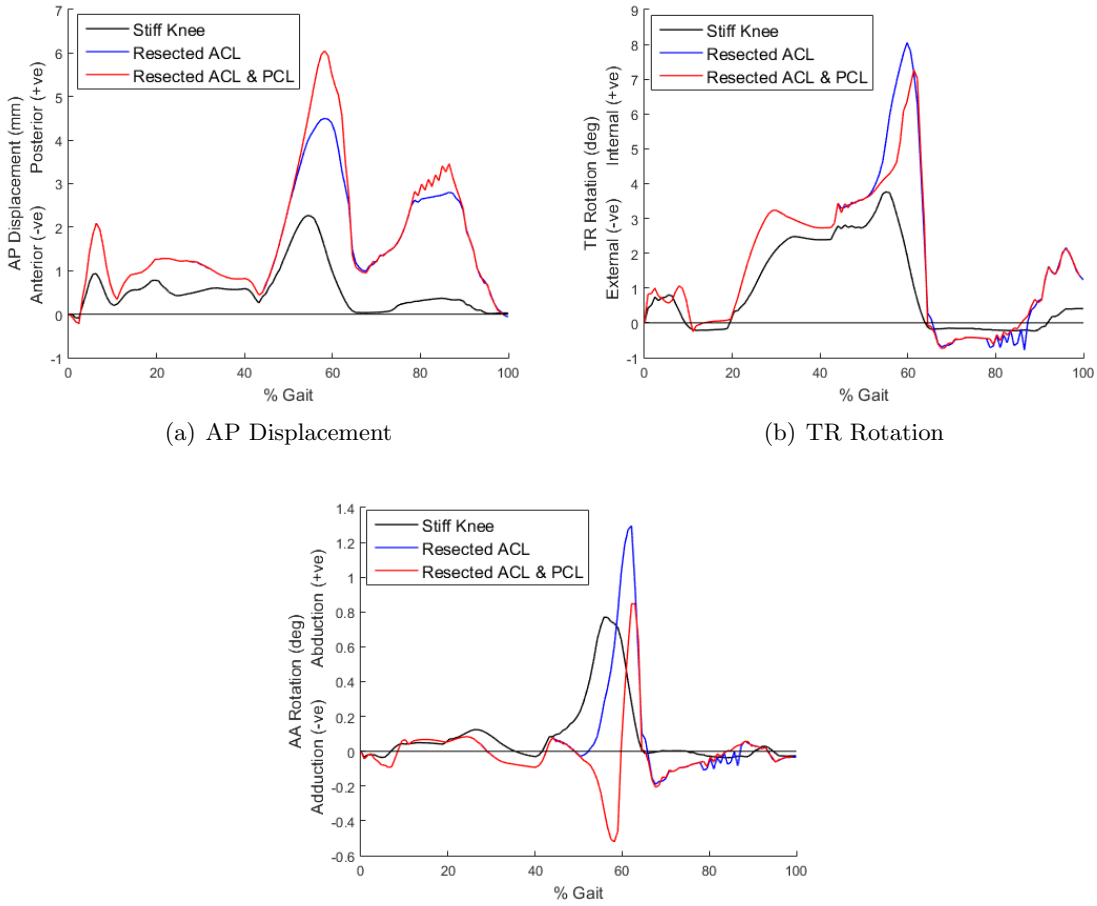

(a) AP Displacement

(b) TR Rotation

(c) AA Rotation

Figure 5.25: The output AP (a), TR (b) and AA (c) displacements under the stiff knee, resected ACL and resected ACL & PCL soft tissue conditions using the computational model

The resected ACL soft tissue condition resulted in a higher peak AA displacement. While the resected ACL & PCL soft tissue condition was the only one to result in both adduction and abduction.

5.6.2 Contact Area

The contact area was determined for all three soft tissue conditions throughout the gait cycle (Figure 5.26). The values of the contact area were very similar between the three soft tissue conditions throughout the gait cycle.

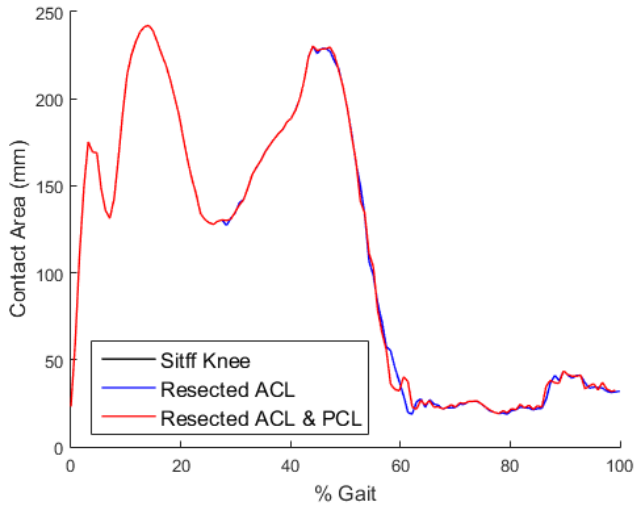

Figure 5.26: The contact area (mm^2) under the stiff knee, resected ACL and resected ACL & PCL soft tissue conditions using the computational model

5.6.3 Peak Contact Pressure

The peak contact pressure was determined for each of the three soft tissue conditions at four points in the gait cycle (Table 5.7). The four points were the same points where the Tekscan measurements were taken in the experimental study. The resected ACL and resected ACL & PCL soft tissue conditions resulted in the same peak pressure values at points 1, 2 and 4 in the cycle. This may be due to the similarities in the kinematics at these points. The stiff knee soft tissue condition resulted in the highest peak pressure at all the measured points compared to the other two soft tissue conditions. At point 3 in the cycle the stiff knee soft tissue condition resulted in the highest peak pressure and the resected ACL & PCL soft tissue condition the lowest. However the differences in the peak pressure values were small at points 1-3 in the cycle; the stiff knee soft tissue condition only resulted in a higher value by up to 3MPa. At point 4 in the cycle there was the greatest difference with the stiff knee soft tissue condition resulting in a value of 23MPa compared to 12.2MPa with the other two soft tissue conditions.

Table 5.7: The peak contact pressure (MPa) under the stiff knee, resected ACL and resected ACL & PCL soft tissue conditions using the computational model at each of the four points in the gait cycle

Point	Stiff Knee	Resected ACL	Resected ACL & PCL
1	29.1	27.4	27.4
2	20.0	19.7	19.7
3	16.3	15.6	13.0
4	23.0	12.2	12.2

5.7 Discussion

This study investigated the effect of soft tissue constraints on the output kinematics, contact pressure and wear of a TKR under mechanical alignment. Three soft tissue conditions were defined in order to represent a knee with a resected ACL, a resected ACL & PCL and a stiff knee. The resected ACL and resected ACL & PCL soft tissue conditions were the ISO standard spring profiles for a CR and a CS TKR respectively [186]. Both soft tissue conditions included a gap around the zero position in order to replicate the non linear behaviour of the soft tissues in vivo. The stiff knee condition meanwhile was based on clinical data in order to represent a patient with a stiffer than average knee. This soft tissue condition did not include the gaps around the zero position in order to replicate a join with no laxity. The definition of all three soft tissue conditions were defined in order to represent the range of conditions that are found in vivo.

The representation of the soft tissues within the knee however is difficult due to a number of factors including the variation between patients and the issues with measurement of the soft tissues while they are in vivo without causing damage. Therefore the validity or appropriateness of the soft tissue conditions are difficult to determine. As the TKR used in this study was a CR TKR the resected ACL soft tissue condition should be the most representative of patients with this TKR. However there may be patients where damage to the soft tissues within the knee may occur during or after surgery, in this case the resected ACL & PCL soft tissue condition may be more representative. Conversely patients with a painful knee for a long period of time may have less laxity of the knee due to the soft tissues becoming tighter. A lack of soft tissue release during surgery or the use of a tibial insert which was too thick for the joint space may also result in a stiff knee. This soft tissue condition may be the least likely to occur out of the three conditions in this study, however it provides an insight into the effects of high tension soft tissue conditions.

5.7.1 Computational Model Validation

The influence of the soft tissue conditions was investigated using both experimental and computational methods. The computational kinematics and contact area were validated against the experimental data under all three soft tissue conditions. The AP and TR displacements were found to have good correlations between the two methods for all the soft tissue conditions. However there was more variation in the AA rotation with poor correlations under all the soft tissue conditions. There were some similarities between the AA rotation profiles with the increase towards to the peak AA rotation occurring with similar gradients and with only a short delay between the computational and experimental methods. There were also similarities in the contact area and position between the two methods. There were some differences in the loading patterns however the static computational model resulted in closer contact positions and contact areas than the dynamic model. This implies that the differences in the contact area between the computational model and the experimental methods may be

due to the static measurement under the experimental methods or due to the differences in the kinematics.

There are many reasons why there may be differences between the computational and experimental results. For example the computational model does not include any internal friction or mass that may occur in the simulator. The only masses included in the system are those from the tibial and femoral components. However in the simulator the mass of the tibial fixture, the friction in the AP bearing system and the mass of the AA arm will have affected the motion. The AA arm in particular had a large mass and may be the reason there was such a difference between the experimental and computational AA rotations.

There may also be some differences in the relative positioning of the femoral and tibial components as the tibial component is cemented into place by hand relative to the femoral component for experimental simulation. In the simulator there may have been some variations in this positioning between the stations and therefore the femoral may not have been perfectly aligned with the tibial dwell point each time. This may be why there were some differences between the computational and experimental data in terms of the positioning of the contact point.

The contact area data from the Tekscan was taken under static loading conditions, this was to prevent the sensor being moved or damaged during the study. In order to verify whether this, or the differences in kinematics, were the cause of the differences in the contact area results a static computational model was run under the experimental output kinematics. The static computational model has shown that the differences in the contact area between methods may be due to the static loading of the Tekscan sensor or due to the differences in the kinematics. The weight and internal friction within the experimental simulator may be the cause of the differences in kinematics. As these are limitations of the experimental simulator these were not included in the computational model.

5.7.2 Stability

The fixed bearing TKR was found to be stable under all the soft tissue conditions studied, including with no springs attached. This showed that there was good stability of the TKR even with no soft tissue constraints applied. This may be due to the conformity of the insert restricting displacements or it could be due to limitations of the simulator. Factors such as the internal friction within the simulator may have resulted in reduced displacements and therefore more stable motion.

5.7.3 Kinematics

The stiff knee soft tissue condition resulted in significantly lower displacements as well as a significantly lower wear rate. This relationship between the soft tissue conditions and the output displacements was similar to that found in the Chapter 4 and in other studies [92, 194]. One previous experimental study of the same TKR resulted in higher displacements under

the lower tension condition as found in this study [92]. The increase in wear rate with the increase in kinematics was also a similar relationship to that found previously [20].

For the first 50% of the gait cycle there was a minimal difference in the AP and TR displacements for the resected ACL and resected ACL & PCL soft tissue conditions; this may be due to a high AF being applied during this period. The increased friction may have resulted in the soft tissue condition having less of an influence on the kinematics. This may also have been due to the AP and TR displacements being within the respective spring gaps during the period. There was a greater difference in the stiff knee soft tissue condition than between the resected ACL and resected ACL & PCL soft tissue conditions, this may be due largely to the differences in the spring gaps. The resected ACL and resected ACL & PCL soft tissue conditions both had a 2.5mm AP and a 6° TR spring gap whereas the stiff knee soft tissue condition had no spring gaps at all. For the TR rotation particularly, where the peak displacement for the resected ACL & PCL soft tissue condition was 8°, this means the springs were only being applied from between around 50-60% gait at the peak TR rotation. Therefore the differences in spring tensions for the resected ACL and resected ACL & PCL soft tissue conditions resulted in minimal differences in the TR rotation. Correspondingly, the stiff knee soft tissue condition had no spring gap so the difference in the output in TR rotation was more significant.

In the experimental study the stiff knee soft tissue condition resulted in a similar AA output profile to the resected ACL soft tissue condition; it resulted in a lower and earlier peak AA rotation. The differences between the profiles again occurred from 50% gait onwards, however there was no significant difference. There was a more obvious difference between the resected ACL and resected ACL & PCL AA rotation profiles; they followed similar shapes however there was an offset of around 1° offset between the two profiles. This was the only kinematic output parameter where the resected ACL and resected ACL & PCL outputs were not similar up until 50% gait. This difference could be due to the fact that there was no AA force applied, therefore there may have been more variation as it was free to move.

However in the computational results there was more variation in the AA displacement profiles. The difference between the experimental and computational results may be due to the weight of the AA arm within the simulator or due to the internal friction influencing the AA rotation. In the computational results the resected ACL & PCL soft tissue condition was the only one to result in both adduction and abduction rotation. This may imply an increase in the instability of the TKR under this soft tissue condition. The resected ACL soft tissue condition resulted in the highest peak AA rotation, however the difference in value was only around 0.4°.

5.7.4 Contact Area and Pressure

The stiff knee soft tissue condition was found to result in the most balanced loading throughout the cycle, closely followed by the resected ACL soft tissue condition which only resulted in unbalanced loading at point 4 in the cycle. However the resected ACL & PCL soft tissue

condition resulted in unbalanced loading with a majority of the contact pressure occurring through the lateral tibial condyle. The other soft tissue conditions were more balanced and tended to result in higher contact areas on the medial side of the tibial insert.

This difference may be caused by the AA position; the resected ACL & PCL soft tissue condition resulted in more adduction and therefore more lateral loading. The imbalanced loading that occurred with the lower tension soft tissue conditions correlates with a different study that found that the lower tension springs were more unstable and resulted in more imbalanced loading patterns [201]. Unbalanced loading could result in instability of the knee, lift off and patient dissatisfaction [88, 153].

The movement of the medial and lateral contact between points 1 and 2 mimicked the motion found in the natural knee, where the medial contact remains relatively stationary. However in this study there was more motion of both the lateral and medial contacts later in the cycle that was not found in the natural knee [117]. Small differences in the AA motion resulted in a significant effect on the contact and the balance between the medial and lateral loading.

In the experimental study the resected ACL & PCL soft tissue condition resulted in lower contact areas at points 1 and 3 in the cycle. However in the computational results there was no difference in the contact areas between the three soft tissue conditions. This difference between the results again may be due to the differences in the AA rotations and the loading patterns. For example at point 3 in the cycle the experimental methods only resulted in lateral contact, while the computational model resulted in both medial and lateral contact.

In the computational results the stiff knee soft tissue condition resulted in the highest peak pressure values at all four points measured, however the difference in values was low for most of the cycle. At points 1-3 in the cycle the difference between the stiff knee soft tissue condition and the other two soft tissue conditions was only 3MPa, however at point 4 in the cycle the difference was 10MPa. The peak pressure under all three soft tissue conditions was higher than the average yield stress of crosslinked UHMWPE [125].

5.7.5 Wear

The wear rate for the stiff knee soft tissue condition was significantly lower than that of the resected ACL and resected ACL & PCL soft tissue conditions; this follows from the kinematics results where the stiff knee soft tissue condition resulting in lower displacements than the resected ACL and resected ACL & PCL soft tissue conditions. The kinematics for the resected ACL and resected ACL & PCL soft tissue conditions were different, with the resected ACL & PCL soft tissue condition resulting in higher peak displacements on both the AP and TR profiles. However there was no significant difference in the range of motion of the AP, TR and AA profiles, this may be why the wear rates were also similar.

The increase in variation in the kinematics between stations with the resected ACL & PCL soft tissue condition may be due to the decrease in spring tensions resulting in differences in friction between stations having a greater effect on the kinematics. With less stabilisation

from the soft tissue condition the differences between the stations resulted in more of an effect on the kinematics. However for all of the wear studies there was found to be no correlation between the differences in kinematics between stations or tibial inserts with the wear rates.

5.7.6 Conclusions

Overall the soft tissue conditions had a significant effect on the output kinematics and wear rates of the TKR in this study. The use of the lower tension resected ACL & PCL soft tissue condition with a CR TKR was to replicate a patient with a damaged or degraded PCL after surgery. Conversely the stiff knee soft tissue condition replicated a patient without enough ligament release during surgery or due to a thicker than necessary tibial insert. The lower tension resected ACL & PCL soft tissue condition resulted in similar wear to the resected ACL condition, however it also resulted in increased displacements and more unbalanced loading. This may result in instability and reduce patient satisfaction.

The stiff knee soft tissue condition resulted in significantly lower wear rates than the resected ACL soft tissue condition, it was also the only soft tissue condition to maintain contact on both sides of the tibial insert at all the points studied.

These results imply that higher tension soft tissue conditions may result in better outcomes for the patient. However this study has only investigated the mechanical impact of the soft tissue conditions and not any impact on patient satisfaction. For example the stiff knee soft tissue condition may result in a restricted range of motion, especially under high flexion conditions, and therefore lower patient satisfaction.

Chapter 6

The Influence of Alignment on the Mechanics and Wear Rate of a TKR

6.1 Introduction

The aim of this study was to investigate the effect of component alignment on the output kinematics, contact area and wear rate of a TKR. In order to do this five alignment conditions were defined in order to represent the range found in vivo; mechanical alignment, 4° varus joint line, 14° femorotibial rotational mismatch, 10° tibial slope and values recommended to achieve kinematic alignment.

All the alignment conditions were studied under the same soft tissue condition; the stiff knee soft tissue condition defined in the previous chapter. These springs were based on clinical data in order to represent a stiff knee and were chosen to provide stability to the alignment conditions, allowing all of them to be studied.

Experimental studies were carried out with a knee simulator in order to find the output AP, TR and AA displacements under each of the alignment conditions. The output displacements were then compared between the alignment conditions in order to determine their effect.

The contact area was also measured at four different points in the gait cycle for each alignment. The four points in the cycle were defined to represent the range of motion and loading that occurred.

Finally four wear studies were run for 2MC with the mechanical, varus, rotated and tibial slope alignment conditions to determine whether the alignments would result in different wear rates.

The computational model was then validated using the experimental data described in this chapter under all the alignment conditions. The output kinematics and contact areas were compared between the experimental and computational data for each alignment condition.

Parametric testing was then carried out with the computational model to investigate the effect of a further set of alignment conditions; 4° and 2° varus, 14°, 8° and 4° rotational mismatch, 10° and 4° posterior tibial slope as well as the experimental kinematic alignment

values and half the kinematic alignment values used for the experimental study. The output kinematics, contact pressure and contact area were then compared between the alignment conditions and the mechanical alignment condition. These were all carried out under the stiff knee soft tissue condition.

6.2 Materials

All the studies were carried out using DePuy Sigma (DePuy Synthes, Leeds, UK) fixed bearing, right knee components. The tibial inserts were moderately crosslinked UHMWPE (5MRad irradiated and re-melted GUR1020 XLK). The tibial inserts used for the varus, rotated and tibial slope wear studies were new inserts from batches 8466296 and 8466300 (part number 1581-13-110).

The femoral components had been used in previous studies, to ensure this would not affect the wear results the femorals were polished in order to remove any scratches.

The lubricant was 25% bovine serum (Life Technologies, New York, USA) in 0.04% sodium azide solution (Severn Biotech Ltd, Worcestershire, UK) and was changed approximately every 350,000 cycles. The contact area measurements were carried out using a Tekscan (Tekscan Inc., Boston, USA) pressure mapping sensor as detailed in Section 2.2.

The soft tissues were simulated using virtual springs within the simulator, the profiles of the virtual springs were changed to represent different soft tissue constraints. In order to represent different component alignments femoral and tibial fixtures were designed and made that allowed the tibial and femoral components to be inserted into the simulator in the desired positions.

6.3 Methods

6.3.1 Alignment conditions

A literature review was conducted to identify relevant studies which detailed the surgical technique used and reported the post-surgical component position. The studies included used an intramedullary guide for femoral alignment and an extramedullary guide for tibial alignment which is the routine clinical practice. None of the studies included revision surgery or patients with large preoperative varus/valgus, used cadavers and all measured the angles of the components with the same methods.

For coronal alignment the studies included were those where the angles were measured using a weight bearing, long leg radiograph. The angle of the tibial component was defined as the angle between the base of the tibial tray and the anatomical axis of the tibia. The angle of the femur was defined as the angle between the mechanical axis of the leg and the tangent to the femoral condyles. There were eight studies that fit these criteria and the range in tibial, femoral and tibiofemoral component alignments are shown in Table 6.1. A value of 4° was chosen in order to represent the common range of tibial and femoral alignment found

in vivo. This represented a 4° varus joint line where error in the initial tibial bone cut was carried across into the femoral bone cut. A varus angle was also chosen as previous studies had found that varus alignment resulted in worse outcomes than valgus alignment [189, 195].

Table 6.1: Results from studies on the amount of variation in TKR position in the coronal plane. A negative value represents a varus alignment and a positive value valgus

Study	**Number of Subjects**	**Tibial (°)**	**Femoral (°)**
[89]	100	-6 to +2	-4 to +10
[13]	51	-4 to +4	-5 to +5
[38]	50	Not Reported	-5 to +4
[137]	39	-3.7 to +5.1	-6 to +1.8
[48]	29	-3 to +8	-1 to +6
[55]	30	-3 to +5	-6 to +3
[209]	29	-2 to +4	-5 to +8
[59]	50	-3 to +3	-4 to +3

The studies included for the rotational alignment of knee components were those measured using CT scans and using the Perth or Berger CT protocol were included as they use the same methods [33, 50]. The studies that met these criteria and the maximum tibiofemoral rotational mismatch found in each study are shown in Table 6.2. A value of 14° rotational mismatch was chosen for this study in order to represent the ranges found in each of the five studies. The femoral component was rotated 7° internally and the tibial component 7° externally.

Table 6.2: Results from studies on the maximum rotational mismatch of TKR components

Study	**Number of Subjects**	**Tibiofemoral Mismatch (°)**
[127]	159	13
[51]	36	11
[96]	22	13.6
[26]	56	18.6
[148]	26	22.1

For the sagittal alignment the studies included were those where CT scans were used to calculate the alignment angle according to the Perth CT protocol. The surgical guidelines for this TKR are for no tibial slope and the tibial cut to be perpendicular to the tibial axis. The studies included used TKRs with the same guidelines for the tibial slope. The four studies that met these criteria are shown in Table 6.3, in 3 of the 4 studies the maximum posterior tibial slope was 10°, therefore this alignment was chosen.

The final alignment condition was based on clinical data found after using kinematic alignment methods [133]. Kinematic alignment may result in the femoral and tibial components at different angles relative to the mechanical axis of the leg, which could affect the contact patterns and kinematics. For each component alignment the value at 95% CI away from the mean was used as the value for this fixture; 2.5° femoral valgus, 3.4° tibial varus and 4.6° posterior tibial slope.

Table 6.3: Results from studies on the variation in TKR position in the sagittal plane. A negative value represents an anterior tibial slope

Study	**Number of Subjects**	**Tibial Slope (°)**
[127]	159	-1 to +13
[51]	36	+1 to +10
[96]	22	+1 to +10
[101]	27	-1 to +10

Five alignment conditions were studied experimentally; mechanical alignment, 4° varus joint line, 14° femorotibial rotational mismatch, 10° tibial slope and after kinematic alignment during surgery (Table 6.4 and Figures 6.1 and 6.2). The alignment values were chosen to represent the range of alignment found in vivo (Tables 6.1, 6.2 and 6.3).

Table 6.4: The femoral and tibial component positions in the coronal, sagittal and transverse planes relative to mechanical alignment under each alignment condition studied

Condition	Femoral Component			Tibial Component		
	Coronal	Sagittal	Transverse	Coronal	Sagittal	Transverse
Mechanical	0°	0°	0°	0°	0°	0°
Varus	4° varus	0°	0°	4° varus	0°	0°
Rotated	0°	0°	7° internal	0°	0°	7° external
Tibial Slope	0°	0°	0°	0°	10° posterior	0°
Kinematic	2.5° valgus	0°	0°	3.4° varus	4.6° posterior	0°

The varus joint line alignment is a result of the femoral and tibial cuts being made at an angle to the mechanical axis of the leg in the coronal plane (Figure 6.1 (c)). The tibial slope alignment is a result of the tibial cut being made at an angle that is not perpendicular to the mechanical axis of the leg (Figure 6.2 (c)). The kinematic alignment is a combination of the femoral and tibial cuts being made at an angle to the mechanical axis in both the coronal and sagittal planes (Figures 6.1 (d) and 6.2 (d)). While the rotated alignment condition is partially due to the femoral bone cuts being made at an angle to the centre of the femoral (Figure 6.3 (c)) and the tibial component being cemented on to the at an angle to the centre of the tibia. In this study the rotational mismatch was split evenly between the femoral and tibial components, therefore an angle of 7° was applied to both components.

Kinematic alignment methods aim to maintain the natural geometry of the knee, keeping the axes of motion constant and does not include any soft tissue releases. The aim of kinematic alignment is to keep the motion and geometry of the knee as natural as possible. The kinematic alignment condition was based on a study into the postoperative component alignment after kinematic alignment methods were used [133]. For each component alignment a value was taken at the 95% CI away from the mean giving a tibial varus angle of 3.4°, a posterior tibial slope of 4.6° and a femoral valgus angle of 2.5°. These were chosen to represent the range of alignments determined in vivo after kinematic alignment.

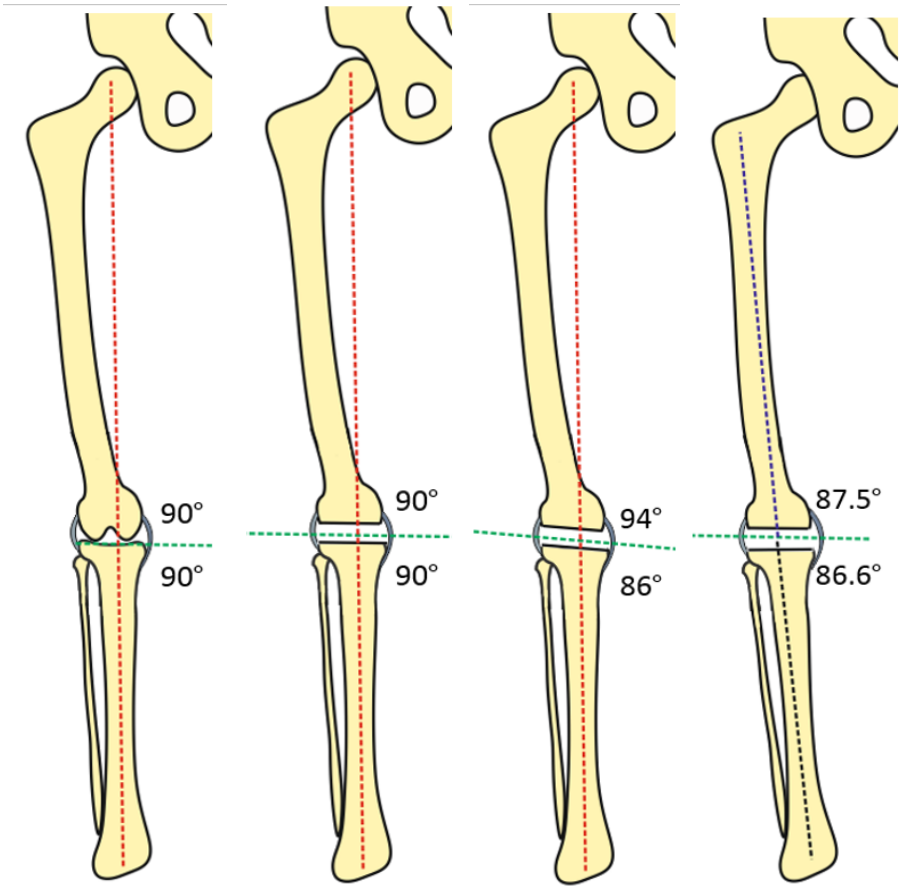

(a) Natural knee (b) Mechanical alignment (c) Varus alignment (d) Kinematic alignment

Figure 6.1: Diagrams showing the natural knee and the mechanical, varus joint line and kinematic alignments after the femoral and tibial bone cuts have been made in the coronal plane. The mechanical axis of the leg is shown with a red dotted line and the collateral ligaments shown in grey. As the mechanical axis of the leg will have changed after surgery for the kinematic alignment condition the pre-surgical mechanical axis is shown in blue for reference to the bone cut angles

6.3.1.1 Mechanical alignment

Under mechanical alignment conditions the femoral component centre of rotation was aligned with the FE axis of the simulator (Figure 6.4). The AA axis passes through the proximal surface of the tibial component and through the centre of the tibial fixture in the medial-lateral direction. The AA axis was also parallel to the proximal tibial fixture surface.

6.3.1.2 4° Varus Joint Line

The varus fixture simulated the effect of a varus initial tibial or femoral cut rather than one perpendicular to the anatomical axis of the leg. The femoral and tibial cuts are made relative to each other so a varus initial cut would result in both of the components at a varus angle relative to the mechanical axis of the leg. The centre of rotation for the femoral component

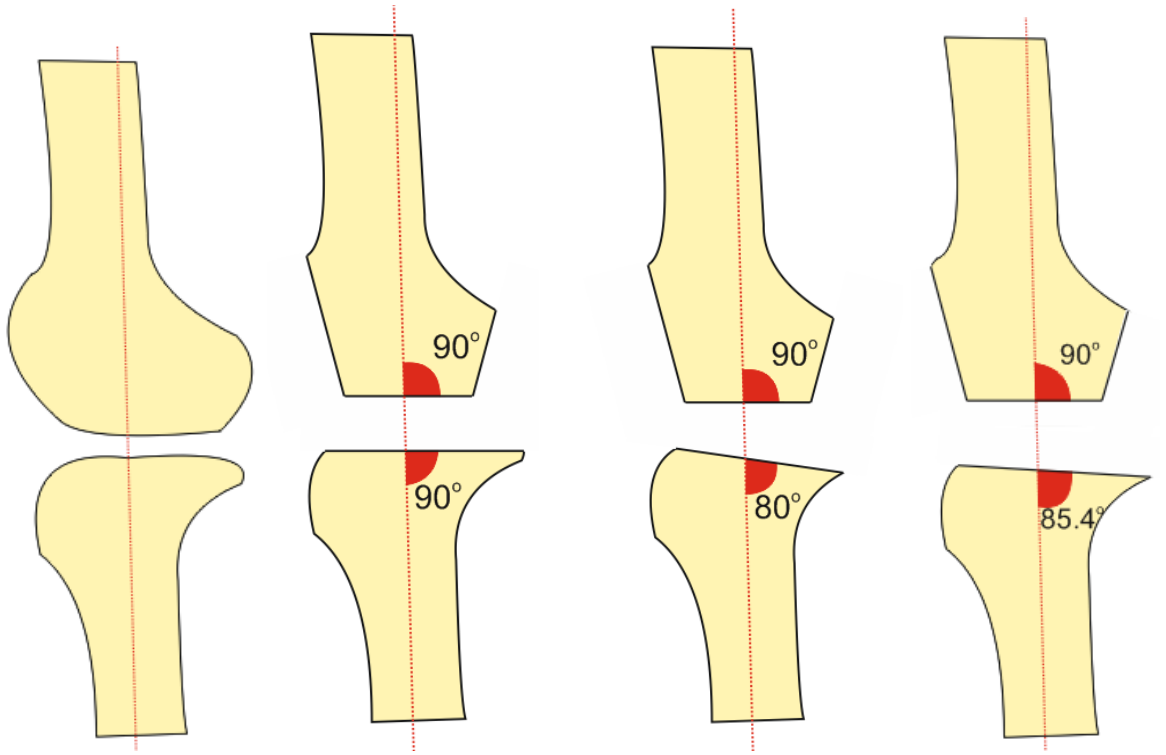

(a) Natural knee (b) Mechanical alignment (c) Tibial slope (d) Kinematic alignment

Figure 6.2: Diagrams showing the natural knee and the mechanical, tibial slope and kinematic alignments after the femoral and tibial bone cuts have been made in the sagittal plane. The mechanical axis of the leg is shown with a red dotted line.

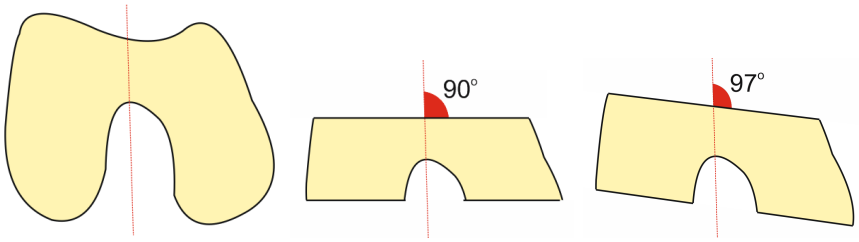

(a) Natural knee (b) Mechanical alignment (c) Rotated alignment

Figure 6.3: Diagrams showing the natural knee and the mechanical and rotated alignments after the femoral bone cuts have been made in the sagittal plane. The centre line of the femoral is shown with a red dotted line

was at a 4° varus angle to the FE axis of the simulator (Figure 6.5). The FE axis crossed the axis of the centre of rotation of the femoral component at the centre of the femoral fixture in the medial-lateral direction. The same alignment was applied to the tibial component so that the tibial and femoral components were parallel. This meant that the tibial component could be cemented into position relative to the femoral component. The AA axis passed through the proximal surface of the tibial insert at the centre of the tibial fixture in the medial lateral direction.

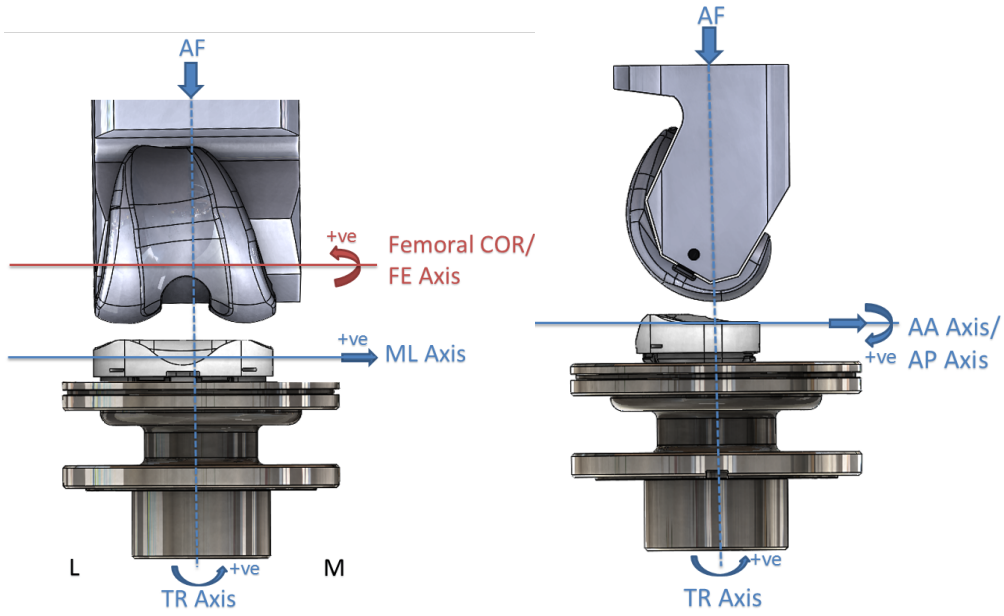

Figure 6.4: Femoral and tibial fixtures for mechanical alignment along with the locations of the FE and AA axes of the simulator and the femoral component centre of rotation

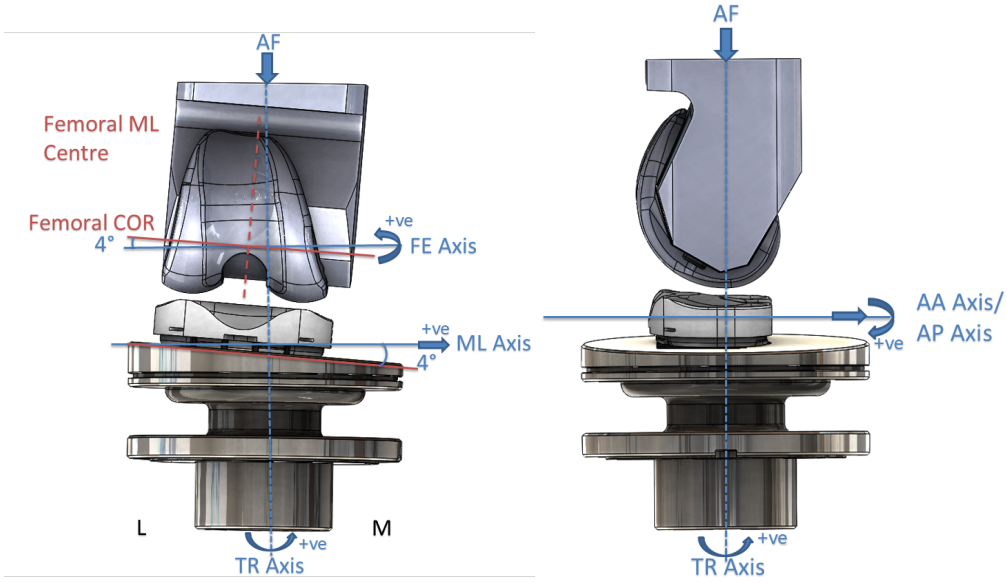

Figure 6.5: Femoral and tibial fixtures for varus alignment along with the locations of the FE and AA axes of the simulator and the femoral component centre of rotation

6.3.1.3 10° Posterior Tibial Slope

The tibial slope alignment simulated the effect of a posteriorly sloped tibial cut rather than perpendicular to the axis of the tibia in the sagittal plane. This did not affect the alignment of the femoral component, which was kept in the mechanical alignment position. The increased tibial slope was achieved using a fixture that resulted in a 10° posterior tibial slope (Figure 6.6). As before the AA axis passed though the medial-lateral centre of the tibial fixture and

through the proximal tibial insert surface at the anterior-posterior centre of the tibial fixture.

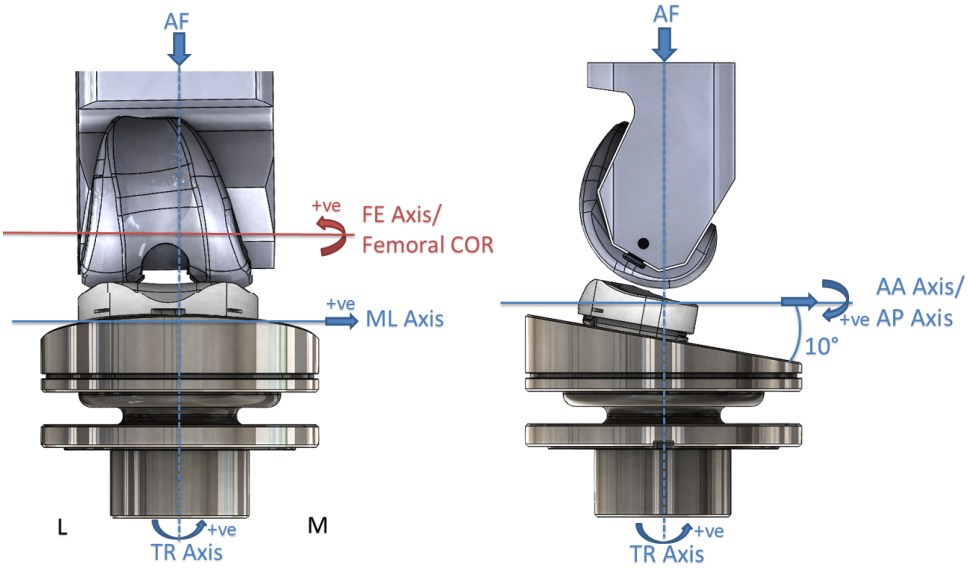

Figure 6.6: Femoral and tibial fixtures for tibial slope alignment along with the locations of the FE and AA axes of the simulator and the femoral component centre of rotation

6.3.1.4 14° Rotational Mismatch

The rotational alignment of the femoral and tibial components can be difficult to ascertain during surgery due to a lack of external landmarks. The rotational mismatch study simulated the effect of the components being rotationally malaligned with respect to each other. The femoral component was rotated 7° internally and the tibial component 7° externally (Figure 6.7).

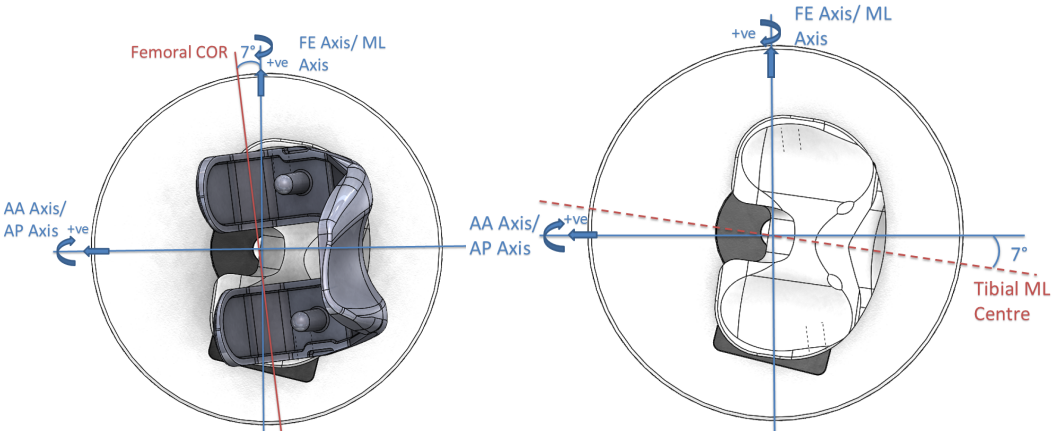

Figure 6.7: Femoral and tibial fixtures for rotated alignment along with the locations of the FE and AA axes of the simulator and the femoral component centre of rotation

The axis of the centre of rotation of the femoral component was at an angle of 7° to the FE axis of the simulator in the transverse plane. Otherwise the femoral component was in the

same position within the simulator. The same was true of the tibial component; it was rotated purely in the transverse plane around the centre of the tibial fixture. In order to cement the tibial component relative to the femoral component the simulator software was used to rotate the tibial component by 14° to be aligned with the femoral component.

6.3.1.5 Kinematic Alignment

The axis of the centre of rotation of the femoral component was at an angle of 2.5° valgus to the FE axis of the simulator in the coronal plane (Figure 6.8). The proximal surface of the tibial fixture had a slope of 4.6° posteriorly and 3.4° medially. The centre of the surface was aligned with the AA axis of the simulator. The centre of the tibial fixture surface remained at the same height as for the mechanical alignment condition.

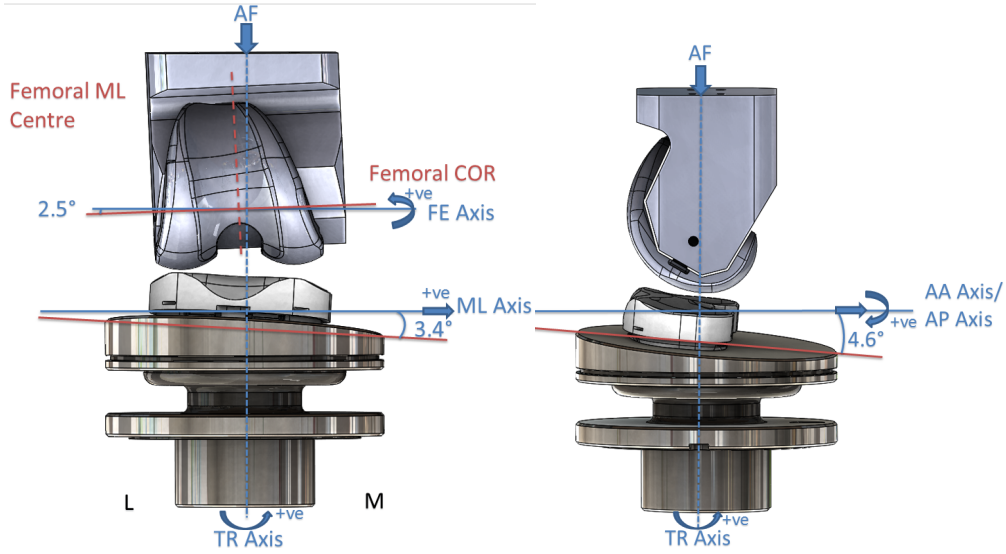

Figure 6.8: Femoral and tibial fixtures for kinematic alignment along with the locations of the FE and AA axes of the simulator and the femoral component centre of rotation

6.3.2 Kinematics

For each of the five alignment conditions 10 consecutive cycles were recorded on each of the 6 stations of the simulator. The output AP, TR and AA profiles were then averaged across the simulator in order to determine the average displacements and 95% CI.

The average output profiles were then compared between the different alignment conditions using minimum and maximum points in the output profiles as defined in Chapter 2 (Figure 6.9). Points A-D were defined in the AP profile, points E-H in the TR profile and points I-K in the AA displacement profile.

The range of motion in the displacement profiles were also compared between studies; this was defined as the difference between the maximum and minimum point in the displacement profile.

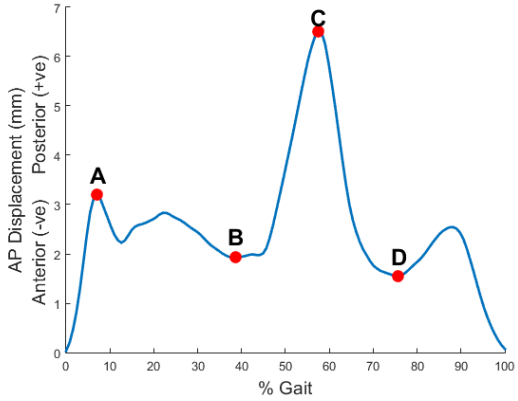

(a) AP Displacement

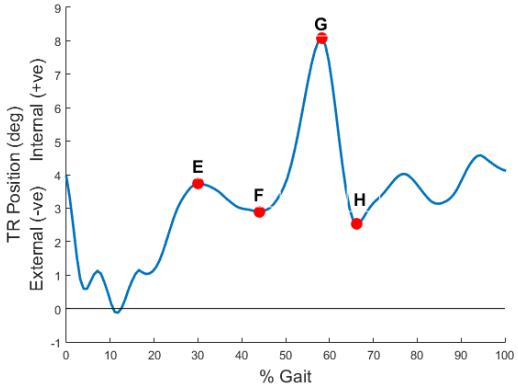

(b) TR Rotation

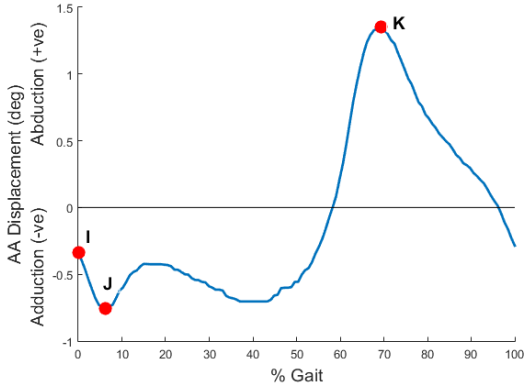

(c) AA Rotation

Figure 6.9: The maximum and minimum points in the AP, TR and AA displacement profiles used for comparison between studies

6.3.3 Contact Area

For each alignment condition four points within the gait cycle were measured using the Tekscan sensor; the first at 5% gait where the initial peak in the AP force occurs, the second at 45% gait where the last peak in the AF occurs, the third at the point in the cycle where the combined AP and TR displacement were at their maximum and the fourth point at 72% gait where the FE was at its peak (Figure 6.10).

The displacements and loads at these points were determined for each spring condition (Tables A.1 to A.5).

The contact area was measured on 5 stations of the simulator at each point in the cycle for each alignment condition. The AA motor was not functional on the 6th station and was therefore not used for the study. The average and 95% CI of the contact area position and size was then determined for each point in the cycle.

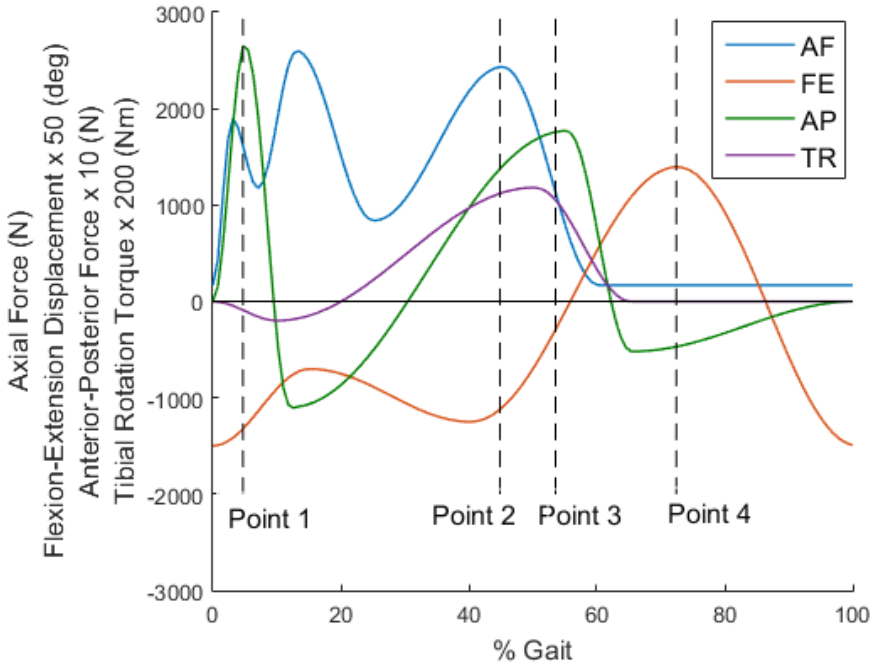

Figure 6.10: The input axial force, flexion-extension, AP force and TR torque profiles with the four points in the cycle where the contact area was measured

6.3.4 Wear rate

In order to investigate the effect of the alignment constraints on the wear rates four different wear studies were carried out. A wear study of 2MC was carried out for each of four alignment conditions; mechanical, varus, rotated and tibial slope. A wear study was not carried out with the kinematic alignment condition as the contact results were not representative of those in vivo.

At the end of each wear study the change in the output kinematics over time was investigated to determine whether the kinematics changed as the wear scar was formed. The wear rates between each of the inserts were then compared to determine whether there were similar differences in the wear rates over time as described in Section 2.3.7.

The variation between the stations was also investigated. Any significant differences in the kinematics were then compared to the wear rates on each station to determine whether the differences in kinematics may have affected the wear rates.

The size, position and areas of the wear scars at the end of each wear study were also determined and compared between wear studies.

Before and after each wear study the surface roughness of the superior surface of the tibial inserts and the inferior surface of the femoral components were measured. Any significant change in surface roughness may be due to third body damage to the components. Over time this damage may result in increased wear.

During each wear study the bulk temperature of the serum was measured in order to

determine any differences in running temperatures. The mean and 95% CI of the station and soak serum temperatures were compared between the different wear studies.

A one way ANOVA with significance taken at $p<0.05$ using IBM SPSS Statistics 22 was used. Depending on the homoscedasticity either a post hoc Tukey's test or a Games-Howell test was carried out, with significance taken at $p<0.05$, to determine the differences between the groups.

6.3.5 Validation of Computational Model

The experimental and computational data was compared for each alignment condition studied experimentally; mechanical, varus, rotated, tibial slope and kinematic alignment.

This was first done by comparing the output AP, TR and AA displacements between the experimental and computational results. The correlation between the experimental and computational displacements was determined and a correlation coefficient above a value of 0.7 was determined to be a good correlation.

The contact at the same four points in the gait cycle where the Tekscan sensor was used to measure the contact area experimentally were then found for the computational model. The position of the tibiofemoral contact and the contact area were then compared between the computational and experimental results.

6.3.6 Parametric testing with Computational Model

In order to investigate a wider range of alignment conditions the computational model was used for parametric testing.

Varus alignment with values of 0°, 2° and 4°, rotational mismatch values of 0°, 4°, 8° and 14° and a posterior tibial slope with values of 0°, 4° and 10° were then developed and tested.

Finally the kinematic alignment values were varied in order to represent a range of component positions that may occur after kinematic alignment methods are used during surgery. The component alignments tested experimentally were 95% CI away from the mean values and were therefore the most extreme alignment values tested. Five component positions were tested, these ranged equally from mechanical alignment to the kinematic alignment condition tested experimentally (Table 6.5).

Table 6.5: Kinematic alignment component positions studied computationally

Test	Femoral	Tibial	
	Coronal (° valgus)	Coronal (° varus)	Sagittal (° posterior)
Mechanical	0	0	0
Half Experimental Values	1.2	1.7	2.3
Experimental Values	2.5	3.4	4.6

6.4 Experimental Results

6.4.1 Effect on Kinematics

The mean anterior-posterior, tibial rotation and abduction-adduction displacement profiles were determined for each of the five alignment conditions.

6.4.1.1 AP Displacement

The AP displacement profiles for each component alignment follow a similar profile shape; an initial peak at around 5% gait followed by a larger peak at 60% gait (Figure 6.11). The mechanical, varus and rotated components had the most similar profile shapes with the varus and rotated profiles having a larger amplitude compared to mechanical alignment. The varus and rotated components had a significantly larger initial peak than the other alignments at point A, both with values of 1.6mm ($p<0.01$).

The tibial slope and kinematic alignments had significantly more anterior displacement for most of the cycle at points A, B and C ($p<0.01$). The kinematic and tibial slope alignments were also the only alignment conditions that resulted in anterior displacement, the other alignments had purely posterior displacements.

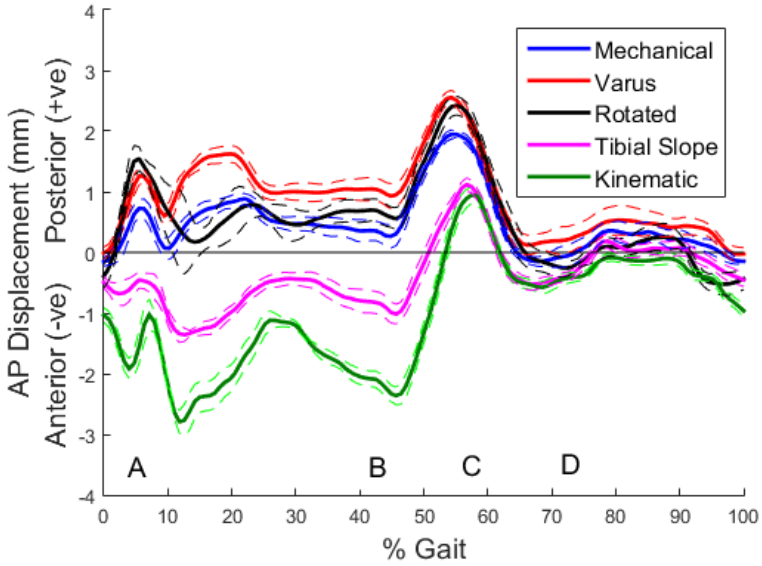

Figure 6.11: Average AP displacement (mm) profiles using the stiff knee soft tissue condition for all alignment conditions with the 95% CI shown in dotted lines

The kinematic alignment resulted in significantly higher range of motion across the whole AP profile of 3.8mm compared to all the other alignments while the mechanical and rotated alignments had significantly lower AP ranges of motion than the varus and tibial slope alignments ($p<0.01$).

6.4.1.2 TR rotation

The mechanical and varus components had similar TR rotation output profiles; there was no significant difference between the two profiles at any point in the cycle (Figure 6.12).

The tibial slope and kinematic alignments also resulted in similar profile shapes but with different peak TR rotations. The rotated alignment condition however had a different profile shape which was not centred around zero, unlike all the other alignment conditions.

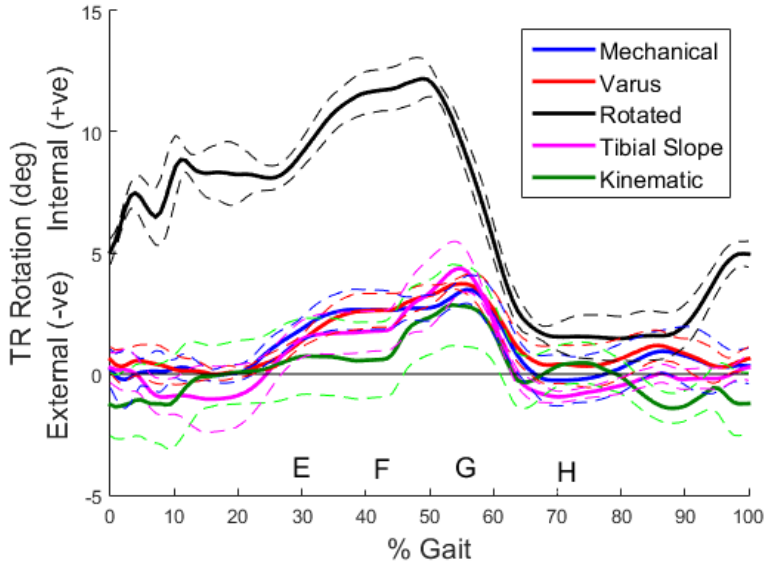

Figure 6.12: Average TR rotation (°) profiles using the stiff knee soft tissue condition for all alignment conditions with the 95% CI shown in dotted lines

Throughout the cycle from points E-G the rotated alignment condition resulted in significantly higher TR rotation than all the other alignment conditions ($p<0.01$).

The tibial slope alignment had a significantly lower TR rotation at points E and F in the cycle than the other alignments ($p<0.01$).

The rotated alignment resulted in a significantly higher range of motion of 11.3° compared to the other alignments ($p<0.01$).

6.4.1.3 AA Rotation

The mechanical, varus and tibial slope alignments resulted in similar AA rotation profiles. The kinematic alignment resulted in a similar profile shape but with around 2° more abduction motion throughout the cycle. The rotated alignment had higher peak AA rotations as well as having a larger range of motion than the other profiles.

At point I the rotated components had a significantly higher AA rotation compared to the other alignments ($p<0.04$), the kinematic alignment also resulted in a significantly higher AA rotation compared to the mechanical and tibial slope conditions ($p<0.05$).

At point J the kinematic alignment had a significantly higher AA rotation of 2.4° compared

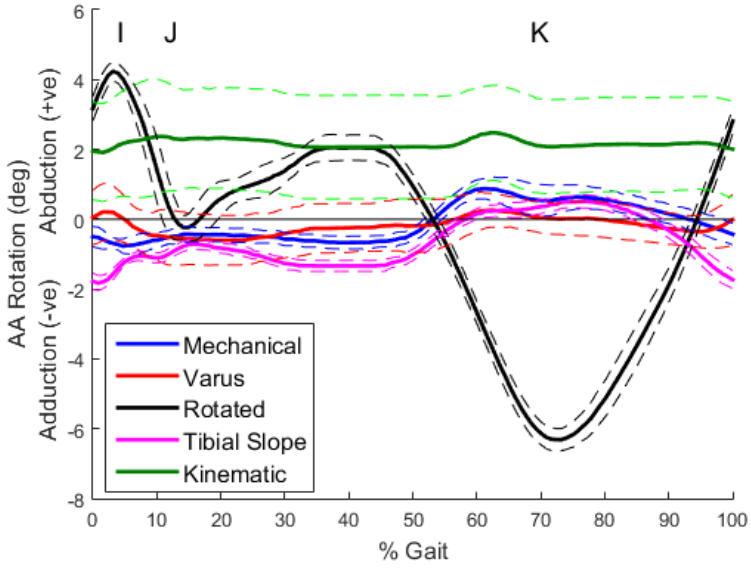

Figure 6.13: Average AA rotation (°) profiles using the stiff knee soft tissue condition for all alignment conditions with the 95% CI shown in dotted lines

to all the other alignments which had adduction motion at this point ($p<0.04$). At point K the rotated alignment had a significantly higher adduction displacement compared to the other alignment conditions ($p<0.01$).

The rotated alignment had a significantly higher range of motion across the cycle compared to all the other alignments ($p<0.01$). The kinematic and varus alignments had significantly lower ranges of motion than all the other alignments ($p<0.01$).

6.4.2 Effect on Contact Area

The contact area of each alignment condition was measured using a Tekscan sensor at four points in the gait cycle, the forces and displacements at each of these points is shown in Table A.5.

Table 6.6 and Figure 6.14 show the mean contact areas for each alignment condition along with the 95% CI (n=5).

Table 6.6: The contact area (mm^2) on the tibial insert at each point in the cycle for each alignment condition (mean±95%CI, n=5)

Point	Mechanical	Varus	Rotated	Kinematic	Tibial Slope
1	91.3±4.2	89.1±24.4	92.1±15.2	84.3±12.5	125.4±34.9
2	139.8±3.6	181.9±18.3	154.3±22.6	120.0±13.9	153.1±85.6
3	45.4±1.6	62.6±35.1	128.3±22.3	42.9±9.7	29.0±11.3
4	15.6±2.5	7.1±5.0	6.0±4.3	14.5±4.5	35.7±63.6

At point 1 most of the alignment conditions resulted in similar contact areas however the tibial slope alignment resulted in a significantly higher total contact area than all the other

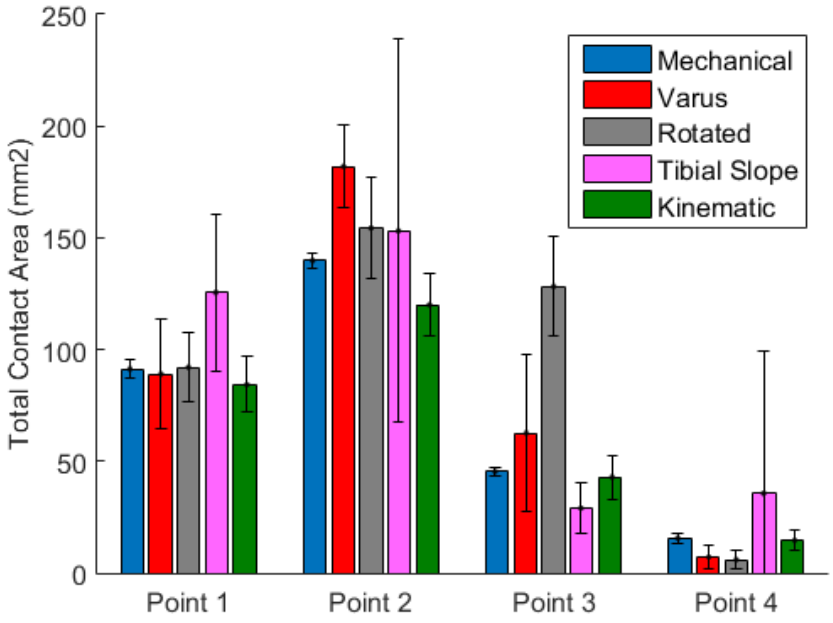

Figure 6.14: The average contact area for all the alignment conditions with the stiff knee soft tissue condition at each measured point in the gait cycle with error bars showing the 95% CI (n=5)

alignments at this point ($p<0.01$).

For all the alignment conditions there was more variation in the contact areas at point 2 in the cycle between the alignment conditions. The tibia slope alignment condition resulted in a high 95% CI.

At point 3 the rotated alignment had a significantly higher total contact area than all other alignments ($p<0.02$). The varus alignment resulted at a higher 95% CI than the other alignment conditions at this point.

At point 4 the rotated alignment had a significantly lower total contact area than the mechanical or kinematic alignments ($p<0.04$). The tibial slope alignment resulted in the highest contact area, however it also had a very high 95% CI therefore there was no significant difference.

Figure 6.15 shows the position of the average contact areas for each alignment condition with the 95% CI shown with dotted lines.

The mechanical alignment condition resulted in both medial and lateral contact at each of the four points in the cycle. There was also no contact on the edge of the tibial insert.

However under the varus alignment condition there was only medial contact at point 2 in the cycle. This suggests that the varus alignment condition resulted in unbalanced tibial loading.

The rotated alignment condition resulted in more posterior medial contact and more anterior lateral contact than the other alignment conditions. The rotated alignment condition

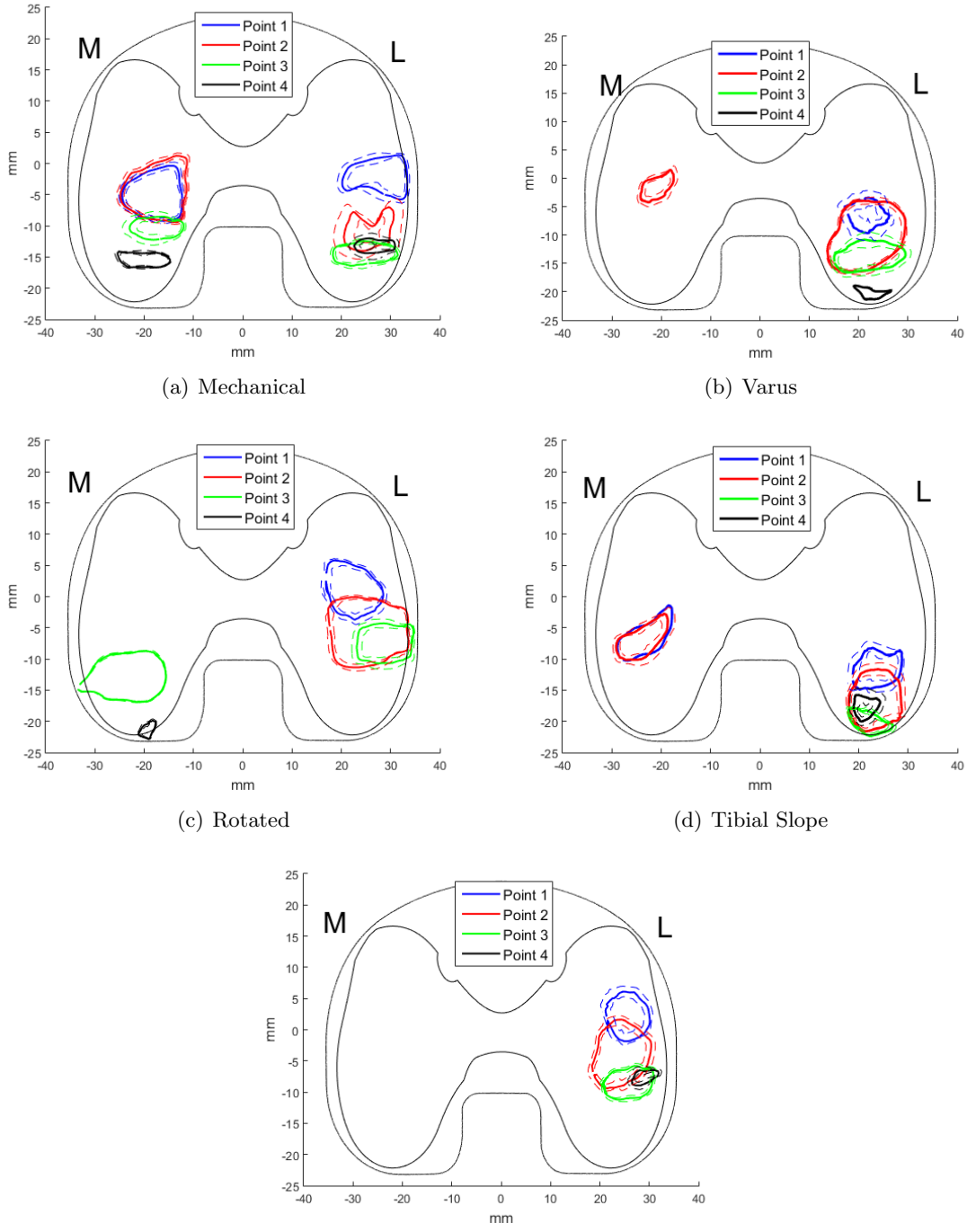

(a) Mechanical

(b) Varus

(c) Rotated

(d) Tibial Slope

(e) Kinematic

Figure 6.15: The average contact areas with 95% CI shown in dotted lines (n=5) for each alignment condition at each point in the cycle with the stiff knee soft tissue condition

also resulted in unbalanced loading with only lateral contact in the first half of the cycle and only medial contact at the end of the cycle.

The tibial slope alignment resulted in more posterior tibiofemoral contact than the other alignment conditions. There was medial and lateral contact for the first half of the cycle but

then only lateral contact at points 3 and 4.

The kinematic alignment did not result in any medial contact and was the only alignment to do so. The lateral contacts were all central in the tibial condyle and did not get close to the tibial edge. As the gait cycle progressed the contact areas were more posterior than the previous one.

The mechanical and kinematic alignment conditions were the only ones where the contact did not occur close to the posterior edge of the tibial insert at the end of the gait cycle.

6.4.3 Effect on Wear

Wear studies were carried out for 2MC with the mechanical, varus, rotated and tibial slope alignment conditions. Wear studies were not carried out with the kinematic alignment condition as the contact was not representative of the conditions in vivo.

6.4.3.1 Wear rates

The wear rates for the mechanical, varus, rotational mismatch and tibial slope alignments were 1.58±1.20mm^3/MC, -0.10±1.00mm^3/MC, 10.05±4.37mm^3/MC and 9.24±2.80mm^3/MC respectively (Figure 6.16). The wear rates for the rotated and tibial slope alignments were significantly higher than the other alignment conditions ($p<0.01$). The varus alignment also resulted in a significantly lower wear rate than all the other alignment conditions ($p<0.04$). The negative wear value under the varus alignment is due to the wear rate being too low to be measured accurately rather than an actual increase in weight.

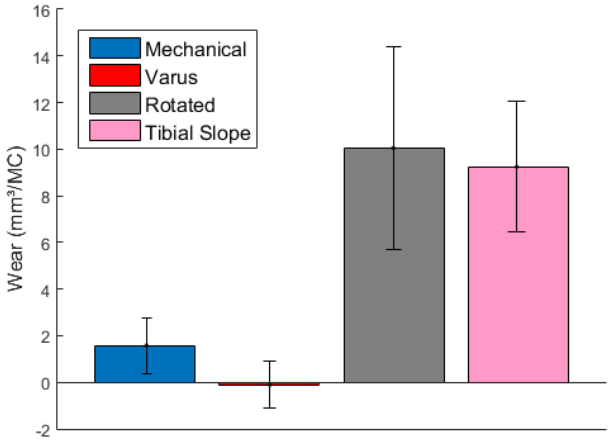

Figure 6.16: Wear rates over 2MC with the stiff knee soft tissue condition for mechanical, 4° varus, 14° rotational mismatch and 10° tibial slope alignment conditions with 95% CI

The wear volume over the wear study under mechanical alignment for each station on the simulator and each tibial insert are shown in Figure 6.17 (a). On all the inserts that ran for the full study under the mechanical alignment condition the wear volume was higher after

2MC than after 1MC (Figure 6.17 (b)). Station 4 was only run for the first MC in this study and could not be run for the second MC due to issues with the station. This difference in wear volume could be due to the formation of wear scars during the study. After 2MC insert 1 and insert 5 resulted in higher wear rates of 2.7mm^3/MC and 2.0mm^3/MC than the other inserts which resulted in values of around 1mm^3/MC.

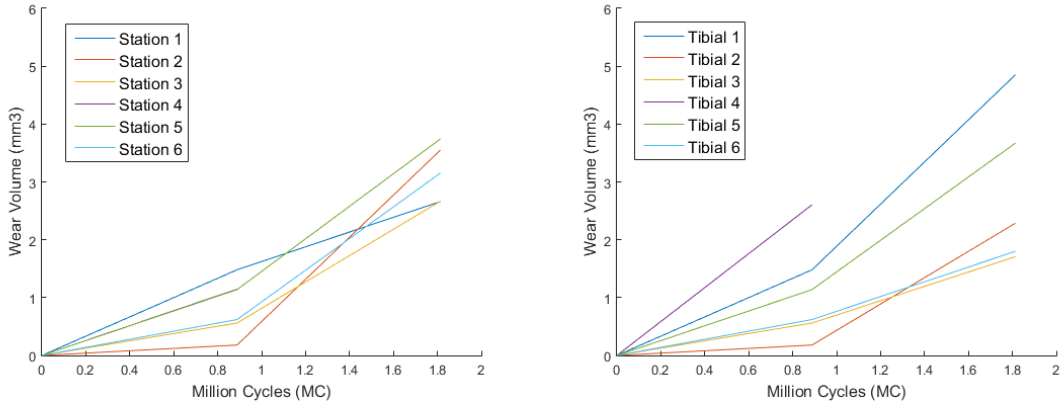

(a) Station Wear Volumes

(b) Tibial Insert Wear Volumes

Figure 6.17: The wear volumes (mm3) for each tibial insert and each station on the simulator over 1MC and over 2MC with the mechanical alignment and stiff knee soft tissue condition

The wear volume for each station of the simulator under the varus alignment and stiff knee soft tissue condition were determined at 1MC and 2MC (Figure 6.18 (a)). There was variation between the stations of the simulator with station 1 resulting in the highest wear volume throughout the study. After 1MC stations 2, 4, 5 and 6 resulted in negative wear volumes. This suggests that the wear volume is too low to be measured accurately and may be the cause of the variation between the stations. However after 2MC only stations 4 and 5 resulted in a negative wear volume. Three stations resulted in a higher wear rate over the second MC, while two resulted in a lower wear rate.

Tibial insert 1 resulted in a much higher wear volume than any of the other inserts (Figure 6.18 (b)). All the other inserts resulted in negative wear volumes at the end of the study. Again this suggests that the wear volume is too low to be measured accurately.

With the rotated alignment after the first MC stations 1 and 4 had higher wear volumes of 14.5mm^3 and 14.2mm^3 respectively (Figure 6.19 (a)).

However in the second MC station 4 was not running and the wear rate on station 1 was lower resulting in an overall wear volume of 22.6mm^3 over the whole study. Of the five stations that ran for 2MC three stations resulted in a higher wear rate after 2MC than after 1MC.

After 1MC inserts 3 and 6 had higher wear rates than the other inserts (Figure 6.19 (b)), however their wear rates then decreased after 2MC but remained higher than the other three inserts. Inserts 3 and 6 had higher wear volumes than the other inserts.

After the first MC with the tibial slope alignment there there was a range in the wear volume between stations from 0.9mm^3 to 13.7mm^3 (Figure 6.20 (a)). This variation then

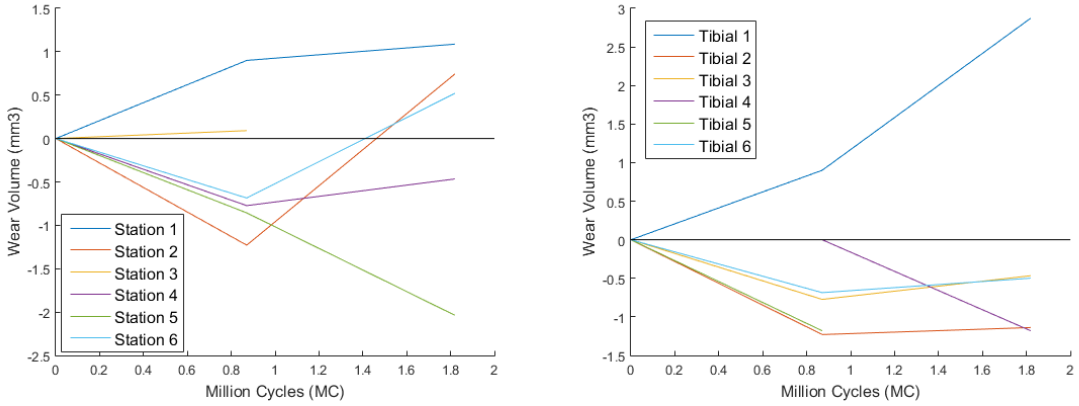

(a) Station Wear Volumes (b) Tibial Insert Wear Volumes

Figure 6.18: The wear volumes (mm3) for each tibial insert and each station on the simulator over 1MC and over 2MC with the varus alignment and stiff knee soft tissue condition

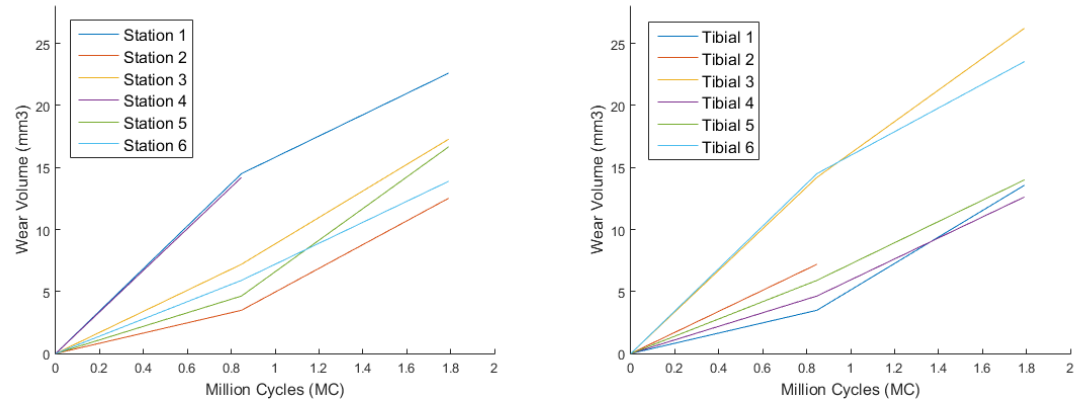

(a) Station Wear Volumes (b) Tibial Insert Wear Volumes

Figure 6.19: The wear volumes (mm3) for each tibial insert and each station on the simulator over 1MC and over 2MC with rotated alignment and stiff knee soft tissue condition

increased after 2MC to varying between 1.8mm^3 and 22.9mm^3. Station 4 had the lowest wear rate throughout the study while station 2 had the highest wear rate.

A similar relationship occurred with the tibial inserts, however the wear rate of tibial insert 3 decreased during the second MC compared to the first MC (Figure 6.20 (b)). There was a range in the wear volume of 1.8mm^3 to 25.0mm^3 at the end of the study.

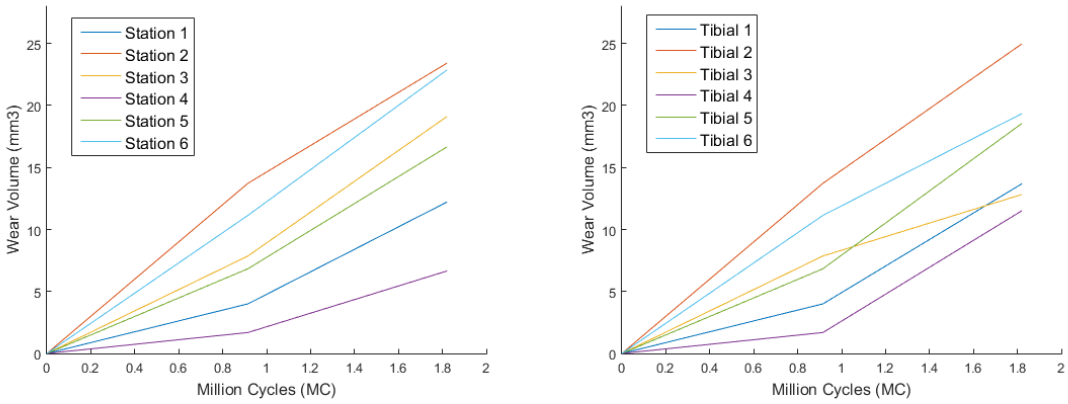

(a) Station Wear Volumes

(b) Tibial Insert Wear Volumes

Figure 6.20: The wear volumes (mm3) for each tibial insert and each station on the simulator over 1MC and over 2MC with the tibial slope alignment and stiff knee soft tissue condition

6.4.3.2 Kinematic variation during simulation

Under the mechanical alignment condition there was no significant change in the AP range of motion during the wear study (p=0.47). However the range of motion of the TR rotation was significantly lower at 1MC with a value of 3.0° compared to 3.5° at 0MC and 3.3° at 2MC (p<0.01). The AA range of motion was significantly higher at 2MC with a value of 1.2° compared to 0.8° and 0.9° at 0MC and 1MC respectively (p<0.01). The differences in the range of motion during the wear study were small and did not follow an obvious trend.

Under the varus alignment condition there were only small changes in the AP and TR ranges of motion during the study. The AP range of motion at 0MC was significantly higher than the value at 1MC with values of 2.6mm and 2.5mm respectively (p=0.02). The TR range of motion was significantly higher at 2MC compared to 0MC with values of 3.7° and 3.2° respectively (p=0.05). There was no significant difference in the AA range of motion during the study (p=0.08) and the differences in AP and TR motion were small.

With the rotated alignment condition there was no significant difference in the AP range of motion during the wear study (p=0.64). The TR range of motion was significantly higher at 0MC with a value of 11.9° compared to at 2MC with a value of 11.4° which was a small change in value (p=0.02). The difference in the TR range of motion was small and would have had a negligible impact on the wear. However at 2MC the AA range of motion resulted in a significantly higher value of 5.3° compared to 3.6° and 3.5° at 0MC and 1MC respectively (p<0.01).

With the tibial slope alignment condition there was no significant difference in the AP range of motion during the wear study (p=0.97). However the range of TR motion was significantly lower at 0MC with a value of 3.5° compared to 3.9° at 1MC and 4.2° at 2MC (p<0.01).

The range of AA motion was significantly lower at 2MC with a value of 0.4° compared to

0.9° at 0MC and 0.8° at 1MC (p<0..01). However the differences in the TR and AA motion were small.

6.4.3.3 Station variation during simulation

Under the mechanical alignment condition three stations; stations 1, 2 and 5, resulted in significantly higher AP ranges of motion (p<0.01). There was more variation in the TR and AA ranges of motion. However there was no positive correlation between the differences in wear rate and the differences in the ranges of motion between stations or between tibial inserts (Figure 6.21).

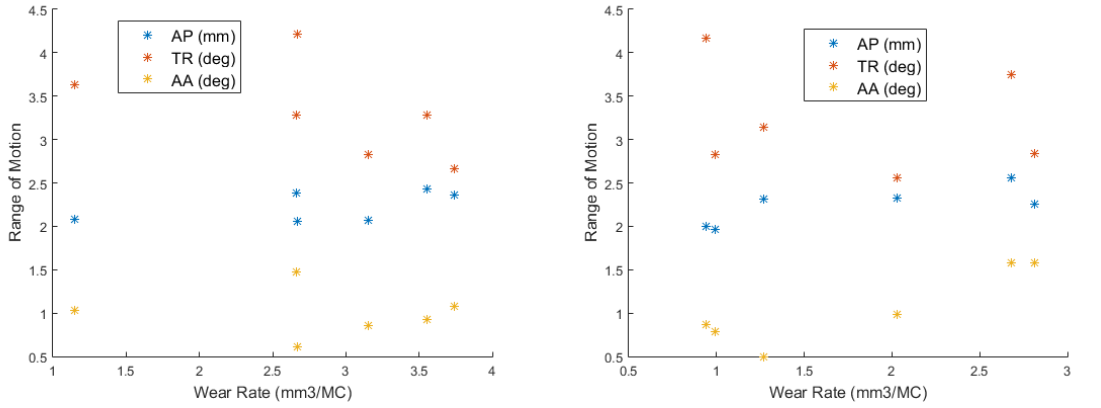

(a) Station Range of Motion vs Wear Rate (b) Tibial Insert Range of Motion vs Wear Rate

Figure 6.21: The correlation between the wear rate and range of motion under the mechanical alignment condition for the stations (a) and the tibial inserts (b)

With the varus alignment condition stations 1 and 3 resulted in significantly higher AP ranges of motion (p<0.01). Stations 3 and 4 resulted in significantly higher TR ranges of motion, while station 1 resulted in a significantly lower value (p<0.01). However stations 1 and 6 resulted in significantly higher AA ranges of motion (p<0.01). There was some correlation with a decrease in the TR range of motion and an increase in the AA range of motion as the wear rate increased (Figure 6.22 (a)). However this mainly occurred over a wear rate range of 0 - 0.6mm^3/MC and the differences in the ranges of motion were small. A similar correlation between the ranges of motion and wear rates of each tibial insert (Figure 6.22 (b)).

With the rotated alignment condition all the stations resulted in significantly different ranges of AP motion with the values increasing from 2.2mm to 5.6mm in the order of station 1, 2, 3, 4, 5 and 6 (p<0.01). All the stations apart from stations 2 and 6 again resulted in significantly different TR ranges of motion ranging from 10.6° on station 1 to 12.8° on station 3 (p<0.01). There was less variation in the AA range of motion with station 1 and 2 resulting in significantly higher values than stations 3, 4 and 5 (p<0.01). This alignment condition resulted in the most significant differences between the stations of the simulator. However there was no positive correlation between the differences in the ranges of motion between each

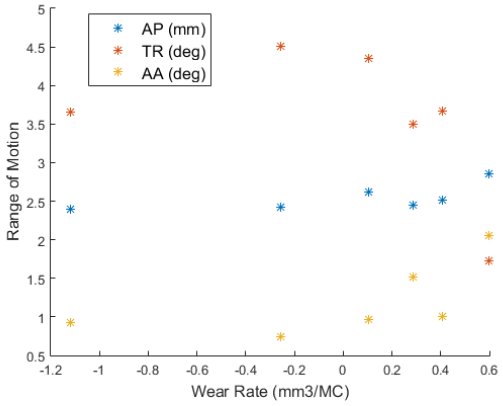

(a) Station Range of Motion vs Wear Rate

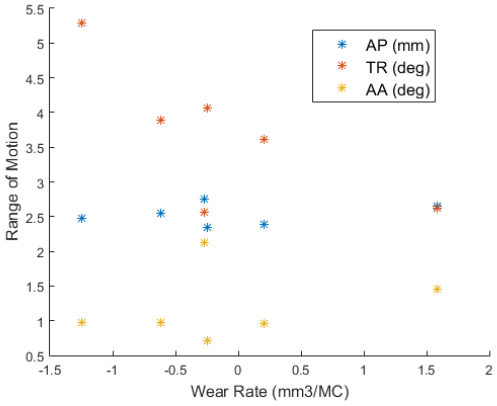

(b) Tibial Insert Range of Motion vs Wear Rate

Figure 6.22: The correlation between the wear rate and range of motion under the varus alignment condition for the stations (a) and the tibial inserts (b)

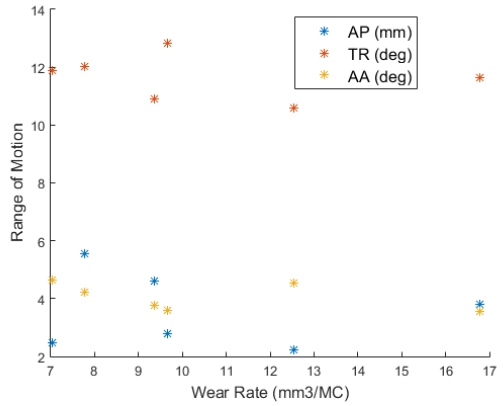

(a) Station Range of Motion vs Wear Rate

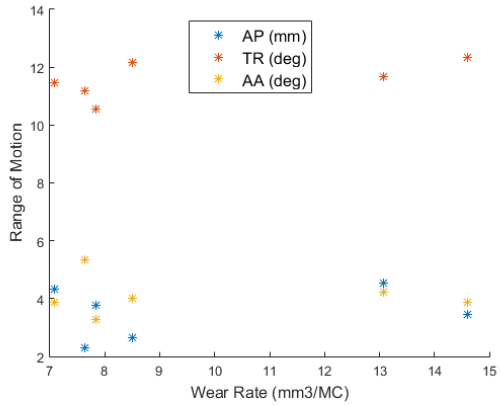

(b) Tibial Insert Range of Motion vs Wear Rate

Figure 6.23: The correlation between the wear rate and range of motion under the rotated alignment condition for the stations (a) and the tibial inserts (b)

station and the wear rates (Figure 6.23 (a)). There was also no positive correlation between the ranges of motion and wear rates of each tibial insert (Figure 6.23 (b)).

With the tibial slope alignment condition there was a significant difference in the AP range of motion between all of the stations with values ranging from 2.4mm to 6.9mm ($p<0.01$). Stations 3 and 5 resulted in significantly higher TR ranges of motion with values of 4.7° compared to values ranging from 2.5° to 4.0° on the other stations ($p<0.01$). There was less variation in the AA range of motion with stations 1, 2, 3 and 5 resulting in higher values than station 6 ($p<0.01$).

However there was no positive correlation between the differences in the ranges of motion between each station and the wear rates (Figure 6.24 (a)). There was also no positive correlation between the ranges of motion and wear rates of each tibial insert (Figure 6.24 (b)).

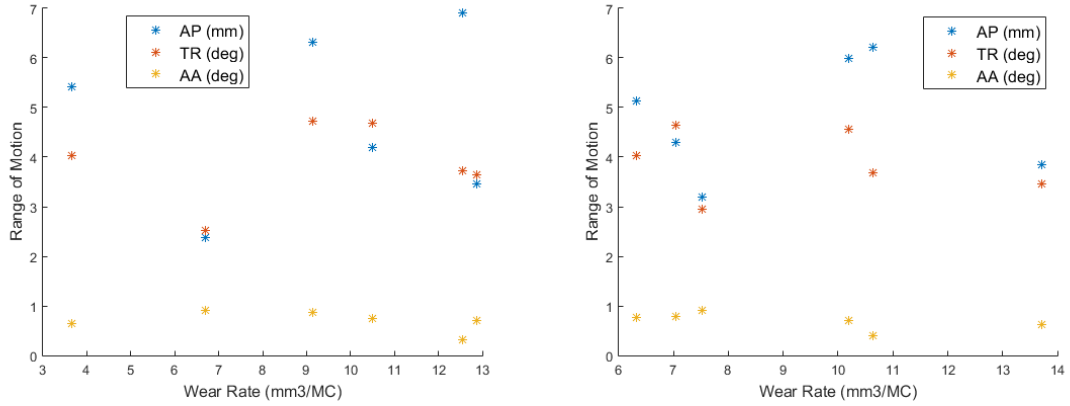

(a) Station Range of Motion vs Wear Rate (b) Tibial Insert Range of Motion vs Wear Rate

Figure 6.24: The correlation between the wear rate and range of motion under the tibial slope alignment condition for the stations (a) and the tibial inserts (b)

6.4.3.4 Wear scars

The average wear scars on the varus, rotational mismatch and tibial slope studies were determined (Figure 6.25). As the mechanical alignment study was not carried out on new tibial inserts the wear scars for this study were not able to be analysed.

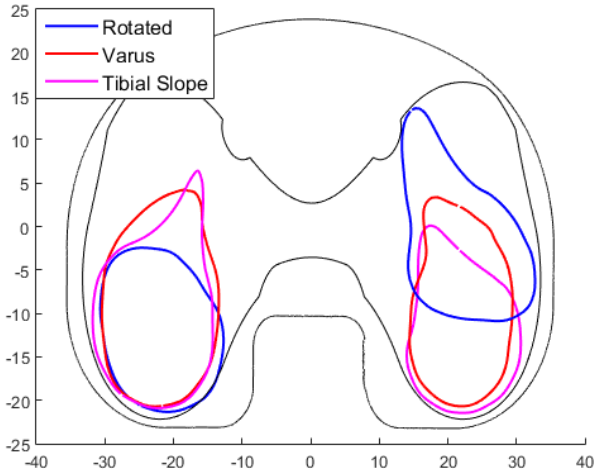

Figure 6.25: Average wear scar outlines after 2MC with stiff knee soft tissue condition for 4° varus, 14° rotational mismatch and 10° tibial slope

The rotational mismatch alignment resulted in less symmetrical wear scars; the lateral wear scar was more anterior and asymmetrical. The lateral wear scar for the rotated components was more anterior than for the other alignments. However with the varus and tibial slope alignments the medial and lateral wear scars were more similar in shape and position.

The area of each wear scar was determined for each alignment condition (Table 6.7); the varus alignment resulted in a significantly larger medial wear scar than the rotational

Table 6.7: Wear scar areas (mm^2) for each alignment condition after 2MC with the stiff knee soft tissue condition (mean±95%CI, n=6)

Alignment	Lateral	Medial	Total
Rotational Mismatch	308.6±63.11	280.4±18.19	589.0±75.97
Varus	290.9±33.94	350.5±23.63	641.3±28.63
Posterior Tibial Slope	270.0±35.2	331.2±16.12	601.2±43.1

mismatch and tibial slope alignments ($p<0.01$).

For the varus and tibial slope alignments the area of the medial wear scar was determined to be significantly higher than the lateral wear scar ($p<0.01$). There was no significant difference between the areas of the medial and lateral wear scars using the rotated components.

The varus alignment did not result in any overlap between the wear scar and the edge of the tibial insert. However with the tibial slope components there was overlap with the edge of the tibial insert on 3 components; 2 on the medial side and 1 on the lateral side. The overlap was small for two of the components; $0.01mm^2$ and $1.27mm^2$ on the third component. With the rotated alignment there was also overlap between the wear scar and the edge of the tibial insert on four of the components. One was on the lateral anterior side of $2.77mm^2$ and the other three were on the medial, posterior side of the insert with areas of $3.8mm^2$, $3.75mm^2$ and $0.8mm^2$.

6.4.3.5 Running Temperature

During each wear study the bulk temperature of the serum in each station was measured in order to determine any differences in running temperature (Table 6.8). For each study the running temperatures across the stations and soak controls were similar with the station temperatures being within 0.7°c of each other and the soak controls being within 0.3°c of each other.

Table 6.8: Mean running temperature (°C) with the 95% CI across the simulator of the stations and soak controls during each wear study under the CS springs

Study	Station	Soak
Mechanical	28.7±0.3	26.5±0.6
Varus	28.5±0.3	26.2±0.5
Rotated	28.4±0.3	26.2±0.8
Tibial Slope	29.1±0.4	26.3±0.5

During each study the station temperatures were hotter than the soak controls by around 2°C, this was due to the friction and heat generated in each of the stations.

6.4.3.6 Surface roughness

The surface roughness of the femoral and tibial contact surfaces were measured at the start and end of each wear study (Table 6.9). New tibial inserts were used for the rotated, varus and tibial slope wear studies.

Before the wear studies the average surface roughness of the tibials were similar, but the mechanical alignment had higher tibial Ra values at the start of the test. There was also no significant difference between the surface roughness of the femorals for the mechanical, varus and tibial slope alignments. The surface roughness of the rotated femorals was determined but they were then polished before testing in order to remove scratching, the approximate surface roughness value was based on other femorals after polishing was 0.02±0.01 (n=3).

Table 6.9: Average surface roughness values (µm) for the femoral and tibial components at the start and end of each wear study (mean±95%CI, n=6)

Alignment Condition	Femoral		Tibial	
	Start	End	Start	End
Mechanical	0.053±0.026	0.053±0.035	0.329±0.178	0.338±0.160
Varus	0.036±0.004	0.045±0.018	0.215±0.007	0.317±0.114
Rotated	approx. 0.02±0.01	0.028±0.010	0.221±0.028	0.232±0.155
Tibial Slope	0.044±0.024	0.117±0.028	0.229±0.016	0.303±0.065

The rotated tibial inserts also had some damage that was not due to wear; there were small indents in the tibial surface mainly on the lateral edge. This may have occurred during start up of the simulator; during the first 10 cycles only the AF and FE profiles were applied while the AF was increased gradually to its peak value. As there were no TR or AP forces the rotated components would remain at 14° rotational mismatch, the femoral may have been impacting the lateral side of the tibial insert as the AF and FE profiles were applied resulting in the indentation.

After the wear study using the varus alignment there was an increase in the surface roughness of the tibial components but there was no change in the femoral components. The rotated alignment wear study resulted in no significant change in the tibial or femoral components. The tibial slope wear study resulted in a large increase in the surface roughness of the tibial inserts and the femoral components.

There was no large difference in the roughness of the tibial inserts at the end of each wear study however the tibial slope alignment had significantly rougher femoral components at the end of the wear study than any of the other conditions.

6.5 Validation of Computational Model Under Different Alignment Conditions

In order to validate the computational model under each of the alignment conditions studied experimentally the output kinematics and contact area were compared to the experimental results. Validation of the computational model under the mechanical alignment condition was carried out in the previous chapter. In this chapter the validation was carried out under the remaining alignment conditions; 4° varus, 14° rotational mismatch, 10° posterior tibial slope and kinematic alignment under the stiff knee soft tissue condition.

The mean experimental AP, TR and AA displacements were compared to the computa-

tional predictions and the correlation between the two results determined. The position and area of the tibiofemoral contact was also compared between the experimental results using the Tekscan sensor to the computational model at four points in the cycle.

6.5.1 Varus Alignment Condition

The femoral component was rotated 4° around it's centre of rotation in order to generate a varus alignment. The tibial component was then rotated 4° around it's centre of rotation to generate varus alignment. The tibial centre of rotation was determined in the same way as with the mechanical alignment condition.

6.5.1.1 Kinematics

The computational prediction of the AP, TR and AA displacements were compared to the experimental values of the mean and 95% CI (Figure 6.26).

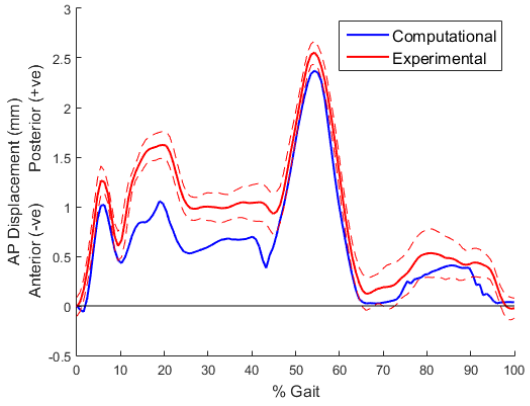

(a) AP Displacement

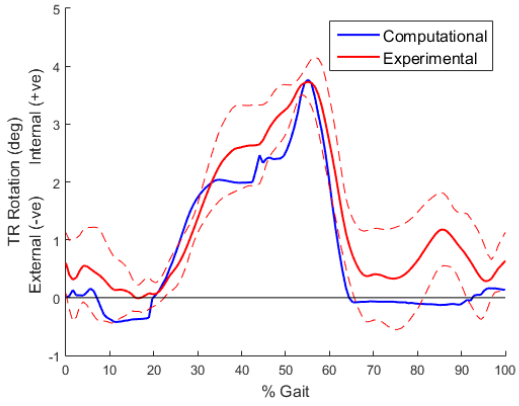

(b) TR rotation

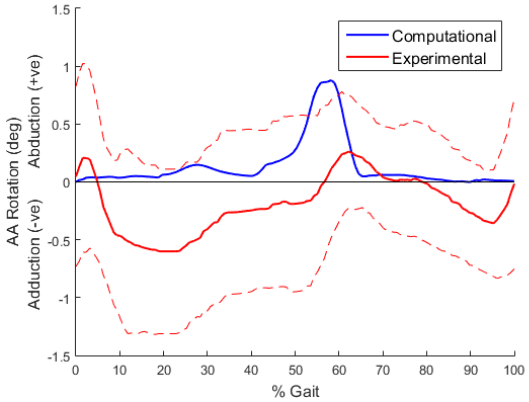

(c) AA Rotation

Figure 6.26: The AP (a), TR (b) and AA (c) displacements under the varus alignment condition and stiff soft tissue condition using the experimental methods (mean with 95% CI shown with dotted lines) and using the computational model

The shape of the AP profiles between the two methods were similar, however the experimental methods resulted in a higher initial peak. The computational prediction of the AP displacement was consistently lower than the experimental result. From 50-100% gait the computational prediction was within the 95% CI of the experimental data, however there was more variation at the start of the gait cycle, particularly from 10-50% gait.

The computational prediction of the TR rotation profile was similar to the experimental results and was within the 95% CI for most of the cycle. There was some variation between the profile shapes; for example the computational prediction resulted in a sharper increase to the peak value at 60%. The experimental results also resulted in a small peak in TR at around 85% gait which was not present in the computational prediction.

There was the greatest difference between the computational and experimental results in the AA rotation profiles. The computational prediction resulted in a peak at around 55% that was lower and occurred later in the cycle with the experimental results. However for most of the gait cycle the computational prediction was within the 95% CI of the experimental data.

There was a strong correlation in the AP displacement values between the computation prediction and the experimental results; the correlation coefficient was 0.96 (Figure 6.27 (a)). The gradient of the linear fit was 0.86 showing that the computational prediction of the AP displacement was lower than the experimental result.

There was also a good correlation in the TR rotation between the results with an r-squared value of 0.95 and a gradient of the linear fit of 0.95 (Figure 6.27 (b)). There was some variation with the computational data resulting in higher TR rotation however the computational prediction was still within the 95% CI of the experimental data for most of the cycle.

However there was poor correlation in the AA rotation between the two results, with a gradient of 0.25 and a correlation coefficient of 0.28 (Figure 6.27 (c)). The computational prediction resulted in an AA rotation close to 0° from 0-40% gait and 70-100% gait. Between 40-70% gait there was a peak in the AA rotation profile. The profile shape of the AA rotation was different in the experimental data, with a minima at around 15% gait and a smaller peak at around 65% gait. There was therefore a weak correlation between the two. However the AA rotation profile was within the 95% CI for most of the gait cycle.

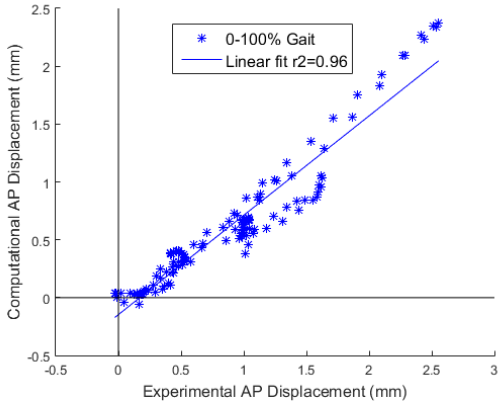

(a) AP Displacement gradient = 0.86

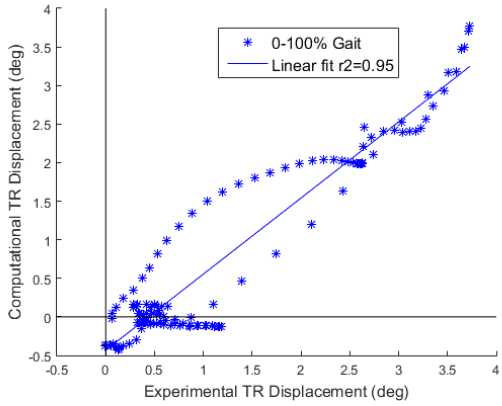

(b) TR rotation gradient =0.99

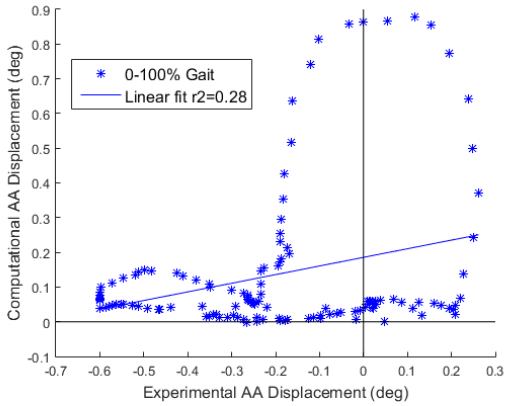

(c) AA Rotation gradient = 0.25

Figure 6.27: Correlation between the computational and experimental output kinematics for the varus alignment condition under the stiff soft tissue condition

6.5.1.2 Contact Area

At points 1, 3 and 4 in the gait cycle the computational model resulted in both medial and lateral contact which did not occur experimentally (Figure 6.28). The positions of the lateral contact point were similar; it was centrally located in the lateral tibial condyle.

At point 2 both methods resulted in similar contact positions however the lateral experimental contact area was larger.

The difference in loading between the two methods may be due to the differences in the AA rotations; the experimental methods resulted in more adduction and therefore may have caused more lateral loading.

The average contact area at each point in the cycle under the experimental and computational methods was determined (Table 6.10).

At all points in the cycle the computational prediction of the contact area was higher than that determined experimentally. However both sets of results followed a similar trend with the highest contact area occurring at point 2 in the cycle and the lowest at point 4. At points

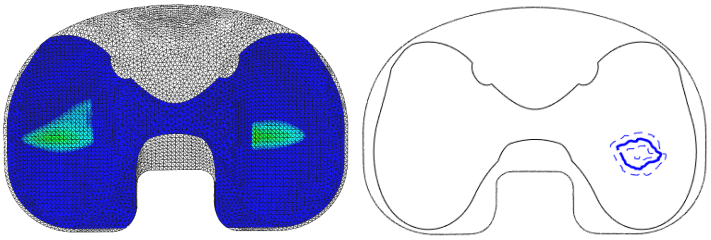

(a) Point 1

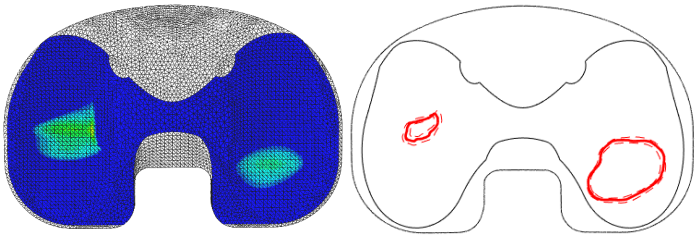

(b) Point 2

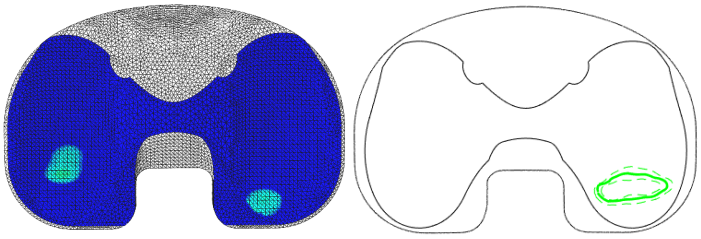

(c) Point 3

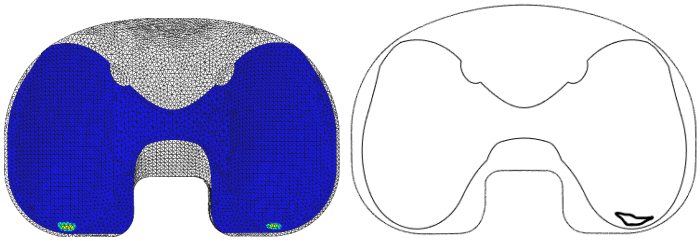

(d) Point 4

Figure 6.28: Contact area under the varus alignment condition and the stiff knee soft tissue condition at each point in the cycle using the computational (left with a red value showing 40MPa) and experimental methods right)

Table 6.10: The contact area (mm^2) at each point in the cycle under the varus alignment condition and stiff knee soft tissue condition using the computational and experimental (mean±95%CI) methods

Point	Experimental	Computational
1	89.1±24.4	161.9
2	181.9±18.3	226.2
3	62.6±35.1	88.5
4	7.1±5.0	8.2

3 and 4 the computational prediction was also within the 95% CI of the experimental data.

6.5.2 Rotated Alignment Condition

The femoral component was rotated 7° internally around it's centre of rotation. The tibial component was then rotated 7° externally around it's centre of rotation. This was determined in the same was as with the mechanical alignment condition.

6.5.2.1 Kinematics

The AP displacement profiles were similar using both the experimental and computational methods (Figure 6.29 (a)).

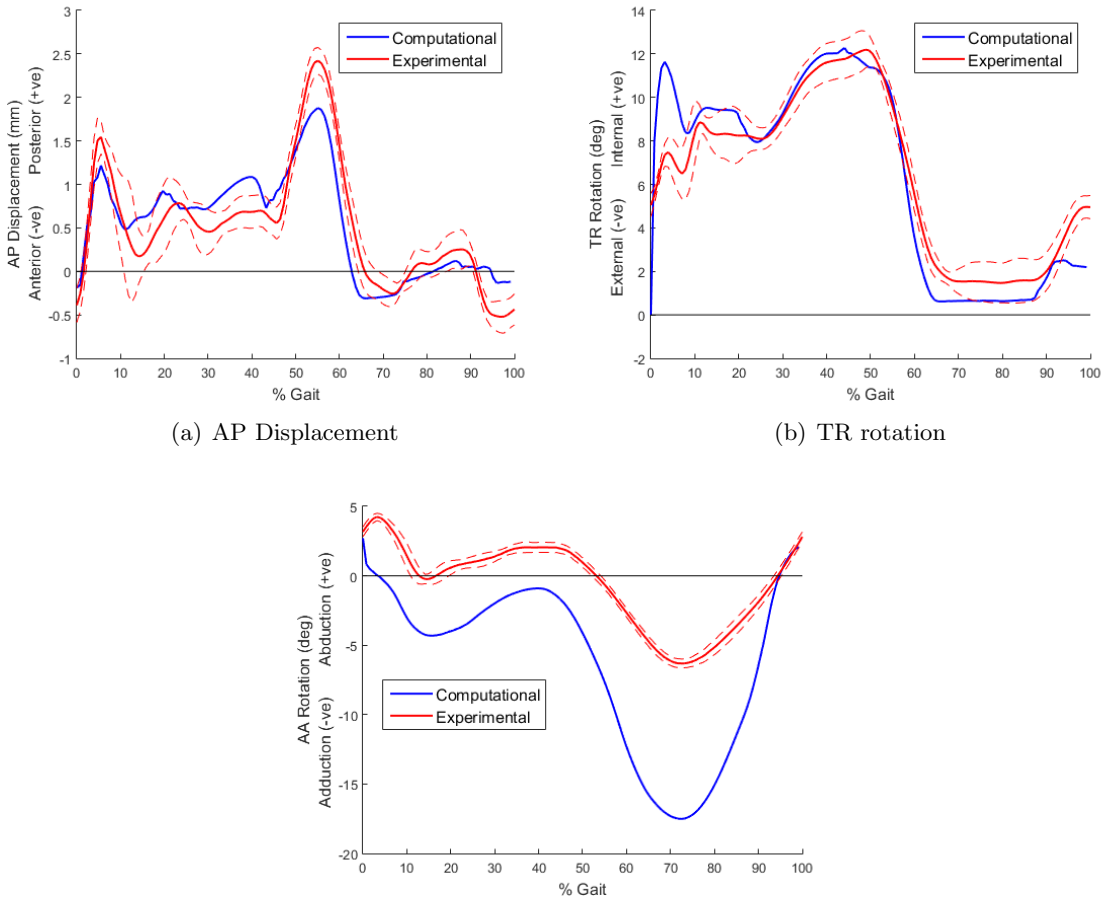

(a) AP Displacement

(b) TR rotation

(c) AA Rotation

Figure 6.29: The AP (a), TR (b) and AA (c) displacements under the rotated alignment condition and stiff knee soft tissue condition using the experimental methods (mean with 95% CI shown with dotted lines) and using the computational model

However the computational prediction resulted in a lower peak AP displacement and lower peak AP displacement at 5% gait. From 10% to 50% gait the computational prediction was

higher than the experimental results. However from 50% to 90% gait the computational prediction was lower than the experimental data.

For 10% to 60% the computational prediction of the TR rotation was within the 95% CI of the experimental data (Figure 6.29 (b)). However the computational prediction did result in a higher peak TR rotation at around 5% gait than the experimental data, which may be due to the momentum of the tibial component rotating as the AF is applied. As the computational prediction resulted in a lower TR rotation at the end of the gait cycle there may have been higher momentum on the tibial component which resulted in a higher displacement.

The AA profile shapes between the computational and experimental data were similar with minima at around 10% gait and around 70% gait with a maxima at 40% gait (Figure 6.29 (c)). However the computational prediction resulted in higher adduction throughout the gait cycle, which may be due to the weight of the AA arm in the experimental simulator as discussed previously.

There was a strong correlation in the AP displacements between the computational and experimental methods (Figure 6.30 (a)).

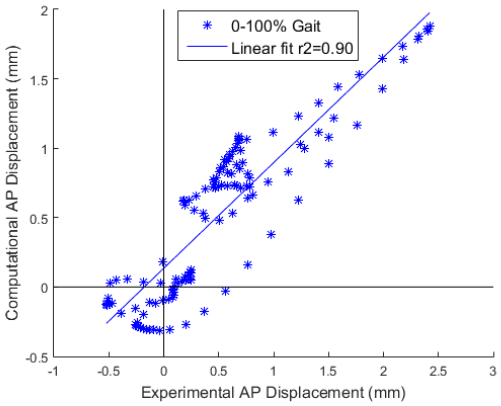

(a) AP Displacement gradient = 0.76

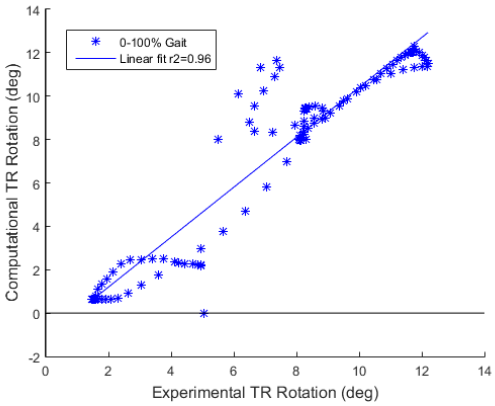

(b) TR rotation gradient = 0.96

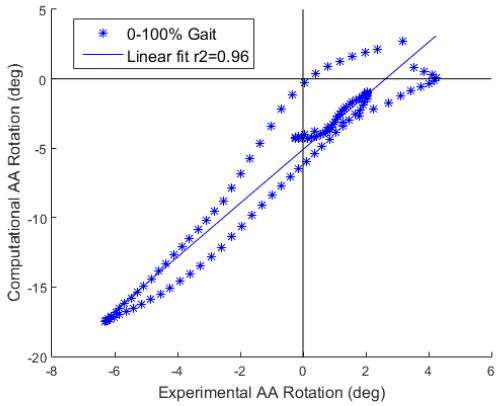

(c) AA Rotation gradient = 1.93

Figure 6.30: Correlation between the computational and experimental output kinematics for the rotated alignment condition under the stiff knee soft tissue condition

The linear fit of the data had a gradient of 0.76 and an r-squared value of 0.9. This implies that at higher experimental AP displacement values the computational prediction resulted in lower values; this corresponds to the computational prediction resulting in a lower peak AP displacement.

There was also a strong correlation in the TR rotations between the two methods with a gradient of 0.96 and an r-squared value of 0.96. There was some variation between the two results where the computational TR rotation was between 8° and 12°. This section corresponds to the initial peak at 5% gait that occurred in the computational prediction that was not present in the experimental results.

There was also a strong correlation between the AA rotations with an r-squared value of 0.96. However the gradient of the linear fit was 1.9 showing that the computational prediction resulted in higher AA rotation values than the experimental results throughout the gait cycle.

6.5.2.2 Contact Area

The contact area under the computational and experimental methods are shown for each point in the cycle under the rotated alignment condition in Figure 6.31.

At points 1 and 2 in the cycle the positions of the medial and lateral contacts were different between the two methods; the experimental data only resulted in a lateral contact whereas the computational model resulted in both medial and lateral contact. This difference may be due to the differences in kinematics at this point; the experimental data resulted in higher AA rotation which may have resulted in just lateral contact. This difference in the AA rotation may also have resulted in the different shaped lateral contact areas.

At points 3 and 4 the contact points were more similar between the two methods. At point 3 the computational data resulted in a higher pressure on the medial condyle, again this may be due to the differences in the AA rotation as the computational data resulted in more adduction.

At point 4 the computational method resulted in a small, low pressure lateral contact on the lateral edge of the tibial insert. This did not occur using the experimental methods, however this could be due to the sensitivity or position of the Tekscan sensor.

The average contact area at each point in the cycle under the experimental and computational methods was determined (Table 6.11). At each point the computational model resulted in higher contact areas, however the values and the trend across the cycle were similar. The highest contact area values occurred at points 2 and 3 in the cycle and the lowest at point 4. At points 2 and 4 in the cycle the computational prediction was also within the 95% CI of the experimental data. Differences in the AA rotation and therefore the loading distribution on the tibial insert may have resulted in some of the differences in contact area.

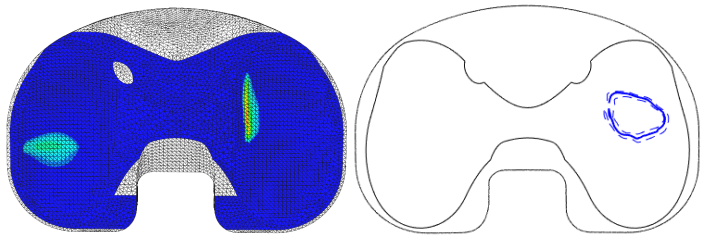

(a) Point 1

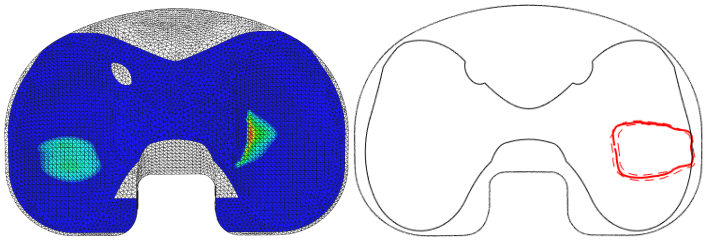

(b) Point 2

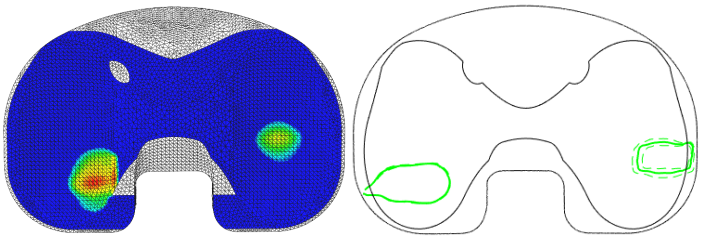

(c) Point 3

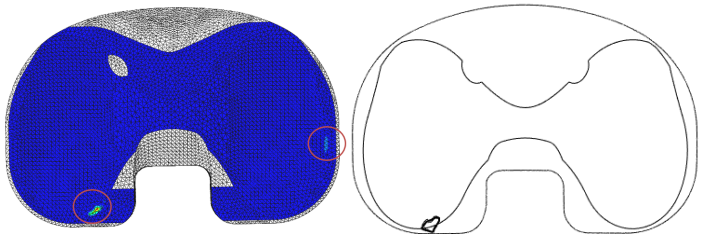

(d) Point 4

Figure 6.31: Contact area under the rotated alignment condition and the stiff knee soft tissue condition at each point in the cycle using the computational (left with a red value for 85MPa and blue for 0MPa) and experimental methods (right)

Table 6.11: The average contact area (mm^2) at each point in the cycle under the rotated alignment condition and stiff knee soft tissue condition using the computational and experimental methods

Point	Experimental	Computational
1	92.1±15.2	114.7
2	154.3±22.6	174.1
3	128.3±22.3	179.3
4	6.0±4.3	8.2

6.5.3 Tibial Slope Alignment Condition

The tibial component was rotated 10° around it's centre of rotation to generate a posterior tibial slope. The position of the tibial centre of rotation was determined in the same way as with the mechanical alignment condition.

6.5.3.1 Kinematics

The computational prediction of the AP displacement profile was a similar shape as the experimental results (Figure 6.32 (a)). During the first half of the gait cycle the computational prediction resulted in a higher AP displacement than the experimental results. However in the second half of the gait cycle the computational prediction was close to the experimental data.

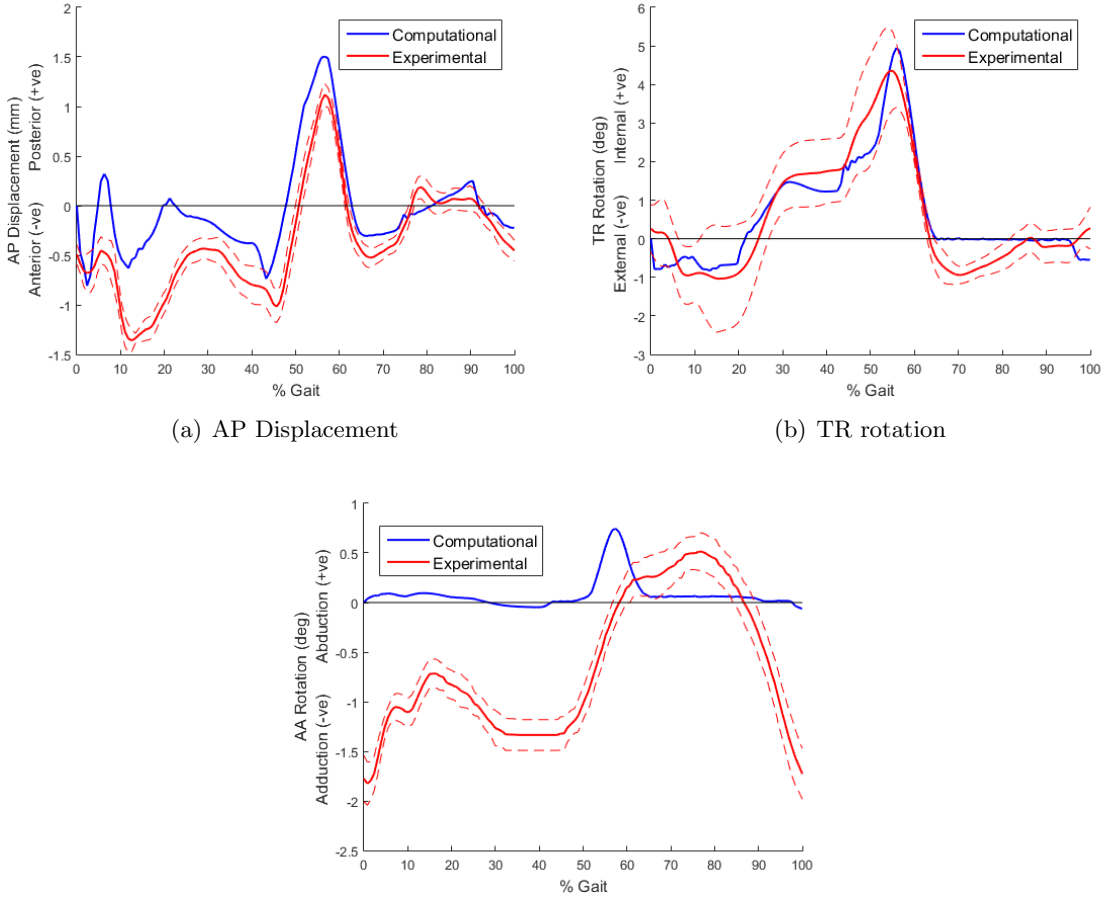

(a) AP Displacement

(b) TR rotation

(c) AA Rotation

Figure 6.32: The AP (a), TR (b) and AA (c) displacements under the tibial slope alignment condition and stiff knee soft tissue condition using the experimental methods (mean with 95% CI shown with dotted lines) and using the computational model

The computational prediction of the TR rotation was very similar to the experimental results (Figure 6.32 (b)). The computational prediction resulted in a higher peak TR rotation

however it was within the 95% CI of the experimental data for most the gait cycle.

The greatest difference between the two methods was with the AA rotation profile; the computational prediction resulted in an AA rotation close to 0° for most of the cycle with a peak at around 60% gait (Figure 6.32 (c)). The experimental methods resulted in a very different profile shape with a maxima at 15%, a minima at 40% gait and a peak at 80% gait. As discussed previously the difference in the AA rotation may be due to the weight of the AA arm in the experimental simulator.

There was a good correlation between the AP displacement values from the computational and experimental data with an r-squared value of 0.84 and a gradient of 0.75. (Figure 6.33 (a)) The higher predicted AP values during the first half of the gait cycle are shown by the line of points crossing through (0,0.6). Otherwise the points in the cycle follow a strong correlation between the two data sets.

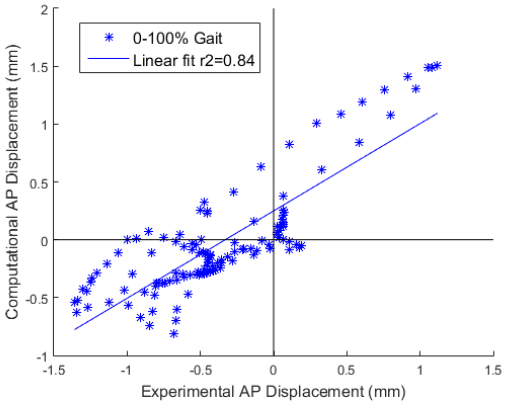

(a) AP Displacement gradient = 0.75

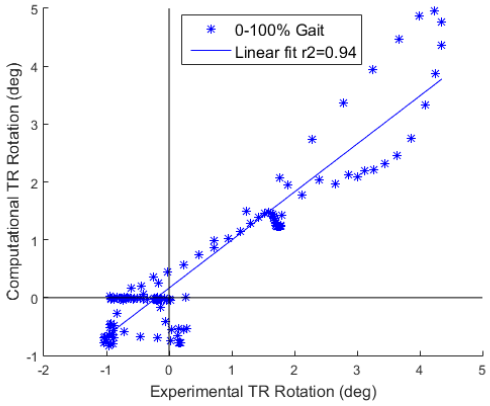

(b) TR rotation gradient = 0.83

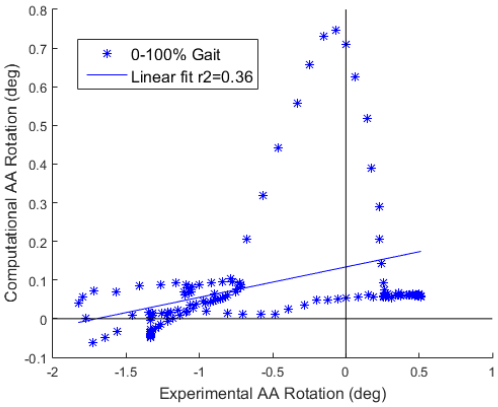

(c) AA Rotation gradient = 0.08

Figure 6.33: Correlation between the computational and experimental output kinematics for the tibial slope alignment condition under the stiff knee soft tissue condition

There was also a strong correlation in the TR rotation; the linear fit had a gradient of 0.83 and an r-squared value of 0.94 (Figure 6.33 (b)). The area with the greatest difference between the two data sets occurred at high TR rotation values. This corresponds to the higher

peak TR rotation that occurred with the computational prediction.

As with the other alignment conditions there was a weak correlation in the AA rotation values between the experimental and computational values (Figure 6.33 (c)). The linear fit had a gradient of 0.08 and an r-squared value of 0.36, this reflects the differences in the AA rotation profile shapes and values between the two methods.

6.5.3.2 Contact Area

At point 1 in the cycle the computational method resulted in a more anterior lateral contact compared to the experimental methods, this difference may be due to differences in the TR rotation at this point (Figure 6.34).

At points 2, 3 and 4 in the cycle the position of the contact points between the two methods were similar but at all points the computational model resulted in a more medial contact. This difference may be due to the differences in the AA rotation between the two methods at this point.

The average contact area was determined at each point under the tibial slope alignment using the experimental and computational methods (Table 6.12).

As with the other alignment conditions the computational prediction for the contact area was higher than the experimental result for most of the points. However the two sets of results follow a similar trend. At points 2 and 4 in the gait cycle the computational prediction was within the 95% CI of the experimental data. Some of the differences in the contact area may be due to the differences in the loading patterns of the tibial insert.

Table 6.12: The average contact area (mm^2) at each point in the cycle under the tibial slope alignment condition and stiff knee soft tissue condition using the computational and experimental methods

Point	Experimental	Computational
1	125.4±34.9	178.2
2	153.1±85.6	237.7
3	29.0±11.3	76.7
4	35.7±63.6	3.3

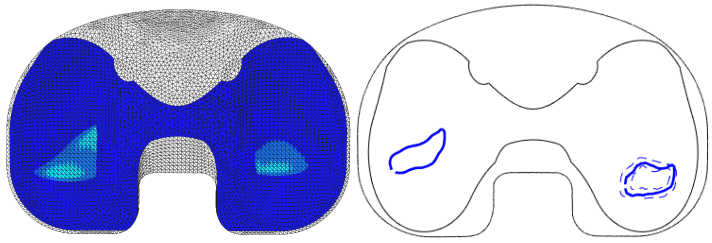

(a) Point 1

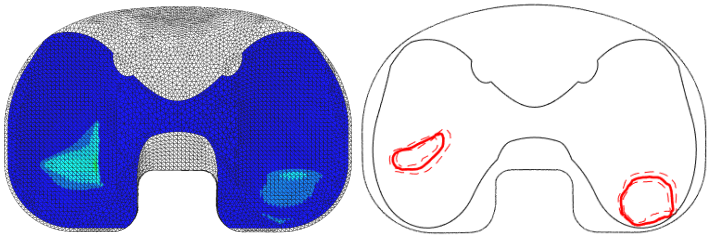

(b) Point 2

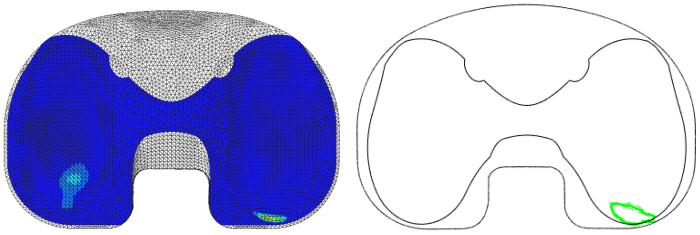

(c) Point 3

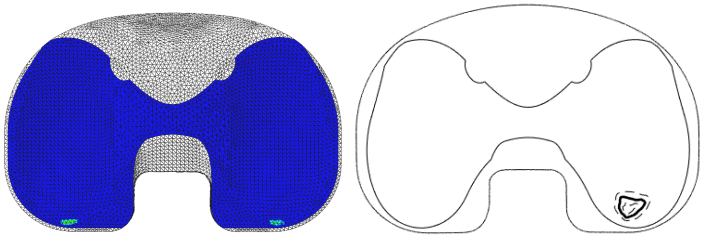

(d) Point 4

Figure 6.34: Contact area under the tibial slope alignment condition and the stiff knee soft tissue condition at each point in the cycle using the computational (left with a red value for 70MPa and a blue value for 0MPa) and experimental methods (right)

6.5.4 Kinematic Alignment Condition

The femoral component was rotated 2.5° around it's centre of rotation to result in valgus alignment. The tibial component was rotated 4.6° around it's centre of rotation to generate a posterior tibial slope and 3.4° to generate a varus alignment. The position of the tibial centre of rotation was determined in the same way as with the mechanical alignment condition.

6.5.4.1 Kinematics

The computational prediction resulted in an AP displacement profile with a similar shape to that determined experimentally (Figure 6.35 (a)). However the computational model resulted in more anterior displacement, especially during the first half of the cycle. This resulted in a higher computational prediction of the peak AP displacement.

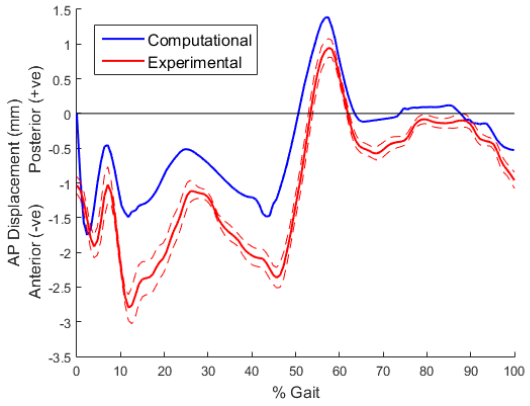

(a) AP Displacement

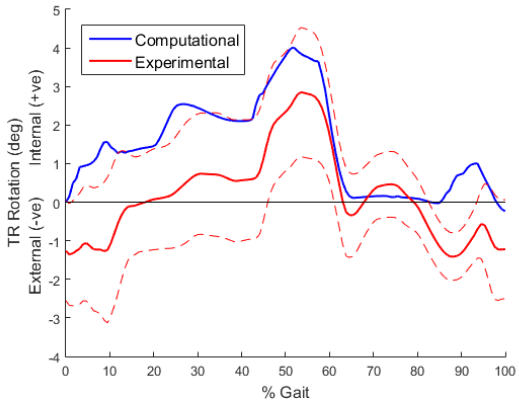

(b) TR rotation

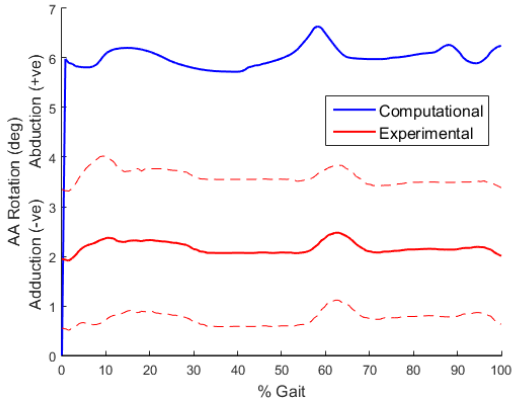

(c) AA Rotation

Figure 6.35: The AP (a), TR (b) and AA (c) displacements under the kinematic alignment condition and stiff knee soft tissue condition using the experimental methods (mean with 95% CI shown with dotted lines) and using the computational model

The computational prediction of the TR rotation profile was a similar shape to that determined experimentally and was within the 95% CI for most of the cycle (Figure 6.35 (b)). However it resulted in higher TR rotation throughout the cycle, especially during the first half of the gait cycle, as with the AP displacement.

The experimental AA rotation was centred around 2° abduction which resulted in only lateral contact on the tibial insert throughout the cycle (Figure 6.35 (c)). However the computational prediction resulted in the AA rotation profile centred around 6° abduction. This difference in the AA rotation profiles may be due to the weight of the AA arm in the simulator

restricting the AA rotation. The computational prediction may be a more accurate representation of kinematic alignment in vivo as it resulted in both medial and lateral contact. This difference in the contact may also have resulted in differences in the AP displacement and TR rotation profiles due to the extra contact on the medial condyle in the computational model.

Three was a strong correlation in the AP displacements between the two data sets with a linear fit of gradient 0.7 and r-squared value of 0.93 (Figure 6.36). This showed the strong correlation in the profile shape between the two results despite the higher displacement values determined with the computational model.

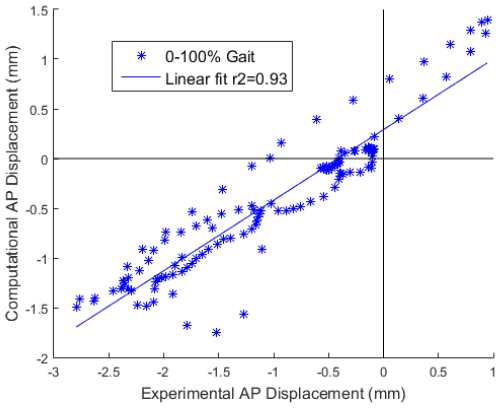

(a) AP Displacement gradient = 0.71

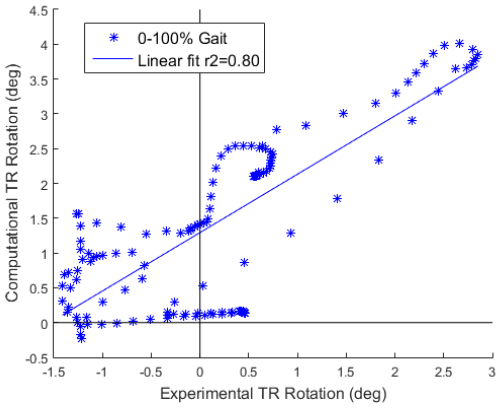

(b) TR rotation gradient = 0.84

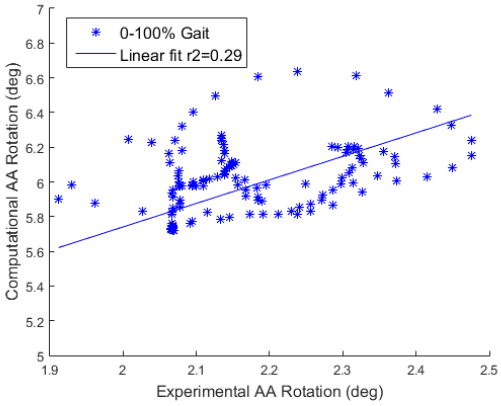

(c) AA Rotation gradient = 1.35

Figure 6.36: Correlation between the computational and experimental output kinematics for the kinematic alignment condition under the stiff knee soft tissue condition

There was also a good correlation in the TR rotations with a linear fit with gradient of 0.84 and an r-squared value of 0.8. Again this showed the good correlation between the TR rotation profile shapes between the two methods.

As with the other alignment conditions there was a weak correlation in the AA rotation values between the computational and experimental results. The linear fit had a gradient of 1.35 and an r-squared value of 0.29. This showed that along with the offset between the two

displacement profiles there was also a difference in the profile shape.

6.5.4.2 Contact Area

Under the experimental methods there was only lateral contact between the femoral and tibial components throughout the gait cycle which may be due to the weight of the AA arm in the simulator restricting the AA rotation (Figure 6.37).

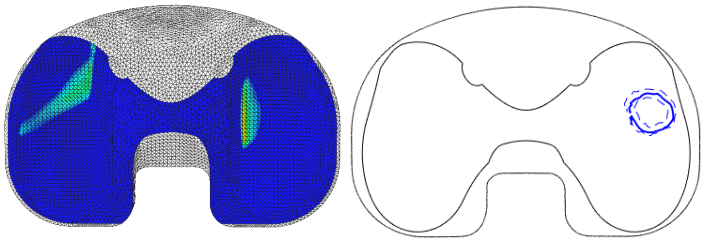

(a) Point 1

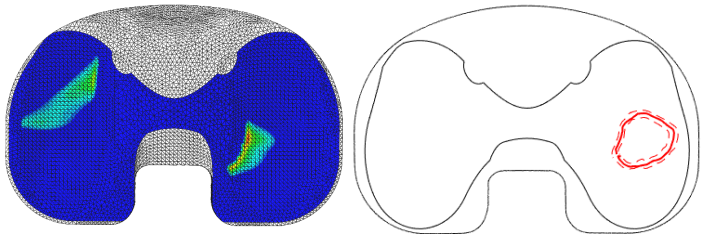

(b) Point 2

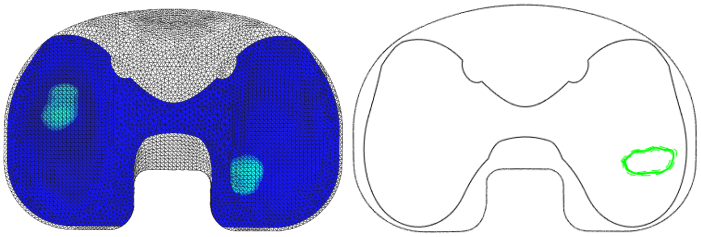

(c) Point 3

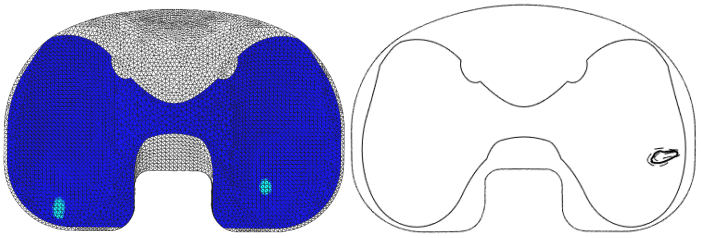

(d) Point 4

Figure 6.37: Contact area under the kinematic alignment condition and the stiff knee soft tissue condition at each point in the cycle using the computational (left with a red value showing 45MPa) and experimental methods (right)

The computational prediction resulted in higher AA rotation and more balanced loading between the tibial condyles. This may therefore be a more accurate representation of kinematic

alignment in vivo.

At point 1 in the cycle the computational prediction resulted in a smaller and more narrow lateral contact compared to the experimental data.

At point 2 in the cycle the experimental methods resulted in a more posterior lateral contact than at point 1. The computational prediction also resulted in a more posterior lateral contact, which again was a different shape to that determined experimentally.

At point 3 in the cycle the experimental data resulted in a smaller and slightly more posterior lateral contact than at the previous step. The computational model also resulted in a more posterior lateral contact than at point 2 in the cycle.

At the final point in the cycle the experimental data resulted in a small contact area, the computational prediction also resulted in a small lateral contact area at this point.

The average contact area was determined at each point under the tibial slope alignment using the experimental and computational methods (Table 6.13). For the kinematic alignment during experimental simulation there was only ever contact on the lateral tibial condyle, however under computational methods there was both medial and lateral contact. This may be due to the weight of the AA arm in the experimental simulator reducing the AA rotation and therefore resulting in just lateral contact. Therefore the computational prediction of the contact area was greater than the experimentally measured value at each point in the cycle.

Table 6.13: The average contact area (mm^2) at each point in the cycle under the kinematic alignment condition and stiff knee soft tissue condition using the computational and experimental methods

Point	Experimental	Computational
1	84.3±12.5	139.8
2	120.0±13.9	174.3
3	42.9±9.7	139.7
4	14.5±4.5	21.4

6.6 Computational Results

Once the computational model was validated parametric testing was carried out in order to find the kinematics and contact pressure under different alignment conditions.

The computational model was run under one additional varus alignment condition of 2° femoral and tibial varus.

The rotated alignment model was run under two additional rotational mismatch values of 8° and 4° in order to generate results between mechanical alignment and 14° rotational mismatch. Each time the femoral and tibial components were rotated in opposite directions by equal amounts e.g. for 8° rotational mismatch the femoral component was rotated 4° internally and the tibial component 4° externally.

The tibial slope alignment condition was run under one additional condition of 4° posterior tibial slope.

Finally one additional kinematic alignment conditions was run; this was defined as half the alignment values that were studied experimentally (Table 6.5).

For each alignment condition the effect on the kinematics, contact pressure and contact area will be investigated.

6.6.1 Varus Alignment Condition

The varus alignment condition was studied under 4° and 2° femoral and tibial varus and the output kinematics, contact pressure and contact area compared to mechanical alignment.

6.6.1.1 Kinematics

The output AP, TR and AA kinematics were determined for both the varus alignment conditions and compared to mechanical alignment (Figure 6.38).

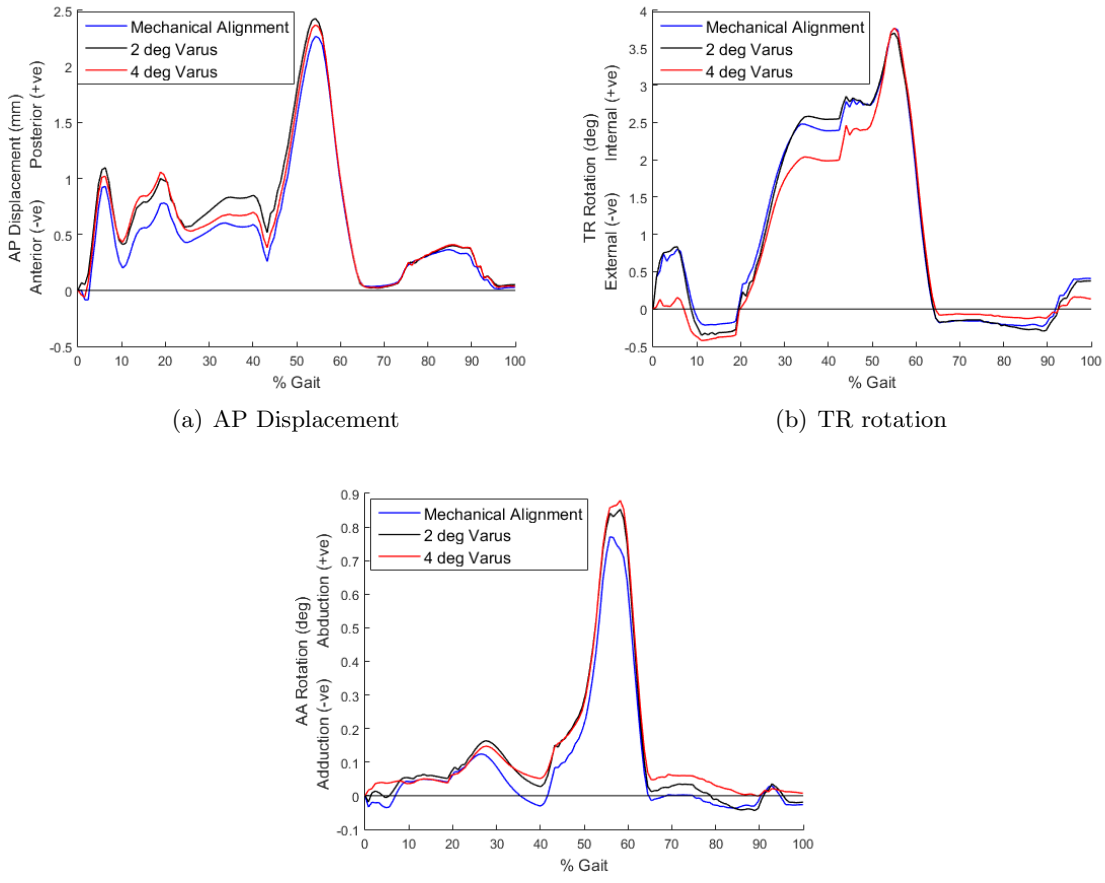

(a) AP Displacement

(b) TR rotation

(c) AA rotation

Figure 6.38: The output AP (a), TR (b) and AA (c) displacements from the computational model under mechanical alignment, 2° varus and 4° varus alignment conditions under the stiff knee soft tissue condition

There was a minimal difference in the AP displacement profiles between the three alignment conditions studied, especially from 50% gait onwards. The 4° and 2° varus alignment

conditions resulted in similar profiles with more posterior displacement in the first half of the cycle compared to mechanical alignment. The offset between the profiles at this point was around 0.25mm. Between 25% and 40% gait the 2° varus alignment condition resulted in a higher posterior displacement compared to both the other alignment conditions. This was the point in the cycle with the greatest difference between the 2° and 4° alignment conditions. However the offset between them was still small with a value of around 0.15mm.

The mechanical alignment and 2° varus alignment conditions resulted in very similar TR rotation profiles. The 4° varus alignment condition resulted in a lower initial peak at 5% gait and resulted in lower TR rotations between 25% and 50% gait. This section of the gait cycle is the same section where the 2° varus alignment condition resulted in more AP displacement than the 4° varus alignment condition. From 50% gait onwards the three TR rotation profiles were very similar.

As with the AP displacement profile the 4° varus and 2° varus alignment conditions resulted in very similar AA rotation profiles. Whereas the mechanical alignment condition resulted in lower AA rotation from 25% to 60% gait. However the differences in the AA rotations were small with the mechanical alignment resulted in a peak around 0.1° lower than the other alignment conditions.

6.6.1.2 Contact Area and Pressure

The pressure distribution was determined for the mechanical alignment, 2° varus and 4° varus alignment conditions at four points in the gait cycle (Figure 6.39). These points were the same four points where the contact area was measured experimentally.

Due to the similar kinematics between the alignment conditions the contact positions were similar at all four points investigated. There was no clear difference in contact position between the alignment conditions.

The peak contact pressure was determined at each of the four points in the cycle for each of the three alignment conditions (Table 6.14).

Table 6.14: The peak contact pressure (MPa) from the computational model under mechanical alignment, 2° varus and 4° varus alignment conditions under the stiff knee soft tissue condition at four points in the gait cycle

Point	Mechanical Alignment	2° Varus	4° Varus
1	29.10	28.51	22.30
2	19.96	20.15	23.28
3	16.31	18.25	14.36
4	22.96	23.84	27.63

At the first point in the cycle the 4° varus alignment condition resulted in a lower value than the mechanical and 2° varus alignment conditions. This difference may be due to the more medial position of the lateral contact point under the mechanical and 2° varus alignment conditions, resulting in a higher contact pressure on the medial side of the lateral condyle.

At point 2 in the cycle the 4° varus alignment condition resulted in a higher contact

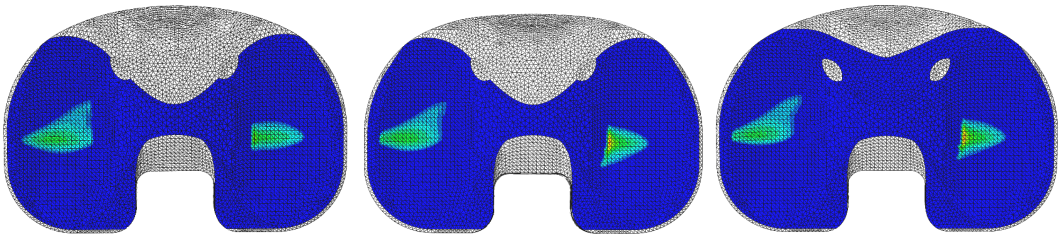

(a) Point 1

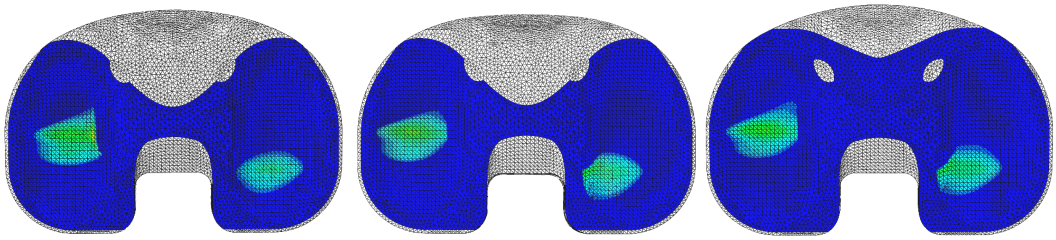

(b) Point 2

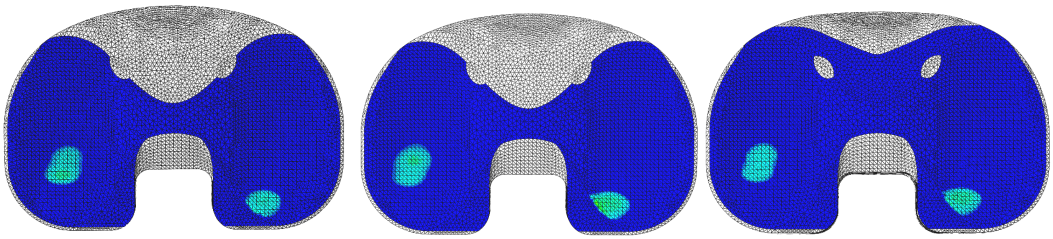

(c) Point 3

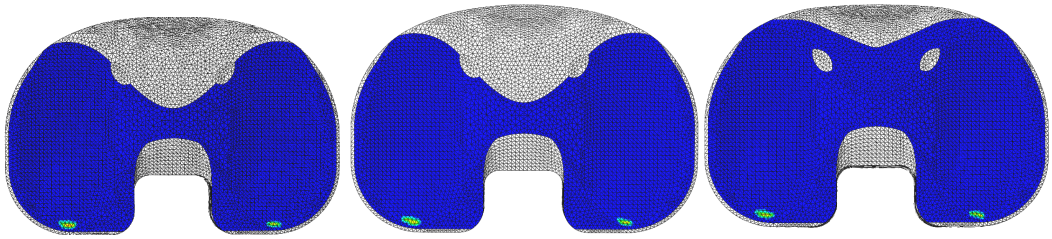

(d) Point 4

Figure 6.39: Computational prediction of the contact pressure under 4° varus (left), 2° varus (centre) and mechanical alignment (right) under the stiff knee soft tissue condition (0MPa blue, 40MPa red)

pressure. The increased varus alignment may have resulted in more medial than lateral loading and therefore a higher peak contact pressure on the medial tibial condyle.

At point 3 in the cycle the 2° varus alignment condition resulted in a higher value compared to the other two alignment conditions. The 2° and 4° varus alignment conditions resulted in increased AP displacements at this point in the cycle which may have resulted in a higher lateral pressure at this point due to the position of the femorotibial contact. The increased varus alignment of 4° may have resulted in more medial loading as discussed previously which may have resulted in a higher peak lateral pressure with the 2° varus alignment compared to

the 4° varus alignment.

At point 4 in the cycle. The 4° varus alignment resulted in a higher value compared to the mechanical and 2° varus alignment conditions. This again may be due to the loading of the 4° varus alignment condition resulting in a higher medial pressure.

The contact area for each of the three alignment conditions was determined throughout the gait cycle (Figure 6.40).

There was a minimal difference in the contact area between the three alignment conditions at all points in the cycle. The 2° and 4° varus alignment conditions did result in a higher contact area between 10% and 20% gait however this difference was minimal. This difference may be due to the differences in loading between the alignment conditions resulting in different contact areas.

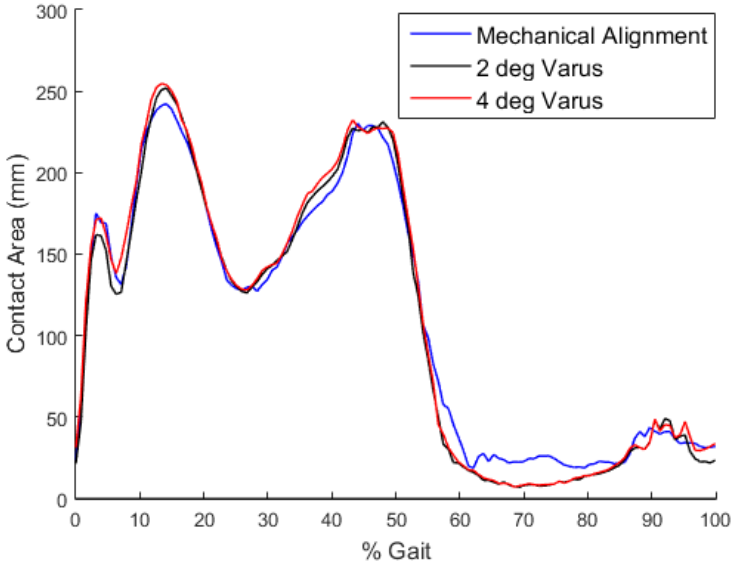

Figure 6.40: The contact area (mm²) from the computational model under mechanical alignment, 2° varus and 4° varus alignment conditions under the stiff knee soft tissue condition

6.6.2 Rotated Alignment Condition

The rotated alignment condition was studied under 14°, 8° and 4° rotational mismatch and the output kinematics, contact pressure and contact area compared to mechanical alignment.

6.6.2.1 Kinematics

The mechanical alignment, 8° and 4° rotational mismatch alignment conditions resulted in similar AP displacement profiles (Figure 6.41 (a)). The 14° rotational mismatch alignment condition resulted in lower peak AP displacement than the other alignment conditions, however the difference was in value was small.

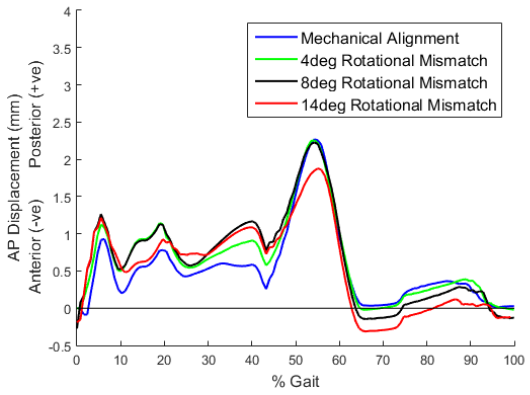

(a) AP Displacement

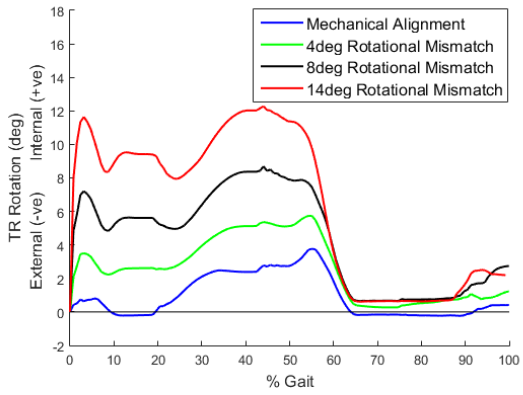

(b) TR rotation

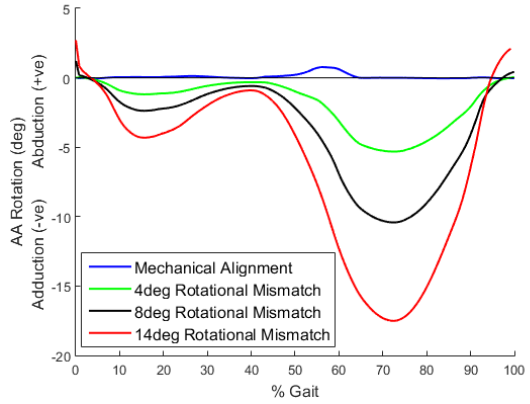

(c) AA rotation

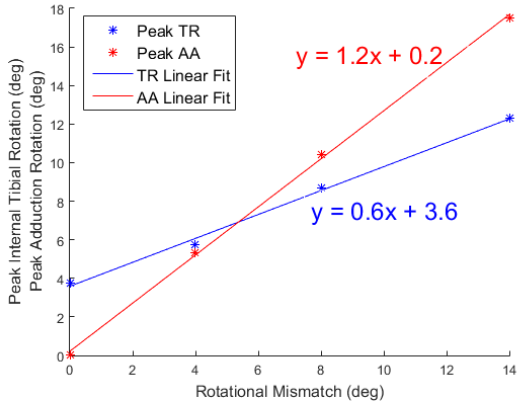

(d) Peak TR and AA vs Rotational Mismatch

Figure 6.41: The output AP (a), TR (b) and AA (c) displacements from the computational model under mechanical alignment, 8° rotational mismatch and 14° rotational mismatch alignment conditions under the stiff knee soft tissue condition. Relationship between the rotational mismatch and the peak internal TR and adduction rotation was also found (d)

The 14° and 8° rotational mismatch alignment conditions resulted in a similar shape TR rotation profile, however the amplitude under the 8° mismatch condition was lower (Figure 6.41 (b)). The 14° rotational mismatch alignment condition reached a peak of around 12° compared to 8° under the 8° rotational mismatch alignment condition. With the 4° rotational mismatch alignment condition the shape of the TR rotation profile was similar to that under mechanical alignment, however the amplitude was higher. There was a linear relationship between the peak TR rotation and the rotational mismatch of the components (Figure 6.41 (d)). The gradient of this relationship was less than one, which suggests that the conformity of the insert or the soft tissue condition may be restricting the peak TR rotation.

All the rotational mismatch alignment conditions resulted in similar AA rotation profile shapes but with different amplitudes (Figure 6.41 (c)). The 14° mismatch condition resulted in a peak of -17.5° compared to -10.4° with the 8° mismatch and -5.3° with the 4° rotational mismatch alignment condition. As with the TR rotation there was a linear relationship

between the rotational mismatch and the peak adduction rotation (Figure 6.41 (d)). The gradient of the linear fit was higher for the AA rotation, therefore the AA rotation was more sensitive to changes in the rotational alignment. Unlike the AP and TR displacement profiles the greatest difference between the alignment conditions occurred in the second half of the gait cycle. This may be due to the decrease in the TR rotation down to around 1° in the second half of the gait cycle. This would result in there being no correction of the rotational mismatch of each alignment condition and therefore may have resulted in increased AA rotations due to the poor conformity of the femoral and tibial components.

6.6.2.2 Contact Pressure and Area

At point 1 in the gait cycle the 14° and 8° rotational mismatch alignment conditions resulted in similar contact areas (Figure 6.42). The lateral contact for both alignment conditions was narrow and longer than the lateral contact under mechanical alignment. The 14° rotational mismatch condition resulted in the longest contact area which came close to the anterior edge of the tibial insert. For points 1-3 the 4° mismatch alignment condition resulted in similar contact positions to those found under mechanical alignment conditions.

At point 2 in the cycle the 14° rotational mismatch alignment condition resulted in a more anterior lateral contact and more posterior medial contact than the other two rotated alignment conditions. The mechanical alignment meanwhile resulted in the opposite; a more anterior medial and more posterior lateral contact. This difference may be due to the differences in the TR rotations between the alignment conditions.

At point 3 in the cycle the 14° rotational mismatch alignment condition again resulted in a more posterior medial and more anterior lateral contact. The medial contact was close to the centre of the tibial insert, resulting in high contact pressures. The 8° rotational mismatch condition resulted in the medial and lateral contacts in similar positions, while the mechanical alignment again resulted in a posterior lateral and anterior medial contact. As before this may be due to the differences in the TR rotations.

At point 4 in the cycle all four alignment conditions resulted in contact on the posterior edge of the tibial insert. The mechanical alignment condition however was the only one to result in both medial and lateral contact. This difference in loading may be due to the differences in the AA rotations at this point.

At all the points in the cycle the 14° rotational mismatch alignment condition resulted in higher peak pressure values than all the other alignment conditions (Table 6.15). At points 1 and 2 in the cycle this may be due to the lateral contact position occurring closer to the centre of the tibial insert, resulting in higher stresses. At point 3 this may have been due to the position of the medial contact occurring closer towards the centre of the tibial insert again resulting in higher stress, At point 4 in the cycle the difference may be due to the increased AA rotation resulting in an increased pressure on the medial side of the tibial insert.

The 8° rotational mismatch alignment condition resulted in higher peak pressures at points 1, 2 and 4 than the mechanical alignment condition. The reason for this may be the same as

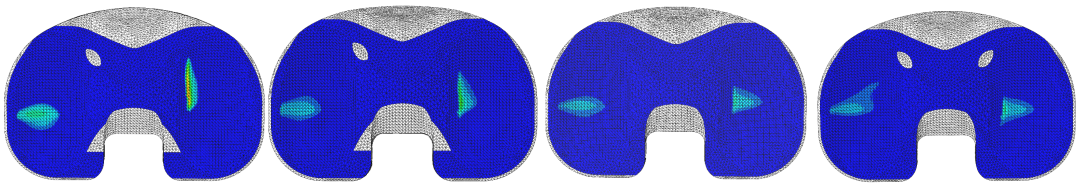

(a) Point 1

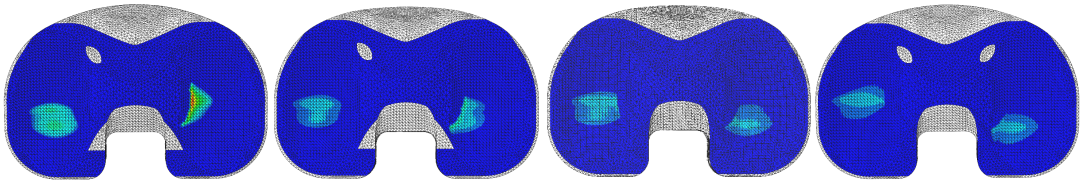

(b) Point 2

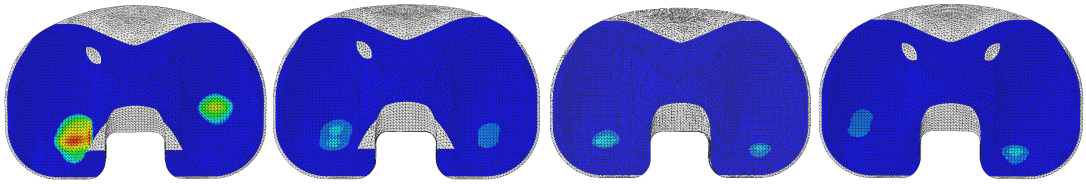

(c) Point 3

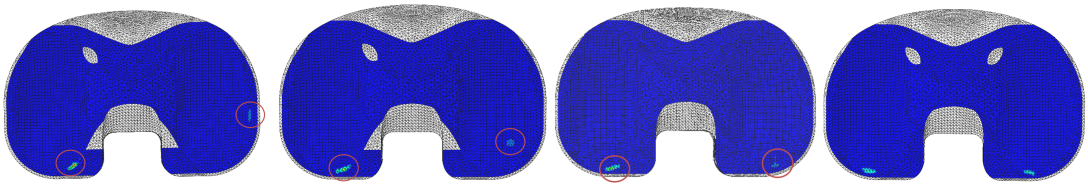

(d) Point 4

Figure 6.42: Computational prediction of the contact pressure under 14°, 8°, 4° and 0° rotational mismatch (from left to right) under the stiff knee soft tissue condition (0MPa blue, 85MPa red)

Table 6.15: The peak contact pressure (MPa) from the computational model under mechanical alignment, 4° rotational mismatch, 8° rotational mismatch and 14° rotational mismatch alignment conditions under the stiff knee soft tissue condition at four points in the gait cycle

Point	Mechanical Alignment	4° Rotational Mismatch	8° Rotational Mismatch	14° Rotational Mismatch
1	29.10	28.0	39.38	39.67
2	19.96	17.4	28.53	38.25
3	16.31	18.5	14.60	19.39
4	22.96	43.0	39.64	56.67

for the 14° rotational mismatch alignment condition. At point 3 in the cycle the TR rotation is at 8° and therefore has corrected the mismatch in the alignment condition. The 8° rotational mismatch alignment condition resulted in a similar peak pressure to the mechanical alignment condition.

The 4° rotational mismatch alignment condition resulted in similar peak pressure values

to the mechanical alignment condition at points 1-3, however due to the purely medial contact at point 4 it resulted in a much higher pressure at the end of the cycle.

The contact area was determined for the 14°, 8° and 4° rotational mismatch and mechanical alignment conditions throughout the gait cycle (Figure 6.43).

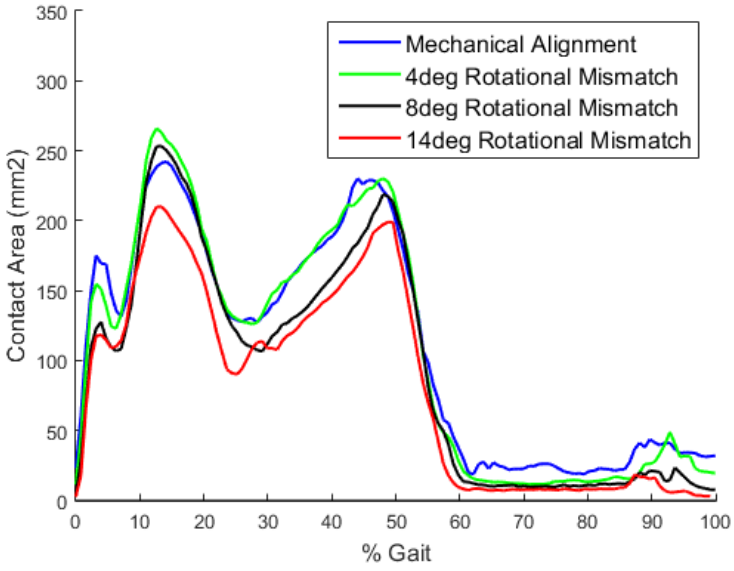

Figure 6.43: The contact area (mm^2) from the computational model under mechanical alignment, 4° rotational mismatch, 8° rotational mismatch and 14° rotational mismatch alignment conditions under the stiff knee soft tissue condition

For the first 10% of the gait cycle the mechanical alignment condition resulted in a higher contact area than the rotational mismatch alignment conditions. However from 10% to 25% gait the 14° rotational mismatch condition resulted in a lower contact area.

From 25% to 55% gait the mechanical alignment and 4° rotational mismatch alignment condition again resulted in higher contact area while the two other rotational mismatch alignment conditions resulted in similar values to each other.

From 50% gait onwards there was no obvious difference between the three alignment conditions. During this section of the gait cycle there was the least difference in the AP and TR displacements which may be why the contact areas are similar. The mechanical alignment resulted in a higher contact area which may be due to the contact on both the medial and lateral condyles as determined at Point 4.

The 14° rotational mismatch alignment condition consistently resulted in a lower contact area than the mechanical alignment condition. This may be due to the rotational mismatch resulting in poor conformity between the femoral and tibial components and therefore a lower contact area.

6.6.3 Tibial Slope Alignment Condition

The tibial slope alignment condition was studied under 10° and 4° posterior tibial slope and the output kinematics, contact pressure and contact area compared to mechanical alignment.

6.6.3.1 Kinematics

The AP, TR and AA displacement profiles were determined for the 10° tibial slope, 4° tibial slope and mechanical alignment conditions (Figure 6.44).

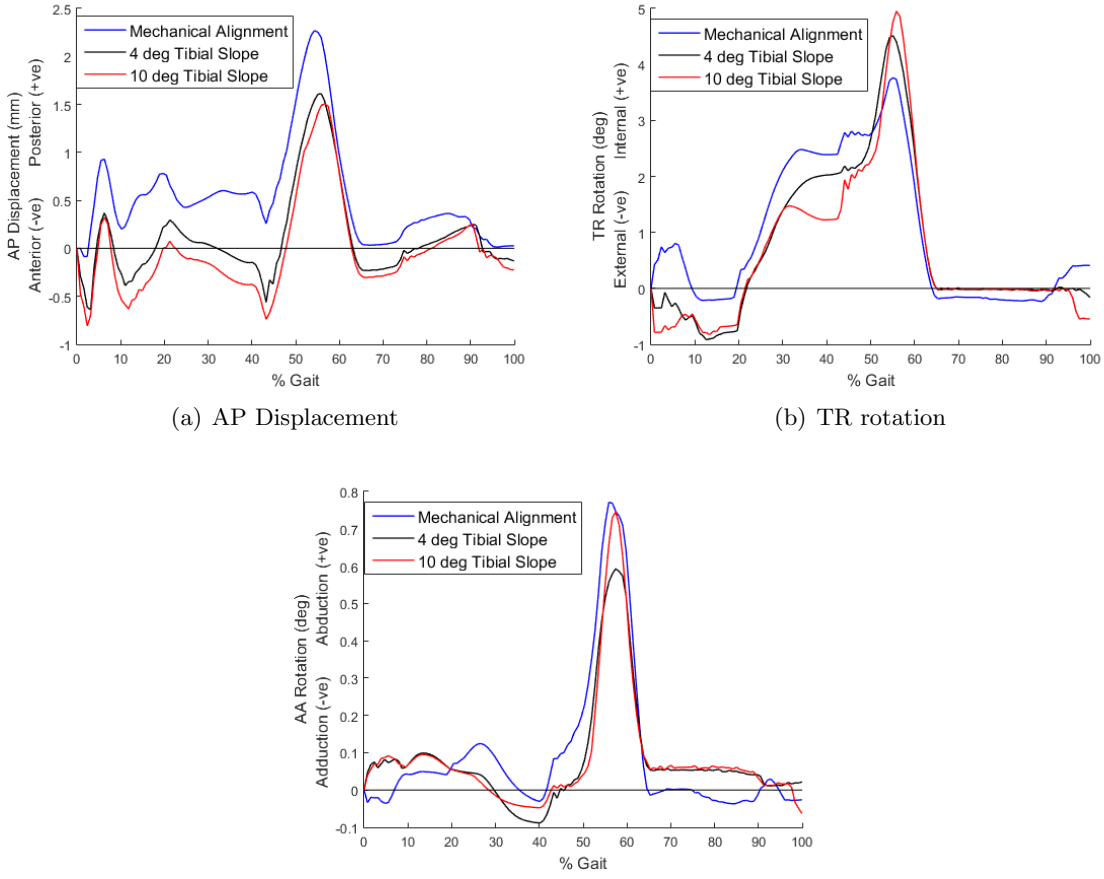

(a) AP Displacement

(b) TR rotation

(c) AA rotation

Figure 6.44: The output AP (a), TR (b) and AA (c) displacements from the computational model under mechanical alignment, 4° posterior tibial slope and 10° posterior tibial slope alignment conditions under the stiff knee soft tissue condition

The 10° and 4° tibial slope alignment conditions resulted in similar AP displacement profiles. They resulted in more anterior displacement than the mechanical alignment condition throughout the gait cycle. The 4° tibial slope alignment condition did result in more posterior displacement compared to the 10° tibial slope alignment from 5% to 55% gait, however the difference was low.

As with the AP displacement profiles the two tibial slope alignment conditions resulted in similar TR rotation profiles. For the first half of the gait cycle the tibial slope alignment

conditions resulted in lower TR rotations compared to the mechanical alignment condition. However they then resulted in a higher peak TR rotation at around 60% gait. The 4° tibial slope alignment condition resulted in higher TR rotation from 30% to 40% gait compared to the 10° tibial slope alignment condition however it also resulted in a lower peak TR rotation. From 30% to 60% gait the 4° tibial slope alignment resulted in TR rotation values between those of mechanical and 10° tibial slope alignment conditions. The reduced TR rotation from 30% to 40% gait may be due to the increase in posterior displacement resulting in the conformity of the tibial insert restricting the TR rotation. As the AP displacement then increased from 50% gait this restriction is reduced resulting in a sharp increase in the TR rotation. The lower AP displacement under the tibial slope alignments may have resulted in the higher peak TR rotation due to the femorotibial contact being more central in the tibial insert.

The three alignment conditions resulted in similar AA rotation profiles. The 4° tibial slope alignment condition did result in a lower peak AA rotation compared to the other two alignment conditions however the difference in the AA rotation was small; around 0.2°.

6.6.3.2 Contact Pressure and Area

The pressure distribution was determined at four points in the gait cycle under the 10° and 4° tibial slope alignment conditions and compared to the mechanical alignment condition (Figure 6.45). The four points in the cycle were the same points where the experimental contact area measurements were carried out.

At point 1 in the cycle the more anterior AP displacements under the tibial slope alignment conditions have resulted in more posterior contact points. Otherwise the contact points were similar between the three alignment conditions.

At point 2 in the cycle the more anterior AP displacement under the tibial slope alignment conditions again resulted in more posterior contact, this time close to the posterior edge of the tibial insert. The increased TR rotation under the mechanical alignment condition has also resulted in a more anterior medial contact.

At point 3 in the cycle the tibial slope alignment conditions again resulted in more posterior contact points, on the posterior edge of the tibial insert. While the mechanical alignment condition did not result in edge contact. The 4° posterior tibial slope alignment condition also resulted in more medial loading than the 10° tibial slope alignment condition. This may be due to the lower peak AA rotation under the 4° tibial slope alignment condition.

At point 4 in the cycle all three alignment conditions resulted in similar contact points, with medial and lateral contact on the posterior edge of the tibial insert.

The peak contact pressure was determined for each alignment condition at the same four points in the gait cycle as those measured experimentally (Table 6.16).

At point 1 in the cycle the mechanical alignment condition resulted in the highest pressure value and the 10° tibial slope alignment condition the lowest. This may be due to the more anterior displacement under the tibial slope alignment conditions resulting in more central

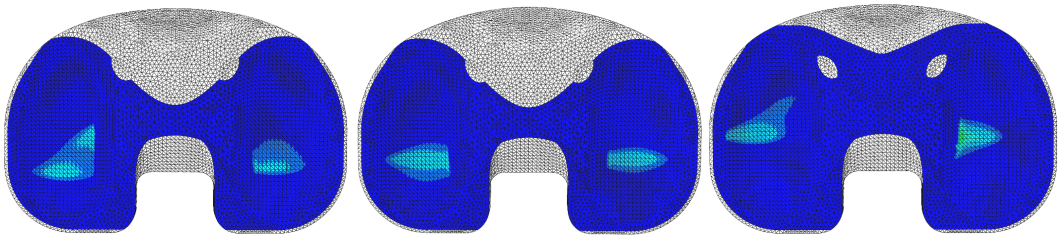

(a) Point 1

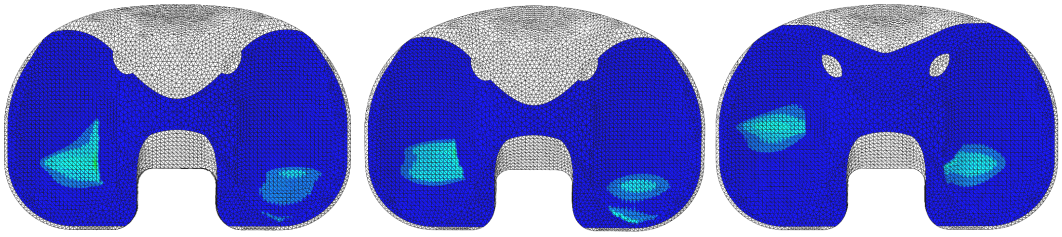

(b) Point 2

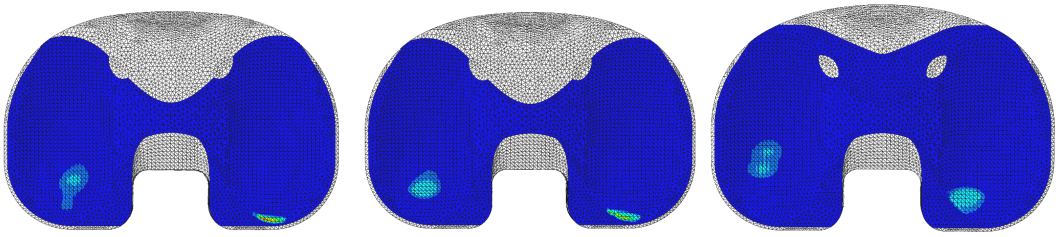

(c) Point 3

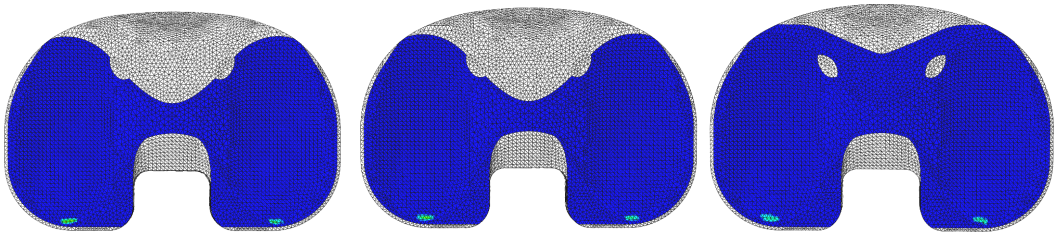

(d) Point 4

Figure 6.45: Computational prediction of the contact pressure under 10° (left), 4° (centre) and 0° (right) posterior tibial slope under the stiff knee soft tissue condition (0MPa blue, 70MPa red)

Table 6.16: The peak contact pressure (MPa) from the computational model under mechanical alignment, 4° posterior tibial slope and 10° posterior tibial slope alignment conditions under the stiff knee soft tissue condition at four points in the gait cycle

Point	Mechanical Alignment	4° Tibial Slope	10° Tibial Slope
1	29.10	17.39	16.74
2	19.96	23.58	28.59
3	16.31	37.28	55.13
4	22.96	26.92	32.74

tibiofemoral contact points.

At points 2 to 4 in the cycle the mechanical alignment condition resulted in the lowest contact pressure and the 10° tibial slope alignment condition resulted in the highest value. This may have been due to the anterior displacement under the tibial slope alignment conditions resulted in contact on the posterior edge of the tibial insert and therefore higher contact pressures.

The greatest range in peak pressure values between the three alignment conditions occurred at point 3 in the cycle, this may be due to the edge loading under the tibial alignment conditions. The higher range in pressures at point 3 compared to point 4 may be due to a higher applied AF at point 3.

The contact area for each of the three alignment conditions was determined throughout the gait cycle (Figure 6.46). All three alignment conditions resulted in similar contact areas throughout the cycle. The mechanical alignment condition resulted in higher contact area from 60% to 90% gait which may be due to the edge contact that occurred with the tibial slope alignments resulting in lower contact areas.

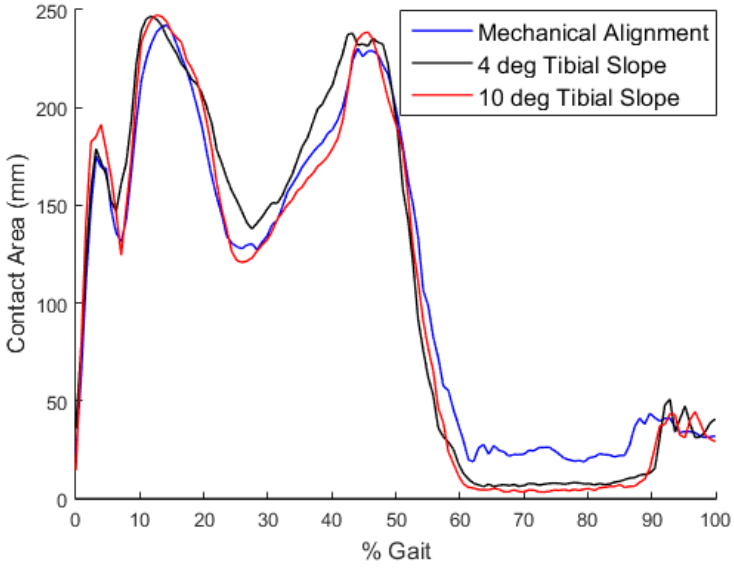

Figure 6.46: The contact area (mm^2) from the computational model under mechanical alignment, 4° posterior tibial slope and 10° posterior tibial slope alignment conditions under the stiff knee soft tissue condition

6.6.4 Kinematic Alignment Condition

The kinematic alignment condition was studied under the values studied experimentally and half the experimental values. The output kinematics, contact pressure and contact area compared to mechanical alignment.

6.6.4.1 Kinematics

The AP, TR and AA displacement profiles were determined for the experimental kinematic alignment values, half the experimental kinematic alignment values and under mechanical alignment conditions (Figure 6.47).

The shape of the AP displacement profiles were similar for each alignment condition. The two kinematic alignment conditions however resulted in more anterior AP displacements with the experimental kinematic alignment resulting in the most anterior displacement.

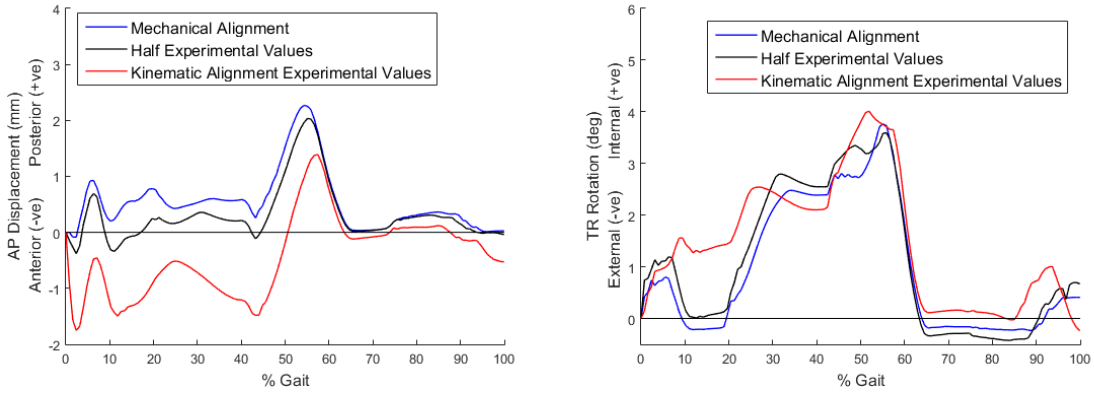

(a) AP Displacement

(b) TR rotation

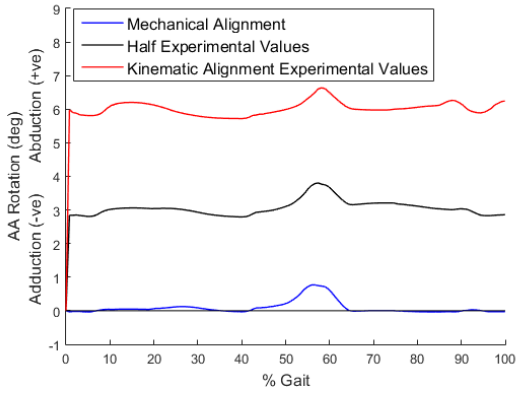

(c) AA rotation

Figure 6.47: The output AP (a), TR (b) and AA (c) displacements from the computational model under mechanical alignment, half the experimental values and the experimental kinematic alignment conditions under the stiff knee soft tissue condition

All three alignment conditions also resulted in similar TR rotation profiles. The experimental kinematic alignment condition however did result in higher TR rotation from 10% to 30% gait and resulted in a higher peak TR rotation than the other alignment conditions.

The largest difference in kinematics between the alignment conditions occurred in the AA rotation profiles. The experimental kinematic alignment condition resulted in an AA profile centred around 6° compared to 3° for half the experimental kinematic values and 0° under mechanical alignment. These values represent the differences in angle between the femoral

and tibial components in the coronal plane; the experimental kinematic alignment condition had 2.5° femoral valgus and 3.4° tibial valgus which corresponds to 5.9° difference in angle. While for the half experimental values alignment condition this corresponded to a difference of 2.9°.

6.6.4.2 Contact Pressure and Area

The pressure distribution for the two kinematic alignment conditions and mechanical alignment condition were determined at four points in the cycle (Figure 6.48).

At point 1 in the cycle the kinematic alignment conditions resulted in larger and more anterior medial contact points compared to the mechanical alignment condition. The lateral contact areas were also narrower under the kinematic alignment conditions compared to the mechanical alignment condition. These differences may be due to the differences in the AA rotation profiles resulting in different loading on the tibial insert.

At points 2 and 3 in the cycle the kinematic alignment conditions again resulted in larger and more anterior medial contact areas compared to the mechanical alignment condition.

At point 4 in the cycle the kinematic alignment condition of half the experimental values and the mechanical alignment condition both resulted in medial and lateral contact areas on the posterior edge of the tibial insert. The experimental kinematic alignment condition however resulted in a more anterior lateral contact. This may be due to the higher TR rotation that occurred under the experimental kinematic alignment condition at this point in the gait cycle.

The anterior contact on the kinematic alignment conditions may be due to the posterior tibial slope resulting in contact between the anterior femoral surface and the anterior tibial surface. This contact may be what causes the anterior displacement of the tibial insert.

Due to the AA rotation there was more loading on the lateral side of the tibial insert. This is converse to what occurred under the posterior tibial slope alignment where the tibial slope and anterior displacement resulted in a more posterior contact point. These differences may be due to the differences in the loading between the alignment conditions.

The high AA rotation around the centre of rotation would change the position of the tibiofemoral contacts, resulting in more medial contact. This medial contact may have resulted in the difference in contact points on the femoral components (Figure 6.49). The off centre and more medial position of the tibial centre of rotation may also have resulted in the medial and lateral tibiofemoral contact points occurring less centrally compared to the mechanical alignment condition. The differences due to the TR rotation and the AA rotation may have resulted in the differences in contact position under the kinematic alignment condition in comparison to the tibial slope alignment condition despite the similarities in the alignment conditions.

The peak pressure values were found at the same four points in the gait cycle. At points 1 and 2 the mechanical alignment condition resulted in the lowest pressure values and at points 3 and 4 in the cycle the experimental kinematic alignment condition resulted in the lowest

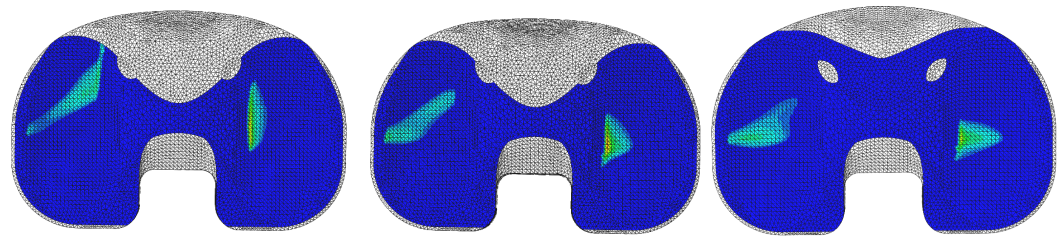

(a) Point 1

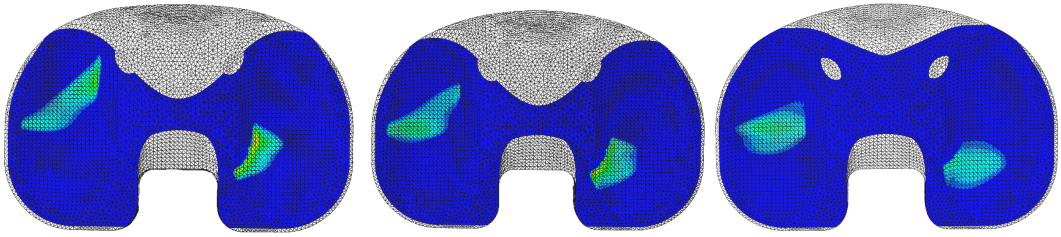

(b) Point 2

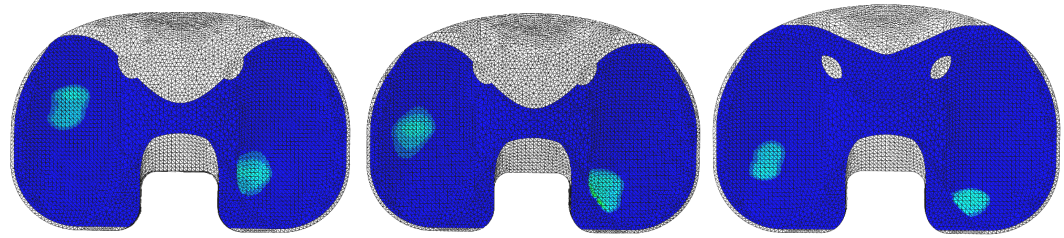

(c) Point 3

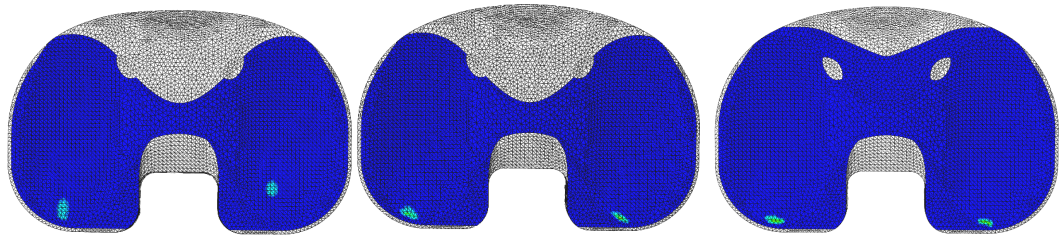

(d) Point 4

Figure 6.48: Computational prediction of the contact pressure under the experimental kinematic aliment values (left), half the experimental values (centre) and mechanical alignment (right) under the stiff knee soft tissue condition (0MPa blue, 50MPa red)

pressure values (Table 6.17).

At point 1 in the cycle the kinematic alignment with half the experimental values resulted in the highest peak pressure. The position of the peak pressure for both kinematic alignment conditions occurred on the lateral tibial condyle close to the centre of the tibial insert. This may be due to the higher AA rotations in combination with an off centre, more medial tibial centre of rotation.

At point 2 in the cycle the two kinematic alignment conditions resulted in similar peak pressure values. The position of the peak pressure occurred in a similar position to at point

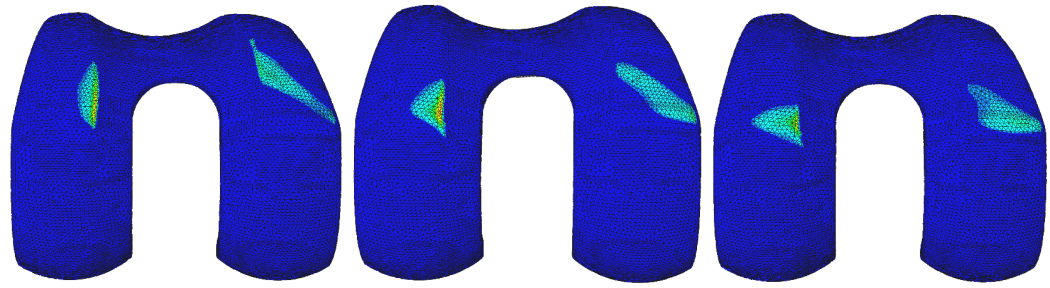

(a) Point 1

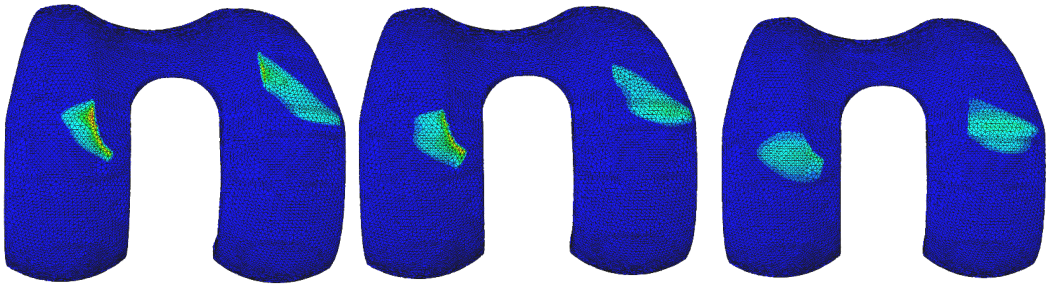

(b) Point 2

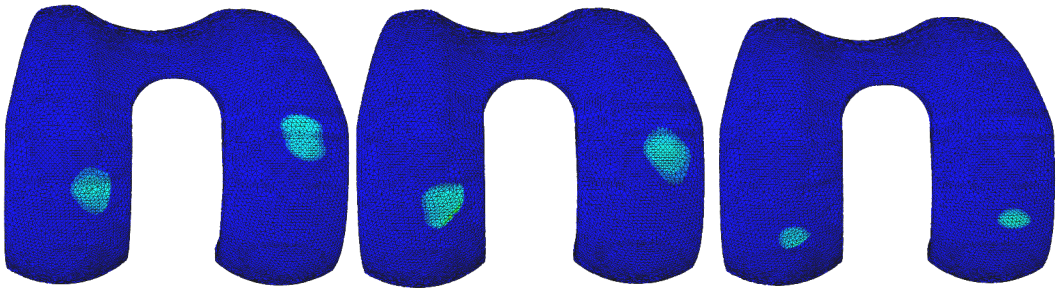

(c) Point 3

(d) Point 4

Figure 6.49: Computational prediction of the contact pressure on the femoral component under the experimental kinematic aliment values (left), half the experimental values (centre) and mechanical alignment (right) under the stiff knee soft tissue condition (0MPa blue, 50MPa red)

1 in the gait cycle.

At point 3 in the kinematic alignment condition based on half the experimental values

Table 6.17: The peak contact pressure (MPa) from the computational model under mechanical alignment, half the experimental values and the experimental kinematic alignment conditions under the stiff knee soft tissue condition at four points in the gait cycle

Point	Mechanical Alignment	Half Experimental Values	Experimental Kinematic Alignment Values
1	29.10	35.86	31.62
2	19.96	35.33	36.70
3	16.31	21.87	14.28
4	22.96	23.72	11.0

resulted in a higher peak pressure value compared to the mechanical and experimental kinematic alignment conditions. The slightly lower AP displacement compared to the mechanical alignment condition may have resulted in the lateral contact occurring at the corner of the edge of the tibial insert. While the lower AP displacement under the experimental kinematic alignment condition resulted in the lateral contact pressure occurring more anteriorly than the corner of the tibial insert edge. This may be why this alignment condition resulted in the highest pressure at this point.

At point 4 in the cycle the mechanical alignment condition and the kinematic alignment condition based on half the experimental values resulted in similar pressure values. The experimental alignment condition however resulted in a lower peak pressure which may have been due to the higher TR rotation resulting in less edge contact.

The contact area for each of the three alignment conditions was determined throughout the gait cycle (Figure 6.50).

In the second half of the gait cycle there was no difference between the three alignment conditions. However in the first half of the gait cycle the mechanical alignment condition resulted in the highest contact area. The two kinematic alignment conditions resulted in similar contact areas. The experimental kinematic alignment condition resulted in a slightly lower contact area for most of the first half of the cycle. This difference in the contact area may be due to the differences in the AA rotation affecting the load distribution on the tibial insert. This difference in loading may have resulted in different contact areas.

6.7 Discussion

This study experimentally and computationally investigated the effect of component alignment on the kinematics, contact area and wear of a TKR under one soft tissue condition.

The alignment conditions studied experimentally were mechanical alignment, 4° varus, 14° rotational mismatch, a 10° posterior tibial slope and alignment based on the use of kinematic alignment techniques during surgery. The rotational mismatch and posterior tibial slope alignments resulted in significantly higher wear rates, while the varus alignment resulted in a significantly lower wear rate than under mechanical alignment.

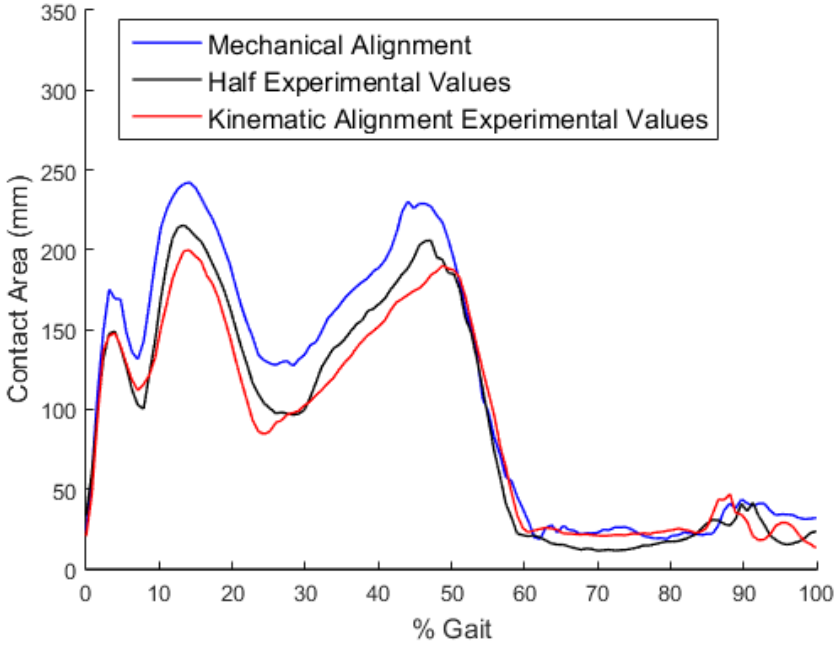

Figure 6.50: The contact area (mm^2) from the computational model under mechanical alignment, half the experimental values and the experimental kinematic alignment conditions under the stiff knee soft tissue condition

6.7.1 Computational Model Validation

The computational model was validated under the same alignment conditions as those studied experimentally. The output AP, TR and AA kinematics were compared between the experimental and computational methods as well as the contact area at four points in the cycle.

There was good correlation between the AP and TR displacements between the experimental and computational results. As with the mechanical alignment condition the greatest difference in the kinematics occurred with the AA rotation. This may be due to the weight of the AA arm in the simulator, which was not represented in the computational model. The weight of the AA arm is not an accurate representation of the conditions in vivo and therefore was not included in the computational model. However the computational prediction resulted in a similar AA profile shape to the experimental results under the rotated alignment condition. This alignment condition had the highest AA rotation and therefore would have had the greatest momentum on the AA arm. This momentum may have resulted in increased AA displacements despite the weight of the AA arm.

The computational prediction also resulted in similar contact positions as the experimental results, however it did result in more medial loading. The difference in loading may also be due to the difference in the AA rotation profiles. The computational model resulted in higher values of the contact area, however it resulted in a similar trend as determined experimentally. Differences in the contact area may also be due to the differences in the loading of the tibial

insert.

The greatest difference occurred with the kinematic alignment condition due to the difference in loading on the tibial insert. The experimental study resulted in just lateral loading however the computational model predicted much higher abduction than occurred experimentally. This resulted in loading on both the medial and lateral condyles which also did not occur in the experimental results. This suggests that the computational model may be a more realistic representation of the kinematic alignment in vivo. Due to the large differences in the loading of the tibial insert there were also differences in the contact position and the contact area between the two methods.

Overall there was good correlation in the AP and TR rotation profiles for all the alignment conditions. There was more of a difference in the AA profile due to the design of the simulator. The differences in the AA rotation profiles also resulted in differences in the loading of the tibial insert, especially under the kinematic alignment condition, along with differences in the contact areas.

The computational model was then used to run parametric testing on different alignment conditions to those studied experimentally. Alignment conditions between those studied experimentally and the mechanical alignment condition were generated and the output kinematics, contact pressure and contact area determined.

6.7.2 Varus Joint Line Alignment Condition

In the experimental and computational study the varus alignment conditions resulted in similar output kinematics to mechanical alignment, which was similar to the result of a previous study using the same TKR [92]. However in the experimental study it also resulted in more unbalanced loading of the tibial compartment, with most of the contact occurring on the lateral condyle. Lateral loading of the tibial compartment has been shown to result in increased peak bone strains on the medial compartment [162], which may result in tibial implant migration.

The lateral loading under varus alignment is converse to what has been found previously in other studies [52, 151, 189] and to what was found with the computational model. The difference in loading under the experimental methods may be due to differences in the AA rotation due to the weight of the AA arm within the simulator. This may be why the computational model, where this limitation was not present, resulted in more medial loading. Previous studies have also simulated a varus leg alignment rather than a varus joint line. Clinically a varus leg alignment has been found to result in a medial shift in the joint force [154], however in this study the axial force was applied in the same position as under mechanical alignment conditions.

The varus alignment condition was run using the computational model under the 4° tibial and femoral varus studied experimentally and under 2° tibial and femoral varus. There was more medial loading as the varus angle increased. This resulted in different contact positions and different contact pressures between the alignment conditions.

There was found to be significantly lower wear under the varus alignment condition than under mechanical alignment, however previous studies have found that >3° varus alignment resulted in double the wear rates [66, 184]. This could be due to the design of the TKRs used in the study, due to the tibial inserts not being crosslinked or due to the simulation of a varus leg alignment rather than a varus joint line. One was a retrievals study, therefore patient factors such as BMI could have resulted in higher wear rates [184]. Another study found that healthy soft tissues within the knee can counteract the effect of alignment [201], therefore the stiff knee soft tissue condition may have reduced the influence of the varus alignment condition on the kinematics and wear in this study.

6.7.3 Rotated Alignment Condition

The rotated alignment condition resulted in a significantly higher TR rotation under the experimental and computational studies. For the 14° mismatch condition the TR rotation profile was shifted internally. This shift in the TR rotation was similar to that found in a previous study with the same TKR [92]. In the computational study the TR rotation increased in order to correct the rotational mismatch and there was found to be a linear relationship between the rotational mismatch and the peak TR rotation. Internal rotation of the tibia increases the Q angle in the knee, which may lead to patellar instability and increased pain as discussed previously in Section 1.6.

The rotated alignment condition resulted in a higher TR range of motion and a higher AA range of motion As with the TR rotation there was a linear relationship between the rotational mismatch and the peak adduction rotation. The gradient of the linear fit for the AA rotation was higher than that for the peak TR rotation, suggesting that the AA rotation was more sensitive to changes in the rotational alignment. An increased adduction moment within the knee may also contribute to the development of knee pain; the adduction moment was correlated with a compressive force on the medial compartment [170]. The peak adduction moment during gait has also been related to surgical outcome pain relief in patients with knee OA [102].

The rotated alignment also resulted in unbalanced loading in the experimental study, with mainly lateral loading in the first half of the gait cycle, followed by mainly medial loading in the second half. Imbalance in the medial and lateral loading may result in instability of the knee, lift off and patient dissatisfaction [88, 153]. A study by Wasielewski et al found that if the loading between the medial and lateral tibial compartments were comparable there was no lift off greater than 1mm [199].

There was also contact and damage that occurred on the medial posterior edge of the tibial insert during the wear study. This damage resulted in plastic deformation on the posterior tibial edge, which over an increased time period could result in early failure or instability of the TKR.

In the computational study the increase in the rotational mismatch also resulted in an increase in the peak contact pressure as well as a decrease in the contact area. This may be

due to more loading on the posterior edge of the tibial insert. The higher pressure found under the rotational mismatch alignment condition with the computational model corresponded to previous studies [52, 53].

The rotated alignment condition resulted in a significantly higher wear rate than the mechanical alignment condition, this could be due to the increase in kinematics or due to the contact on the edge of the tibial insert. As there was damage caused to the rotated tibials that was not due to wear and may have been due to the start up process this suggests that the wear rate in vivo may be different. In vivo the wear rate could be higher as the motion would be less continuous than in the simulator, therefore there may be the potential for more damage as the mismatched components come into contact. A previous computational study found that alignment in the transverse plane resulted in the greatest increase in wear rates, which is similar to that found in this study [135]. Internal rotation of the tibial insert was also found to result in loading on the edge of the tibial insert, as in this study [134].

In the computational results the 4° rotational mismatch alignment condition resulted in similar AP and TR profiles to the mechanical alignment condition. It also resulted in similar peak contact pressure values and contact area for most of the gait cycle. Rotational mismatch should be minimised in order to reduce the potential for pain and patient dissatisfaction. This study suggests that the mismatch should be kept within 4° of neutral in order to maintain similar mechanics as under mechanical alignment conditions.

6.7.4 Tibial Slope Alignment Condition

In the experimental and computational studies the posterior tibial slope resulted in anterior AP displacement throughout the gait cycle and resulted in more posterior contact including contact on the posterior tibial edge. The increased anterior tibial motion and a more posterior tibiofemoral contact point correlated with a previous computational study into the effect of a posterior tibial slope [114].

A posterior tibial slope may be beneficial for a CR TKR; there tends to be more anterior motion of the femur on the tibia in CR knees [153] compared to rollback of the femur which occurs in natural knees, one study determined that there was 80% of the femoral translation of the natural knee with a TKR at 120° flexion [142]. As the posterior tibial slope resulted in anterior motion of the tibia relative to the femur in this study, a posterior tibial slope may help to counteract the paradoxical motion found in CR knees. This matches that found by previous studies [179] and a positive correlation has been found between femoral-rollback and higher clinical and functional scores [67]. Another study found that for every mm of additional posterior femoral translation there was a resulting increase of 1.4° more flexion [19]. However in this study the flexion was fixed as it was displacement controlled, therefore the effect of the posterior tibial slope on flexion could not be investigated.

In the computational study there was a greater difference between the 4° tibial slope alignment condition and the mechanical alignment condition than the 4° and 10° tibial slope alignment conditions. This may be due to the conformity of the tibial insert restricting motion.

The posterior tibial slope alignment also resulted in significantly higher wear rates than the mechanical and varus alignments as well as damage to the posterior edge of the tibial insert. The increased wear rate due to the posterior tibial slope is similar to a previous computational study on the effect of component alignment [135]. Over a longer study this may have resulted in increased wear rates as more damage occurred to the edge of the tibial insert.

There was more lateral than medial loading particularly during the second half of the gait cycle. There was also more variation in the medial and lateral contact with this alignment condition than with the others in the experimental study, this could be due to the tibial slope causing instability and therefore more variation between the stations. In the computational study the higher tibial slope alignment of 10° resulted in the highest pressure for most of the cycle. This may be due to the contact occurring near to the edge of the tibial insert.

For this TKR the surgical guidelines are for no tibial slope. The posterior tibial slope should be kept lower than 10° as this resulted in significantly higher wear rates compared to mechanical alignment conditions. A tibial slope of 4° was found to result in increased anterior motion which may be beneficial for CR knees, however this alignment resulted in edge loading and higher peak pressure values than mechanical alignment and there may result in increased wear rates,

6.7.5 Kinematic Alignment Condition

The kinematic alignment condition resulted in more anterior AP displacement in the experimental study than all of the other alignment conditions studied. It also resulted in the AA rotation profile being centred around 2° in the experimental study, which resulted in only lateral contact.

However in the computational model there was both medial and lateral contact as there were increased AA displacements. The AA rotation profile was centred around the difference in angle between the femoral and tibial components in the coronal plane. The AA rotation increased in order for the femoral and tibial components to become parallel. Therefore the purely lateral contact found experimentally may be due to the weight of the AA arm in the simulator restricting the AA rotation, as discussed previously. The computational results for this alignment condition may be more representative of the conditions in vivo as there was both medial and lateral contact throughout the cycle.

However this high AA rotation can lead to a valgus leg alignment which increases the Q angle,which makes the quadriceps muscle less efficient and results in a lateral pull on the patella. This may cause knee pain, instability and patella maltracking [22, 43, 64, 138, 153, 169, 175]. A previous study found that the mean Q angle was significantly higher for patients with knee pain than those without [64].

Component alignment with a valgus femoral and varus tibial may also result in asymmetrical instability; this will result in a progressing valgus deformity along with an increase in the lateral joint line stresses [153]. This imbalance and consequential gap between the medial tibial and femoral surfaces may also result in the medial collateral ligament lengthening over

time, which would result in coronal instability [153].

In the computational results the kinematic alignment condition based on half the experimental values resulted in the highest peak pressure at most of the points studied. In the first half of the gait cycle the AA rotation around the more medial tibial centre of rotation may have resulted in the higher pressures. This may have resulted in the lateral contact occurring towards the centre of the tibial insert, resulting in high pressures on both the kinematic alignment conditions. At point 3 in the cycle the differences in contact pressure may be due to the position of the lateral contact in relation to the curved edge of the tibial insert. At the last point in the cycle the increased TR rotation under the experimental kinematic alignment condition resulted in less edge contact and therefore lower pressures. The kinematic alignment conditions also resulted in lower contact areas throughout the cycle which may have resulted in higher peak pressures compared to the mechanical alignment condition.

The study on the kinematic alignment condition has shown that the combination of alignments in different planes results in a more complicated analysis; the effect on the kinematics and contact pressure are not equal to the effect the alignment in each plane would have combined. For example the kinematic alignment condition had a smaller posterior tibial slope than the tibial slope alignment condition yet resulted in more anterior AP displacement. Neither the varus or rotational mismatch alignment conditions resulted in a shift in the AP displacement. Therefore the combined effect of alignments in multiple planes must have resulted in the shift in the AP displacement.

Further study of the effect of different alignment conditions is required in order to fully understand the effect of kinematic alignment. However in order to reduce the AA rotation, and therefore the potential for knee pain and instability, the angle between the femoral and tibial components in the coronal plane should be minimised.

6.8 Conclusions

Overall the experimental study determined that the varus alignment condition resulted in similar kinematics and lower wear but resulted in more unbalanced loading than the mechanical alignment. The rotated and tibial slope alignment conditions resulted in significantly higher wear rates and mechanics that may result in instability and knee pain in vivo. The kinematic alignment condition resulted in purely lateral loading, however due to the limitations of the experimental simulation this may not be an accurate representation of how it would behave in vivo.

The computational study determined that each of the alignment conditions responded differently under different alignment values. For varus alignment the main difference was increased medial loading as the varus angle increased.

Whereas the rotational mismatch resulted in increased TR and AA rotations, as well as higher peak pressures as the rotational mismatch increased. The rotational mismatch of the TKR should be kept within 4° in order to minimise the TR and AA rotations.

As the posterior tibial slope increased the AP displacement became more anterior resulting in more posterior tibiofemoral contact points. This resulted in more edge loading and higher peak pressures.

The kinematic alignment conditions resulted in higher AA rotations as the alignment angles increased. The angle between the femoral and tibial components in the coronal plane should be minimised in order to reduce the AA rotation and the Q angle.

Alignment conditions had a significant effect on the output kinematics, contact area and wear of the TKR studied. In order to represent the range of outcomes that occur in vivo a range of component alignment conditions should be studied pre-clinically.

Chapter 7

The Influence of Soft Tissue Constraints and Surgical Alignment on Kinematics, Mechanics and Wear

7.1 Introduction

This study was carried out to investigate the influence of different soft tissue constraints on the kinematics and wear rates under different alignment conditions. Chapter 5 investigated the effect of soft tissue constraints under mechanical alignment and Chapter 6 investigated the effect of alignment under a single soft tissue condition. This chapter will investigate the influence of the combination of soft tissues and alignment on a TKR.

The effect of the soft tissues on the kinematics was determined for each alignment condition by finding the average AP, TR and AA output profiles under each of the soft tissue conditions. The ISO standard force control input profiles and centre of rotation were used [186]. The contact areas were also determined in order to investigate the effect on the femorotibial contact. Finally wear studies were carried out for 2MC each with the highest and lowest tension soft tissue conditions.

Three soft tissue conditions were applied within the simulator to each alignment condition in order to represent a knee with a resected ACL and PCL, with an intact PCL and resected ACL and to represent a stiff knee. These were the same three spring conditions used in Chapter 5 to investigate the effect of the soft tissue constraints under mechanical alignment.

In the first section of the experimental results the effect of the soft tissues on three alignment conditions were investigated; 4° varus joint line, 14° rotational mismatch and kinematic alignment. The effect of the soft tissues under mechanical alignment was investigated in Chapter 5 therefore mechanical alignment was not included in these results. The 10° posterior tibial slope alignment was determined to be too unstable to be run under the two lower tension soft tissue conditions so the effect of the soft tissue constraints on the kinematics and wear rates could not be determined.

In the second part of the experimental results the different alignment conditions will be compared to each other, under all three soft tissue conditions.

The computational model was validated under mechanical alignment conditions in Chapter 5 and under all other alignment conditions and the stiff knee soft tissue condition in Chapter 6. The next part of this chapter will validate the computational predictions of kinematics and contact area against the experimental data under the remaining alignment and soft tissue combinations.

The final results section will detail the results of the computational parametric study that simulated a wider range of alignment condition under the same three soft tissue conditions.

7.2 Materials

All the studies were carried out using DePuy Sigma fixed bearing, right knee, size 3 (DePuy Synthes, Leeds, UK) components. The tibial inserts were moderately crosslinked UHMWPE (5MRad irradiated and re-melted GUR1020 XLK, n=6). The tibial inserts used for the varus, rotated and tibial slope wear studies were new inserts from batches 8466296 and 8466300 used in Chapter 6 (part number 1581-13-110).

The femoral components had been used in previous studies, to ensure this would not affect the wear results the femorals were polished in order to remove any scratches.

The lubricant was 25% bovine serum (Life Technologies, New York, USA) in 0.04% sodium azide solution (Severn Biotech Ltd, Worcestershire, UK) and was changed approximately every 350,000 cycles. The contact area measurements were carried out using a Tekscan (Tekscan Inc., Boston, USA) pressure mapping sensor as detailed in Section 2.2.

The soft tissues were simulated using virtual springs within the simulator, the profiles of the virtual springs were changed to represent different soft tissue constraints. In order to represent different component alignments femoral and tibial fixtures were designed and made that allowed the tibial and femoral components to be inserted into the simulator in the desired positions.

7.3 Methods

The effect of the soft tissue constraints on the different alignment conditions were studied experimentally using a 6 station knee simulator. The simulator was run under force control condition to allow the kinematics to change in response to the alignment and soft tissue constraints.

Three soft tissue conditions were used for the study; the resected ACL soft tissue condition, the resected ACL & PCL soft tissue condition and stiff knee soft tissue condition based on clinical data to represent a stiff knee as described in Chapter 5 (Table 7.1).

The alignment conditions investigated are defined relative to mechanical alignment of a TKR in Table 7.2. The influence of the soft tissue conditions under mechanical alignment was

Table 7.1: The AP and TR spring tensions and spring gaps for the three soft tissue conditions studied

Condition	AP		TR	
	Gap (mm)	Tension (N/mm)	Gap (°)	Tension (Nm/°)
Resected ACL (ISO CR)	±2.5	44 posteriorly, 9.3 anteriorly	±6	0.36
Resected ACL & PCL (ISO CS)	±2.5	9.3	±6	0.13
Stiff	0	127	0	0.7

detailed in Chapter 5 and the tibial slope alignment condition could only be run under the stiff knee soft tissue condition. Therefore this chapter will focus on the varus joint line, rotated and kinematic alignment conditions. These alignments are the same alignment conditions that were specified in Chapter 6.

Table 7.2: The femoral and tibial component positions in the coronal, sagittal and transverse planes relative to mechanical alignment under each alignment condition studied

Condition	Femoral Component			Tibial Component		
	Coronal	Sagittal	Transverse	Coronal	Sagittal	Transverse
Mechanical	0°	0°	0°	0°	0°	0°
Varus	4° varus	0°	0°	4° varus	0°	0°
Rotated	0°	0°	7° internal	0°	0°	7° external
Tibial Slope	0°	0°	0°	0°	10° posterior	0°
Kinematic	2.5° valgus	0°	0°	3.4° varus	4.6° posterior	0°

7.3.1 Stability

In order to determine the stability of the TKR under a wider range of soft tissue conditions the TKR was studied under more extreme soft tissue conditions. Two other soft tissue conditions were studied; the resected ACL & PCL spring tensions with increased spring gaps of ±5mm and ±9° for the AP and TR springs respectively along with applying no spring restraints at all. The motion of the TKR was observed and any signs of lift off, dislocation of the joint or loading on the edges of the tibial insert were noted. Lift off was defined as any point where the femoral and tibial components were not in contact during the gait cycle.

The TKR was run with Vaseline used as lubricant and without the gaiters attached so that the mechanics of the joint could be observed.

7.3.2 Kinematics

The mean kinematics for each alignment and soft tissue condition were determined by averaging the output AP, TR and AA displacement profiles across the simulator.

The average output profiles were then compared between different soft tissue conditions using minimum and maximum points in the profiles as defined in Chapter 2 (Figure 7.1).

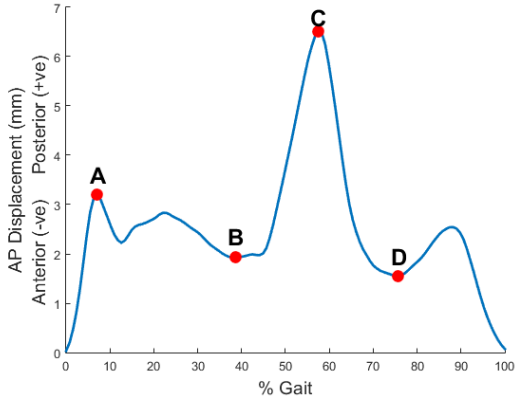

(a) AP Displacement

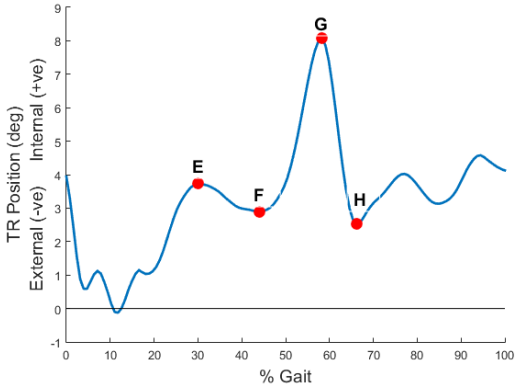

(b) TR Rotation

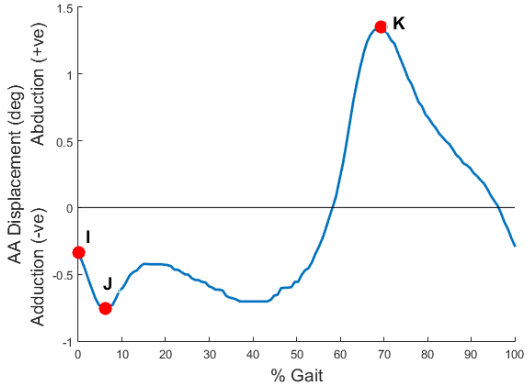

(c) AA Rotation

Figure 7.1: Maximum and minimum points on the AP, TR and AA displacement profiles that were used for statistical comparison between tests

Points A-D were defined in the AP profile, points E-H in the TR profile and points I-K in the AA rotation profile.

The range of motion in the displacement profiles was also compared between studies. The range of motion was defined as the difference between the maximum and minimum point in the displacement profile.

A one way ANOVA with significance taken at $p<0.05$ using IBM SPSS Statistics 22 was used. Depending on the homoscedasticity either a post hoc Tukey's test or a Games-Howell test was carried out, with significance taken at $p<0.05$, to determine the differences between the groups.

7.3.3 Contact Area

In order to investigate the effect of the soft tissue conditions on the contact area of the TKR a Tekscan pressure sensor was used.

The contact area was measured at four points in the gait cycle; point 1 was at 5% gait where the initial peak in the AP force occurs, the second at 45% gait where the last peak in the

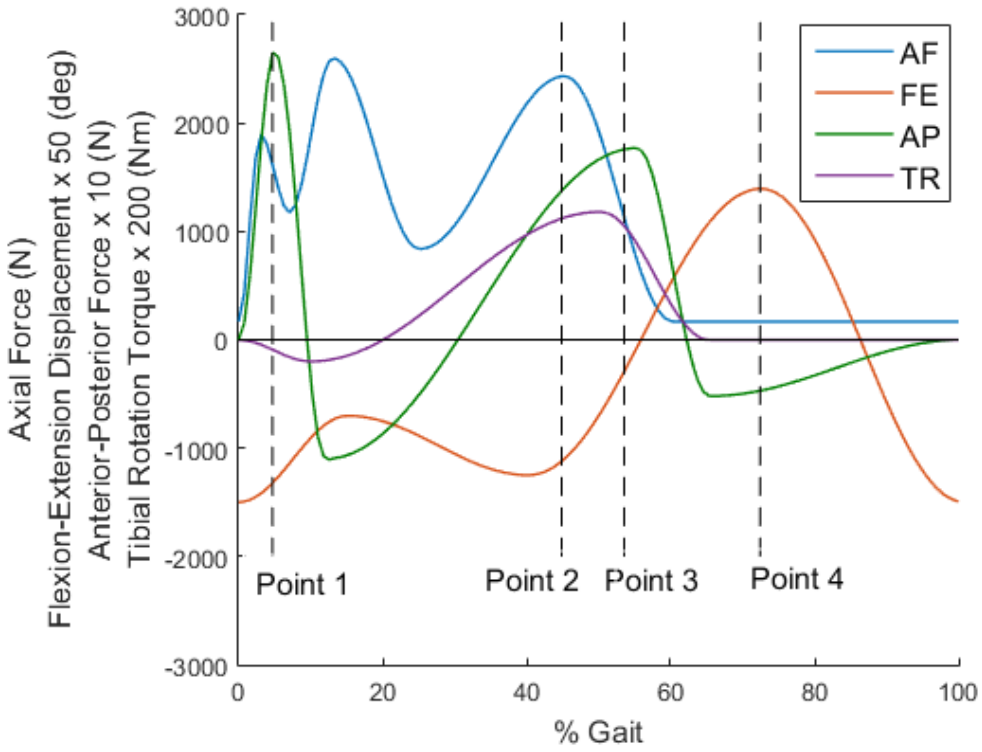

Figure 7.2: The input axial force, flexion-extension, AP force and TR torque profiles with the four points in the cycle where the contact area was measured

AF occurs, the third at the point in the cycle where the combined AP and TR displacement were at their maximum and the fourth point at 72% gait where the FE was at its peak (Figure 7.2).

The displacements and forces at these points for each of the three soft tissue conditions are shown in Tables A.1 to A.5.

The contact area was measured on 5 of the stations of the simulator for each soft tissue condition and the mean contact areas found for each point in the gait cycle. The AA motor was not functional on the 6th station and was therefore not used for the study. The mean contact area was found by calculating the area of the sensor where the pressure value was greater than 0MPa and accounting for the curvature of the insert at that point. The average and 95% CI of the contact area position and size was then determined for each point in the cycle.

A one way ANOVA with significance taken at $p<0.05$ using IBM SPSS Statistics 22 was used. As with the kinematic data either a post hoc Tukey's test was carried out or a Games Howell test depending on the variance between groups.

7.3.4 Wear studies

In order to investigate the effect of the soft tissue constraints on the wear rate of the tibial insert different wear simulation studies were carried out. With the varus joint line and rotational mismatch alignments wear studies each of 2MC were carried out with the stiff knee and the resected ACL & PCL soft tissue conditions. The wear rates with the two different soft tissue conditions were then compared to determine the effects on wear.

Wear studies were not carried out with the kinematic alignment condition as the experimental simulation also resulted in only lateral tibial contact and was therefore not a clinically relevant study. As the tibial slope alignment condition could not be run under the resected ACL & PCL soft tissue condition a wear study was run just under the stiff knee soft tissue condition.

At the end of each wear study the change in the output kinematics over time was investigated. This was to determine whether the kinematics were changing as the wear scar was formed. The wear rates between each of the inserts used in the study were then compared in order to determine whether there were similar differences in the wear rates over time.

The variation between the stations was also investigated. Any differences in the kinematics were then compared to the wear rates on each station to determine whether the differences in kinematics may have affected the wear rates.

The average wear scar outline and areas at the end of each wear study were also determined. The size and positions of the wear scars were then compared between wear studies.

Before and after each wear study the surface roughness of the superior surface of the tibial insert and contact surface of the femoral were measured. The surface roughness values and the change in the values were compared between the wear studies to investigate whether any of the alignment and soft tissue conditions resulted in damage to the contact surfaces.

A one way ANOVA with significance taken at $p<0.05$ using IBM SPSS Statistics 22 was used. s with the kinematic and contact area data either a post hoc Tukey's test was carried out or a Games Howell test depending on the variance between groups.

7.3.5 Computational Model Validation

In previous chapters the effect of different soft tissue constraints under mechanical alignment using the computational model has been validated by comparison with the experimental data (Chapters 4 and 5). The computational model has also been validated under all the alignment conditions and the stiff knee soft tissue condition (Chapter 6).

In order to validate the computational model under different alignment and soft tissue conditions the output AP, TR and AA displacements from the computational model were compared to the experimental data. The correlation coefficients were found between the computational and experimental predictions, a coefficient of greater than 0.7 was considered a good correlation.

The position of the contact points were also compared to those found experimentally.

Finally the computational value of the contact area was compared to the experimental results at the same four points in the gait cycle.

7.3.6 Computational Results

In this section the computational model was used in order to find the effect of the stiff knee, resected ACL and resected ACL & PCL soft tissue conditions on a wider range of alignment conditions. The output AP, TR and AA kinematics were found for each alignment and soft tissue condition. The peak contact pressure values were also found at the same four points in the cycle where the contact pressure was measured experimentally. The contact area was found for each alignment and soft tissue condition throughout the cycle.

The rotational mismatch alignment was run under values of 14°, 8° and 4°. The varus joint line alignment condition was run under values of 4° and 2°. The tibial slope alignment condition was run under values of 10° and 4° posterior tibial slope. Finally the kinematic alignment condition was run under the same alignment values studied experimentally and half the experimental values (Table 7.3).

Table 7.3: Kinematic alignment component positions studied computationally

Test	Femoral	Tibial	
	Coronal (° valgus)	Coronal (° varus)	Sagittal (° posterior)
Mechanical	0	0	0
Half Experimental Values	1.2	1.7	2.3
Experimental Values	2.5	3.4	4.6

7.4 Experimental Results

7.4.1 Stability

The stability of each alignment condition was determined under a range of soft tissue conditions, including with increased AP and TR gap sizes of 5mm and 9° and with no springs applied. Lift off was defined as loss of contact between the femoral and tibial components during gait.

The mechanical alignment condition was stable under all the soft tissue conditions applied, with no lift off occurring.

With the varus joint line alignment condition there was some lift off, with external tibial rotation resulting in the femorotibial contact moving to the posterior edge of the insert. This occurred with the 5mm and 9° gap soft tissue condition and with no springs applied.

The rotated alignment also resulted in some lift off; the femorotibial contact moved up the posterior edge of the tibial insert as with the varus alignment. This occurred with the large gap soft tissue condition and with no springs applied. There was then an impact as the femoral component came back into contact with the tibial insert as it came off the posterior edge. When no springs were applied this impact was more severe.

The TKR with a posterior tibial slope dislocated under all the soft tissue studies apart from the stiff knee soft tissue condition. The external rotation of the femoral component caused the lateral femoral condyle to come off the posterior side of the tibial insert in all other soft tissue conditions.

With the kinematic alignment the TKR was stable during all studies, however the contact between the femoral and tibial components was very posterior during flexion using all but the stiff knee soft tissue condition.

7.4.2 Effect on kinematics

The average anterior-posterior, tibial rotation and abduction-adduction displacement profiles were determined for each of the three soft tissue conditions for the varus joint line, rotated and kinematic alignment conditions as follows.

7.4.2.1 Varus Joint Line Alignment Condition

The average output kinematics with all three different soft tissue conditions were determined for the varus alignment condition. For the AP and TR displacements the profile shapes were similar, with the two lower tension soft tissue conditions (resected ACL and resected ACL & PCL) resulting in higher amplitudes.

For the first half of the gait cycle the resected ACL and resected ACL & PCL soft tissue conditions resulted in very similar AP displacement values but the stiff knee soft tissue condition resulted in significantly lower AP displacements ($p<0.01$) (Figure 7.3 (a)).

All three soft tissue conditions resulted in significantly different peak AP displacements ($p<0.01$). For the second half of the gait cycle the resected ACL & PCL soft tissue condition resulted in a higher AP displacement than the resected ACL soft tissue condition at all points, however this was not significant.

All three soft tissue conditions also resulted in significantly different ranges of AP motion; 7.0mm, 5.5mm and 2.6mm for the resected ACL & PCL, resected ACL and stiff knee soft tissue conditions ($p<0.01$).

As with the AP displacement the resected ACL and resected ACL & PCL soft tissue conditions resulted in very similar TR displacements during the first half of the gait cycle (Figure 7.3 (b)). There was no significant difference in the TR rotation between the soft tissue conditions in the first half of the gait cycle ($p>0.18$). However the stiff knee soft tissue condition resulted in a significantly lower peak TR rotation ($p<0.02$). The resected ACL & PCL soft tissue condition also resulted in a higher peak TR rotation than the resected ACL soft tissue condition and then resulted in a sharper decrease in TR from 60-70% gait. At point H the resected ACL soft tissue condition resulted in a significantly higher TR rotation than the resected ACL & PCL soft tissue condition ($p=0.04$).

There was no significant difference in the range in TR motion between the resected ACL and resected ACL & PCL soft tissue conditions, however the stiff knee soft tissue conditions resulted in a significantly lower range of motion ($p<0.01$).

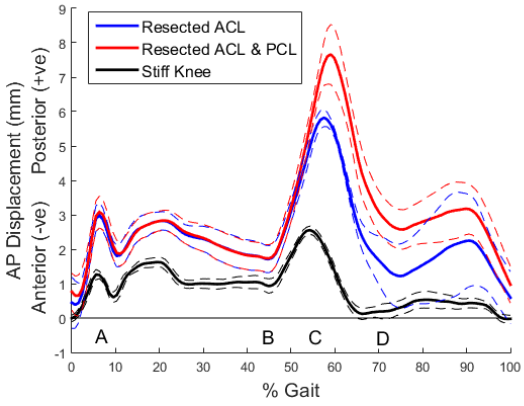

(a) AP Displacement

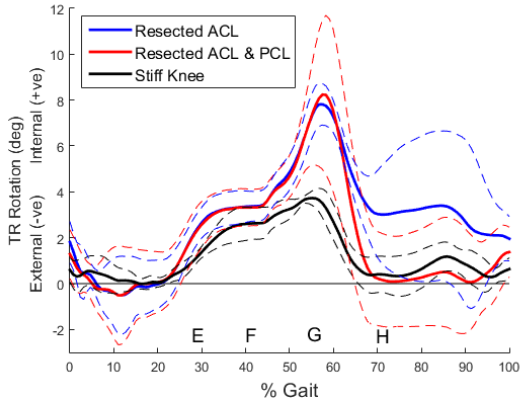

(b) TR Rotation

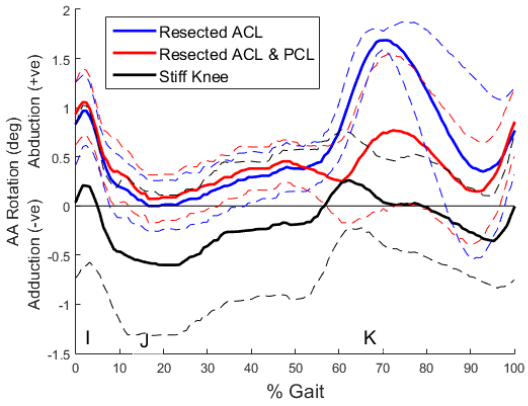

(c) AA Rotation

Figure 7.3: The average AP, TR and AA displacements for the varus joint line alignment condition with the stiff knee, resected ACL and resected ACL & PCL soft tissue conditions

The resected ACL and resected ACL & PCL soft tissue conditions resulted in similar AA displacements for the first half of the gait cycle (Figure 7.3 (c)). The resected ACL and resected ACL & PCL soft tissue conditions also resulted in AA motion that was centred around 1° whereas the stiff knee soft tissue condition resulted in AA rotation centred around 0°. At point I the stiff knee soft tissue condition resulted in a significantly lower AA rotation compared to the resected ACL and resected ACL & PCL soft tissue conditions ($p=0.03$). At 50% gait the AA displacement then decreased with the resected ACL & PCL soft tissue condition, while the resected ACL soft tissue condition resulted in an increase in the AA rotation. The stiff knee soft tissue condition resulted in a significantly lower peak AA rotation than the resected ACL soft tissue condition ($p<0.01$), there was also a significant difference between the resected ACL and resected ACL & PCL soft tissue conditions at this point ($p=0.04$). The peak AA rotation also occurred earlier in the cycle for the stiff knee soft tissue condition than for the resected ACL or resected ACL & PCL soft tissue conditions. This was also true of the peak AP and TR displacements. The stiff knee soft tissue condition resulted in a significantly lower range in AA motion than the resected ACL soft tissue condition ($p=0.01$).

7.4.2.2 Rotated Alignment Condition

Under the rotated alignment condition the AP displacement profiles were similar to those under varus joint line alignment; under the resected ACL and resected ACL & PCL soft tissue conditions there were similar AP displacements for the first 50% gait (Figure 7.4 (a)). The stiff knee soft tissue condition resulted in a significantly lower AP displacement at point A ($p<0.01$). At point B the stiff knee soft tissue condition resulted in a significantly lower AP displacement compared to the resected ACL & PCL soft tissue condition. All three soft tissue conditions resulted in significantly different peak AP displacements of 7.9mm, 5.8mm and 2.4mm for the resected ACL & PCL, resected ACL and stiff knee soft tissue conditions respectively ($p<0.03$).

The three soft tissue conditions resulted in significantly different AP ranges of motion of 2.0mm, 6.5mm and 8.6mm for the stiff knee, resected ACL and resected ACL & PCL soft tissue conditions respectively ($p<0.04$).

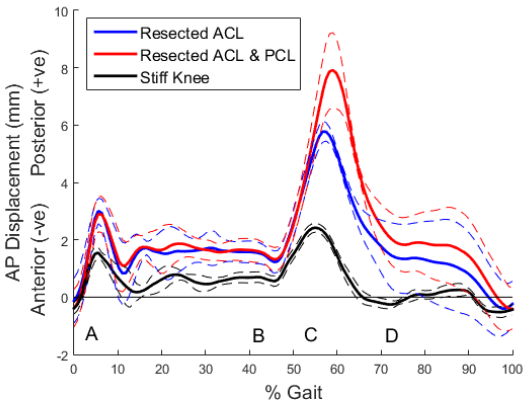

(a) AP Displacement

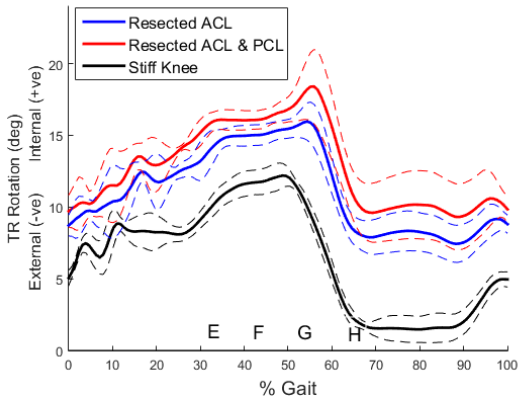

(b) TR Rotation

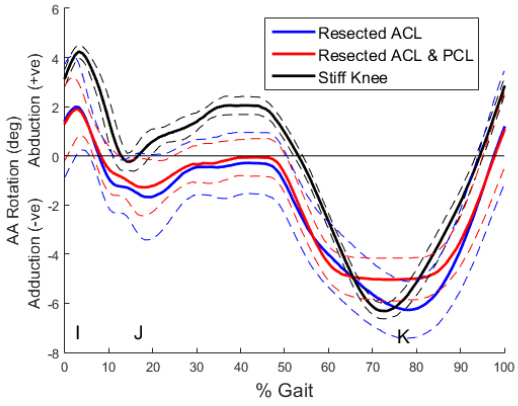

(c) AA Rotation

Figure 7.4: The average AP, TR and AA displacements for the rotated alignment condition with the stiff knee, resected ACL and resected ACL & PCL soft tissue conditions

All of the soft tissue conditions resulted in similar TR profile shapes, however there was an offset between them; the resected ACL & PCL soft tissue condition resulted in the highest

TR rotation at all points and the resected ACL soft tissue condition resulted in a higher displacement than the stiff knee soft tissue condition (Figure 7.4 (b)). The stiff knee soft tissue condition resulted in a TR rotation centred around 5° whereas the resected ACL and resected ACL & PCL soft tissue conditions were centred around 9° and 10° respectively. At points E-H the stiff knee soft tissue condition resulted in significantly lower TR rotation than the other two soft tissue conditions ($p<0.01$). The stiff knee soft tissue condition resulted in a significantly higher range of TR motion than the resected ACL soft tissue condition ($p=0.03$) .

The soft tissue conditions also resulted in similar AA rotation profiles with maximum and minimum peaks at 5% and 70% gait (Figure 7.4 (c)). The stiff knee soft tissue condition resulted in a significantly higher AA rotation at point I in the cycle ($p<0.05$) and a significantly lower peak AA rotation at point K than the resected ACL & PCL soft tissue condition ($p=0.04$). The range in AA was significantly different between all three soft tissue conditions with the stiff knee soft tissue condition resulting in the highest value and the resected ACL & PCL soft tissue condition resulting in the lowest value ($p<0.01$).

7.4.2.3 Kinematic Alignment Condition

With the kinematic alignment condition there was more anterior displacement than any of the other alignment conditions (Figure 7.5 (a)). The resected ACL and resected ACL & PCL soft tissue conditions resulted in very similar AP displacements throughout the cycle with the AP displacement centred around -5mm. With the stiff knee soft tissue condition there was lower displacement with the AP profiles centred around -2mm. This shift in the AP displacement under different soft tissue conditions only occurred with the kinematic alignment. The stiff knee soft tissue condition resulted in significantly higher AP displacement than the other two soft tissue conditions at points A, B and D and significantly lower peak AP displacement at point C in the cycle ($p<0.01$). There was no significant difference between the resected ACL and resected ACL & PCL soft tissue conditions at any point. The stiff knee soft tissue condition resulted in a significantly lower AP range of motion than the other two soft tissue conditions ($p<0.01$).

As with the AP displacement the resected ACL and resected ACL & PCL soft tissue conditions resulted in very similar TR rotation profiles (Figure 7.5 (b)). The stiff knee soft tissue condition resulted in lower TR displacements and resulted in a different profile shape, with the peak TR rotation occurring earlier in the cycle. At points E-G in the cycle the stiff knee soft tissue condition resulted in a significantly lower displacement than the other soft tissue conditions ($p<0.05$). At point H, near the end of the cycle, there was no significant difference between any of the soft tissue conditions ($p=0.86$). The stiff knee soft tissue condition also resulted in a significantly lower range in TR than the other soft tissue conditions ($p<0.02$).

All the soft tissue conditions resulted in AA profiles with different offsets; the resected ACL soft tissue profile was centred around 1°, the resected ACL & PCL soft tissue condition around 1.5° and the stiff knee soft tissue condition around 2° (Figure 7.5 (c)). The stiff knee

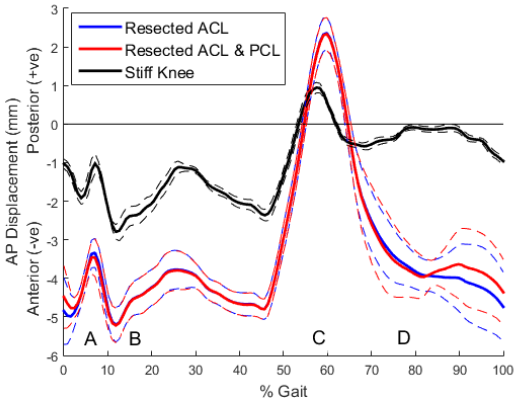

(a) AP Displacement

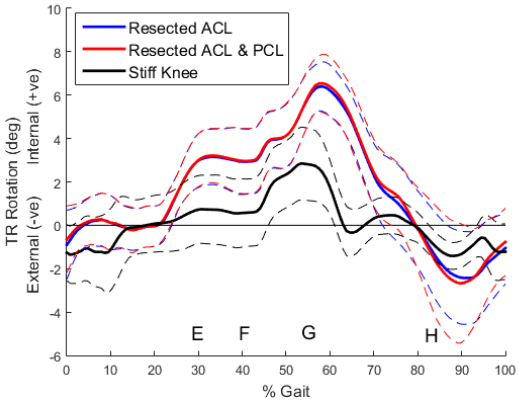

(b) TR Rotation

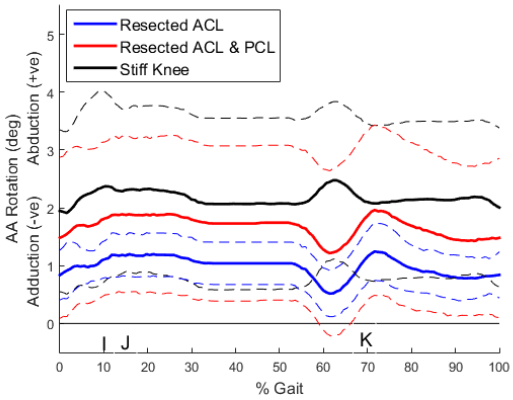

(c) AA Rotation

Figure 7.5: The average AP, TR and AA displacements for the kinematic alignment condition with the stiff knee, resected ACL and resected ACL & PCL soft tissue conditions with the 95% CI shown with dotted lines

soft tissue condition also resulted in a different profile shape with the AA rotation increasing rather than decreasing at around 55% gait and with the peak occurring earlier in the cycle than the other soft tissue conditions at around 60% gait. There was however no significant difference in the AA displacements at any point in the cycle or the range of motion ($p>0.09$).

7.4.2.4 Comparison between alignment conditions

The mean AP displacement for each alignment condition was determined for each of the three soft tissue conditions; stiff knee, resected ACL and resected ACL & PCL (Figure 7.6). All the alignment and soft tissue conditions resulted in a similar AP displacement profile with the peak displacement occurring at 60% gait. The lower tension resected ACL and resected ACL & PCL springs, with gaps around the zero position, resulted in higher peak AP displacements compared to the stiff knee springs. There was a smaller difference in the peak AP displacements between the resected ACL and resected ACL & PCL springs than with the stiff knee springs for all the alignment conditions.

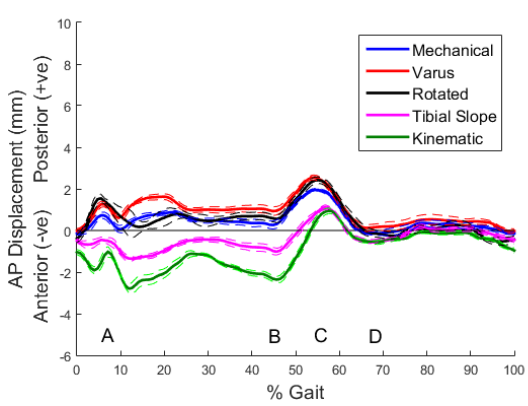

(a) Stiff Knee

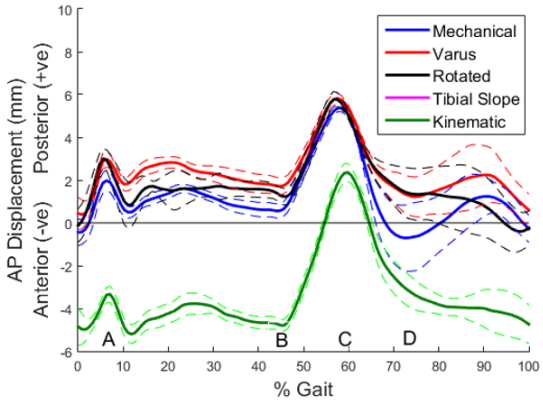

(b) Resected ACL

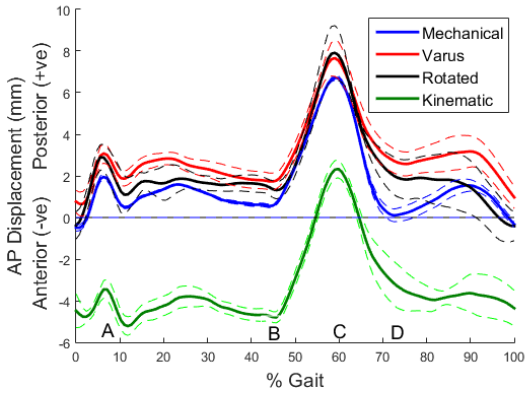

(c) Resected ACL and PCL

Figure 7.6: The mean output AP displacement for each alignment condition under the stiff knee, resected ACL and resected ACL & PCL soft tissue conditions with the 95% CI shown with dotted lines

The tibial slope alignment condition was too unstable to run under the resected ACL and resected ACL & PCL springs. Under the stiff knee soft tissue condition it resulted in significantly more anterior displacement than the mechanical, varus joint line and rotated alignment conditions at points A-C ($p<0.01$).

Under the resected ACL and resected ACL & PCL springs the kinematic alignment condition resulted in significantly more anterior displacement than all the other alignment conditions at all points in the cycle ($p<0.01$).

Under all the soft tissue conditions the varus alignment resulted in a similar AP displacement profile as the mechanical and rotated alignment conditions. The varus and rotated alignment conditions resulted in higher peak AP displacements than mechanical alignment under all the soft tissue conditions, however the difference in values was small.

The range of motion in the AP displacement was determined from the difference in the minimum and maximum points in the gait cycle (Figure 7.7). For all the alignment conditions the lowest range of motion occurred under the stiff knee soft tissue condition with similar values

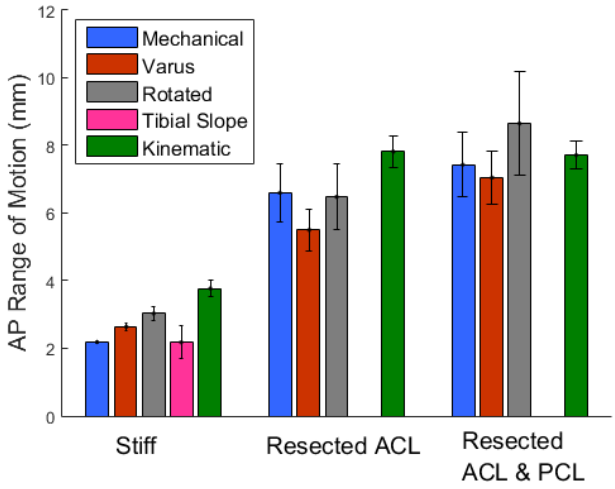

Figure 7.7: The mean and 95% confidence interval of the range of motion in the AP displacement for each alignment and soft tissue condition

under the resected ACL and resected ACL & PCL soft tissue conditions. There was more variation in the range of motion under the lower tension soft tissue conditions than under the stiff knee soft tissue condition.

The mechanical, varus, kinematic and tibial slope alignment conditions resulted in similar TR rotation output profiles; an increase after 20% gait followed by a plateau and peak displacement at 60% gait (Figure 7.8).

The varus and tibial slope alignment conditions resulted in similar peak displacements as the mechanical alignment condition for all the soft tissue conditions and for the stiff knee soft tissue condition under the tibial slope alignment.

Under the stiff knee springs the kinematic alignment condition resulted in a lower initial plateau at around 30% gait, and a slightly lower peak TR rotation than the mechanical, varus and tibial slope alignment conditions (Figure 7.8 (a)). However under the other two soft tissue conditions this difference did not occur.

The rotated alignment condition resulted in a different output profile under all the soft tissue conditions compared to the other alignment conditions. The initial plateau was present under the stiff knee springs but occurred earlier in the cycle, while under the lower tension springs it was not present at all. For the resected ACL and resected ACL & PCL springs there was a gradual increase in TR rotation for the first half of the cycle. After this point it resulted in a similar profile shape to the other alignment conditions (Figure 7.8 (b) and (c)). The peak TR rotation under the rotated alignment condition resulted in significantly higher TR displacements than the other alignment conditions for all the soft tissue conditions ($p<0.01$) and occurred earlier in the cycle.

The mean and 95% CI for the range of TR motion was determined for each alignment and soft tissue condition (Figure 7.9).

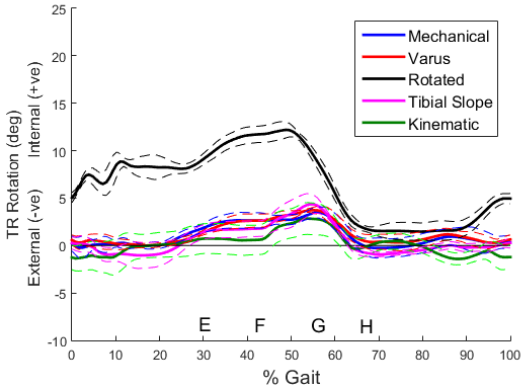

(a) Stiff Knee

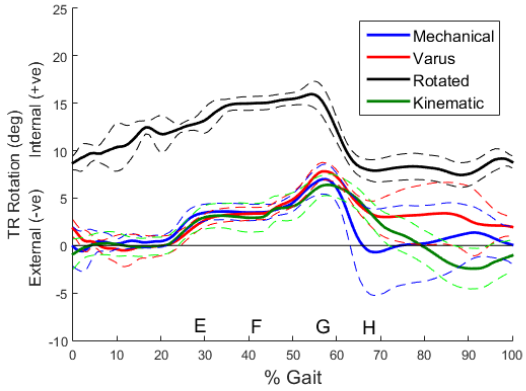

(b) Resected ACL

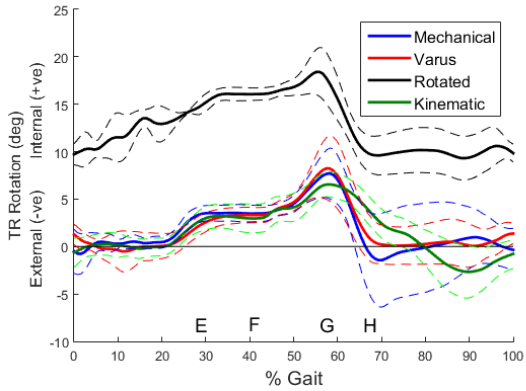

(c) Resected ACL and PCL

Figure 7.8: The mean output TR rotation for each alignment condition under the stiff knee, resected ACL and resected ACL & PCL soft tissue conditions with the 95% CI shown with dotted lines

Under the stiff knee springs the rotated alignment condition resulted in significantly higher range of motion of 11.3° compared to the other alignment conditions ($p<0.01$). However under the other two soft tissue conditions the range of TR rotation was similar across all the alignment conditions.

As with the AP range of motion there was more variation in the TR range of motion under the resected ACL and resected ACL & PCL springs, particularly with the mechanical alignment condition. This was partly due to the increased inter-station variation that occurred under the lower tension springs and partly due to the variation at the end of the cycle. The end of the cycle, where the AF was at it's lowest point, was where the most variation occurred and was often the minimum displacement point during the cycle. Therefore this variation resulted in an affect on the range of motion, increasing its confidence interval.

The mechanical, varus and tibial slope alignment conditions resulted in similar AA rotation profiles, with the peak displacement occurring at around 60% gait (Figure 7.10).

The mechanical alignment condition resulted in significantly higher peak AA rotation than the varus alignment condition under the stiff knee springs ($p<0.01$) (Figure 7.10 (a)).

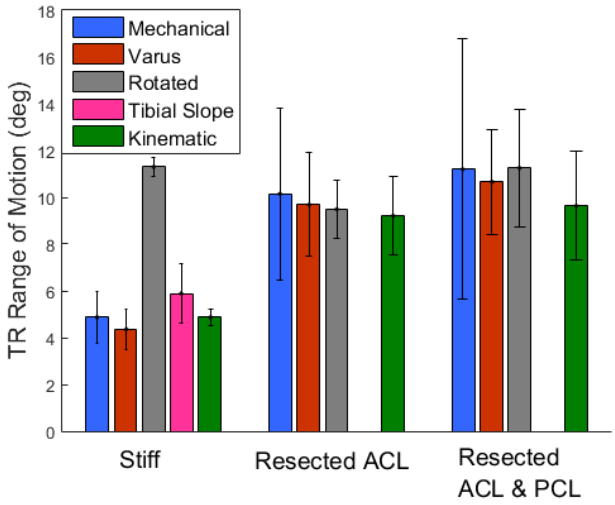

Figure 7.9: The mean and 95% confidence interval of the range of motion in the TR rotation for each alignment and soft tissue condition

The rotated alignment condition resulted in a different AA profile; there was a peak at the start of the gait cycle followed by a decrease then plateau from 10-50% gait then a large peak in adduction at around 70% gait. Both the shape and amplitude of the AA profile was different for the rotated alignment condition.

The kinematic alignment condition also resulted in a different profile shape to the other alignment conditions with the AA rotation being around 2° higher than the other alignment conditions at all points in the cycle.

Under all the soft tissue conditions the rotated alignment condition resulted in a significantly higher AA range of motion ($p<0.01$) (Figure 7.11).

Under the resected ACL springs the range of motion for the mechanical, varus and kinematic alignment components increased to 2.3°, 2.0° and 0.8° respectively. However with the rotated alignment condition the range of motion decreased by 1.93° to a value of 8.67°, this was significantly higher than the other alignment conditions ($p<0.01$). The kinematic alignment condition resulted in a significantly lower range of AA motion under the resected ACL springs than the other alignment conditions ($p<0.03$).

Under the resected ACL & PCL springs the range of motion for the mechanical, varus and rotated alignment conditions decreased to 2.2°, 1.23° and 7.22° respectively. While the kinematic alignment condition resulted in a small increase in the range of motion to 0.9°. The kinematic alignment condition again resulted in a significantly lower range of motion compared to the mechanical alignment condition ($p<0.01$).

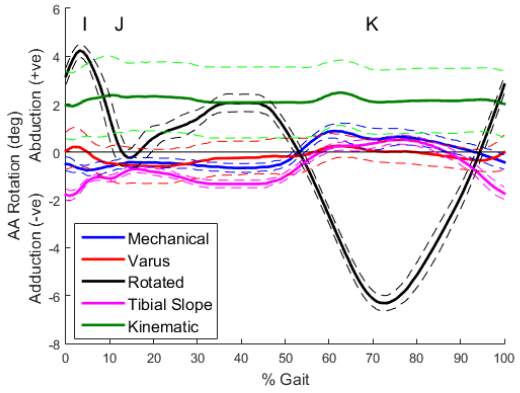

(a) Stiff Knee

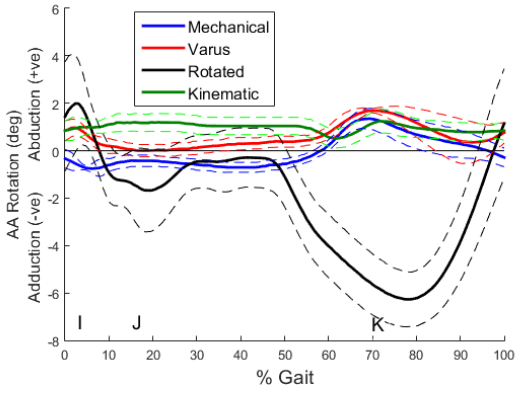

(b) Resected ACL

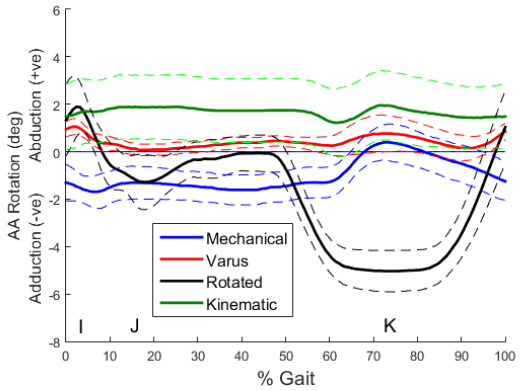

(c) Resected ACL and PCL

Figure 7.10: The mean output AA rotation for each alignment condition under the stiff knee, resected ACL and resected ACL & PCL soft tissue conditions with the 95% CI shown with dotted lines

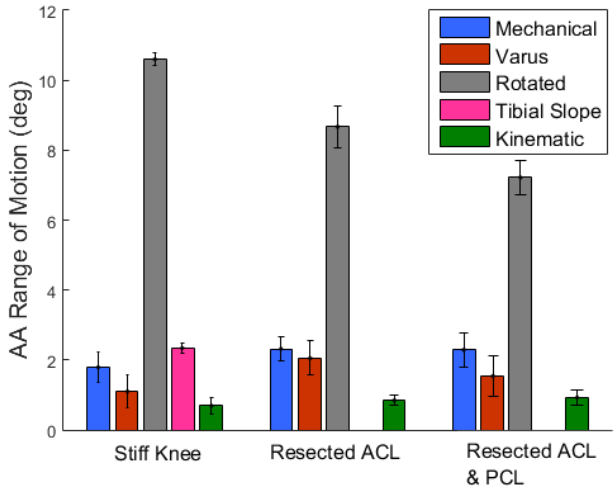

Figure 7.11: The mean and 95% confidence interval of the range of motion in the AA rotation for each alignment and soft tissue condition

7.4.3 Effect on contact area

A Tekscan pressure sensor was used to measure the contact between the tibial and femoral components at four points in the gait cycle. The loads and displacements at these points were determined using the kinematic data for each soft tissue condition.

7.4.3.1 Varus Joint Line Alignment Condition

Figure 7.12 shows the average contact area and 95% CI for each point measured using the varus joint line alignment condition.

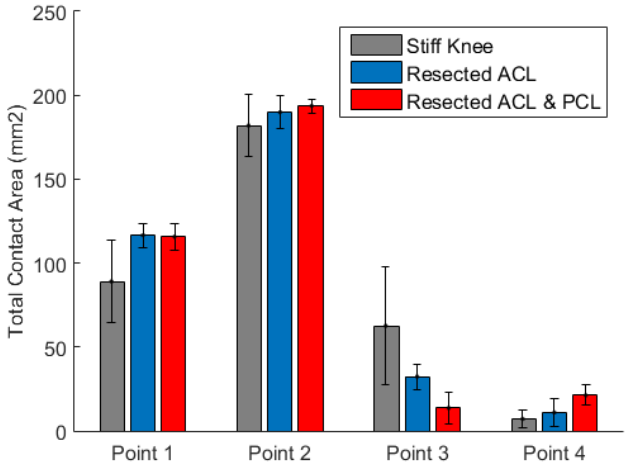

Figure 7.12: The average contact area (mm2) with error bars showing the 95% CI (n=5) for the varus alignment condition combined with the stiff knee, resected ACL and resected ACL & PCL soft tissue conditions at each point in the cycle

At point 1 the stiff knee soft tissue condition resulted in a significantly lower total contact area ($p<0.01$) and a significantly higher contact area at point 3 ($p=0.04$). However at point 2 there was no significant difference in the total contact areas for each soft tissue condition ($p=0.20$).

The resected ACL soft tissue condition also resulted in a significantly higher total contact area than the resected ACL & PCL soft tissue condition at point 3 ($p<0.01$).

At point 4 the resected ACL & PCL soft tissue condition resulted in a significantly higher contact area at this point compared to the stiff knee soft tissue condition ($p<0.01$).

The average contact area outlines with the 95% CI shown in dotted lines for each point in the cycle are shown in Figure 7.13 for the varus alignment and each of the soft tissue conditions.

Under the stiff knee soft tissue condition the varus alignment condition resulted in mostly lateral contact (Figure 7.13 (a)). At the end of the cycle the lateral contact was also small and close to the posterior edge of the tibial insert.

Under the resected ACL soft tissue condition there was more medial loading than under

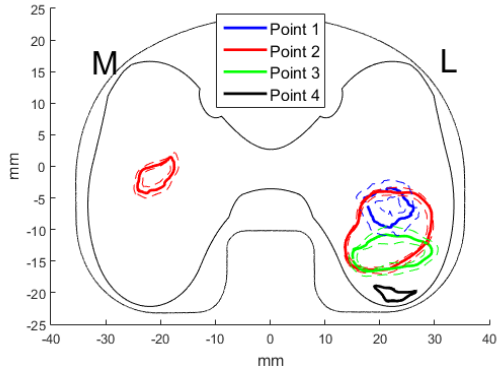

(a) Stiff Knee

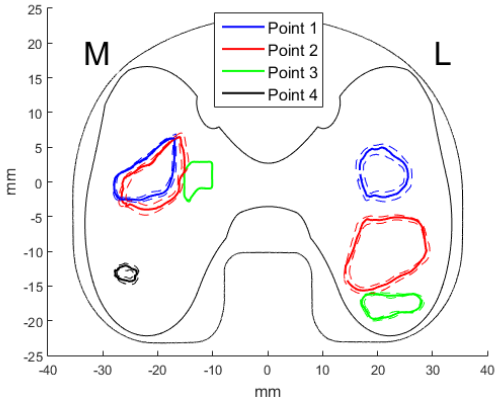

(b) Resected ACL

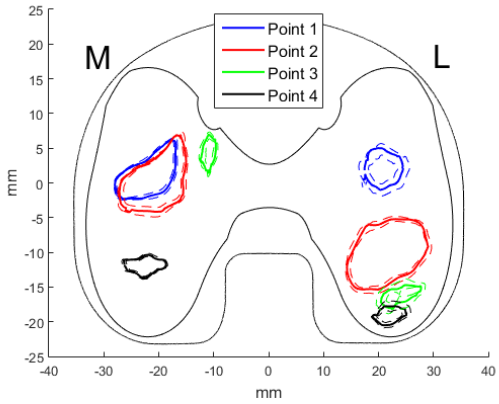

(c) Resected ACL and PCL

Figure 7.13: The average contact area with the 95% CI shown in dotted lines (n=5) for the varus alignment condition with the stiff knee, resected ACL and resected ACL & PCL soft tissue conditions

the stiff knee soft tissue condition (Figure 7.13 (b)). There was medial contact at all points in the cycle and lateral contact at all points apart from at point 4, at the end of the cycle. The contact points at the start of the cycle, especially point 1, were more anterior than under the stiff knee soft tissue condition. The contact was also further from the posterior edge of the tibial insert.

Under the resected ACL & PCL soft tissue condition there was both medial and lateral contact at all points in the cycle (Figure 7.13 (c)). The position of the contact points were similar to those under the resected ACL soft tissue condition. However the contact at point 4 was close to the posterior tibial edge of the insert.

7.4.3.2 Rotated Alignment Condition

The average contact area across the simulator was found under the rotated alignment condition and each of the three soft tissue conditions (Figure 7.14).

There was no significant difference in the contact area between the resected ACL and

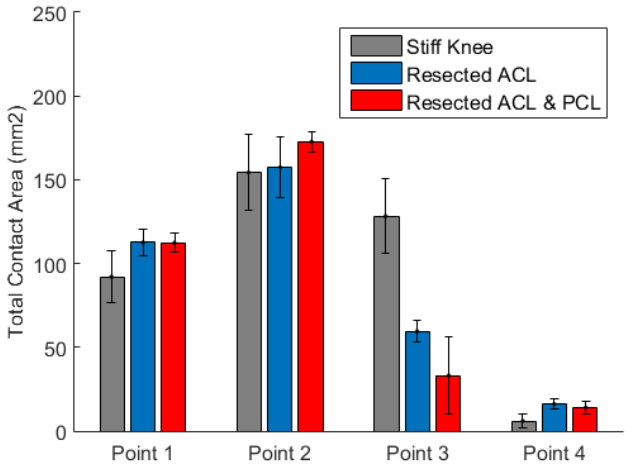

Figure 7.14: The average contact area (mm2) with error bars showing the 95% CI (n=5) for the rotated alignment condition combined with the stiff knee, resected ACL and resected ACL & PCL soft tissue conditions at each point in the cycle

resected ACL & PCL soft tissue conditions at any point in the cycle.

The soft tissue condition resulted in a significantly lower contact area at points 1 and 4 ($p<0.04$ and $p<0.01$) but resulted in a significantly higher contact area at point 3 ($p<0.01$).

Figure 7.15 shows the position of the contact areas for each point in the cycle and each soft tissue condition.

With the stiff knee soft tissue condition there was more lateral loading in the first half of the cycle and more medial loading in the second half of the cycle (Figure 7.15 (a)). At point 4 the contact also overlapped with the posterior edge of the tibial insert.

With the resected ACL soft tissue condition there was more medial loading at the start of the cycle, however the loading was still unbalanced (Figure 7.15 (b)). The contact positions however were further from the edge of the tibial insert than under the stiff knee soft tissue condition.

With the resected ACL & PCL soft tissue condition there was more medial loading throughout the cycle and no contact close to the posterior edge of the tibial insert (Figure 7.15 (c)).

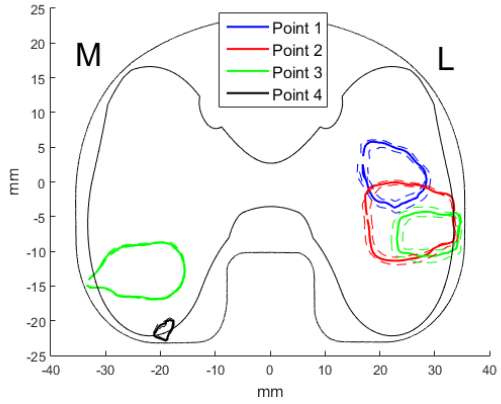

(a) Stiff Knee

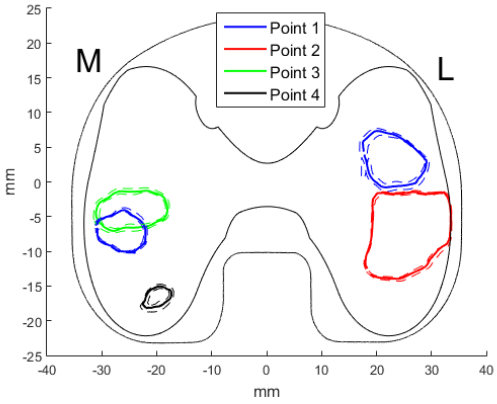

(b) Resected ACL

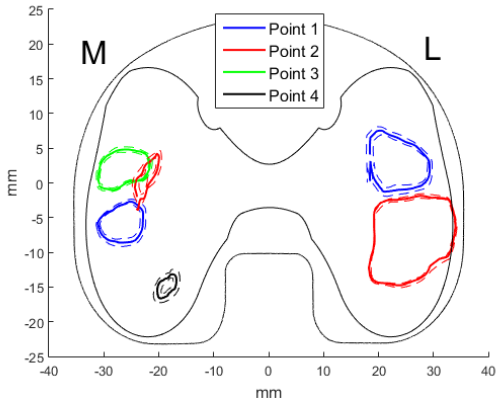

(c) Resected ACL and PCL

Figure 7.15: The average contact area with the 95% CI shown in dotted lines (n=5) for the rotated alignment condition combined with the stiff knee, resected ACL and resected ACL & PCL soft tissue conditions at each point in the cycle

7.4.3.3 Kinematic Alignment Condition

Figure 7.16 shows the average contact areas for the kinematic alignment condition at each measured point in the cycle with all three soft tissue conditions. The contact area was similar at each point in the cycle for all soft tissue conditions.

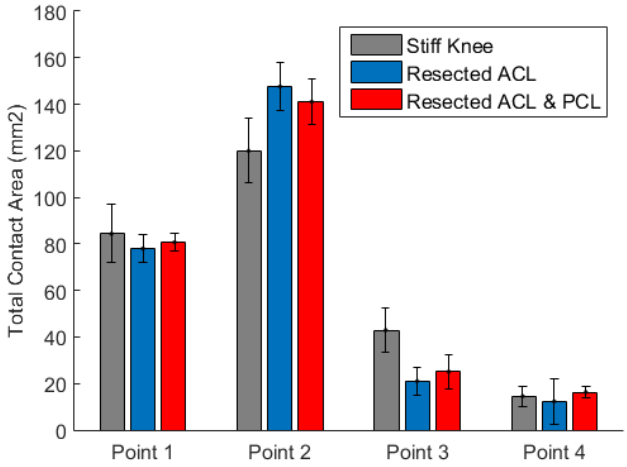

Figure 7.16: The average contact area (mm2) with error bars showing the 95% CI (n=5) for the kinematic alignment condition combined with the stiff knee, resected ACL and resected ACL & PCL soft tissue conditions at each point in the cycle

At points 1 and 4 there was no significant difference between the contact area with the different soft tissue conditions ($p=0.36$ and $p=0.48$). At point 2 however the stiff knee soft tissue condition resulted in a significantly lower total contact area ($p<0.03$).

At point 3 the stiff knee soft tissue condition resulted in a significantly higher total contact area ($p<0.01$).

The positions of the contact areas are shown along with the 95% CI in Figure 7.17 for all of the soft tissue conditions with the kinematic alignment. For all of the soft tissue conditions there was only ever lateral contact at all points in the cycle.

With the stiff knee soft tissue condition the contact was more anterior throughout the gait cycle compared to the other two soft tissue conditions (Figure 7.17 (a)).

The contact areas were similar with the resected ACL and resected ACL & PCL soft tissue conditions (Figure 7.17 (b) and (c)). The contacts were all more posterior with the resected ACL and resected ACL & PCL soft tissue conditions than they were with the stiff knee soft tissue condition, however there was no contact near to the posterior tibial edge.

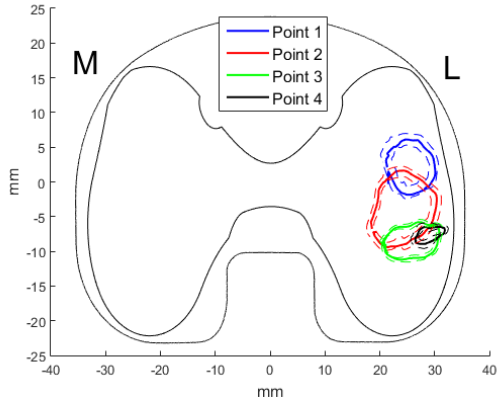

(a) Stiff Knee

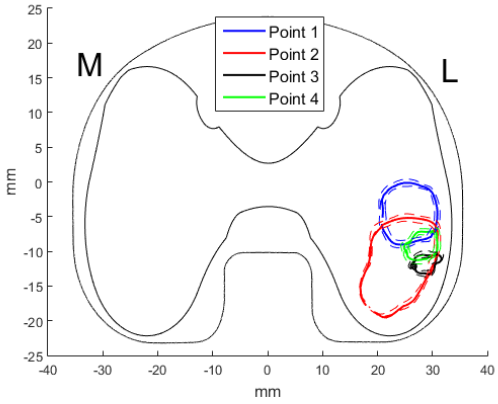

(b) Resected ACL

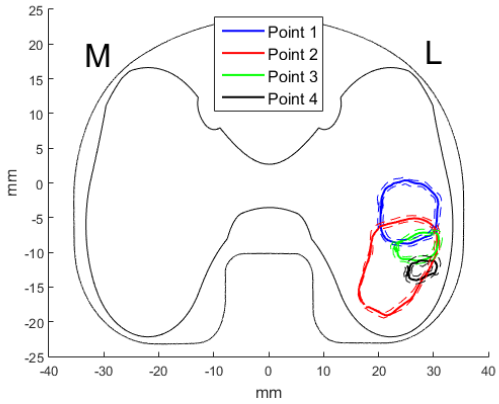

(c) Resected ACL and PCL

Figure 7.17: The average contact area with the 95% CI shown in dotted lines (n=5) for the kinematic alignment condition combined with the stiff knee, resected ACL and resected ACL & PCL soft tissue conditions at each point in the cycle

7.4.3.4 Comparison in Contact Area Between Alignment Conditions

The comparison in the contact area between the alignment conditions was carried out under the stiff knee soft tissue condition in Chapter 6. In this section the contact area between the alignment conditions will be compared under the resected ACL and resected ACL & PCL soft tissue conditions.

The mean contact area for each alignment condition at each point in the cycle under the resected ACL and resected ACL & PCL soft tissue conditions are shown in Figures 7.18 and 7.19. For all the alignment conditions the highest contact areas occurred at point 2 in the cycle, where the AF was at its peak. The contact areas at points 1 and 2 were much higher than those later in the cycle, when the AF was at its lowest.

At point 1 in the cycle, at 5% gait, under both soft tissue conditions the varus and rotated alignment conditions resulted in significantly higher total contact areas than the mechanical and kinematic alignment conditions ($p<0.01$).

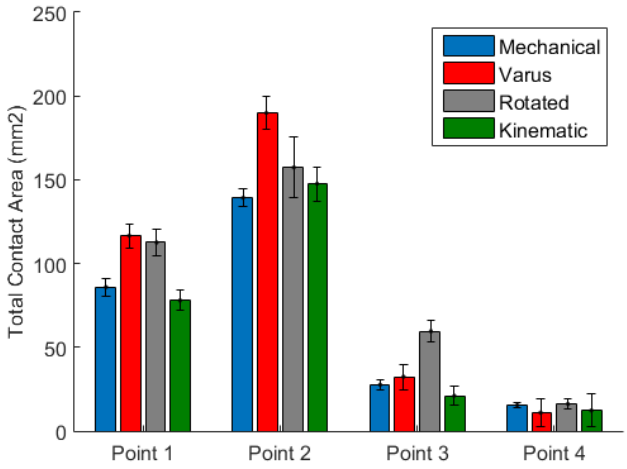

Figure 7.18: The mean contact area for all the alignment conditions under the resected ACL soft tissue condition at each measured point in the gait cycle with error bars showing the 95% CI (n=5)

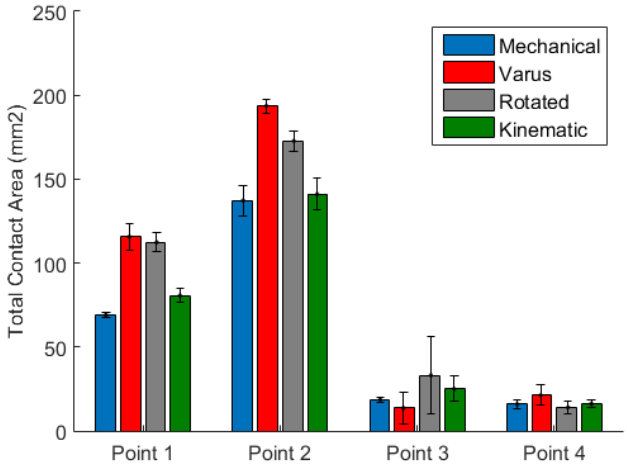

Figure 7.19: The mean contact area for all the alignment conditions under the resected ACL & PCL soft tissue condition at each measured point in the gait cycle with error bars showing the 95% CI (n=5)

The varus alignment condition also resulted in a significantly higher total contact area than all the other alignment conditions at point 2 in the cycle under both soft tissue conditions ($p<0.02$).

Under the resected ACL soft tissue condition the rotated alignment condition resulted in a significantly higher total contact area at point 3 compared to the other alignment conditions ($p<0.01$).

At the end of the cycle the contact areas across all the alignment conditions were at their lowest and similar in value.

7.4.4 Effect on wear

Seven wear studies were carried out each for 2MC with the different alignment and soft tissue conditions. Wear studies were carried out with the mechanical, varus and rotated alignments with the resected ACL & PCL and the stiff knee soft tissue conditions. Only one wear study was carried out with the tibial slope alignment under the stiff knee soft tissue condition as it could not be run under the resected ACL & PCL soft tissue condition, therefore this data was not included in this chapter. No wear studies were carried out using the kinematic alignment as the purely lateral contact found under the experimental simulation may not be representative of the conditions in vivo.

7.4.4.1 Wear rates

The mean wear rates with 95% CI for the mechanical, varus and rotational mismatch alignments under the resected ACL & PCL soft tissue condition were 3.06±1.57mm^3/MC, 1.79±1.64mm^3/MC and 7.33±3.05mm^3/MC respectively (Figure 7.20).

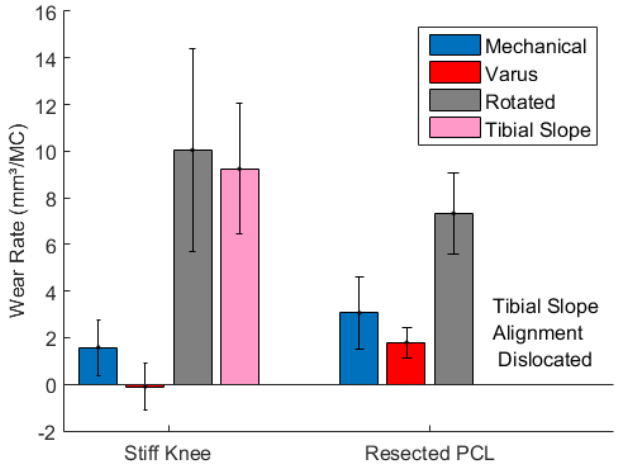

Figure 7.20: Wear rates over 2MC with 95% CI under the "stiff knee" and resected ACL & PCL soft tissue conditions for mechanical, 4° varus, 14° rotational mismatch and 10° tibial slope alignment conditions

With the resected ACL & PCL soft tissue condition the wear rates were higher for the mechanical and varus alignment conditions compared to the wear rates with the stiff knee soft tissue condition, however this was not significant. With the rotated components the wear rate was lower for the resected ACL & PCL soft tissue condition than for the stiff knee soft tissue condition but again this difference in wear was not significant.

Under the stiff knee springs the rotated and tibial slope alignments resulted in significantly higher wear than the mechanical and varus alignments. While the varus alignment resulted in significantly lower wear compared to the mechanical alignment.

Under the resected ACL & PCL springs the rotated alignment still resulted in a signi-

ficantly higher wear rate than the mechanical and varus alignments ($p<0.03$). There was however no significant difference between the wear rates with the mechanical and varus alignment conditions ($p=0.36$).

The investigation into the variation in kinematics and wear during the wear studies under the stiff knee soft tissue condition was carried out in Chapter 6, in this chapter the wear studies under the resected ACL & PCL soft tissue condition will be investigated.

Under the varus alignment condition and the resected ACL & PCL soft tissue condition, after 1MC and 2MC one insert resulted in a much higher wear volume than the others (Figure 7.21 (b)). There was a similar wear rate across all the inserts after 1MC of 1.7mm^3/MC than 1.8mm^3/MC after 2MC.

The wear volume of each station of the simulator and each tibial insert after 1MC and after 2MC are shown in Figure 7.21 (a). As with the tibial inserts one station resulted in a much higher wear volume than the other five stations. Station 6 resulted in a very low wear volume over the first MC, however this then increased during the second MC.

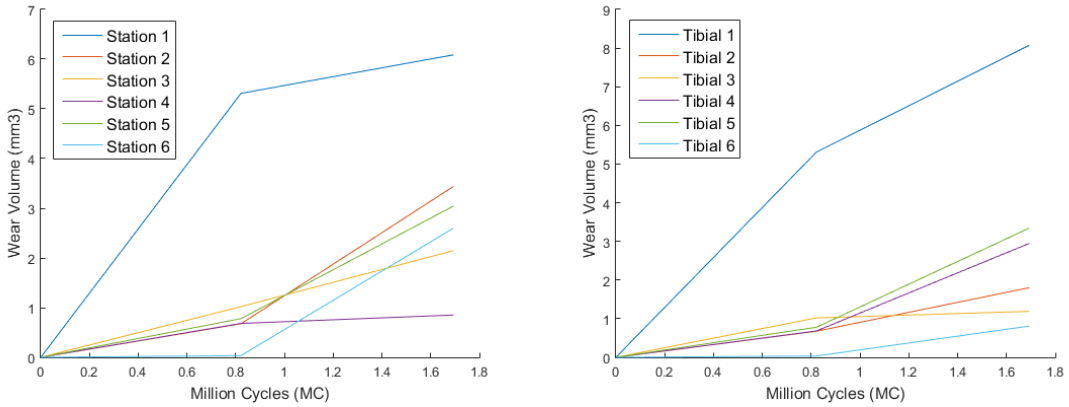

(a) Station Wear Volume

(b) Insert Wear Volume

Figure 7.21: The wear volume (mm3) for each tibial insert and each station on the simulator over 1MC and over 2MC with the varus alignment and resected ACL & PCL soft tissue condition

After 1MC under the rotated alignment condition and the resected ACL & PCL soft tissue condition the wear volumes of the tibial inserts ranged from 1.9mm^3 to 10.2mm^3 (Figure 7.22 (b)). Three of the six tibial inserts resulted in lower wear rates in the first MC compared to the second; inserts 1, 2 and 3, 4. The overall wear rate was similar after 1MC compared to after 2MC; 6.1mm^3/MC compared to 7.3mm^3/MC.

The wear volume of each station of the simulator and each tibial insert at 1MC and 2MC is shown in Figure 7.22 (a). After 1MC station 4 resulted in the highest wear volume of 10.2mm^3. Stations 3 and 6 resulted in similar wear volumes of 7.8mm^3/MC and 7.3mm^3/MC respectively while the other stations resulted in lower wear volumes of 1.9mm^3, 2.2mm^3 and 4.2mm^3 for stations 1, 2 and 5 respectively. After 2MC station 4 still resulted in a high wear volume compared to the other stations of 20.5mm^3, however stations 1,2, 3 and 5 had similar

values. While the wear rates of stations 6 was still lower than the other stations despite having a higher wear rate after 2MC.

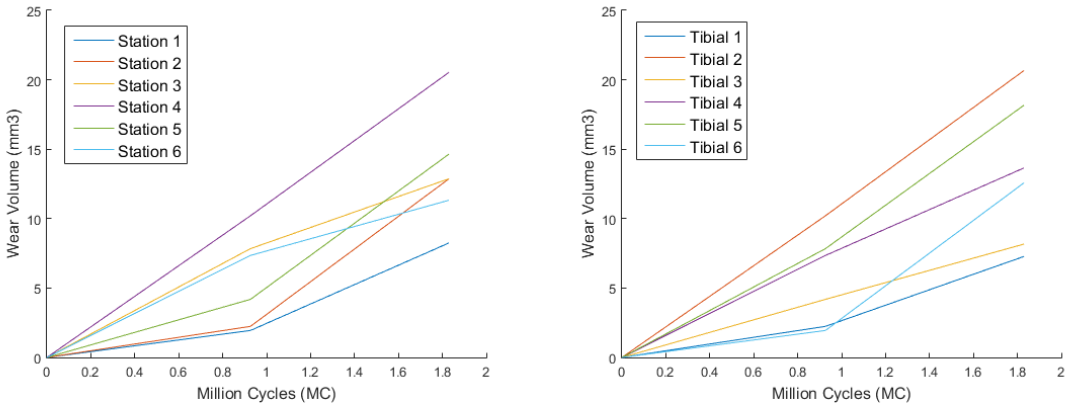

(a) Station Wear Volume

(b) Insert Wear Volume

Figure 7.22: The wear volume (mm3) for each tibial insert and each station on the simulator over 1MC and 2MC with the rotated alignment and resected ACL & PCL soft tissue condition

7.4.4.2 Kinematic variation during studies

The variation in the kinematics during the mechanical alignment wear studies were detailed in Chapter 6 and are therefore not repeated here. The variation in the varus and rotated wear studies with the stiff knee soft tissue condition were also detailed previously in Chapter 6. This section investigated the variation in kinematics in the remaining wear studies; the rotated and varus alignment conditions under the resected ACL & PCL soft tissue condition.

With the varus components there was no significant difference in the AP range of motion during the study ($p=0.84$). However the TR range of motion was significantly higher at 1MC with a value of 10.0° compared to a value of 8.1° at 2MC ($p<0.01$). The AA range of motion was found to be significantly higher at 0MC compared to 1MC with values of 1.2° and 1.0° respectively ($p<0.01$). However this difference in the AA range of motion was small.

Under the rotational mismatch alignment condition there was a significantly different AP range of motion at 0MC, 1MC and 2MC with values of 8.4mm, 7.6mm and 7.1mm respectively ($p<0.01$). At 0MC the TR range of motion was significantly higher with a value of 11.7° compared to 8.4° and 9.1° at 1MC and 2MC respectively ($p<0.01$). The AA range of motion was also significantly higher at 1MC than 0MC however the difference in values was only 0.3° ($p=0.04$).

7.4.4.3 Station variation during studies

With the varus alignment and resected ACL & PCL soft tissue condition there was variation in the kinematics between the 6 stations of the simulator. Stations 2, 4 and 5 resulted in significantly higher AP ranges of motion with values between 6.8mm and 7.0mm compared to

values ranging from 5.7mm to 6.5mm on the other three stations ($p<0.01$). All of the stations resulted in significantly different TR ranges of motion, but stations 2, 4 and 5 resulted in the lowest three values ranging from 5.2° to 8.7° compared to 10.0° to 12.1° on the other stations ($p<0.01$). There was less variation in the AA range of motion but stations 2 and 5 resulted in significantly higher ranges of motion compared to stations 3 and 4 ($p<0.01$).

There was no correlation between the ranges of motion in the AP, TR or AA axes with the wear rate of each station or tibial insert (Figure 7.23).

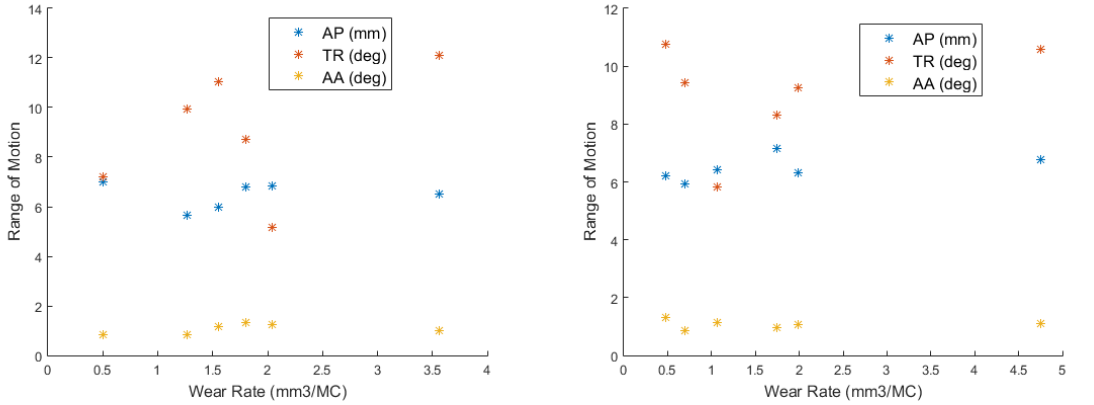

(a) Station Range of Motion vs Wear Rate

(b) Tibial Insert Range of Motion vs Wear Rate

Figure 7.23: The correlation between the wear rate and range of motion under the varus alignment condition and the resected ACL & PCL soft tissue condition for the stations (a) and the tibial inserts (b)

Under the rotational mismatch alignment condition stations 1, 2 and 4 resulted in significantly higher AP ranges of motion with values between 7.8mm and 8.9mm compared to the other three stations with values from 6.8mm to 7.1mm ($p<0.01$). Station 6 resulted in the highest TR range of motion of 14.3°, which was significantly higher than stations 3 - 5 with values between 10.2° and 10.8° and stations 1 and 2 with values of 5.7° and 6.6° respectively ($p<0.01$). There was less variation in the AA range of motion but station 6 had the highest value of 6.9° and station 5 the lowest of 5.6°.

There was no correlation between the ranges of motion in the AP, TR or AA axes with the wear rate of each station or tibial insert (Figure 7.24).

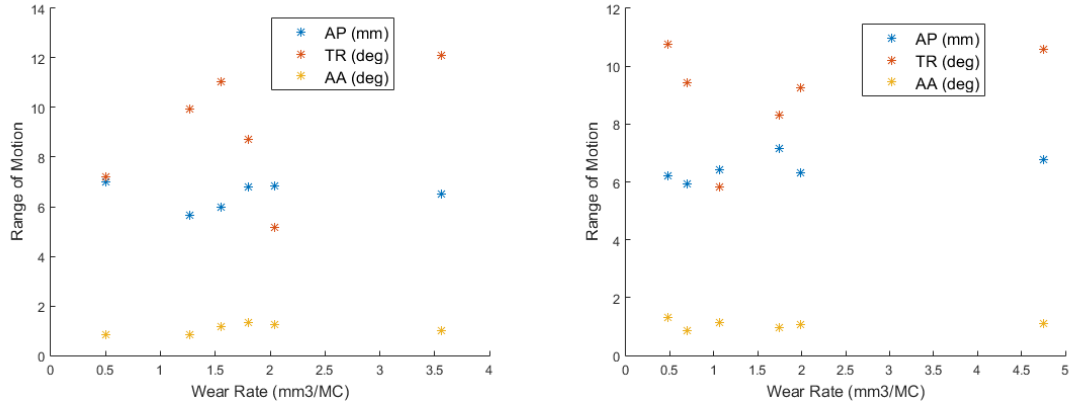

(a) Station Range of Motion vs Wear Rate

(b) Tibial Insert Range of Motion vs Wear Rate

Figure 7.24: The correlation between the wear rate and range of motion under the rotated alignment condition and the resected ACL & PCL soft tissue condition for the stations (a) and the tibial inserts (b)

7.4.4.4 Wear scars

The average wear scars from the varus and rotational mismatch studies under the resected ACL & PCL soft tissue condition were determined (Figures 7.25 and 7.26). As the mechanical alignment study was not carried out on new inserts the wear scar for this study was not able to be analysed.

The same tibial inserts were used for the resected ACL & PCL wear studies as for the stiff knee soft tissue condition wear study with the resected ACL & PCL study being carried out second.

The wear scar areas were determined for the medial and lateral condyles as well as the total area (Table 7.4). The varus alignment did not result in any overlap between the wear scar and the edge of the tibial insert. However with the rotated components there was some overlap on four of the six tibial inserts. This may be the same overlap that was determined after the stiff knee soft tissue wear study.

Table 7.4: Wear scar areas (mean±95%CI, n=6) after the resected ACL & PCL studies

Alignment	Lateral Area (mm^2)	Medial Area (mm^2)	Total Area (mm^2)
Rotational Mismatch	415.4±19	490.8±13	906.2±25
Varus	342.5±26	425.8±17	768.3±32

Both the rotated and varus wear scars resulted in significantly larger medial wear scar areas than lateral ($p<0.01$). The rotated alignment resulted in significantly larger lateral, medial and total wear scar areas than the varus alignment ($p<0.01$).

Figure 7.25 shows the average wear scars for the rotated tibial inserts after each wear study. The same tibial inserts were used for both studies, therefore the wear scar after the resected ACL & PCL soft tissue study was the wear scar after 2MC with the stiff knee soft tissue condition and 2MC with the resected ACL & PCL soft tissue condition. After the

resected ACL & PCL soft tissue study the lateral wear scar resulted in a similar shape as before but with more posterior wear. The medial wear scar resulted in much more anterior wear than after the stiff knee wear study. This resulted in the medial and lateral wear scars being more central in the tibial insert and being more similar to each other in terms of size and shape. After the resected ACL & PCL wear study the medial, lateral and total wear scar areas were significantly higher than after the stiff knee soft tissue study ($p<0.01$).

Figure 7.26 shows the average wear scars for the varus tibial inserts after each wear study.

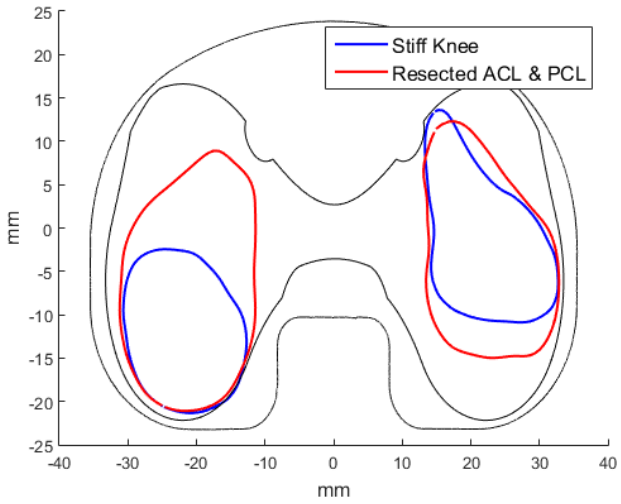

Figure 7.25: The average wear scar for the rotated tibial components after 2MC with the "stiff knee" soft tissue condition and after 2MC with the resected ACL & PCL soft tissue condition, the same tibial components were used for each study

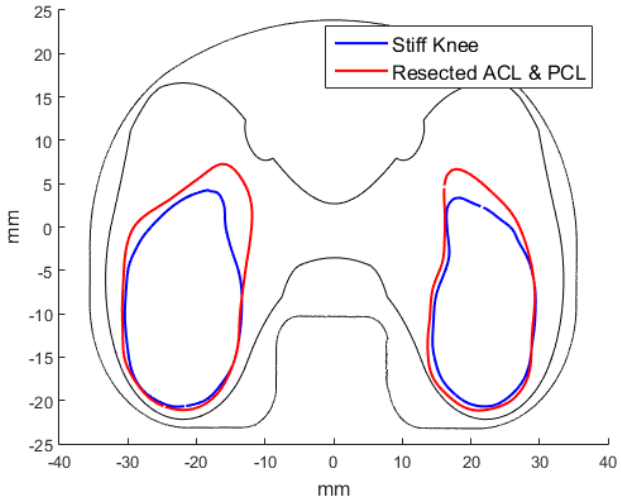

Figure 7.26: The average wear scar for the varus tibial components after 2MC with the "stiff knee" soft tissue condition and after 2MC with the resected ACL & PCL soft tissue condition, the same tibial components were used for each study

As with the rotated components the same tibial inserts were used for both studies, therefore the wear scar after the resected ACL & PCL soft tissue study was the wear scar after both wear studies. After the resected ACL & PCL wear study both the lateral and medial wear scars significantly increased in area (p=0.011). Both particularly increased in size in the anterior direction, however the wear scar shape was similar to that after the stiff knee soft tissue condition wear study.

7.4.4.5 Running Temperature

During each wear study the bulk temperature of the serum in each station was measured in order to determine any differences in running temperature. The values for the wear tests under the resected ACL & PCL soft tissue condition are shown in Table 7.5. For each study the running temperatures across the stations and soak controls were very similar with the station temperatures being within 0.4°c of each other and the soak controls being within 0.5°c of each other.

Table 7.5: Mean running temperature (°c) with the 95% CI across the simulator of the stations and soak controls during each wear study under the resected ACL & PCL soft tissue condition

Study	Station	Soak
Mechanical	29.0±0.4	26.7±0.4
Varus	29.4±0.2	26.8±0.2
Rotated	29.1±0.3	26.3±0.4

During each study the station temperatures were higher than the soak controls by around 3°c, this was due to the friction and heat generated in each of the stations.

7.4.4.6 Surface roughness

The surface roughness of the femoral and tibial contact surfaces were measured at the start and end of each wear study (Table 7.6).

Table 7.6: Average surface roughness values (Ra) (µm) (mean±95%CI, n=6) for the femoral and tibial contact surfaces at the start and end of each wear study with the resected ACL & PCL soft tissue condition

Alignment Condition	Femoral		Tibial Insert	
	Start	End	Start	End
Mechanical	0.051±0.025	0.053±0.026	0.427±0.168	0.339±0.175
Varus	0.045±0.018	0.050±0.019	0.317±0.114	0.266±0.095
Rotated	0.028±0.010	0.037±0.015	0.227±0.145	0.156±0.067

The surface roughness values of the femoral components were similar at the start and end of each study. There was more variation in the surface roughness of the tibial inserts. The rotated alignment condition had the lowest Ra value at the start and at the end of the studies. The Ra value of the tibial inserts however decreased by a similar amount; during the mechanical alignment study it decreased by 0.09µm, by 0.05µm with the varus alignment condition and

by 0.07µm with the rotated alignment condition. The rotated alignment condition may have resulted in the lowest Ra value for the tibial insert due to the higher wear rate that occurred in the first wear study under the stiff knee soft tissue condition.

7.5 Computational Model Validation

In the previous chapter the varus, rotated, tibial slope and kinematic alignment conditions were validated against the corresponding experimental data under the stiff knee spring condition. The mechanical alignment condition was validated under all the soft tissue conditions in Chapter 5.

The tibial slope alignment condition was too unstable to be able to be studied experimentally under the resected ACL and resected ACL & PCL soft tissue conditions, therefore no further validation can be carried out. In this section the varus, rotated and kinematic alignment conditions will be validated under the resected ACL and resected ACL & PCL soft tissue conditions.

7.5.1 Varus Alignment Condition

The computational result for the AP displacement under the resected ACL and resected ACL & PCL soft tissue conditions resulted in similar profile shapes to those determined experimentally (Figure 7.27 (a)).

The computational model however resulted in lower AP displacements in the first half of the gait cycle and resulted in lower peak AP displacements. However as with the experimental results there was no difference in the computational AP displacement under the resected ACL and resected ACL & PCL soft tissue conditions for the first 50% gait, the resected ACL & PCL soft tissue condition then resulted in a higher peak displacement value.

The computational TR rotation profiles were again similar in shape to the experimental results (Figure 7.27 (b)). However the TR rotation was lower from 30% - 50% gait and resulted in a slightly later peak TR rotation with the computational methods compared to the experimental results.

As before the greatest difference in kinematics occurred with the AA rotation profiles (Figure 7.27 (c)).

The correlation in the AP, TR and AA displacements between the computational and experimental methods were determined for both soft tissue conditions (Figure 7.28 (a)).

For both spring conditions there was a good correlation in the AP displacement and TR rotation with R-squared values above 0.76 and gradients from 0.7 and above (Figure 7.28 (b)). There was a much weaker correlation in the AA rotation between methods, as found previously with the stiff knee soft tissue condition, with r-squared values of 0.18 and 0.08 (Figure 7.28 (c)).

Under both the resected ACL and resected ACL & PCL soft tissue conditions the computational and experimental contact positions were similar under the varus alignment condition

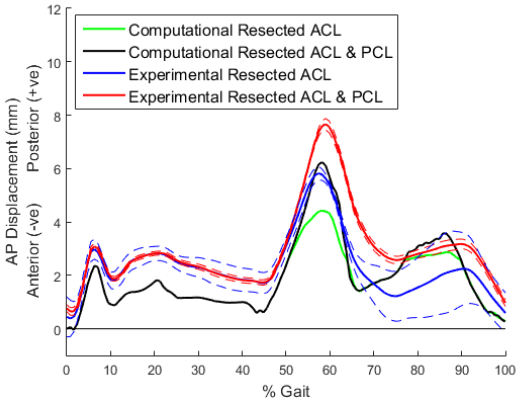

(a) AP Displacement

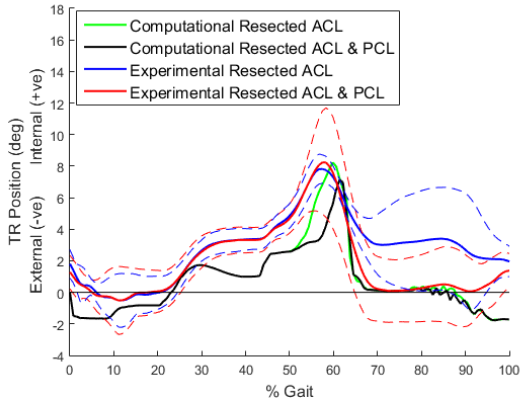

(b) TR Rotation

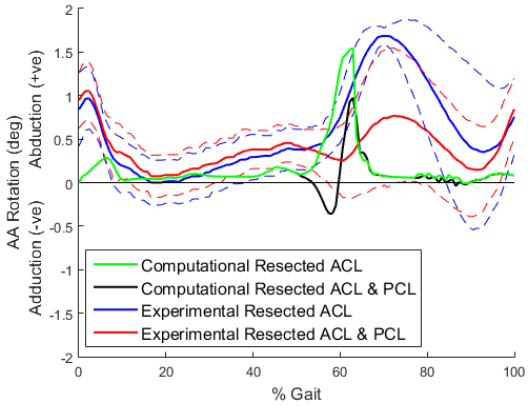

(c) AA Rotation

Figure 7.27: The AP (a), TR (b) and AA (c) displacements under the varus alignment condition and resected ACL and resected ACL & PCL soft tissue conditions using the experimental methods (mean with 95% CI shown with dotted lines) and using the computational model

(Figures 7.29 and 7.30). As before there were some differences in the loading of the medial and lateral compartments due to the differences in the AA rotation between the methods.

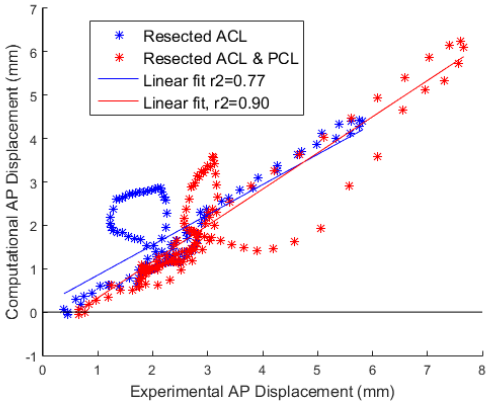

(a) AP Displacement gradient = 0.70 and 0.83

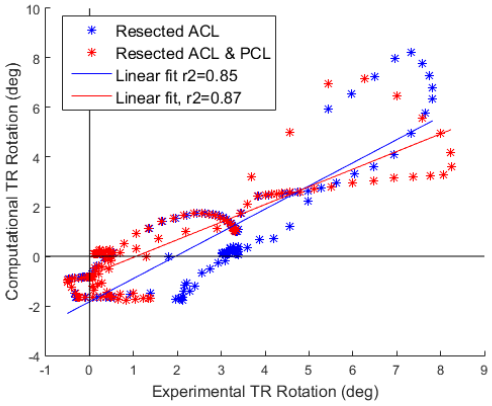

(b) TR Rotation gradient = 0.93 and 0.71

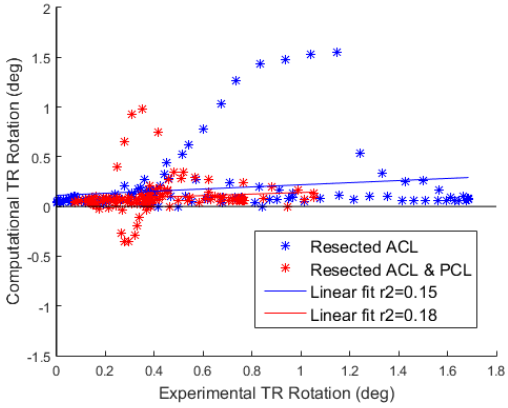

(c) AA Rotation gradient = 0.11 and 0.08

Figure 7.28: Correlation between the computational and experimental output kinematics for the varus alignment condition under the resected ACL and resected ACL & PCL soft tissue conditions

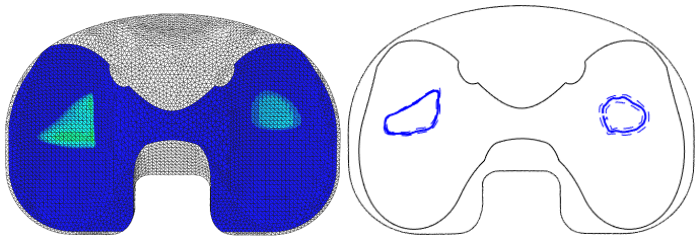

(a) Point 1

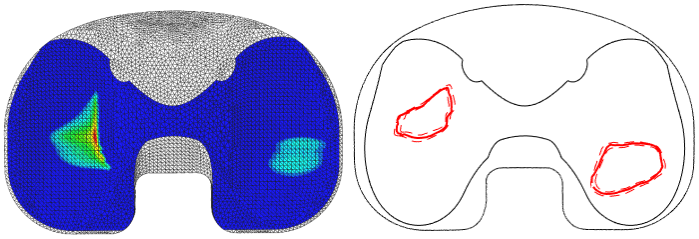

(b) Point 2

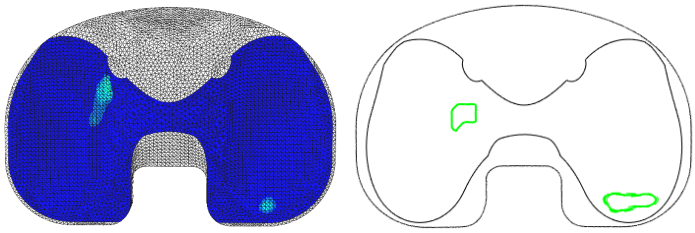

(c) Point 3

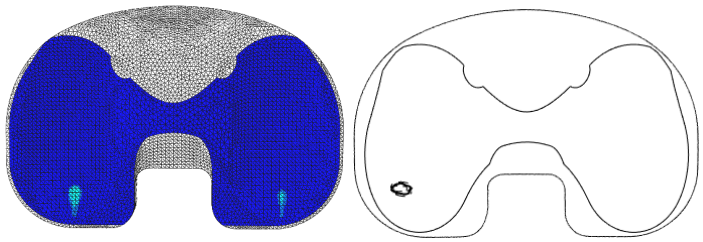

(d) Point 4

Figure 7.29: Contact area under the varus alignment condition and the resected ACL soft tissue condition at each point in the cycle using the computational (left with a red value showing 40MPa) and experimental methods (right)

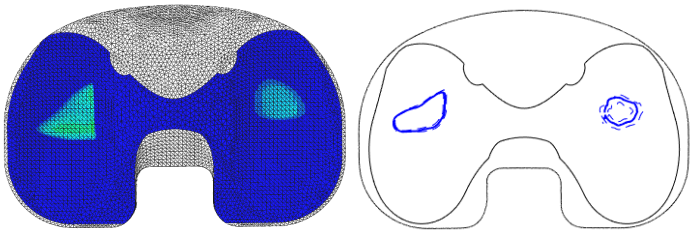

(a) Point 1

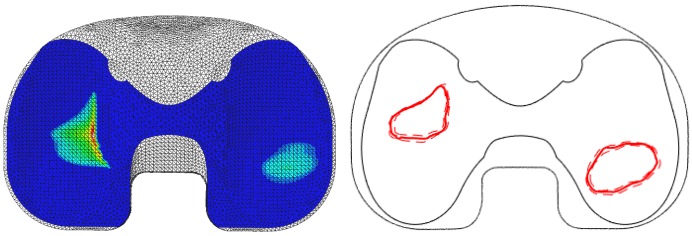

(b) Point 2

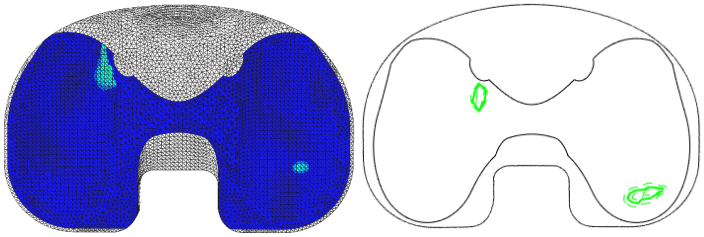

(c) Point 3

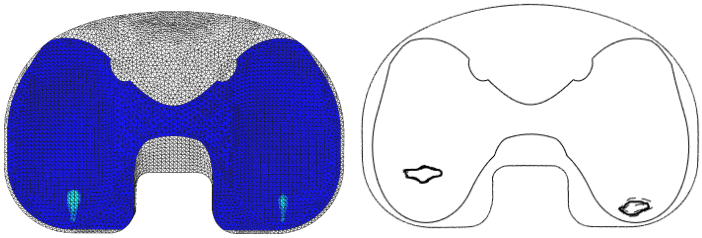

(d) Point 4

Figure 7.30: Contact area under the varus alignment condition and the resected ACL & PCL soft tissue condition at each point in the cycle using the computational (left, 0MPa blue, 40MPa red) and experimental methods (right)

The contact area at four points in the gait cycle was determined using both the experimental and computational methods (Table 7.7). Under both the resected ACL and resected ACL & PCL soft tissue conditions the computational contact area was higher than the experimental result. However there was a similar trend in the contact areas between the two methods, with the contact area at points 1 and 2 being much higher than those at points 3 and 4 and with the highest contact area occurring at point 2 in the cycle.

Table 7.7: The contact area (mm^2) at each point in the cycle under the varus alignment condition and stiff knee soft tissue condition using the computational and experimental (mean±95%CI) methods

Point	Resected ACL		Resected ACL & PCL	
	Experimental	Computational	Experimental	Computational
1	116.6±7.1	190.4	115.7±7.9	190.4
2	189.9±10.1	200.6	193.6±4.1	200.6
3	32.4±7.6	61.8	13.7±9.3	36.3
4	11.0±8.3	23.4	21.2±6.1	25.5

7.5.2 Rotated Alignment Condition

For the first half of the gait cycle the AP displacement profiles for the rotated alignment condition under both the resected ACL and resected ACL & PCL soft tissue conditions resulted in similar displacement values using the experimental and computational methods (Figure 7.31 (a)).

The computational methods resulted in lower peak AP displacements under both soft tissue conditions and resulted in a minima in the AP displacement at around 70% gait. This minima did not occur under the experimental methods which may be due to differences in the loading pattern due to the different AA rotations at this point. It may also be due to the internal friction within the simulator reducing the AP displacement.

The TR rotation was similar between both the experimental and computational methods for both of the soft tissue conditions (Figure 7.31 (b)). However the computational methods did result in a peak TR rotation before 5% gait, which did not occur using the experimental methods, and resulted in lower peak TR displacements.

The computational and experimental methods resulted in similar AA rotation profile shapes however the computational methods resulted in higher AA rotation values throughout the cycle (Figure 7.31 (c)). This increase in the AA rotation may be due to the lack of mass and internal friction in the computational model, as discussed previously. This may also have resulted in the minima in the AP displacement with the computational model, due to the increased AA rotation at this point in the cycle.

Due to the minima in the AP displacement in the second half of the cycle with the computational model that did not occur under the experimental methods there was poor correlation between the computational and experimental AP displacement values with r-squared values below 0.31 (Figure 7.32 (a)).

However there was good correlation with both the TR and AA rotations between the two methods with r-sqaured values above 0.8 (Figure 7.32 (b)). The gradient of the linear fit of the AA rotation was 2.1 and 2.2 for the resected ACL and resected ACL & PCL soft tissue conditions respectively (Figure 7.32 (c)). This shows the difference in amplitude between the two methods.

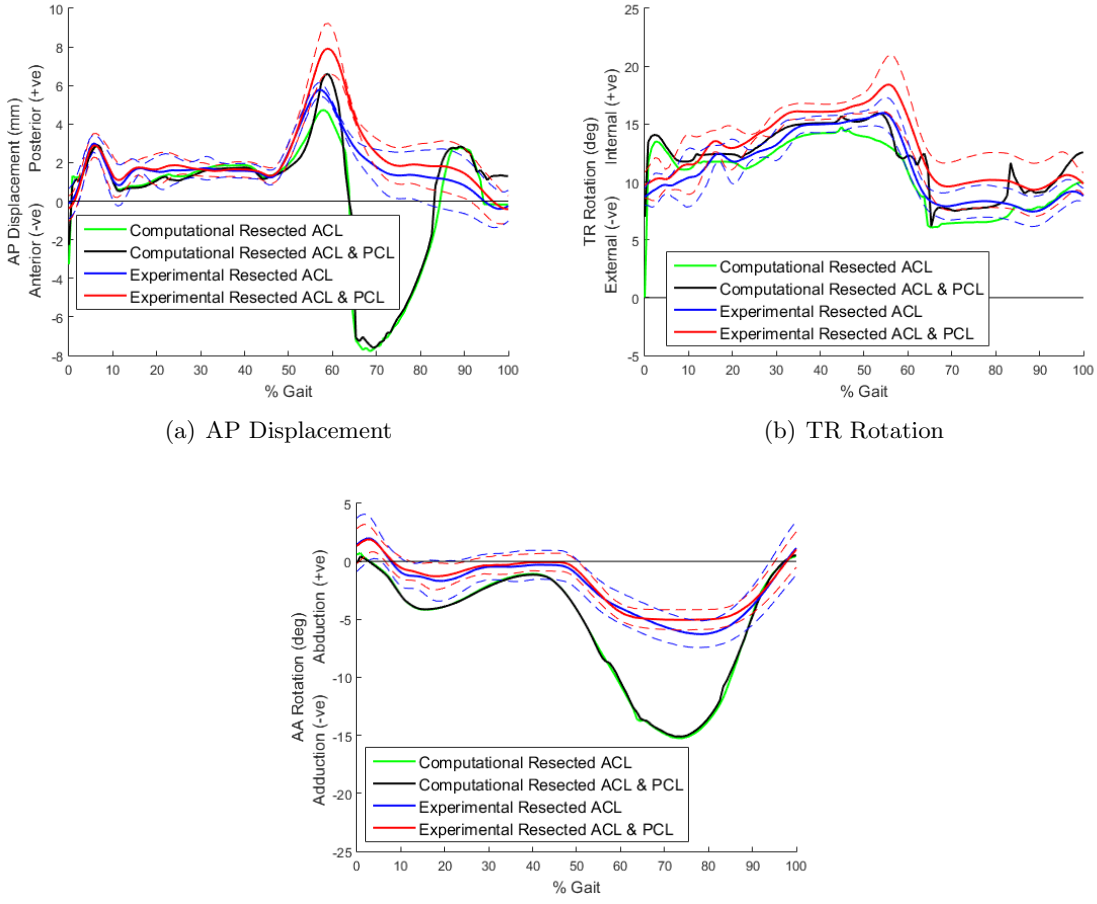

(a) AP Displacement

(b) TR Rotation

(c) AA Rotation

Figure 7.31: The AP (a), TR (b) and AA (c) displacements under the rotated alignment condition and resected ACL and resected ACL & PCL soft tissue conditions using the experimental methods (mean with 95% CI shown with dotted lines) and using the computational model

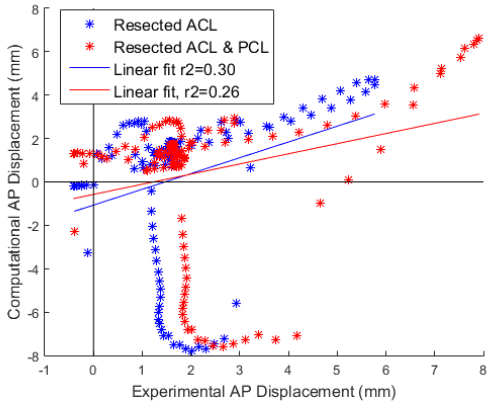

(a) AP Displacement gradient = 0.73 and 0.47

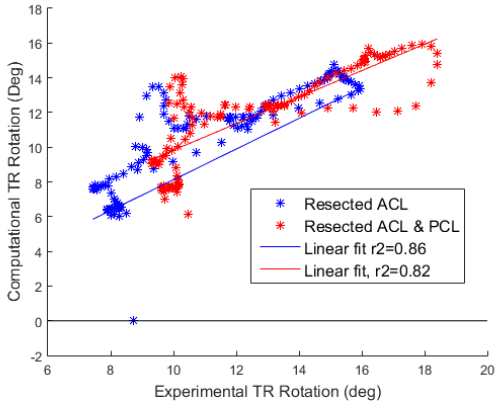

(b) TR Rotation gradient = 0.88 and 0.76

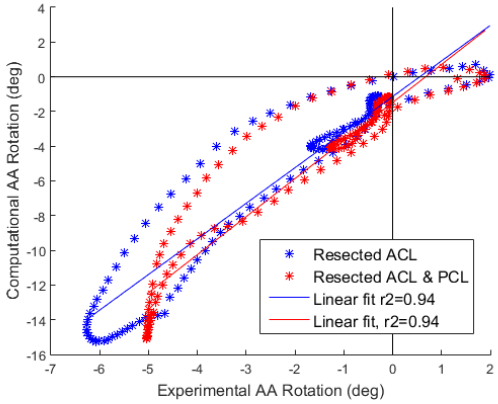

(c) AA Rotation gradient = 2.05 and 2.19

Figure 7.32: Correlation between the computational and experimental output kinematics for the rotated alignment condition under the resected ACL and resected ACL & PCL soft tissue conditions

Under both the resected ACL and resected ACL & PCL soft tissue conditions the computational and experimental contact positions were similar under the rotated alignment condition (Figures 7.33 and 7.34). As before there were some differences in the loading of the medial and lateral compartments due to the differences in the AA rotation between the methods and due to differences in the AP displacement between methods.

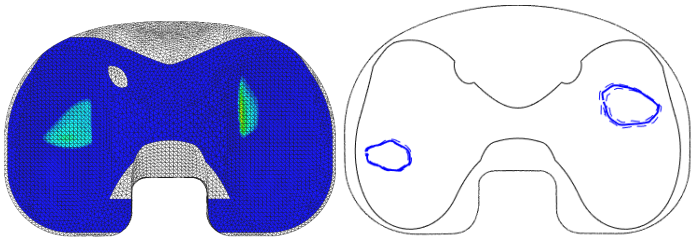

(a) Point 1

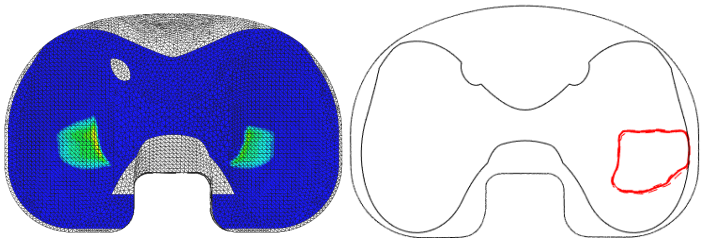

(b) Point 2

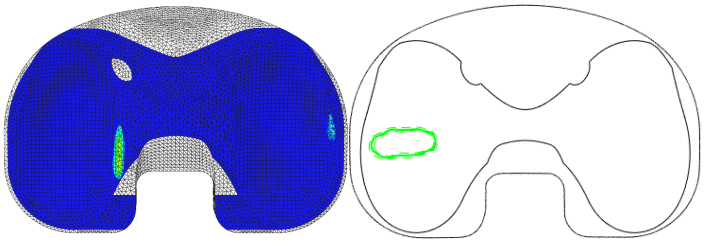

(c) Point 3

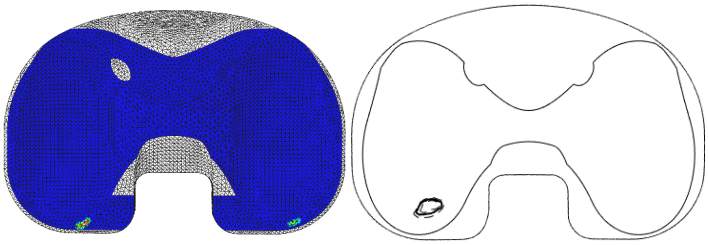

(d) Point 4

Figure 7.33: Contact area under the rotated alignment condition and the resected ACL soft tissue condition at each point in the cycle using the computational (left with a red value showing 45MPa) and experimental methods (right)

The experimental and computational methods resulted in a similar trend in the contact area throughout the cycle for both the resected ACL and resected ACL & PCL soft tissue conditions (Table 7.8). Again the computational model resulted in higher contact area values than the experimental methods however with both methods the highest contact area occurred at point 2 in the cycle and the lowest at point 4.

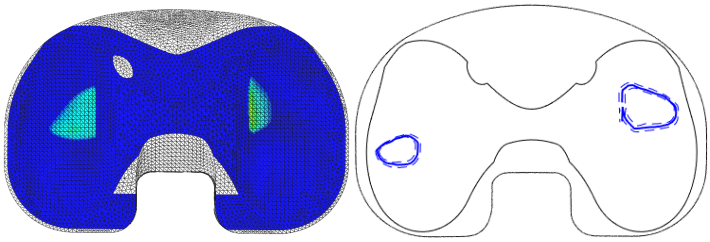

(a) Point 1

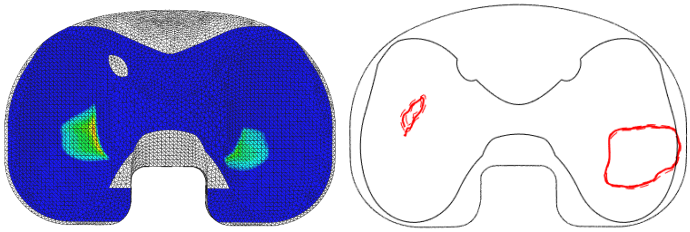

(b) Point 2

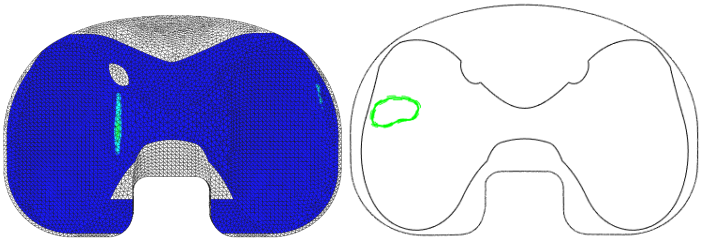

(c) Point 3

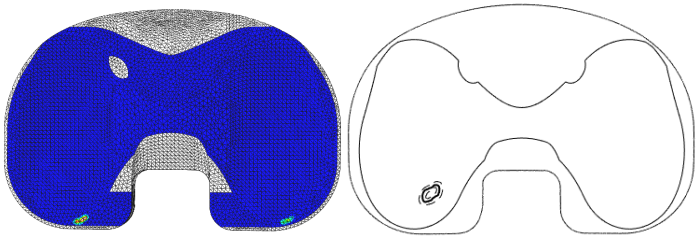

(d) Point 4

Figure 7.34: Contact area under the rotated alignment condition and the resected ACL & PCL soft tissue condition at each point in the cycle using the computational (left, 0MPa blue, 45MPa red) and experimental methods (right)

Table 7.8: The contact area (mm^2) at each point in the cycle under the rotated alignment condition and stiff knee soft tissue condition using the computational and experimental (mean±95%CI) methods

Point	Resected ACL		Resected ACL & PCL	
	Experimental	Computational	Experimental	Computational
1	112.6±7.7	136.2	112.4±5.9	137.4
2	157.4±17.9	160.2	172.8±5.9	159.4
3	59.6±6.2	52.8	33.1±23.1	23.3
4	16.1±3.3	5.0	14.0±3.8	4.8

7.5.3 Kinematic Alignment Condition

The AP displacement and TR rotation profiles were similar under both the experimental and computational methods for the resected ACL and resected ACL & PCL soft tissue conditions (Figure 7.35 (a) and (b)).

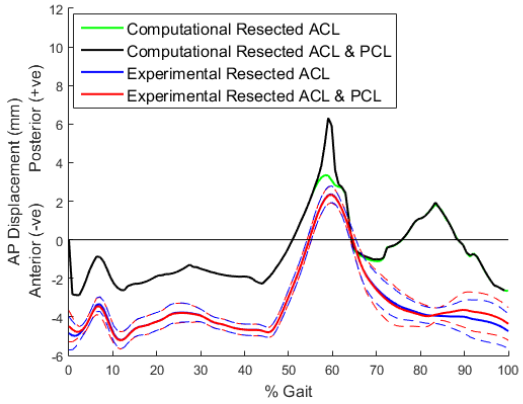

(a) AP Displacement

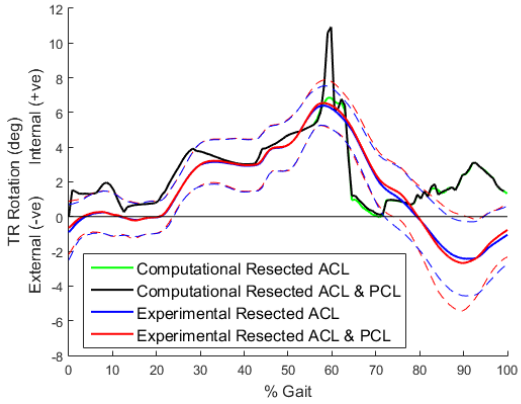

(b) TR Rotation

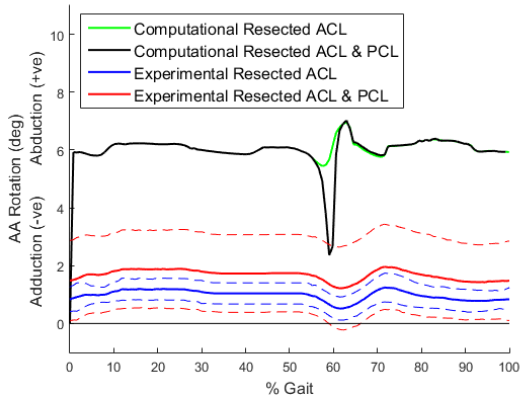

(c) AA Rotation

Figure 7.35: The AP (a), TR (b) and AA (c) displacements under the kinematic alignment condition and resected ACL and resected ACL & PCL soft tissue conditions using the experimental methods (mean with 95% CI shown with dotted lines) and using the computational model

However the computational results under the resected ACL & PCL soft tissue conditions resulted in a spike in both the AP displacement and TR rotation at around 60% gait. At this point in the cycle the tibiofemoral contact was on the medial, anterior edge of the tibial insert resulting in a spike in the AA rotation (Figure 7.35 (c)).

This spike in AA rotation may have resulted in the sudden change in the AP displacement and TR rotations. As before there was also an offset in the AA rotation between the experimental and computational methods of around 6°, this may be due to the weight of the AA arm in the experimental simulator which was not included in the computational model.

There was good correlation in the AP displacement between the two methods with r-

squared values greater than 0.78 and gradients of 0.68 and 0.81 for the resected ACL and resected ACL & PCL respectively (Figure 7.36 (a)).

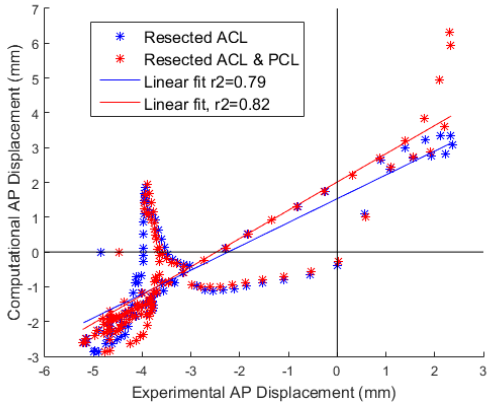

(a) AP Displacement gradient = 0.68 and 0.81

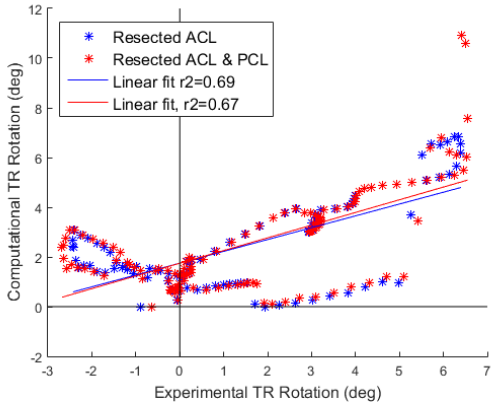

(b) TR Rotation gradient = 0.48 and 0.51

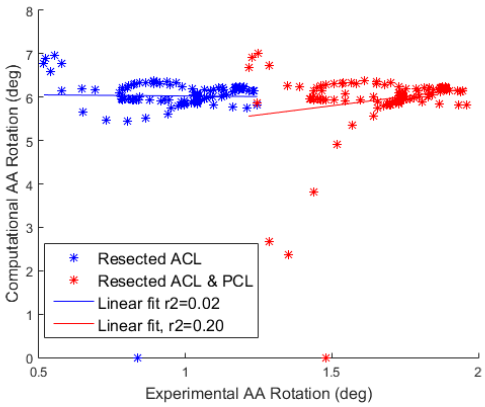

(c) AA Rotation gradient = -0.05 and 0.85

Figure 7.36: Correlation between the computational and experimental output kinematics for the kinematic alignment condition under the resected ACL and resected ACL & PCL soft tissue conditions

The correlation in the TR rotation was less strong with r-squared values of 0.69 and 0.67 (Figure 7.36 (b)). The weaker correlation may be due to the greater differences in profile shape between the two methods for example from 60% to 70% gait. However for most of the cycle the computational results were within the 95% CI of the experimental data.

There was a very weak correlation in the AA rotation between the two methods, which as before may be due to the lack of mass and internal friction within the computational model (Figure 7.36 (c)).

Under both the resected ACL and resected ACL & PCL soft tissue conditions the computational and experimental contact positions were quite different under the kinematic alignment condition (Figures 7.37 and 7.38).

This may be due to the large differences in loading between the computational and experimental methods due to the mass of the AA arm in the experimental simulator. This

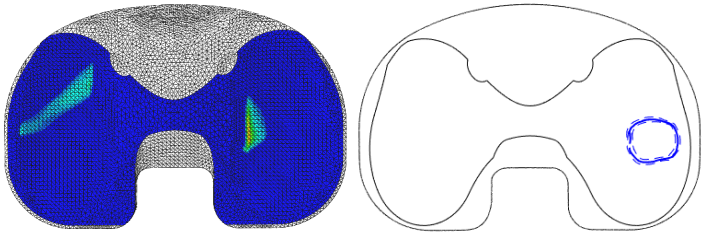

(a) Point 1

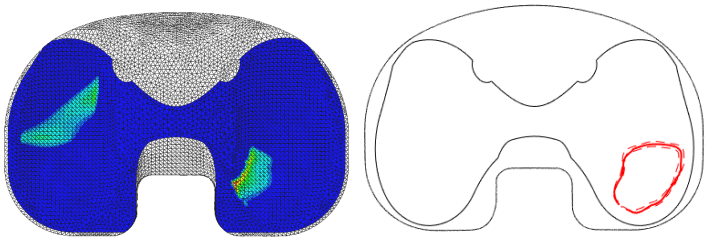

(b) Point 2

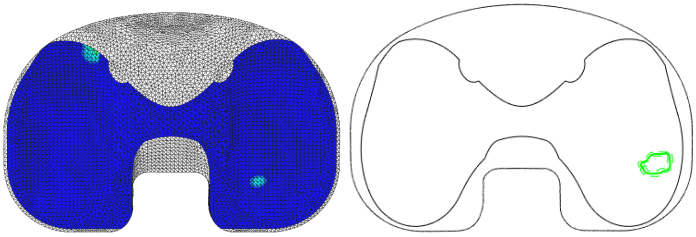

(c) Point 3

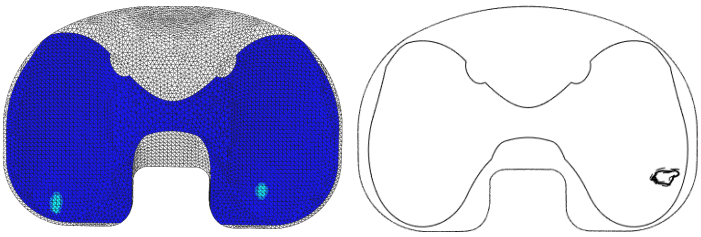

(d) Point 4

Figure 7.37: Contact area under the kinematic alignment condition and the resected ACL soft tissue condition at each point in the cycle using the computational (left with a red value showing 50MPa) and experimental methods (right)

resulted in only lateral contact in the experimental simulation, which is not representative of the conditions in vivo.

As with the other alignment conditions the computational methods resulted in higher contact area values than the experimental methods (Table 7.9). However the values of the contact area follow a similar trend, with the highest contact area occurring at point 2 and the lowest at point 4 in the cycle.

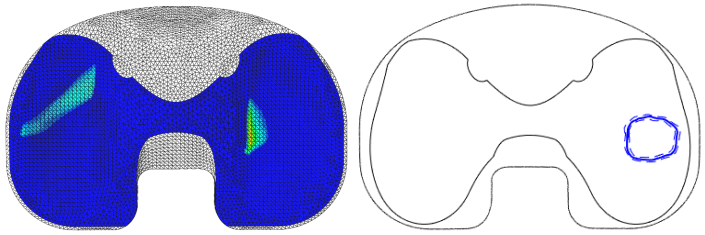

(a) Point 1

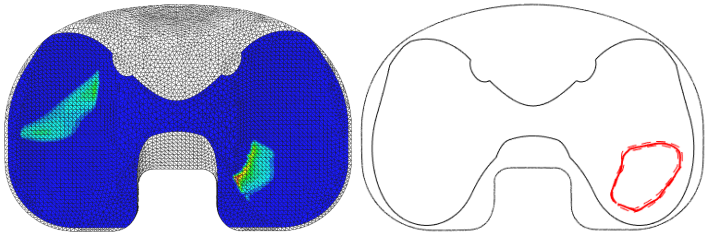

(b) Point 2

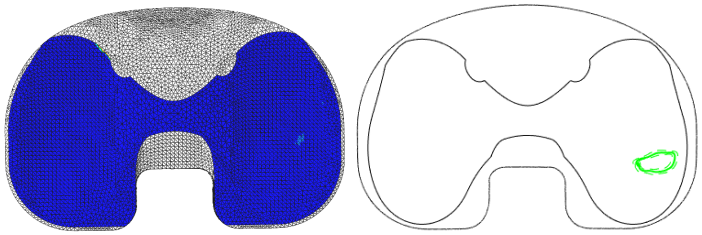

(c) Point 3

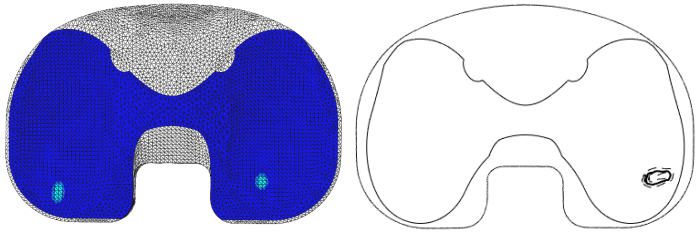

(d) Point 4

Figure 7.38: Contact area under the kinematic alignment condition and the resected ACL & PCL soft tissue condition at each point in the cycle using the computational (left with a red value showing 50MPa) and experimental methods (right)

Table 7.9: The contact area (mm^2) at each point in the cycle under the kinematic alignment condition and stiff knee soft tissue condition using the computational and experimental (mean±95%CI) methods

Point	Resected ACL		Resected ACL & PCL	
	Experimental	Computational	Experimental	Computational
1	78.0±5.9	141.3	80.7±4.0	141.3
2	147.6±10.2	178.9	141.1±9.7	178.9
3	21.0±5.8	28.8	25.0±7.5	20.7
4	12.3±9.7	16.1	16.3±2.3	20.5

7.6 Computational Results

7.6.1 Varus Joint Line Alignment Condition

The varus alignment condition was run using the computational model under all three soft tissue conditions and under 4°, 2° and 0° varus angles.

7.6.1.1 Kinematics

The different soft tissue conditions had a greater effect on the output kinematics than the different varus angles studied (Figures 7.39 - 7.41).

There was a minimal difference in the AP displacement and AA rotation profiles between the varus alignment conditions (Figure 7.39 and 7.40).

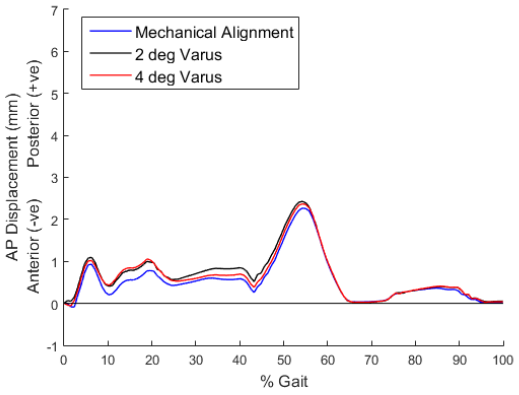

(a) Stiff Knee

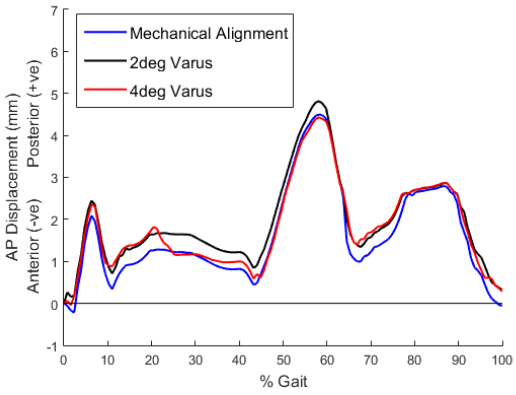

(b) Resected ACL

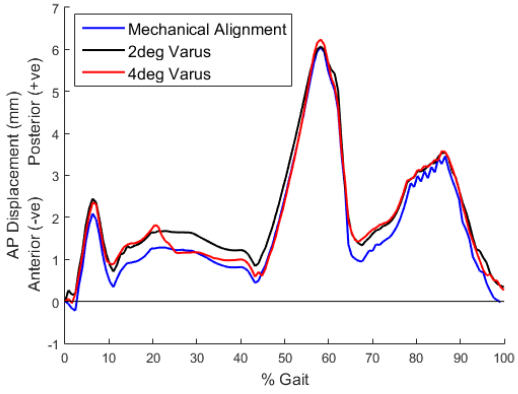

(c) Resected ACL and PCL

Figure 7.39: The AP displacement under 4°, 2° and 0° varus alignment conditions and the stiff knee (a), resected ACL (b) and resected ACL & PCL (c) soft tissue conditions

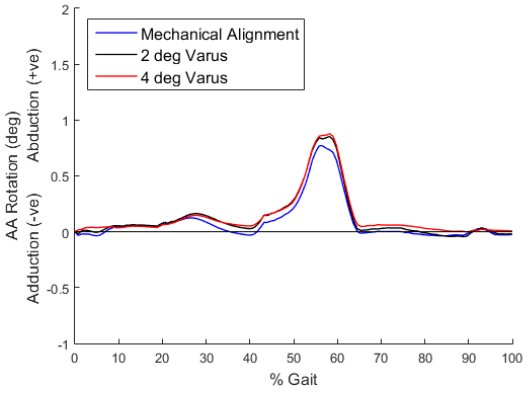

(a) Stiff Knee

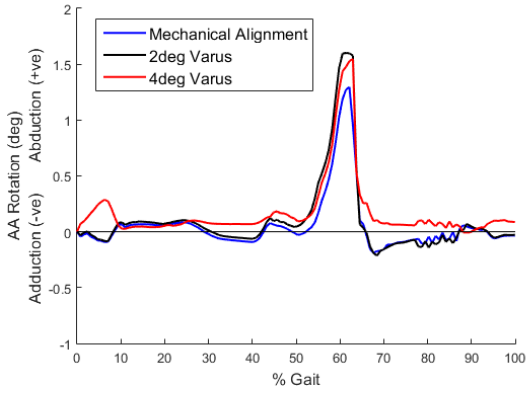

(b) Resected ACL

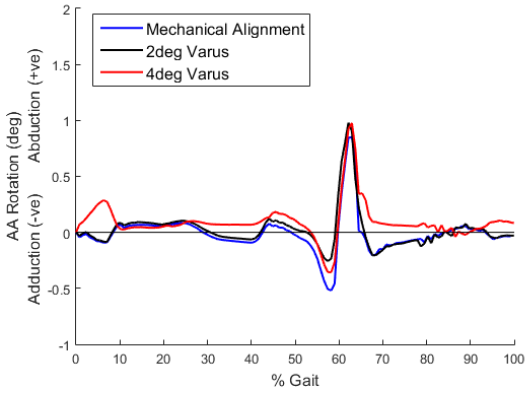

(c) Resected ACL and PCL

Figure 7.40: The AA rotation under 4°, 2° and 0° varus alignment conditions and the stiff knee (a), resected ACL (b) and resected ACL & PCL (c) soft tissue conditions

The 4° varus alignment condition resulted in a lower TR displacement than the 2° and 0° varus alignments between 30% and 50% gait under the stiff knee soft tissue condition (Figure 7.41 (a)). Under the other two soft tissue conditions the 4° varus alignment condition resulted in a lower TR rotation for the first half of the gait cycle (Figure 7.41 (b) and (c)). Otherwise there was a minimal difference in the TR rotation between the varus alignment conditions.

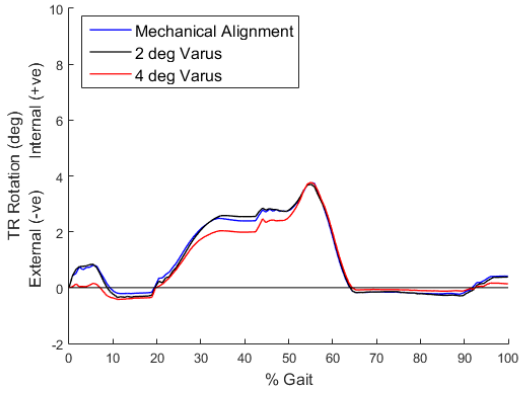

(a) Stiff Knee

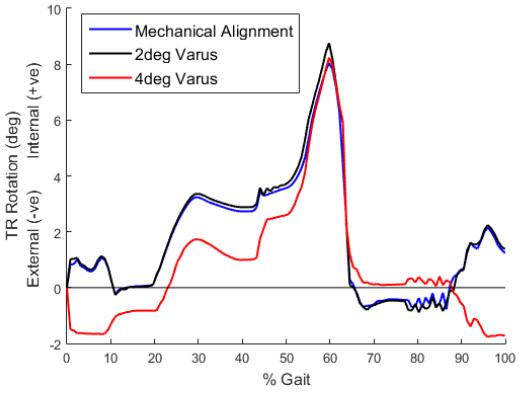

(b) Resected ACL

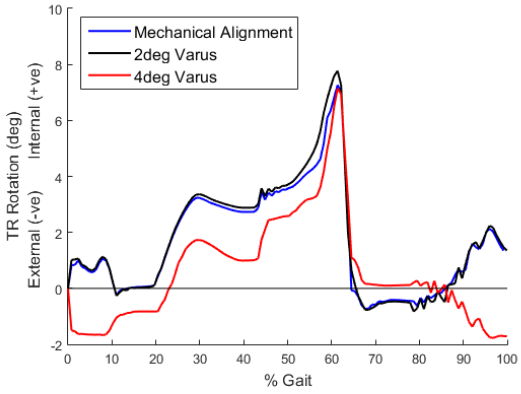

(c) Resected ACL and PCL

Figure 7.41: The TR rotation under 4°, 2° and 0° varus alignment conditions and the stiff knee (a), resected ACL (b) and resected ACL & PCL (c) soft tissue conditions

7.6.1.2 Contact Pressure

The contact pressure was found at the same four points in the gait cycle where the contact area was measured experimentally under the resected ACL and resected ACL & PCL soft tissue conditions (Figures 7.42 and 7.43).

The 4° varus alignment resulted in more medial loading than the 2° and 0° varus alignment conditions under both the resected ACL and resected ACL & PCL soft tissue conditions. This is similar to what was found previously under the stiff knee soft tissue condition.

The contact at point 3 in the cycle was close to the anterior edge of the tibial insert, especially with the mechanical alignment condition, under the resected ACL & PCL soft tissue condition.

The peak contact pressure at each point in the cycle was found under the resected ACL and resected ACL & PCL soft tissue conditions (Tables 7.10 and 7.11). For both of the soft tissue conditions the 4° varus alignment condition resulted in the lowest pressure out of the alignment conditions at point 1 in the cycle, however it also resulted in the highest pressure of the varus alignment conditions at point 2 in the cycle. The 2° and 0° varus alignment

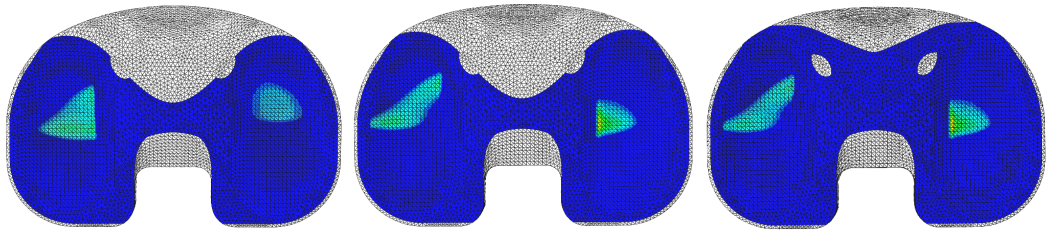

(a) Point 1

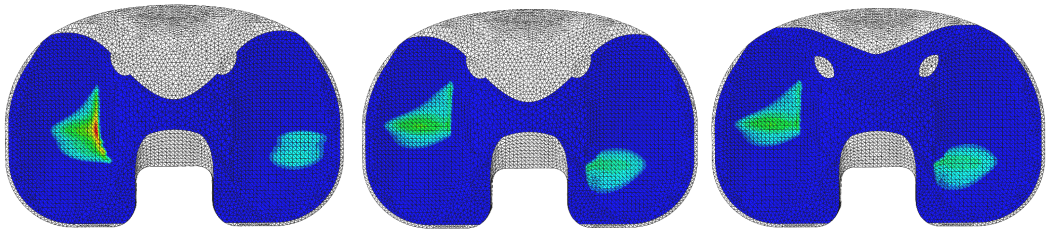

(b) Point 2

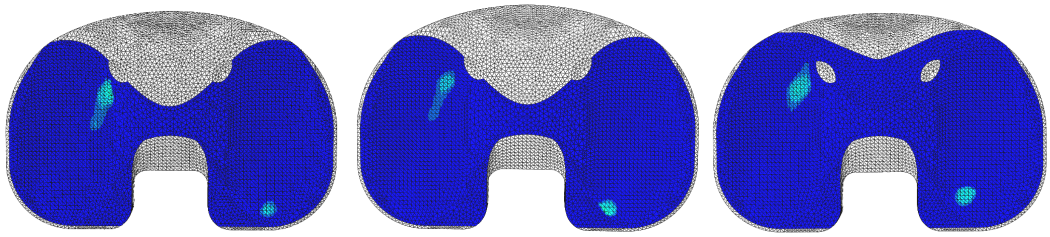

(c) Point 3

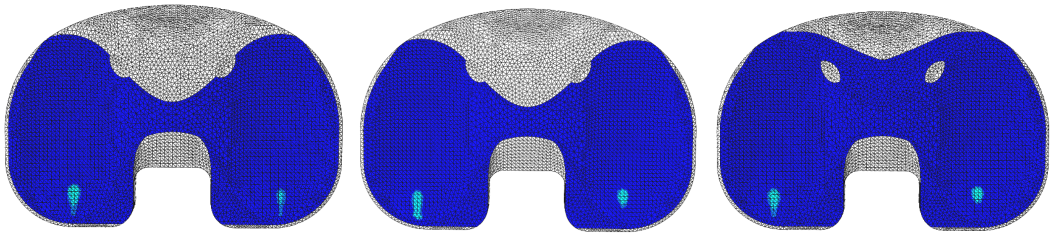

(d) Point 4

Figure 7.42: Computational prediction of the contact pressure under 4° varus (left), 2° varus (centre) and mechanical alignment (right) under the resected ACL soft tissue condition (0MPa blue, 40MPa red)

conditions resulted in the peak pressure occurring at point 1 in the cycle and decreasing during the rest of the gait cycle. However for the 4° varus alignment the pressure increased to its peak at point 2.

This may be due to the position of the peak contact pressure; at point 1 in the cycle for the 2° and 0° varus alignments this occurred on the lateral condyle, therefore the increased medial loading with the 4° varus alignment resulted in a lower overall peak pressure.

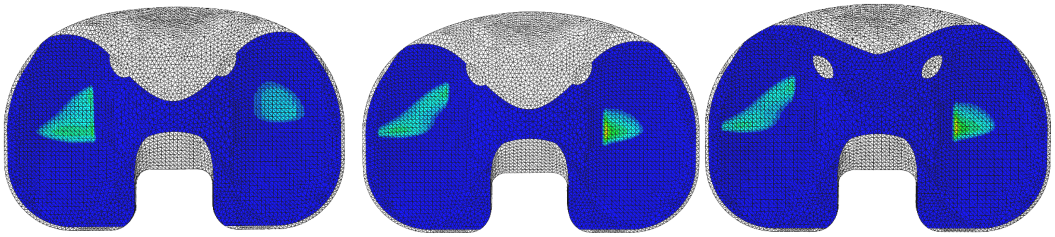

(a) Point 1

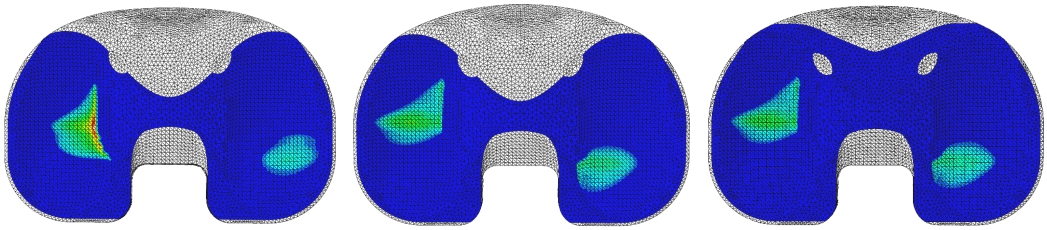

(b) Point 2

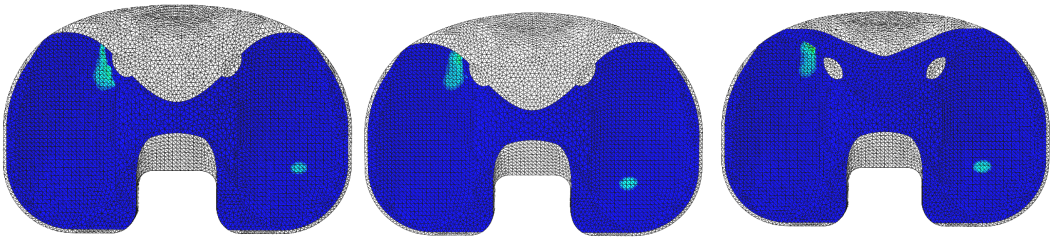

(c) Point 3

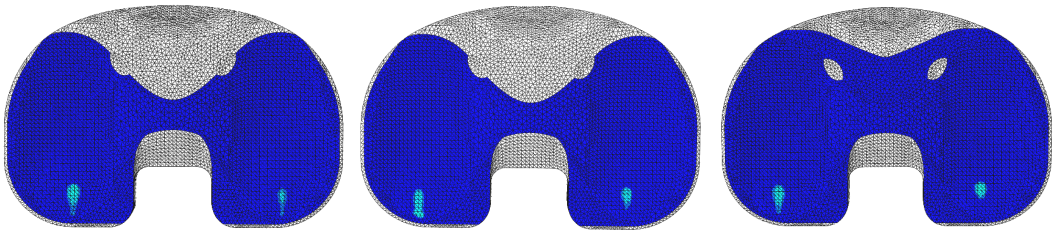

(d) Point 4

Figure 7.43: Computational prediction of the contact pressure under 4° varus (left), 2° varus (centre) and mechanical alignment (right) under the resected ACL & PCL soft tissue condition (0MPa blue, 40MPa red)

Table 7.10: The peak contact pressure (MPa) for the 4°, 2° and 0° varus alignment conditions under the resected ACL soft tissue condition

Point	4°	2°	0°
1	15.3	25.6	27.4
2	34.4	20.1	19.7
3	12.7	12.5	15.6
4	11.2	9.9	12.2

Table 7.11: The peak contact pressure (MPa) for the 4°, 2° and 0° varus alignment conditions under the resected ACL & PCL soft tissue conditions

Point	4°	2°	0°
1	15.4	25.6	27.4
2	37.0	20.1	19.7
3	13.4	15.0	13.0
4	11.1	11.8	12.2

However at point 2 in the cycle the peak contact pressure was on the medial tibial condyle for the 2° and 0° varus alignments, therefore the increased medial loading resulted in a higher peak pressure under the 4° varus alignment condition.

7.6.1.3 Contact Area

The contact area throughout the gait cycle was found for all three varus alignment and soft tissue conditions (Figure 7.44).

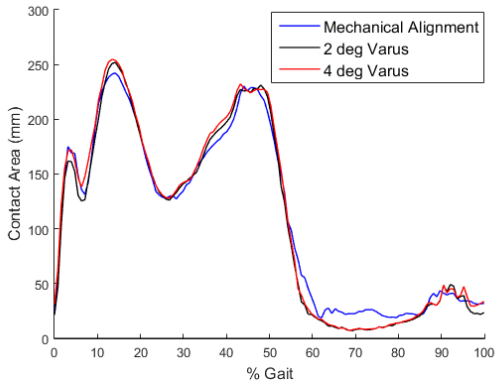

(a) Stiff Knee

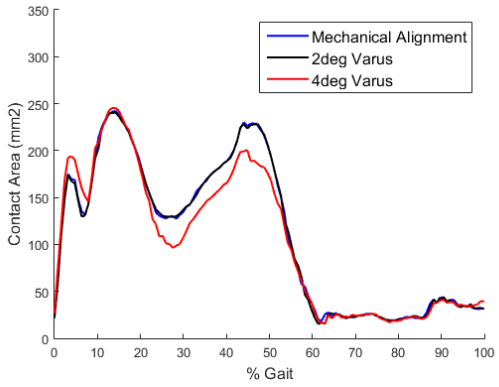

(b) Resected ACL

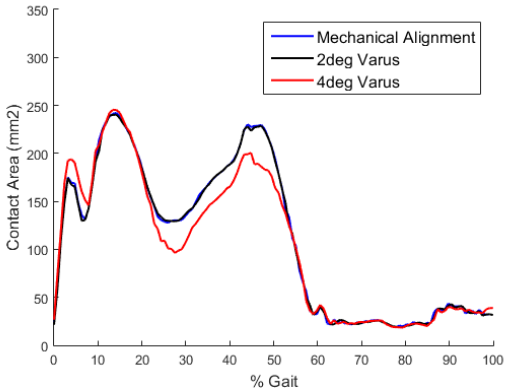

(c) Resected ACL and PCL

Figure 7.44: The contact area (mm^2) under 4°, 2° and 0° varus alignment conditions under the stiff knee (a), resected ACL (b) and resected ACL & PCL (c) soft tissue conditions

The contact area under the 4° varus alignment condition and the resected ACL and resected

ACL & PCL soft tissue conditions had a higher initial peak and was then lower than the others studied between 20% and 50% gait (Figure 7.44 (b) and (c)). Otherwise there was a minimal difference in the contact area between the varus alignment and soft tissue conditions. This difference in contact area may be due to the differences in loading between the varus alignment conditions.

7.6.2 Rotated Alignment Condition

The rotated alignment condition was run using the computational model under all three soft tissue conditions and under 14°, 8°, 4° and 0° rotational mismatch.

7.6.2.1 Kinematics

The soft tissue conditions had a greater effect on the AP displacement than the rotational mismatch alignment conditions (Figure 7.45).

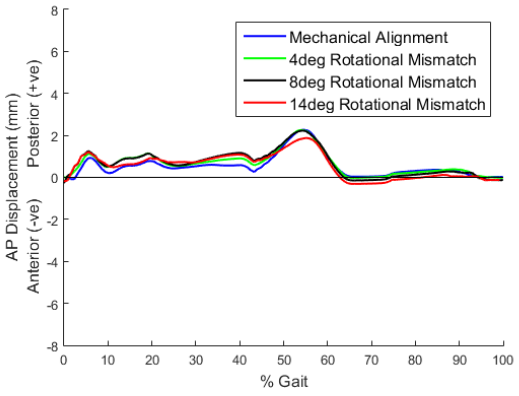

(a) Stiff Knee

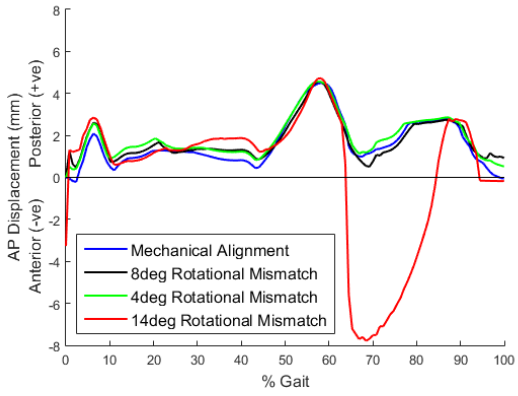

(b) Resected ACL

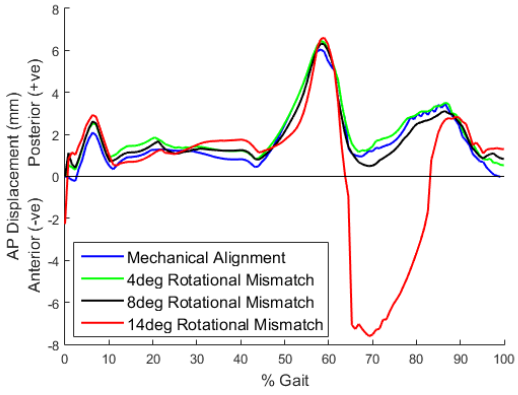

(c) Resected ACL and PCL

Figure 7.45: The AP displacement under 14°, 8°, 4° and 0° rotational mismatch alignment conditions and the stiff knee (a), resected ACL (b) and resected ACL & PCL (c) soft tissue conditions

However under the 14° rotational mismatch alignment condition there was a minima of -7°

at around 70% gait under the resected ACL and resected ACL & PCL soft tissue conditions which did not occur in any of the other displacement profiles (Figure 7.45 (b) and (c)).

This spike in the anterior displacement may be due to the high AA rotation that occurred at this point under the same alignment condition (Figure 7.46).

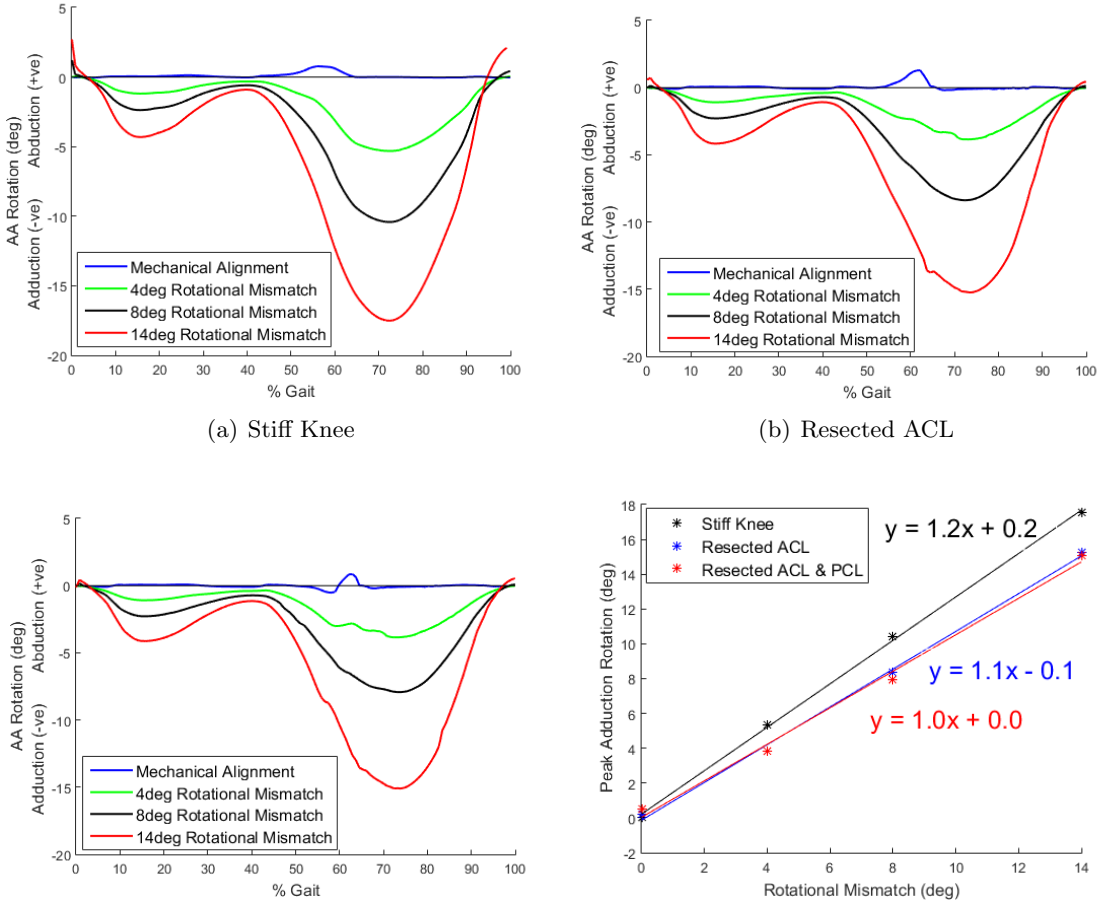

(a) Stiff Knee

(b) Resected ACL

(c) Resected ACL and PCL

(d) Peak Adduction vs Rotational Mismatch

Figure 7.46: The AA rotation under 14°, 8°, 4° and 0° rotational mismatch alignment conditions and the stiff knee (a), resected ACL (b) and resected ACL & PCL (c) soft tissue conditions. The relationship between the peak adduction rotation and the rotational mismatch was found for each soft tissue condition (d)

Under mechanical alignment conditions the AA rotation was low and was mainly abduction. However all the rotational mismatch alignment conditions resulted in more adduction rotation, with peaks at 15% and 70% gait.

The amplitude of this profile increased linearly as the rotational mismatch increased (Figure 7.46 (d)). With the resected ACL and resected ACL & PCL soft tissues conditions the gradient of the linear fit was lower, resulting in a lower increase in the peak adduction as the rotational mismatch increased.

The TR rotation profile had a similar shape under 4° rotational mismatch and under mechanical alignment conditions, with a plateau from 25% to 50% gait followed by a peak

at around 60% gait (Figure 7.47). However the profile shapes under 8° and 14° rotational mismatch did not have this initial plateau or peak.

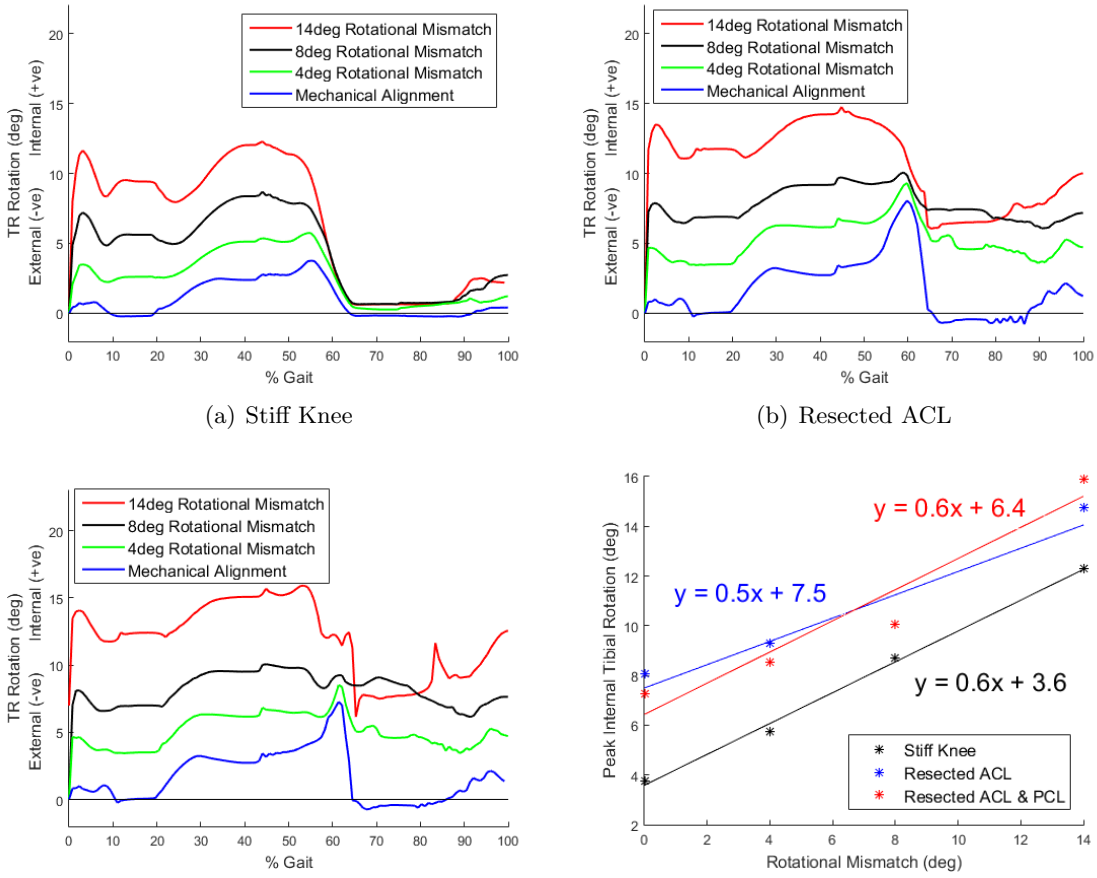

(a) Stiff Knee

(b) Resected ACL

(c) Resected ACL and PCL

(d) Peak TR vs Rotational Mismatch

Figure 7.47: The TR rotation under 14°, 8°, 4° and 0° rotational mismatch alignment conditions and the stiff knee (a), resected ACL (b) and resected ACL & PCL (c) soft tissue conditions. The relationship between the peak internal TR rotation and the rotational mismatch was found for each soft tissue condition (d)

The higher the rotational mismatch the greater the offset between the TR rotation profiles, as the rotational mismatch increased so did the peak TR (Figure 7.47 (d)).

The linear fit of this relationship resulted in a similar gradient for all three soft tissue conditions, however the resected ACL and resected ACL & PCL soft tissue conditions resulted in a higher y-intercept value. This shift in the linear fit replicates the increase in peak TR due to the change in soft tissue condition. This shift may be due to the spring gap of ±6° with these soft tissue conditions.

7.6.2.2 Contact Pressure

The contact pressure was found at the same four points in the gait cycle where the contact area was measured experimentally under the resected ACL and resected ACL & PCL soft

tissue conditions (Figures 7.48 and 7.49).

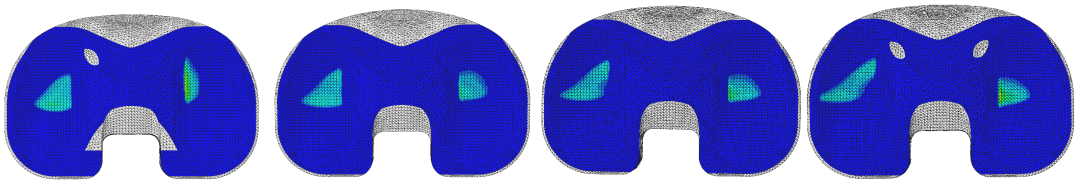

(a) Point 1

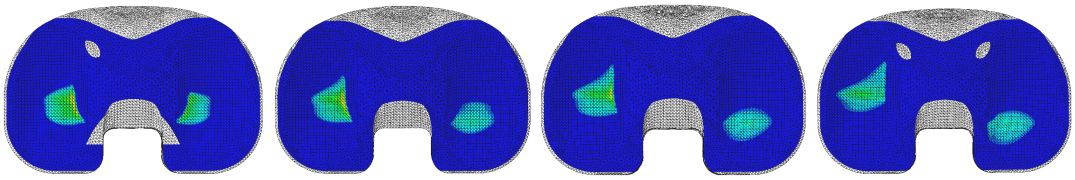

(b) Point 2

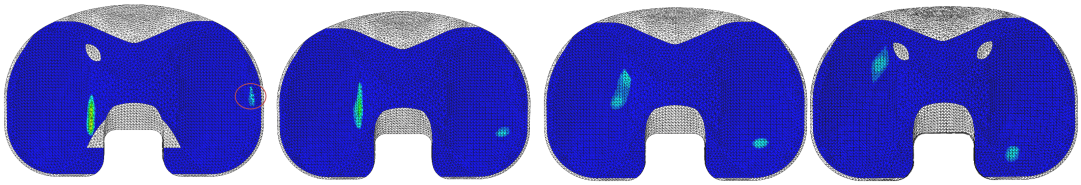

(c) Point 3

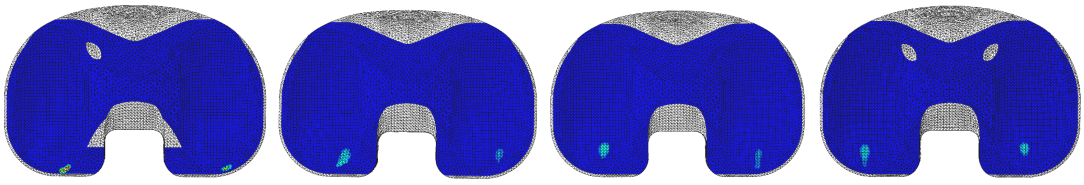

(d) Point 4

Figure 7.48: Computational prediction of the contact pressure under 14°, 8°, 4° and 0° rotational mismatch (from left to right) under the resected ACL soft tissue condition (0MPa blue, 45MPa red)

Under both soft tissue conditions the tibiofemoral contact points were similar across all the rotational mismatch conditions at points 1 and 2 in the cycle. However at point 3 in the cycle the 14° and 8° rotational mismatch alignment conditions resulted in a narrow medial contact close to the centre of the tibial insert. At point 4 in the cycle they also resulted in contact on the posterior edge of the tibial insert.

Under the resected ACL & PCL soft tissue condition the 4° rotational mismatch and mechanical alignment condition resulted in contact on the anterior edge of the tibial insert. While under both soft tissue conditions the 14° rotational mismatch alignment condition resulted in contact on the posterior edge of the tibial insert at the end of the cycle, which may be due to the peak in anterior displacement at this point.

The peak contact pressure at each point in the cycle was found under the resected ACL and resected ACL & PCL soft tissue conditions (Tables 7.12 and 7.13).

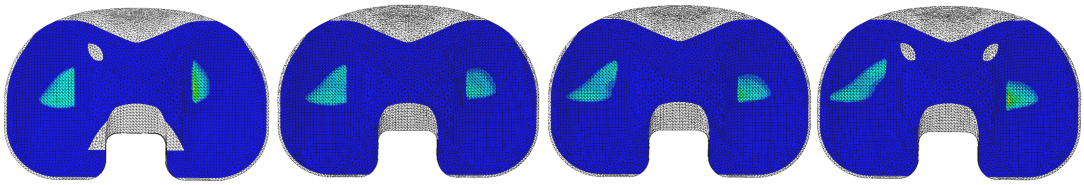

(a) Point 1

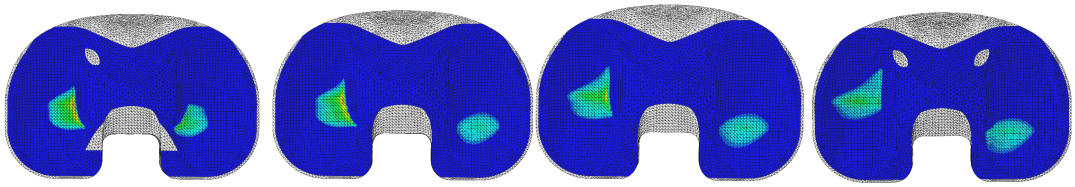

(b) Point 2

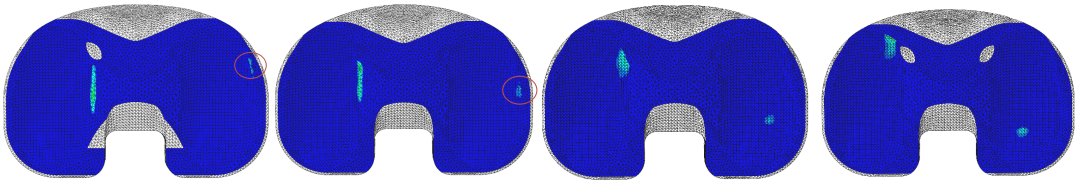

(c) Point 3

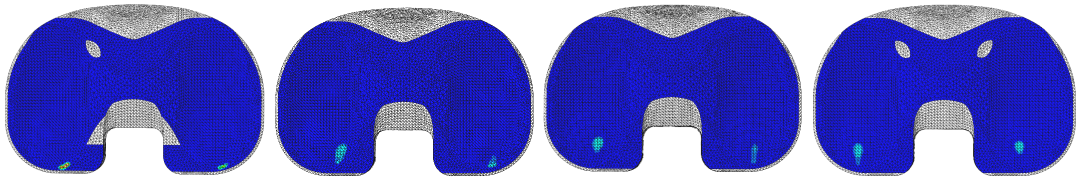

(d) Point 4

Figure 7.49: Computational prediction of the contact pressure under14°, 8°, 4° and 0° rotational mismatch (from left to right) under the resected ACL & PCL soft tissue condition (0MPa blue, 45MPa red)

Table 7.12: The peak contact pressure (MPa) under 14°, 8°, 4° and 0° rotational mismatch alignment conditions under the resected ACL soft tissue condition

Point	14°	8°	4°	0°
1	25.7	16.3	19.4	27.4
2	31.5	32.3	30.2	19.7
3	26.1	21.3	13.8	15.6
4	41.1	13.0	12.5	12.2

Under both soft tissue conditions the 14° rotational mismatch alignment condition resulted in the highest peak contact pressure out of the alignment conditions. This peak contact occurred at point 4 in the cycle and may be due to contact on the posterior edge of the tibial insert. On all the other alignment conditions the contact pressure at this point was low; below 15MPa.

At point 1 in the cycle under both soft tissue conditions the 14° rotational mismatch and

Table 7.13: The peak contact pressure (MPa) under 14°, 8°, 4° and 0° rotational mismatch alignment conditions under the resected ACL & PCL soft tissue conditions

Point	14°	8°	4°	0°
1	26.7	16.2	19.3	27.4
2	34.7	33.8	26.3	19.7
3	17.3	21.1	18.9	13.0
4	39.8	10.2	12.5	12.2

mechanical alignment conditions resulted in similar contact pressures, higher than those found under the 8° and 4° rotational mismatch alignment conditions. This peak pressure occurred on the lateral condyle, close to the centre of the tibial insert and its positioning may be why the contact pressure was higher than the other alignment conditions where the lateral contact was more central with respect to the lateral condyle.

At points 2 and 3 in the cycle under the resected ACL soft tissue condition and at point 2 under the resected ACL & PCL soft tissue condition the contact pressure increased as the rotational mismatch increased. Again this may be due to the position of the contact point.

7.6.2.3 Contact Area

The contact area throughout the gait cycle was found for all rotational mismatch alignment and soft tissue conditions (Figure 7.50).

Under all the soft tissue conditions the 14° rotational mismatch alignment condition resulted in a lower contact area, especially from 30% to 50% gait. The 8° rotational mismatch alignment condition resulted in a slightly lower contact area at this point in the cycle as well, though the difference in contact area was small.

7.6.3 Tibial Slope Alignment Condition

The tibial slope alignment condition was run using the computational model under all three soft tissue conditions and under 10°, 4° and 0° posterior tibial slope.

7.6.3.1 Kinematics

Unlike with the experimental simulation the 10° posterior tibial slope alignment condition could be run under the resected ACL and resected ACL & PCL soft tissue conditions using the computational model, despite being unstable.

The 4° posterior tibial slope alignment condition resulted in similar AP, TR and AA output kinematics as the mechanical alignment condition for the first 60% of the gait cycle (Figures 7.51 - 7.53). However after 60% gait there was a sharp increase in anterior displacement, internal rotation and adduction rotation under the resected ACL and resected ACL & PCL soft tissue conditions.

There was an anterior shift in the AP profile with the 4° tibial slope alignment compared to the mechanical alignment condition (Figure 7.51). However under the 10° posterior tibial

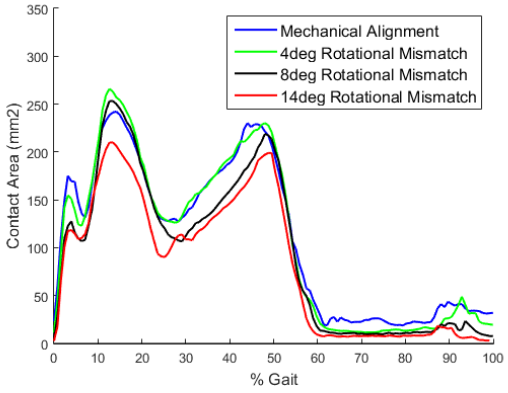

(a) Stiff Knee

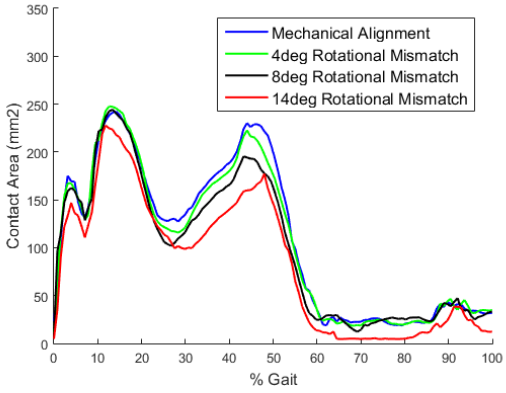

(b) Resected ACL

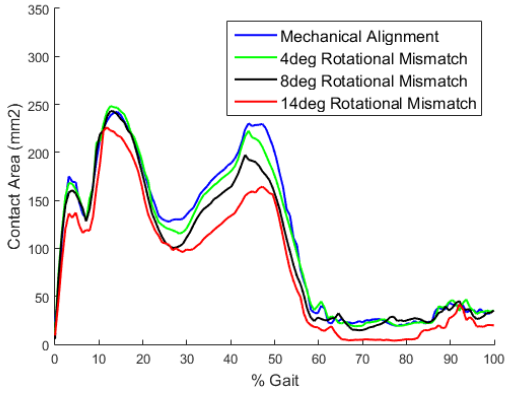

(c) Stiff Knee

Figure 7.50: The contact area (mm^2) under 14°, 8°, 4° and 0° rotational mismatch alignment conditions under the stiff knee (a), resected ACL (b) and resected ACL & PCL (c) soft tissue conditions

slope alignment condition there was a greater shift in the AP displacement profile.

With the 10° tibial slope alignment the AP displacement profiles was shifted around 4mm anteriorly under the resected ACL and resected ACL & PCL soft tissue conditions, under the stiff knee soft tissue condition this shift was lower. Unlike the mechanical and 4° tibial slope alignment conditions there was no increase in the peak AP displacement under the resected ACL & PCL soft tissue condition compared to the resected ACL soft tissue condition under the 10° tibial slope condition. This may be due to the AP spring gap of ±2.5mm and the peak AP displacement of 2.4mm under the 10° tibial slope and resected ACL soft tissue condition.

The 10° posterior tibial slope alignment resulted in a lower peak anterior displacement than the 4° tibial slope alignment condition. This higher anterior displacement at this point in the cycle may be due to the higher posterior displacement at 50% gait under the 4° tibial slope alignment; the increased displacement would have resulted in a higher anterior force from the virtual spring and increased momentum as the anterior displacement increased.

The 10° posterior tibial slope also resulted in a different shape TR rotation profile under

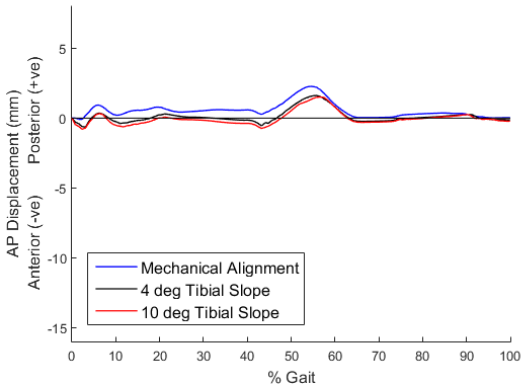

(a) Stiff Knee

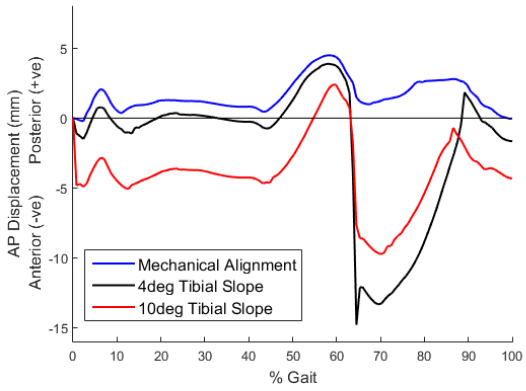

(b) Resected ACL

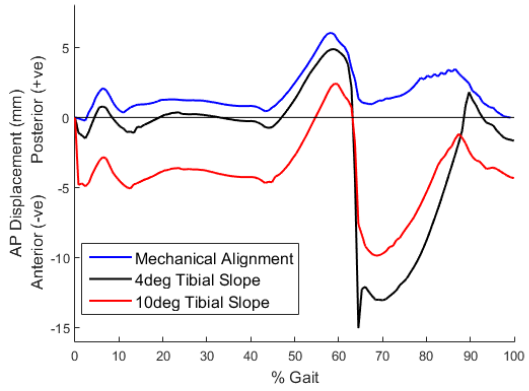

(c) Resected ACL and PCL

Figure 7.51: The AP displacement under 10°, 4° and 0° posterior tibial slope alignment conditions and the stiff knee (a), resected ACL (b) and resected ACL & PCL (c) soft tissue conditions

the resected ACL and resected ACL & PCL soft tissue conditions (Figure 7.52 (b) and (c)).

There was no peak at 60% gait, instead there was a plateau followed by a spike in the TR displacement at around 65% gait, which suggests instability. This spike in the TR rotation also occurred under the 4° tibial slope alignment condition. This spike was higher under the resected ACL & PCL soft tissue condition with a peak value of around 15°. The 10° tibial slope alignment condition also resulted in a much higher TR rotation between 65% to 85% gait under the resected ACL and resected ACL & PCL soft tissue conditions compared to the mechanical alignment condition.

The 10° tibial slope also resulted in a different shape AA rotation profile under the resected ACL and resected ACL & PCL soft tissue conditions (Figure 7.53 (b) and (c)). The minimum and maximum in the AA rotation profiles occurred much later in the cycle compared to the other alignment conditions. This shift in the AA rotation profile may be due to the different TR rotation profile shapes.

The 4° tibial slope alignment condition resulted in a sudden increase in the adduction rotation after 60% gait under the resected ACL and resected ACL & PCL soft tissue conditions.

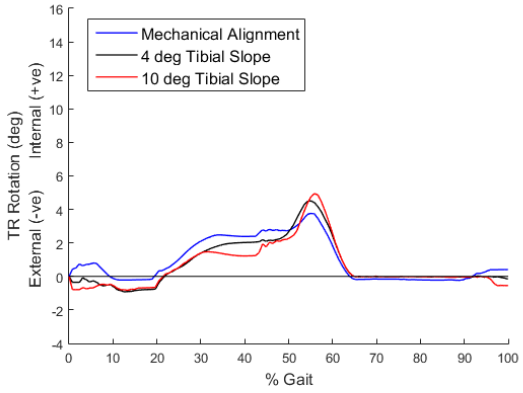

(a) Stiff Knee

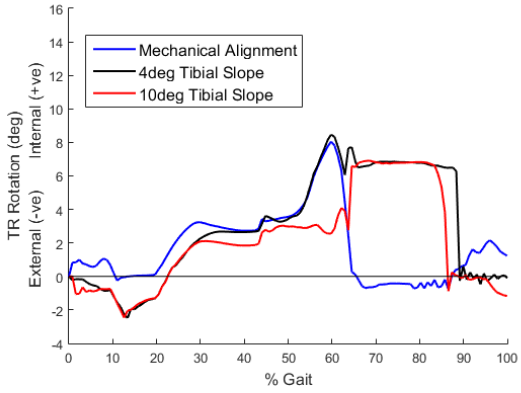

(b) Resected ACL

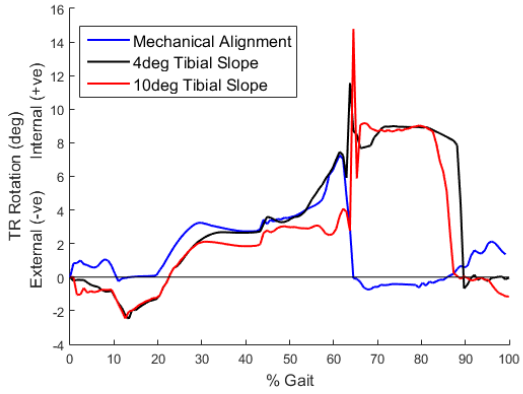

(c) Resected ACL and PCL

Figure 7.52: The TR rotation under 10°, 4° and 0° posterior tibial slope alignment conditions and the stiff knee (a), resected ACL (b) and resected ACL & PCL (c) soft tissue conditions

This was at the same point in the cycle where there was a sudden increase in the anterior displacement.

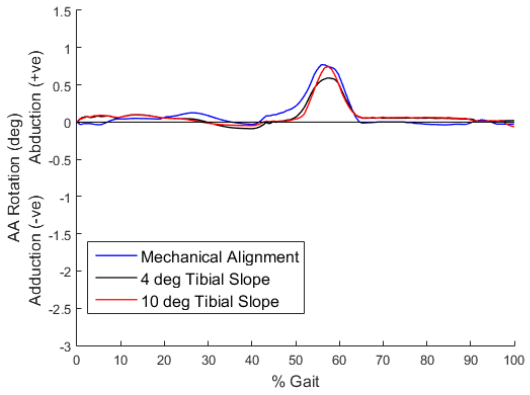

(a) Stiff Knee

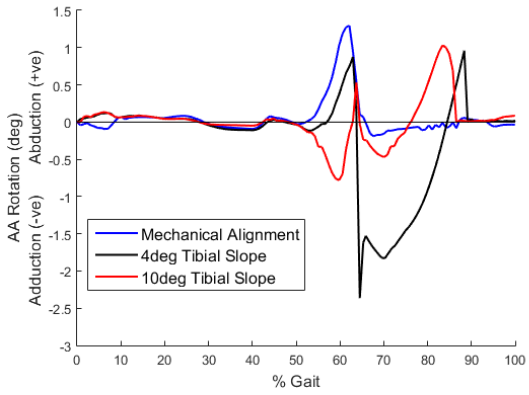

(b) Resected ACL

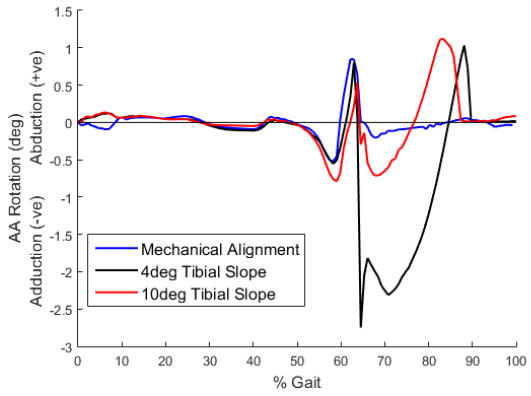

(c) Resected ACL and PCL

Figure 7.53: The AA rotation under 10°, 4° and 0° posterior tibial slope alignment conditions and the stiff knee (a), resected ACL (b) and resected ACL & PCL (c) soft tissue conditions

7.6.3.2 Contact Pressure

The contact pressure was found at the same four points in the gait cycle where the contact area was measured experimentally (Figures 7.54 and 7.55).

At points 1 and 2 in the cycle the 10° and 4° posterior tibial slope alignment conditions resulted in similar contact positions under both soft tissue conditions. The contact was central in the tibial insert at the start of the gait cycle however there was contact on the lateral posterior edge of the tibial insert at point 2 in the cycle. Whereas with the mechanical alignment condition there was no edge contact. This may be due to the increased anterior displacement under the tibial slope alignment.

The 4° tibial slope alignment condition resulted in edge contact on the posterior, lateral edge of the tibial insert at point 3 in the cycle under the resected ACL soft tissue condition. However under the resected ACL & PCL soft tissue condition there was no edge contact. This difference may be due to the difference in AP displacement at this point in the cycle; there was more posterior tibial displacement under the resected ACL & PCL soft tissue condition.

For the 10° and 4° tibial slope alignment conditions there was edge contact at point 4 in

the cycle for both the soft tissue conditions. For the 4° tibial slope alignment condition this contact was slightly more posterior than the 10° tibial slope alignment condition which may be due to the higher anterior displacement at this point.

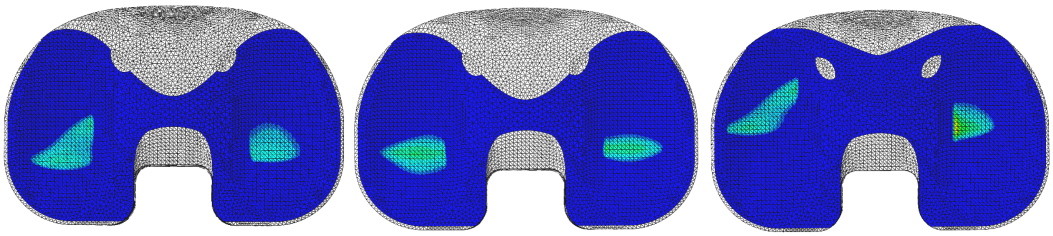

(a) Point 1

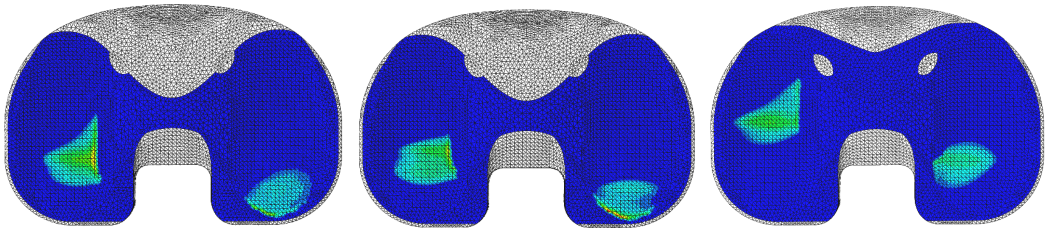

(b) Point 2

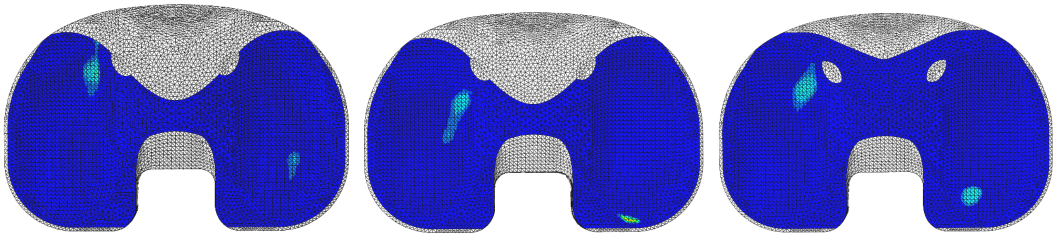

(c) Point 3

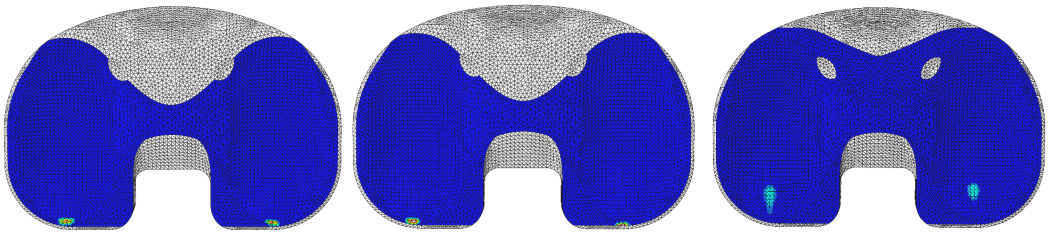

(d) Point 4

Figure 7.54: Computational prediction of the contact pressure under 10° posterior tibial slope (left), 4° posterior tibial slope (centre) and mechanical alignment (right) under the resected ACL soft tissue condition (0MPa blue, 40MPa red)

The peak contact pressure at each point in the cycle was found under the resected ACL and resected ACL & PCL soft tissue conditions (Tables 7.14 and 7.15).

At point 1 in the cycle the mechanical alignment condition had the highest peak pressure and the 10° tibial slope condition the lowest for both soft tissue conditions

At point 2 in the cycle the mechanical alignment condition had the lowest peak pressure

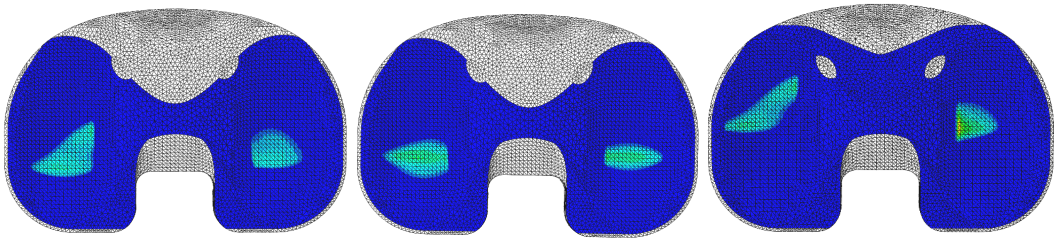

(a) Point 1

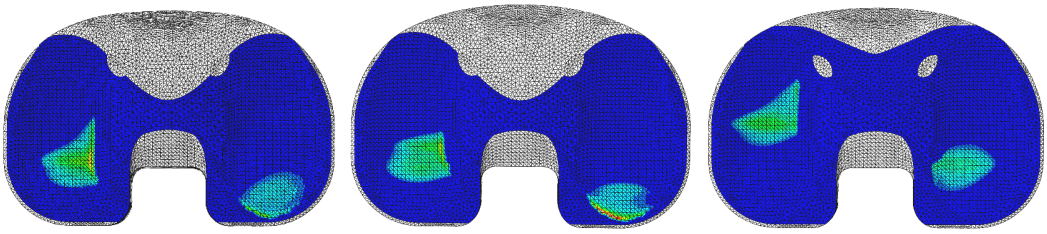

(b) Point 2

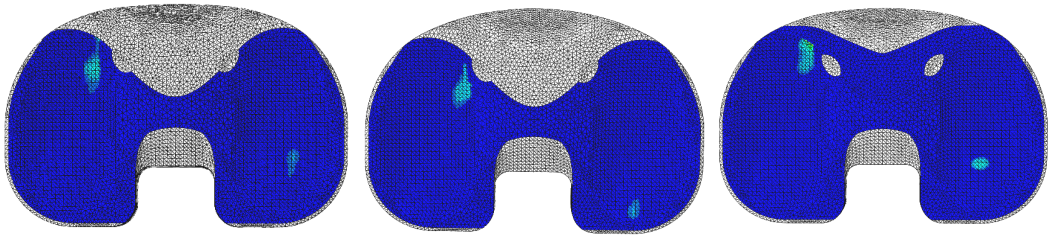

(c) Point 3

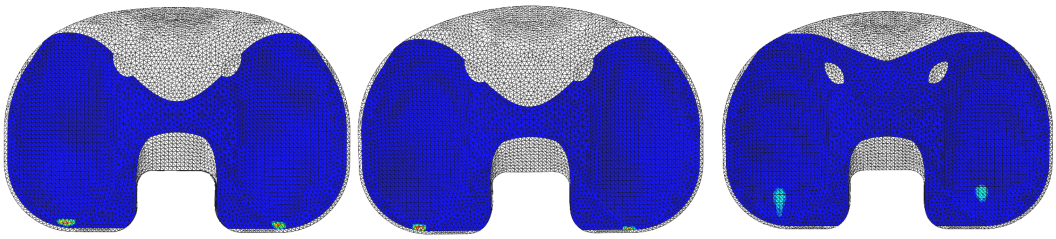

(d) Point 4

Figure 7.55: Computational prediction of the contact pressure under 10° posterior tibial slope (left), 4° posterior tibial slope (centre) and mechanical alignment (right) under the resected ACL & PCL soft tissue condition (0MPa blue, 40MPa red)

due to there being no contact on the posterior edge of the tibial insert. The pressure for both the tibial slope alignment conditions was similar for both soft tissue conditions.

At point 3 in the cycle the 4° tibial slope alignment condition resulted in the highest peak pressure under the resected ACL soft tissue condition due to the contact on the posterior edge of the tibial insert. However under the resected ACL & PCL soft tissue condition the peak pressure value was similar between both tibial slope alignment conditions.

At point 4 in the cycle the 10° and 4° tibial slope alignment condition resulted in the high peak pressure values due to the edge contact on the tibial insert. However due to the more

posterior contact under the 4° tibial slope the peak pressure under this alignment condition was highest.

Table 7.14: The peak contact pressure (MPa) for 10° posterior tibial slope, 4° posterior tibial slope and mechanical alignment conditions under the resected ACL soft tissue condition

Point	10°	4°	0°
1	13.5	16.5	27.4
2	30.5	29.1	19.7
3	7.6	24.0	15.6
4	29.9	38.5	12.2

Table 7.15: The peak contact pressure (MPa) for 10° posterior tibial slope, 4° posterior tibial slope and mechanical alignment conditions under the resected ACL & PCL soft tissue conditions

Point	10°	4°	0°
1	13.9	16.5	27.4
2	30.5	34.4	19.7
3	10.9	9.2	13.0
4	29.7	35.4	12.2

7.6.3.3 Contact Area

The contact area throughout the gait cycle was found for the tibial slope alignment and soft tissue conditions (Figure 7.56). For all the alignment and soft tissue conditions the contact area was similar, however under the resected ACL and resected ACL & PCL soft tissue conditions the tibial slope alignment conditions resulted in a lower contact area at around 15% gait compared to the mechanical alignment. This decrease may be due to edge loading on the tibial insert.

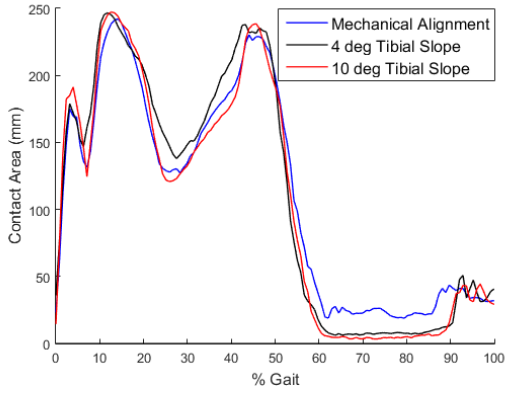

(a) Stiff Knee

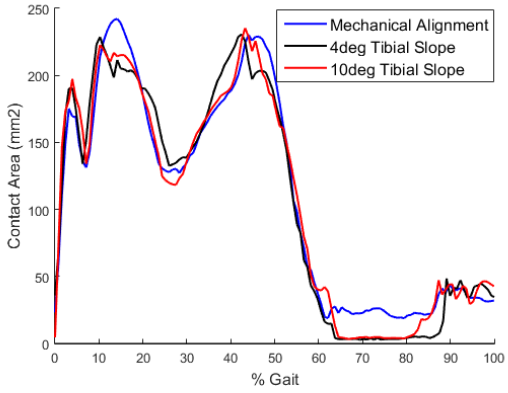

(b) Resected ACL

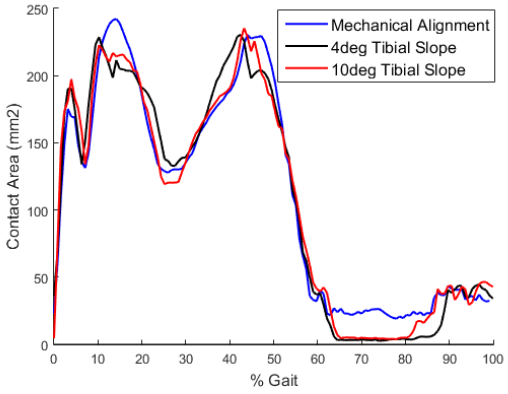

(c) Resected ACL and PCL

Figure 7.56: The contact area (mm^2) under 10° posterior tibial slope, 4° posterior tibial slope and mechanical alignment conditions under the stiff knee (a), resected ACL (b) and resected ACL & PCL (c) soft tissue conditions

7.6.4 Kinematic Alignment Condition

The kinematic alignment condition was run using the computational model under all three soft tissue conditions and under the same kinematic alignment as that studied experimentally, half the experimentally studied angles and mechanical alignment conditions.

7.6.4.1 Kinematics

The mechanical alignment condition and the kinematic alignment condition with half the values studied experimentally resulted in similar AP displacement profiles (Figure 7.57). The kinematic alignment with the values studied experimentally resulted in more anterior displacement during all of the gait cycle. For all the kinematic alignment conditions the different soft tissue conditions affected the amplitude of the displacement profiles.

The soft tissue conditions had more of an effect on the TR rotation than the different kinematic alignment conditions (Figure 7.58). The kinematic alignment condition studied

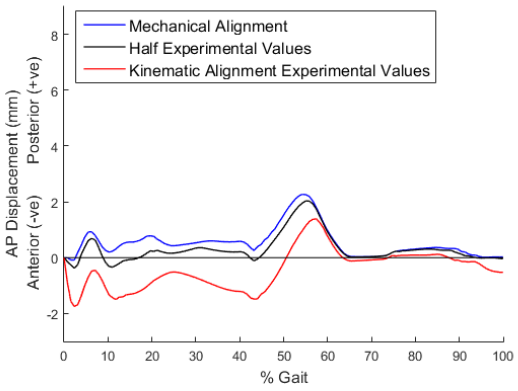

(a) Stiff Knee

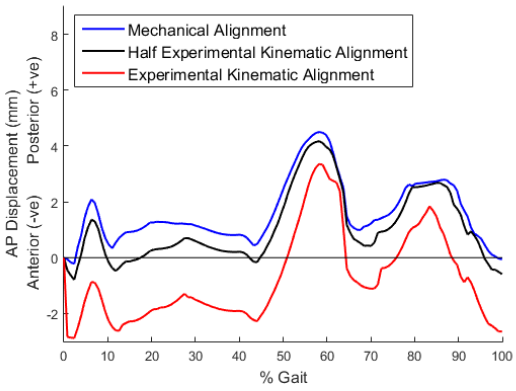

(b) Resected ACL

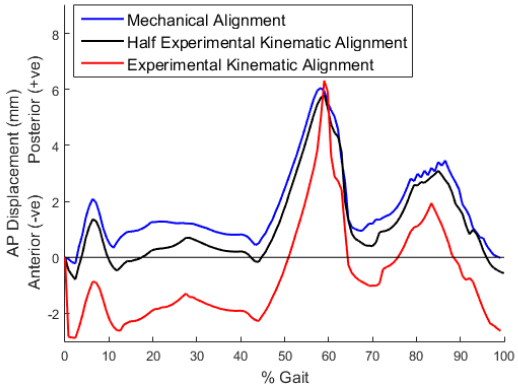

(c) Resected ACL and PCL

Figure 7.57: The AP displacement under the kinematic alignment studied experimentally, alignment with half the angles studied experimentally and mechanical alignment conditions and the stiff knee (a), resected ACL (b) and resected ACL & PCL (c) soft tissue conditions

experimentally however resulted in a spike in the TR rotation resulting in a higher peak TR rotation than the other alignment conditions under the resected ACL & PCL soft tissue condition. This spike in the TR rotation suggests that there may be some instability under this alignment and soft tissue condition.

There was an offset in the AA rotation between the three kinematic alignment conditions; with the AA rotation centred around 6° with the experimental values, around 3° with half the experimental values and around 0° under the mechanical alignment condition (Figure 7.59).

These values of this offset were equal to the difference in angle between the femoral and tibial components in the coronal plane. The shape of the AA rotation profiles was similar between the mechanical alignment and half experimental values alignment conditions for all the soft tissue conditions; the resected ACL & PCL soft tissue condition resulted in more adduction than the other soft tissue conditions.

However under the kinematic alignment condition studied experimentally there was a minima in the AA rotation at around 60% gait with both the resected ACL and resected

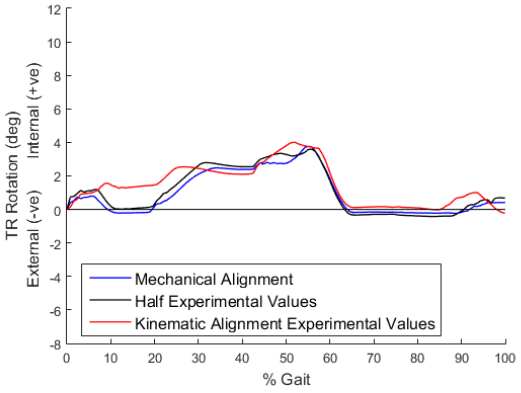

(a) Stiff Knee

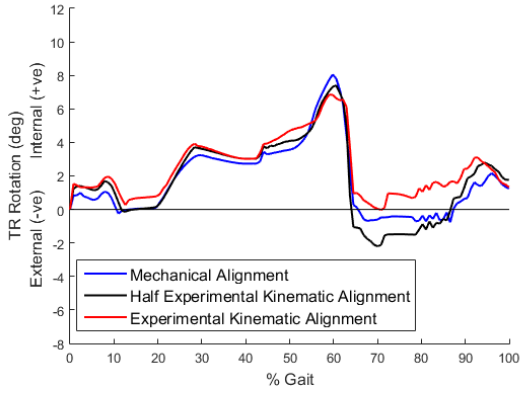

(b) Resected ACL

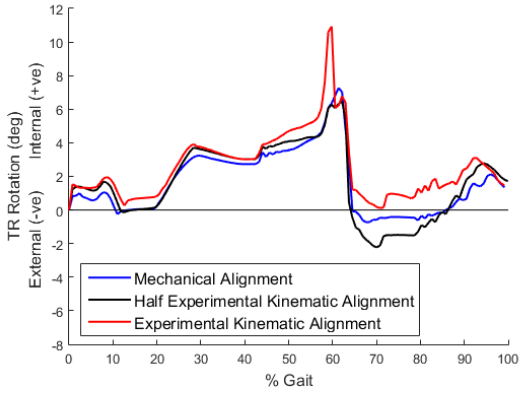

(c) Resected ACL and PCL

Figure 7.58: The TR rotation under the kinematic alignment studied experimentally, alignment with half the angles studied experimentally and mechanical alignment conditions and the stiff knee (a), resected ACL (b) and resected ACL & PCL (c) soft tissue conditions

ACL & PCL soft tissue conditions. With the resected ACL & PCL soft tissue condition this minima was lower and corresponds with the peak in the TR rotation. These spikes may be due to the contact on the anterior edge of the tibial insert at this point in the cycle.

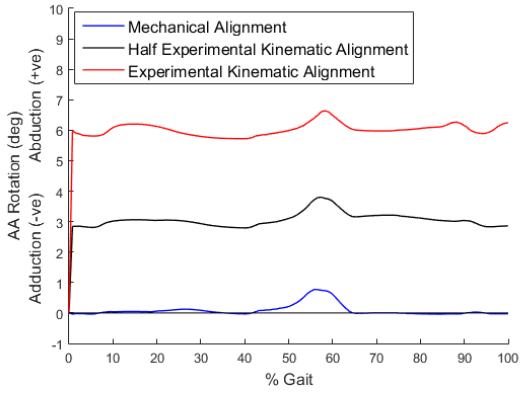

(a) Stiff Knee

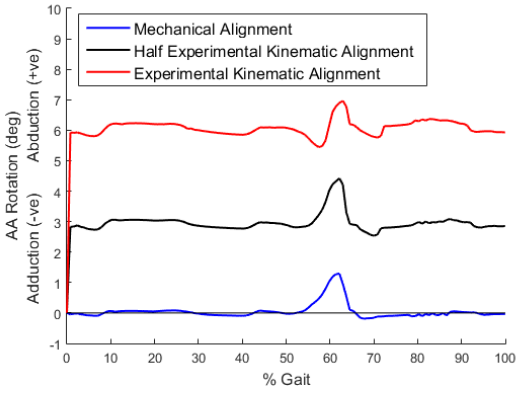

(b) Resected ACL

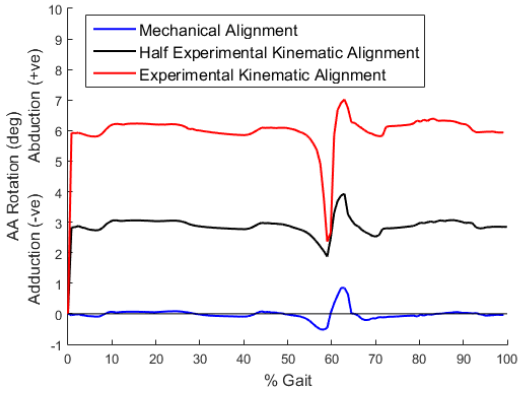

(c) Resected ACL and PCL

Figure 7.59: The AA rotation under the kinematic alignment studied experimentally, alignment with half the angles studied experimentally and mechanical alignment conditions and the stiff knee (a), resected ACL (b) and resected ACL & PCL (c) soft tissue conditions

7.6.4.2 Contact Pressure

The contact pressure was found at the same four points in the gait cycle where the contact area was measured experimentally under the resected ACL and resected ACL & PCL soft tissue conditions (Figures 7.60 and 7.61).

Under both the resected ACL and resected ACL & PCL soft tissue conditions the tibiofemoral contact position was similar across all three kinematic alignment conditions. At point 3 in the cycle however the kinematic alignment condition studied experimentally resulted in contact on the medial, anterior edge of the tibial insert. This also occurred with the kinematic alignment with half the values studied experimentally under the resected ACL & PCL soft tissue condition.

The peak contact pressure at each point in the cycle was found under the resected ACL and resected ACL & PCL soft tissue conditions (Tables 7.16 and 7.17).

Under the resected ACL soft tissue condition the kinematic alignment conditions resulted

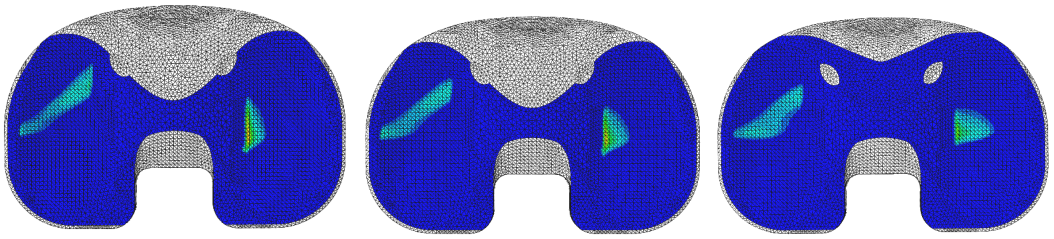

(a) Point 1

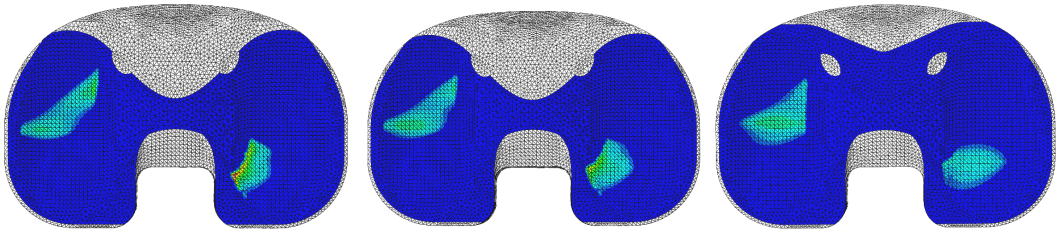

(b) Point 2

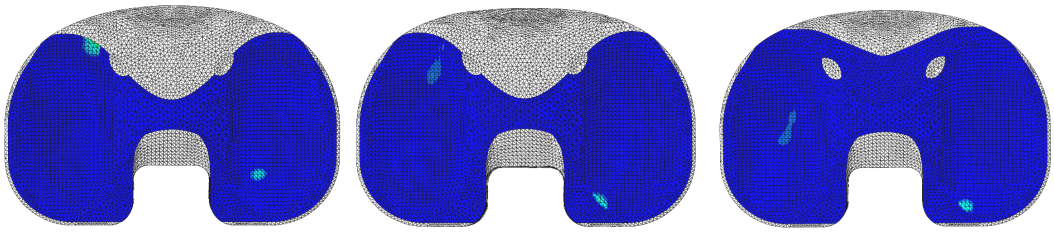

(c) Point 3

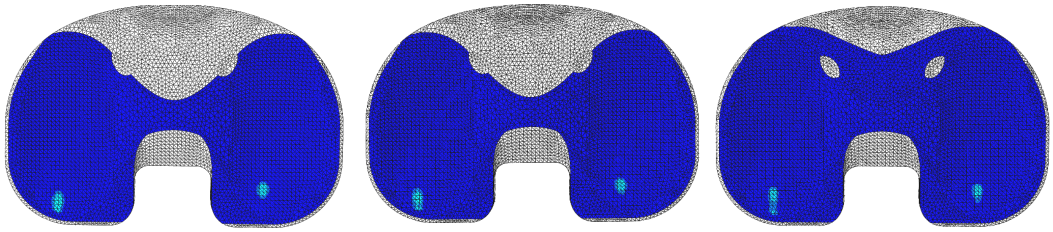

(d) Point 4

Figure 7.60: Computational prediction of the contact pressure under kinematic alignment studied experimentally (left), alignment with half the angles studied experimentally (centre) and mechanical alignment (right) under the resected ACL soft tissue condition (0MPa blue, 50MPa red)

in higher contact pressures than the mechanical alignment condition at points 1-3 in the cycle. While with the resected ACL & PCL soft tissue condition the experimental kinematic alignment condition resulted in the highest pressure at points 1 and 2 but the lowest pressure at point 3. The low pressure value at point 3 in the cycle may be due to the position of the contact as it was on the edge of the measured area, this is a limitation of this model. Due to the instability of the alignment condition increasing the area of the tibial surface where the contact pressure was calculated resulted in a significant increase in the model running time, which was not able to be carried out.

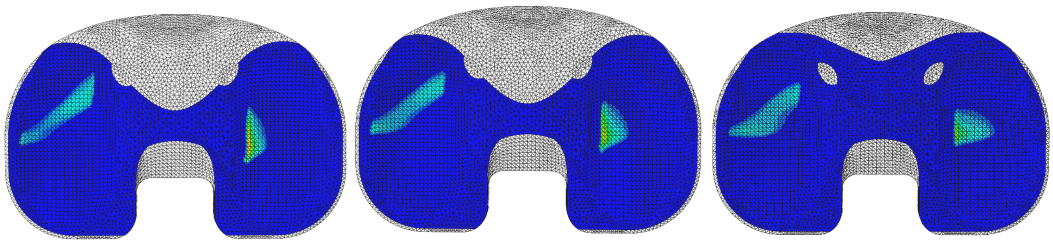

(a) Point 1

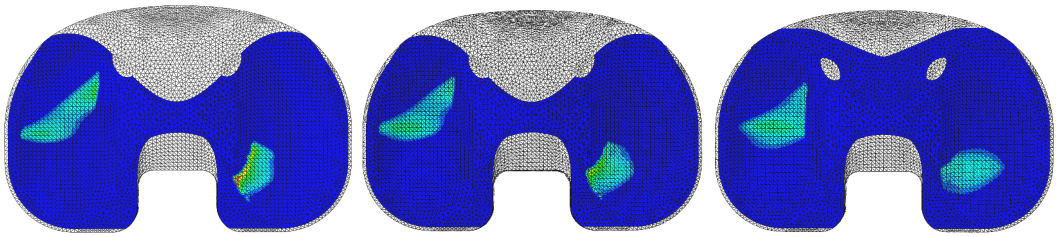

(b) Point 2

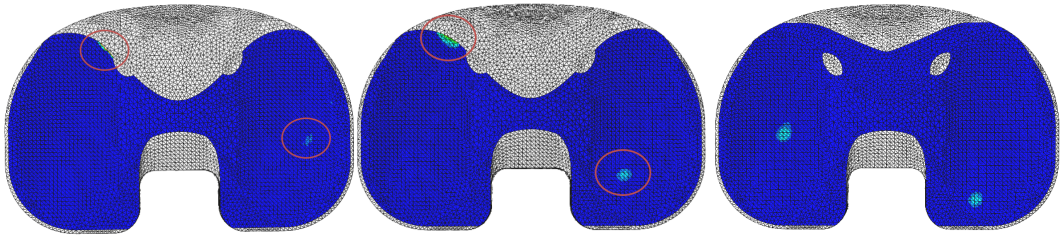

(c) Point 3

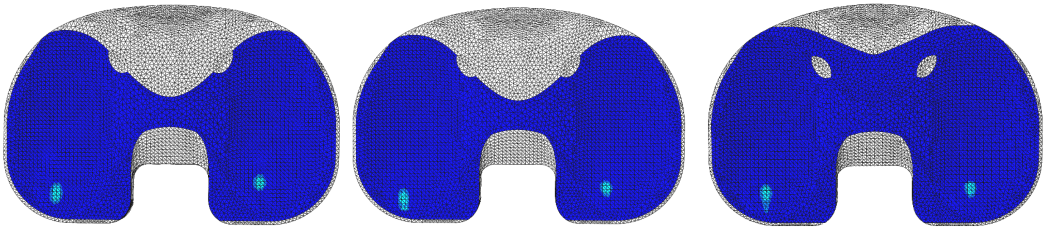

(d) Point 4

Figure 7.61: Computational prediction of the contact pressure under kinematic alignment studied experimentally (left), alignment with half the angles studied experimentally (centre) and mechanical alignment (right) under the resected ACL & PCL soft tissue condition (0MPa blue, 50MPa red)

Table 7.16: The peak contact pressure (MPa) for the kinematic alignment studied experimentally, alignment with half the angles studied experimentally and mechanical alignment conditions under the resected ACL soft tissue condition

Point	Experimental Alignment	Half Experimental Alignment	Mechanical Alignment
1	36.4	33.7	27.4
2	45.6	32.5	19.7
3	23.4	17.6	15.6
4	10.5	10.9	12.2

Table 7.17: The peak contact pressure (MPa) for the kinematic alignment studied experimentally, alignment with half the angles studied experimentally and mechanical alignment conditions under the resected ACL & PCL soft tissue conditions

Point	Experimental Alignment	Half Experimental Alignment	Mechanical Alignment
1	34.6	33.7	27.4
2	45.6	32.5	19.7
3	8.5	26.6	13.0
4	10.3	10.9	12.2

7.6.4.3 Contact Area

The contact area throughout the gait cycle was found for the kinematic alignment and soft tissue conditions (Figure 7.62).

The mechanical alignment condition resulted in higher contact area for the first half of the gait cycle than both the kinematic alignment conditions under all the soft tissue conditions studied, which may result in increased wear rates.

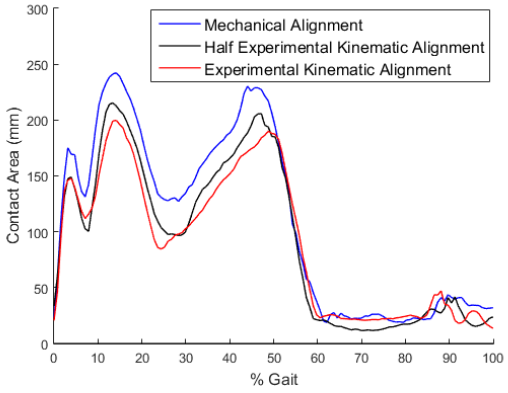

(a) Stiff Knee

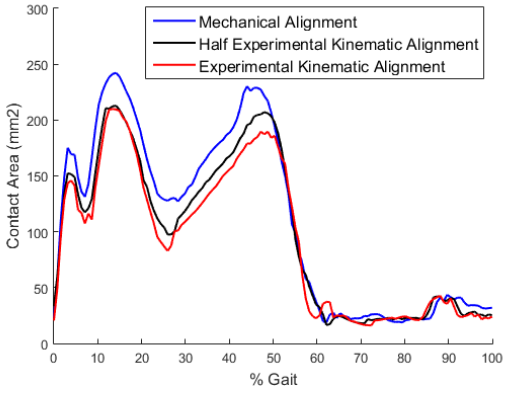

(b) Resected ACL

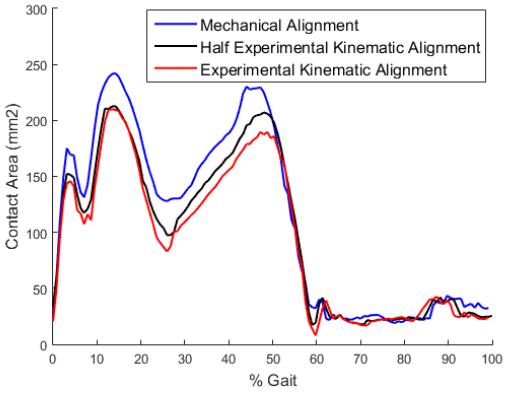

(c) Resected ACL and PCL

Figure 7.62: The contact area (mm^2) under the kinematic alignment studied experimentally, alignment with half the angles studied experimentally and mechanical alignment conditions under the stiff knee (a), resected ACL (b) and resected ACL & PCL (c) soft tissue conditions

7.7 Discussion

In this study the effect of the soft tissue conditions in combination with the varus, rotated, kinematic and tibial slope alignment conditions were investigated on the output kinematics, contact pressure and wear rates. Each alignment condition responded differently to the changes in the soft tissues.

7.7.1 Varus Joint Line Alignment Condition

Under the varus joint line alignment condition the different soft tissue conditions had a similar effect on the kinematics as under mechanical alignment; the lower tension soft tissue conditions resulted in increased displacements, with all the displacement profiles centred around zero. One previous study found that a varus or valgus component alignment had a minimal effect on the output AP and TR kinematics, which confirms this finding [92].

However unlike the mechanical alignment the lower tension springs also resulted in more balanced loading across the tibial compartments due to an increase in medial loading. The increase in medial loading under the varus alignment condition compared to the mechanical alignment is again similar to what has been found previously [52, 151, 189, 201]. However some previous studies have simulated a varus leg alignment rather than the varus joint line simulated in this study [52, 189, 201]. Clinically a varus leg alignment would result in a more medial joint force [154] which was not simulated in this study.

Under the resected ACL & PCL soft tissue condition the mechanical alignment resulted in contact on the anterior edge of the tibial insert. However under the varus alignment conditions the contact was more central, reducing the potential for damage on the edge of the insert.

The soft tissue conditions had a greater influence on the output kinematics than the varus alignment conditions. In the computational study the difference in varus angle between 4°, 2° and 0° had a minimal effect on the output kinematics. However the higher varus alignment of 4° resulted in more medial tibial loading and a higher peak contact pressure compared to the 2° and 0° alignment conditions.

Under the resected ACL & PCL soft tissue condition the varus alignment resulted in higher wear than under the stiff knee soft tissue condition, this increase in wear is similar to that determined under mechanical alignment, however as the wear rate was so low this may not be significant. In this study the medial wear scar was found to be larger than the lateral wear scar under the varus alignment condition. This increase in medial wear under varus alignment conditions was also similar to a previous study [195].

However other studies have found that an angle of 3° varus resulted in double the wear rate which is the opposite found in this study [66, 184]. Differences in the wear rate found in this study to previous studies may be due to the use of explants or may be due to differences in the UHMWPE; for example the level of cross-linking. One of these studies was also a retrieval study therefore a range of other factors, such as BMI may have affected the wear rates.

During the wear study there was more variation in the kinematics, especially the TR and the AA displacements, with the varus components compared to the mechanical alignment wear studies. With mechanical alignment the differences over time were small, where as with the varus alignment some of the differences in displacement values were much higher. This may be due to an increased variation between stations or may be due to increased variation due to some instability of the alignment condition.

Variation in the AA rotation may also have been due to it's measurement; the AA rotation was measured using a potentiometer which zeroed every time the simulator was initialised. Therefore any variation in the AA position as the simulator was initialised would result in an offset in the AA measurement.

Under the lower tension resected ACL & PCL soft tissue condition the varus alignment resulted in more balanced loading and less contact on the edge of the tibial insert. Therefore for patients where the ligaments have been damaged or removed a varus component alignment

may result in better patient satisfaction. The 4° varus alignment condition also resulted in a lower contact area during the gait cycle, which may help reduce surface wear rates. The wear rate under the resected ACL & PCL soft tissue condition was found to be lower than the mechanical alignment condition.

7.7.2 Rotated Alignment Condition

Under the rotated alignment condition the lower tension springs had a similar effect on the AP displacement as under the varus and mechanical alignment conditions. The soft tissue conditions had a greater effect on the AP displacement than the rotational mismatch conditions. However under the 14° rotational mismatch alignment there was a peak in anterior displacement that did not occur in the other alignment conditions and may be a sign of instability.

The rotational mismatch had more of an effect on the TR rotation. The TR range of motion did not vary between the rotational mismatch and soft tissue conditions; instead there was a shift in the displacement profile. This shift in the displacement rather than an increase in the range of motion was similar to another study using the same TKR [92].

As the rotational mismatch between the components increased so did the offset between the TR rotation profiles. The shape of the TR rotation profile was similar to the mechanical alignment condition under the 4° rotational mismatch alignment condition, however as the rotational mismatch increased to 8° and 14° the shape of the profile changed significantly, removing the peak at 60% gait. As discussed previously internal rotation of the tibia clinically can result in an increased Q angle, leading to pain and instability [22, 43, 64, 138, 153, 169, 175]. In this study the lower tension resected ACL and resected ACL & PCL soft tissue conditions and the rotational mismatch resulted in increased internal tibial rotation.

The rotated alignment condition also resulted in more AA rotation than the other alignments. The peak adduction rotation increased as the rotational mismatch of the components increased. The lower tension soft tissue conditions also resulted in lower AA displacements, which may have been due to the shift in the tibial rotation. The conformity of the tibial insert and the off centre contact point may result in an AA moment due to the curvature of the tibial insert. As the mismatch between the components reduced there may have been a more central contact point and therefore a lower AA moment. An increased adduction moment may contribute to the development of knee pain [170] and the lower tension soft tissue conditions resulted in lower adduction.

In the experimental study with the rotated alignment the contact for the first half of the cycle was on the lateral condyle of the tibial insert, this then shifted to being mainly on the medial condyle in the second half of the cycle. This may be due to the change from abduction to adduction resulting in a change in the loading. As the rotated alignment resulted in the largest change in the AA rotation this may be why this pattern was only seen with this alignment condition. There was imbalanced loading of the tibial insert under all the soft tissue conditions resulting in just medial loading at the end of the cycle. However the lower tension

resected ACL & PCL soft tissue condition resulted in the most balanced loading, especially during the first half of the gait cycle.

There was more instability under lower tension soft tissue conditions, resulting in some lift off when no soft tissue restraints were applied. Under the stability testing, with lower tension soft tissue conditions, lift off occurred, as the medial femoral condyle moved up the posterior lip of the tibial insert. The lower tension springs resulted in more internal rotation throughout the cycle, reducing the rotational mismatch between the tibial and femoral components.

As with the varus alignment condition during the wear study there was more variation in the kinematics, especially the TR and the AA rotations. Again this may be due to an increased variation between stations or may be due to increased variation due to the instability of the alignment condition. There was a linear relationship between the peak AA and TR rotations with the rotational mismatch. The AA rotation was more sensitive under the soft tissue condition than the lower tension conditions to changes in the rotational alignment of the components.

In the computational study under both the resected ACL and resected ACL & PCL soft tissue conditions the 14° rotational mismatch alignment resulted in higher peak pressures than the 8° and 4° rotational mismatch and mechanical alignment conditions. This occurred at the end of the gait cycle, where the contact was on the posterior edge of the tibial condyle. For most of the points measured as the rotational mismatch increased so did the contact pressure.

The 14° rotational mismatch alignment condition resulted in significantly higher wear rates than the mechanical and varus alignment conditions under both the soft tissue conditions studied. This is similar to a previous computational study that found that rotational alignment resulted in high wear rates [135]. Unlike the mechanical and varus alignment conditions the rotated alignment condition resulted in a lower wear rate under the resected ACL & PCL soft tissue condition than under the stiff knee soft tissue condition, however the difference in wear was not significant. This may be due to the lower tension soft tissue condition allowing the TR rotation to increase and reduce the rotational mismatch between the components.

The rotational mismatch alignment conditions resulted in similar AP displacement to the mechanical alignment condition, however the peak TR and AA rotations increased as the rotational mismatch increased. Under just 4° rotational mismatch the shape and range of the TR rotation profile was similar to under mechanical alignment conditions. There was an increased AA rotation and peak pressure values under 4° rotational mismatch compared to mechanical alignment conditions, however these were small. Rotational mismatch of the femoral and tibial components should therefore be kept within 4° in order to keep the shape and range of motion of the TR rotation and to minimise the peak contact pressure and AA moment.

7.7.3 Tibial Slope Alignment Condition

The posterior tibial slope alignment condition could not be studied experimentally under the resected ACL or resected ACL & PCL soft tissue conditions as it was too unstable. Under

these soft tissue conditions the femoral component would dislocate off the posterior side of the tibial insert before the input profiles could be tuned properly. The instability of the tibial slope alignment may have been partially due to the anterior tibial displacement causing a more posterior contact point.

However the computational simulation was able to run with the 10° posterior tibial slope alignment condition under both lower tension soft tissue conditions. Under these soft tissue conditions however the 10° and 4° posterior tibial slope alignment conditions were unstable resulting in sudden changes in the output displacements. The profile shape for the TR rotation was also very different to that found under the stiff knee soft tissue condition.

Under the 4° tibial slope the kinematics were similar for both the resected ACL and resected ACL & PCL soft tissue conditions. For the first 60% of the gait cycle the kinematics were similar to those under mechanical alignment. However after this point there was a sudden increase in the anterior displacement, internal rotation and adduction rotation.

There was a greater increase in the anterior displacement under the 4° tibial slope alignment condition than the 10° tibial slope condition, this may be due to the higher peak posterior displacement before this point resulting in a greater anterior force from the virtual springs. This consequently may have resulted in the increased instability due to the femorotibial contact occurring right on the posterior edge of the tibial insert.

The AP displacement profile for the 10° posterior tibial slope alignment was shifted around 4mm anteriorly under the resected ACL and resected ACL & PCL soft tissue conditions. The increased anterior displacement is similar to that found under the stiff knee soft tissue condition as well as previous studies [114] As discussed previously this increase in anterior displacement may be beneficial for CR knees in providing femoral rollback [179]. However there was also some instability with spikes in the TR rotation profiles.

In the computational study the 10° and 4° tibial slope alignment conditions resulted in different shaped TR and AA rotation profiles under the resected ACL and resected ACL & PCL soft tissue conditions compared to the mechanical alignment condition. Under the lower tension soft tissue conditions there was a sharp increase in the TR rotation and a later peak in the AA rotation profile under the 10° tibial slope alignment condition. While under the 4° tibial slope there was a higher peak adduction rotation. This increase in the peak TR and AA rotations may result in knee pain and instability clinically due to the increase in the Q angle [22, 43, 64, 138, 153, 169, 175].

Both tibial slope alignment conditions resulted in higher peak contact pressure values than under mechanical alignment conditions due to edge contact on the tibial insert. This edge contact could result in damage to the tibial insert in vivo and higher wear rates over a long term study.

The surgical guidelines for this TKR are no tibial slope. Under the 4° posterior tibial slope alignment condition there was edge contact and instability during the cycle under the lower tension soft tissue conditions. This suggests that for this TKR the posterior tibial slope should be less than 4° in order to prevent instability or damage occurring on the edge of the

tibial insert. There was an increase in the anterior displacement, which may be beneficial for a CR patient, however for patients with low tension soft tissue conditions this tibial slope value was too high, causing instability.

7.7.4 Kinematic Alignment Condition

The kinematic alignment condition with half the values studied experimentally resulted in a similar AP displacement profile as the mechanical alignment condition. However with the kinematic alignment condition studied experimentally there was a shift in the AP displacement profile in the anterior direction. This AP shift only occurred experimentally with the kinematic alignment condition. This may be due to the posterior tibial slope and the soft tissue gaps that occurred in the resected ACL and resected ACL & PCL soft tissue conditions, resulting in a more posterior tibiofemoral contact. The TR rotation profiles were similar across all alignment conditions.

In the experimental study the kinematic alignment condition resulted in very similar AP displacement and TR rotation profiles under the resected ACL and resected ACL & PCL soft tissue conditions. This may have been due to the size of the soft tissue gaps; the TR springs had a gap of 6° and the peak TR rotation for the resected ACL and resected ACL & PCL soft tissue conditions was 6.4° and 6.6° respectively. Therefore the TR springs were only applied over a very small section of the cycle. The AP springs had a gap of 2.5mm, the peak AP displacements were 2.4mm and 2.3mm for the resected ACL and resected ACL & PCL soft tissue conditions. Therefore the springs were only applied when the AP displacement was higher than 2.5mm in the anterior direction. This was mainly at the start of the cycle when the AF was at its highest. The stiff knee soft tissue condition, which had no soft tissue gaps, resulted in very different AP and TR displacement profiles. However in the computational study the lower tension resected ACL & PCL soft tissue condition resulted in a higher peak AP displacement. This difference in response could be due to the differences in loading between the two methods.

In the experimental study the kinematic alignment only resulted in lateral contact, this was the only alignment condition that only resulted in contact on one side of the tibial compartment. However kinematic alignment has resulted in good clinical outcomes, which contradict the purely lateral loading determined in this study. This may be due to the limitations in the experimental simulation of this alignment method as discussed previously such as the weight of the AA arm. In the computational study, where this mass was not included, the contact occurred on both the lateral and medial condyles. The contact positions were similar between the kinematic and mechanical alignment conditions, however the kinematic alignment resulted in contact on the anterior edge of the tibial insert under the lower tension soft tissue conditions.

The lower tension soft tissue conditions resulted in increased TR rotation and a shift in the AA rotation profile. The AA rotation was centred around 2°, 1.5° and 1° for the stiff knee, resected ACL & PCL and resected ACL soft tissue conditions respectively in the

experimental study. However in the computational model the AA rotation shifted due to the different alignment conditions rather than the soft tissue conditions. The AA rotation was centred around the difference in angle between the femoral and tibial components in the coronal plane. For example under the kinematic alignment condition studied experimentally the femoral component was at a valgus angle of 2.5° and the tibial component at a varus angle of 3.4° and the AA rotation profile was centred around 6°.

In the computational study the kinematic alignment condition that was studied experimentally also resulted in higher contact pressures. However if the contact pressure remains below the yield stress of the UHMWPE then this may not result in increased fatigue wear. Both the kinematic alignment conditions resulted in lower contact areas during the gait cycle than the mechanical alignment condition. This reduction in contact area may result in a lower surface wear rate.

The increased AA rotation that occurred under the kinematic alignment conditions may result in knee pain [170], therefore the difference in angle between the femoral and tibial components in the coronal plane should be kept to a minimum. Restricted kinematic alignment methods ensure that kinematic alignment results in a mechanical axis of the leg within a defined range in order to ensure good patient satisfaction. The angle between the components in the coronal plane will affect the mechanical axis of the leg and this should be considered during surgery.

Under the lower tension soft tissue conditions the kinematic alignment condition was found to be stable under the experimental study, however in the computational study it was found to result in contact on the anterior edge of the tibial component. The spikes in the TR and AA rotations under the kinematic alignment condition studied experimentally under the resected ACL & PCL soft tissue condition also suggests that the combination of alignment and soft tissue conditions resulted in unstable motion. Therefore with kinematic alignment the soft tissue conditions should also be taken into consideration in order to ensure stability.

7.7.5 Conclusions

The varus joint line alignment resulted in more medial loading and more balanced loading under the lower tension soft tissue conditions compared to the mechanical alignment condition.

The rotated alignment condition resulted in significantly higher TR and AA rotations, which may lead to knee pain and reduced patient satisfaction. The rotated alignment also resulted in significantly higher wear rates under both the soft tissue conditions, however unlike the other alignment conditions the wear rate was lower under the resected ACL & PCL soft tissue conditions. With rotational mismatch the lower restraints allowed the TR rotation to increase and reduce the mismatch between components, reducing the damage and contact pressures.

The tibial slope alignment resulted in some instability and contact on the posterior edge of the tibial insert. However the increase in anterior tibial displacement may be beneficial for CR knees.

The kinematic alignment conditions resulted in a shift in the AA rotation equal to the difference in component alignment in the coronal plane. The higher AA rotation may result in knee pain and therefore should be minimised where possible. Under the lower tension soft tissue conditions there was also some instability with contact on the edge of the tibial insert. The conditions of the soft tissues within the knee should therefore be taken into consideration when performing kinematic alignment methods to ensure stability.

Component alignment and soft tissue conditions should be considered in combination during TKR surgery in order to maintain stability and reduce wear rates.

Chapter 8

Discussion and Further Work

8.1 Introduction

The aim of this research was to investigate the effect of surgical alignment in combination with different soft tissue conditions on the kinematics and wear of a TKR. Both the component alignment and soft tissue conditions were found to have a significant effect on the kinematics and wear of the TKR studied.

Experimental studies were carried out using a DePuy Sigma CR TKR under a range of alignment and soft tissue conditions. The effect on the kinematics was determined by finding the average AP, TR and AA displacements during gait. The contact area was found using a Tekscan pressure sensor. Finally wear studies were carried out over 2MC under each alignment condition and a range of soft tissue conditions.

A computational finite element model was developed using Abaqus 6.14 to model the TKR within the experimental simulator. The computational model was validated by comparing the kinematics and contact area results with the experimental data. The model was then used to investigate the effect of additional alignment conditions on the kinematics and contact mechanics of the TKR.

Previous studies have determined that poor alignment can result in knee pain, lower knee scores or early failure [26, 56, 68, 181]. Some studies found that a knee with a mechanical axis $>3^{\circ}$ from neutral resulted in lower knee scores or that internal rotation resulted in knee pain [26, 56]. However alignment of the TKR may not result in early failure, often failure occurs due to a combination of factors such as alignment and BMI [32].

One cadaveric study investigating varus-valgus alignment determined that changes in the load distribution of the TKR were proportional to the angle of the component alignment [201]. But that the cadaveric specimens with tight ligaments resulted in more balanced loading. This study suggested that alignment on its own may not result in imbalanced loading, but that it is the combination of alignment and the soft tissue conditions within the knee that are important.

No previous studies have investigated the range of conditions in this study, and none have used both experimental and computational methods to do so. The use of both experimental

and computational methods has also allowed the computational model to be independently validated using the experimental results. Previous studies have investigated the effect of soft tissues within the knee and the effect of component alignment as individual variables but not in combination. The combination of both of these factors may help to explain why poor alignment may not necessarily lead to early failure.

8.2 Experimental Methods

All of the experimental investigations were carried out with a 6 station ProSim electro-mechanical knee simulator.

The simulator was validated under both displacement control and force control conditions in Chapter 2. This was carried out by verifying that the applied forces and displacements were close to the input profiles. Under displacement control there was good profile following with the applied values within ±5% of the input profiles. The wear rates under displacement control were similar to those found under the same test conditions on a different, same generation simulator.

Under force control conditions there was more deviation from the input profiles for the AP force and TR torque. Tuning was carried out to minimise this deviation, however there were still oscillations which may have been due to the movement of the TKR and the other applied forces. For example the most oscillations in the TR torque occurred at the start of the gait cycle where the AP force increased sharply from 0N to 270N. This increase in the AP force may have impacted the application or measurement of the TR torque resulting in oscillations. There was more variation between the stations of the simulator in the output AP displacement and TR torque profiles. This may have been due to small differences in the internal friction of each station, resulting in different displacements. However the wear rate found under force control conditions was around the value expected compared to the wear under displacement control, having accounted for the differences in kinematics. Despite the increased variation in the applied forces and inter-station variation there was not a significant increase in the 95% CI of the wear rate compared to displacement control.

Virtual springs were used within the simulator in order to represent the soft tissues within the natural knee by applying restraints to the AP displacement and TR rotation. The profile of each spring was uploaded onto the simulator, the displacement value from the previous step was used to determine the correct spring force to apply. The use of virtual rather than physical springs allowed the use of non-linear profiles and the ability to change both the spring gap and tensions to any desired value. However the limitation of the virtual springs was the delay in the force application; the virtual spring applied the spring force that would have occurred in the previous step under a physical spring.

A Tekscan pressure sensor was used to take contact area measurements at four points in the gait cycle. The use of the pressure sensor allowed the measurement of the position and area of the tibiofemoral contact. Initially the pressure sensor was going to be used to

investigate the effect on the contact pressure. However the measurement of the applied force was poor and therefore the values of the force and contact pressure were not used (Section 2.7). During calibration the measured force value was accurate however this was not the case during the gait cycle measurements. This difference may be due to the small contact areas during the gait cycle compared to the much larger contact area necessary during calibration.

The weight of the tibial fixture was also found to have an impact on the output kinematics under force control conditions (Section 2.5.6). One of the main limitations of the experimental simulation was the weight of the AA arm, which affected the AA rotation. As force control simulation had not been carried out before the effect of the weight of the parts within the simulator had not previously been an issue. The weight of the AA arm was unable to be varied however the weights of all the tibial fixtures used were kept as close to each other as possible in order to remove variation due to weight.

Wear studies were carried out for 2MC and the average wear scar outlines were found using a Matlab script. The Matlab script was developed in order to compare the shape and position of the wear scars between studies more effectively and to calculate an accurate wear scar area. Previously the outlines of the wear scars on each tibial insert were photographed, with the contact area calculated using Image Pro-Plus. The Matlab code however allowed for each outline to be digitised and normalised in terms of size, position and orientation relative to the outer edge of the tibial insert. The average outline for each wear study could then be calculated along with the 95% CI.

The alignment conditions studied in the experimental simulation were chosen to represent the range found in vivo. This was based on previous studies in to component alignment, which all used the same alignment method during surgery and a consistent post surgical measurement method. The alignment conditions chosen reflected the “worst case” alignment conditions that were found in these studies.

The use of the experimental simulation allowed the influence of the soft tissues and component alignment to be studied. Despite the limitations of the experimental simulation, the greatest being the weight of the AA arm, the experimental results allowed for the data for the validation of the computational model as well as the determination of different wear rates.

8.3 Computational Methods

A finite element model was developed of the TKR in order to replicate the conditions within the simulator. The output kinematics and contact area from the computational model were validated by comparing the results with the experimental data.

Some computational studies have previously been carried out into the effect of component alignment, mainly into the influence on the contact pressure of the tibial insert. There are three computational studies that have investigated the effect of varus-valgus alignment on the contact pressure, varus alignment was found to result in higher stresses than under valgus alignment [52, 126, 189]. One previous computational study investigated the effect of the

posterior tibial slope on the kinematics and contact pressure of a TKR [114]. Another previous study determined that rotational alignment resulted in the highest wear rate compared to varus-valgus and posterior tibial slope alignment conditions [135]. However in this study the computational results were validated across a range of component alignment and soft tissue conditions using experimental data.

There was good agreement between the computational and experimental methods. There were some differences which may have been due to a number of issues, for example the weight and internal friction of the simulator was not included within the computational model. This resulted in significant differences in the AA rotation profiles. This was especially clear with the kinematic alignment condition, where there was only lateral contact during the experimental study but both medial and lateral contact in the computational model. There was also a slight time delay in the output kinematics under the experimental simulation compared to the computational simulation. Some of the output profiles resulted in similar peaks between the two methods, however the peak in the computational simulation occurred slightly earlier in the cycle.

The differences in the kinematics, especially the differences in the AA rotation resulted in different contact areas on the tibial insert. Some of the differences in the contact area and position may also have been due to the static measurement that was used in the experimental simulation, in order to prevent damage of the Tekscan sensor, compared to the dynamic computational model. In order to verify this a static computational model was run using the experimental output kinematics (Section 5.5.1.3). The resulting contact areas were closer to those found experimentally than the original computational model.

Under the lower tension soft tissue conditions there were greater differences between the computational and experimental kinematics. These differences under the lower tension soft tissue conditions may have been due to the higher displacement values that occurred under these conditions. Therefore there may have been greater differences in the contact area or contact position and differences in friction may have had more of an effect.

The computational model allowed the generation of kinematics without the weight and internal friction inherent in the experimental simulator. It also allowed the accurate calculation of the contact area and the peak contact pressure during the gait cycle. The tibial slope alignment condition was also only able to be run experimentally under the stiff knee soft tissue condition due to its instability. However in the computational model it was able to be run under all of the soft tissue conditions. This allowed the collection of data that was too unstable to be generated experimentally as the input profiles could not be tuned before the TKR dislocated. The computational simulation of the kinematic alignment condition also resulted in more representative motion than that found experimentally; the experimental study only resulted in lateral contact throughout the cycle.

The use of the computational model resulted in a wider range of alignment conditions to be studied along with the calculation of the peak contact pressure. The model also showed the potential effect of the limitations of the simulator, such as the weight and internal friction.

8.4 Soft Tissue Conditions and Insert Design

This research experimentally investigated the effect of different soft tissue conditions on the kinematics of the TKR. There are a range of soft tissue conditions that occur in vivo and this range had not been simulated experimentally previously.

Measurement of the soft tissues within the knee is difficult in vivo. One study found that the results of measurements of the soft tissues taken during and after TKR surgery were different due to relaxation of the soft tissues over time [27]. Most studies that measure the tension of the ACL and PCL ligaments do so on cadaveric specimens, which may not be an accurate representation of the ligaments in vivo. Therefore the understanding of the properties and stiffness of the ligaments and soft tissues within the knee is slightly limited. There are a wide range of soft tissue conditions that occur in vivo and the soft tissues or ligaments could vary over time.

One previous study investigated the effect of TR torque on the resulting TR rotation and translation of cadaveric knees [113]. The TR torque was increased from 0Nm to 10Nm on knees with an intact and resected ACL. The greatest effect of the ACL was determined to be on the translation of the tibia rather than the rotation. Another study applied an anterior force to cadaveric knees and measured the resulting AP displacement [73]. The resulting displacement was determined to vary as the flexion of the knee varied. Therefore the restraint applied by the ligaments within the knee also varies during flexion and extension

Many studies have used the experimental simulation of TKRs in order to determine the kinematics or wear rate. There are a range of spring profiles that have been used under force control conditions. One study compared two spring tensions of 7.24N/mm (soft) and 33.8N/mm (hard) to cadaveric knee joints using a knee simulator [194]. With the ACL and PCL resected the cadaveric knee resulted in increased AP displacement and TR rotation. With the hard springs and the resected ACL & PCL there was near normal AP displacement however it reduced the TR rotation. Therefore the determination of the spring tensions within the knee simulator may be a compromise. However the knee simulator used for the previous study did not have separate AP and TR springs as in this study, instead the same springs are used to restrict both motions.

In this study three different tibial insert designs were experimentally investigated to find the effect of the tibial insert design on the output kinematics. The design of the tibial insert particularly affected the TR position. A lower conformity insert had a higher peak position which occurred earlier in the cycle. This was due to the lower conformity inserts allowing the TR position to follow the shape of the TR torque profile more closely. The lower conformity inserts also resulted in more anterior AP displacement.

The spring gaps and tensions affected the peak displacements in both the AP and TR positions, particularly in the second half of the cycle when the axial force was at its minimum. The lower conformity tibial insert was more sensitive to changes in the soft tissue conditions with changes in the spring gap and spring tension resulting in larger changes in the kinematics.

A previous study [92] investigated the effect of different spring tensions and gaps on the

output kinematics under force control on the same TKR. High tension springs (anterior restraint of 7.24N/mm and posterior restraint of 33.8N/mm) were tested with a 2.5mm and 0mm gap. Low tension springs (anterior and posterior restraint of 7.24N/mm) with a 2.5mm gap were also studied to investigate the effect of spring tension.

The spring gap tests had similar results to this study. The low tension spring resulted in a similar kinematic profile but with a higher amplitude. For the low tension TR springs the maximum TR position in the previous study was higher than that determined in this study. This may have been due to an offset between the sets of results of around 6°. However there was less of a difference between the previous study and this study's peak TR rotation for a high tension spring with a 0mm or 2.5mm gap.

Differences in the results between studies may be due to differences in the test conditions and simulators. For example this study used virtual springs rather than the two physical springs used previously to apply both AP and TR restraint. Different knee simulators have also been used; this study used a ProSim simulator compared to the Instron-Stanmore simulator used in the previous study. The Instron-Stanmore simulator is pneumatic [197] compared to the electro-mechanical simulator used for this study. Electro-mechanical simulators can provide better kinematic following than the first generation pneumatic simulators [7].

In this study three different soft tissue conditions were defined in order to represent a stiff knee, a knee with a resected ACL and a knee with a resected ACL & PCL. The representation of the soft tissues within the knee is difficult due to a number of factors. These include the variation between patients and the issues with measurement of the soft tissues while they are in vivo. Therefore the validity or appropriateness of the soft tissue conditions are difficult to determine. As the TKR used in this study was a CR TKR the resected ACL soft tissue condition should be the most representative of patients with this TKR. However there may be patients where damage to the soft tissues within the knee may occur during or after surgery, in this case the resected ACL & PCL soft tissue condition may be more representative. Conversely patients with a painful knee for a long period of time may have less laxity of the knee due to the soft tissues becoming tighter. A lack of soft tissue release during surgery or the use of a tibial insert which was too thick for the joint space may also result in a stiff knee. This soft tissue condition may be the least likely to occur out of the three conditions in this study, however it provides an insight into the effects of high tension soft tissue conditions.

The effect of the soft tissue conditions on the kinematics and wear rates were determined. The higher tension soft tissue conditions, representing a stiff knee, resulted in significantly lower AP and TR displacements. The stiff knee condition also resulted in a significantly lower wear rate than the resected ACL spring condition.

The stiff knee soft tissue condition was found to result in the most balanced loading throughout the cycle, closely followed by the resected ACL soft tissue condition which only resulted in unbalanced loading at the end of the cycle. However the resected ACL & PCL soft tissue condition resulted in unbalanced loading with a majority of the contact pressure

occurring through the lateral tibial condyle. The imbalanced loading that occurred with the lower tension soft tissue conditions correlates with a different study that found that the lower tension springs were more unstable and resulted in more imbalanced loading patterns [201]. Unbalanced loading could result in instability of the knee, lift off and patient dissatisfaction [88, 153]. Small differences in the AA motion resulted in a significant effect on the contact and the balance between the medial and lateral loading.

In the computational study the stiff knee soft tissue condition resulted in the highest peak pressure values at all four points measured, however the difference in values was low for most of the cycle.

The wear rate for the stiff knee soft tissue condition was significantly lower than that of the resected ACL and resected ACL & PCL soft tissue conditions. This follows from the kinematics results where the stiff knee soft tissue condition resulted in lower displacements than the resected ACL and resected ACL & PCL soft tissue conditions. The kinematics for the resected ACL and resected ACL & PCL soft tissue conditions were different, with the resected ACL & PCL soft tissue condition resulting in higher peak displacements on both the AP and TR profiles. However there was no significant difference in the range of motion of the AP, TR and AA profiles, this may be why the wear rates were also similar.

The lower tension resected ACL & PCL soft tissue condition resulted in similar wear to the resected ACL condition, however it also resulted in increased displacements and more unbalanced loading. This may result in instability and reduce patient satisfaction.

The stiff knee soft tissue condition resulted in significantly lower wear rates than the resected ACL soft tissue condition, it was also the only soft tissue condition to maintain contact on both sides of the tibial insert at all the points studied. The stiff knee soft tissue condition also resulted in higher peak pressures compared to the other two soft tissue conditions, however the difference in the peak pressure values were low for most of the cycle.

These results imply that higher tension soft tissue conditions may result in better outcomes for the patient. However this study has only investigated the mechanical impact of the soft tissue conditions and not any impact on patient satisfaction. For example the stiff knee soft tissue condition may result in a restricted range of motion, especially under high flexion conditions, and therefore lower patient satisfaction.

Simulating the average soft tissue tensions will not represent the variation across different patients. Patient variation should be represented in experimental simulation; in order to simulate a patient with increased laxity in the knee an increased spring gap should be used. The difference in spring tensions were found to have a lower effect on the high conformity tibial inserts. To ensure a test is clinically relevant the spring conditions should be considered with the tibial insert design in mind. For example a low conformity insert would not be used in a patient with high laxity. In order to replicate the range of outcomes that occur in vivo, experimental simulation must include a range of patient factors such as different soft tissue constraints.

8.5 Varus Joint Line Alignment Condition

In the experimental and computational study the varus joint line alignment conditions resulted in similar output kinematics to mechanical alignment, which was similar to the result of a previous study using the same TKR [92].

In this study there was found to be significantly lower wear under the varus alignment condition than under mechanical alignment, however previous studies have found that >3° varus alignment resulted in double the wear rates [66, 184]. This could be due to the design of the TKRs used in the study or due to differences in the simulation of the varus leg alignment compared to the varus joint line alignment in this study.

However the greatest effect of the varus alignment was on the loading pattern of the tibial insert. The mechanical alignment condition resulted in balanced loading under the stiff knee soft tissue condition and more unbalanced loading, with more lateral than medial compartment loading, under the other two soft tissue conditions. However the varus alignment resulted in unbalanced, mostly lateral loading under the stiff knee soft tissue condition and more balanced loading under the lower tension, resected ACL and resected ACL & PCL soft tissue conditions. Lateral loading of the tibial compartment has been shown to result in increased peak bone strains on the medial compartment [162], an increase in the bone stress may result in tibial implant migration.

The lateral loading under the stiff knee soft tissue condition and varus alignment was converse to what has been found previously in other studies and to what was found using the computational model [52, 151, 189]. However, previous studies simulated a varus leg alignment rather than a varus joint line. The difference in loading under the experimental methods may be due to differences in the AA rotation due to the weight of the AA arm within the simulator. This may be why the computational model, where this limitation was not present, resulted in more medial loading.

The difference in varus alignment angle between 4° and 2° had a minimal effect on the kinematics, the difference in soft tissue conditions was more influential. The increase in varus angle however did result in an increase in the medial compartment loading.

Under the stiff knee soft tissue condition the varus alignment conditions resulted in more unbalanced loading than under mechanical alignment (Table 8.1). However under lower tension soft tissue conditions, such as in patients where the ligaments have been damaged or removed a varus component alignment may result in more balanced loading. However as a varus leg alignment results in a more medial joint force, which was not replicated in this study, the loading conditions in vivo may be different to those found in this study. The varus component alignment also resulted in lower wear rates compared to the mechanical alignment condition under both the stiff knee and resected ACL & PCL soft tissue conditions studied.

Table 8.1: Table showing the effect of combinations of varus alignment and different soft tissue conditions, ranging from green (no adverse effects) to red (adverse mechanical and trichological conditions)

	0°	2°	4°
Stiff Knee			
Resected ACL			
Resected ACL & PCL			

8.6 Rotational Mismatch Alignment Condition

The rotated alignment condition resulted in a significantly higher TR rotation under the experimental and computational studies. The TR rotation profile shifted resulting in more internal rotation, but the same range of motion, as the rotational mismatch increased. This shift in the TR rotation was similar to that found in a previous study with the same TKR [92].

The increase in rotational mismatch between the components also resulted in an increase in the amplitude of the AA rotation profile. There was a linear relationship between the rotational mismatch of the components and the peak TR and AA rotations.

Internal rotation of the tibia increases the Q angle in the knee, this makes the quadriceps muscle less efficient and results in a lateral pull on the patella which may lead to patellar instability and increased pain. This follows with a previous study that found that internal rotation of the TKR components correlated with knee pain [26]. An increased adduction moment within the knee may also contribute to the development of knee pain [170].

The rotated alignment also resulted in unbalanced loading in the experimental study, with mainly lateral loading in the first half of the gait cycle, followed by mainly medial loading in the second half. Imbalance in the medial and lateral loading may result in instability of the knee, lift off and patient dissatisfaction [88, 153]. This occurred under all the soft tissue conditions studied.

There was also contact and damage that occurred on the medial posterior edge of the tibial insert during the wear study. This damage resulted in plastic deformation on the posterior tibial edge, which over an increased time period could result in early failure or instability of the TKR.

As the rotational mismatch increased so did the peak contact pressure, while there was a decrease in the contact area. This may be due to more loading on the posterior edge of the tibial insert. The higher pressure found under the rotational mismatch alignment condition corresponds to previous studies [52, 53].

The rotated alignment condition resulted in a significantly higher wear rate than the mechanical alignment condition, this could be due to the increase in kinematics or due to the contact on the edge of the tibial insert. This is similar to what was found in a previous computational study [135].

The rotational mismatch of the components should be reduced as much as possible during

surgery in order to keep the peak TR and AA rotations at a minimum. The change in the rotational mismatch of the components had a greater effect than the differences in the soft tissue conditions. However under the stiff knee soft tissue condition the restraint on the motion resulted in the off centre contact and loading on the edge of the tibial condyle. The rotational mismatch should be kept within 4°, at this angle the shape of the AP displacement and TR rotation profiles were similar to those under mechanical alignment conditions (Table 8.2). There was only a small increase in the peak AA rotation and in the peak contact pressures compared to the mechanical alignment condition. Therefore TKRs with rotational mismatch within 4° should not result in higher patient dissatisfaction. This is the case regardless of the soft tissue conditions within the knee.

Table 8.2: Table showing the effect of combinations of rotated alignment and different soft tissue conditions, ranging from green (no adverse effects) to red (adverse mechanical and trichological conditions)

	0°	4°	8°	14°
Stiff Knee				
Resected ACL				
Resected ACL & PCL				

8.7 Posterior Tibial Slope Alignment Condition

In the experimental and computational studies the posterior tibial slope resulted in anterior AP displacement throughout the gait cycle and resulted in more posterior contact including contact on the posterior tibial edge. The increased anterior tibial motion and a more posterior tibiofemoral contact point also correlates with previous studies into the effect of a posterior tibial slope [114, 179].

A posterior tibial slope may be beneficial for a CR TKR; there tends to be more anterior motion of the femur on the tibia in CR knees [153] compared to rollback of the femur which occurs in natural knees. A positive correlation has been found between femoral-rollback and higher clinical and functional scores [67]. In the computational study there was a greater difference between the 4° tibial slope alignment condition and the mechanical alignment condition than the 4° and 10° tibial slope alignment conditions under the stiff knee soft tissue condition.

However in the experimental study the 10° posterior tibial slope alignment condition was too unstable to be studied with the resected ACL or resected ACL & PCL soft tissue conditions. With the computational methods the 10° tibial slope alignment condition was able to run with these soft tissue conditions however there was still instability and an increase in the peak TR rotation.

Under the stiff knee soft tissue condition the 10° and 4° posterior tibial slope alignment conditions resulted in an increase in the peak TR rotation. This increase in the peak TR

rotation could result in pain and instability clinically as discussed previously [22, 43, 64, 138, 153, 169, 175].

The posterior tibial slope alignment resulted in significantly higher wear rates than the mechanical and varus alignments. There was more variation in the loading with this alignment condition than with the others, this could be due to the tibial slope causing instability. In the computational study the higher tibial slope alignment of 10° resulted in a higher contact pressure than the 4° or mechanical alignment conditions for most of the cycle. This may be due to the contact occurring near to the edge of the tibial insert.

The 4° tibial slope alignment condition resulted in more similar output kinematics as under mechanical alignment conditions under the resected ACL and resected ACL & PCL soft tissue conditions for the first half of the gait cycle. However after this point there was a sudden increase in the anterior displacement resulting in edge contact and instability. There was increased anterior displacement which may be beneficial for CR knees however the instability under the low tension soft tissue conditions suggests 4° is too high a tibial slope for this design. There was also increased TR and adduction rotations under the 4° tibial slope alignment condition which may result in pain and instability clinically.

Both of the tibial slope alignment conditions resulted in higher contact pressure values and contact on the edge of the tibial insert under all of the soft tissue conditions. This did not occur under the mechanical alignment condition.

This study suggests that although a posterior tibial slope could be beneficial in providing more anterior tibial displacement for this design a value less than 4° should be chosen (Table 8.3). This is to reduce the instability and edge contact on the tibial insert under lower tension soft tissue conditions. Under the stiff knee soft tissue condition the 4° tibial slope alignment condition was more stable but did not result in anterior displacement, therefore may not provide any benefit for CR patients.

Table 8.3: Table showing the effect of combinations of tibial slope alignment and different soft tissue conditions, ranging from green (no adverse effects) to red (adverse mechanical and trichological conditions)

	0°	4°	10°
Stiff Knee			
Resected ACL			
Resected ACL & PCL			

8.8 Kinematic Alignment Condition

In this study we were not able to measure wear rates in kinematic alignment as there was only lateral contact in the experimental study. Kinematic alignment has received good clinical results, the purely lateral contact found in this study may be due to the difficulty in pre clinical testing of kinematic alignment. For example the alignment studied was based on clinical data for the average positions and CI of the femoral and tibial components. The values used

were those taken one standard deviation away from the mean, therefore this combination of the femoral and tibial alignments may not occur in vivo. The main difference between the mechanical and kinematic alignment methods is that under kinematic alignment the collateral ligaments are never released, however in the simulator used for this study the soft tissues are represented by displacement constraints in the AP and TR directions with no restraints in the AA direction. Therefore the differences in the soft tissues between these two methods was not able to be represented.

However in the computational study the mass of the AA arm in the experimental simulator was not included, this allowed higher AA rotations resulting in contact on both the medial and lateral tibial condyles. The computational simulation of the kinematic alignment condition was therefore more representative of the conditions in vivo.

The kinematic alignment condition resulted in more anterior AP displacement in the experimental and computational studies than most of the other alignment conditions studied.

The AA rotation profile was centred around the difference in angle between the femoral and tibial components in the coronal plane so that the femoral and tibial components were parallel. However this lead to a valgus leg alignment which increases the Q angle, which may cause knee pain, instability and patella maltracking [22, 43, 64, 138, 153, 169, 175]. This angle between the femoral and tibial components should therefore be reduced in order to minimise the AA rotation that occurs during gait.

Restricted kinematic alignment methods ensure that kinematic alignment results in a mechanical axis of the leg within a defined range in order to ensure good patient satisfaction. The angle between the components in the coronal plane will affect the mechanical axis of the leg and this should be considered during surgery.

In the computational results at most points in the cycle studied the kinematic alignment condition based on half the experimental values resulted in the highest peak pressure under the stiff knee soft tissue condition. This may be due to the AA rotation around the more medial tibial centre of rotation resulting in higher pressures. Both the kinematic alignment conditions also resulted in lower contact areas throughout the cycle which may have resulted in higher peak pressures compared to the mechanical alignment condition. However under the lower tension soft tissue conditions the experimental kinematic alignment condition resulted in higher peak pressures.

Under the lower tension soft tissue conditions the kinematic alignment condition was found to be stable in the experimental study, however in the computational study it was found to result in contact on the anterior edge of the tibial component. The spikes in the TR and AA rotations under the kinematic alignment condition studied experimentally under the resected ACL & PCL soft tissue condition also suggests that the combination of alignment and soft tissue conditions resulted in unstable motion (Table 8.4). Therefore with kinematic alignment the soft tissue conditions should also be taken into consideration in order to ensure stability. The increased AA rotation under both kinematic alignment conditions studied may result in knee pain and instability clinically. Restricted kinematic alignment methods may reduce this

risk.

Table 8.4: Table showing the effect of combinations of kinematic alignment and different soft tissue conditions, ranging from green (no adverse effects) to red (adverse mechanical and trichological conditions)

	Ideal	Half Experimental Values	Experimental Values
Stiff Knee			
Resected ACL			
Resected ACL & PCL			

8.9 Clinical Significance

Currently in mechanical alignment of TKRs the aim is to keep the mechanical axis of the leg within 3° of neutral. However this envelope of 3° has not been proven to be the desired range of higher patient satisfaction and may also vary between different TKR designs.

Rotational alignment of the TKR is carried out using bony landmarks, which can be difficult to determine. This can result in a range of rotational alignments, as shown in the range of rotational mismatch values found in vivo (Section 1.11).

The tibial slope is defined as perpendicular to the mechanical axis of the tibia, which is found using an extramedullary rod. However the angle of the rod will vary depending on the attachment to the bony landmarks at the ankle and knee. Therefore there is some variation in the angle of the tibial slope.

A literature review was carried out in order to determine the alignment of TKRs in vivo (Section 6.3). The least variation in alignment was found in the coronal plane, with most TKRs within 4° of the mechanical axis. The range of alignments was found to be up to 10° in the sagittal plane and 14° in the transverse plane. The surgical guidelines for the TKR studied were for no tibial slope, literature studies for alignment in the sagittal plane were included if they had TKRs with similar guidelines. The alignment of most TKRs was lower than these values and would have occurred closer to the desired axis. The aim of this study was to investigate the range of alignments found in vivo therefore the high values of alignment were chosen.

Our understanding of the effects of different alignment conditions on patient satisfaction and early failure is not completely understood. Kinematic alignment is becoming more prevalent and results in a range of component alignments designed to keep the geometry of the natural knee the same. One of the questions associated with kinematic alignment is whether there should be a limit to the component alignment positions. For example that kinematic alignment will be carried out but the mechanical alignment of the leg should still remain within 3° of neutral. The effect of kinematic alignment on the mechanics of the TKR is debated. The mechanical effect of the TKR components being at different alignments with respect to

each other is also not known. Current preclinical studies investigate the mechanics and wear of TKRs under mechanical alignment, which is mechanical alignment rather than kinematic. Therefore the femoral and tibial components are only studied when they are parallel to each other which may not be the case under kinematic alignment.

This study has found that the effect of varus joint line alignment of the femoral and tibial components resulted in similar kinematics, lower wear rates and different loading patterns. The varus alignment resulted in more medial tibial loading. Varus alignment may be beneficial in patients with lower tension soft tissue conditions such as the resected ACL & PCL soft tissue condition studied as this resulted in more balanced tibial loading than mechanical alignment.

The rotational mismatch alignment condition resulted in much higher TR and AA rotations which may cause a range of issues such as knee pain and patella maltracking. There was also significantly higher wear rates with 14° rotational mismatch compared to mechanical alignment under both the soft tissue conditions studied. Regardless of the soft tissue condition the rotational mismatch may result in low patient satisfaction. Current methods of rotational alignment during TKR surgery may need to be improved in order to reduce the rotational mismatch than occurs in vivo.

A posterior tibial slope may be beneficial for a CR TKR as it may help to result in a more posterior femorotibial contact. In this study a posterior tibial slope of 10° was found to be unstable and resulted in significantly higher wear rates than the mechanical alignment condition. However a lower posterior tibial slope may be beneficial in restoring more natural motion of the knee. Even under the 4° tibial slope alignment condition the shift in the anterior displacement was only around 1mm and there was instability therefore a lower tibial slope may be more stable but not provide a benefit to the patient.

The experimental simulation of the kinematic alignment condition proved to be difficult and more realistic results were found using the computational model. Simulation of kinematic alignment is difficult due to the relationship between the soft tissues in the knee and the alignment of the TKR components which cannot be replicated within the simulator; the "correct" alignment will vary between patients. The kinematic alignment condition resulted in a lower contact area compared to mechanical alignment, which may result in lower wear rates. However the kinematic alignment also resulted in high AA rotation, which may lead to knee pain [170]. However the value of the AA rotation will depend on the angle of the femoral and tibial components in the coronal plane. In order to reduce the AA rotation limited kinematic alignment could be defined in order to keep the difference in angle of the femoral and tibial components within a certain range.

8.10 Limitations

Some of the limitations of the experimental and computational simulations have already been discussed. One of the main limitations are the mass and friction of the experimental simulation, which particularly affected the AA rotation.

One of the limitations in the experimental simulation was the variation between the stations of the simulator with respect to the kinematics, contact area and the wear rates. In some cases this made the results less clear between studies, particularly under the lower tension soft tissue conditions. This variation may be due to differences between the stations such as differences in internal friction.

Another limitation is the simulation of the soft tissue conditions. As mentioned previously the soft tissues within the knee are difficult to measure in vivo, meaning the range and material properties that occur in the population is unknown. The use of the virtual springs within the simulator is an approximation of the response of the soft tissues. However the natural tissues have a more complex response, for example the change in response as the knee flexes and extends. The AP and TR springs profiles are designed in order to represent all of the soft tissues within the knee, however in the natural knee there would not just be restraints in the AP and TR directions; the collateral ligaments would apply a restraint on the AA rotation.

The choice of the alignment conditions studied was based on previous research into alignment in vivo. The studies included were reduced to try to remove variations in surgical procedure and measurement of the alignment. However these studies investigated a range of TKR designs and therefore the alignment may not be representative of the TKR used in this study. A more conforming TKR may result in less variation in alignment while a TKR with lower conformity may result in a wider variation.

This study simulated a varus joint line rather than a varus leg alignment. Clinically a varus leg alignment has been found to result in a more medial joint force, which was not replicated in this study with the application of the axial force. Therefore the loading patterns found in this study under the varus joint line alignment condition may be different to those for a varus leg alignment.

The experimental simulation of the kinematic alignment condition was also a major limitation. The weight of the AA arm restricted the AA rotation resulting in only lateral contact on the tibial insert. The simulation of kinematic alignment is difficult to carry out as the component alignment depends so heavily on the natural geometry of the patient's knee as well as the soft tissue conditions within the knee. In this study values of the femoral and tibial alignments were taken from a study where they were not recorded in relation to each other. Therefore the combination of the valgus femoral and varus tibial alignments may not have occurred in vivo in the same patient. The choice of the kinematic alignment values is therefore an estimation of what could happen in vivo but is not an accurate representation of any particular patient.

This study also determined that the response to different soft tissue conditions was influenced by the geometry of the tibial insert. Therefore a different TKR design may respond completely differently to the same alignment and soft tissue conditions in this study. The effect of the alignment and soft tissue conditions can not be generalised to all TKRs, especially those of fundamentally different designs such as posterior stabilising TKRs.

This study investigated the mechanical impact of the alignment and soft tissue conditions

on the TKR. The effect of these conditions on the patient satisfaction was not investigated and can only be suggested based on other research. For example the effect of the component alignment and soft tissue conditions on the patient's range of movement and pain were not possible to identify. The higher tension soft tissue conditions may have mechanically better outcomes, however may also result in poor range of motion and therefore poor patient satisfaction.

This research carried out a systematic investigation into the combined effect of component alignment and soft tissue conditions within the knee. Both experimental and computational methods were used in order to determine the effect of a number of alignment and soft tissue conditions. The computational model was independently validated using the experimental data. No previous studies have investigated the effect of alignment in the coronal, transverse and sagittal planes and not in combination with soft tissue conditions,

8.11 Conclusions and Further Work

This research investigated the effect of component alignment and soft tissue conditions of a TKR on the kinematics and wear. Surgical alignment and soft tissue tensions significantly affected the kinematics and wear rates in this study. Rotational mismatch and a large posterior tibial slope resulted in the most adverse effects in terms of the mechanics of the TKR. The 4° varus alignment was found to be beneficial under lower tension soft tissue conditions on the kinematics and loading of the tibial insert. Rotational mismatch should be minimised in order to prevent anterior knee pain and instability due to high TR and AA rotation. A posterior tibial slope may be beneficial for CR knees however for this TKR the tibial slope should be kept lower than 4° in order to prevent instability. The angle between components in the coronal plane should be minimised in kinematic alignment methods in order to reduce the AA rotation and prevent knee pain.

Further investigations should be carried out into the effects of alignment in combination with soft tissue constraints to determine the most adverse biomechanical conditions and causes of early failure. In this study only a set number of alignment conditions were investigated and this was only carried out on one design of TKR. Further study into combinations of alignment conditions in multiple planes should also be carried out in order to determine the effect of their interaction.

Investigations into different designs of TKRs would also determine what variations there are between TKR designs in terms of their response towards component alignment and soft tissue conditions. For example a TKR with higher conformity may result in less variation in kinematics due to the soft tissue conditions but higher contact pressures due to changes in component alignment.

The use of actual patient data in the simulation of kinematic alignment may also result in more realistic simulations. As the component angles depend on the soft tissues of the particular patient both the post surgical alignment and soft tissue tensions should be considered together

in the simulation.

Reductions in the limitations of both the experimental and computational methods may also aid this. The mass of the AA arm in particular in the experimental simulation had a large influence on the loading of the tibial insert, especially the kinematic alignment condition. A more reliable method for experimental measurement of the contact pressure would also be beneficial as the Tekscan sensor was not able to measure the contact over the small contact areas in this TKR.

The computational model could also be improved in order to get output kinematics closer to those found experimentally. The computational simulation could also be extended in order to predict the wear rate of the TKR alignment and soft tissue condition. As experimental wear studies require a long time this would provide a much quicker estimation of the wear rate.

Bibliography

[1] Shape-fit cutting guides for total knee replacement lower operating time, raise patient satisfaction. Accessed 06.11.2015.

[2] M. Abdel. Measured resection versus gap balancing for total knee arthroplasty. *Clinical Orthopaedics and Related Research*, 472:2016 – 2022, 2014.

[3] M.P. Abdel and S.B. Haas. The unstable knee: Wobble and buckle. *The Bone and Joint Journal*, 96(B):112–114, 2014.

[4] M.P. Abdel, S.P. Parratte, and N.C. Budhiparama. The patella in total knee arthroplasty: to resurface or not is the question. *Curr Rev Musculoskelet Med.*, 7(2):117–124, 2014.

[5] A. Abdelgaied, C. Brockett, F. Liu, L. Jennings, J. Fisher, and Z. Jin. Quantification of the effect of cross-shear and applied nominal contact pressure on the wear of moderately cross-linked polyethylene. *Proceedings of the Institution of Mechanical Engineers. Part H: Journal of Engineering in Medicine*, 227(1):18 – 26, 2013.

[6] A. Abdelgaied, C. Brockett, F. Liu, L. Jennings, Z. Jin, and J. Fisher. The effect of insert conformity and material on total knee replacement wear. *The Journal of Engineering in Medicine*, 228:98–106, 2014.

[7] A. Abdelgaied, J. Fisher, and L.M. Jennings. A comparison between electromechanical and pneumatic-controlled knee simulators for the investigation of wear of total knee replacements. *Proceedings of the Institution of Mechanical Engineers, Part H: Journal of Engineering in Medicine*, 2017.

[8] A. Abdelgaied, J. Fisher, and L.M. Jennings. A comprehensive combined experimental and computational framework for pre-clinical wear simulation of total knee replacements. *Journal of the Mechanical Behavior of Biomedical Materials*, 78:282 – 291, 2018.

[9] A. Abdelgaied, F. Liu, C. Brockett, L. Jennings, J. Fisher, and Z. Jin. Computational wear prediction of artificial knee joints based on a new wear law and formulation. *Journal of Biomechanics*, 44:1108–1116, 2011.

[10] S. Affatato. Displacement or force control knee simulators? variations in kinematics and in wear. *Artificial Organs*, 40(2):195 – 201, 2016.

[11] S. Affatato, B. Bordini, C. Fagnano, P. Taddei, A. Tinti, and A. Toni. Effects of the sterilisation method on the wear of uhmwpe acetabular cups tested in a hip joint simulator. *Biomaterials*, 23:1439 – 1446, 2002.

[12] M. Al-Hajjar, I. Leslie, J. Tipper, S. Williams, J. Fisher, and L. Jennings. Effect of cup inclination angle during microseparation and rim loading on the wear of biolox delta ceramic-on-ceramic total hip replacement. *Journal of Biomedical Materials Research Part B: Applied Biomaterials*, 95(2):263 – 268, 2010.

[13] K. Anderson, K. Buehler, and D. Markel. Computer assisted navigation in total knee arthroplasty. *The Journal of Arthroplasty*, 20:132–138, 2005.

[14] T.P. Andriacchi, E.J. Alexander, M.K. Toney, C. Dyrby, and J. Sum. A point cluster method for in vivo motion analysis: applied to a study of knee kinematics. *Journal of biomechanical engineering*, 120:743–749, 1998.

[15] J. Archard. Contact and rubbing of flat surfaces. *Journal of Applied Physics*, 24(8):981 – 988, 1953.

[16] H. Asano, A. Hoshino, and T.J. Wilton. Soft tissue tension in total knee arthroplasty. *The journal of arthroplasty*, 19:558–561, 2004.

[17] P.I. Babazadeh, J.D. Stoney, K. Lim, and P.F.M. Choong. The relevance of ligament balancing in total knee arthroplasty: how important is it? a systematic review of the literature. *Orthop Rev (Pavia)*, 1, 2009.

[18] D. Baker, A. Bellare, and L. Pruitt. The effects of degree of crosslinking on the fatigue crack initiation and propagation resistance of orthopedic-grade polyethylene. *Journal of Biomedical Materials Research*, 66A:146–154, 2003.

[19] S.A. Banks, M.K. Harman, J. Bellemans, and W.A. Hodge. Making sense of knee arthroplasty kinematics: news you can use. *J Bone Joint Surg Am*, 85-A(Suppl 4):64–72, 2003.

[20] P. Barnett and J. Fisher. Comparison of wear in a total knee replacement under different kinematic conditions. *Journal of Materials Science: Materials in Medicine*, 12:1039 – 1042, 2001.

[21] P. Barnett, H. McEwen, D. Auger, M. Stone, E. Ingham, and J. Fisher. Investigation of wear of knee prostheses in a new displacement/force-controlled simulator. *Proceedings of the Institution of Mechanical Engineers, Part H: Journal of Engineering in Medicine*, 216(1):51 – 61, 2002.

[22] R. Barrack, T. Schrader, A. Bertot, M. Wolfe, and L. Myers. Component rotation and anterior knee pain after total knee arthroplasty. *Clinical Orthopaedics and Related Research*, 392:46–55, 2001.

[23] D. Bartel, J. Rawlinson, A. Burstein, C. Ranawat, and W. Flynn. Stresses in polyethylene components of contemporary total knee replacements. *Clinical Orthopaedics and Related Research*, 317:76–82, 1995.

[24] H. Bathis, L. Perlick, M. Tingart, C. Luring, D. Zurakowski, and J. Grifka. Alignment in total knee arthroplasty: A comparison of computer-assisted surgery with the conventional technique. *The Journal of Bone and Joint Surgery*, 86-B:682–687, 2014.

[25] L.E. Bayliss, D. Culliford, A.P. Monk, S. Glyn-Jones, D. Prieto-Alhambra, A. Judge, C. Cooper, A.J. Carr, N.K. Arden, and D.J. Beard. The effect of patient age at intervention on risk of implant revision after total replacement of the hip or knee: a population-based cohort study. *The Lancet*, 389:1424–1430, 2017.

[26] S. Bell, P. Young, C. Drury, J. Smith, I. Anthony, B. Jones, M. Blyth, and A. McLean. Component rotational alignment in unexplained painful primary total knee arthroplasty. *The Knee*, 21:272–277, 2014.

[27] J. Bellemans, P. D'Hooghe, H. Vandenneucker, G.V. Damme, and J. Victor. Soft tissue balance in total knee arthroplasty: does stress relaxation occur perioperatively? *Clinical Orthopaedics and Related Research*, 452:49–52, 2006.

[28] M.G. Benedetti, F. Catani, T.W. Bilotta, M. Marcacci, E. Mariani, and S. Giannini. Muscle activation pattern and gait biomechanics after total knee replacement. *Clinical Biomechanics*, 18:871–876, 2003.

[29] D.L. Benoit, D.K. Ramsey, M. Lamontagne, L. Xu, P. Wretenberg, and P. Renstrom. In vivo knee kinematics during gait reveals new rotation profiles and smaller translations. *Clinical orthopaedics and related research*, 454:81–88, 2007.

[30] M. Berend, M. Ritter, H. Hyldahl, J. Meding, and R. Redelman. Implant migration and failure in total knee arthroplasty is related to body mass index and tibial component size. *Journal of Arthroplasty*, 23(6):104–109, 2008.

[31] M. Berend, M. Ritter, J. Meding, P. Faris, E. Keating, R. Redelman, G. Faris, and K. Davis. The chitranjan ranawat award: Tibial component failure mechanisms in total knee arthroplasty. *Clinical Orthopaedics and Related Research*, 428:26–34, 2004.

[32] M. Berend, M. Ritter, J. Meding, P. Faris, M. Keating, R. Redelman, G. Faris, and K. Davis. Tibial component failure mechanisms in total knee arthroplasty. *Clinical Orthopaedics and Related Research*, 428:26–34, 2004.

[33] R. Berger, H. Rubash, J. Michael, W. Thompson, and S. Lawrence. Determining the rotational alignment of the femoral component in total knee arthroplasty using the epicondylar axis. *Clinical Orthopaedics and Related Research*, 286:40–47, 1993.

[34] R.A. Berger, L.S. Crossett, J.J. Jacobs, and H.E. Rubash. Malrotation causing patellofemoral complications after total knee arthroplasty. *Clinical Orthopaedics and Related Research*, 356:144–153, 1998.

[35] D. Bertolini, G. Nedwin, T. Bringman, D. Smith, and G. Mundy. Stimulation of bone resorption and inhibition of bone formation in vitro by human tumour necrosis factors. *Nature*, 319:516–518, 1986.

[36] K.H. Bloemker, T.M. Guess, L. Maletsky, and K. Dodd. Computational knee ligament modelling using experimentally determined zero-load lengths. *Open Biomed Eng J.*, 6:33–41, 2012.

[37] G. Blunn, E. Brach del Preva, L. Costa, J. Fisher, and A. Freeman. Ultra high molecular-weight polyethylene (uhmwpe) in total knee replacement: Fabrication, sterilisation and wear. *The Journal of Bone and Joint Surgery*, 84:946–949, 2002.

[38] M. Bolognesi and A. Hofmann. Computer navigation versus standard instrumentation for tka. *Clinical Orthopaedics and Related Research*, 440:162–169, 2005.

[39] F. Bookstein. Landmark methods for forms without landmarks: morphometrics of group differences in outline shape. *Medical Image Analysis*, 1(3):225–243, 1996.

[40] F. Bookstein, editor. *Morphometric Tools for Landmark Data: Geometry and Biology.* Cambridge University Press, 1997.

[41] P. Bracco, V. Brunella, M. Luda, E. Brach del Prever, M. Zanetti, and L. Costa. Oxidation behaviour in prosthetic uhmwpe components sterilised with high energy radiation in a low oxygen environment. *Journal of Othropaedic Traumatology*, 91:3057–3064, 2006.

[42] E. Brach del Prever, A. Bistolfi, P. Bracco, and L. Costa. Uhmwpe for arthroplasty: Past or future? *Journal of Othropaedic Traumatology*, 10:1–8, 2009.

[43] G.W. Brick and R.D. Scott. The patellofemoral component of total knee arthroplasty. *Clinical Orthopaedics and Related Research*, 231:163–178, 1988.

[44] C.L. Brockett, A. Abdelgaied, T. Haythornthwaite, C. Hardaker, J. Fisher, and L.M. Jennings. The influence of simulator input conditions on the wear of total knee replacements: An experimental and computational study. *Proceedings of the Institution of Mechanical Engineers, Part H: Journal of Engineering in Medicine*, 230:429–439, 2016.

[45] N. Budhiparama, M. Abdel, and S. Parratte. Icl 19: The importance of surgical technique in the outcome of tkr gap balancing vs measured resection technique for tkr: with specific reference to final outcome, 2015. International Society of Arthroscopy, Knee Surgery and Orthopaedic Sports Medicine.

[46] B. Carr and T. Goswami. Knee implants- review of models and biomechanics. *Materials and Design*, 30:398–413, 2009.

[47] Arianna Cerquiglini, Johann Henckel, Harry S. Hothi, Lorenzo Dall'Ava, Paul Shearing, Michael T. Hirschmann, and Alister J. Hart. Computed tomography techniques help understand wear patterns in retrieved total knee arthroplasty. *The Journal of Arthroplasty*, 33(9):3030 – 3037, 2018.

[48] C. Chang and C. Yang. Kinematic navigation in total knee replacement - experience from the first 50 cases. *Journal of the Formosan Medical Association*, 105(6):468–474, 2006.

[49] E. Chao, R. Laughman, E. Shneider, and R. Stauffer. Normative data of knee joint motion and ground reaction forces in adult level walking. *Journal of Biomechanics*, 16(3):219 – 233, 1983.

[50] S. Chauhan, G. Clark, S. Lloyd, R. Scott, W. Breidahl, and J. Sikorski. Computer-assisted total knee replacement. *The Journal of Bone and Joint Surgery*, 86-B(6):818–823, 2004.

[51] S. Chauhan, R. Scott, W. Breidahl, and R. Beaver. Computer-assisted knee arthroplasty versus a conventional jig-based technique. *The Journal of Bone and Joint Surgery*, 86-B(3):372–377, 2004.

[52] Z. Chen, L. Wang, Y. Liu, J. He, Q. Lian, D. Li, and Z. Jin. Effect of component mal-rotation on knee loading in total knee arthroplasty using multi-body dynamics modeling under a simulated walking gait. *Journal of Orthopaedic Research*, 33(9):1287–1296, 2015.

[53] C. Cheng, C. Huang, J. Liau, and C. Huang. The influence of surgical malalignment on the contact pressures of fixed and mobile bearing knee prostheses - a biomechanical study. *Clinical Biomechanics*, 18(3):231–236, 2003.

[54] A. Cheung, S.K. Goh, A. Tang, and T.B. Keng. Complications of total knee arthroplasty. *Current Orthopaedics*, 22(4):274–283, 2008.

[55] P. Chin, K. Yang, S. Yeo, and N. Lo. Randomized control trial comparing radiographic total knee arthroplasty implant placement using computer navigation versus conventional technique. *The Journal of Arthroplasty*, 20(5):618–626, 2005.

[56] P. Choong, M. Dowsey, and J. Stoney. Does accurate anatomical alignment result in better function and quality of life? comparing conventional and computer-assisted total knee arthroplasty. *The Journal of Arthroplasty*, 24(4):560–569, 2009.

[57] J. Collier, D. Sperling, J. Currier, L. Sutula, K. Saum, and M. Mayor. Impact of gamma sterilization on clinical performance of polyehtylene in the knee. *The Journal of Arthroplasty*, 11(4):377 – 389, 1996.

[58] B. Daines and D. Dennis. Gap balancing vs. measured resection technique in total knee arthroplasty. *Clinics in Orthopedic Surgery*, 6:1 – 8, 2014.

[59] F. Daubresse, C. Vajeu, and J. Loquet. Total knee arthroplasty with conventional or navigated technique: Comparison of the learning curves in a community hospital. *Acta Orthopaedica Belg*, 71:710–713, 2005.

[60] A. Demulder, S.V. Suggs, K.M. Zsebo, T. Scarcez, and G.D. Roodman. Effects of stem cell factor on osteoclast-like cell formation in long-term human marrow cultures. *Journal of Bone and Mineral Research*, 7(11):1337–1344, 1992.

[61] D. Dennis, R. Komistek, R. Kim, and A. Sharma. Gap balancing versus measured resection technique for total knee arthroplasty. *Clinical Orthopaedics and Related Research*, 468:102–107, 2010.

[62] J. DesJardins, P. Walker, H. Haider, and J. Perry. The use of a force-controlled dynamic knee simulator to quantify the mechanical performance of total knee replacement designs during functional activity. *Journal of Biomechanics*, 33:1231–1242, 2000.

[63] H. Dossett, N. Estrada, G. Swartz, G. LeFevre, and B. Kwasman. A randomised controlled trial of kinematically and mechanically aligned total knee replacements. *The Bone and Joint Journal*, 96-B(7):907–913, 2014.

[64] M-J. Emami, M-H. Ghahramani, F. Abdinejad, and H. Namazi. Q-angle - an invaluable parameter for evaluation of anterior knee pain. *Archives of Iranian Medicine*, 10(1):24–26, 2007.

[65] K. Ezzet, J. Hermida, C. Colwell Jr, and D. D'Lima. Oxidized zirconium femoral components reduce polyethylene wear in a knee wear simulator. *Clinical Orthopaedics and Related Research*, 428:120–124, 2004.

[66] K. Ezzet, J. Hermida, N. Steklov, and D. D'Lima. Wear of polyethylene against oxidized zirconium femoral components. *The Journal of Arthroplasty*, 27(1):116–120, 2012.

[67] S. Fantozzi, F. Cantani, A. Ensini, A. Leardini, and S. Giannini. Femoral rollback of cruciate-retaining and posterior-stabilized total knee replacements: in vivo fluoroscopic analysis during activities of daily living. *Journal of Orthopaedic Surgery and Research*, 24(12):2222–2229, 2006.

[68] E. Feng, S. Stulberg, and R. Wixon. Progressive subluxation and polyethylene wear in total knee replacements with flat articular surfaces. *Clinical Orthopaedics and Related Research*, 299:60–71, 1994.

[69] J. Fisher, L. Jennings, A. Galvin, Z. Jin, M. Stone, and E. Ingham. Polyethylene wear in total knees. *Clinical Orthopaedics and Related Research*, 468:12–18, 2010.

[70] J. Fisher, H.M.J McEwen, J. Tipper, A.L. Galvin, J. Ingram, A. Kamali, M.H. Stone, and E. Ingham. Wear, debris, and biologic activity of cross-linked polyethylene in the knee: Benefits and potential concerns. *Clinical Orthopaedics and Related Research*, 428:114–119, 2004.

[71] B. Fregly, C. Marquez-Barrientos, S. Banks, and J. DesJardins. Increased conformity offers diminishing returns for reducing total knee replacement wear. *Journal of Biomechanical Engineering*, 182:021007–021007–7, 2010.

[72] Benjamin J. Fregly, W.Gregory Sawyer, Melinda K. Harman, and Scott A. Banks. Computational wear prediction of a total knee replacement from in vivo kinematics. *Journal of Biomechanics*, 38(2):305 – 314, 2005. Knee Mechanics: An Update of Theoretical and Experimental Analyses.

[73] T. Fukubayashi, P.A. Torzilli, M.F. Sherman, and R.F. Warren. An in vitro biomechanical evaluation of anterior-posterior motion of the knee. *Journal of Bone and Joint Surgery*, 64-A:258–264, 1982.

[74] J.R. Funk, G.W. Hall, J.R. Crandall, and W.D. Pilkey. Linear and quasi-linear viscoelastic characterization of ankle ligaments. *Journal of Biomechanical Engineering*, 122(1):15–22, 1999.

[75] A. Galvin, L. Kang, J. Tipper, M. Stone, E. Ingham, Z. Jin, and J. Fisher. Wear of crosslinked polyethylene under different tribological conditions. *Journal of Materials Science: Materials in Medicine*, 17:235–243, 2006.

[76] A. Galvin, L. Kang, I. Udofia, L. Jennings, H. McEwen, Z. Jin, and J. Fisher. Effect of conformity and contact stress on wear in fixed-bearing total knee prostheses. *Journal of Biomechanics*, 42:1898–1902, 2009.

[77] A. Galvin, J. Tipper, E. Ingham, and J. Fisher. Nanometre size wear debris generated from crosslinked and non-crosslinked ultra high molecular weight polyethylene in artificial joints. *Wear*, 259:977–983, 2006.

[78] S. Gencur, C. Rimnac, and S. Kurtz. Failure micromechanisms during uniaxial tensile fracture of conventional and highly crosslinked ultra-high molecular weight polyethylenes used in total joint replacements. *Biomaterials*, 24:3947–3954, 2003.

[79] J. Giffin, K. Stabile, T. Zantop, T. Vogrin, S. Woo, and C. Harner. Importance of tibial slope for stability of the posterior cruciate ligament-deficient knee. *The American Journal of Sports Medicine*, 35(9):1443–1449, 2007.

[80] J. Giffin, T. Vogrin, T. Zantop, T. Vogrin, S. Woo, and C. Harner. Effects of increasing tibial slope on the biomechanics of the knee. *The American Journal of Sports Medicine*, 32(2):376–382, 2004.

[81] A.C. Godest, M. Beaugonin, E. Huang, M. Taylor, and P.J. Gregson. Simulation of a knee joint replacement during a gait cycle using explicit finite element analysis. *Journal of Biomechanics*, 35(2):267–275, 2002.

[82] A. Gomoll, T. Wanich, and A. Bellare. J-integral fracture toughness and tearing modulus measurement of radiation cross-linked uhmwpe. *Journal of Orthopaedic Research*, 20:1152–1156, 2002.

[83] F.A. Gottschalk, S. Kourosh, M. Stills, B. McClellan, and J. Roberts. Does socket configuration influence the position of the femur in above-knee amputation? *Journal of Prosthestics and Orthotics*, 2(1):94, 1989.

[84] M. Gowen, D. Wood, E. Ihrie, M. McGuire, and G. Russel. An interleukin 1 like factor stimulates bone resorption in vitro. *Nature*, 306:378–380, 1983.

[85] D. Grecu, I. Antoniac, O. Trante, M. Niculescu, and O. Lupescu. Failure analysis of retrieved polyethylene insert in total knee replacement. *Biomaterials*, 6:12–15, 2016.

[86] F.M. Griffin, J.N. Insall, and G.R. Scuderi. Accuracy of soft tissue balancing in total knee arthroplasty. *The Journal of Arthroplasty*, 15:970–973, 2000.

[87] Y. Gu, J. Roth, S. Howell, and M. Hull. How frequently do four methods for mechanically aligning a total knee arthroplasty cause collateral ligament imbalance and change alignment from normal in white patients? *The Journal of Bone and Joint Surgery*, 96-A(12), 2014.

[88] K.A. Gustke, G.J. Golladay, M.W. Roche, G.J. Jerry, L.C. Elson, and C.R. Anderson. Increased satisfaction after total knee replacement using sensor-guided technology. *The Bone and Joint Journal*, 96-B(10):1333–1338, 2014.

[89] R. Haaker, M. Stockheim, M. Kamp, G. Proff, J. Breitenfelder, and A. Ottersbach. Computer-assisted navigation increases precision of component placement in total knee arthroplasty. *Clinical Orthopaedics and Related Research*, 433:152–159, 2005.

[90] H. Haider, L. Alberts, M. Laurent, T. Johnson, J. Yao, L. Gilbertson, P. Walker, J. Neff, and K. Garvin. Comparison between force-controlled and displacement-controlled in-vitro wear testing on a widely used tkr implant. In *Transactions of the annual meeting - orthopaedic research society*, pages 1007–1007, 2002.

[91] H. Haider, T. Sekundiak, and K. Garvin. Analysis and recommendations for the optimum spring configurations for soft tissue restraint in force-control knee simulator testing. *48th Annual Meeting of Orthopaedic Research Society*, 2002.

[92] H. Haider, P. Walker, J. DesJardins, and G. Blunn. Effects of patient and surgical alignment variables on kinematics in tkr simulation under force-control. *Journal of ASTM International*, 3(10):3–16, 2006.

[93] Hani Haider. Chapter 26 - tribological assessment of uhmwpe in the knee. In Steven M. Kurtz, editor, *UHMWPE Biomaterials Handbook (Second Edition)*, pages 381 – 408. Academic Press, Boston, second edition edition, 2009.

[94] J. Halloran, A. Petrella, and P. Rullkoetter. Explicit finite element modeling of total knee replacement mechanics. *Journal of Biomechanics*, 38:323–331, 2005.

[95] M. Harman, J. DesJardins, S. Banks, L. Benson, M. Laberge, and W. Hodge. Damage patterns on polyethylene inserts after retrieval and after wear simulation. *47th Annual Meeting, Orthopaedic Research Society. Implant Wear.*, 2001.

[96] P. Harvie, K. Sloan, and R. Beaver. Computer navigation vs conventional total knee arthroplasty; five-year functional results of a prospective randomized trial. *The Journal of Arthroplasty*, 27(5):667–672, 2012.

[97] W. Healy, R. Lorio, and M. Lemos. Athletic activity after joint replacement. *The American Journal of Sports Medicine*, 3(29):377–388, 2001.

[98] P.F. Hill, V. Vedi, A. Williams, H. Iwaki, V. Pinkserova, and M.A.R. Freeman. Tibiofemoral movement 2: the loaded and unloaded living knee studied by mri. *The Journal of Bone and Joint Surgery*, 82(B):1196–1198, 2000.

[99] S. Howell, S. Papadopoulos, K. Kuznik, and M. Hull. Accurate alignment and high function after kinematically aligned tka performed with generic instruments. *Knee Surgery, Sports Traumatology, Arthroscopy*, 0942-2056, 2013.

[100] H. Hsu, A. Garg, P. Walker, M. Spector, and F. Ewald. Effect of knee component alignment on tibial load distribution with clinical correlation. *Clinical Orthopaedics and Related Research*, 248:135–144, 1989.

[101] T. Huang, L. Kuo, K. Peng, M. Lee, and R. Hsu. Computer tomography evaluation in total knee arthroplasty: Computer-assisted navigation versus conventional instrumentation in patients with advanced valgus arthritic knees. *The Journal of Arthroplasty*, 29:2363–2368, 2014.

[102] D.E Hurwitz, A.B Ryals, J.P Case, J.A Block, and T.P Andriacchi. The knee adduction moment during gait in subjects with knee osteoarthritis is more closely correlated with static alignment than radiographic disease severity, toe out angle and pain. *Journal of Orthopaedic Research*, 20(1):101 – 107, 2002.

[103] E. Ingham and J. Fisher. Biological reactions to wear debris in total joint replacement. *Proceedings of the Institution of Mechanical Engineers, Part H: Journal of Engineering in Medicine*, 214(1):21–37, 2000.

[104] M. Ishikawa, S. Kuriyama, H. Ito, M. Furu, S. Nakamura, and S. Matsuda. Kinematic alignment produces near-normal knee motion but increases contact stress after total knee arthroplasty: A case study on a single implant design. *The Knee*, 22:206–212, 2015.

[105] H. Iwaki, V. Pinskerova, and M.A.R. Freeman. Tibiofemoral movement 1: the shapes and relative movements of the femur and tibia in the unloaded cadaverknee. *The Journal of Bone and Joint Surgery*, 82(B):1189–1195, 2000.

[106] Faezeh Jahani. Modelling of dynamic edge loading in total hip replacements with ceramic on plyethylene bearings. *PhD Thesis*, 2017.

[107] L. Jennings, M. Al-Hajjar, C. Brockett, S. Williams, J. Tipper, E. Ingham, and J. Fisher. Enhancing the safety and reliability of joint replacement implants. *Orthopaedics and Trauma*, 26(4):246 – 252, 2012.

[108] Z. Jin, M. Stone, E. Ingham, and J. Fisher. Biotribology. *Current Orthopaedics*, 20:32 – 40, 2006.

[109] T. Johnson, M. Laurent, J. Yao, and L. Gilbertson. The effect of displacement control input parameters on tibiofemoral prosthetic knee wear. *Wear*, 250:222 – 226, 2001.

[110] H. Jojima, L. Whiteside, and K. Ogata. Effect of tibial slope or posterior cruciate ligament release on knee kinematics. *Clinical Orthopaedics and Related Research*, 426:194–198, 2004.

[111] M. Jones and D. Scott, editors. *Industrial Tribology: The Practical Aspects of Friction, Lubrication and Wear*. North Holland [Imprint], 1983.

[112] Cynthia A. Kahlenberg, Benedict U. Nwachukwu, Alexander S. McLawhorn, Michael B. Cross, Charles N. Cornell, and Douglas E. Padgett. Patient satisfaction after total knee replacement: A systematic review. *HSS Journal Â®*, 14(2):192–201, Jul 2018.

[113] A. Kanamori, J. Zeminski, T.W. Rudy, G. Li, F.H. Fu, and S.L-Y. Woo. The effect of axial tibial torque on the function of the anterior cruciate ligament: a biomechanical study of a simulated pivot shift test. *Arthroscopy: The Journal of Arthroscopic and Related Surgery*, 18:394–398, 2002.

[114] Kyoung-Tak Kang, Yong-Gon Koh, Juhyun Son, Oh-Ryong Kwon, Jun-Sang Lee, and Sae-Kwang Kwon. Influence of increased posterior tibial slope in total knee arthroplasty on knee joint biomechanics: A computational simulation study. *The Journal of Arthroplasty*, 2017.

[115] K. Kato and K. Adachi, editors. *Modern Tribology Handbook, Chapter 7. Wear Mechanisms*. CRC Press, 2001.

[116] L. Knight, S. Pal, J. Coleman, F. Bronson, H. Haider, D. Levine, M. Taylor, and P. Rullkoetter. Comparison of long-term numerical and experimental total knee replacement wear during simulated gait loading. *Journal of Biomechanics*, 40:1550–1558, 2006.

[117] R. Komistek, D. Dennis, and M. Mahfouz. In vivo fluoroscopic analysis of the normal human knee. *Clinical Orthopaedics and Related Research*, 410:69–81, 2003.

[118] D. Kopeliovich. Mechanisms of wear. Accessed 28.01.2016.

[119] S. Kurtz, editor. *The UHMWPE Handbook*. Elsevier, 2004.

[120] S. Kurtz, editor. *UHMWPE Biomaterials Handbook: Ultra High Molecular Weight Polyetheylene in Total Joint Replacement and Medical Devices*. Elsevier, 2016.

[121] S. Kurtz, C. Jewetta, J. Bergstroma, J. Fouldsa, and A. Edidin. Miniature specimen shear punch test for uhmwpe used in total joint replacements. *Journal of Biomaterials*, 23:1907–1919, 2002.

[122] S. Kurtz, K. Ong, E. Lau, F. Mowat, and M. Halpern. Projections of primary and revision hip and knee arthroplasty in the united states from 2005 to 2030. *JBJS*, 89:780–785, 2007.

[123] M. Lafortune, P. Cavanagh, H. Sommer, and A. Kalenak. Three-dimensional kinematics of the human knee during walking. *Journal of Biomechanics*, 25(4):347 – 357, 1992.

[124] Yong Seuk Lee, Stephen M. Howell, Ye-Yeon Won, O-Sung Lee, Seung Hoon Lee, Hamed Vahedi, and Seow Hui Teo. Kinematic alignment is a possible alternative to mechanical alignment in total knee arthroplasty. *Knee Surgery, Sports Traumatology, Arthroscopy*, 25(11):3467–3479, Nov 2017.

[125] G. Lewis. Properties of crosslinked ultra-high-molecular-weight polyethylene. *Biomaterials*, 22:371–401, 2001.

[126] J. Liau, C. Cheng, C. Huang, and W. Lo. The effect of malalignment on stresses in polyethylene component of total knee prostheses - a finite element analysis. *Clinical Biomechanics*, 17:140–146, 2002.

[127] L. Longstaff, K. Sloan, N. Stamp, M. Scaddan, and R. Beaver. Good alignment after total knee arthroplasty leads to faster rehabilitation and better function. *The Journal of Arthroplasty*, 24(4):570–578, 2009.

[128] J. Lorenzo, S. Sousa, J. Foriseca, J. Hock, and E. Medlock. Colony-stimulating factors regulate the development of multinicleated osteoclasts from recently replicated cells in vitro. *Journal of Clinical Investigation*, 80:160–164, 1987.

[129] S. Maruyuna, S. Yoshiya, N. Matsui, R. Kuroda, and M. Kurosaka. Functional comparison of posterior cruciate-retaining versus posterior stabilized total knee arthroplasty. *Journal of Arthroplasty*, 19:349–353, 2004.

[130] J. Mason, T. Fehring, R. Estok, D. Banel, and K. Fahrbach. Meta-analysis of alignment outcomes in computer-assisted total knee arthroplasty surgery. *The Journal of Arthroplasty*, 22:1097–1106, 2007.

[131] P. Massin and A. Gournay. Optimization of the posterior condylar offset, tibial slope, and condylar roll-back in total knee arthroplasty. *The Journal of Arthroplasty*, 21(6):889–896, 2006.

[132] H. McEwen, P. Barnett, C. Bell, R. Farrar, D. Auger, M. Stone, and J. Fisher. The influence of design, materials and kinematics on the in vitro wear of total knee replacements. *The Journal of Biomechanics*, 38:357–365, 2005.

[133] Peter J. McNair, Mark G. Boocock, Nicholas D. Dominick, Richard J. Kelly, Bill J. Farrington, and Simon W. Young. A comparison of walking gait following mechanical and kinematic alignment in total knee joint replacement. *The Journal of Arthroplasty*, 33(2):560 – 564, 2018.

[134] S.P. Mell, S. Fullam, M.A. Wimmer, and H.J. Lundberg. Sensitivity of total knee replacement wear to tibial component malrotation. In *Transactions of the annual meeting - orthopaedic research society*, 2009.

[135] S.P. Mell, M.A. Wimmer, J.J. Jacobs, and H.J. Lundberg. Total knee replacement wear is most sensitive to transverse plane alignment - a parametric finite element study. In *Transactions of the annual meeting - orthopaedic research society*, 2009.

[136] R.L. Merkow, M. Soudry, and J.N. Insall. Patellar dislocation following total knee replacement. *The Journal of Bone and Joint Surgery, American Volume*, 67(9):1321–1327, 1985.

[137] H. Mizu-uchi, S. Matsuda, H. Miura, K. Okazaki, Y. Alasaki, and Y. Iwamoto. The evaluation of postoperative alignment in total knee replacement using a ct-based navigation system. *The Journal of Bone and Joint Surgery*, 90-B(8):1025–1031, 2008.

[138] Y. Mizuno, M. Kumagai, S.M. Mattessich, J.J. Elias, N. Ramrattan, A.J. Cosgarea, and E.Y.S. Chao. Q-angle influences tibiofemoral and patellofemoral kinematics. *Journal of Orthopaedic Research*, 19(5):834–840, 2001.

[139] Matthew F. Moran, Safia Bhimji, Joseph Racanelli, and Stephen J. Piazza. Computational assessment of constraint in total knee replacement. *Journal of Biomechanics*, 41(9):2013 – 2020, 2008.

[140] J. Moreland. Mechanisms of failure in total knee arthroplasty. *Clinical Orthopaedics and Related Research*, 226:49–64, 1988.

[141] J. Morrison. The mechanics of the knee joint in relation to normal walking. *Journal of Biomechanics*, 3:51–61, 1970.

[142] E. Most, S. Zayontz, G. Li, E. Otterberg, K. Sabbag, and H.E. Rubash. Femoral rollback after cruciate-retaining and stabilizing total knee arthroplasty. *Clinical Orthopaedics and Related Research*, 410:101–113, 2003.

[143] A. Mouttet and V. Sourdet. Europ total knee prosthesis with or without posterior cruciate ligament retention? comparative study at mid-term follow-up. *Orthopaedics and Traumatology: Surgery and Research*, 100:895–900, 2014.

[144] V. Musahl, K.M. Bell, A.G. Tsai, R.S. Costic, R. Allaire, T. Zantop, J.J. Irrgang, and F.H. Fu. Development of a simple device for measurement of rotational knee laxity. *Knee Surgery, Sports Traumatology, Arthroscopy*, 15:1009–1012, 2007.

[145] Y. Nagano, K. Naito, Y. Saho, S. Torii, T. Ogata, K. Nakazawa, M. Akai, and T. Fukubayashi. Association between in vivo knee kinematics during gait and the severity of knee osetoarthritis. *The Knee*, 19:628–632, 2012.

[146] S. Nakagawa, Y. Kadoya, S. Todo, A. Kobayashi, H. Sakamoto, M.A.R. Freeman, and Y. Yamano. Tibiofemoral movement 3: full flexion in the living knee studied by mri. *The Journal of Bone and Joint Surgery*, 82(B):1199–1200, 2000.

[147] J. Nevelos, E. Ingham, C. Doyle, A. Nevelos, and J. Fisher. The influence of acetabular cup angle on the wear of "biolox forte" alumina ceramic bearing couples in a hip joint simulator. *Journal of Materials Science: Materials in Medicine*, 12:141 – 144, 2001.

[148] D. Nicoll and D. Rowley. International rotational error of the tibial component is a major cause of pain after total knee replacement. *The Journal of Bone and Joint Surgery*, 92-B:1238–1244, 2010.

[149] NJR. National joint registry for england, wales, northern ireland and the isle of man: 13th annual report. 2006.

[150] NJR. National joint registry for england, wales, northern ireland and the isle of man: 15th annual report. 2018.

[151] T.L. Norman, J. Hutchison, M.R. Gardner, and J.D. Blaha. Knee loading due to varus and external rotation in gait supports medial compartment wear in total knee arthroplasty. *The Scientific Pages of Orthopedics and Rheumatism*, 1(1):8–18, 2017.

[152] W. Norman Scott, editor. *Insall and Scott Surgery of the Knee*. Elsevier, 5 edition, 2012.

[153] W. Norman Scott, editor. *Insall and Scott Surgery of the Knee, Volume II*. Elsevier, 6 edition, 2018.

[154] O.D. Noyes, F.R. abd Schipplein, T.P. Andriacchi, S.R. Saddemi, and M. Welse. The anterior cruciate ligament-deficient knee with varus alignment: An analysis of gait adaptations and dynamic joint loadings. *The American Journal of Sports Medicine*, 20(6):707–716, 1992.

[155] Knee Restoration Center of Indiana. Anatomy. Accessed 28.01.19.

[156] C. Olcott and R. Scott. Femoral component rotation during total knee arthroplasty. *Clinical Orthopaedics and Related Research*, 367:39–42, 1999.

[157] M.W. Pagnano, A.D. Hanssen, D.G. Lewallen, and M.J. Stuart. Flexion instability after primary posterior cruciate retaining total knee arthroplasty. *Clinical Orthopaedics and Related Research*, 356:39–46, 1998.

[158] J. Parizi, R.M. Nunley, K.R. Berend, A.V. Lombardi Jr, E.L. Ruth, and J.C. Clohisy. High level of residual symptoms in young patients after total knee arthroplasty. *Clinical Orthopaedics and Related Research*, 472(1):133–137, 2014.

[159] S. Parratte and M.W. Pagnano. Effect of postoperative mechanical axis alignment on the fifteen year survival of modern cemented total knee replacements. *The Journal of Bone and Joint Surgery*, 92(12):2143–2149, 2010.

[160] E. Pena, B. Calvo, M.A. Martinez, and M. Doblare. A three-dimensional finite element analysis of the combined behavior of ligaments and menisci in the healthy human knee joint. *Journal of Biomechanics*, 39(9):1686 – 1701, 2006.

[161] D. Pereira, F. Jaffe, and C. Ortiguera. Posterior cruciate ligament-sparing versus posterior cruciate ligament-sacrificing arthroplasty. *Journal of Arthroplasty*, 13:138–144, 1998.

[162] A. Perillo-Marcone and M. Taylor. Effect of varus/valgus malalignment on bone strains in the proximal tibia after tkr: An explicit finite element study. *Journal of Biomechanical Engineering*, 129(1):1–11, 2006.

[163] S. Pickering and D. Armstrong. Alignment in total knee replacement. *The Journal of Bone and Joint Surgery*, 468, 2012. URL http://www.boneandjoint.org.uk/content/focus/alignment-total-knee-replacement Accessed 27.10.2015.

[164] C. Plaskos, A. Hodgson, K. Inkpen, and R. McGraw. Bone cutting errors in total knee arthroplasty. *The Journal of Arthroplasty*, 17(6):698–705, 2002.

[165] Tobias Pohlen. Fourier descriptor. Accessed 19.12.17.

[166] L. Pruitt. Deformation, yielding, fracture and fatigue behaviour of conventional and highly cross-linked ultra high molecular weight polyethylene. *Biomaterials*, 26:905–915, 2005.

[167] S. Puloski, R. McCalden, S. MacDonald, C. Rorabeck, and R. Bourne. Tibial post wear in posterior stabilized total knee arthroplasty. *Journal of Bone and Joint Surgery*, 83:390–397, 2001.

[168] E. Rabinowicz. The least wear. *Wear*, 100:533 – 541, 1984.

[169] C.S. Ranawat. The patellofemoral joint in total condylar knee arthroplasty. pros and cons based on five- to ten-year follow-up observations. *Clinical Orthopaedics and Related Research*, 205:93–99, 1986.

[170] Amin S., N. Luepongsak, C.A. McGibbon, M.P. LaValley, D.E. Krebs, and D.T. Felson. Knee adduction moment and development of chronic knee pain in elders. *Arthritis and Rheumatism (Arthritis care and research)*, 51(3):371–376, 2004.

[171] T. Sando, R. McCalden, R. Bourne, S. MacDonald, and L. Somerville. Ten-year results comparing posterior cruciate-retaining versus posterior cruciate-substituting total knee arthroplasty. *Journal of Arthroplasty*, 30:210–215, 2015.

[172] W. Schroer, K. Berend, A. Lombardi, C. Barnes, M. Bolognesi, M. Berend, M. Ritter, and R. Nunley. Why are total knees failing today? etiology of total knee revision in 2010 and 2011. *The Journal of Arthroplasty*, 28:116–119, 2013.

[173] T. Schwenke, C. Kaddick, E. Schneider, and M. Wimmer. Fluid composition impacts standardized testing protocols in ultrahigh molecular weight polyethylene knee wear testing. *Proceedings of the Institution of Mechanical Engineers. Part H, Journal of Engineering in Medicine*, 219(6):457 – 64, 2005.

[174] T. Schwenke, D. Orozco, E. Schneider, and M. Wimmer. Differences in wear between load and displacement control tested total knee replacements. *Wear*, 267(5-8):757 – 762, 2009.

[175] G.R. Scuderi and J.N Insall. Total knee arthroplasty. current clinical perspectives. *Clinical Orthopaedics and Related Research*, 276:26–32, 1992.

[176] SharcNet. Choosing between linear and higher order elements. Accessed 14.11.18.

[177] SharcNet. Degenerated shape elements. Accessed 14.11.18.

[178] P. Sharkey, W. Hozack, R. Rothman, S. Shastri, and S. Jacoby. Why are total knee arthroplasties failing today? *Clinical Orthopaedics and Related Research*, 404:7–13, 2002.

[179] K. Shelburne, H. Kim, W. Sterett, and M. Pandy. Effect of posterior tibial slope on knee biomechanics during functional activity. *Journal of Orthopaedic Research*, 29:223–231, 2011.

[180] R. Shenoy, P.S. Pastides, and D. Nathwani. (iii) biomechanics of the knee and tkr. *Orthopaedics and Trauma*, 27(6):364 – 371, 2013.

[181] Omer Slevin, Anna Hirschmann, Filippo F. Schiapparelli, Felix Amsler, Rolf W. Huegli, and Michael T. Hirschmann. Neutral alignment leads to higher knee society scores after total knee arthroplasty in preoperatively non-varus patients: a prospective clinical study using 3d-ct. *Knee Surgery, Sports Traumatology, Arthroscopy*, Oct 2017.

[182] C.R Smith, M.F. Vifnos, R.L. Lenhart, J. Kaiser, and D.G. Thelen. The influence of component alignment and ligament properties on tibiofemoral contact forces in total knee replacement. *Journal of Biomechanical Engineering*, 138(2), 2016.

[183] H.J. Sommer. Polygeom.m. Accessed 29.01.18.

[184] A. Srivastava, G. Lee, N. Steklov, C. Colwell Jr., K. Ezzet, and D. D'Lima. Effect of tibial component varus on wear in total knee arthroplasty. *The Knee*, 19(5):560–563, 2012.

[185] British Standard. Geometric product specifications (gps) - surface texture: Profile method - nominal characteristics of contact (stylus) instruments. *ISO*, 3274, 1998.

[186] British Standard. *Implants for Surgery - Wear of Total Knee-joint Prostheses, Part 1: Loading and displacement parameters for wear-testing machines with load control and corresponding environmental conditions for test*, 2009. 14243-1.

[187] British Standard. *Implants for Surgery - Wear of Total Knee-joint Prostheses, Part 2: Methods of Measurement*, 2009. 14243-2.

[188] British Standard. *Implants for Surgery - Wear of Total Knee-joint Prostheses, Part 3: Loading and displacement parameters for wear-testing machines with displacement control and corresponding environmental conditions for test*, 2014. 14243-3.

[189] D-S. Suh, K-T. Kang, J. Son, O-R. Kwon, C. Baek, and Y-G. Koh. Computational study on the effect of malalignment of the tibial component on the biomechanics of total knee arthroplasty. *Bone and Joint Research*, 6(11), 2017.

[190] M. Sundfelt, L. Carlsson, C. Johansson, P. Thomsen, and C. Gretzer. Asceptic loosening, not only a question of wear. *Acta Orthopaedica*, 77:177–197, 2006.

[191] M. Tanzer. Posterior stabilized versus cruciate retaining total knee arthroplasty. *Journal of Arthroplasty*, 17:813–819, 1970.

[192] P. Trent and P. Walker. Wear and conformity in total knee replacement. *Wear*, 36:175–187, 1976.

[193] K. Valkering, S. Breugem, M. van den Bekerom, W. Tuinebreijer, and R. van Geenen. Effect of rotational alignment on outcome of total knee arthroplasty. *Acta Orthopaedica*, 86(4):432–439, 2015.

[194] M. Van Houtem, R. Clough, A. Khan, M. Harrison, and G. Blunn. Validation of the soft tissue restraints in a force-controlled knee simulator. *Proceedings of the Institution of Mechanical Engineers, Part H: Journal of Engineering in Medicine*, 220(3):449–456, 2006.

[195] Pieter-Jan T.K. Vandekerckhove, Matthew G. Teeter, Douglas D.R. Naudie, James L. Howard, Steven J. MacDonald, and Brent A. Lanting. The impact of coronal plane alignment on polyethylene wear and damage in total knee arthroplasty: A retrieval study. *The Journal of Arthroplasty*, 32(6):2012 – 2016, 2017.

[196] P. Walker and H. Haider. Characterizing the motion of total knee replacements in laboratory tests. *Clinical Orthopaedics and Related Research*, 410:54–68, 2003.

[197] P.S. Walker, G.W. Blunn, D.R. Broome, J. Perry, A. Watkins, S. Sathasivam, M.E. Dewar, and J.P. Paul. A knee simulating machine for performance evaluation of total knee replacements. *Journal of Biomechanics*, 30:83–89, 1997.

[198] P.S. Warren, T.K. Olanlokun, A.G. Cobb, P.S. Walker, and B. Iverson. Laxity and function in knee replacements: A comparative study of three prosthetic designs. *Clinical Orthopaedics and Related Research*, 305:200–228, 1994.

[199] R.C. Wasielewski, D.D. Galat, and R.D. Komistek. Correlation of compartment pressure data from an intraoperative sensing device with postoperative fluoroscopic kinematic results in tka patients. *Journal of Biomechanics*, 38(2):333–339, 2005.

[200] G. Waslewski, B. Marson, and J. Benjamin. Early, incapacitating instability of posterior cruciate ligament-retaining total knee arthroplasty. *Journal of Arthroplasty*, 13:763–767, 1998.

[201] F. Werner, D. Ayers, L. Maletsky, and P. Rullkoetter. The effect of varus/valgus malalignment on load distribution in total knee replacements. *Journal of Biomechanics*, 38:349–355, 2005.

[202] S. White, R. Paxson, M. Tanner, and L. Whiteside. Effects of sterilization on wear in total knee arthroplasty. *Clinical Orthopaedics and Related Research*, (331):164 – 171, 1996.

[203] R. Willing and I. Kim. Three dimensional shape optimization of total knee replacements for reduced wear. *Journal of Structural and Multidisciplinary Optimization, Medical and Bioengineering Application*, 38:405–414, 2008.

[204] R. Willing and I.Y. Kim. A holistic numerical model to predict strain hardening and damage of uhmwpe under multiple total knee replacement kinematics and experimental validation. *Journal of Biomechanics*, 42(15):2520–2527, 2009.

[205] Huseyin S. Yercan, Tarik Ait Si Selmi, Tahir S. Sugun, and Philippe Neyret. Tibiofemoral instability in primary total knee replacement: A review, part 1: Basic principles and classification. *The Knee*, 12(4):257–266, 2005.

[206] J. Yim, E. Song, M. Khan, Z. Sun, and J. Seon. A comparison of classical and anatomical total knee alignment methods in robotic total knee arthroplasty. *The Journal of Arthroplasty*, 28:932–937, 2013.

[207] D. Zhao, H. Sakoda, W. Sawyer, and B. Fregly. Predicting knee replacement damage in a simulator machine using a computational model with a consistent wear factor. *Journal of Biomechanical Engineering*, 130, 2008.

[208] M. Zihlmann, A. Stacoff, J. Romero, I. Quervain, and E. Stussi. Biomechanical background and clinical observations of rotational malalignment in tka: Literature review and consequences. *Clinical Biomechanics*, 20:661–668, 2005.

[209] M. Zumstein, L. Frauchiger, D. Wyss, R. Hess, and P. Ballmer. Is restricted femoral navigation sufficient for accuracy of total knee arthroplasty? *Clinical Orthopaedics and Related Research*, 451:80–86, 2006.

Appendix

Table A.1: Gait cycle points and the AF and FE, AP, TR and AA displacements at which the contact pressure and area measurements were taken for the **ideal** alignment condition

Soft Tissue Condition	Point	AF (N)	FE (°)	AP (mm)	TR (°)	AA (°)
Stiff Knee	1	1402	-25.3	0.7	0.1	-0.7
	2	2433	-22.4	0.3	2.6	-0.6
	3	624	0.1	1.9	3.5	0.4
	4	168	27.9	-0.1	-0.2	0.6
Resected ACL	1	1402	-25.3	1.9	0.4	-0.7
	2	2433	-22.4	0.6	3.6	-0.7
	3	367	4	5.4	7.0	-0.1
	4	168	27.9	-0.7	-0.3	1.2
Resected ACL & PCL	1	1402	-25.3	1.9	0.5	-1.7
	2	2433	-22.4	0.6	3.6	-1.6
	3	275	6	6.6	7.7	-1.3
	4	168	27.9	0.1	-0.9	0.4

Table A.2: Gait cycle points and the AF and FE, AP, TR and AA displacements at which the contact pressure and area measurements were taken for the **varus** alignment condition

Soft Tissue Condition	Point	AF (N)	FE (°)	AP (mm)	TR (°)	AA (°)
Stiff Knee	1	1402	-25.3	1.3	0.5	-0.1
	2	2433	-22.4	0.9	2.7	-0.2
	3	952	-3.9	2.6	3.7	-0.1
	4	168	27.9	0.2	0.4	0.0
Resected ACL	1	1402	-25.3	2.9	0.2	0.6
	2	2433	-22.4	1.7	3.6	0.3
	3	367	4.1	5.8	7.8	0.5
	4	168	27.9	1.3	3.0	1.7
Resected ACL & PCL	1	1402	-25.3	3.0	-0.1	0.6
	2	2433	-22.4	1.7	3.6	0.4
	3	275	6.1	7.6	8.2	0.3
	4	168	27.9	2.7	0.1	0.8

Table A.3: Gait cycle points and the AF and FE, AP, TR and AA displacements at which the contact pressure and area measurements were taken for the **rotated** alignment condition

Soft Tissue Condition	Point	AF (N)	FE (°)	AP (mm)	TR (°)	AA (°)
Stiff Knee	1	1402	-25.3	1.5	7.0	1.6
	2	2433	-22.4	0.6	11.8	0.6
	3	1682	-11.5	1.8	11.8	1.8
	4	168	27.9	-0.3	1.5	-0.3
Resected ACL	1	1402	-25.3	3.0	9.7	3.0
	2	2433	-22.4	1.3	15.1	1.3
	3	624	0.1	5.6	15.7	5.6
	4	168	27.9	1.4	8.1	1.4
Resected ACL & PCL	1	1402	-25.3	2.9	10.3	2.9
	2	2433	-22.4	1.4	16.2	1.4
	3	367	4.1	7.6	17.7	7.6
	4	168	27.9	2.0	9.8	2.0

Table A.4: Gait cycle points and the AF and FE, AP, TR and AA displacements at which the contact pressure and area measurements were taken for the **kinematic** alignment condition

Soft Tissue Condition	Point	AF (N)	FE (°)	AP (mm)	TR (°)	AA (°)
Stiff Knee	1	1402	-25.3	-1.6	-1.1	2.2
	2	2433	-22.4	-2.3	1.1	2.1
	3	484	2.1	0.9	2.7	2.1
	4	168	27.9	-0.4	0.4	2.1
Resected ACL	1	1402	-25.3	-3.7	0.2	1.0
	2	2433	-22.4	-4.8	3.5	1.0
	3	210	8.1	2.3	6.4	0.7
	4	168	27.9	-3.0	1.5	1.2
Resected ACL & PCL	1	1402	-25.3	-3.7	0.2	1.7
	2	2433	-22.4	-4.8	3.6	1.7
	3	210	8.1	2.3	6.5	1.4
	4	168	27.9	-3.1	1.8	1.9

Table A.5: Gait cycle points and the AF and FE, AP, TR and AA displacements at which the contact pressure and area measurements were taken for the **tibial slope** alignment condition

Soft Tissue Condition	Point	AF (N)	FE (°)	AP (mm)	TR (°)	AA (°)
Stiff Knee	1	1402	-25.3	-0.5	-0.5	-1.1
	2	2433	-22.4	-1.0	2.1	-1.3
	3	624	0.1	1.1	4.2	-0.3
	4	168	27.9	-0.4	-0.9	0.4